THE PHYSICAL REVIEW

VOLUME 89 Second Series NUMBER 6

MARCH 15, 1953

Published for the

AMERICAN PHYSICAL SOCIETY

by the

AMERICAN INSTITUTE OF PHYSICS

Incorporated

LANCASTER, PA., AND NEW YORK, N. Y.

THE PHYSICAL REVIEW

A journal of experimental and theoretical physics established by E. L. Nichols in 1893

Published by the American Institute of Physics
for the
AMERICAN PHYSICAL SOCIETY

Officers

President

ENRICO FERMI
Institute for Nuclear Studies
University of Chicago
Chicago 37, Illinois

Vice-President

H. A. BETHE
Cornell University
Ithaca, New York

Secretary

K. K. DARROW
Bell Telephone Laboratories
Office:
Columbia University
New York 27, New York

Treasurer

G. B. PEGRAM
Columbia University
New York 27, New York

Local Secretary
for the Pacific Coast

J. KAPLAN
University of California at Los Angeles
Los Angeles, California

Managing Editor

S. A. GOUDSMIT
Brookhaven National Laboratory
Upton, Long Island
New York

BOARD OF EDITORS

Editor

S. A. GOUDSMIT

Associate Editor

H. Fesbach

Associate Editors

1953–1955	1953–1954	1953–1956
E. L. Chaffee	W. P. Allis	W. A. Fowler
H. Feshbach	F. G. Brickwedde	Kenneth Greisen
M. Goldhaber	W. B. Fretter	Charles Hutter
C. H. Johnson	Conyers Herring	R. E. Marshak
J. Sawyer	H. W. Lewbenz	W. K. H. Panofsky
C. H. Townes	Arnold Nordsieck	V. F. Weisskopf

Manuscripts for publication should be submitted to S. A. Goudsmit, Brookhaven National Laboratory, Upton, Long Island, New York. The authors' institutions are requested to pay a publication charge of $15 per page printed. If honored, entitles them to 100 free reprints. Instructions will be sent with galley proofs.

Proof and all correspondence concerning papers in the process of publication should be addressed to the Publication Manager, American Institute of Physics, 57 East 55 Street, New York 22, New York.

Subscription Price

United States and Canada.....$20.00
Elsewhere.....$22.00

Back Numbers[1]

Purely back number rate when complete year is available:
Prior to 1918: $25.00
Thereafter: $15.00
Single copies: $2.50 each, prior to July, 1929;
$1.50 each, July, 1929–December, 1941;
$2.00 each, January, 1942–December, 1945;
$2.50 each, thereafter.
Current Index, 1951–1952: $4.00.

Subscriptions, renewals, and orders for back numbers should be addressed to the American Institute of Physics, 57 East 55 Street, New York 22, New York.

Changes of address in the case of members of the American Physical Society should be addressed to the Treasurer; in the case of other subscribers to the American Institute of Physics.

[1] The Ryan Library of Physics Department, Cornell University, Ithaca, New York.

The Physical Review is published semimonthly at Prince and Lemon Streets, Lancaster, Pennsylvania.

Entered as second-class matter March 6, 1917, at the Post Office at Lancaster, Pennsylvania, under the Act of March 3, 1879.

Acceptance for mailing at special rate of postage provided for in paragraph (d-2), section 34.40, P. L. & R. of 1948, authorized January 27, 1925.

THE
PHYSICAL REVIEW

A journal of experimental and theoretical physics established by E. L. Nichols in 1893

SECOND SERIES, VOL. 89, NO. 6 MARCH 15, 1953

Mean Excitation Potentials*

DONALD C. SACHS, *Stanford Research Institute, Stanford, California*

AND

J. REGINALD RICHARDSON, *Department of Physics, University of California, Los Angeles, California*

(Received September 22, 1952)

Previous experimental results of the present authors on the energy loss of 18-Mev protons in aluminum are corrected to give a value for the mean excitation potential $I=168$ ev. It is pointed out that recent work on the range-energy relationship for protons in aluminum may indicate a variation of I with proton energy which is considerably larger than that to be attributed to the nonparticipation of the K electrons.

THE results of a measurement of the absolute energy loss of protons upon passing through various materials have been recently published.[1] Since that time, it has become evident that an out-of-date and inaccurate value of the constant e^2/mc^2 was used[2] in computing the mean excitation potentials of these materials. In the light of new work[3-5] that has been done in the field of proton ranges and excitation potentials, it was thought worth while to correct the previous computations.

In Bethe's energy loss formula,[6]

$$-dE/dx=(4\pi NZ^2e^4/mv^2)B, \quad B=Z\ln(2mv^2/I)-C_k,$$

the atomic stopping number B can be obtained from the experimentally determined $dE/d\sigma$ by using the relation

$$B=\frac{\beta^2 A}{4\pi mc^2 r_0^2 N_0}\left(\frac{-dE}{d\sigma}\right).$$

Here $\beta=v/c$, $r_0=e^2/mc^2$, $A=$atomic weight of the absorber, $N_0=$Avogadro's number, and $-dE/d\sigma$ is the energy loss per unit surface density of the absorbing foil. Negligible error is introduced in this experiment by using the average value of β^2 during the energy loss. Also the mean excitation potential

$$I=2\beta^2mc^2\exp[(-B+C_k)/Z].$$

It is to be noted from these relations that a half-percent error in r_0 will be reflected as a six percent error in I.

Using the value 2.818×10^{-13} cm for r_0 we obtain the corrected results for aluminum which are shown in Table I. The values of the other constants used are $mc^2=0.5108$ Mev, $N_0=6.0228\times10^{23}$ atoms per gram atom (chemical scale), $A=26.98$ g for aluminum. The weighted average for aluminum becomes $I=168$ electron volts.

TABLE I. Mean excitation potential of aluminum.

Surface density (mg/cm²)	Most probable energy loss (Mev)	Mean excitation potential (ev) (with probable error)
7.153	0.153	179.3±21.5
14.054	0.301	181.3±13.6
21.432	0.465	172.7± 8.6
21.532	0.470	167.0± 9.6
33.875	0.737	175.8± 7.0
38.395	0.839	173.8± 5.0
47.457	1.048	168.7± 8.3
57.493	1.276	168.6± 5.9
67.294	1.515	160.9± 5.4
76.849	1.737	161.6± 4.1

* This work was supported in part by the joint program of the U. S. Office of Naval Research and the U. S. Atomic Energy Commission.

[1] D. C. Sachs and J. R. Richardson, Phys. Rev. **83**, 834 (1951).

[2] We are greatly indebted to Dr. Joseph E. Perry for bringing this discrepancy to our attention.

[3] N. Bloemberger and P. J. van Heerden, Phys. Rev. **83**, 561 (1951).

[4] K. B. Mather and E. Segrè, Phys. Rev. **84**, 191 (1951).

[5] E. L. Hubbard and K. R. MacKenzie, Phys. Rev. **85**, 107 (1952).

[6] M. S. Livingston and H. A. Bethe. Revs. Modern Phys. **9**, 262 (1937). See this paper for notation.

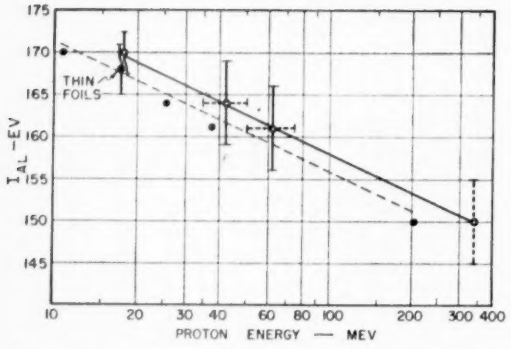

FIG. 1. Mean excitation potential of aluminum as a function of proton energy. The solid curve connects points obtained from proton range-energy experiments. The dotted curve represents an approximate thin-foil energy loss function.

Table II presents a summary of the results of recent experiments[7] which determined the mean excitation potential of aluminum. Our experiment (Sachs-Richardson) was performed with thin foils of material where the loss of proton energy in the foils was a small fraction of the incident energy (see Table I). In contrast, the remaining experimenters measured the complete proton ranges in aluminum. Assuming for the moment that there is a real variation of I with proton energy, Kaus has calculated the value of the proton energy which represents an effective value for the entire energy loss. He assumes that

$$I(E)=I_0-a\log E$$

is the functional relationship between I and the proton energy and that $a/I_0\lesssim 0.1$. From this, one obtains the result that $E_{\text{eff}}\simeq 0.6E_{\text{inc}}$. This E_{eff} for each experiment is shown in column 3 of Table II. Of course, for thin foils we have $E_{\text{eff}}\simeq E_{\text{inc}}$. In column 4 of this table, the I_{Al} values (with standard deviations) are listed. The standard deviations to the excitation potentials were obtained from the respective papers with the exception of that of Mather and Segrè. In this case the standard deviation had to be computed from their statements[8] of the approximate deviations (i.e., about 1 Mev for the energy and 0.2 g/cm² for the ranges).

Figure 1 shows a semi-log plot of the mean excitation potential of aluminum *vs* proton energy. The open circles refer to the incident proton energies (column 2 of Table II), while the solid circles represent the effective energies as defined above. The point corresponding to the thin foil result is not changed when account is taken of the effective proton energy. Upon consideration of the results in the figure, it is clear that better experimental data would be desirable before deciding that the variation of I with energy is real. It should also be pointed out that the effect of I of the nonparticipation of K electrons[6] has been taken into account in the treatment of the experimental data when use is made of C_k. Even if these calculated corrections were ignored entirely, the apparent variation of I over this energy range would only be of the order of 6 ev, which is small compared to the indicated experimental variation.

The thin foil mean ionization potentials for some other materials are shown in Table III. These results were computed using C_k, C_l, $\cdots=0$, i.e., no corrections for nonparticipating electrons were made. These corrections, if they were known, would tend to lower the values of the potentials.

TABLE II. The results of recent experiments which measured the mean excitation potential of aluminum.

Experiment	Incident proton energy (Mev)	Effective proton energy (Mev)	Mean excitation potential of aluminum (ev)
Sachs-Richardson[a]	17.8	17.8	168±3
Hubbard-MacKenzie[b]	18.0	10.8	170±2.5
Bloembergen-van Heerden[c]	35–50	21–30	164±5
	50–75	30–45	161±5
Mather-Segrè[d]	340	204	150±5

[a] See reference 1.
[b] See reference 5.
[c] See reference 3.
[d] See reference 4.

[7] See also D. H. Simmons, Proc. Phys. Soc. (London) **A65**, 454 (1952).

TABLE III. Weighted averages of the mean excitation potentials of various materials.

Material	Weighted average mean excitation potential (ev)
Nickel	399
Copper	435
Rhodium	799
Silver	796
Cadmium	792
Tin	853
Tantalum	1148
Gold	1383
Nylon	41.3

[8] See reference 4, p. 193.

Scattering of Neutrons by Deuterons*

R. K. ADAIR, A. OKAZAKI, AND M. WALT†
University of Wisconsin, Madison, Wisconsin
(Received November 21, 1952)

Angular distributions and total cross sections for neutrons scattered by deuterons were measured at various neutron energies ranging from 220 kev to 3 Mev. A proportional counter filled with deuterium was irradiated with monoenergetic fast neutrons produced by bombarding thin lithium and tritium-filled zirconium targets with protons from the electrostatic generator. Angular distributions of the neutrons scattered by deuterons were determined by measuring the distribution in energy of the recoiling deuterons with a differential discriminator. Total neutron-deuteron cross sections were measured by comparing the neutron transmission of heavy water with ordinary water. Phase shifts determined from an analysis of the data were not in agreement with theoretical conclusions of Buckingham and Massey or of Verde.

I. INTRODUCTION

THE lack of any marked success in determining the properties of the nucleon-nucleon interaction in odd states, and hence the exchange character of nuclear forces, from nucleon-nucleon scattering experiments has led to an interest in the scattering of neutrons and protons by deuterons. Because of the large radius of the deuteron, relatively low energy neutrons and protons are strongly scattered in states of angular momentum greater than zero. Detailed calculations by Buckingham, Massey, and Hubbard[1,2] and by Verde[3] have shown that, in particular, the sign and magnitude of the P-wave phase shifts should be strongly affected by the exchange character of nuclear forces.

Although there have been many determinations of neutron-deuteron angular distributions[4–10] and total cross sections,[11–13] it has been difficult to reach any definite conclusions as to the role of exchange forces in the $n-d$ interaction. Since the theoretical calculations are based on nuclear force models which do not adequately explain nucleon-nucleon scattering, one should not expect phase shifts calculated in this way to be more than qualitatively reliable. The differential cross sections are a sensitive function of the combination of at least six phase shifts at energies at which the main experimental results exist; therefore it is difficult to learn much from comparisons of theoretical and experimental differential cross sections.

It would be preferable to compare calculated phase shifts with phase shifts determined from analysis of the experimental results. However, even disregarding experimental uncertainties, which are not small in these measurements, neutron-deuteron differential cross section measurements cannot determine a unique set of phase shifts unless restrictions are imposed on the phase shifts from other considerations than the data alone. Recent measurements[14,15] concerning the neutron-deuteron scattering lengths have made it possible to make reliable estimates of S-wave phase shifts up to neutron energies of a few Mev by using an effective range approximation.[16] It then appeared that angular distribution and total cross section measurements at low energies where D-waves would not be important, might determine P-wave phase shifts which could be compared with phase shifts calculated by using various exchange force prescriptions.

II. TOTAL CROSS SECTION MEASUREMENTS

Measurements of the difference between the total neutron-deuteron cross section and the neutron-proton cross section were made by comparing the transmissions for monoenergetic neutrons of brass cans filled with heavy water and similar cans filled with the same number of molecules per cm² of ordinary water. The heavy water, obtained from Stuart Oxygen Company, was stated to be 99.8 percent pure by the supplier; a measurement of the density confirmed this value within an error of one percent. Transmissions were determined in a manner similar to that previously reported.[17]

For measurements at neutron energies greater than 900 kev, monoenergetic neutrons were produced by bombarding thin tritium-filled zirconium targets with protons from the electrostatic generator. The target was found to be 25 kev thick for 3.5-Mev protons by measuring the experimental width of the 2.08-Mev neutron scattering resonance in carbon.[17] This level has

* Work supported by the U. S. Atomic Energy Commission and the Wisconsin Alumni Research Foundation.
† U. S. Atomic Energy Commission Predoctoral Fellow.
[1] R. Buckingham and H. Massey, Proc. Roy. Soc. (London) **A179**, 123 (1941).
[2] Buckingham, Hubbard, and Massey, Proc. Roy. Soc. (London) **A211**, 183 (1952).
[3] M. Verde, Helv. Phys. Acta **22**, 339 (1949).
[4] J. H. Coon and H. H. Barschall, Phys. Rev. **70**, 592 (1946).
[5] J. H. Darby and J. B. Swann, Australian J. Sci. Research **A1**, 18 (1948).
[6] E. Wantuch, Phys. Rev. **84**, 169 (1951).
[7] Hamouda, Halter, and Sherrer, Phys. Rev. **79**, 539 (1950).
[8] I. Hamouda and G. Montmoulin, Phys. Rev. **83**, 1277 (1951).
[9] J. H. Coon and R. F. Taschek, Phys. Rev. **76**, 710 (1949).
[10] Griffith, Remley, and Kruger, Phys. Rev. **79**, 443 (1950).
[11] Nuckolls, Bailey, Bennett, Bergstralh, Richards, and Williams, Phys. Rev. **70**, 805 (1946).
[12] H. Aoki, Proc. Phys. Soc. Japan **21**, 232 (1939).
[13] Poss, Salant, Snow, and Yuan, Phys. Rev. **87**, 11 (1952).
[14] D. G. Hurst and W. F. Alcock, Can. J. Research **29**, 36 (1951).
[15] Wollan, Schull, and Koehler, Phys. Rev. **83**, 700 (1951).
[16] H. A. Bethe, Phys. Rev. **76**, 38 (1949).
[17] Bockelman, Miller, Adair, and Barschall, Phys. Rev. **84**, 69 (1951).

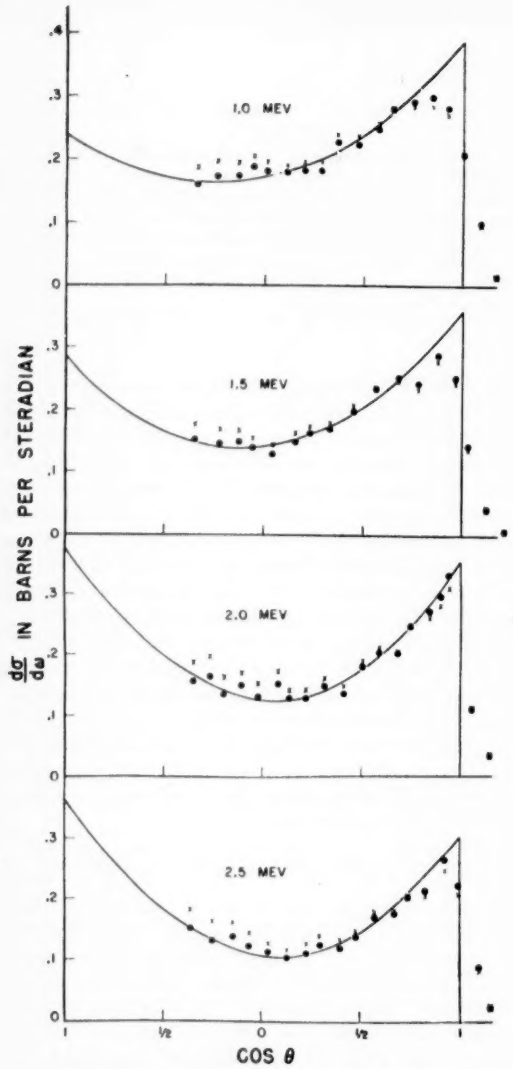

FIG. 1. Angular distributions in the center-of-mass system of neutrons scattered by deuterons at neutron bombardment energies of 1 Mev, 1.5 Mev, 2 Mev, and 2.5 Mev. The crosses represent the uncorrected data. The solid circles represent the data corrected for end effects and wall effects. The solid curve shows the distribution calculated from the phase shifts of Fig. 4.

been found to have a natural width of less than 10 kev. The neutrons were detected by a cylindrical pulse ionization chamber which had an active volume $\frac{1}{16}$ in. in diameter and 4 in. long. For detection of high energy neutrons the counter was filled with 43 atmospheres of purified hydrogen. A pulse-height discriminator eliminated pulses of less than one-half the incident neutron energy, in this way reducing the background, which is mainly caused by room-scattered neutrons, to less than one percent.

Below 900 kev it seemed advantageous to make use of the larger flux available from the Li(p, n) reaction. It was necessary to operate the counter at reduced pressures to improve the signal-to-noise ratio. Presumably the increased mobility of the electrons results in a larger voltage change during the time determined by the clipping time constant of the amplifier. The thickness of the target was found to be 25 kev by measuring the apparent width of the narrow 820-kev scattering resonance in beryllium.[17]

The cylindrical brass cans were constructed from 0.032 in. brass. Various lengths were used throughout the measurements in an effort to keep the transmission of the can containing ordinary water above 40 percent, thereby reducing uncertainties from multiple scattering into the detector. The scatterer was placed 7 in. from the source and 7 in. from the detector. With this geometry, the attenuation of the beam results from removal of all neutrons scattered through angles greater than 8° by the scatterer. Corrections, which considered the probable angular distribution of the scattered neutrons, were made for neutrons scattered into the counter.

The second column of Table I presents the measured cross section differences and their probable errors. Uncertainties in the inscattering corrections, the number of nuclei per cm^2, and the statistical standard deviation were considered in estimating the probable error. Column b shows the neutron-proton cross section calculated from the effective range theory[18] using as parameters[18,19] $A_s = -23.7\times10^{-13}$ cm, $A_t = 5.38\times10^{-13}$ cm, $\rho_t = 1.704\times10^{-13}$ cm, and $\rho_s = 2.5\times10^{-13}$ cm. Cross sections calculated from these parameters are in agreement with the results of measurements recently made in this laboratory.[20] Column c represents the neutron-deuteron cross section calculated from columns a and b. Probable errors can be considered to be about equal to those in column a.

The values are in agreement with early work of Aoki[12] and of the Minnesota group.[11]

III. ANGULAR DISTRIBUTIONS

Angular distributions of neutrons scattered by deuterons were determined using a method similar to that previously reported.[21] Monoenergetic neutrons were used to bombard deuterium in a proportional counter and the angular distribution of the scattered neutrons was determined by measuring the distribution in energy of the deuteron recoils. Barschall and Kanner[22] have pointed out that this distribution is proportional to the differential scattering cross section per unit solid angle as a function of $\cos\vartheta$, where ϑ is the angle of scattering in the center-of-mass system. The propor-

[18] Burgy, Ringo, and Hughes, Phys. Rev. **84**, 1160 (1951).
[19] E. E. Salpeter, Phys. Rev. **82**, 60 (1951).
[20] Fields, Becker, and Adair, Bull. Am. Phys. Soc. **27**, No. 5, 23 (1952).
[21] R. K. Adair, Phys. Rev. **86**, 155 (1952).
[22] H. H. Barschall and M. H. Kanner, Phys. Rev. **58**, 590 (1940).

tional counter was the same as used previously. Pulse-height distributions were measured with a single-channel differential discriminator. A channel width of 2½ volts was used. The position of the bottom of the channel could be varied from 0 to 50 volts.

Measurements of the $n-d$ angular distributions at neutron energies of 1 Mev, 1.5 Mev, 2 Mev, and 2.5 Mev were made by irradiating the counter with fast neutrons from the T(p, n) reaction. The tritium target was the same as used for the total cross section measurement. For these measurements the counter was filled with 20 cm of deuterium, and sufficient argon was added to reduce the recoil track length of deuterons scattered in the forward direction to about 9 mm. The total pressure, therefore, was varied with the neutron energy. A gas multiplication of about ten was obtained with about 3000 volts on the center wire and 800 volts between the wire and guard sleeve. A set of ten $B^{10}F_3$ filled proportional counters encased in paraffin was used to monitor the neutron flux. Measurements were made with the active volume of the counter in line with the proton beam and about 7 in. from the source. Backgrounds, determined by interposing a 10-in. cone of paraffin between the counter and the source, were found to be negligible. The crosses on Fig. 1 indicate the pulse-height distributions obtained in this way; the ordinate of each point is proportional to the number of counts in the channel per unit neutron flux, and the abscissa is proportional to the bias voltage measured to the center of the channel.

Slightly different procedures were used to obtain the angular distributions at energies of 220 kev, 500 kev, and 750 kev. Since the low energy group of neutrons from the Li(p, n) reaction will not interfere with measurements at these energies, it seemed again advantageous to make use of the greater flux from this reaction. For measurements at 220 kev the chamber was filled with 78 cm of deuterium and operated at a gas multiplication of about 30. The crosses in Fig. 2 show the distributions obtained with the neutrons produced by bombarding a 25-kev thick lithium target with protons from the electrostatic generator.

TABLE I. Total neutron cross section of deuterium. Column a gives the experimental difference in the neutron-proton and neutron-deuteron cross section in barns for 9 values of neutron energy in Mev. Column b gives the $n-p$ cross section calculated from effective range theory. Column c is obtained by subtracting column a from column b.

E_n	a	b	c
0.262	5.25–0.11	8.47	3.22
0.593	2.62–0.10	5.60	2.98
0.872	1.67–0.08	4.57	2.90
1.178	1.18–0.10	3.89	2.71
1.505	0.82–0.09	3.41	2.59
1.772	0.49–0.05	3.11	2.62
2.185	0.34–0.04	2.76	2.42
2.598	0.21–0.04	2.49	2.28
2.962	0.19–0.03	2.30	2.11

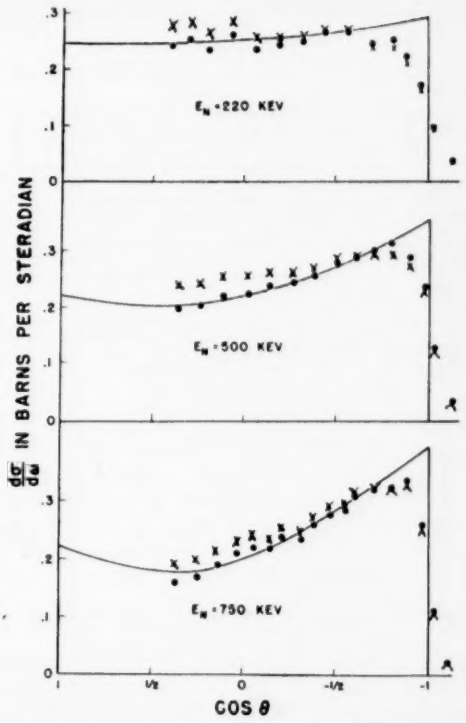

FIG. 2. Angular distributions in the center-of-mass system of neutrons scattered by deuterons at neutron bombardment energies of 220 kev, 500 kev, and 750 kev. The crosses represent the uncorrected data. The solid circles represent the data corrected for end effects and wall effects. The solid curve shows the distribution calculated from the phase shifts of Fig. 4.

Corrections must be made to pulse-height distributions before one can relate them to differential cross sections. In particular, allowance must be made for tracks which enter or leave the active volume expending only part of their energy in this volume. Recoils of each energy E are lost when deuterons of this energy strike the walls or leave the active volume of the counter by passing out of the end. Spurious pulses of energy E are produced when recoils of energy greater than E leave the active volume of the counter after losing only the fraction of this energy equal to E in the active volume. In computing corrections for these effects it was assumed, for simplicity, that the active volume ended sharply at planes normal to the center wire intercepting the ends of the guard sleeves. Corrections were then calculated numerically using deuteron range-energy curves. The uncertainty in the correction is estimated to be equal to about one-third of the correction and is of the same magnitude as the purely statistical errors.

The solid circles on Fig. 1 and Fig. 2 represent the corrected pulse-height distributions. Since the pulse-height distribution is proportional to the angular distribution, the circles also represent differential cross

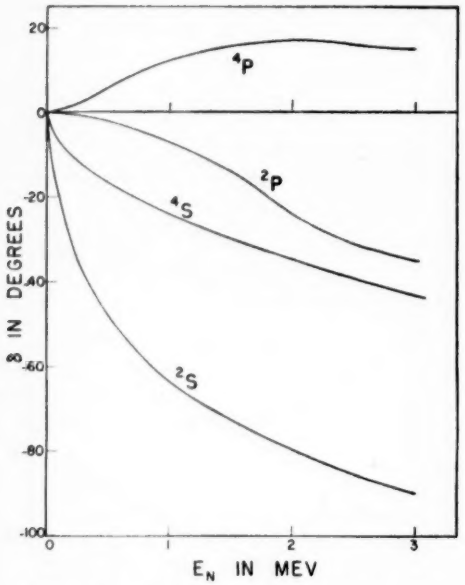

FIG. 3. Phase shifts for neutron-deuteron scattering.

sections. The ordinate is scaled so that a reasonable extension of the distribution to small angles results in a total cross section in agreement with the measured values. We estimate that the differential cross sections determined in this way are reliable to within about 15 percent, except at 180° where the poor resolution of the counter may give too low a value by a somewhat larger factor.

The results at 2.5 Mev are in excellent agreement with the measurements of Coon and Barschall.[4]

IV. INTERPRETATION

If we assume that the total spin of the system and its Z component are conserved, we can write the differential cross section for the scattering of neutrons by deuterons as

$$d\sigma/d\omega = k^{-2}[\tfrac{1}{3}|\textstyle\sum_l (2l+1)^2 A_l P_l(\cos\vartheta)|^2 + \tfrac{2}{3}|\textstyle\sum_l (2l+1)^4 A_l P_l(\cos\vartheta)|^2], \quad (1)$$

where $A_l = e^{i\delta_l}\sin\delta_l$ is the complex scattering amplitude for partial waves associated with orbital angular momentum l, the superscript on A represents the spin multiplicity, and δ is the scattering phase shift. At low energies we can assume that only S and P waves are scattered appreciably, and the cross section takes the form

$$d\sigma/d\omega = k^{-2}(A + B\cos\vartheta + C\cos^2\vartheta), \quad (2)$$

where

$$A = \tfrac{1}{3}\sin^2{}^2\delta_0 + \tfrac{2}{3}\sin^2{}^4\delta_0,$$

$$B = 2\sin^2\delta_0\sin^2\delta_1\cos({}^2\delta_0 - {}^2\delta_1) + 4\sin^4\delta_0\sin^4\delta_1\cos({}^4\delta_0 - {}^4\delta_1),$$

$$C = 3\sin^2{}^2\delta_1 + 6\sin^2{}^4\delta_1.$$

It is obviously not possible to extract the four phase shifts from the three parameters, A, B, and C, available from the experimental measurements.

It appears possible, however, to make a unique determination of the phase shifts by requiring them to behave in a physically plausible manner, and to be consistent with the zero energy scattering lengths. The antisymmetrization of the wave function required by the Pauli principle results in effective regions of repulsion in ${}^4S$, ${}^2P$, ${}^4D$ states, etc. These phase shifts might then be expected to be less positive than the ${}^2S$, ${}^4P$, ${}^2D$ phases. Since there exists a state of the doublet system bound by about 6 Mev, the ${}^2S$ radial wave function should have a node at about the triton radius. The ${}^2S$ phase shift should, therefore, lie in the second quadrant and the scattering length should be positive and of the same magnitude as the triton radius.

Two sets of scattering lengths are consistent with the low energy neutron-deuteron scattering data;[14,15] ${}^2a = 0.7\pm0.3\times10^{-13}$ cm, ${}^4a = 6.38\pm0.06\times10^{-13}$ cm, and ${}^2a = 8.26\pm0.12\times10^{-13}$ cm, ${}^4a = 2.6\pm0.2\times10^{-13}$ cm. Only the latter set is in agreement with the existence of a nearby bound state of the triton.

Gordon[23] has pointed out that if one accepts the charge symmetry of nuclear forces, the low energy proton-deuteron scattering measurements establish this choice of scattering lengths. Theoretical calculations by Troesch and Verde[24] are in good agreement with these values, though the results of Buckingham and Massey are less satisfactory in this respect.

It is possible to estimate the S-wave phase shifts by using the scattering lengths and the effective range approximation,[16] $k\cot\delta = -1/a + \frac{1}{2}\rho k^2$. The scattering lengths[14,15] used were ${}^2a = 8.3\times10^{-13}$ cm and ${}^4a = 2.7\times10^{-13}$ cm. The phases are not very sensitive to the range ρ, which was taken, rather arbitrarily, as 5×10^{-13} cm. Since scattering amplitudes are not affected by a shift of 180°, the ${}^2S$ phases are represented in the fourth quadrant for convenience.

An interesting characteristic of the scattering is the shift in the asymmetry of the angular distribution with energy. At low energies back scattering is predominant, while at higher energies there is some indication that most of the scattering is in the forward direction. Other workers[5,8–10] have shown that this trend continues to higher energies. Since the S-wave phase shifts are both negative, Eq. (2) shows that back scattering is the result of interference between the S waves and P waves which have a positive phase shift. Forward scattering must be due to the interference effects of S waves and P waves with a negative phase shift. The angular distribution at 1.5 Mev has a large P-wave contribution quadratic in $\cos\vartheta$, but is nearly symmetric about 90°. This can only occur if the asymmetric $S-P$ interference terms from doublet and quartet states are of opposite signs and cancel. This will occur if the ${}^2P$ and

[23] M. M. Gordon, Phys. Rev. **80**, 1111 (1950).
[24] A. Troesch and M. Verde, Helv. Phys. Acta **24**, 39 (1951).

^4P waves are of opposite sign. From our considerations regarding the effects of the exclusion principle, we see that the ^4P-wave phase shift must be positive and the ^2P-wave phase shift negative. At low energies the $^4P^4S$ interference term, resulting in back scatterings, is more important than the $^2P^2S$ term which gives rise to preferential scattering in the forward direction. At higher energies the $^2P^2S$ term is dominant. Figure 3 shows S- and P-wave phase shifts as a function of energy. They were adjusted by trial and error to best fit the data. The phase shifts were required to change smoothly with energy and to vary[25] as $E^{(2l+1)/2}$ at low energies. Above 750 kev, S-wave phases a little smaller than calculated by the effective range parameters best fit the data. The solid curves on Fig. 1 and Fig. 2 show differential cross sections calculated with these phase shifts. The solid curve on Fig. 4 shows the total cross section calculated from the phase shifts, while the points represent the experimental determinations.

At the higher energies the effects of D waves probably will not be negligible. These effects may be most evident in $P-D$ interference terms in $\cos^3\vartheta$. Since the neutron-deuteron angular distributions are particularly unreliable at 180° where the D-wave contributions might be large, any estimate of the D-wave phase shifts must be obtained from another source. Measurements[26] of the proton-deuteron differential scattering cross section are quite accurate. If nuclear forces are charge symmetric the proton-deuteron phase shifts should differ from the neutron-deuteron phase shifts only because of Coulomb forces. While it is not possible to calculate the effects of Coulomb forces without a detailed understanding of the interaction, it is probable that the proton-deuteron phase shifts will be somewhat smaller than the neutron-deuteron phase shifts at the same energy. The points on Fig. 5 show the experimental values for the proton-deuteron differential cross section at 2.53 Mev. The solid curve is calculated from phase shifts similar to but smaller than the neutron-deuteron phase shifts at 2.5 Mev. The phase shifts were adjusted to fit the experimental results at 125° and 55°, angles where the D wave vanishes. The dotted curve shows the differential cross section with the added contributions of a ^2D-wave phase shift of $+7°$ and a ^4D-wave phase shift of $+1°$. Cumulative effects of uncertainties in the approximations made are sufficiently great so that the values of the D-wave phase shifts are of only qualitative significance.

It can be shown that the measurements of Wantuch[6] at 4.5 Mev and 5.5 Mev are not in contradiction with an interpretation in terms of phase shifts resulting from an extrapolation of the phases in Fig. 3. Though this conclusion is in disagreement with the statement of Latter and Latter[27] that the S-wave phase shifts are

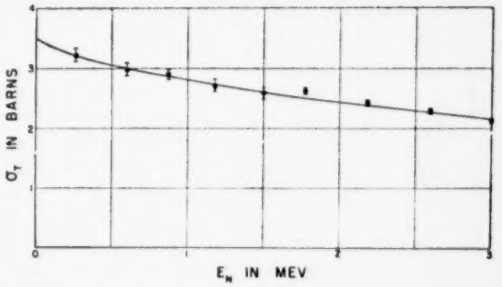

FIG. 4. The neutron-deuteron total cross section as a function of neutron bombarding energy. The points represent the experimental values while the solid curve represents values calculated from the phase shifts of Fig. 3.

"almost certainly positive," it is not in contradiction with the careful survey made by these authors of the possible combinations of phase shifts which could fit both the neutron-deuteron and proton-deuteron data. Slight adjustments of the phase shifts listed as $u=1$ $(1+-)$ in the notation of their article are consistent both with our low energy conclusions and the 5-Mev data.

It has been assumed in this discussion that the Z component of the total spin of the system is a good quantum number. In view of the strong spin orbit interactions observed in other neutron scattering experiments[21] and the importance of tensor forces in nuclear interactions, it would appear that the neglect of spin orbit coupling may not be realistic. Considering only S and P waves, the differential scattering cross section, with spin orbit coupling, takes the form

$$\begin{aligned}\frac{d\sigma}{d\omega}=\frac{1}{3k^2}\Big[&\left|{}^4A_0^{3/2}+\left(\frac{6}{5}{}^4A_1^{5/2}+\frac{9}{5}{}^4A_1^{3/2}\right)\cos\vartheta\right|^2\\&+\left|\frac{3\sqrt{3}}{5}{}^4A_1^{3/2}-\frac{3\sqrt{3}}{5}{}^4A_1^{5/2}\right|^2\sin^2\vartheta\\&+\left|{}^4A_0^{3/2}+\left(\frac{9}{5}{}^4A_1^{5/2}+\frac{1}{5}{}^4A_1^{3/2}+{}^4A_1^{1/2}\right)\cos\vartheta\right|^2\\&+\left|\frac{1}{2}{}^4A_1^{1/2}+\frac{2}{5}{}^4A_1^{3/2}-\frac{9}{10}{}^4A_1^{5/2}\right|^2\sin^2\vartheta\\&+\left|\frac{3\sqrt{3}}{10}{}^4A_1^{5/2}+\frac{\sqrt{3}}{5}{}^4A_1^{3/2}-\frac{\sqrt{3}}{2}{}^4A_1^{1/2}\right|^2\sin^2\vartheta\\&+\left|{}^2A_0^{1/2}+(2\,{}^2A_1^{3/2}+{}^2A_1^{1/2})\cos\vartheta\right|^2\\&\qquad+\left|{}^2A_1^{1/2}-{}^2A_1^{3/2}\right|^2\sin^2\vartheta\Big],\end{aligned}\tag{3}$$

where the added right-hand superscript on the scattering amplitudes represents the total angular momentum of the scattered wave. The general effect of spin orbit forces on the differential cross section is to add to the

[25] E. P. Wigner, Phys. Rev. **73**, 1002 (1948).
[26] Sherr, Blair, Kratz, Bailey, and Taschek, Phys. Rev. **72**, 662 (1947).
[27] A. L. Latter and R. Latter, Phys. Rev. **86**, 727 (1952).

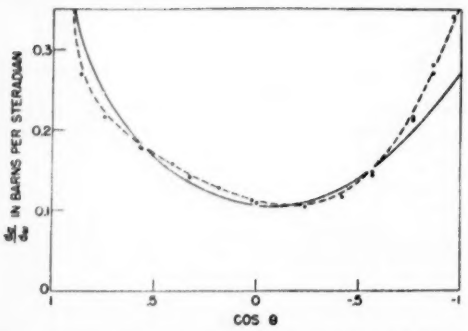

FIG. 5. Proton-deuteron angular distribution at 2.53 Mev. The points represent the experimental values of reference 26. The solid curve shows the angular distribution calculated using: $\delta(^1S)=-31°$, $\delta(^3S)=-80°$, $\delta(^3P)=-27°$, $\delta(^1P)=+15°$. The dotted curve shows the angular distribution calculated using the same S- and P-wave phases and $\delta(^1D)=+1°$ and $\delta(^3D)=+7°$.

isotropic part of the cross section and subtract from the terms which are quadratic in $\cos\vartheta$. The magnitudes of the terms in $\sin^2\vartheta$ of Eq. (3) are a measure of the kinematic importance of spin orbit forces. If the splitting, or angular difference, between the P waves associated with the same spin multiplicity but different total angular momentum be represented by Δ, the effect on the differential cross section will be of the order of $k^{-2}\sin^2\Delta$. This will be quite small compared to the isotropic term, unless the splitting Δ is of the same magnitude as the phase shifts of the P waves themselves. There is some evidence that the ^3P splittings are not large. Gamma-rays produced by the capture of protons by deuterons are emitted in a nearly pure $\sin^2\vartheta$ distribution.[28] and Wilkinson[29] has shown that they are almost completely polarized. This is explained as the result of an electric dipole transition from ^3P to ^3S state. In order that the angular distribution be nearly pure $\sin^2\vartheta$ it is necessary for $^3P_1$ and $^3P_1$ waves to be captured in the ratio of their statistical weights, an improbable occurrence if the two waves were refracted very differently.

It appears that little error is introduced in assuming the conservation of spin. Doublet-quartet transitions can only occur if the orbital angular momentum changes two units. Since only S and P waves are expected to be important at the energies under consideration in this experiment, it would seem justifiable to neglect the effects of such transitions. At higher energies $^4S \rightleftarrows {}^2D$, and $^2S \rightleftarrows {}^4D$ transitions may be important. Their effect on the angular distribution would be to increase the isotropic part of the cross section at the expense of the angular dependent part.

V. DISCUSSION

Qualitatively the neutron-deuteron angular distributions at 1.5 Mev and above are quite similar to the proton-deuteron angular distributions, and it appears from Fig. 5 that both sets of data can be fitted with similar phase shifts, a result which is in agreement with the equivalence of neutron-neutron and proton-proton forces.[30] Critchfield[31] has analyzed the proton-deuteron scattering using an auxiliary assumption, from the theoretical conclusions of Buckingham and Massey, that the ^2S and ^4S phases are equal. Though the validity of this assumption has since been shown to be dubious by the low energy neutron-deuteron scattering data, the P-wave phases extracted by Critchfield should not be strongly affected by this. Since these phase shifts are very similar to those derived here from the neutron-deuteron scattering data, the general conclusions of Critchfield are in agreement with this work.

A direct comparison of the phase shifts derived from these data with those calculated by Buckingham, Massey, and Hubbard[2] reveals rather considerable differences. As was evident from the scattering lengths, their S-wave phase shifts do not adequately represent the experimental data. The P-wave phase shifts should, in general, be less positive for exchange forces than for ordinary forces as the nucleon-nucleon potentials are repulsive in the antisymmetric space states which occur in P-wave interactions.

Both of the measured P-wave phases are more negative than theoretical values calculated for ordinary forces, and the ^2P-wave phase shift is much more negative than even the phase calculated for exchange forces. S-wave phase shifts derived by Troesch and Verde[24] are in good agreement with the phases in Fig. 3 for both ordinary and exchange forces. However, the P waves calculated by these authors at 2.5 Mev do not appear to adequately represent the data.

It was shown that the kinematic effects of spin orbit forces are not likely to change these conclusions appreciably. Of course, this does not exclude the importance of such forces on the dynamics of the interaction. Such forces may account for some of the discrepancy between the theoretical work which was calculated on the basis of central forces, and the conclusions from the experimental data.

[28] Fowler, Lauritsen, and Tollestrup, Phys. Rev. **76**, 1767 (1949).
[29] D. H. Wilkinson, Phil. Mag. **341**, 659 (1952).
[30] G. Breit, Phys. Rev. **80**, 1110 (1950).
[31] C. L. Critchfield, Phys. Rev. **73**, 1 (1948).

The Approach to Saturation in Dilute Ferromagnetics*

ALAN D. FRANKLIN AND AMI E. BERKOWITZ
Franklin Institute Laboratories for Research and Development, Philadelphia, Pennsylvania
(Received September 12, 1952)

The law of approach to magnetic saturation in finely divided and diluted iron powders has been studied. For samples containing volume fractions of iron greater than about 0.6, Néel's theory of fluctuation-controlled approach is valid. As the concentration of iron decreases, the deviation from the theory increases in the direction of steeper approach.

THE approach to magnetic saturation in "soft" ferromagnetic materials for field strengths between 500 and 10 000 oersteds usually follows a law of the form

$$I = I_s(1 - A/H), \tag{1}$$

where I is the intensity of magnetization, and I_s is its value when the magnetic field strength H becomes infinitely large. A is a constant, sometimes called the coefficient of magnetic hardness. Néel[1] has shown that this behavior is probably due to the presence of nonmagnetic inclusions in the material, and has derived an equation for the dependence of I upon H and upon V, the volume fraction of the sample occupied by the inclusions. In the field strength region in which $1 \leqslant 4\pi I_s/H \leqslant 5$, Néel's equation reduces approximately to Eq. (1), with

$$A = \tfrac{1}{2}(0.067)4\pi I_0 V, \tag{2}$$

where I_0 is the saturation magnetization of the ferromagnetic phase.

The theory considers only materials containing small amounts of inclusions, and has been verified[1] for sintered iron compacts containing up to 0.4 volume fraction of voids. For higher values, the theory cannot be expected to hold. Since this more dilute region should be of importance in studying the properties of very fine ferromagnetic powders, experimental data on the approach to saturation in this region are presented here.

The pressed specimens, $\frac{1}{4}$ in.$\times\frac{1}{4}$ in.$\times 1$ in., contained two micron carbonyl iron powder[2] mixed with 50A silica powder, and were cemented with a thermosetting resin. Magnetic measurements were made in a Sanford-Bennett[3] isthmus permeameter, with the field along the long direction of the samples, perpendicular to the pressing direction. The maximum field strengths used were of the order of 6000 oersteds. The volume fractions of the specimens were determined from the saturation magnetization and are accurate to within about 5 percent.

The values for the constant A in Eq. (1) were determined by least-squares calculations from the original $I-H$ data, weighting each value of I with H^2 to emphasize the high field points. These values are displayed in Fig. 1, plotted as a function of $(1-V)$. The solid line represents Néel's theory, in the form of Eq. (2). The figure also includes the data of Néel and Lorin, as reported by Néel,[1] on sintered iron compacts.

The experimental points begin to deviate from the theoretical line for samples containing about 40 percent by volume of voids. Below this figure, Néel's theory is applicable; above it, it appears that some other mechanism controls the approach to saturation.

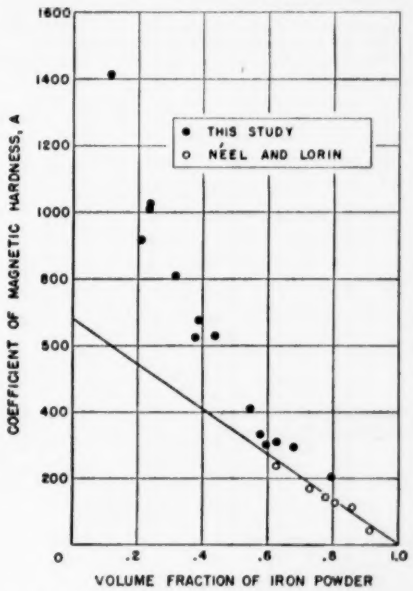

FIG. 1. Coefficient of magnetic hardness, A, as a function of the volume fraction of iron powder, $1-V$.

* The work described herein was performed under the auspices of the U. S. Office of Naval Research.
[1] L. Néel, J. phys. et radium **9**, 184 (1948).
[2] Provided through the generosity of the General Aniline and Film Corporation.
[3] R. L. Sanford and E. G. Bennett, J. Research Natl. Bur. Standards **10**, 567 (1933).

An Experimental Investigation of the Nucleon Cascade in Water

C. B. A. McCusker, H. Messel,* D. D. Millar† and N. A. Porter
Dublin Institute for Advanced Studies, Dublin, Ireland
(Received October 31, 1952)

The nucleon cascade in water produced by primaries of energy greater than 20×10^9 ev has been examined using an array of Geiger-Müller counters and a 31-channel hodoscope. Over 15 000 showers have been studied. Transition curves for various primary energies, barometric coefficients for various multiplicities and at different depths, root mean square lateral spreads, and intensities at different depths are given. The experimental results are compared with the theory of the nucleon cascade developed by Messel and his co-workers. In particular, the variation of lateral spread with depth substantiates their conclusion that the differential cross section for nucleon-nucleon collision at high energies has a very peaked form in the forward direction.

INTRODUCTION

THE apparatus described in this paper was originally set up to investigate the production of mesons in high energy nuclear encounters. The method used was to study local penetrating showers from water, paraffin, carbon, and lead using an array of Geiger-Müller counters operating a 31-channel hodoscope. While the experiment was in progress the theory of the nuclear cascade was considerably developed by Messel, Green, and their co-workers.[1,2] In this paper the results obtained from an examination of 15 000 penetrating showers from water are compared with this theory.

I. THE EXPERIMENTAL ARRANGEMENT

A sketch of the apparatus is given in Fig. 1. Trays A, B, C, D, and E each consisted of 12 Geiger-Müller counters 50 cm long by 3.8 cm wide. The axes of counters in tray A were at 90° to those of tray B. To provide a master pulse, at least 2 counters in each of trays B, C, and D had to be discharged, i.e., the master pulse was at least a sixfold coincidence. Each counter in trays A and B operated its own neon lamp. For the purpose of the hodoscope, the counters in tray D were connected in adjacent pairs. Each pair then operated a neon lamp. Finally the extended tray E, working with all its counters in parallel, operated a single neon lamp.

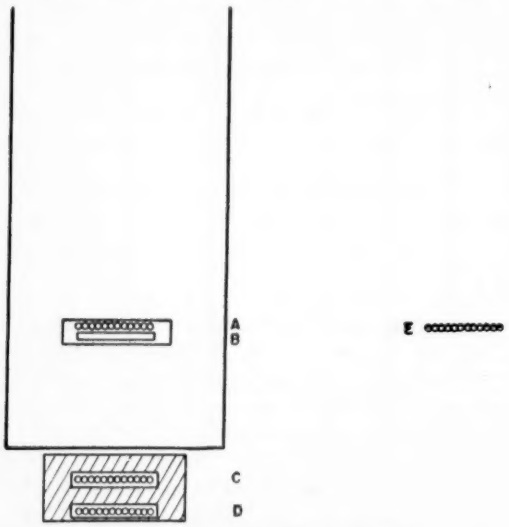

FIG. 1. The experimental arrangement.

Trays A and B were contained in a water tight sheet steel box. This box was itself inside an iron tank of height 8 ft and base 4 ft×4 ft. At the start of the experiment the water in the tank was just level with the top of the box (zero position). The water level was then raised in steps until a maximum depth of 180 cm over the box was reached, then reduced in similar steps and finally a second reading at the zero level was taken. This took 6 months.

Trays C and D were contained in a lead pile beneath the tank. Each counter in these trays was wrapped in lead sheet $\frac{1}{10}$ in. thick to reduce the effect of μ meson knock-ons. Above C the lead was 7.5 cm thick, between C and D 5 cm thick, and between D and the concrete floor 2.5 cm thick. On all sides there were 15 cm of lead. The extensive tray E was 2 m from the center line of the tank. The whole apparatus was housed in a wooden hut with a light roof.

II. ANALYSIS OF THE DATA

(1) Method

Complete details of each individual shower were punched on Hollerith cards. This was essential since it would be quite impossible to sort by hand the 15 000 showers already obtained in the various ways necessary to get all the information possible from the crude data. There are, of course, various ways of specifying the showers. One particularly useful and simple description is that of the "multiplicity" in terms of counters discharged in trays A and B. If, in these two trays, there are m and n counters discharged, $m>n$, the shower is called an m fold event; m is obviously the minimum number of particles necessary to produce this event.

* Now at the University of Sydney, Sydney, Australia.
† Now at the University of Manchester, Manchester, England.
[1] H. Messel, Commun. of the Dublin Institute for Advanced Studies (1951), Series A, No. 7.
[2] H. Messel, *Progress in Cosmic Ray Physics*, Vol. II (1953) (to be published).

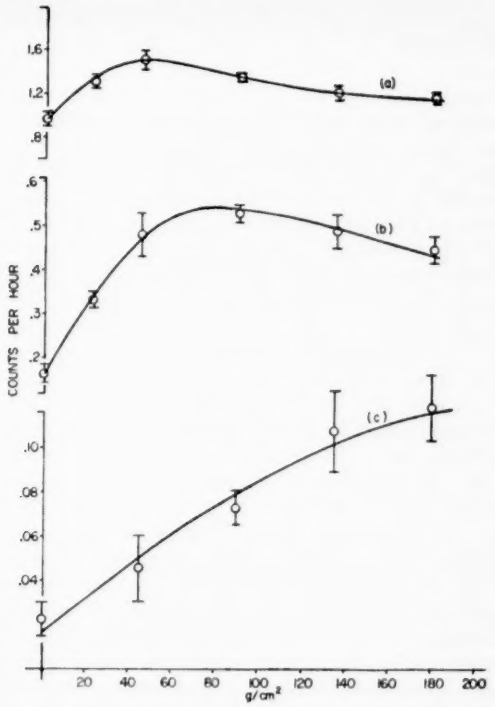

FIG. 2. The transition curves for (a) 2-fold, (b) 4-fold, and (c) 12-fold local showers.

Generally, the actual number of particles in the shower will be greater.

(2) The Extensive Showers

Of all the showers recorded, a fraction between $\frac{1}{3}$ and $\frac{1}{5}$, depending on the depth, discharged the extensive tray. The multiplicity distribution of these showers for the zero position is given in Table I. Multiplicity distributions for other thicknesses were not much different. In order to see if these showers were of the normal type (with $\gamma=1.5$, $k=1/40$) or not, the expected multiplicity distribution was calculated for such showers falling on an array consisting of two unshielded trays, one of 12 separate counters of which at least two must be discharged, the other of 12 counters in parallel, and a shielded tray of 12 counters of which at least two must be discharged. This array is an approximation to the real arrangement. Probably the greatest error is introduced by specifying that two penetrating particles are necessary. In extensive showers about $\frac{1}{3}$ of the penetrating particles are nucleons, and one nucleon if it interacts in the lead is sufficient to discharge the real shielded arrangement.

TABLE I. Multiplicity distribution for extensive showers.

Multiplicity		2	3	4	5	6	7	8	9	10	11	12
No. of showers	Expt.	130	109	116	86	84	66	81	76	70	98	342
	Calc.	72	70	68	68	68	71	75	84	101	141	442

The calculated distribution is given in Table I. The agreement between theoretical and calculated distributions is sufficiently good to make it likely that all the extensive showers recorded were of the normal type—the disagreement being due to the approximations in the calculation. It is, at first sight, surprising to find that it is possible to select showers of quite normal type which are represented on the apparatus by only two π-mesons or nucleons.[3]

(3) Transition Curves

For the local showers, transition curves for all multiplicities, 2-fold to 12-fold, were plotted (in this as in all other cases, the rates were corrected to a barometric pressure of 1000 millibars). Curves for 2 folds, 4 folds, and 12 folds are given in Fig. 2. Figure 3 shows the variation of the position of the cascade maximum with the number of particles at the maximum. This number was determined by the procedure given in the next section.

(4) Intensities of Charged Particles

It is possible to estimate the intensity of charged particles at a given depth caused by the single nucleons incident on the top of the water. To do this we must determine the number of charged particles which, on the average, produces the discharge of m and n counters on trays A and B [an (m, n) event] where $m>n$.

Let $P(N, n, m)$ be the probability that N particles produce an (n, m) event. A method of calculating these probabilities for a single tray assuming random distribution of the particles on the tray has been given by Schrödinger.[4] The extension to two crossed trays is elementary. The effect of the lack of randomness amongst the shower particles has been examined by Sitte and his co-workers[3] and found to be small. Now if $Q(N)$ is the probability of N particles occurring, the

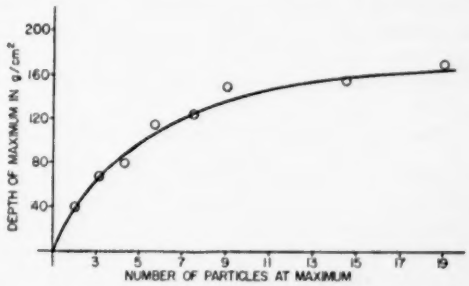

FIG. 3. The variation of the depth of the cascade maximum with the number of particles at the maximum for the complete cascade.

[3] Froehlich, Harth, and Sitte, private communication (1952).
[4] E. Schrödinger, Proc. Phys. Soc. (London) **A64**, 1040 (1951).

TABLE II. Intensities of all charged particles at different depths.

Depth in cm H_2O	22.5	45	90	135	180
No. of charged particles per hour	4.6	8.7	15.0	17.2	16.6

TABLE III. Corrected root mean square lateral spread of showers.

Depth (cm)	Spread corrected for background (cm)	Spread corrected for background, finite size of tray and angle of incidence (cm)
22.5	6.4	8.0
45	8.5	12.4
90	10.2	17.1
135	11.4	21.3
180	12.1	24.9

absolute probability of an (n, m) event is

$$\sum_{N=m}^{\infty} Q(N)P(N, n, m).$$

If we know the value of $Q(N)$ for all N, we can use the above formula to calculate the average number of particles $\bar{N}$, associated with any given n, m event. Then, if $R(n, m)$ is the rate of any given (n, m) event and $\bar{N}(n, m)$ is the associated average number of particles, the intensity for a particular depth is

$$\sum_{(n, m)} R(n, m)\bar{N}(n, m).$$

This must then be corrected for the background intensity.

Strictly it is necessary to know $Q(N)$ in order to calculate the averages and hence the intensity. However, the intensities are rather insensitive to the form of $Q(N)$ because, for small N, $P(N, n, m)$ approximates to a δ-function and the form of $Q(N)$ is then unimportant, and secondly, events of large N are comparatively rare.

This insensitivity was shown by first calculating the intensities assuming that $Q(N) \propto 1/N$, which is probably a reasonable approximation to reality. The result of this is given in Table II. Then the calculation was again performed assuming that $Q(1)=Q(2)=Q(3)$, etc., a physically impossible case. The difference in the final intensities was in all cases less than 6 percent.

(5) Lateral Spread of Showers

The total spread of each shower at the level A, B can be determined by measuring the distances between the extreme counters discharged on each tray. The product of the distances gives the square spread and the root mean square spread for all the showers at that depth can be obtained at once. A number of corrections must be applied before these results can be compared with theory.

First a correction must be made for the background showers which come from the air and the surroundings. To do this the mean square spread was found for the zero position. Then for all subsequent depths the contribution of these showers to the run in question was calculated (normalized both to time and the average barometric pressure over the runs) and subtracted from the total spread for the run. The remainder was taken to be the spread due to the genuine locally produced showers for that depth. The results corrected in this way are given in the second column of Table III.

A second correction is necessary for the angle of incidence of the primary. Because the apparatus itself constitutes a vertical telescope and because the high energy nucleon component at sea level is strongly peaked in the vertical direction[5] the correction is not large. If we take the variation of intensity with angle to be $\cos^6\theta$, then the average angle to the vertical of the showers is 17.5° and all spreads must be multiplied by 0.95 (=cos 17.5°).

Thirdly, a correction must be made for the finite size of the detecting trays. This has been done assuming that (a) if a shower has a spread of n counters, all counters within the spread are discharged; and (b) showers produced near the edge of apparatus have an equal chance of discharging the apparatus as centrally produced showers. The correction was then made by finding the recorded spread of every possible shower of a given real spread, including those striking the edges (remembering that at least 2 counters in tray B must be discharged). The recorded spreads were averaged and compared with the assumed spread, and the resulting correction table was used (together with the correction for angle of incidence) to give the results in the third column of Table III.

It is worth considering the effects produced by the breakdown of assumptions (a) and (b). If either of these assumptions is not fulfilled, the correction to be applied will be smaller, since in both cases it will be showers hitting the edge of trays which will be affected.

As a check on our method of measuring the root mean square spread we have measured the spread for the extensive showers for the zero position. The result was 18.2 cm which is to be compared with the 21.0 cm which would be produced if all the showers were of infinite extent and density. For such large spreads the correction table is necessarily inaccurate but the value given is >70 cm.

The further corrections which may be applied are: (a) A correction for the finite width of individual counters (3.8 cm). Since at least 2 counters in B must be discharged, showers whose spread is less than 3.8 cm will tend to be missed and hence the recorded average will be greater than the real average. (b) The complete cascade is measured, and it is obvious from the method of measurement that the effect of this inclusion of the nonnucleonic component can only be to increase the

[5] M. G. Mylroi and J. G. Wilson, Proc. Phys. Soc. (London) **A64**, 404 (1951).

measured spread. The true spread of the nucleon cascade will, if anything, be less than the measured spread.

(6) Barometric Effects

The barometric coefficient was determined for various multiplicities at various depths for both extensive and nonextensive showers. All gave values close to -10 percent per cm Hg with the exception of the nonextensive 2 folds at 0 and 90 cm. For these the values were -0.57 ± 1.0 percent per cm Hg and -4.2 ± 0.6 percent per cm Hg.

III. DISCUSSION OF RESULTS

Throughout the discussion which follows a number of points should be kept in mind; the intensities and results obtained in our experiment are necessarily for *all* ionizing particles capable of penetrating the sheet steel ($\frac{1}{16}$-in.) box. That is to say the intensity due to the complete cascade of nucleons, mesons, and electrons is measured. This cascade is probably started by the energetic sea-level nucleon component of the cosmic radiation. In order, therefore, to carry out a completely satisfactory comparison between theory and experiment, it would be necessary to measure the various effects of the different components separately, and secondly to compare the results obtained with those which would be given by a mixed-cascade theory. It is obvious that both of these tasks are formidable, and not likely to be achieved immediately.[6] The comparisons which follow should therefore be treated as qualitative, bringing out the main features of the various phenomena involved in the cascade process.

(1) Transition Curves and Intensities of Charged Particles

The lower limit to the energy of the particles measured must lie somewhere in the range 10^7–10^8 ev since they need only have sufficient energy to penetrate the steel box.

The minimum triggering energy of the apparatus, on the other hand is probably about 20.10^9 ev. This may be estimated in two ways. Firstly, Salant *et al.*[7] and the Bristol group[8] have shown that stars with two shower particles are produced on average by primaries of about 5×10^9 ev energy. A π-meson is classified as a shower particle if its energy is greater than 80×10^6 ev. Our apparatus, on the other hand, requires at least two penetrating particles of energy greater than 300×10^6 ev. This suggests that the minimum triggering energy is greater than 10×10^9 ev. Secondly, we can estimate the flux of energetic protons and neutrons through the apparatus using the intensity of protons and the exponent of the energy spectrum given by Mylroi and Wilson. Assuming the number of protons and neutrons to be equal, the calculated number of nucleons greater than 10×10^9 ev is 8 per hour. But at the maximum of our total transition curve we got 2.3 showers per hour over background. Thus, it seems reasonable to estimate that the minimum triggering energy is of the order of 20×10^9 ev.

The transition curves for local penetrating showers produced in water have been determined by Wataghin and his co-workers.[9] The arrangement used was a simple fourfold coincidence, and the single curve had a cascade maximum at 75 g/cm² (see Fig. 2). An examination of our results given in Fig. 2 reveals that as one passes from twofold to twelvefold events the depth at which the cascade maximum is attained increases. In other words there is a shift in the position of the maximum towards greater depths, with increasing primary energy (fixed secondary energy) or with decreasing secondary energy and a fixed primary energy. This behavior is in accordance with that predicted by cascade theory. From Messel's[5] work on the nucleon cascade it may easily be shown that the position of the cascade maximum for particles with energies $>E$ due to a primary nucleon of energy E_0 is given by $\theta_{max}\approx0.72\{\log_{10}(E_0/E)-0.79\}$ interaction lengths, whereas for a primary nucleon power law spectrum with exponent γ and particle energies $>E<E_c$ (E_c is the cut-off energy), $\theta_{max}\approx0.72\{\log_{10}(E_c/E)-0.79+0.43/(\gamma-0.55)\}$ interaction lengths. The corresponding expressions for electrons produced by a photon or spectrum of photons are given by

$$x_{max}=2.3\{\log_{10}(E_0/E)-0.32\}\text{ cascade lengths,}$$
$$x_{max}=2.3\{\log_{10}(E_c/E)-0.32+0.43/(\gamma-1)\}\text{ cascade lengths,}$$

respectively.[10] For energies $E>E_c$, in the case of a primary power law spectrum, no maximum occurs, since the intensity now decreases monotonically with increasing depth. The interpretation of Fig. 2 by means of the above theoretical results is now obvious, and qualitatively at least agreement between theory and experiment on this point is good.

It is now interesting to use the expression for θ_{max} in the case of nucleons and the result in Fig. 2 for the twofolds to obtain an estimate for the minimum triggering energy required by the apparatus. Taking $\gamma=1.8$ we find $E_c=68E$. The minimum energy E of the 2 folds is about 3×10^8 ev, since 12.5 cm of lead must be traversed

[6] Messel, Potts, and McCusker, Phil. Mag. **43**, 889 (1952) have recently set up and solved completely the equations for a mixed cascade forming within a nucleus, for various schemes of meson production. Master equations have also been formulated by Messel for a mixed-cascade developing in a finite absorber; numerical results for this last case are, however, unlikely to appear for some time because of the heavy computations involved.

[7] Salant, Hornbostel, Fisk, and Smith, Phys. Rev. **79**, 184 (1950).

[8] Camerini, Davies, Fowler, Franzinetti, Muirhead, Lock, Perkins, and Yekutieli, Phil. Mag. **42**, 1241 (1951).

[9] Meyer, Schwachheim, Wataghin, and Wataghin, Phys. Rev. **76**, 598 (1949).

[10] See, for instance, L. Janossy and H. Messel, Proc. Roy. Irish Acad. **A54**, 217 (1951).

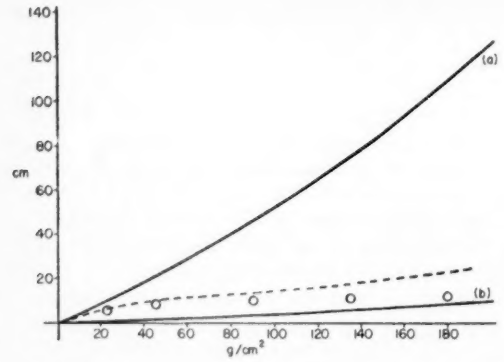

FIG. 4. The lateral spread of the complete cascade at different depths. Curve (a) gives the calculated curve for the nucleon cascade from the Messel-Green theory assuming a quasi-isotropic differential cross section; curve (b) that assuming a cross section of exponential form. The circles give the experimental points corrected for background, and the dashed curve is the estimated experimental upper limit.

in order to obtain a sixfold coincidence. The minimum triggering energy is therefore 2×10^{10} ev.

In Fig. 3 we have given the depth of the transition curve maximum plotted against the total number of charged particles at the shower maximum. This curve was obtained from our experimental results by the method discussed in the previous section of this paper. We note that as the depth at which the cascade maximum is attained increases, the number of charged particles at the maximum point of shower development increases. For showers which attain their maximum development at small depths, the number of particles at the maximum is small; this remains so until depths of the order of 160 g/cm² are attained. For showers which attain their maximum development beyond this depth, the number of particles at the maximum increases very rapidly. Agreement between these experimental facts and predictions by cascade theory is again very good. For instance, the average number of protons at the cascade maximum for the two cases discussed previously is given by

$$N_p(E_0, E; \theta_{\max}) \approx 0.36(E_0/E)^{0.55}\{9.36\log(E_0/E)-4.08\}^{-\frac{1}{2}},$$

and

$$N_p(E_c, E; \theta_{\max}) \approx \frac{0.36}{\gamma-0.55}\left(\frac{E_c}{E}\right)^{0.55}\left\{9.36\log(E_c/E) -4.08+\frac{4.05}{\gamma-0.55}+\frac{1}{(\gamma-0.55)^2}\right\}^{-\frac{1}{2}}.$$

In case of the electrons we have

$$N_e(E_0, E; x_{\max}) \approx 0.09(E_0/E)\{\log(E_0/E)-0.25\}^{-\frac{1}{2}},$$

and

$$N_e(E_c, E; x_{\max}) \approx \frac{0.09}{\gamma-1}(E_c/E)\left\{\log(E_c/E)-0.25 +\frac{0.43}{\gamma-1}+\frac{0.28}{(\gamma-1)^2}\right\}^{-\frac{1}{2}}.$$

Hence, with increasing ratio (E_0/E) or (E_c/E), both the depth of the cascade maximum and number of particles at this maximum increases. This phenomenon occurs for both the electrons and the nucleons separately. The experimental curve given in Fig. 3 must, therefore, consist of a *weighted* average of these two results. A further difficulty in making a quantitative comparison in this instance arises because of the low energies of the particles considered. The expressions for N_p and N_e are only valid for high energies where energy loss by ionization is included. If these losses are taken into account, the average number of particles at the cascade maximum given by N_p and N_e may be decreased by a factor of 2 or 3 depending upon the secondary energy considered. A rough calculation has been carried out taking ionization losses into account. The results obtained agree quantitatively with those found experimentally, provided a sufficiently low secondary energy E and a reasonable value of the weights to be applied to the average numbers are chosen.

(3) The Lateral Spread

The solid curves in Fig. 4 give the calculated lateral spread of the nucleon cascade in water for secondaries of energy 500 Mev and an incident power law of exponent 1.1 according to the theory of Messel and Green.[11] The upper curve is for a quasi-isotropic cross section, the lower for a cross-section exponential in the laboratory system. Also displayed on the graph are the experimental points corrected for the background showers and the experimental curve (shown dashed) corrected also for the angle of incidence of the primary and the finite size of the detecting tray. No correction for the finite size of the counters or for the nonnucleonic component has been made. Since the further corrections to be applied all tend to reduce the spread, it seems likely that the dashed curve gives an upper limit for the spread of the cascade in water. It will be seen that the experimental curve strongly favors a differential cross section much more strongly peaked than the quasi-isotropic form.

There are two further effects to consider. It seems likely that the exponent of the proton spectrum at sea level is higher than 1.1,[5] and it also seems likely that particles of less than 500 Mev would be detected by

[11] H. S. Green and H. Messel, Phys. Rev. **85**, 679 (1952); Proc. Phys. Soc. (London) **A65**, 245 (1952); Phys. Rev. **88**, 331 (1952).

our apparatus. Both of these effects would increase the calculated spread for a given depth thus increasing the agreement between the experimental points and the curve calculated for the exponential form of the differential cross section. Evidence in favor of this form of differential cross section has already been given by Messel and Green,[11] and Hazen *et al.*[12] has shown that the Fermi distribution tends to give lateral spreads of extensive air showers considerably greater than those reported experimentally.

CONCLUSION

We have been able to determine experimentally the variation of the intensity of charged particles with depth, the variation of the lateral spread with depth, and the variation of the number of charged particles at the maximum of the transition curve with the depth of that maximum for the nucleon induced cascade in water. In all cases there is qualitative agreement with theory. Whereas in some cases the theory of the complete cascade is not sufficiently developed for a quantitative comparison to be possible, in the case of the lateral spread our results make it seem very likely that the differential cross section in high energy nucleon-nucleon collisions cannot have a quasi-isotropic form. On the other hand the exponential form suggested by Messel and Green gives good agreement.

We wish to thank Professor E. Schrödinger and Dr. R. C. Geary for their help and advice, Professor L. W. Pollak for allowing us the use of his meteorological records, and Messrs. A. Guinness, Son and Co. Ltd. for the loan of a large iron tank.

[12] Hazen, Heineman, and Lennox, Phys. Rev. **86**, 198 (1952).

PHYSICAL REVIEW VOLUME 89, NUMBER 6 MARCH 15, 1953

Relativistic Corrections to the Magnetic Moments of Nuclear Particles*

G. Breit and R. M. Thaler
Yale University, New Haven, Connecticut
(Received December 10, 1952)

A re-examination of the problem is reported. The results for the vector and scalar cases in the case of the deuteron are explained in terms of known correction factors for the one-body problem. For the vector equation part of the result is caused by an induction effect which is the meson theoretic generalization of Faraday's law of induction. In the scalar case the relation to the one-body result is made in a form employing an effective change in mass caused by the presence of the scalar. These interpretations are substantiated by an analysis in terms of plane waves. Simple forms are obtained for one particle in a pseudoscalar field and a tentative application to the deuteron is made and criticized.

1. INTRODUCTION AND NOTATION

RELATIVISTIC corrections to the magnetic moment of a single Dirac particle in a central potential field have been discussed by Breit[1] and by Margenau.[2] The latter has pointed out that an application of the formula applicable to the one-electron case to the deuteron problem gives effects comparable with the change of the magnetic moment expected on account of the admixture of a D-wave to the ground state of H^2. Caldirola[3] was the first to consider the relativistic correction for the case of a particle having an intrinsic magnetic moment in Pauli's sense. Caldirola's signs are either inconsistently used or applied with a misunderstanding regarding the correction factor for the proton, which differs from unity by an amount which is too small in absolute value under his postulated assumptions having been obtained as $-0.667+0.596=-0.071$ rather than $-0.667-0.596$. Since there is an almost compensating error for the neutron, the result for the deuteron is practically unaffected by this ambiguity. In view of this situation and the fact that Caldirola's work considered the particle with intrinsic Pauli moment to be in a central field, a condition which is not satisfied in the deuteron, the problem was again briefly treated by Breit.[4] In this discussion the correction for the intrinsic moment has the form

$$1-\langle T_\sigma\rangle/Mc^2,$$

where T_σ is the part of the kinetic energy owing to motion along the direction of the particle spin. The character of the field enters the result only through T_σ, and this part of the correction may therefore be used directly for the deuteron. The relativistic factor for a single charged particle in a central scalar field was also contained in this work. It was pointed out in the same note that a single particle treatment does not suffice for the calculation of effects stemming from the Dirac current of the particle's charge; the contribution to the relativistic correction arising from the charge of the

* Assisted by the joint program of the U. S. Office of Naval Research and the U. S. Atomic Energy Commission.
[1] G. Breit, Nature **122**, 649 (1928).
[2] H. Margenau, Phys. Rev. **57**, 383 (1940).
[3] P. Caldirola, Phys. Rev. **69**, 608 (1946).
[4] G. Breit, Phys. Rev. **71**, 400 (1947).

proton may in fact be affected by the two-body character of the problem.

This aspect has been treated by Sachs[5] and by Breit and Bloch,[6] the papers being concerned with hypothesized scalar and vector interactions. The calculations of Breit and Bloch contain an error in manipulation as has been ascertained for the scalar case by Adams[7] and confirmed by Breit.[8] The corrected result agrees with that obtained by Sachs[5] for the same field. The error just mentioned affected the results for the vector field as well, the same erroneously evaluated integral having entered both cases. The corrected vector case factor turned out to be unity in disagreement with the result of Sachs. The procedure used by Sachs was not convincing; the effective Hamiltonians were not covariant and the employment of momentum operators for current was made in such a way as to omit part of the effect of spin currents in the vector case. On the other hand, the main point brought out in the discussions of Breit,[4] Sachs,[5] Breit and Bloch,[6] and Primakoff[9] has been that it was not possible to make relativistic corrections with certainty and there existed considerable uncertainty in attempts at quantitative conclusions regarding the fractional content of the ^3D state in the ground state of the deuteron. From this viewpoint the result of Sachs for the vector case may be regarded as an illustration of the flexibility which could be attained if one invented a vector meson field in which coupling to the nuclear spin current would be absent. The papers mentioned have not considered the pseudoscalar interaction which appears at present to be the most probable one. In view of the absence of a consistent and error free treatment of the two-body problem it appeared desirable to reexamine the subject, establishing more obvious connections between single particle and two-body results and removing some of the uncomfortable dependence on involved calculations which has been necessary so far. A discussion of the pseudoscalar interaction is included. The answer in this case is especially simple, the correction factor being Mc^2/E for a single particle. The small magnitude of this correction suggests agreement with experiment for the deuteron, where $(\mu_N+\mu_P)-\mu_D=0.879-0.857=0.022$. Here μ_N, μ_P, μ_D are the magnetic moments of the neutron, the proton, and the deuteron, respectively. However, such an identification is difficult to justify since it involves the assumption of additivity of nucleon moments.[10–12] The possibility of additional corrections having their origin in distorting or exchange effects between nucleons is not denied, but the percentage of D state arrived at by Lévy[13] from the *PSps* theory and from nuclear two-body data does not definitely indicate its presence.

[5] R. G. Sachs, Phys. Rev. **72**, 91 (1947).
[6] G. Breit and I. Bloch, Phys. Rev. **72**, 135 (1947).
[7] E. N. Adams II, Phys. Rev. **81**, 1 (1951).
[8] See footnote 20 of E. N. Adams (reference 7). The authors wish to thank Dr. Adams for his correspondence relating to this matter and for making available some of his calculations.
[9] H. Primakoff, Phys. Rev. **72**, 118 (1947).
[10] H. Miyazawa, Prog. Theoret. Phys. **7**, 207 (1952).
[11] R. Osborn and L. Foldy, Phys. Rev. **79**, 795 (1950).
[12] R. G. Sachs, Phys. Rev. **74**, 433 (1948).

Notation

I, II . . . subscripts designating the two particles. For the deuteron, I designates the proton, II the neutron.

1, 2 . . . subscripts designating respectively values of a quantity for a one-body and two-body problem; these subscripts are used only when a distinction between the two cases is necessary.

E = energy including rest mass energies.

$\mathbf{p}$ = momentum (variable canonically conjugate to coordinate).

$\boldsymbol{\alpha}=(\alpha_x, \alpha_y, \alpha_z)$ = Dirac's four-row square matrix vector.

$\boldsymbol{\alpha}=\rho_1(\sigma_x, \sigma_y, \sigma_z)$, where the σ are Dirac's four-row spin matrices.

β = Dirac's $\alpha_4=\rho_3$.

$\boldsymbol{\sigma}$ = Pauli's two-row square matrix vector when it occurs in a nonrelativistic approximation.

ψ = Dirac's spinor wave function having four components per particle.

Φ = column matrix formed by first two components ("small" components) of ψ in one body problem; employment of Dirac's original representation of the α_μ is presupposed. In the two body problem Φ is operated on by spinor index matrices like the direct product of the corresponding quantities for the two particles.

Ψ, χ_{I}, χ_{II} are quantities similar to Φ with Ψ "large" in both particles; χ_{I} "small" in I and "large" in II; χ_{II} "large" in I and "small" in II.

W = energy excluding rest mass energies; W is negative for the deuteron.

M = mass of nucleon.

T = kinetic energy in nonrelativistic approximation, excluding rest mass energies.

J = negative of potential energy in nonrelativistic approximation.

$\mathbf{u}$ . . . arbitrary fixed unit vector.

u . . . index used for designation of components along $\mathbf{u}$.

$f=dJ/rdr$.

$[A, B]_+=AB+BA$.

$\mathbf{r}$ = position vector in the one-body case. In the two-body case $\mathbf{r}=\mathbf{r}_{\mathrm{I}}-\mathbf{r}_{\mathrm{II}}$.

$r=|\mathbf{r}|$.

$\mathfrak{A}$ = mesic vector potential.

$\mathcal{J}=\mathcal{J}(|\mathbf{p}-\mathbf{p}'|)$ = momentum transform of J, see Eq. (12.4).

$\mathcal{J}'=(d\mathcal{J}(x)/dx)_{x=|\mathbf{p}-\mathbf{p}'|}$.

$\mathfrak{L}(\mathbf{p})C(\mathbf{p})$ = wave function in momentum space.

$\mathfrak{L}(\mathbf{p})=(E^a+Mc^2)\beta+c(\boldsymbol{\alpha}\mathbf{p})$.

$E^a=|(M^2c^4+p^2c^2)^{\frac{1}{2}}|$.

C = four-component amplitude column matrix, describing spin orientation and sign of energy.

[13] M. Lévy, Phys. Rev. **88**, 725 (1952). The authors are grateful to Dr. Lévy for making available to them a preprint of this paper.

C_- = two-component amplitude column matrix, corresponding to negative energy, consisting of the first and second components of C.

C_+ = two-component amplitude column matrix, corresponding to positive energy, consisting of the third and fourth components of C.

$\mathbf{L}=[\mathbf{r}\times\mathbf{p}]$.

$\mathbf{v}=[\mathbf{u}\times\mathbf{r}]$.

$\mathcal{C}$ = two-body wave function in momentum space.

g = pseudoscalar coupling constant.

χ = pseudoscalar nonquantized wave field.

2. LIMITATIONS OF PREVIOUS FORMAL TREATMENTS

(a) The Treatment of Sachs[5]

In this discussion the scalar and vector interactions are considered, employing explicitly a nonquantized meson field. The field produced by I is used in static approximation, and the terms corresponding to it are included in the part of the two-body Hamiltonian which belongs to II in the uncoupled problem. The Hamiltonian is then symmetrized in I and II. The assumption is made that it suffices to use a static approximation for the meson field produced by I in the process just described and that in the vector case one may substitute for $\boldsymbol{\alpha}_\mathrm{I}$ the approximate representation by $\mathbf{p}_\mathrm{I}$.

The approximation mentioned last neglects the effect of the particle spin current of I. This current carries with it a current of mesic charge. Its neglect is analogous to disregarding the magnetic field caused by the spin magnetic moment of one electron in a calculation of the magnetic moment of the second electron. According to Lenz' law one expects the spin current of the second electron to change in such a direction as to oppose the change of magnetic flux through a fixed closed curve produced by the first electron.

The Hamiltonians used by Sachs include some corrections of order v^2/c^2 but omit corrections for retardation which are formally of the same order of magnitude. Without a demonstration of the absence of effects of retardation on the magnetic moments one cannot arrive at a definite conclusion regarding the value of the magnetic moment.

The construction of Hamiltonians by the procedure described can at most establish them to the second order of the interaction constant. The treatment of the deuteron to this order is not sufficient for the reproduction of experimental results as is clear from the fact that a calculation of p-n scattering by the first Born approximation would be very inaccurate. The corrections dealt with cannot be believed in, therefore, for the whole interaction unless an additional justification can be made.

(b) The Treatment of Breit and Bloch[6]

This work makes use of the possibility of formally correcting some types of wave equations for lack of relativistic invariance of their predictions. It employs Hamiltonians thus set up employing all terms literally. While consistent from the formal viewpoint of covariance, the method lacks justification in the following respects.

No proof has been given that in addition to the terms which have been added to the Hamiltonians in order to secure covariance there are not present other terms of relative order v^2/c^2. It is well known that requirements of covariance alone do not determine a two-body Hamiltonian but only restrict the choice of possibilities. To be sure the vector equation is a rather immediate extension of the special case of electromagnetic interaction. But in this case the terms of the form

$$\tfrac{1}{2}[(\boldsymbol{\alpha}_\mathrm{I}\boldsymbol{\alpha}_\mathrm{II})J-(\boldsymbol{\alpha}_\mathrm{I}\mathbf{r})(\boldsymbol{\alpha}_\mathrm{II}\mathbf{r})(dJ/rdr)]$$

have been established[14] only to the extent of representing the energy correction through their expectation value. It is in fact possible to obtain wrong results in radiation problems by employing these terms to calculate the wave function. In the magnetic moment problem the magnetic interaction-retardation terms yield a nonvanishing contribution, and a justification of the employment of the approximate Hamiltonian therefore has to be given. A complete treatment would consist in a calculation avoiding the use of a two-body Hamiltonian, except possibly as an intermediate step, but based otherwise on a consistent field theory. Since such a theory is not available a perfect treatment is impossible. The scalar equation used by Breit and Bloch is subject to a similar criticism.

It is especially unclear and uncertain that the problem may be stated with sufficient accuracy in terms of a two-particle Hamiltonian with correction terms having a universal form in terms of J. Thus, e.g., if the correct treatment were capable of being formulated in terms of an expansion of observables in powers of J, then each term in the expansion could conceivably require different forms of relativistic corrections. The large value of the interaction constant usually denoted by f or g makes it impossible to disregard this possibility on the grounds of rapid convergence of the series in powers of J. The work of Salpeter and Bethe[15] indicates the likelihood of such effects since in hyperfine structure calculations they find additional terms of relative order $\alpha m/M$ with α, m, M standing for the fine structure constant and the masses of the particles.

3. VECTOR INTERACTION

A straightforward application of the method used by Breit and Bloch[6] gives for an S state of the deuteron system the correction factor to the proton moment owing to the proton charge as

$$(CF)_{V^{(2)}}=1-\langle(\sigma_\mathrm{I}-\sigma_\mathrm{II})_s\rangle[\langle T_2\rangle/(3Mc^2)], \qquad (1)$$

[14] G. Breit, Phys. Rev. **51**, 248 (1937).

[15] E. E. Salpeter, Phys. Rev. **87**, 328 (1952).

the two spins being supposedly oriented along the z axis, with T_2 representing the energy of relative motion. Subscripts I, II refer to the proton and neutron, respectively. For the parallel spin orientation in the ^3S state the whole factor reduces to

$$(CF)_V{}^{(2)}=1. \tag{1.1}$$

This result may be understood as follows. For the single particle problem the factor[2]

$$(CF)_V{}^{(1)}=1-2\langle T_1\rangle/(3Mc^2) \tag{2}$$

is applicable in this case. Here the nonrelativistic approximation to T_1 suffices. In this approximation

$$\langle T_2\rangle=2\langle T_1\rangle, \tag{2.1}$$

questions of frames of reference being irrelevant within the accuracy of the calculation. Thus the correction factor is expected to be

$$1-\langle T_2\rangle/(3Mc^2). \tag{2.2}$$

The mesic field induction effect is omitted, however, in this estimate. This effect arises from the fact that particle II (neutron) produces a mesic vector potential

$$\mathfrak{A}_I$$

at the location of particle I. The vector potential modifies the single particle Hamiltonian for I by the correction

$$\delta H_I=-(\boldsymbol{\alpha}_I\mathfrak{A}_I) \tag{2.2'}$$

in the interaction energy,

$$H_I'=-J+\delta H_I, \tag{2.2''}$$

which represents the interaction of particle I with the meson field. As in the electromagnetic case,

$$\mathfrak{A}_I=-\boldsymbol{\alpha}_{II}J$$

and

$$H_I'=-J[1-(\boldsymbol{\alpha}_I\boldsymbol{\alpha}_{II})]. \tag{2.3}$$

Taking into account additional terms arising from the inclusion of δH_I in the calculation of the one-body problem, one obtains an addition to the expression representing small components in terms of large ones, *viz.*,

$$\delta\Phi_I=(J/2Mc^2)(\boldsymbol{\sigma}_I\boldsymbol{\alpha}_{II})\Psi_I, \tag{2.4}$$

the subscripts I on Φ and Ψ indicating a one-body treatment of the proton (i.e. I). This change in Φ_I produces a change

$$\delta(\psi_I{}^*[\mathbf{r}_I\times\boldsymbol{\alpha}_I]_u\psi_I)=(J/Mc^2)(\Psi_I{}^*[\mathbf{r}_I\times\boldsymbol{\alpha}_{II}]_u\Psi_I) \tag{2.5}$$

which is found to be expressible approximately as the mean value of

$$(\hbar/2M^2c^3)[\boldsymbol{\sigma}_{II}(\mathbf{r}_I\mathbf{r})-\mathbf{r}(\mathbf{r}_I\boldsymbol{\sigma}_{II})]f, \tag{2.6}$$

with

$$f=dJ/rdr \tag{2.7}$$

and

$$\mathbf{r}=\mathbf{r}_I-\mathbf{r}_{II},\quad r=|\mathbf{r}|. \tag{2.7'}$$

For s terms the expression yields Eq. (1.1). In the above account of the work the presentation is such as though the two-body wave function were a product of one-body functions for particles I and II. The calculations have been carried, however, also for linear combinations of products, so as to apply also in configuration space. The limitations existing at this stage will become more apparent in the analysis of the problem in terms of plane waves.

The results obtained by the separate consideration of the two particles agree with calculations made by employing the covariant Hamiltonians as in the work of Breit and Bloch.[6] In the notation of this reference and in units making $\hbar=c=1$,

$$(\psi,[\mathbf{r}_I\times\boldsymbol{\alpha}_I]\psi)_{Vrc}$$
$$=\left(\Psi^{(1)},\left\{\left[-\frac{1}{M}+\frac{W+J}{2M^2}+\frac{p_I{}^2-p_{II}{}^2}{4M^3}\right](\mathbf{L}_I+\boldsymbol{\sigma}_I)-\mathbf{D}+\frac{\mathbf{C}_V}{4M^2}\right\}\Psi^{(1)}\right), \tag{3}$$

where

$$\mathbf{D}=\{i[\mathbf{r}_I\times\boldsymbol{\nabla}_IJ]+(\boldsymbol{\nabla}_IJ)(\mathbf{r}_I\boldsymbol{\sigma}_I)-\boldsymbol{\sigma}_I(\mathbf{r}_I\boldsymbol{\nabla}_IJ)\}/(4M^2), \tag{3.1}$$

$$[A,B]_+=AB+BA, \tag{3.2}$$

$$\mathbf{C}_V=[(\boldsymbol{\sigma}_{II}\mathbf{p}_{II}),[X,[\mathbf{r}_I\times\boldsymbol{\sigma}_I]]_+]_+ \tag{3.2'}$$

$$X=-\tfrac{1}{2}(\boldsymbol{\sigma}_I\boldsymbol{\sigma}_{II})J+\tfrac{1}{2}(\boldsymbol{\sigma}_I\mathbf{r})(\boldsymbol{\sigma}_{II}\mathbf{r})f, \tag{3.3}$$

$$\Psi^{(1)}=(\Psi,\Psi)^{-\frac{1}{2}}\Psi$$
$$=[1+(p_I{}^2+p_{II}{}^2)/8M^2+\cdots]\Psi. \tag{3.3'}$$

Calculation gives for s terms

$$\langle\mathbf{D}\rangle=-\langle r^2f\boldsymbol{\sigma}_I\rangle/(12M^2)=\langle T_2\boldsymbol{\sigma}_I\rangle/(6M^2), \tag{3.4}$$

$$\left(\Psi^{(1)},\left[\left(-\frac{1}{M}+\frac{W+J}{2M^2}+\frac{p_I{}^2-p_{II}{}^2}{4M^3}\right)(\mathbf{L}_I+\boldsymbol{\sigma}_I)-\mathbf{D}\right]\Psi^{(1)}\right)=-\frac{1}{M}\left\langle\left(1-\frac{T_2}{3M}\right)\boldsymbol{\sigma}_I\right\rangle, \tag{3.5}$$

and in general

$$\langle\mathbf{C}_V\rangle=2\langle[\boldsymbol{\sigma}_{II}(\mathbf{r}\mathbf{r}_I)-\mathbf{r}(\boldsymbol{\sigma}_{II}\mathbf{r}_I)]f\rangle \tag{3.6}$$

which becomes

$$\langle\mathbf{C}_V\rangle=-(4/3)\langle T_2\boldsymbol{\sigma}_{II}\rangle,\quad (s\text{ terms}). \tag{3.7}$$

These calculations differ from corresponding steps in the work of Sachs[5] through the consistent use of the operators $\boldsymbol{\alpha}$ and from the work of Breit and Bloch[6] through the correct evaluation of $\mathbf{C}_V$. Inserting the values listed in Eqs. (3.4), (3.5), (3.7) into Eq. (3)

there results

$$\langle[\mathbf{r}_I\times\boldsymbol{\alpha}_I]\rangle_{Vec}=-\frac{1}{M}\left\langle\left(1-\frac{T_2}{3M}\right)\boldsymbol{\sigma}_I\right\rangle-\frac{\langle T_2\boldsymbol{\sigma}_{II}\rangle}{3M^2}, \quad (4)$$

which is seen to agree with Eq. (1).

Comparing Eq. (3.5) with Eqs. (2), (2.2) one sees that all terms in the two body treatment with the exclusion of $\mathbf{C}_V$ account for the one-body effects caused by I (proton) being exposed to the action of J and without inclusion of effects of α_I which are treated in Eqs. (2.2′), (2.2″), (2.3), (2.4), and (2.5). The correction for the generalization of the magnetic induction effect treated in these equations corresponds in the two-body calculation to the terms arising from $\mathbf{C}_V$. These terms arise from X of Eq. (3.3), and this term arises from the generalization of the magnetic interaction between two charges with inclusion of the correction for retardation in the action of the electrostatic potential. The values in Eqs. (2.6), (3.6) agree. The two ways of obtaining $(CF)_V{}^{(2)}$ are thus closely related contributions arising from the same physical effects contributing equal amounts in both considerations. The effect of the correction for retardation is seen to be immaterial for the present problem.

4. SCALAR INTERACTION

A calculation along the lines of Breit and Bloch[6] gives in units for which $\hbar=c=1$,

$$(\psi,[\mathbf{r}_I\times\boldsymbol{\alpha}_I]\psi)_{Sc}$$
$$=\left(\Psi^{(1)},\left\{\left[-\frac{1}{M}+\frac{W-J}{2M^2}+\frac{p_I{}^2-p_{II}{}^2}{4M^3}\right](\mathbf{L}_I+\boldsymbol{\sigma}_I)+\mathbf{D}+\frac{\mathbf{C}_{Sc}}{4M^2}\right\}\Psi^{(1)}\right), \quad (5)$$

where $\mathbf{D}$ is as in Eqs. (3.1), (3.4), while

$$\mathbf{C}_{Sc}=[(\boldsymbol{\sigma}_{II}\mathbf{p}_{II}),[Y,[\mathbf{r}_I\times\boldsymbol{\sigma}_I]]_+]_+ \quad (5.1)$$

with

$$Y=\tfrac{1}{2}J(\boldsymbol{\sigma}_I\boldsymbol{\sigma}_{II})+\tfrac{1}{2}(\boldsymbol{\sigma}_I\mathbf{r})(\boldsymbol{\sigma}_{II}\mathbf{r})f. \quad (5.2)$$

A straightforward rearrangement gives

$$\langle(\mathbf{u}\cdot\mathbf{C}_{Sc})\rangle=\langle(\boldsymbol{\sigma}_{II}\cdot\mathbf{curl}_{II}\{J\mathbf{u}_I+f\mathbf{r}(\mathbf{u}_I\mathbf{r})\})\rangle, \quad (5.3)$$

where

$$\mathbf{u}_I=[\mathbf{u}\times\mathbf{r}_I], \quad (5.4)$$

with $\mathbf{u}$ standing for an arbitrary fixed unit vector. The two parts in curly braces on the right side of Eq. (5.3) contribute equal and opposite amounts so that

$$\langle\mathbf{C}_{Sc}\rangle=0. \quad (5.5)$$

Collecting terms one finds with the aid of Eqs. (3.4), (3.5), (5.5) by substitution into Eq. (5) that

$$\langle[\mathbf{r}_I\times\boldsymbol{\alpha}_I]\rangle_{Sc}=-\frac{1}{M}\left\langle\left(1-\frac{W}{M}+\frac{T_2}{3M}\right)\boldsymbol{\sigma}_I\right\rangle, \quad (6)$$

in agreement with Eq. (14) of Sachs.[5] The difference from Breit and Bloch[6] is caused by an error in the calculation of $\langle\mathbf{C}_{Sc}\rangle$. On the other hand, the calculation of Sachs has left out of consideration the effect of C_{Sc} which arises from corrections for lack of covariance of the two-body equation if one employs only the term in $\beta_I\beta_{II}J$. If one omitted the corrections for covariance in the vector case the effect of $\mathbf{C}_V$ would have been absent. It is thus seen that the inclusion of corrections for covariance is essential in the general case. The agreement of Eq. (6) with the result of Sachs is seen to arise from Eq. (5.5) which has not been discussed in the literature before and explains the apparently accidental correctness of the answer in the work of Sachs.

On the other hand Eq. (5.5) may be seen to mean directly that the addition to the Hamiltonian of a term proportional to

$$H''=(\boldsymbol{\alpha}_I\boldsymbol{\alpha}_{II})J+(\boldsymbol{\alpha}_I\mathbf{r})(\boldsymbol{\alpha}_{II}\mathbf{r})f \quad (7)$$

has no effect on the magnetic moment to within terms of relative order v^2/c^2. This term contains the same combinations as the term which has to be added to the interaction $(1-\boldsymbol{\alpha}_I\boldsymbol{\alpha}_{II})J$ to obtain the Hamiltonian used by Breit and Bloch and in the present paper for the discussion of the vector case. It was found for the latter that the same result can be obtained by the procedure used in Eqs. (2)$\cdots$(2.6) as by that used in Eqs. (3)$\cdots$(4). The latter includes the generalization of electrodynamic retardation effects as in Eq. (7) which are again seen to have made no difference for the magnetic moment problem. The fact that terms of this type have no effect could have been deduced from the fact that

$$H''=-(\boldsymbol{\alpha}_I\boldsymbol{\nabla}_I)(\boldsymbol{\alpha}_{II}\boldsymbol{\nabla}_{II})K, \quad (7.1)$$

where

$$K=\int^r rJdr.$$

The introduction of a term of form

$$(\boldsymbol{\alpha}_I\boldsymbol{\nabla}_I)G \quad (7.2)$$

can be counterbalanced by making

$$\psi=\exp(-iG/\hbar c)\psi'. \quad (7.3)$$

Since G is in this case free of the α_I and β_I, the calculation of $[\mathbf{r}_I\times\boldsymbol{\alpha}_I]$ is unaffected by the change from ψ to ψ' and the retardation terms cannot affect the magnetic moment.

The form of the two-body result for the scalar case can be explained in terms of the one-body result.[4] The latter is

$$(CF)_{Sc}{}^{(1)}=1-\langle T_1/3Mc^2\rangle-W_1/Mc^2, \quad (8)$$

while Eq. (6) gives

$$(CF)_{Sc}{}^{(2)}=1+\langle T_2/3Mc^2\rangle-W_2/Mc^2. \quad (8.1)$$

The connection becomes more obvious by eliminating

W by means of

$$W_i=\langle T_i-J\rangle, \quad (i=1,2). \tag{8.2}$$

One then has expressions equivalent to Eqs. (8), (8.1)

$$(CF)_{Se}^{(1)}=1-\langle 4T_1/3Mc^2\rangle+\langle J_1/Mc^2\rangle, \tag{8.3}$$

$$(CF)_{Se}^{(2)}=1-\langle 2T_2/3Mc^2\rangle+\langle J_2/Mc^2\rangle. \tag{8.4}$$

Noting that T_2 includes the kinetic energy of the neutron and comparing the one- and two-body answers for the same mean kinetic energies of the proton one has Eq. (2.1). With this identification it follows from Eqs. (8.3), (8.4) that

$$(CF)_{Se}^{(2)}/(CF)_{Se}^{(1)}=\langle Mc^2-J_1\rangle/\langle Mc^2-J_2\rangle, \tag{8.5}$$

corresponding to expectation, since for the one-body scalar equation J occurs in the Hamiltonian only in the term

$$-\beta(Mc^2-J), \tag{8.6}$$

and since the nonrelativistic magnetic moment contains the factor $1/M$. The part of the effect of J which is not explicitly taken into account in the kinetic energy is the change of the mass M to the effective mass $M-\langle J/c^2\rangle$.

Comparing this interpretation with the corresponding conditions for the vector case which have been discussed in relation to Eqs. (2), (2.1), (2.2) one sees that in both cases the one-body answers when supplemented by the argument concerning absence of retardation effects either in the form of Eqs. (7) to (7.3) or of Eqs. (5.3) to (5.5) give a complete account of the situation for vector and scalar interactions. It is essential here that in the two-body problem J may be considered as playing the same role for the motion of I as though the motion of II were not part of the problem.

5. PLANE WAVE REPRESENTATIONS

Comparison of one-body results as in Eqs. (2) and (8.3) shows the occurrence of an extra factor 2 in the correction term containing T in the answer for the scalar interaction. The work described in the present section has been done in order to obtain a clearer understanding of the reason for this difference. It turned out that a classification of contributions from terms diagonal and nondiagonal in the sign of energy gives a simple account of the facts. The wave function ψ can be represented by

$$\psi_\mu(\mathbf{r})=h^{-1}\int(\mathfrak{L}(\mathbf{p})C(\mathbf{p}))_\mu e^{i\mathbf{k}\mathbf{r}}d\mathbf{p}, \tag{9}$$

where

$$\mathbf{k}=\mathbf{p}/\hbar, \quad c=1, \tag{9.1}$$

$$\mathfrak{L}(\mathbf{p})=(E^a+M)\beta+\boldsymbol{\alpha}\mathbf{p}, \quad E^a=|(M^2+p^2)^{\frac{1}{2}}|, \tag{9.2}$$

$$(\mathfrak{L}(\mathbf{p})C(\mathbf{p}))_\mu=\mathfrak{L}_{\mu\nu}(\mathbf{p})C_\nu(\mathbf{p}). \tag{9.3}$$

The convention of omitting summation signs over common indices is used and units are adjusted so as to have $c=1$. The 4-row column matrix C describes the probability of a state with specified spin orientation and sign of energy, provided the reference system for $\boldsymbol{\alpha}$ and β is such as to make β diagonal. The representation used below is such that

$$\beta_{\mu\mu}=1, \quad (\mu=1,2); \quad \beta_{\mu\mu}=-1, \quad (\mu=3,4). \tag{9.4}$$

Accordingly C_1, C_2 are relative probability amplitudes for $E<0$ while C_3, C_4 are similar amplitudes for $E>0$. The notation

$$(C_-)=\begin{pmatrix}C_1\\C_2\end{pmatrix}, \quad (C_+)=\begin{pmatrix}C_3\\C_4\end{pmatrix} \tag{9.5}$$

shows this relationship to the sign of E. The probability of finding the particle in the momentum range $d\mathbf{p}$ with specified spin and energy sign designated by σ is

$$N^2|C_\sigma(\mathbf{p})|^2d\mathbf{p}, \tag{9.6}$$

where N^2 arises from

$$(\mathfrak{L}^2)_{\mu\nu}=N^2\delta_{\mu\nu} \tag{9.7}$$

and is given by

$$N^2=2E^a(E^a+M). \tag{9.8}$$

Charge conjugation is not needed and is therefore not used. The wave function in momentum space in the usual sense is seen to be

$$\mathfrak{L}(\mathbf{p})C(\mathbf{p})$$

and multiplication of $\psi_\mu(\mathbf{r})$ by a Cartesian coordinate y is equivalent to the application of $-\hbar\partial/i\partial p_y$ to the momentum space wave function.

It is convenient to employ the quantity

$$\mathbf{v}=[\mathbf{u}\times\mathbf{r}] \tag{10}$$

where $\mathbf{u}$ is an arbitrary fixed unit vector. In terms of $\mathbf{v}$ the component

$$[\mathbf{r}\times\boldsymbol{\alpha}]_u=(\mathbf{v}\boldsymbol{\alpha}). \tag{10.1}$$

The evaluation of the expectation value of this quantity yields the magnetic moment arising from the Dirac current. It is seen from Eq. (9) that this evaluation when put in terms of the C_σ involves the quantity $\mathfrak{L}(\mathbf{v}\boldsymbol{\alpha})\mathfrak{L}$, a general form for which can be obtained by direct calculation. One finds

$$\begin{aligned}\mathfrak{L}(\mathbf{v}\boldsymbol{\alpha})\mathfrak{L}=&2\rho_3(E^a+M)(L_u+\hbar\sigma_u)\\&+\rho_3(\hbar/E^a)[(\boldsymbol{\sigma}\mathbf{p})p_u-p^2\sigma_u]+\rho_1\{[(\boldsymbol{\sigma}\mathbf{p}),L_u]_+\\&+2\hbar p_u-[E^a(E^a+M),[\mathbf{r}\times\boldsymbol{\sigma}]_u]_+\},\end{aligned} \tag{10.2}$$

where the component of orbital angular momentum enters as

$$L_u=(\mathbf{L}\mathbf{u}), \quad \mathbf{L}=[\mathbf{r}\times\mathbf{p}] \tag{10.3}$$

and components of other quantities along $\mathbf{u}$ are similarly designated by the subscript u. In Eq. (10.2) the first two terms contain $\rho_3=\beta$ and are, therefore, diagonal in the sign of energy. The remaining part of $\mathfrak{L}(\mathbf{v}\boldsymbol{\alpha})\mathfrak{L}$ contains the 4-row square matrices only as ρ_1 and $\boldsymbol{\sigma}$ and is nondiagonal in the sign of energy.

For $(C_-)=0$, taking into account the normalization convention of Eqs. (9.6), (9.8), it follows from Eq. (10.2) that

$$-\langle(\mathbf{v}\boldsymbol{\alpha})\rangle=\left\langle\frac{L_u+h\sigma_u}{E^a}+h\frac{(\boldsymbol{\sigma}\mathbf{p})p_u-p^2\sigma_u}{2(E^a)^2(E^a+M)}\right\rangle_{NC},\qquad(C_-=0),\quad(11)$$

where the calculation of the expectation value of the right side is supposed to be done by inserting the operator occurring on the right side between $N(C_+^*)^T$ and $N(C_+)$, multiplying by $h^{-3}d\mathbf{p}$ and integrating; the superscript T stands for transposition. It may be shown that for s terms, i.e. states for which Dirac's $k=-1$, where $k=\pm(j+\frac{1}{2})$, the quantity $C_+(\mathbf{p})$ is spherically symmetric in $\mathbf{p}$ space. In this specialization the contribution to $-\langle(\mathbf{v}\boldsymbol{\alpha})\rangle$ arising from positive energy plane waves is

$$\begin{aligned}-\langle(\mathbf{v}\boldsymbol{\alpha})\rangle_{++}&=\left\langle\frac{h\sigma_u}{E^a}-\frac{hp^2\sigma_u}{3(E^a)^2(E^a+M)}\right\rangle_{NC}\\&\cong(h/M)\langle[1-(2p^2/3M)]\sigma_u\rangle_{NC}\\&=(h/M)\langle[1-(4T/3M)]\sigma_u\rangle_{NC},\end{aligned}\qquad(s\text{ terms}).\quad(11.1)$$

The inherent relativistic correction factor for the positive energy part of the wave function is seen to be $1-4\langle T\rangle/(3Mc^2)$.

The results for the one-body scalar interaction problem are now readily interpretable. The correction factor apart from the effect of $\langle J\rangle$ in Eq. (8.3) is accounted for by the effect of states with $E>0$. The term in $\langle J\rangle$ must be caused therefore by cross product terms between C_+ and C_-. One finds in fact that the wave equation takes the form

$$\begin{aligned}(E_0+E^a)(C_-)&=\int(\mathcal{J}/N^2)\{A(\mathbf{p},\mathbf{p}')(C_-')\\&\qquad+B(\mathbf{p},\mathbf{p}')(C_+')\}d\mathbf{p}',\\(E_0-E^a)(C_+)&=\int(\mathcal{J}/N^2)\{B(\mathbf{p},\mathbf{p}')(C_-')\\&\qquad-A(\mathbf{p},\mathbf{p}')(C_+')\}d\mathbf{p}',\end{aligned}\qquad(12)$$

where

$$(C_+')=[C_+(\mathbf{p}')]\qquad(12.1)$$

and similarly for the other (C). The other quantities in the Schrödinger equation needing explanation are

$$A(\mathbf{p},\mathbf{p}')=(E^a+M)(E'^a+M)-(\boldsymbol{\sigma}\mathbf{p})(\boldsymbol{\sigma}\mathbf{p}'),\quad(12.2)$$

$$B(\mathbf{p},\mathbf{p}')=(E^a+M)(\boldsymbol{\sigma}\mathbf{p}')+(E'^a+M)(\boldsymbol{\sigma}\mathbf{p}),\quad(12.3)$$

$$\mathcal{J}=h^{-3}\int J(\mathbf{r})\exp\{i(\mathbf{k}-\mathbf{k}')\mathbf{r}\}d\mathbf{r},\qquad(12.4)$$

$$E_0=\text{energy of stationary state}.\qquad(12.5)$$

Solving for (C_-) from the first line of Eq. (12) one has

$$(C_-)\cong(1/4M^2)\int(\boldsymbol{\sigma}(\mathbf{p}+\mathbf{p}'))\mathcal{J}(C_+')d\mathbf{p}',\qquad(12.6)$$

and employing this form in the ρ_1 containing part of Eq. (10.2) one obtains three terms arising from the three parts inside the curly braces. The last term gives the largest contribution on account of the factor $E^a(E^a+M)$. A simplification takes place in the evaluation of the effect of this term because $[\mathbf{r}\times\boldsymbol{\sigma}]$ operating on $\mathcal{J}$ gives an odd function in $\mathbf{p}-\mathbf{p}'$ while the remainder of the integrand is even. For this reason the only contributions to be considered come from $[\mathbf{r}\times\boldsymbol{\sigma}]$ applied to $\boldsymbol{\sigma}\mathbf{p}$. One has thus by means of Eq. (12.6)

$$\begin{aligned}&-\langle\rho_1[E^a(E^a+M),[\mathbf{r}\times\boldsymbol{\sigma}]_u]_+\rangle\\&\quad=-(4/4M^2)\int C_+^{*T}(\mathbf{p})(-h/i)[-\boldsymbol{\sigma}\times\boldsymbol{\sigma}]_u\\&\qquad\qquad\times\mathcal{J}E^a(E^a+M)C_+(\mathbf{p}')d\mathbf{p}d\mathbf{p}'\\&\quad=-(1/M^2)\int C_+^{*T}(\mathbf{p})Nh\sigma_u\mathcal{J}NC_+(\mathbf{p}')d\mathbf{p}d\mathbf{p}'\\&\qquad=-(h/M^2)\langle\sigma_uJ\rangle.\end{aligned}\qquad(12.7)$$

Here the first factor 4 takes account of repeated doubling coming from double order once for $C_-^{*T}C_+$ and $C_+^{*T}C_-$ and once for $[\ ]_+$. Adding the right side of Eq. (12.7) to the value of $\langle(\mathbf{v}\boldsymbol{\alpha})\rangle_{++}$ as in Eq. (11.1) the correction factor of Eq. (8.3) is reproduced. The term in $\langle J\rangle$ has thus been verified to be caused by matrix elements nondiagonal in the sign of energy.

For the vector case the Schrödinger equation in the C_+, C_- form takes the form

$$\begin{aligned}(E_0+E^a)(C_-)&=-\int(\mathcal{J}/N^2)\{A_V(\mathbf{p},\mathbf{p}')(C_-')\\&\qquad+B_V(\mathbf{p},\mathbf{p}')(C_+')\}d\mathbf{p}',\\(E_0-E^a)(C_+)&=-\int(\mathcal{J}/N^2)\{-B_V(\mathbf{p},\mathbf{p}')(C_-')\\&\qquad+A_V(\mathbf{p},\mathbf{p}')(C_+')\}d\mathbf{p}',\end{aligned}\qquad(13)$$

where

$$A_V(\mathbf{p},\mathbf{p}')=(E^a+M)(E'^a+M)+(\boldsymbol{\sigma}\mathbf{p})(\boldsymbol{\sigma}\mathbf{p}'),\quad(13.1)$$

$$B_V(\mathbf{p},\mathbf{p}')=(E^a+M)(\boldsymbol{\sigma}\mathbf{p}')-(E'^a+M)(\boldsymbol{\sigma}\mathbf{p}),\quad(13.2)$$

and the notation is otherwise as for Eq. (12). From the first line of Eq. (13) there follows the approximation

$$(C_-)\cong(1/4M^2)\int(\boldsymbol{\sigma}(\mathbf{p}-\mathbf{p}'))\mathcal{J}(C_+')d\mathbf{p}'.\quad(13.3)$$

A procedure similar but slightly more laborious than that in Eq. (12.7) gives

$$\langle(\mathbf{v}\boldsymbol{\sigma})\rangle_{+-}\cong(h/2M^2)\int(C_+^{*T})\{2\sigma_u\mathcal{J}+[\sigma_u(\mathbf{p}-\mathbf{p}')^2+(p_u'-p_u)(\boldsymbol{\sigma}(\mathbf{p}-\mathbf{p}'))]\mathcal{J}'/|\mathbf{p}-\mathbf{p}'|\}(C_+')d\mathbf{p}d\mathbf{p}',\quad(13.4)$$

with the understanding that both orders $C_+^{*T}C_-$ and $C_-^{*T}C_+$ are included and with

$$\mathcal{J}'=(d\mathcal{J}(x)/dx)_{x=|\mathbf{p}-\mathbf{p}'|}. \tag{13.5}$$

Inserting the value for (C_-) available in Eq. (13.3) into the second line of Eq. (13) one obtains the C space transform of the nonrelativistic Schrödinger equation. From this equation there follows the relation

$$[(p^2/M)+(E^a-E_0)(\mathbf{p}\nabla_p)](C_+)$$
$$=\int[p^2-(\mathbf{p}\mathbf{p}')][\mathcal{J}'/|\mathbf{p}-\mathbf{p}'|](C_+')dp', \tag{13.6}$$

which when used with Eq. (13.4) gives a contribution canceling $\frac{1}{2}$ of the term $-4\langle T/3Mc^2\rangle$ in the correction factor.

The representation of the answer in terms of plane waves has been used so far only for the one-body problem. It will now be made use of for the two-body case. It is fortunately not necessary to make a new calculation because it is possible to justify the adoption of Eq. (11.1) for the two-body case, with T standing for the kinetic energy of the proton. Similarly one can justify the employment of Eq. (12.7) with J standing for $J(|\mathbf{r}_\mathrm{I}-\mathbf{r}_\mathrm{II}|$ essentially on the grounds that Eq. (12.6) can be carried over to the two-particle case with a slightly changed meaning. The somewhat intuitive approach used in connection with Eq. (8.5) can be thus explained in terms of J causing transitions to (C_-) and the form of the correction factor remaining the same for the scalar case provided the variables used are the kinetic energy of the proton and the mean J. Similarly in the vector case Eq. (13.3) shows how J is responsible for the existence of (C_-) and cancellation of half of $4\langle T\rangle/(3Mc^2)$ occurs because the contribution in terms of $\mathcal{J}$ happens to be expressible in terms of T with the aid of Eqs. (13.4), (13.5), (13.6).

In the argument just presented there are some gaps which were left in order to present the essential features concisely and which will now be filled in. The two-body 16-component ψ is analyzed as

$$\psi=h^{-3}\int \mathfrak{C}(\mathbf{p}_\mathrm{I},\mu_\mathrm{I};\mathbf{p}_\mathrm{II},\mu_\mathrm{II})$$
$$\times\exp\{i(\mathbf{k}_\mathrm{I}\mathbf{r}_\mathrm{I}+\mathbf{k}_\mathrm{II}\mathbf{r}_\mathrm{II})\}d\mathbf{p}_\mathrm{I}d\mathbf{p}_\mathrm{II}, \tag{14}$$

the spin index μ being indicated as an argument of the wave function in momentum space. The function $\mathfrak{C}$ can be represented as

$$\mathfrak{C}(\mathbf{p}_\mathrm{I},\mu_\mathrm{I};\mathbf{p}_\mathrm{II},\mu_\mathrm{II})$$
$$=[\mathfrak{L}(\mathbf{p}_\mathrm{I})C^\mathrm{I}(\mathbf{p}_\mathrm{I})]_{\mu_\mathrm{I}}[\mathfrak{L}(\mathbf{p}_\mathrm{II})C^\mathrm{II}(\mathbf{p}_\mathrm{II})_{\mu_\mathrm{II}}, \tag{14.1}$$

because only states restricted by

$$\mathbf{p}_\mathrm{I}+\mathbf{p}_\mathrm{II}=0 \tag{14.2}$$

need to be considered. For each value of the relative momentum there enter in the representation four possibilities regarding sign of energy, two for each particle, corresponding to C_+^I, C_-^II, etc. Since one is concerned with the calculation of the expectation value of a single particle operator, *viz.* $[\mathbf{r}_\mathrm{I}\times\boldsymbol{\alpha}_\mathrm{I}]$, the only combinations that matter are those diagonal in the sign of C^II. For this reason J and $\mathcal{J}$ affect the cross product terms in a manner analogous to that in the one-particle case. It will be noted that $\mathcal{J}$ in the present case is precisely of the same form as in the one-body problem since it comes in through the introduction of the relative momentum. The quantity C^II takes no part in the operations and the one-body result for cross terms can be transferred to the two-body case. Another point needing mention is the slight change regarding the operator L_u^I for $+,+$ combinations. This operator has no effect in the one body problem on account of spherical symmetry of C_+ for s states. In the two-body case it also has no effect to the order that matters, provided the presence of the D state is disregarded. The authors have not succeeded in reducing this part of the argument to a simple form. It is based on the possibility of separating spin and angular variables for the ${}^3S_1$ state in the general manner used by Critchfield.[16]

6. PSEUDOSCALAR INTERACTION

The single particle problem has been calculated by means of the Hamiltonian

$$H=-c(\boldsymbol{\alpha}\mathbf{p})-Mc^2\beta-ig\beta\gamma^5\chi, \tag{15}$$

where χ is the pseudoscalar nonquantized field and the conventions

$$\begin{aligned}&\gamma^4=-\beta, &&\gamma^k=-i\beta\alpha_k=\rho_2\sigma_k,\\ &\gamma^5=\gamma^1\gamma^2\gamma^3\gamma^4=\rho_1, &&-i\beta\gamma^5=\rho_2\end{aligned} \tag{15'}$$

are used. Expressing the "small components" Φ in terms of the "large components" Ψ one finds by straightforward calculation

$$\int(\psi^{*T}[\mathbf{r}\times\boldsymbol{\alpha}]\psi)d\mathbf{r}\Big/\int(\psi^{*T}\psi)d\mathbf{r}$$
$$=-(c/E)\int(\Psi^{*T}(\mathbf{L}+\hbar\boldsymbol{\sigma})\Psi)d\mathbf{r}\Big/\int(\Psi^{*T}\Psi)d\mathbf{r}$$
$$=-(c/E)\langle\mathbf{L}+\hbar\boldsymbol{\sigma}\rangle_\Psi, \tag{16}$$

where it is supposed that the energy of the state ψ is E and the subscript Ψ indicates averaging in terms of the two-component function Ψ. The result is independent of the pseudoscalar field except insofar as Ψ is affected by it. Although Eq. (16) suggests that the correction factor to the magnetic moment is Mc^2/E, the special character of the pseudoscalar interaction makes it necessary to exercise caution in applications.

It appears probable that Eq. (16) will be more useful in applications to heavy nuclei because the approxi-

[16] C. L. Critchfield, Phys. Rev. **71**, 258 (1947).

mation of a fixed field is presumably more justifiable in such cases than for the deuteron. If one were to form a model of a heavy nucleus by analogy with atomic models the simplest hypothesis would consist in making χ spherically symmetric. If one did, stationary states containing mixtures of wave functions of even and odd parity would result showing the inconsistency of such an assumption with the pseudoscalar character of χ. The simple *a priori* reasons for considering L to be a good quantum number can thus hardly be transferred from atomic theory to the present case. It is nevertheless customary to assume that L is not far from being a good quantum number and the L meant in this connection is usually defined in terms of Ψ rather than ψ, nuclear theory being customarily stated nonrelativistically. Within the limitations of these assumptions there is a definite meaning to a statement that a nuclear particle is in an s-state when the nucleus as a whole is in a stationary state. Under such conditions Eq. (16) gives the simple correction factor

$$Mc^2/E \tag{16.1}$$

to the nonrelativistic moment. This factor, as well as the general result in the form of Eq. (16), means that the relation between the magnetic moment and the energy which applies to free particles is not disturbed by the introduction of the pseudoscalar interaction.

It may be shown that a relation similar to Eq. (16) holds in terms of the four component wave function ψ. The wave equation corresponding to the Hamiltonian of Eq. (15) is

$$-(E/c)\psi=[(\boldsymbol{\alpha}\mathbf{p})+Mc\beta-(g/c)\rho_2\chi]\psi. \tag{17}$$

Multiplying by $(\mathbf{v}\boldsymbol{\alpha})$ it becomes

$$-(E/c)(\mathbf{v}\boldsymbol{\alpha})\psi =\{(\mathbf{v}\boldsymbol{\alpha})(\boldsymbol{\alpha}\mathbf{p})-[Mc\beta-(g/c)\rho_2\chi](\mathbf{v}\boldsymbol{\alpha})\}\psi. \tag{17.1}$$

Multiplying by ψ^{*T}, integrating over $\mathbf{r}$, and employing the complex conjugate of Eq. (17) to eliminate the combination $Mc\beta-(g/c)\rho_2\chi$ one obtains

$$-2(E/c)(\psi,(\mathbf{v}\boldsymbol{\alpha})\psi) =(\psi,[(\mathbf{v}\boldsymbol{\alpha})(\boldsymbol{\alpha}\mathbf{p})+(\boldsymbol{\alpha}\mathbf{p})(\mathbf{v}\boldsymbol{\alpha})]\psi). \tag{17.2}$$

Linearizing the operator on the right side of the last equation with respect to the Dirac σ's and employing commutation relations for coordinates and momenta, one finds after a short calculation

$$(\psi,[\mathbf{r}\times\boldsymbol{\alpha}]\psi)=-(c/E)(\psi,[\mathbf{L}+\hbar\boldsymbol{\sigma}]\psi). \tag{18}$$

The form of this result is similar to that of Eq. (16). For two states with different energies E, E' one obtains by employing ψ'^{*T} in place of ψ^{*T}

$$(\psi',[\mathbf{r}\times\boldsymbol{\alpha}]\psi)=-[2c/(E+E')](\psi',[\mathbf{L}+\hbar\boldsymbol{\sigma}]\psi), \tag{18'}$$

which furnishes nondiagonal matrix elements. The last result shows the presence of vanishing denominators between states with the same absolute value but opposite signs of E and is nugatory in such cases. The existence of Eq. (18) shows that the relationships to conditions in heavy nuclei which have been discussed in connection with Eq. (16) are more general than the usual nonrelativistic approximation.

The usefulness of Eq. (16) in applications to the deuteron is questionable. If it were justifiable to consider the ground state of this nucleus as a linear combination of wave functions consisting of products of proton and neutron wave functions and if these states contained only proton functions with energies between approximately $W+Mc^2$ and Mc^2, one would be justified in employing a mean E in place of E in Eq. (16.1). The discussion of other cases in the section concerned with plane waves has shown however that states with $E<0$ matter, so that this simple procedure is not correct in the general case.

By analogy with the cases of the scalar and vector interactions one can attempt to estimate the correction factor for the deuteron by attributing the difference between the factor $1-4\langle T_1\rangle/(3Mc^2)$ and

$$Mc^2/E_1=1-W_1/(Mc^2) \tag{19}$$

as arising from cross product terms between states with opposite signs of energy. This difference corresponds to the inclusion of a factor

$$1+[4\langle T_1\rangle/3-W_1]/(Mc^2) =1+[\langle T_1\rangle/3-(W_1-\langle T_1\rangle)]/(Mc^2) \tag{19.1}$$

in the one-body case, as an allowance for the effect of cross terms. If one replaces $W_1-\langle T_1\rangle$ by $W_2-\langle T_2\rangle$ on the grounds that the mean potential energy must be responsible for the proportion of states with $E<0$ and if one supposes that $\langle T_1/3\rangle$ is present in Eq. (19.1) as a direct property of the proton, then the correction factor for the deuteron should be

$$[1-2\langle T_2\rangle/(3Mc^2)]\{1+\langle T_2\rangle/6-(W_2-\langle T_2\rangle)\} =1+[\langle T_2\rangle/2-W_2]/(Mc^2). \tag{19.2}$$

This formula is subject to considerable uncertainties and doubts. The interaction between the particles is inherently not of the central field type. It is therefore rather questionable that there is a simple connection between the properties of a one-particle s state and the ^3S state of the two-particle system. There is no proof that the latter does not contain linear combinations of products of wave functions corresponding to vector coupling of states with $L>0$. For a nonquantized pseudoscalar field the sources of the $e^{-\kappa r}/r$ terms are in fact proportional to

$$\partial(\psi_\alpha{}^{*T}\sigma_{\alpha\beta}{}^i\psi_\beta)/\partial x^i$$

and are decidedly directional in character. The fact[13] that for the two-body problem the net result of the quantized pseudoscalar theory is to give a relatively small proportion of the ^3D state does not remove this difficulty. Furthermore there is no proof that the

contributions of L_u arising from C_+ are sufficiently small in the present case to be neglected. There is besides no assurance that the formation of virtual nucleon pairs which is known to be important in applications to nuclear forces does not appreciably affect the conclusions. This question is so closely connected with the perturbing influence between nucleons that it becomes hard to separate it from the general question of additivity of nuclear moments.[10–12] It is necessary therefore to regard Eq. (19.1) as a speculation.

7. THE DIAMAGNETIC EFFECT AND CONCLUDING REMARKS

In addition to the relativistic effects, the comparison of calculated with measured values should include the consideration of the diamagnetic effect caused by the shielding of a nuclear moment by the current system of the deuteron. This effect is related to the diamagnetic effect calculated for atoms by Lamb.[17] It has been apparently omitted in previous discussions. Formally such an omission amounts to disregarding magnetic interaction terms between the particles. While these terms produce smaller effects on the mutual energy between the particles they produce, nevertheless, effects which are formally of the same order of magnitude as the relativistic corrections. It is estimated to be smaller than the direct effects of $\langle T\rangle$ or $\langle J\rangle$ but not necessarily negligible in comparison with W/Mc^2. In the general case it is necessary to consider the difference in the rates of precession of $\mathbf{L}$ and $\boldsymbol{\sigma}$. For s terms in the single body case only the precession of the spin matters and the effect is then very similar to that calculated by Lamb. Estimates made on this basis indicate that this effect is small compared to the others considered here. On the other hand there is an obvious inconsistency in applying a one-body treatment to this problem. Some of the smallness of the effect results from the spherical symmetry of the s term and this condition is not satisfied on account of the tensor force.

The treatment of relativistic corrections has been discussed in the present paper in terms of somewhat arbitrary assumptions concerning the form of the two-body equations, the primary object being to explain the differences between the different results in terms of effects which can be described in simple language. The existence of additional effects is, of course, not excluded by the fact that the formal calculations have been interpreted in another way. The fact that two of the Hamiltonians used are covariant to the relative order v^2/c^2 is not a sufficient condition for their correctness and the results may not be regarded as final. In fact the more detailed discussion has brought out reasons for believing that additional terms including the interaction constant with the meson field will occur in a more complete treatment. In this connection it may be especially desirable to draw attention to the fact that the possibility of clearly distinguishing between relativistic corrections and nonadditivity of nuclear moments has not been established. The effect of the tensor force has been omitted on the grounds that the deuteron is probably predominantly in the ^3S state. The errors committed at this point have not been ascertained and are probably impossible to separate from the questions raised in connection with the pseudoscalar interaction.

[17] W. E. Lamb, Jr., Phys. Rev. **60**, 817 (1941).

Study of Elastic Pion-Hydrogen Scattering in Photographic Emulsions*†

GERSON GOLDHABER
Columbia University, New York, New York
(Received November 19, 1952)

Pion-hydrogen elastic scattering events were observed in photographic emulsions exposed to the 75±5 Mev negative and positive pion beams of the Nevis synchrocyclotron. The methods of identification, based on the energy momentum conservation in the interaction, are described. The cross section measured for the elastic scattering of negative and positive pions from hydrogen at 75±5 Mev are ~3 mb and 41±15 mb, respectively.

THE elastic scattering of π-mesons from hydrogen has been studied in photographic emulsions. The events can be identified because of energy-momentum conservation in the interaction.

The elastic π+H scattering events (Fig. 1) are characterized by the following four criteria:

1. Coplanarity.
2. Angular correlation between scattered meson and recoil proton.
3. Range-angle correlation for the recoil proton (Fig. 3).
4. Identification of the grey prong (Fig. 1) as a meson by grain density measurements.

Ilford G5 emulsions were exposed to the 75±5 Mev negative and positive pion beams of the Nevis synchrocyclotron.

The emulsions were scanned "by area" (10×45 oil objective). The total path length in hydrogen was calculated from the total area scanned, the hydrogen concentration and a sampling of the meson track density (correcting for beam contamination).[1-3] To insure a high scanning efficiency for the one-prong events, each proton beginning in the emulsion was examined closely to determine whether a meson was associated with it. There is reasonable agreement between the total number of meson interactions found and the number calculated from the total pion path length and the known cross sections[2-4] when corrections are made for scanning efficiency ($e=0.85$) and the types of interaction missed by area scanning.[5]

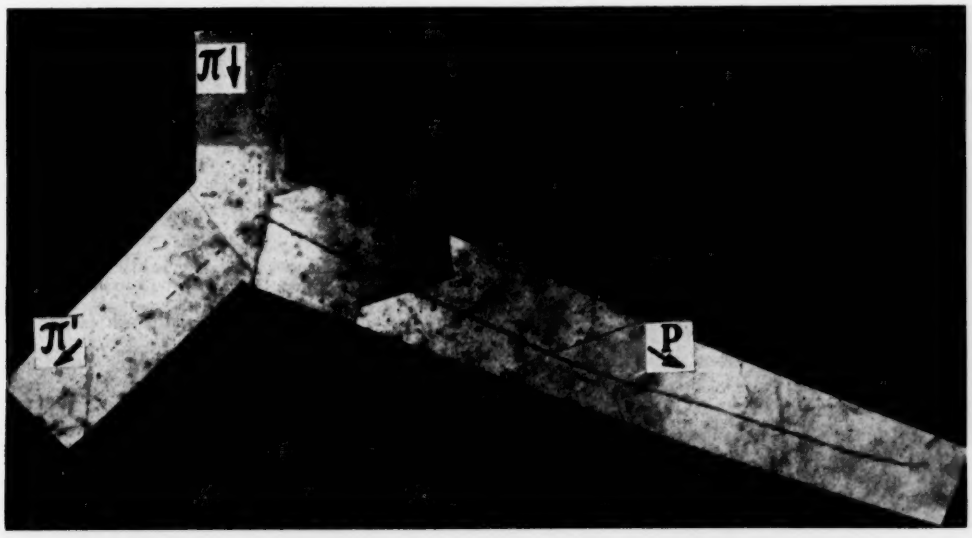

FIG. 1. Microphotograph of a π^++H scattering event. The recoil proton range is 370μ (observer, Mrs. E. Arase).

* A preliminary report of this work was presented at the 1952 Washington meeting of the American Physical Society [Phys. Rev. 87, 222 (1952)].
† This research was supported by the joint program of the U. S. Office of Naval Research and the U. S. Atomic Energy Commision.
[1] Bernardini, Booth, Lederman, and Tinlot, Phys. Rev. 82, 105 (1951).
[2] Bernarding, Booth, and Lederman, Phys. Rev. 83, 1075 (1951).
[3] G. Bernardini and F. Levy, Phys. Rev. 84, 610 (1951).
[4] Chedester, Isaacs, Sachs, and Steinberger, Phys. Rev. 82, 958 (1951).
[5] Stops, elastic scatterings, inelastic scatterings without heavy prongs, stars with very short prongs (<20μ), stars with one single grey prong.

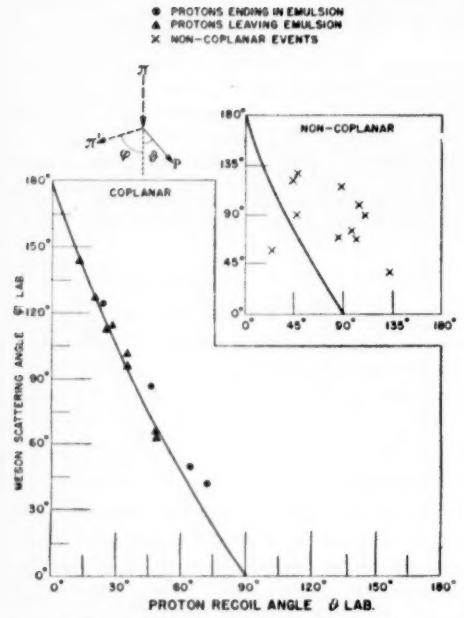

FIG. 2. The correlation between meson scattering angle ϕ_{lab} and recoil proton angle θ_{lab} evaluated for $\pi+H$ scattering at 75 Mev. The coplanar $\pi^+ + H$ events are given on the main plot. The noncoplanar events on the inset.

For negative pions, ordinary and water-loaded[6] emulsions were exposed and scanned. In scanning an area of emulsion corresponding to a traversal of π^- mesons through 630 ± 100 g/cm^2 of hydrogen, only one $\pi^- + H$ scattering event was found. This corresponds to a cross section of ~ 3 mb. Such a low cross section for the elastic scattering is consistent with the measurements by Shutt and co-workers.[7]

For positive pions, ordinary emulsions were used, and an area of emulsion corresponding to a traversal of π^+ mesons through 580 ± 100 g/cm^2 of hydrogen was scanned. In this area 234 meson interactions were found, of which 23 were one-prong scattering events. Of these, 12 were identified as $\pi^+ + H$ scatterings. The other 11 one-prong scattering events were inelastic scatterings from other nuclei in the emulsion.

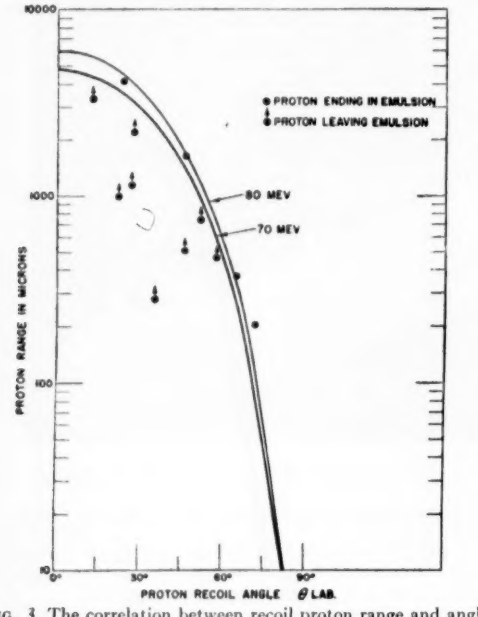

FIG. 3. The correlation between recoil proton range and angle (θ_{lab}) evaluated for $\pi+H$ scattering in Ilford emulsions at 70 and 80 Mev.

[6] S. Goldhaber and G. Goldhaber, Phys. Rev. **87**, 185 (1952).

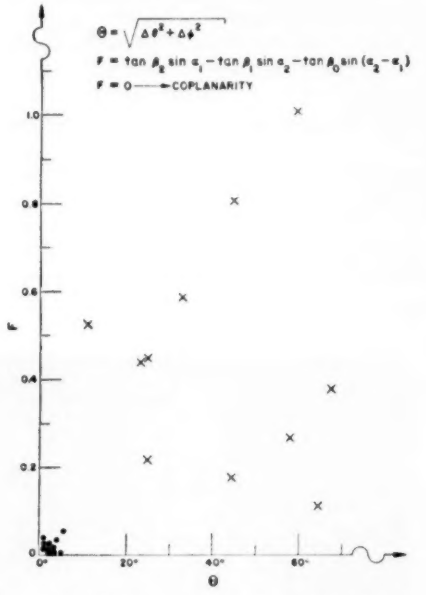

FIG. 4. The deviation from coplanarity $|F|$ plotted *versus* $|\Theta|$, the deviation from the angular correlation for $\pi^+ + H$ scattering. The black dots represent the identified elastic scattering events; the crosses represent the inelastic scatterings.

When ϕ_{lab} the meson scattering angle is plotted *versus* θ_{lab} the proton recoil angle, all the coplanar scattering events lie close to the calculated angular correlation curve for $\pi+H$ scattering (Fig. 2). The noncoplanar scattering events show no such clustering around the calculated curve (inset Fig. 2). Figure 3 gives calculated correlation curves between recoil proton range and angle, as well as the points corresponding to the coplanar π^+ scattering events. Within the experimental limits the points agree with the calculated range for events with recoil protons ending in the emulsion, or lie below the calculated range for protons leaving the emulsion. The condition for coplanarity of three prongs (incoming meson, scattered meson, and recoil proton)

[7] Shutt, Fowler, Miller, Thorndike, and Fowler, Phys. Rev. **84**, 1247 (1951).

is given by $F=0$, where $F=\tan\beta_2 \sin\alpha_1-\tan\beta_1 \sin\alpha_2 -\tan\beta_0 \sin(\alpha_2-\alpha_1)$. Here α_1, α_2 are the projected angles of the two outgoing prongs in the plane of the emulsion, β_1, β_2, are the corresponding dip angles, and β_0 is the dip angle of the incoming meson.[8] The deviation from coplanarity $|F|$ is plotted (Fig. 4) *versus* $|\Theta|$, the deviation from the angular correlation curve for $\pi+$H scattering. $\Theta=(\Delta\theta^2+\Delta\phi^2)^{\frac{1}{2}}$, where $\Delta\theta$ and $\Delta\phi$ represent the respective angular deviations of each event from the calculated $\pi+$H scattering curve as obtained from Fig. 2.

The distribution of the π^++H scattering between the forward and backward direction in the center-of-mass system is

$$d\sigma_{\text{c.m.}}=2.7\pm1.3 \text{ mb/steradian for } \phi_{\text{c.m.}}=35-90°,$$

and

$$d\sigma_{\text{c.m.}}=4.4\pm1.6 \text{ mb/steradian for } \phi_{\text{c.m.}}=90-180°.$$

As the scanning efficiency drops off for recoil prongs shorter than $\sim 50\mu$, a cutoff was taken at a recoil proton length of 100μ, which corresponds to a meson scattering angle of $\phi_{\text{c.m.}}=35°$. The asymmetry of the differential cross section with a peak in the backward direction found by Anderson and co-workers[9] at π^+ energies of 135 Mev and 110 Mev appears to be still evident in the present work at 75 Mev. From the work of Shutt and co-workers,[10] there is very little asymmetry at 53 Mev. The total cross section for π^++H scattering obtained is 41 ± 15 mb for $\phi_{\text{c.m.}}>35°$. This is in agreement with other measurements.[11]

The author would like to express his appreciation to Professor G. Bernardini and Dr. D. Bodansky, who participated in the initial stages of this work, to Mrs. E. Arase and Mrs. C. Major for their efforts in scanning the plates, and to Dr. S. Goldhaber and Dr. T. A. Green for discussions in connection with this work. Thanks are also due Mrs. J. Bielk for help in the development of the emulsions, and Mr. J. Spiro and the Nevis Cyclotron staff for their invaluable assistance.

[8] This relation holds for either the original dip angles or the final dip angles in the shrunk emulsion. In Fig. 4, $|F|$ is plotted in the form using the final dip angles.

[9] Anderson, Fermi, Nagle, and Yodh, Phys. Rev. **86**, 793 (1952).

[10] Fowler, Fowler, Shutt, Thorndike, and Whittemore, Phys. Rev. **86**, 1053 (1952).

[11] Anderson, Fermi, Long, and Nagle, Phys. Rev. **85**, 936 (1952).

PHYSICAL REVIEW VOLUME 89, NUMBER 6 MARCH 15, 1953

The Occurrence of Singularities in the Elastic Frequency Distribution of a Crystal

LÉON VAN HOVE
Institute for Advanced Study, Princeton, New Jersey
(Received December 5, 1952)

It is shown that for a crystal, under the assumption of harmonicity for the interatomic forces and as a consequence of the periodic structure, the frequency distribution function of elastic vibrations has analytic singularities. In the general case, the nature of the singularities depends only on the number of dimensions of the crystal. For a two-dimensional crystal, the distribution function has logarithmically infinite peaks. In the three-dimensional case, the distribution function itself is continuous whereas its first derivative exhibits infinite discontinuities. These results are elementary consequences of a theorem of Morse on the existence of saddle points for functions defined on a torus.

I. INTRODUCTION

IT is well known that the shape of the frequency distribution function $g(\nu)$ of a crystal (defined as the number of elastic frequencies per unit frequency interval, divided by the total number of frequencies) determines an important part of the thermodynamical properties of the crystal. The frequency distribution of two- and three-dimensional crystals, as predicted by the Born-von Karman theory of crystal dynamics, has been extensively studied by approximate methods based on the use of a finite sample of elastic vibrations.[1] A smooth distribution function was obtained in all cases, showing for small frequencies a behavior in full agreement with the Debye continuum theory, tending continuously to zero at the maximum frequency and displaying for intermediate frequencies a few finite maxima.[2]

The analytical nature of the frequency distribution function, or rather of its asymptotic form for a crystal of infinite extension, has recently attracted attention as a consequence of an exact calculation by Montroll for a two-dimensional square lattice.[3] As found by

[1] M. Blackman, Repts. Prog. Phys. **8**, 11 (1941) and references there quoted; E. Montroll, J. Chem. Phys. **10**, 219 (1942); E. Montroll and D. Peaslee, J. Chem. Phys. **12**, 98 (1944); H. M. J. Smith, Trans. Phil. Soc. **A241**, 105 (1948); W. V. Houston, Revs. Modern Phys. **20**, 161 (1948); R. B. Leighton, Revs. Modern Phys. **20**, 165 (1948).

[2] The frequency distribution obtained by Leighton (reference **1**), has at the maximum frequency of each branch a singularity very similar to some of the singularities we shall show to exist in three dimensions. The singularities obtained by Houston (reference 1) are entirely spurious.

[3] E. Montroll, J. Chem. Phys. **15**, 575 (1947).

Montroll, for arbitrary values of the constants describing the forces between particles, the frequency distribution function has two logarithmically infinite peaks, one for each branch of the spectrum. These singularities were of course bound to remain undetected in the previous approximate investigations, in which the infinite peaks were approximated by finite maxima. Montroll's result has been extended by Smollett to the case of a two-dimensional ionic lattice, taking into account the long range Coulomb forces between ions.[4]

As noticed by Smollett, the logarithmic peaks obtained for the two-dimensional lattices considered are a simple consequence of the existence of saddle points for the function $\nu(\mathbf{q})$ expressing the frequency of an elastic plane wave in terms of its wave vector. The main object of the present paper is to point out that the existence of such saddle points in the $\nu(\mathbf{q})$ function, far from being accidental, is necessarily implied by the periodic structure of the lattice. According to a general theorem of M. Morse, any function of more than one independent variable which, as $\nu(\mathbf{q})$, is periodic in all its variables has at least a certain number of saddle points; this number is determined by topological considerations and depends only on the number of independent variables. It is this mathematical fact which accounts for the occurrence of logarithmic peaks in the $g(\nu)$ function; it implies that such peaks will appear quite generally for two-dimensional lattices.

For three-dimensional crystals, the theorem of Morse implies again the existence of saddle points in the $\nu(\mathbf{q})$ function. As will be shown below, saddle points of $\nu(\mathbf{q})$ produce, however, weaker singularities in the distribution function, no longer connected with its maxima: $g(\nu)$ remains continuous whereas $dg/d\nu$ has infinite discontinuities. In contradiction with a prediction by Smollett,[4] no logarithmic infinities are therefore in general to be expected for three-dimensional lattices, although some could possibly occur when the forces between particles satisfy special conditions, not implied by the symmetry properties of the crystal.

II. TYPES OF SINGULARITIES

We shall now analyze in somewhat more detail the two elements which by their combination account for the occurrence of analytic singularities in the frequency distribution $g(\nu)$ of a crystal, namely, the rather elementary fact that saddle points of $\nu(\mathbf{q})$, and more generally points where $\operatorname{grad}\nu(\mathbf{q})=0$, produce singularities in the $g(\nu)$ function, and the more fundamental theorem of Morse according to which the periodicity of the crystal implies the existence of saddle points for $\nu(\mathbf{q})$. The former fact will be discussed in this section, whereas Sec. III will deal with the application of Morse's theorem.

As is known from lattice dynamics,[5] under the assumption of harmonicity for the forces between particles, the elastic vibrations of a crystal are superpositions of normal modes, each of which is a plane wave vibration with a definite frequency ν and a wave vector $2\pi\mathbf{q}$ defined up to the addition of an arbitrary vector $2\pi\sum_\alpha n_\alpha\mathbf{h}_\alpha$; here the n_α are integers and the $\mathbf{h}_\alpha$ are the basic vectors of the reciprocal lattice, related to the basic vectors $\mathbf{s}_\beta$ of the crystal cell by

$$(\mathbf{h}_\alpha\cdot\mathbf{s}_\beta)=\begin{cases}1 & \text{for } \alpha=\beta\\ 0 & \text{for } \alpha\neq\beta.\end{cases}$$

For a crystal with Z atoms per cell, and in l dimensions (the cases $l=2$ and 3 will be discussed here),[6] there are lZ independent plane wave vibrations for each wave vector $\mathbf{q}$, and their frequencies $\nu(\mathbf{q})$ are the positive square roots of the eigenvalues of a positive-definite symmetric matrix with lZ rows and columns; the coefficients of this matrix are periodic functions of $\mathbf{q}$ with the periodicity of the reciprocal lattice. The frequency $\nu(\mathbf{q})$ is therefore an lZ valued function satisfying

$$\nu\Big(\mathbf{q}+\sum_{\alpha=1}^{l}n_\alpha\mathbf{h}_\alpha\Big)=\nu(\mathbf{q}),\quad (n_\alpha \text{ integers}). \tag{1}$$

It consists of lZ branches, some of which may become equal for special values of $\mathbf{q}$. Such equalities will be referred to as contacts between branches. According to (1), it is sufficient to consider $\nu(\mathbf{q})$ as defined in one single cell of the reciprocal lattice.

In terms of the multivalued $\nu(\mathbf{q})$ function, the frequency distribution function $g(\nu)$ for a crystal of infinite extension is given by

$$g(\nu)d\nu=(v_0/Zl)\int d_l\mathbf{q},$$

the integral being extended to the region within one cell of reciprocal space where $\nu\leqslant\nu(\mathbf{q})\leqslant\nu+d\nu$; an easy calculation gives then

$$g(\nu)=\frac{v_0}{Zl}\sum\int_{S(\nu)}\Big[\sum_{\alpha=1}^{l}\Big(\frac{\partial\nu(\mathbf{q})}{\partial q_\alpha}\Big)^2\Big]^{-\frac{1}{2}}dS; \tag{2}$$

v_0 is the volume of the crystal cell, and the q_α's are the components of $\mathbf{q}$. The summation $\sum$ extends over all branches of $\nu(\mathbf{q})$. For each of them $S(\nu)$ is the line (for $l=2$) or surface (for $l=3$) of reciprocal space defined by the equation $\nu(\mathbf{q})=\nu$ and limited to one cell of the reciprocal lattice; dS is the length or area of an infinitesimal portion of $S(\nu)$. Equation (2) remains valid after any change of coordinates in $\mathbf{q}$ space leaving invariant the area or volume element $d_l\mathbf{q}$ of reciprocal space.

[4] M. Smollett, Proc. Phys. Soc. (London) **A65**, 109 (1952).

[5] See for example M. Born and M. Goeppert-Mayer, *Handbuch der Physik* (J. Springer, Berlin, 1933), **24**, No. 2, Chap. IV.

[6] In one dimension, $l=1$, the frequency distribution is known to have no singularity apart from infinities at the extreme frequencies of each branch. See F. Seitz, *Modern Theory of Solids* (McGraw-Hill Book Company, Inc., New York, 1940), p. 123.

It is now clear that the analytic singularities of $g(\nu)$ originate from the so-called critical points of $\nu(\mathbf{q})$, i.e., the points where all derivatives $\partial\nu/\partial q_\alpha$ vanish. Let us investigate the singularity produced in $g(\nu)$ by a critical point $\mathbf{q}_c$ of $\nu(\mathbf{q})$, in the general case where the determinant $|\partial^2\nu/\partial q_\alpha \partial q_\beta|$ does not vanish at $\mathbf{q}_c$ (as is usual in mathematics, such a critical point will be called nondegenerate). Putting $\nu(\mathbf{q}_c)=\nu_c$, we may write in first approximation for $\mathbf{q}$ near $\mathbf{q}_c$, and after a convenient change of coordinates preserving $d_l\mathbf{q}$,

$$\nu=\nu_c+a\sum_{\alpha=1}^{l}\epsilon_\alpha\xi_\alpha^2+\cdots,\quad \epsilon_\alpha=\pm 1,\quad \xi=\mathbf{q}-\mathbf{q}_c,\quad a>0. \tag{3}$$

Restricting the summation in (2) to the branch with the critical point and the integration to a neighborhood of $\mathbf{q}_c$, we use (3) in (2) and obtain the following singularities in $g(\nu)$ for ν near ν_c.

Two-Dimensional Crystal

$(M, i=0)\quad \epsilon_1=\epsilon_2=-1,$

$$g(\nu)=\begin{cases} C+(\pi v_0/Zla)+0(\nu-\nu_c) & \text{for}\quad \nu<\nu_c \\ C+0(\nu-\nu_c) & \text{for}\quad \nu>\nu_c \end{cases}$$

$(S, i=1)\quad \epsilon_1=-\epsilon_2=\pm 1,$

$$g(\nu)=C-\frac{v_0}{Zla}\log\left|1-\frac{\nu}{\nu_c}\right|+0(\nu-\nu_c)$$

$(m, i=2)\quad \epsilon_1=\epsilon_2=1,$

$$g(\nu)=\begin{cases} C+0(\nu-\nu_c) & \text{for}\quad \nu<\nu_c \\ C+(\pi v_0/Zla)+0(\nu-\nu_c) & \text{for}\quad \nu>\nu_c. \end{cases}$$

Three-Dimensional Crystal

$(M, i=0)\quad \epsilon_1=\epsilon_2=\epsilon_3=-1,$

$$g(\nu)=\begin{cases} C+(2\pi v_0/Zla^{\frac{1}{2}})(\nu-\nu_c)^{\frac{1}{2}}+0(\nu-\nu_c) & \text{for}\quad \nu<\nu_c \\ C+0(\nu-\nu_c) & \text{for}\quad \nu>\nu_c \end{cases}$$

$(S_1, i=1)\quad \epsilon_{\alpha 1}=\epsilon_{\alpha 2}=-\epsilon_{\alpha 3}=-1,$

$$g(\nu)=\begin{cases} C+0(\nu-\nu_c) & \text{for}\quad \nu<\nu_c \\ C-(2\pi v_0/Zla^{\frac{1}{2}})(\nu-\nu_c)^{\frac{1}{2}}+0(\nu-\nu_c) & \text{for}\quad \nu>\nu_c, \end{cases}$$

$(S_2, i=2)\quad \epsilon_{\alpha 1}=\epsilon_{\alpha 2}=-\epsilon_{\alpha 3}=1,$

$$g(\nu)=\begin{cases} C-(2\pi v_0/Zla^{\frac{1}{2}})(\nu-\nu_c)^{\frac{1}{2}}+0(\nu-\nu_c) & \text{for}\quad \nu<\nu_c \\ C+0(\nu-\nu_c) & \text{for}\quad \nu>\nu_c, \end{cases}$$

$(m, i=3)\quad \epsilon_1=\epsilon_2=\epsilon_3=1,$

$$g(\nu)=\begin{cases} C+0(\nu-\nu_c) & \text{for}\quad \nu<\nu_c \\ C+(2\pi v_0/Zla^{\frac{1}{2}})(\nu-\nu_c)^{\frac{1}{2}}+0(\nu-\nu_c) & \text{for}\quad \nu>\nu_c. \end{cases}$$

The symbols M and m refer to maxima and minima, respectively. S refers to saddle points in the two-dimensional case, whereas for three dimensions, the saddle points are of two different types, denoted by S_1 and S_2. The number i is the so-called index of the critical point, to be used later. In all expressions C is a constant and $O(\nu-\nu_c)$ denotes a rest term of the order of $\nu-\nu_c$ for $\nu\to\nu_c$. Higher singularities would be produced by critical points for which $|\partial^2\nu/\partial q_\alpha\partial q_\beta|=0$, in particular by a continuous family of critical points. Such cases are to be considered exceptional as compared to the general case just discussed: it can be shown that they occur only when the constants describing the forces between particles satisfy special relations not implied by the crystal symmetries.

III. APPLICATION OF MORSE'S THEOREM

According to the periodicity condition (1), it is natural to consider the $\nu(\mathbf{q})$ function as defined in one cell of the reciprocal lattice, and to identify points $\mathbf{q}$, $\mathbf{q}'$ of the boundary of the cell for which

$$\mathbf{q}'=\mathbf{q}+\sum_{\alpha=1}^{l}n_\alpha\mathbf{h}_\alpha,\quad (n_\alpha \text{ integers}).$$

The domain of definition thus obtained for $\nu(\mathbf{q})$ is an l dimensional torus.

We now state the theorem of Morse under elementary and too restrictive assumptions: consider a function f defined on a closed topological manifold satisfying convenient conditions of differentiability and regularity; assume f to be three times continuously differentiable and to have no degenerate critical points. Call index of a nondegenerate critical point the number of positive eigenroots of the quadratic form in the Taylor expansion of f near the critical point [number of positive terms in the sum in (3)]. Under these conditions, the number of critical points of index i is at least equal to the Betti number R_i of the manifold for the dimension i.[7]

For $l=2$, the two-dimensional torus has Betti numbers $R_0=1$, $R_1=2$, $R_2=1$. If a branch of $\nu(\mathbf{q})$ satisfies the above conditions, it has therefore at least one maximum, two saddle points and one minimum. The corresponding singularities in $g(\nu)$ were listed in Sec. II. By reason of symmetry the two saddle points may often correspond to the same value of $\nu(\mathbf{q})$; they will then produce one single logarithmic peak in $g(\nu)$.

In three dimensions, the Betti numbers of the torus are $R_0=1$, $R_1=3$, $R_2=3$, $R_3=1$. For a branch of $\nu(\mathbf{q})$ satisfying the above conditions, there are at least one maximum, three saddle points of each type and one

[7] For an elementary exposition and examples, see M. Morse, Am. Math. Monthly **49**, 358 (1942), Sec. 5. For details and proofs, see M. Morse, Trans. Am. Math. Soc. **27**, 345 (1925); *Calculus of Variations in the Large, Colloquium Lectures* (American Mathematical Society, Providence, 1934), Chap. VI; *Mémorial Sciences Mathématiques*, "Functional Topology and Abstract Variational Theory" (Gauthier-Villars, Paris, 1939), Fascciule 92. Regarding the definition of the Betti numbers, for our purpose it is sufficient to say that R_i is the maximum number of closed i dimensional surfaces on the manifold which cannot be transformed into one another or into a point by continuous deformation on the manifold.

minimum. Saddle points of the same type will often correspond to the same frequency. The branch considered produces therefore in $g(\nu)$ at least one singularity of each of the four types listed in the previous section for $l=3$.

To determine the net number of singularities to be expected in the frequency distribution $g(\nu)$, one has now to take into account two important factors. Firstly, singularities produced in $g(\nu)$ by various branches may compensate each other. Inspection of the list of singularities in Sec. II shows that for $l=2$ such compensations can occur for the singularities produced in $g(\nu)$ by a maximum and a minimum of $\nu(\mathbf{q})$, whereas cancellations are impossible for the logarithmic peaks resulting from saddle points. For $l=3$ compensations can take place between a maximum and a saddle point of type S_2 (i.e., of index 2), as well as between a minimum and a saddle point of type S_1 (i.e., of index 1).

Secondly, the assumptions made above for the branches of the $\nu(\mathbf{q})$ function are too restrictive: both the behavior of $\nu(\mathbf{q})$ for small ν and certain contacts between branches prevent them from being fulfilled. Before entering into general considerations, let us discuss the region of very small frequencies. It is reached for the l acoustical branches near $\mathbf{q}=0$ (long wavelengths), where the Debye continuum theory of solids is applicable. For each acoustical branch $\nu(\mathbf{q})$ has its absolute minimum $\nu(0)=0$ at $\mathbf{q}=0$. As is well known, this minimum does not have the same properties as the critical points considered up to now. The Taylor expansion (3) is not valid in its neighborhood and is replaced by an expression

$$\nu=|q|\cdot\varphi(\mathbf{q}/|q|)+O(|q|^2) \tag{4}$$

for $|q|$ small; φ is a positive function of the direction of $\mathbf{q}$, which can be determined from the elastic constants of the crystal.[8] According to (4), $|\mathrm{grad}\nu(\mathbf{q})|$ does not tend to zero for $\mathbf{q}\neq 0$ tending to zero, although the gradient is undefined at the point $\mathbf{q}=0$ itself. Therefore this minimum of $\nu(\mathbf{q})$ produces no singularity in $g(\nu)$: from (4) follows the familiar behavior of $g(\nu)$ for small frequencies,

$$g(\nu)\sim\nu^{l-1}.$$

In the same way as $\mathbf{q}=0$ is for the acoustical branches what we may call a generalized minimum, other generalized critical points can occur in $\nu(\mathbf{q})$ at the contacts between branches. For our purpose, the concept of generalized critical point $\mathbf{q}_c$ of index i can be described in the following way: for a one-valued function $f(\mathbf{q})$, one branch of $\nu(\mathbf{q})$ for example, it is a point in the neighborhood of which, although $f(\mathbf{q})$ has no Taylor expansion of type (3), the surfaces $f(\mathbf{q})=f_0$, with f_0 constant and near $f(\mathbf{q}_c)$, have the same topological shape as for the nondegenerate critical points of index i considered above. Just as for the generalized minimum (i.e., critical point of index l) discussed above for the acoustical branches, the generalized critical points to be expected in $\nu(\mathbf{q})$ give rise to an expansion similar to (4)

$$\nu(\mathbf{q})-\nu(\mathbf{q}_c)=|\xi|\cdot\psi(\xi/|\xi|)+O(|\xi|^2),\quad \xi=\mathbf{q}-\mathbf{q}_c.$$

If the directions in which $\psi(\xi/|\xi|)$ vanishes are discrete for $l=2$ or depend on one continuous parameter for $l=3$, such generalized critical points produce in $g(\nu)$ weaker singularities (discontinuities in higher derivatives) than the conventional critical points of same index; moreover the weaker singularities produced by the various branches in contact are likely to compensate each other. On the other hand, if ψ vanishes identically, the quadratic terms of the expansion have to be used. They have the form

$$\nu(\mathbf{q})-\nu(\mathbf{q}_c)=|\xi|^2\psi_1(\xi/|\xi|)+O(|\xi|^3)$$

and, for general values of the forces, they can be shown to produce in $g(\nu)$ the same singularities as the conventional critical points discussed in Sec. II, with again possible compensation between the branches in contact.

The important fact is now that the theorem of Morse is valid under much wider conditions than stated above.[7] For the functions which, like the branches of $\nu(\mathbf{q})$, may have generalized critical points, its prediction is that the number of critical points of index i, the generalized ones included, is at least equal to the Betti number R_i. We have therefore to discuss under what conditions generalized critical points can occur, and which critical points may be expected not to be of generalized type and hence to produce in $g(\nu)$ the singularities predicted for them in Sec. II. The absolute minimum $\nu=0$ of $\nu(\mathbf{q})$, reached in the acoustical branches, is already known to be of generalized type. Other generalized critical points can be produced only by contacts between branches and will now be discussed for the most common types of contacts.

The condition of having two eigenvalues equal decreases by two the number of parameters on which a real symmetric matrix depends.[9] For two-dimensional crystals, the contacts between branches occur therefore in general in isolated points of reciprocal space. If we define the various branches $\nu_1(\mathbf{q})$, $\nu_2(\mathbf{q})$, $\cdots$, $\nu_{lZ}(\mathbf{q})$ by the increasing order of their frequencies for each $\mathbf{q}$:

$$\nu_1(\mathbf{q})\leqslant\nu_2(\mathbf{q})\leqslant\cdots\leqslant\nu_{lZ}(\mathbf{q}), \tag{5}$$

an algebraic discussion shows that at an isolated point of contact a maximum of one branch can coincide with a minimum of the subsequent branch, and both can be of generalized type. No generalized saddle points are to be expected for arbitrary force constants.

For $l=3$ on the contrary, contacts between branches, occurring along curves or in isolated points of $\mathbf{q}$ space, often affect saddle points as well as extrema. Certain contacts are a consequence of crystal symmetries, others do not follow from symmetry and are therefore

[8] H. A. Jahn, Proc. Roy. Soc. (London) **A179**, 320 (1941).

[9] J. von Neumann and E. Wigner, Physik. Z. **30**, 467 (1929).

called accidental. Both types have been carefully discussed for energy bands of electrons in a crystal; this discussion applies without essential change to crystal vibrations.[10] Using again (5), let us consider two branches $\nu_i(\mathbf{q})$ and $\nu_{i+1}(\mathbf{q})$ in contact along a curve C, which is necessarily a closed circuit when taken on the three-dimensional torus. Let the maximum of $\nu_i(\mathbf{q}) = \nu_{i+1}(\mathbf{q})$ on C be reached at $\mathbf{q}_1$, its minimum at $\mathbf{q}_2$. The point $\mathbf{q}_1$ can be a maximum of ν_i and a saddle point of index 2 for ν_{i+1}, and these critical points can be of generalized type. The same holds for $\mathbf{q}_2$ which can be a saddle point of index 1 for ν_i and a minimum for ν_{i+1}.[11] For contacts of two or more branches in an isolated point $\mathbf{q}\neq 0$ of reciprocal space, the generalized critical points which are most likely to appear are a generalized maximum for the lower branch and a generalized minimum for the upper branch, although more complicated situations are not excluded.

Apart from the absolute minimum $\nu=0$, the critical points which can be of generalized type are seen to belong to pairs of critical points of equal frequency. The pairs are maximum-minimum for $l=2$ or 3, maximum-saddle point of index 2 and minimum-saddle point of index 1 for $l=3$. Apart from maximum-minimum for $l=3$, these are also the pairs of critical points which can produce compensating singularities in $g(\nu)$. For $l=2$, all saddle points and the absolute maximum of $\nu(\mathbf{q})$ will therefore remain unaffected by the contacts between branches and they will produce in $g(\nu)$ the singularities predicted for them in Sec. II. No compensation can take place between these singularities, but as noted already in Sec. II, the logarithmic peaks resulting from saddle points belonging to the same branch may coincide as a consequence of crystal symmetries. *This gives for the $g(\nu)$ function of a two-dimensional crystal at least one logarithmic peak per branch and at least a finite discontinuity, occurring at the upper end of the spectrum.* The results obtained by Montroll[3] and Smollett[4] clearly illustrate this conclusion.

For $l=3$, according to our discussion of the most common contacts between branches, the only critical points of $\nu(\mathbf{q})$ which are never affected by such contacts are the absolute maximum of $\nu(\mathbf{q})$, the saddle points of index 2 of the branch with lowest maximum frequency and the saddle points of index 1 of the branch with largest minimum frequency. These points contribute to $g(\nu)$ the singularities predicted for them in Sec. II. No compensation is possible between these singularities, but the crystal symmetries may imply the coincidence of singularities produced by various saddle points belonging to the same branch and having the same index. *The general prediction we can make for three-dimensional crystals is therefore that, $g(\nu)$ being continuous, $dg/d\nu$ has at least two infinite discontinuities, and takes the value $-\infty$ at the upper end of the spectrum.* In many cases, of course, especially when the crystal symmetry is not too high, the number of infinite discontinuities in $dg/d\nu$ will be considerably larger. For the detailed analytical nature of these discontinuities, the reader is referred to the list of singularities in Sec. II, from where it is obtained by mere differentiation of $g(\nu)$ near ν_e.

IV. CONCLUDING REMARKS

As was emphasized several times, the whole discussion carried out in this paper is of a general nature. In each step we tried to handle the case of greatest generality, leaving out various exceptions. Most exceptional cases arise when the force constants strictly satisfy special relations not following from crystal symmetry; hence these cases have no physical interest; they will exhibit in $g(\nu)$ stronger singularities than predicted above, for example logarithmic peaks in three dimensions. The only exceptional case which has not been excluded for general values of the force constants is that of three-dimensional crystals with more complicated contacts between branches than considered above; for them the number or strength of the singularities, if affected at all, could only be reduced.

In regard to the numerical determination of frequency distributions for crystals, the above discussion shows that great attention has to be paid to location and shape of the critical points of $\nu(\mathbf{q})$. This information can be obtained from the shape of the contours of constant frequency in reciprocal space, as was done by Smollett for a two-dimensional ionic lattice.[4]

Finally, it is worth mentioning that the discussion presented in this paper also applies to the Bloch theory of electrons in crystal lattices. The energy of the electron, which is here taking the place of the square of the vibration frequency, is a periodic function of the wave vector and has therefore at least the minimum numbers of critical points predicted by the theorem of Morse, with the same consequences as above for the distribution function (density) of states in energy.[12]

The author would like to express his gratitude to Professor J. R. Oppenheimer for his kind hospitality at the Institute for Advanced Study. He is indebted to Professor M. Morse for his interest in the mathematical aspects of this problem, and to Dr. C. Herring, Dr. M. Kac, Dr. E. Montroll, and Dr. G. Placzek for valuable remarks and suggestions.

[10] Contacts resulting from symmetry are treated by group-theoretical methods by Bouckaert, Smoluchowski, and Wigner, Phys. Rev. **50**, 58 (1936), and by C. Herring, Phys. Rev. **52**, 361 (1937). For accidental contacts, see C. Herring, Phys. Rev. **52**, 365 (1937). The author is indebted to Dr. C. Herring for bringing to his attention the whole question of contacts between branches.

[11] From a mathematical standpoint, the separation of the branches ν_i and ν_{i+1} according to (5) is unnatural: along a path through a point of C, the natural continuation of ν_i is ν_{i+1} and vice versa. This can be avoided by considering the multivalued $\nu(\mathbf{q})$ function as a univalued function on a convenient covering manifold of the torus.

[12] The density of states of an electron in a two-dimensional layer of graphite has been calculated by C. A. Coulson and R. Taylor, Proc. Phys. Soc. (London) **A65**, 815 (1952). In agreement with our predictions, it has two logarithmic infinities for intermediate energies and finite discontinuities at both ends of the energy range.

Neutron-Proton Scattering Using Organic Crystal Scintillation Detectors*†‡

M. E. REMLEY,§ W. K. JENTSCHKE, AND P. G. KRUGER
University of Illinois, Urbana, Illinois
(Received October 20, 1952)

The angular distribution of protons recoiling from neutrons of 13.7 Mev and 28.4 Mev has been investigated in the region of 0° to 90° in the center-of-mass system. Organic scintillation crystals of anthracene and stilbene were used as both sources and detectors of the recoil protons. The angular distribution observed at 13.7 Mev is consistent with spherically symmetric scattering, while the results at 28.4 Mev show an anisotropy with a favoring of scattering of the neutrons in the backward direction.

I. INTRODUCTION

THE experimental study of neutron-proton scattering has long been expected to be a fruitful source of information leading to knowledge of nuclear forces. Consequently, a very large amount of both experimental and theoretical work covering a wide variation in energy has been performed on the neutron-proton scattering problem. It is now generally accepted that the scattering is isotropic in the center-of-mass system (without preclusion of an asymmetry of approximately five percent) for energies below about 15 Mev.[1] At approximately 20 Mev,[2] there are indications of an asymmetry favoring scattering in the backward direction. This is definitely confirmed at 27 Mev[3] and becomes more pronounced at the higher energies of 40, 90,[4] and 260 Mev.[5] In the present experimental work, the scattering of fast neutrons by protons has been studied by the observation of recoil protons in an organic scintillation crystal which was used as both source and detector of the recoils.

II. EXPERIMENTAL APPARATUS AND PROCEDURE

The neutrons for the present experiments were obtained from the $D(d,n)He^3$ and the $T(d,n)He^4$ nuclear reactions. Because of the very low yield of high energy neutrons from the $T(d,n)He^4$ reaction, a technique of using an organic scintillation crystal as both a source and detector of recoil protons was employed. Since this technique was at the time unexploited, it was deemed desirable to check it at a lower energy, where the angular distribution is known to be isotropic.

A plan view of the physical arrangement of the experimental apparatus is shown in Fig. 1. Deuterons of 11.75 ± 0.12 Mev[6] accelerated by the University of Illinois cyclotron were collimated by a set of lead slits, passed through a thin gas target, and were stopped in a 0.030-inch lead foil approximately 13 feet from the target. A scintillation counter was accurately positioned in a light-tight copper box such that a line from the center of the gas target to the crystal made an angle of $11.69°\pm0.05°$ with the deuteron beam direction.

The gas target used by Laughlin and Kruger[1] was used to contain the deuterium for the source of neutrons from the $D(d,n)He^3$ reaction. A somewhat similar target, shown in Fig. 2, was filled to about 25 cm of Hg pressure with a tritium-hydrogen mixture of 60 percent tritium for the second neutron source. When not in use, the tritium was stored as uranium tritide in the small iron container. Filling the target was accomplished by heating the UT_3 to approximately 450°C, which produced decomposition and resulted in essentially complete evolution of the tritium gas into the target chamber.[7] The gas volume was emptied by opening the bellows valve between the target chamber and the uranium container. This permitted the tritium to react with the uranium forming the UT_3 and emptying the target volume to a pressure of approximately 10^{-4} mm of Hg.

Because of the finite size of the target, the angle of emission of the neutrons from the nuclear reactions varied over 7.6°, and this plus the degradation of the deuteron energy in passing through the gas in the target resulted in a finite energy spread in the neutrons which

* This investigation was supported jointly by the U. S. Atomic Energy Commission and the U. S. Office of Naval Research.

† This report is part of a thesis (M.E.R.) submitted in partial fulfillment of the requirements for the degree of Doctor of Philosophy at the University of Illinois, 1952.

‡ A preliminary report of this work was given at the Denver meeting of the American Physical Society in July, 1952 [Phys. Rev. **88**, 162 (1952)].

§ Now at North American Aviation, Inc., Downey, California.

[1] Kruger, Shoupp, and Stallman, Phys. Rev. **52**, 678 (1937); W. F. Caplehorn and G. P. Rundle, Proc. Phys. Soc. (London) **A64**, 546 (1951); J. S. Laughlin and P. G. Kruger, Phys. Rev. **73**, 197 (1948); H. H. Barshall and R. F. Taschek, Phys. Rev. **75**, 1819 (1949).

[2] E. W. Baldwin, Phys. Rev. **83**, 495 (1951).

[3] Brolley, Coon, and Fowler, Phys. Rev. **82**, 190 (1951).

[4] Hadley, Kelly, Leith, Segrè, Wiegand, and York, Phys. Rev. **73**, 1114 (1948); Brueckner, Hartsough, Hayward, and Powell, Phys. Rev. **75**, 555 (1949).

[5] Kelly, Leith, Segrè, and Wiegand, Phys. Rev. **79**, 96 (1950).

[6] This energy was determined by measuring the range of the deuterons in air. This was done by passing the beam through a monitor consisting of a double-end-window proportional counter, whose stopping power was known, and then into a thin zinc sulfide screen placed on the end of a movable 5819 photomultiplier tube. This second detector had a threshold detection energy as measured with a polonium alpha-source of less than 30 kev. This measurement was checked by determining the range in photographic emulsion of protons accelerated by the cyclotron. The energy of the protons was determined from the range-energy relation in emulsion given by J. Rotblatt, Nature **167**, 550 (1951), and the energy of the deuterons was derived from this value of the proton energy.

[7] For a description of the properties of uranium tritide, see F. H. Spedding *et al.*, Nucleonics **4**, No. 1, 4 (1949).

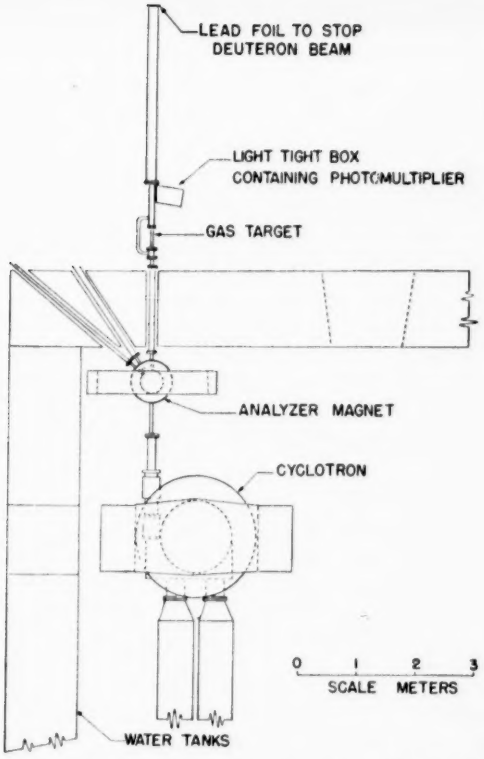

FIG. 1. Arrangement of experimental apparatus. The amplifier, discriminator, and associated electronic equipment were located in the cyclotron control room.

were to be scattered. The neutrons from the $T(d,n)He^4$ reaction had a mean energy of 28.4 Mev with a spread of 0.50 Mev, while those from the $D(d,n)He^3$ reaction were of mean energy 13.7 Mev with a spread of 0.80 Mev.

The hydrogenous radiator and detector consisted of an organic scintillation crystal of either anthracene or stilbene mounted in contact with the photosensitive surface of a selected RCA 5819 photomultiplier tube. The crystal was covered with a thin aluminum reflecting foil. The photomultiplier tube was magnetically shielded with four concentric cylindrical shields of annealed Permalloy, magnetically insulated from each other. The integrated output pulses from the photomultiplier were applied through a cathode follower to a Los Alamos type model 100 linear pulse amplifier,[8] through a pulse shaping circuit and into a twelve-channel pulse amplitude analyzer. The discriminator levels of the analyzing system were set by feeding pulses of known height into the system from an electronic pulse generator. Several checks on the stability of the electronic system showed the discriminator levels to be constant to within ± 0.05 volt over periods as long as 24 hours with the levels set at approximately 7 volts apart. This shift in the levels included the net effects of possible variations in the pulse generator, amplifier, pulse shaping circuit, and analyzer.

The voltage to the dynodes of the photomultiplier tube was supplied by a voltage dividing network of precision resistors connected across the output of a negative electronic power supply. This output voltage was monitored with an auxiliary circuit, and the voltage was maintained constant to within ± 0.1 volt by manual adjustment of the supply during the taking of data.

In order to obtain an absolute energy response of the scintillation detectors, pulse-height distributions from a well-collimated polonium alpha-particle source were taken in a standard geometry before and after each experimental run. The response of the counter to these alpha-particles had been normalized to the response of protons of known energy from the cyclotron. Thus, knowing the relative pulse height *vs* energy relation for the crystals used in addition to the above normalization factor, the response of the counters during any experimental run could immediately be converted to the energy of the protons originating the fluorescence.

Because of the large amount of background radiation produced by the cyclotron, the experimental data were obtained in a series of "runs," half of which were taken with the gas target filled, while the others were background runs taken with the gas target evacuated. During these runs, the integrated cyclotron beam to the main target was measured with a charge measuring circuit; the neutron flux inside the cyclotron shielding tanks was monitored with small gold foils using the well-known reaction

$$Au^{197}+n \rightarrow Au^{198} \rightarrow \beta^- + Hg^{198};$$

the gamma-intensity in the vicinity of the neutron source was measured with a Geiger counter in a standard geometry. These three measurements were all relative, and they were sufficient to determine the background

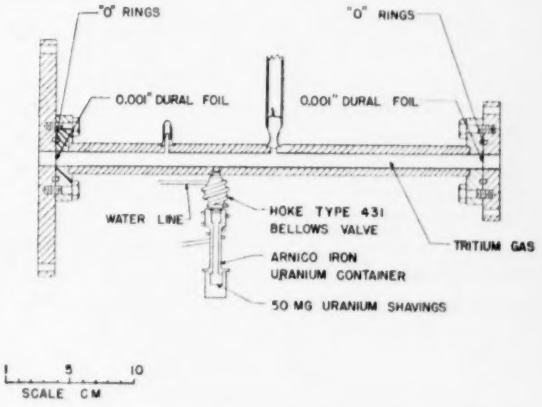

FIG. 2. Gas target used to contain tritium gas for source of high energy neutrons.

[8] W. C. Elmore and M. Sands, *Electronics* (McGraw-Hill Book Company, Inc., New York, 1949).

TABLE I. Angular distribution data at 13.7 Mev.

Center-of-mass recoil angle	Number of counts in recoil angular interval	Correction factor for finite size of crystal	Center-of-mass solid angle	Relative No. of recoils per steradian
15.7±2.1	5734	1.169	0.1456	0.61±0.16
36.1±3.7	6510	1.148	0.0990	1.00±0.021
45.0±2.8	6526	1.124	0.0990	0.98±0.027
52.8±2.4	6833	1.100	0.1077	0.92±0.024
60.2±2.0	7518	1.080	0.1063	1.01±0.035
67.0±1.8	7509	1.056	0.1049	1.00±0.036
73.4±1.6	8191	1.038	0.1047	1.07±0.040
79.7±1.4	7764	1.012	0.1080	0.96±0.055
86.3±1.2	9898	0.9965	0.1220	1.07±0.086

with a precision of ±5 percent plus the normal statistical variations.

III. ANALYSIS OF DATA

The data were analyzed in three groups which can be described as follows:

(1) the data for 13.7-Mev neutrons incident on anthracene;
(2) the data for 28.4-Mev neutrons incident on anthracene;
(3) the data for 28.4-Mev neutrons incident on stilbene.

The treatment included the determination of the actual number of counts in each pulse-height interval resulting from the incidence on the crystal of the nearly monoergic neutrons from the source. This was done by subtracting the proper background from the data taken with the target filled with gas. For the data at 28.4 Mev, the background counting rate in the pulse-height interval corresponding to protons recoiling at 47° in the laboratory system was approximately two-thirds of the total counting rate and decreased to about one-half and one-third of the total counting rate at recoil angles of 43° and 37°, respectively. At recoil angles of less than 33°, the background was quite small, being only about 3 to 4 percent of the total counting rate. For the data at 13.7 Mev, the background counting rate was about one-half of the total counting rate at proton recoil angles of 43° in the laboratory system and decreased to about 30 percent of the total counting rate at recoil angles of 36°. At recoil angles of less than 30°, the background rate varied between 5 and 20 percent of the total rate. The pulse-height intervals as set by the discriminator levels in the pulse analyzer were then converted to recoil proton energy intervals by making use of the pulse height *vs* energy relations for the crystals along with the energy normalization factor obtained with the polonium alpha-particles. The proton energies corresponding to the discriminator settings could immediately be converted to laboratory recoil angles by means of the following equation:[9]

$$\cos^2\theta = E_P/E_n,$$

where E_p = recoil proton energy; E_n = mean neutron energy. An angular distribution in center-of-mass coordinates was then obtained in the usual manner, with the small relativistic correction for the data at 28.4 Mev included for rigor.

The response curve for the anthracene counter was taken from known results[10–12] for energies up to 16.4 Mev, plus an extrapolation from this energy through a point obtained at 29.2 Mev by observation of the pulse heights resulting from the maximum energy protons recoiling from neutrons of 29.2 Mev. This continuation of the curve was found to agree with that predicted by Birks,[13] if the constants in his equation are calculated from the well-investigated lower energy region.

The presently available data for stilbene response[10,12] extend up to about 14.7 Mev. To extend this response curve to the energy needed for analysis of these data, the response of stilbene at 28.7 Mev was measured with neutrons of that energy. The response curve was also calculated for the energy region 5.5 to 30 Mev after the method of Birks.[13] These two curves were found to be in essential agreement, and the calculated curve was used in the analysis.

A correction to the number of counts in each recoil angular interval was required because of the finite size of the crystals. This is complicated by the fact that the recoil protons which originate at points in the crystal such that they pass out of the crystal produce pulses of smaller size than those recoils of the same energy completely stopped in the crystal. These smaller pulses are then subject to confusion with the pulses from recoil protons of less energy wholly stopped in the crystal. The

TABLE II. Angular distribution data at 28.4 Mev taken with anthracene crystal.

Center-of-mass recoil angle	Number of counts in recoil angular interval	Correction factor for finite size of crystal	Correction factor for (n,p) reaction protons	Center-of-mass solid angle	Relative No. of recoils per steradian
11.3±3.3	1776	2.146	1.00	0.0764	1.50±0.58
29.3±5.0	2462	1.919	1.00	0.1145	1.24±0.037
41.0±3.4	2521	1.720	1.00	0.1117	1.17±0.039
50.3±2.6	2778	1.517	1.00	0.1186	1.07±0.032
58.8±2.2	3140	1.366	1.00	0.1227	1.05±0.043
66.5±2.1	3415	1.237	1.00	0.1139	1.11±0.045
73.5±1.6	3873	1.136	1.00	0.1160	1.14±0.059
80.2±1.4	4058	1.049	0.959	0.1119	1.10±0.077
87.0±1.2	5343	0.9914	0.780	0.1242	1.00±0.083
94.2±0.9	6012	0.9345	0.714	0.1257	0.96±0.15

[9] Relativistic corrections will modify this equation slightly for the 28.4-Mev data, but the corrections to the values of θ are of the order of less than 0.5 percent.

[10] Taylor, Jentschke, Remley, Eby, and Kruger, Phys. Rev. **84**, 1034 (1951).

[11] Franzen, Peele, and Sherr, Phys. Rev. **79**, 742 (1950).

[12] W. G. Cross, private communication.

[13] J. B. Birks, Phys. Rev. **84**, 364 (1951); Proc. Phys. Soc. (London) **A64**, 874 (1951).

determination of these contributions was calculated[14] by first finding the fraction of the proton recoils in each recoil angular interval which were not completely stopped in the crystal. This was done by obtaining an expression for this quantity in terms of the recoil angle, the differential cross section for the neutron-proton scattering process, the length of the recoil in the crystal (which is a function of the recoil angle), and the dimensions of the crystal. This expression was then numerically integrated over the recoil angular intervals to give a correction factor for each angular interval. In the evaluation of the integrals, the differential cross section in the center-of-mass system was taken as a constant at 13.7 Mev, and at 28.4 Mev the relative cross section given at 27.2 Mev by Brolley *et al.*[3] was used. Since these latter two energies are comparable and, further, since the recoil angular intervals were of the order of only four degrees, so that the variation of the cross section over the interval was quite small, this approximation in the second case should certainly be valid.

Those recoils which were not completely stopped in the crystal then gave pulses which corresponded to protons recoiling at larger angles and thus were incorrectly counted in the recoil angular intervals which included these larger angles. To obtain the number of pulses incorrectly counted in each interval, the pulse height actually observed was determined as a function of the recoil angle and of the origin of the proton recoil in the crystal. Then from purely geometrical considerations, since the origin of the recoil is equally probable anywhere in the crystal, the desired correction factor was obtained as a function of the correction factor for the proton recoils which were not completely stopped in the crystal. These two factors were then combined into a single correction factor for each recoil angular interval and are presented in that manner in the experimental results.

Because of the carbon component of the crystals, the effects of possible nuclear reactions resulting from neutrons incident on carbon were considered in the analysis of the data. Possible reactions include $C^{12}(n,\alpha)Be^{9}$, $C^{12}(n,3\alpha)n$, and $C^{12}(n,p)B^{12}$. Because of the large threshold energies required for these reactions and, further, because of the smaller fluorescence efficiency of the crystals for alpha-particles, none of the reaction products from these gave pulses which could be confused with the recoil protons in the angular region investigated at 13.7 Mev. The first two reactions also gave no pulses subject to confusion with the higher energy neutrons, but reaction protons from the $C^{12}(n,p)B^{12}$ reaction can be produced with energies from 16.0 Mev to 9.4 Mev (assuming no excited states in the residual B^{12} nucleus). These protons produced pulses which could be confused with the recoil protons. It had been hoped that if the cross section for this reaction was appreciable, a correction could be made by the taking of data with two crystals with different carbon to hydrogen ratios. Unfortunately, the data were not accurate enough in the appropriate angular intervals to permit a meaningful correction of this type to be determined.

TABLE III. Angular distribution data at 28.4 Mev taken with stilbene crystal.

Center-of-mass recoil angle	Number of counts in recoil angular interval	Correction factor for finite size of crystal	Correction factor for (n,p) reaction protons	Center-of-mass solid angle	Relative No. of recoils per steradian
11.3±3.8	1079	1.640	1.00	0.0764	1.17±0.46
29.3±5.3	1400	1.561	1.00	0.1145	0.96±0.028
41.0±3.5	1621	1.452	1.00	0.1117	1.06±0.030
50.3±2.6	1806	1.343	1.00	0.1186	1.03±0.052
58.8±2.4	1972	1.234	1.00	0.1227	1.00±0.042
66.5±2.0	2147	1.164	1.00	0.1139	1.11±0.052
73.5±1.7	2286	1.085	1.00	0.1160	1.08±0.064
80.2±1.5	2609	1.043	0.976	0.1119	1.20±0.12
87.0±1.3	3398	1.014	0.808	0.1242	1.13±0.14

[14] M. E. Remley, Ph.D. thesis, University of Illinois, Urbana, Illinois, 1952 (unpublished).

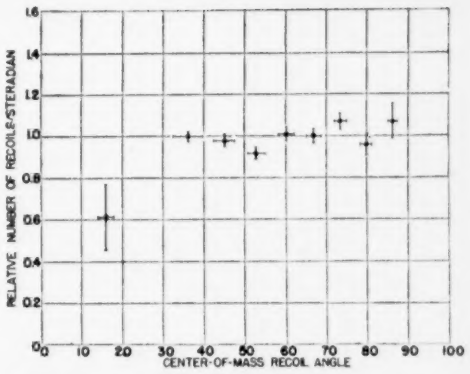

FIG. 3. Experimental angular distribution of recoil protons from 13.7-Mev neutrons; data taken with an anthracene crystal.

Available information from which a feasible correction might be determined is a measurement of the total cross section of the $C^{12}(p,n)N^{12}$ reaction. A value of 0.02 barn ±100 percent for this cross section has been obtained at 32 Mev by the linear accelerator group at the University of California.[15] From a theoretical standpoint this cross section should be approximately the same as that for the $C^{12}(n,p)B^{12}$ reaction. Therefore, a correction was calculated on the assumptions that the total cross section for the (n,p) reaction was 0.02 barn, that the protons were emitted isotropically in the laboratory system, and further that there were no excited states produced in the residual B^{12} nucleus.

IV. RESULTS AND CONCLUSIONS

The results are summarized in Tables I, II, and III and are shown in Figs. 3 and 4 as a function of the proton recoil angle in the center-of-mass system. The uncertainties shown are the probable errors for each

[15] L. Alvarez and H. Tyren, private communications.

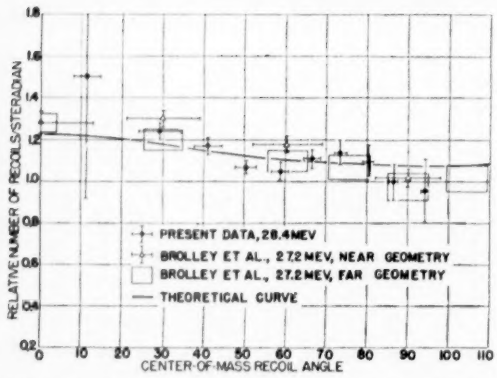
RELATIVE NUMBER OF RECOILS/STERADIAN
CENTER-OF-MASS RECOIL ANGLE
PRESENT DATA, 28.4 MEV
BROLLEY ET AL., 27.2 MEV, NEAR GEOMETRY
BROLLEY ET AL., 27.2 MEV, FAR GEOMETRY
THEORETICAL CURVE

FIG. 4. Experimental angular distribution of recoil protons from 28.4-Mev neutrons; data taken with anthracene crystal. The theoretical curve is one calculated by Christian (see reference 3) for scattering at 27.2 Mev with a Yukawa potential of range 1.35 $\times 10^{-13}$ cm plus a tensor force.

point as determined by combining the probable errors in the various quantities required to obtain the angular distribution by the least square method.

The major sources of uncertainty in each point other than the statistics of counting include that resulting from the background from the cyclotron, the uncertainty in the pulse height *vs* energy curves of the scintillation crystals, and uncertainties in the calculations required by the finite size of the crystal detectors. The uncertainties in the recoil angles and an additional uncertainty in relative cross section at each angle are a result of the experimental errors in determining the energy normalization factor required to convert the response of the scintillation counter to recoil proton energy. The results in the first recoil angular interval are extremely sensitive to this latter factor, and the large uncertainties in this particular interval are primarily owing to the variation in the energy normalization factor.

A study of the results at 13.7 Mev shows that with the exception of the point at 15.7° the distribution is consistent with spherically symmetric scattering. This point is open to serious question because of the extreme dependence on the exact value of the energy normalization factor. The probable error in this normalization factor was 2.7 percent. An analysis of the data was made with a normalization factor different from the experimentally measured factor by 3.0 percent, and the results then gave a completely isotropic angular distribution. Thus, it seems reasonable to conclude that the technique used in this experiment is applicable in the recoil angular region from 0° to 90° in the center-of-mass system, keeping in mind that there will be considerable uncertainty in the results for the first recoil angular interval unless the absolute sensitivity of the apparatus is known with a precision of the order of five times better than that obtained here.

Cross,[16] at Chalk River Laboratory, has also used the technique described here to obtain the angular distribution of neutron-proton scattering at 14 Mev. His results, for which he quotes an uncertainty of ±5 percent, also show spherical symmetry.

The results from the data taken at 28.4 Mev with the anthracene crystal are shown in Fig. 4 along with those of Brolley *et al.*[3] at 27.2 Mev. A study of these shows that the data presented here can be consistent with those at 27.2 Mev. Because of the relatively small difference in energy, the distributions should be expected not to differ radically.

In view of the assumptions under which the corrections for the (n,p) reaction were applied, there must be some doubt placed on the quantitative conclusions that can be drawn from the results of this investigation in the regions in which the reaction protons are confusable with the recoil protons. However, it seems reasonable to conclude that the scattering of the neutrons is anisotropic in the center-of-mass system with a favoring of scattering in the backward direction. The ratio of the differential cross section for backward scattering to that for scattering at 90° can be stated only with a large uncertainty, not only because of the confusable reaction protons, but also because of the inherent large uncertainty in the point at 11.3°. There is an indication, however, that the ratio is greater than that of 1.15 predicted by the calculation of Christian[3] for the scattering at 27.2 Mev using a Yukawa potential plus the inclusion of a tensor force. Also, it appears that the ratio obtained here is certainly greater than the 1.06 reported by Baldwin[2] at 18 to 21 Mev. More definite conclusions must await further knowledge of the (n,p) reaction.

In general, it can be stated that the technique employed here for the study of the scattering does combine the advantages of the continuous sensitivity of the nuclear emulsion and the capacity of simultaneous detection over all solid angles of the cloud chamber. These make it appropriate for use with a low yield. The inherent disadvantages include the fact that the recoil angles must be obtained from an indirect measurement; the pulse analysis must be converted to proton energy intervals (from which the recoil angular intervals are inferred) by means of an additional determination. In addition the large background of neutrons and gamma-rays from the cyclotron results in a high rate of background counting which tends to overshadow the counts from the protons recoiling at larger angles (angles greater than about 40° in this particular experiment) from the monoenergetic neutrons produced in the source. Also, the carbon constituent of the crystals gives rise to nuclear reactions which prevent the obtaining of valid data for the large recoil angles.

The authors would like to express their appreciation to the members of the cyclotron staff for valuable assistance in performing this work. The aid of G. R. Briggs, who designed the pulse generator and discriminator, is most gratefully acknowledged.

[16] W. G. Cross, Phys Rev 87, 223 (1952).

Conservation of Quanta for Nonlocal Fields

CHRISTOPHER GREGORY
University of Hawaii, Honolulu, Hawaii
(Received July 28, 1952)

A definition of spatio and/or temporal integration of nonlocal expressions is set forth. The latter is applied to the computation of the momentum-energy vector and an invariant from nonlocal expressions corresponding to the stress-energy momentum tensor and a four-vector. The latter four-vector is interpreted to be the quantum current density, and the invariant surface integral of this four-vector over a space-like surface is associated with the operator for the number of quanta. Application to a massless boson field leads to the conclusion that only the energy is positive definite, while the operator for the number of quanta is not, even though the boson field is real (Hermitian). In the usual quantum theory of fields a four-vector current exists only for complex fields.

IN a previous report[1] on operator field equations it was shown that there exists a four-vector operator N^μ, which satisfies a conservation principle

$$[p_\mu, N^\mu]_- \equiv p_\mu N^\mu - N^\mu p_\mu = 0, \tag{1}$$

where p^μ is the four-vector displacement operator. In reference 1, N^μ was obtained by exploiting a property of an operator variational principle[2] which led to the so-called quantal field equations. In general, N^μ is nonlocal: $[x^\mu, N^\nu] \neq 0$, where, in the latter, x^μ is the four-vector space-time operator. Hence, it is not clear at once what is meant by spatio and/or temporal integrals of nonlocal expressions. We may define such integrals by introducing a four-vector space-time c-number c^μ into our definition in the following manner:

$$\int \exp(ic_u p^u) A(p, x) \exp(-ic_u p^u) dc, \tag{2}$$

where dc represents any combination of the products of dc^0, dc^1, dc^2, and dc^3. Using (2) as our definition of an integral, we can define the operator for the number of quanta to be, aside from a constant factor,

$$N \equiv \int_\sigma \exp(ic_u p^u) N^\nu \exp(-ic_u p^u) d\sigma_\nu(c), \tag{3}$$

where σ is a space-like surface. N is independent of σ because of (1). In a similar way operators which define the four-vector energy-momentum G^μ may be defined.

As an example let us consider a real (Hermitian) field U which satisfies the operator equation

$$[p_\mu, [p^\mu, U]_-]_- = 0. \tag{4}$$

The stress-energy-momentum tensor $T^{\mu\nu}$ given by

$$4T^{\mu\nu} \equiv \eta^{\mu\nu}[p_\alpha, U]_-[p^\alpha, U]_- - [p^\mu, U]_-[p^\nu, U]_- - [p^\nu, U]_-[p^\mu, U]_-, \tag{5}$$

and N^μ, given by

$$4N^\mu \equiv [U, [U, p^\mu]_-]_-,$$

satisfy conservation equations because of (4). The solution of (4) for U in a representation with the p's diagonal is

$$\langle p' | U | p'' \rangle = H(p', p'')\Delta_+(p' - p'') + iG(p', p'')\Delta_-(p' - p''), \tag{6}$$

where

$$\Delta_\pm(k) \equiv |k|^{-1}\{\delta(k_0 - |k|) \pm \delta(k_0 + |k|)\}, \tag{7}$$

and the δ's are Dirac delta-functions. We will assume $H(p', p'')$ and $G(p', p'')$ to be symmetric in the two arguments and thus real since U is Hermitian. Upon introducing (6) into (5) and computing N and G^μ, we discover that they are diagonal in this representation. When we use Dirac's formalism for second quantization[3] and identify our boson operators to be, aside from certain factors, $\eta(p, p-k) = H(p, p-k) + iG(p, p-k)$, and $\bar{\eta}(p, p-k) = H(p, p-k) - iG(p, p-k)$, G^μ and N work out to be

$$\begin{aligned} G_0 &= \textstyle\sum_k |k| \{n(k^+) + (n(k^-) + 1)\}, \\ G_s &= \textstyle\sum_k k_s \{n(k^+) - (n(k^-) + 1)\}, \\ N &= \textstyle\sum_k \{n(k^+) - (n(k^-) + 1)\}, \end{aligned} \tag{8}$$

where $n = \eta\bar{\eta}$ and $k^\pm$ denotes the four-vector with components $\pm|k|$, k_s with $s = 1, 2, 3$. It will be noticed that our procedure differs from the usual methods which involve Fourier expansions of local fields. Expansions for nonlocal fields[4] can also be effected, but these have not yet been utilized for second quantization. In the local field approximation, U will commute with x^μ if the arbitrary symmetric functions H and G are functions of the differences of the arguments. The $n(k^\pm)$ are known to have positive integral eigenvalues, so that only G_0 in (8) is positive definite. It is interesting to note that for the case considered here we may associate with a *real* system of massless bosons an operator N which has properties similar to the total charge operator which in the usual theory does not exist for *real* but for *complex* fields. It is appropriate to call N the net number of bosons. Other fields of current interest can be treated along similar lines.

[1] C. Gregory, Phys. Rev. **78**, 479 (1950).
[2] C. Gregory, Phys. Rev. **78**, 67 (1950).
[3] P. A. M. Dirac, *Principles of Quantum Mechanics* (Clarendon Press, Oxford, 1947), third edition, pp. 228, 236.
[4] C. Gregory, Proc. Nat. Acad. Sci. **37**, 706 (1951).

Nuclear Reactions with 21-Mev He^3 in a Cyclotron

D. N. KUNDU, T. W. DONAVEN,* M. L. POOL, AND JOHN K. LONG
Ohio State University, Columbus, Ohio

(Received December 8, 1952)

He^3 ions were accelerated to a maximum energy of 21 Mev. Bombardment of Be, C, O, and Ni led to numerous known activities. The relative cross sections of the He^3 reactions involving O and Ni nuclei are evaluated. The half-lives of C^{11} and Zn^{62} were found to be 20.74±0.10 minutes and 8.4±0.2 hours, respectively.

I. INTRODUCTION

IT is well known how each new bombarding particle accelerated in the cyclotron helped in the production of radioisotopes, in the identification of those already produced by other methods and also in the understanding of various features of the mechanism of nuclear reactions. H^3 and He^3 would constitute a special pair of desirable bombarding particles, since they have approximately the same mass but different nucleonic composition. A study of the reactions produced with these nuclei together with a critical comparison of other features like the excitation functions, the cross sections, etc., is expected to be of interest in connection with the mechanisms involved in the effected reactions; for example, with the extent to which Oppenheimer-Phillips mechanism will be operative in the reactions involved.

Both tritium and He^3 are rare materials and have been available only recently in very small quantities. In addition to the acceleration of tritons previously reported,[1] He^3 ions have been accelerated to 13 and 21 Mev in the cyclotron.

In the present paper, the radioactivities produced from a number of target nuclei with He^3 ions will be reported, and the corresponding He^3 reactions based on the identification of the product nuclei will be briefly discussed.

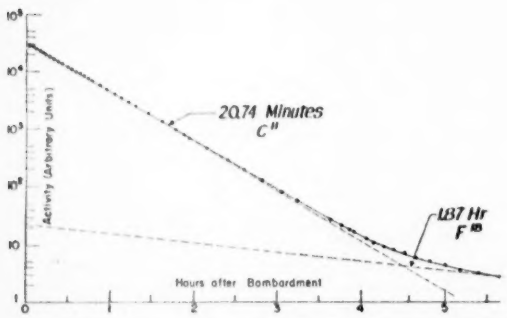

FIG. 1. Decay curve of the C+He^3 bombardment with 21-Mev He^3 beam showing the 20.74-minute C^{11}. The 1.87-hour F^{18} is produced from traces of oxygen in the target.

II. EXPERIMENTAL

A few cubic centimeters of He^3 gas sealed in a glass capsule was procured from the Oak Ridge National Laboratory.[2] Arrangements were made to crush open the capsule inside the cyclotron vacuum system. A recirculation cycle was worked out, the essential features of which are as follows. The main oil diffusion pump was backed by two mercury diffusion pumps in parallel, instead of the usual mechanical pump. These mercury pumps were specially designed to operate with a backing pressure of 5 mm. The gas from the exhaust outlet of the mercury pumps communicated with a ballast tank and was then led into a liquid air trap and later through a set of circulation control valves into a liquid hydrogen trap. The cyclotron vacuum system was so leak-tight that the residual natural leakage amounted to about 0.2 cc per hour. This air leakage was condensed by the liquid hydrogen trap from the outlet of which the gas was reinjected into the cyclotron tank.

The energy of the He^3 particles was 21 Mev as calculated from the frequency, 13.5 Mc per sec, of the cyclotron oscillator. In a different set of bombardments, the frequency of the oscillator was 10.6 Mc per sec corresponding to He^3 particles of 13 Mev. The neutrons and the gamma-rays from an internal probe target of Be were used to detect initially the resonance of the He^3 beam.

III. RESULTS

From among a large number of bombardments on different target elements, a few prominent activities produced are summarized below.

Carbon

A strong positron activity identified as C^{11} was obtained from Hilger carbon of high purity. The decay curve is shown in Fig. 1 in which the activity is followed through 15 half-lives giving a value for the half-life of C^{11} as 20.74±0.10 minutes instead of 20.5 minutes previously reported.[3] The reaction involved is $C^{12}(He^3, \alpha)C^{11}$.

* Now with the General Electric Company, A.N.P. Project, Lockland, Ohio.

[1] D. N. Kundu and M. L. Pool, Phys. Rev. **84**, 481 (1951).

[2] Supplied by the Y-12 plant, Carbide and Carbon Chemical Corporation, through the Isotopes Division, U. S. Atomic Energy Commission, Oak Ridge, Tennessee.

[3] A. K. Solomon, Phys. Rev. **60**, 279 (1941); M. L. Perlman and G. Friedlander, Phys. Rev. **74**, 442 (1948); D. Christian and D. S. Martin, Jr., Phys. Rev. **80**, 1110 (1950).

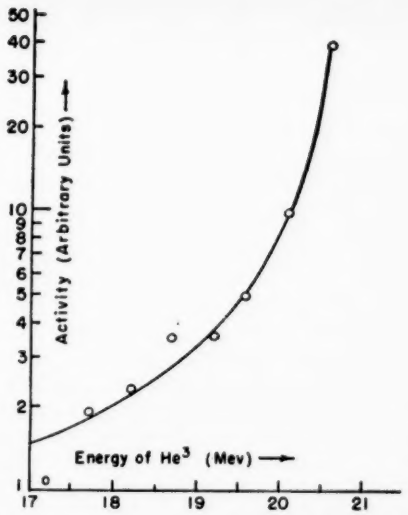

FIG. 2. Energy *vs* yield curve for the 1.8-hour F^{18} activity produced from the O+He^3 bombardment with 21-Mev He^3 beam.

Beryllium

A prominent 20.7-minute positron activity was produced which is ascribed to the reaction $Be^9(He^3, n)C^{11}$. The cross section for this reaction is presumably very high since a bombardment of only a minute gave an estimated initial activity of about 7×10^5 counts per sec. As already indicated, this reaction was used to detect the resonance of the He^3 beam.

Oxygen

From oxygen targets, the 1.97-minute O^{15} and the 1.87-hour F^{18} activities were produced. The former is due to the reaction $O^{16}(He^3, \alpha)O^{15}$, the latter may arise from the reaction $O^{16}(He^3, p)F^{18}$, and/or $O^{16}(He^3, n)Ne^{18}$. Ne^{18} may disintegrate within a very short time by a positron emission into F^{18}. The contention that an $O^{18}(He^3, H^3)F^{18}$ reaction may also explain the F^{18} production is discouraged because of the very low, 0.2039 percent, natural abundance of O^{18}. The ratio of the saturation yields for these activities is approximately 1:1, measured on a bombarded sample of Pb_3O_4.

This F^{18} activity was observed in almost every bombarded sample because of the minute trace of oxygen that remained in the target. For example, the base line of the decay curve for C+He^3 in Fig. 1, shows the 1.87-hour F^{18} activity. One may expect a thin oxide layer on foils of Al, Cu, etc., but hardly on gold. Yet F^{18} activity is in large measurable amounts in Au foils also. This fact was taken advantage of in obtaining the excitation curve for the production of F^{18}. Aluminum is known to have a thin layer of oxide on its surface. A stack of Al foils (0.00035 inch thick), all cut from the same stock foil, was bombarded in a special target piece which was shielded on all sides except for a small hole through which the He^3 beam hit the stack. The F^{18} activity produced in the different foils is plotted in Fig. 2 against the energy of the He^3 particles, as calculated from the range-energy curve for alpha-particles in aluminum.[4]

Nickel

Naturally occurring nickel has five isotopes with the following percent abundances: Ni^{58}(67.76), Ni^{60}(26.16), Ni^{62}(3.66), Ni^{61}(1.25), and Ni^{64}(1.16). He^3 reactions were observed on the first three target isotopes above, but none from the last two where the abundances are quite low. Figure 3 shows the various activities produced in relation to the yield of the individual components. The energy of the He^3 beam in course of this bombardment was 13 Mev. The 1.5-day Ni^{57} is produced from Ni^{58} by the reaction $Ni^{58}(He^3, \alpha)Ni^{57}$. The 24.5-minute activity of Cu^{60} is produced through the reaction $Ni^{58}(He^3, p)Cu^{60}$, and/or $Ni^{58}(He^3, n)Zn^{60}$, where Zn^{60} presumably being short-lived, at once decays into Cu^{60} by a positron emission. The well-known 12.9-hour Cu^{64} is produced from Ni^{62} by a (He^3, p) reaction; a (He^3, n) reaction with this target nucleus would lead to stable Zn^{64}. Ni^{60} yields a prominent 3.4-hour Cu^{61} activity and another activity of 8.4-hour half-life. The latter could be observed only by following the decay through 270 mg/cm² of aluminum which would stop the beta-particles from the strong 12.9-hour Cu^{64} in the composite sample. Based upon decay measurements through four half-lives, a value of 8.4 ± 0.2 hours was obtained for the half-life of Zn^{62}. This is presumably the previously reported[5] 9.5-hour Zn^{62} activity which decays into the 10.1-minute Cu^{62} nucleus. The high energy (2.92 Mev) positrons from Cu^{62} were

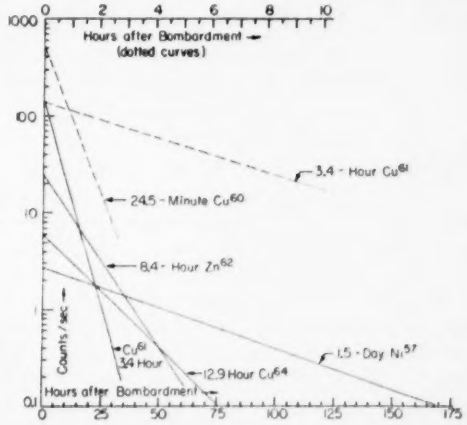

FIG. 3. Comparative magnitudes of the various radioactivities produced from Ni bombarded with 13-Mev He^3 particles. The dotted lines correspond to the horizontal scale at the top.

[4] Aron, Hoffman, and Williams, U. S. Atomic Energy Commission Report AECU-663 (unpublished).

[5] Miller, Thompson, and Cunningham, Phys. Rev. **74**, 347 (1948).

identified by absorption in aluminum long after the disappearance of any Cu^{62} that might have been initially produced during the bombardment through the reaction $Ni^{30}(He^3, p)Cu^{62}$. The reaction involved is therefore $Ni^{60}(He^3, n)Zn^{62}$ for the 8.4-hour activity, whereas for the 3.4-hour activity it is $Ni^{60}(He^3, d)Cu^{62}$ and/or $Ni^{60}(He^3, pn)Cu^{62}$.

From the initial values of the different activities shown in Fig. 3, for which the duration of bombardment was 1 hour, the saturation intensities were calculated. The relative cross sections for production of the above activities were computed after having taken into consideration the decay characteristics of the product nuclei and the efficiency of the measuring equipment for the various radiations emitted. The results are

$$\sigma_{58}(1.5 \text{ days}):\sigma_{68}(24.5 \text{ min}):\sigma_{62}(12.9 \text{ hr}):\sigma_{60}(8.4 \text{ hr}):\sigma_{60}(3.4 \text{ hr})=1:1:10:25:12.$$

The error in the calculation may not exceed 15 percent except in the case of σ_{60}(8.4 hr) where the uncertainty may amount to 50 percent introduced in the process of extrapolating intensities in Fig. 3.

IV. DISCUSSION

The above results, preliminary in nature, show the many radioactivities that are produced through numerous He^3 reactions. Sometimes as in the case of C^{11}, the resulting activity is free from other disturbing activities produced by customary bombarding particles. Activities that are produced with difficulty by $(\alpha, 2n)$ reactions with high energy alpha-particles, are easily produced by (He^3, n) reactions, which reactions, in the present study, are found to be quite prolific.

Grateful acknowledgment is made for an Ohio State University Graduate School Fellowship granted to one of the authors (J.K.L.). Thanks are also due the U. S. Atomic Energy Commission for an AEC predoctoral fellowship given to another (T.W.D.).

PHYSICAL REVIEW VOLUME 89, NUMBER 6 MARCH 15, 1953

Lifetimes of Metastable States of Noble Gases

A. V. PHELPS* AND J. P. MOLNAR
Bell Telephone Laboratories, Inc., Murray Hill, New Jersey

(Received December 10, 1952)

The lifetimes of the lower metastable states of helium, neon, and argon have been studied as a function of the pressure and temperature of the parent gas and the size of the container. The lifetimes were determined from measurements of the decay constant of the radiation absorbed by the metastable atoms. At low metastable concentrations the loss is by diffusion to the walls of the absorption cell and by collisions with neutral atoms within the volume of the cell. The data indicate that at 300°K and sufficiently high pressures, the volume destruction of the lower neon metastable is directly proportional to the pressure as expected for two-body collisions. The volume destruction of the lower neon metastables at 77°K and the helium triplet metastables at 300°K and 77°K is proportional to the square of the pressure as for three-body collisions. The volume loss of the lower argon metastables at 300°K contains both linear and quadratic pressure dependent terms.

INTRODUCTION

THE general principles of the behavior of the metastable atoms of helium, neon, and argon in their parent gases were established by the experiments of Meissner and others.[1] These investigators employed experimental arrangements in which the density of metastables in the afterglow of an interrupted discharge was measured by the optical absorption observed at appropriate wavelengths. Their results were interpreted on the assumption that the metastable atoms were lost by diffusion to the walls of the containing vessel and by excitation to a radiating state in collisions with neutral atoms. The measured diffusion coefficients and excitation cross sections were reasonable except in the case of helium, for which the excitation cross section required to explain Ebbinghaus'[2] results was impossibly large.

Our interest in this problem arose from investigations of the pulsed Townsend discharge by one of us (J.P.M.) in which metastable lifetimes and diffusion coefficients could be measured.[3] An optical experiment similar to that of Meissner was set up with the hope that the destructive processes involving collisions with neutral atoms might be further clarified. The experiment was "modernized" by using a photomultiplier as a light detector in conjunction with electronic timing circuits.[4]

* Now at Westinghouse Research Laboratories, East Pittsburgh, Pennsylvania.

[1] K. W. Meissner and W. Graffunder, Ann. Physik **84**, 1009, (1927); see also summaries by F. M. Penning and N. deGroot *Handbuch der Physik* (Julius Springer, Berlin, 1933), Vol. 23, and A. C. G. Mitchell and M. K. Zemansky, *Resonance Radiation and Excited Atoms* (University Press, Cambridge, 1934).

[2] E. Ebbinghaus, Ann. Physik **7**, 267 (1930).

[3] J. P. Molnar, Phys. Rev. **83**, 933 (1951).

[4] A similar "modernized" experimental arrangement is described by F. A. Grant, Can. J. Research **A28**, 339 (1950), and Phys. Rev. **84**, 844 (1951).

This arrangement enabled us to make observations much more quickly and somewhat more accurately than was possible with the photographic techniques used by earlier workers. The investigations were extended to higher pressures and lower temperatures by one of the authors (A.V.P.) during the summer of 1950. Although circumstances have not permitted us to carry these studies to completion, it is felt that our results lead to a more accurate picture of the processes responsible for the destruction of the metastable atoms than was previously possible.

The results presented in this paper for helium and argon differ qualitatively from those found previously by showing that the dominant destruction process at high pressures is a collision between the metastable and two neutral atoms. The two-body destruction process found previously for neon at 300°K is confirmed but does not dominate at 77°K. In general, the values obtained for the destruction probability of metastables by collisions with neutral atoms were found to be considerably smaller than the values obtained by earlier workers.[6]

THEORY

We propose the following processes to explain the destruction of metastable atoms which results from collisions of metastables with neutral atoms and other metastable atoms:[6]

1. Diffusion and de-excitation on collision with the walls.

2. Two-body collisions with neutral atoms resulting in

(a) excitation to a nearby higher radiating state;[7]

(b) de-excitation to a lower state;

(c) formation of unstable diatomic molecules which may radiate before dissociation, i.e., collision induced radiative transitions.

3. Three-body collisions with two neutral atoms, presumably resulting in the formation of a stable excited molecule.

4. Collisions between pairs of metastable atoms resulting in the ionization of one of the atoms and de-excitation of the other.[8]

Theoretical estimates of the coefficients associated with the various metastable destruction processes are available only in the case of the diffusion of the helium metastables through helium.[9] Accordingly, the separation of the various processes must be based on measurements of the time dependence of the decay of the metastable concentration and the pressure and temperature dependence of the associated decay constants. An estimate of the relative importance of process 2a for the various gases can be obtained from a consideration of the energy spacings of the metastable and nearby radiating states shown for helium, neon, and argon in Fig. 1. In each case the lowest excited state of the atom is metastable because the selection rules prevent electric dipole radiation to the $^1S_0$ ground state. In the cases of neon and argon the lowest radiating state, $^3P_1$, is located less than one-tenth of an electron volt above the lower metastable state, $^3P_2$, so that process 2(a) is energetically possible in thermal collisions. For helium the lowest state which can radiate to the ground state is 1.4 electron volts above the metastable state. Thus, the destruction of helium triplet metastables by process 2(a), as assumed in the interpretation of Ebbinghaus'[1,2] data, seems virtually impossible at room temperatures. The upper metastable state $^3P_0$, in neon and argon can be destroyed by de-excitation to the lower radiating state, $^3P_1$, as well as by excitation to the upper radiating state, $^1P_1$.

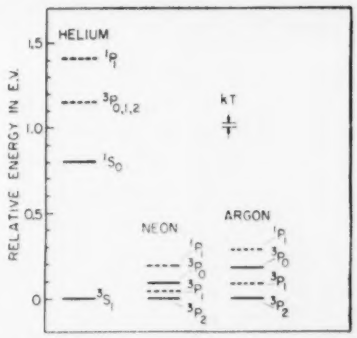

FIG. 1. Relative energy spacings of the states of the lowest excited electron configurations for three of the noble gas atoms. The radiating states are indicated by dashed lines, the metastable by solid lines. The electron configurations are $1s2s$ and $1s2p$ for helium, $2p^53s$ for neon, and $3p^54s$ argon. In each case the lowest state, a metastable state, is taken as the zero of the energy scale. The electron-volt equivalent of kT for 300°K is also indicated.

Here M is the metastable concentration, D_0 is the diffusion coefficient for the metastables at one mm of Hg, p is the pressure in mm of Hg, A is the frequency of destruction by two-body collisions at one mm pressure [processes 2(a), 2(b), and 2(c)], B is the frequency of destruction by three-body collisions at one mm pressure, and α is the ionization frequency per unit metastable concentration.

The rate of change of the metastable concentration as a result of the processes listed above is

$$\partial M/\partial t=(D_0/p)\nabla^2M-ApM-Bp^2M-\alpha M^2. \quad (1)$$

The solution of Eq. (1) for the time dependence of the metastable concentration can be obtained in a

[6] See Mitchell and Zemansky (reference 1).

[7] The loss of metastable atoms due to their natural decay does not appear to be a significant process under the conditions of our experiments.

[7] If the resonance radiation from the radiating state is imprisoned for a sufficient length of time [see T. Holstein, Phys. Rev. **72**, 1212 (1947) and Phys. Rev. **83**, 1159 (1951)], the destruction of the metastables by process 2a will be reduced. Although theoretical estimates indicate that this effect may be appreciable at high pressures in neon, the experimental data are not sufficiently accurate or extensive to permit us to ascribe the observed deviations from Eq. (2) to this process.

[8] Effects of metastable-metastable collisions, as well as independent measurements of diffusion coefficients and cross sections for ionization of impurities, are presented by M. A. Biondi, Phys. Rev. **82**, 453 (1951) and Phys. Rev. **88**, 660 (1952).

[9] R. A. Buckingham and A. Dalgarno, Proc. Roy. Soc. (London) **A213**, 506 (1952).

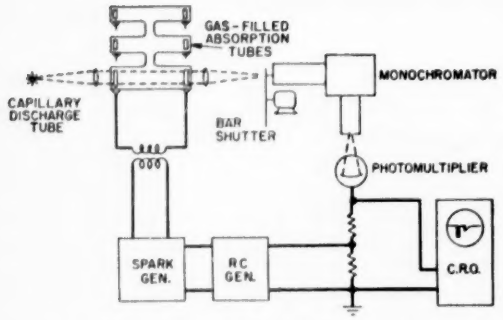

FIG. 2. Schematic diagram of the apparatus used in the metastable decay studies. The Gaertner monochromator had glass lenses and a heavy flint glass prism for high dispersion in the red and infrared.

closed form only in the limits of low and high metastable densities. At low metastable densities the last term of Eq. (1) can be neglected. If we restrict our solution to times sufficiently late in the afterglow, only the lowest diffusion mode will be significant and the metastable density will decay exponentially with time. The decay constant is

$$1/\tau = D_0/(p\Lambda^2) + Ap + Bp^2, \tag{2}$$

where Λ is the diffusion length of the container and for a cylindrical vessel of radius R, and length L is given by $\Lambda = [(\pi/L)^2 + (2.4/R)^2]^{-\frac{1}{2}}$. The parameters D_0, A, and B can be evaluated from measurements of $1/\tau$ as a function of the pressure and the size of the absorption cell. Further details concerning the individual processes can be obtained from studies of the variation of the parameters, D_0, A, B, and α with the gas temperature.

At high metastable densities the destruction of metastables in collisions between pairs of metastable atoms will be large compared to the loss due to diffusion and collisions with neutral particles. The solution of Eq. (1) is then

$$1/M = 1/M_0 + \alpha t, \tag{3}$$

where M_0 is the metastable concentration at the beginning of the afterglow. Thus, if the plot of $1/M$ as a function of time is a straight line over a reasonable range of metastable densities, we can evaluate α and the cross section for collisions between pairs of metastable atoms.

EXPERIMENTAL ARRANGEMENT

A schematic diagram of the experimental apparatus used in these investigations is shown in Fig. 2. The gas to be studied is contained in a cylindrical absorption cell with flat windows and ring electrodes and is broken down periodically (15 to 60 cps) with a pulse from a spark generator lasting approximately 100 microseconds. The line spectrum of the gas being studied is obtained from a hot-cathode discharge tube. The section of the positive column used as the source of radiation is confined by a capillary 0.5 mm in diameter. The radiation which has traversed the absorption cell is passed through a monochromator and detected with a photomultiplier. The output of the photomultiplier is developed across a resistance network and observed with an oscilloscope. The upper oscillograph trace of Fig. 3 shows the output of the photomultiplier under nearly ideal conditions. The downward spike at the left is produced by the interruption of the light by the bar shutter shown in Fig. 2 and indicates 100 percent absorption. This is followed by the sharp rise and slow decay of the absorption due to the metastables produced during the very short discharge pulse.

A simple means for measuring the decay constant of the absorption is provided by using the spark generator to trigger the discharge of a condenser and passing the subsequent current through the resistance network in order to subtract an exponentially varying signal from the output of the photomultiplier. The operation of this exponential comparison circuit is illustrated by the oscilloscope traces shown in Fig. 3. When the exponential signal is adjusted for optimum cancellation of the photomultiplier trace, the lifetime of the metastable atoms can be obtained from the RC time constant of the exponential signal.

The absorption cells were filled from a vacuum system designed to give minimum contamination of the

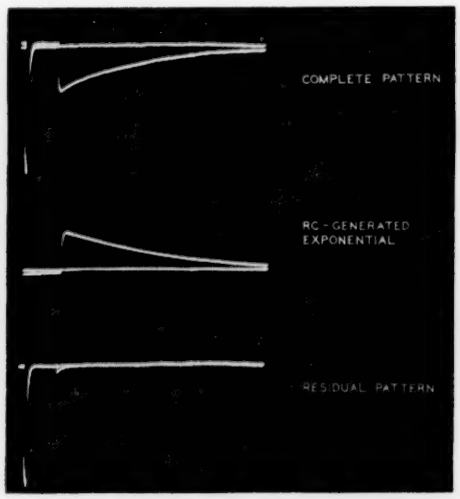

Fig. 3. Oscilloscope traces illustrating the operation of the time constant measuring circuit. The upper trace shows the photomultiplier output. The vertical spike at the left side represents the complete interruption of the light by the bar shutter shown in Fig. 2, and its lowest extension indicates the level of 100 percent absorption. For each trace the repetition rate of the horizontal sweep was set at 30 cps, whereas the sparking rate was set at 15 cps; thus the pattern is initiated by the spark in one sweep and continues through the second. The second trace shows the electronically generated exponential curve. The last trace shows the first two combined, with the second one adjusted in amplitude and time constant for optimum match. The example shown here illustrates operation under conditions of exceptionally low noise.

gas samples. The oil manometer and the stopcocks were separated from the absorption cell by two liquid nitrogen traps. The absorption cells and one trap were baked at 450°C overnight and the electrodes outgassed by induction heating. The gas was obtained from flasks of Airco reagent grade gas and passed over a freshly prepared barium surface. The absorption cells varied in size from six feet long and six inches in diameter to two inches long and 0.4 inch in diameter. The data at 77°K were obtained with a cell that was three feet long and three inches in diameter. It was equipped with a full-length liquid nitrogen-filled jacket. Evacuated end windows were provided to reduce frosting.

A number of precautions were taken to insure reliability in the measurements. The intensity of the light beam used for the absorption measurements in argon and neon was maintained at a level low enough to prevent appreciable destruction of metastables by exciting them to higher levels from which alternate radiative decay paths to the ground state are available. (In helium the $^3S_1$ metastable is immune to such light destruction.) The absorption curves were fitted to the electronically generated exponential curve in the region of 20 percent or less absorption, since only in this region can one assume that the observed absorption is linearly proportional to the density of absorbing atoms.[5]

INTERPRETATION OF ABSORPTION CURVES

Typcial absorption curves obtained for the metastable states and the lower radiating state of neon and argon are shown in Figs. 4 and 5. The absorption by the upper radiating state, $^1P_1$, was very small and is not shown. As illustrated for argon by the curves of Fig. 4, the absorption curves for the $^3P_0$ and $^3P_1$ states in neon and in argon and the $^1S_0$ metastable state in helium either decayed too rapidly for accurate measurements or exhibited a form that varied greatly with spark intensity. We interpret the observed changes in the destruction rate with spark intensity at a given metastable density as indicating destruction of metastables by components other than neutral atoms and metastables, i.e., electrons or positive ions. The decay rates for the helium triplet metastable and the lower metastable states, $^3P_2$, of neon and argon were found to be independent of the spark intensity except at the highest intensities. Therefore, the quantitative data presented in the following section refer only to the lower metastable states of the various gases.

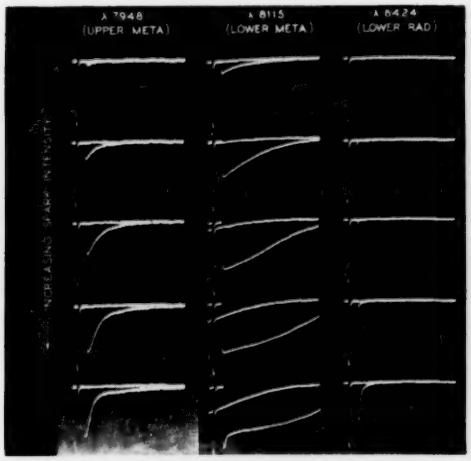

FIG. 4. Absorption curves illustrating the effect of increasing spark intensity for the ^3P states of the $3p^54s$ configuration in argon ($p=1.0$ mm). The left column shows that the decay of the upper metastable ($^3P_0$) density is not simply exponential. At the highest spark intensity a tail develops suggesting a decay rate comparable to that of the lower metastable state ($^3P_2$) shown in the second column. The decay rate of the lower radiating state ($^3P_1$) is very rapid at all spark intensities.

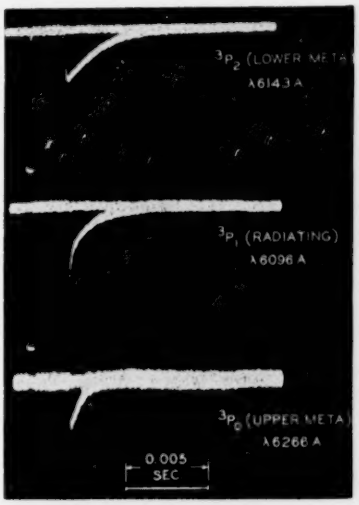

FIG. 5. Absorption traces for the ^3P states in the $2p^53s$ configuration of neon ($p=7.5$ mm). The low noise level present in the neon experiments permits careful examination of the $^3P_1$ decay curve. The second trace shows the 100 percent absorption point produced by the bar shutter, a sharply decaying absorption starting from the 80 percent point, and a more slowly decaying part. The spark intensity was adjusted in each case to give roughly the same amplitude in the absorption curve, e.g., a maximum intensity for the $^3P_1$ case and a minimum intensity for the $^3P_2$.

The absorption curves of Fig. 5 provide qualitative evidence which supports the existence of processes 2(a) and 2(b) discussed under theory. The density of atoms in the lower radiating state, $^3P_1$, can be seen to drop sharply after the termination of the spark and then to decay more slowly. Presumably the rapid initial decay corresponds to loss of these excited atoms by radiation, while the slow decay corresponds to a repopulation of the $^3P_1$ state as a result of de-excitation from the $^3P_0$ state or excitation from the $^3P_2$ state.

Most of our measurements were made in a range of pressure and discharge current such that the light beam traversed mainly the positive column of the dis-

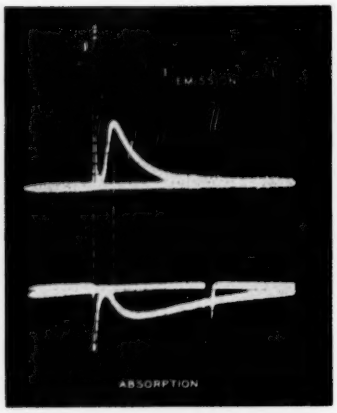

FIG. 6. Emission and absorption curves in the Faraday dark space region of a spark discharge in argon ($p=0.2$ mm). The absorption curve is for the $^3P_2$ state (8115A), while the emission curve represents the integrated light in the red region of the spectrum.

charge set up between the ring electrodes by the original spark. A specially built tube filled with argon at 0.2 mm of Hg was used to examine the absorption curves in various regions of the discharge. The initial metastable destruction rate was especially large in the regions near the cathode and in the striations of the positive column. The absorption curve for the Faraday dark space is shown in Fig. 6. The original metastable density falls almost to zero shortly after the termination of the spark, then builds up, and finally decays with a time constant approximately equal to that found in the positive column. The light generated in this region is shown by the upper curve of Fig. 6 and has the characteristic form of an afterglow. We explain these observations by assuming that fast electrons are present in the discharge after the spark is terminated, and that these destroy the metastables by excitation or ionization. As the electrons lose their initial kinetic energy they recombine with positive ions to produce atoms in the excited states and in the ground state. Radiative decay of the highly excited atoms produces the emitted light as well as metastables so that the maximum emission occurs at the same time as the maximum rate of increase of the metastable density.

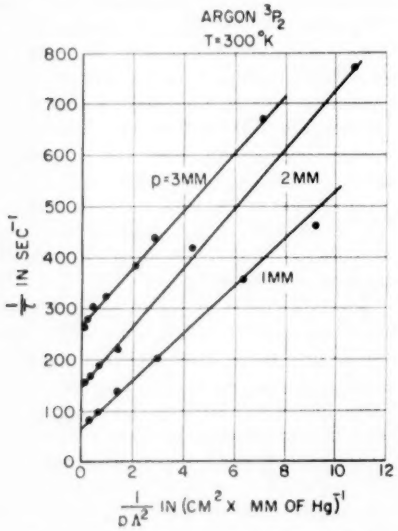

FIG. 7. Data taken with argon ($T=300$°K) illustrating the method for separating the contributions of diffusion loss and volume loss to the measured decay constant, $1/\tau$, by varying the diffusion length Λ. The data were obtained using a set of interconnected absorption cells such as illustrated in Fig. 2.

RESULTS

Most of the quantitative data reported in this paper were obtained at low metastable densities where the absorption appeared to decay exponentially with time. Accordingly, we will analyze the data in terms of the expression for the decay constant, $1/\tau$, given by Eq. (2).

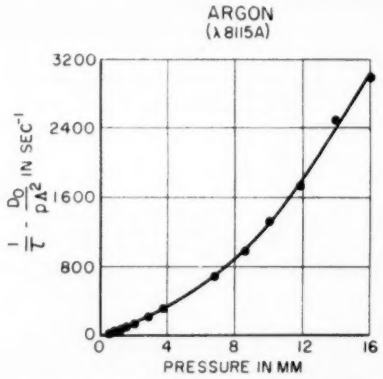

FIG. 8. Volume loss in argon as a function of pressure for the $^3P_2$ state (8115A) for 300°K and $\Lambda^2=2.4$ cm^2.

Figure 7 shows the results of measurements of the lifetimes of the lower argon metastable (using λ8115A) as a function of the size of the absorption cell at various pressures. Equation (2) shows that the slope of the plot of the $1/\tau$ as a function of $1/(p\Lambda^2)$ gives the diffusion coefficient for the metastables at one mm pressure. The average diffusion coefficient at 300°K is 54 cm^2 sec^{-1} compared to 45 cm^2 sec^{-1} obtained from measurements of the transient build-up of a Townsend discharge.[3] The loss of metastables as a result of collisions with neutral gas atoms can be found by subtracting the loss by diffusion from the measured destruction frequencies. Figure 8 shows the results of such a calculation for the lower argon metastable at 300°K. The smooth curve is the result of fitting the sum of a linear and a quadratic term to the experimental data, i.e., $A=40$ sec^{-1} mm^{-1} and $B=9$ sec^{-1} mm^{-2} in Eq. (2). Thus it appears that at 300°K the lower argon metastables are destroyed by both two- and three-body collisions. The data obtained at 77°K were not sufficiently reproducible to be con-

sidered in detail, but suggested a slow variation in the three-body destruction with temperature.

Figure 9 shows the results of a set of time constant measurements obtained from the absorption of the 6143A line by the lower neon metastable. The data at 77°K have been normalized with respect to changes in gas density by multiplying the pressure readings by 300/77. The smooth curves represent a fit of Eq. (2) to the experimental data with $A=50\ \text{sec}^{-1}\ \text{mm}^{-1}$, $B=0$ at 300°K; and $A=0$, $B=5\times10^{-2}\ \text{sec}^{-1}\ \text{mm}^{-2}$ at 77°K. Thus, the loss of the lower neon metastable at 300°K appears to be by diffusion at the lower pressures and by either excitation to a radiating state [process 2(a)] or collision-induced radiation [process 2(c)] at the higher pressures. The measured destruction probability at 77°K shows that within the experimental error the loss of the $^3P_2$ metastables is by diffusion and by destruction in three-body collisions. The average diffusion coefficients at 300°K and 77°K were 150 cm²/sec and 60 cm²/sec at a density corresponding to one mm pressure

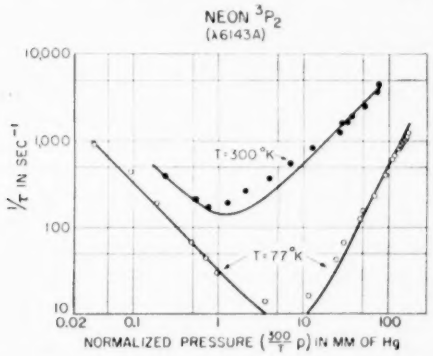

FIG. 9. Data showing $1/\tau$ as a function of normalized pressure in neon for the $^3P_2$ states (6143A) at 77°K and 300°K and for $\Lambda^2=1.9$ cm².

at 300°K. The absence of an approximately linear pressure dependent term in the volume destruction at 77°K requires that the frequency of the process decrease by a factor of at least 200 as the temperature is reduced from 300°K to 77°K. This corresponds to an "activation" energy for the two-body destruction process which is at least as large as the spectroscopic energy difference between the $^3P_2$ and $^3P_1$ states. It should be noted that the decay constants obtained using the λ6402A line were approximately 20 percent lower than the values given in Fig. 9. The departure of the measured decay constants from the analytical curve at intermediate pressures is reproducible[4] but is as yet unexplained.

Figure 10 is a summary of the decay constant measurements for the helium triplet metastable made using the 10 830A line. The plots of the measured values of $1/\tau$ as a function of normalized pressure, though scattered, are consistent with the interpretation that the loss of metastables is characteristic of diffusion at the

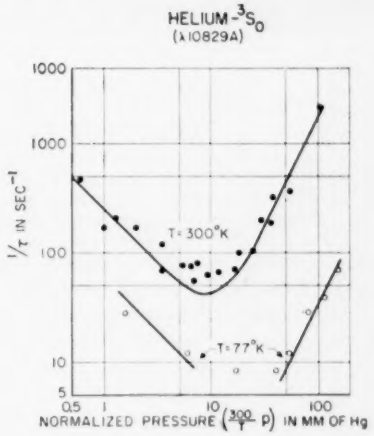

FIG. 10. Data showing $1/\tau$ as a function of normalized pressure in helium for the $^3S_1$ state (10 830A) at 77°K and 300°K for $\Lambda^2=1.9$ cm².

lower pressures and is proportional to the square of the pressure at the higher pressures. The smooth curves were obtained by fitting Eq. (2) to the observed data with $A=0$. The average diffusion coefficient for 300°K and one mm Hg is 410 cm²/sec while that for 77°K and one mm Hg is approximately 130 cm²/sec, showing a somewhat larger variation with temperature than that observed for neon. These values agree satisfactorily with the theoretical values of 370 and 130 cm²/cm obtained by Buckingham and Dalgarno.[9] The diffusion measurements showed that the loss varied as $1/\Lambda^2$ for Λ^2 between 0.04 cm² and 6.3 cm² within the experimental error of approximately 20 percent. The decrease in the volume loss from $0.2p^2\ \text{sec}^{-1}$ to $3\times10^{-3}p^2\ \text{sec}^{-1}$ as the temperature was changed from 300°K to 77°K suggests that the three-body collision process responsible for the destruction of the metastables has

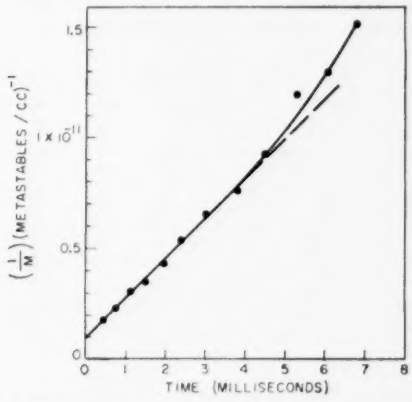

FIG. 11. Plot showing the reciprocal of the metastable density as a function of time. The data were obtained from an analysis of a photograph of the absorption of the 3889A line by helium triplet metastables at 300°K and 10 mm of Hg pressure.

TABLE I. Average cross section for the destruction of metastables of rare gas atoms by various impurities.

Metastable	Impurity	Average cross section, cm²
A ($^3P_2$)	Hg	3×10^{-15}
A ($^3P_2$)	Kr	1×10^{-16}
A ($^3P_2$)	H_2	3×10^{-17}
Ne ($^3P_2$)	A	2×10^{-16}
He ($^3S_1$)	A	3×10^{-17}

an activation energy of the order of 0.03 electron volt. The presence of an activation energy is consistent with the long range repulsive interaction calculated for the helium metastable and a normal helium atom.[9]

The volume loss for the helium triplet metastable obtained from this experiment is less than $\frac{1}{10}$ of that calculated by Ebbinghaus when his rather limited measurements were interpreted in terms of destruction by excitation to the nearest radiating state. The large volume loss of triplet metastables found by Ebbinghaus may well have been due to collisions between pairs of metastable atoms. We were able to estimate the cross section for destructive collisions between pairs of metastable atoms by analyzing a photograph of the absorption curve obtained at high metastable densities where the last term of Eq. (1) dominates the metastable destruction. Thus, Fig. 11 shows that when the nonlinear absorption of the 3889A radiation is taken into account,[10] the reciprocal of the metastable density is a linear function of time over an appreciable range of metastable densities as predicted by Eq. (3). Using the theoretical absorption coefficient[11] to calculate the absolute metastable density, the average cross section for collisions between pairs of helium triplet metastable atoms is found to be 10^{-14} cm² at 300°K. We can now estimate the error in the time constant determinations due to collisions between pairs of metastable atoms. For the measurements summarized in Fig. 10, ten percent absorption corresponds to an average metastable density of 1.5×10^{10} metastable/cc. Therefore, the loss due to collisions between pairs of metastables amounts to about 20 percent of the measured loss at intermediate pressures and 300°K, but becomes negligible at the lower and higher pressures.

[10] A correction for nonlinear absorption was made using the relations developed by Mitchell and Zemansky for Doppler broadening (see reference 1). The effective ratio of the line widths was determined by noting the change in absorption when the absorption path length was doubled. The tables of fractional absorption as a function of the product of the absorption coefficient and the path length have been recomputed and extended for us by R. W. Hamming.

[11] D. R. Bates and A. Damgard, Trans. Roy. Soc. (London) **A242**, 101 (1949).

Destruction of Metastables by Impurities

In order to estimate the effects of foreign gas impurities on the lifetimes of metastable atoms, small amounts of nitrogen, hydrogen, mercury, krypton, and argon were admitted to the absorption cells. Except in the cases of krypton in argon and argon in neon and helium, the foreign gas impurity was "cleaned up" by the discharge and the uncertainty in the admixture fraction is large. Table I gives the average results expressed in terms of the cross section for the destruction of metastables by the impurity atoms at 300°K. The cross sections for argon in helium and neon are in reasonable agreement with those obtained by Biondi from ionization studies.[8] It should be noted that Biondi's measurements of ionization in helium may refer to the helium singlet metastable whereas our data certainly apply to the triplet metastable.

SUMMARY

Our measurements of the lifetimes of metastable atoms at low metastable densities have shown that the destruction of the metastables is by diffusion to the walls at low pressures and by either two-body or three-body collisions at high pressures. These experiments have demonstrated for the first time the importance of three-body collisions as a destruction mechanism for the lower metastable states of argon, neon, and helium. The fact that the observed decay constants for the helium triplet metastable yield reasonable coefficients for the rates of diffusion, three-body collisions, and collisions between pairs of metastables should remove the doubts which have been expressed[5] regarding the validity of the absorption method. In particular, the agreement between the experimental and theoretical diffusion coefficients for the helium triplet metastable should serve to encourage further theoretical and experimental work in this field.

These studies have shown that there are many features of the destruction of the metastables which we could explain only qualitatively. A program directed toward correlated measurements of electron densities and more precise determinations of the metastable densities is being undertaken by one of us (A.V.P.).

The authors wish to express their appreciation to R. G. Brandes, H. C. Geissler, and H. W. Weinhart for their assistance in design and operation of the apparatus, and to P. W. Anderson, J. A. Hornbeck, and A. H. White for many valuable disussions. One of us (A.V.P.) wishes to thank the staff of the Bell Telephone Laboratories for the opportunity to participate in this research during the summer of 1950.

The Macroscopic Theory of Superfluid He^3-He^4 Mixtures*

P. J. PRICE
Institute for Advanced Study, Princeton, New Jersey
(Received November 28, 1952)

The macroscopic hydrodynamic equations to the reversible linear approximation for mixtures are set up and analyzed, without making any assumptions beyond that of the traditional form of the two-fluid model. The equations of wave motion are derived and discussed. A novel feature of them is *appreciable* coupling between pressure and entropy-density fluctuations. It is shown how the constants appearing in the equations may be expressed partly in terms of the measured partial vapor pressures. Pomeranchuk's formula for the velocity of second sound appears as a possible special case; and it is shown how his assumption that the He^3 component is carried entirely with the normal velocity may be tested experimentally. The intervention of isotopic diffusion is briefly discussed.

I. INTRODUCTION

IN recent years experiments with liquid helium containing appreciable fractions of the He^3 isotope have shown that this mixture retains the properties characterizing a superfluid: a lambda transition,[1] superleak transfer of mass,[1] the fountain effect,[2] and "second sound" waves.[3] The study of these macroscopic properties in isotope mixtures may well become of importance to the progress of the microscopic (kinetic) theory of "quantum liquids." For pure[4] He^4 superfluid, an empirical macroscopic theory—the "two-fluid model"[5]—is a virtually indispensable intermediary between the dynamical experiments and microscopic theory: the principal theme of this paper is the construction of such a macroscopic dynamics for *mixtures*, analogous to and generalizing that for pure He^4. (The relation of this paper to other published work on the question is indicated below.)

On the basis of the experiments quoted, it is natural to assume that the two-fluid dynamics gives as correct a description for the superfluid mixtures as for pure He^4.[6] This assumption will be made throughout the present work. Accordingly, the density ρ is divided into two parts associated respectively with two velocity fields $\mathbf{v}_n$, $\mathbf{v}_s$; so that the mass flow $\mathbf{J}$ has two terms, of which the first alone is proportional to the entropy flow $\mathbf{N}$,

$$\rho=\rho_n+\rho_s, \quad \mathbf{J}=\rho_n\mathbf{v}_n+\rho_s\mathbf{v}_s, \quad \mathbf{N}=\rho S\mathbf{v}_n. \tag{1}$$

In the present case of a mixture, the density is also divided between the two chemical components; and we have to assign each of these isotope densities separately between the two velocity fields. Thus,

$$\begin{gathered}\rho=\rho_3+\rho_4, \quad \rho_3=\rho_{3n}+\rho_{3s}, \quad \rho_4=\rho_{4n}+\rho_{4s}, \\ \rho_n=\rho_{3n}+\rho_{4n}, \quad \rho_s=\rho_{3s}+\rho_{4s}.\end{gathered} \tag{2}$$

The ratios ρ_{3n}/ρ_{3s}, ρ_{4n}/ρ_{4s}, will in general depend, like the total density and the other thermodynamic magnitudes, on the concentration of He^3.

We shall find that the precise partition of the He^3 component between the two velocity fields has far-reaching effects on wave propagation. The mass flow vector for the He^3 may be written

$$\begin{aligned}\mathbf{J}_3&=\rho_{3n}\mathbf{v}_n+\rho_{3s}\mathbf{v}_s=\rho_3\mathbf{v}_1+[(\rho_{4s}\rho_{3n}-\rho_{4n}\rho_{3s})/\rho]\mathbf{v}_2 \\ &=\rho w\mathbf{v}_1+(\rho_s w_n-\rho_n w_s)\mathbf{v}_2,\end{aligned} \tag{3}$$

where

$$\rho\mathbf{v}_1=\mathbf{J}=\rho_n\mathbf{v}_n+\rho_s\mathbf{v}_s, \quad \mathbf{v}_2=\mathbf{v}_n-\mathbf{v}_s, \tag{4}$$

and

$$\rho_{3n}=\rho w_n, \quad \rho_{3s}=\rho w_s, \quad w_n+w_s=w=\rho_3/\rho. \tag{5}$$

The $\mathbf{v}_2$ term of (3) represents a flow of He^3 in the reference frame moving with the center-of-gravity velocity $\mathbf{v}_1$, in analogy with the $\mathbf{v}_2$ term in the entropy-flow equation

$$\mathbf{N}=\rho S\mathbf{v}_1+\rho_s S\mathbf{v}_2. \tag{6}$$

This flow of He^3 will give rise, in wave motion involving $\mathbf{v}_2$, to fluctuations of He^3 concentration and hence of the thermodynamic functions in their dependence on the concentration. The consequences of these fluctuations are: (a) an appreciable coupling between pressure and temperature waves, whereas for pure He^4 the coupling is negligible; and (b) a large influence on the dependence on He^3 concentration of the velocity of second sound.[7]

The flow represented by the $\mathbf{v}_2$ term of (3) has been isolated in the "heat flush" experiments of Lane *et al.*,[8] in which "normal" and "super" currents $\rho_n\mathbf{v}_n$ and $\rho_s\mathbf{v}_s$

* This work was begun at Duke University, under contract with the U. S. Office of Naval Research and concluded at the Institute for Advanced Study, where it was supported by a grant-in-aid from the Institute.

[1] Abraham, Weinstock, and Osborne, Phys. Rev. **76**, 864 (1949); J. G. Daunt and C. V. Heer, Phys. Rev. **79**, 46 (1950).

[2] Taconis, Beenakker, and Dokoupil, Phys. Rev. **78**, 171 (1950).

[3] E. A. Lynton and H. A. Fairbank, Phys. Rev. **80**, 1043 (1950).

[4] That is helium from natural sources, containing about one part in 10^7 of He^3.

[5] P. R. Zilsel, Phys. Rev. **79**, 309 (1950).

[6] E. F. Hammel and A. F. Schuch have recently (Schenectady conference, October 1952) described experiments on superleaks which are not obviously consistent with a two-fluid model for mixtures. However, a final interpretation of their results (which seem to contradict those of earlier experiments) must wait on further investigations.

[7] We shall see that $u_2(w)$ is analytic at $w=0$ only if the He^3 component is, like the entropy, carried entirely with the normal velocity $\mathbf{v}_n$.

[8] Lane, Fairbank, Aldrich, and Nier, Phys. Rev. **73**, 256 (1948).

exactly counterbalanced, and in which the He^3 component was found to be carried in the $\mathbf{v}_n$ direction—showing that the coefficient of $\mathbf{v}_2$ is *positive*. Koide and Usui assume,[9] however, that the coefficient of $\mathbf{v}_2$ is zero: that the average velocity of the He^3 atoms is the center-of-gravity velocity $\mathbf{v}_1$. Pomeranchuk's theory,[10] on the other hand, assumes the extreme values $\rho_{3s}=0$, $\rho_{3n}=\rho_3$: that the average velocity of the He^3 atoms is $\mathbf{v}_n$. The object of the present work, on the other hand, is to construct a general theory without making any assumptions beyond those of the traditional form of the two-fluid model (Appendix A). We shall see from the results obtained in Secs. III and IV that the ratios ρ_{3n}/ρ_3 and ρ_{4n}/ρ_4 may (like ρ_n/ρ for pure He^4) be determined empirically by suitable experiments.

Throughout this paper the equations of motion are restricted to their linear approximation, which represents those simpler dynamical effects whose study must be the first objective of the experimental program. We also exclude the linear *irreversible* effects, viscosity and heat conduction, which are known to introduce only inconsiderable refinements into the analysis of the superfluid He^4 phenomena and which may be considered second-level effects in the microscopic theory. Diffusion of He^3 relative to He^4, a linear irreversible effect peculiar to the mixtures, is introduced in a tentative way in the final Sec. V. It is shown there that the effect of diffusion on wave propagation is probably quite negligible, but that diffusion has an essential role in the *generation* of second sound in mixtures, and gives rise to a third mode of wave motion which is highly damped and confined to a thin "skin" round sources and absorbers of second sound.

The two previously published papers on this topic[9,10] make various restrictive assumptions, in addition to those mentioned above. Koide and Usui follow Gorter[11] in supposing that the division of the density between the two velocity fields may be treated as a Gibbsian equilibrium between two phases, and de Boer and Gorter[12] in setting the isotopic mixing term of the Gibbs function equal to that of an ideal solution with isotope densities ρ_3 and ρ_{4n}. Pomeranchuk, whose treatment is confined to dilute solutions ($w\ll 1$) seems to have assumed in his numerical predictions that

$$\rho_n(w)=\rho_n(0)+(m^*/m_3)\rho_3, \quad \rho_s(w)=\rho_s(0),$$

where $m^*/m_3>1$; which makes $\rho(w)>\rho(0)$, contrary to fact.[13]

[9] S. Koide and T. Usui, Prog. Theor. Phys. **6**, 506 (1951).
[10] I. Pomeranchuk, J. Exptl. Theor. Phys. (U.S.S.R.) **19**, 42 (1949).
[11] C. G. Gorter, Physica **15**, 523 (1949).
[12] J. de Boer and C. G. Gorter, Physica **16**, 225 (1950).
[13] In reality, $\rho_s(w)\neq\rho(0)$. One would hence expect ρ_{4s} and ρ_{4n} each to depend on w, even if Pomeranchuk's assumption ($\rho_{3s}=0$, $\rho_{3n}=\rho_3$) is correct. Since the lambda-temperature—where $\rho_s=0$—depends on w,[1] it follows that more generally ρ_s is a function of w.

II. THE REVERSIBLE EQUATIONS OF MOTION

The following equations for the mixture are proposed:

$$\partial\rho/\partial t+\operatorname{div}(\rho_n\mathbf{v}_n+\rho_s\mathbf{v}_s)=0, \tag{7}$$

$$\partial(\rho w)/\partial t+\operatorname{div}(\rho w_n\mathbf{v}_n+\rho w_s\mathbf{v}_s)=0, \tag{8}$$

$$\partial(\rho S)/\partial t+\operatorname{div}(\rho S\mathbf{v}_n)=0, \tag{9}$$

$$\rho_n\partial\mathbf{v}_n/\partial t+\rho_s\partial\mathbf{v}_s/\partial t+\operatorname{grad}P=0, \tag{10}$$

$$\partial\mathbf{v}_s/\partial t+\operatorname{grad}[g-w(\partial g/\partial w)_{P,T}]+(w_s\rho/\rho_s)\operatorname{grad}(\partial g/\partial w)_{P,T}=0, \tag{11}$$

where $g=e+P/\rho-TS$ is the Gibbs function, e and S the internal energy and entropy, per unit mass of mixture. Equations (7), (8), and (9) are the conservation equations corresponding to the formulas (1) and (3) for $\mathbf{J}$, $\mathbf{J}_3$ and $\mathbf{N}$. Equations (10) and (11), the acceleration equations in linear approximation, are derived in Appendix A.

By (A3) and (A6) of the appendix, the energy flux vector $A_n\rho_n\mathbf{v}_n+A_s\rho_s\mathbf{v}_s$ is

$$\mathbf{Q}=(P+\rho e)\mathbf{v}_1+[\rho_s ST+(w_n\rho_s-w_s\rho_n)(\partial g/\partial w)_{P,T}]\mathbf{v}_2. \tag{12}$$

The $\mathbf{v}_2$ ("internal convection") term of (12), which generalizes to mixtures the corresponding term for pure He^4 found by Zilsel,[14] may be written:

$$[\rho_s S(\partial e/\partial S)_{\rho,w}+(\rho_s w_n-\rho_n w_s)(\partial e/\partial w)_{\rho,S}]\mathbf{v}_2,$$

when the exact analogy between the entropy-transport and He^3-transport parts becomes clear.

For pure He^4, the second and third terms of (11) reduce to an irrotational vector, grad$g$. Hence curl$\mathbf{v}_s$ is a constant of motion, and hence it is consistent with the equations of motion to set curl$\mathbf{v}_s=0$ identically. It is of interest to see if this result applies, on our equations, for mixtures. For Pomeranchuk's assumption ($w_s=0$), the third term of (11) vanishes and the result is still true. For the Koide-Usui assumption ($w_s\rho=\rho_s w$), $\partial(\text{curl}\mathbf{v}_s)/\partial t$ is proportional to $\operatorname{grad}(\partial g/\partial w)\times\operatorname{grad}w$. But $\partial w/\partial t=-\mathbf{v}_1\cdot\operatorname{grad}w$ in this case, and hence if grad$w$ is ever zero everywhere (w constant) then it remains zero: and then curl$\mathbf{v}_s$ is constant. However, it is clear that in general, unless $w_s=0$, curl$\mathbf{v}_s$ is not constant and may not be supposed zero over all time.

III. WAVE MOTION

In this section we derive and discuss the wave equations governing macroscopic disturbances of small amplitude. For brevity we write:

$$\epsilon=(w_n\rho_s-w_s\rho_n)/w\rho_s, \quad (\epsilon\leqslant 1) \tag{13}$$

and

$$\bar{S}=S-\epsilon\, w(\partial S/\partial w)_{P,T}. \tag{14}$$

[14] Reference 5, Eq. (3.12).

Equations (7)–(11) give, in linear approximation:[15]

$$S\partial w/\partial t=\epsilon w\partial S/\partial t; \tag{15}$$

$$\partial^2\rho/\partial t^2=\nabla^2 P; \tag{16}$$

$$\partial^2 S/\partial t^2=S(\rho_s/\rho_n)\{(1/\rho)\nabla^2 P-\nabla^2[g-w(\partial g/\partial w)_{P,T}] -(1-\epsilon)w\nabla^2(\partial g/\partial w)_{P,T}\}. \tag{17}$$

Equation (15) integrates to

$$S\delta w/\delta t = \epsilon w\delta S/\delta t; \tag{15'}$$

where the primes denote small deviations from the state at some arbitrary instant. Thus the fluctuations w' and S' are not independent; and hence (16) and (17) represent, as for pure He^4, a wave system with two degrees of freedom. To reduce (16) and (17) to separable form, it is most convenient to transform to the variables P', S'. By straightforward thermodynamics and substituting for w' by (15'), we find (Appendix B):

$$\rho'=\left(\frac{\partial\rho}{\partial P}\right)_{S,w}P'+\left[\bar{S}\left(\frac{\partial\rho}{\partial S}\right)_{P,w}+\epsilon w\left(\frac{\partial\rho}{\partial w}\right)_{P,T}\right]\frac{S'}{S}, \tag{18}$$

$$(1/\rho)P'-[g-w(\partial g/\partial w)_{P,T}]' -(1-\epsilon)w[(\partial g/\partial w)_{P,T}]' =\left[\bar{S}\left(\frac{\partial v}{\partial S}\right)_{P,w}+\epsilon w\left(\frac{\partial v}{\partial w}\right)_{P,T}\right]P' +\left[\bar{S}^2\left(\frac{\partial T}{\partial S}\right)_{P,w}+\epsilon^2 w^2\left(\frac{\partial^2 g}{\partial w^2}\right)_{P,T}\right]\frac{S'}{S}, \tag{19}$$

where

$$v=1/\rho.$$

The wave equations derived from (15), (16), and (17) are hence

$$\partial^2 P/\partial t^2-c_1^2\nabla^2 P=(\rho c_1^2\mu/S)\partial^2 S/\partial t^2, \qquad \partial^2 S/\partial t^2-c_2^2\nabla^2 S=(S\rho_s/\rho\rho_n)\mu\nabla^2 P, \tag{20}$$

where

$$c_1^2=(\partial P/\partial\rho)_{S,w},$$

$$c_2^2=(\rho_s/\rho_n)[(\bar{S})^2 T/C_{P,w}+\epsilon^2 w^2(\partial^2 g/\partial w^2)_{P,T}], \tag{20'}$$

$$\mu=(\bar{S}/C_{P,w})T\alpha_{P,w}+\epsilon(w/v)(\partial v/\partial w)_{P,T}$$

and where

$$C_{P,w}=T(\partial S/\partial T)_{P,w}, \quad \alpha_{P,w}=(1/v)(\partial v/\partial T)_{P,w},$$

as usual.

The equations (20) represent two wave motions, each of coupled pressure and entropy fluctuations, with velocities u_1 and u_2 given by the roots of

$$(u^2-c_1^2)(u^2-c_2^2)=(\rho_s/\rho_n)\mu^2 c_1^2 u^2. \tag{21}$$

The first term of Eq. (20') for the coupling factor μ will be small, as it is for pure He^4, because α_P is small; but we would expect the second term to be appreciable when the concentration w is appreciable. The derivative $\partial v/\partial w$ has not yet been measured;[16] but we have the values for the pure liquids, $v_4=v(0)=6.9$ cm³/g and $v_3=v(1)=12.7$ cm³/g, from which we may take $(1/v)(\partial v/\partial w)$ to be of order unity, and hence

$$\mu\sim\epsilon w\sim w. \tag{22}$$

The factor $(\rho_s/\rho_n)\mu^2$ in (21) will always be finite, since $(\epsilon w)^2(\rho_s/\rho_n)\lesssim\epsilon w(1-w)\lesssim\frac{1}{4}$, but may be large enough at high concentrations for the actual velocities, u_1 and u_2, to deviate appreciably from c_1 and c_2. For small concentrations w, where we are looking for deviations of order w from the pure He^4 values, we may ignore the right-hand side of (21), which is of order w^2.

Appreciable coupling of thermal and acoustic disturbances will considerably complicate the wave phenomena. We set up here the equations needed for making calculations on the coupled waves: Equation (20) gives, for a wave motion of either mode, the equivalent formulas:

$$(u^2-c_1^2)P'=\mu\rho c_1^2 u^2(S'/S), \qquad \rho(u^2-c_2^2)(S'/S)=\mu(\rho_s/\rho_n)P', \tag{23}$$

where $u=u_1$ or u_2, which are supplemented by the relation [Appendix B, Eq. (B3)],

$$T'=(T/C_{P,w})[\bar{S}(S'/S)+(\alpha_{P,w}/\rho)P']. \tag{24}$$

The mass and entropy flux vectors are given, for a general motion, by

$$-\partial\mathbf{J}/\partial t=\mathrm{grad}P, \qquad -\partial\mathbf{N}/\partial t=\rho c_2^2\,\mathrm{grad}S+\mu(\rho_s/\rho_n)S\,\mathrm{grad}P. \tag{25}$$

From (24) and (25) we may write down an acceptance (inverted impedance) matrix,[17] for a plane traveling wave of either mode, according to:

$$\begin{pmatrix}\mathbf{u}\cdot\mathbf{J}\\ \mathbf{u}\cdot\mathbf{N}\end{pmatrix}=\begin{pmatrix}1 & 0\\ [\mu-\alpha_{P,w}(c_2^2\rho_n/\bar{S}\rho_s)]S(\rho_s/\rho_n) & \rho c_2^2 C_{P,w}S/T\bar{S}\end{pmatrix}\begin{pmatrix}P'\\ T'\end{pmatrix}, \tag{26}$$

[15] In the equations which follow, the equals sign is to be understood as within this qualification, which will not be repeated.

[16] The curves of $v(w)$, when they are determined, will be of interest apart from the bearing indicated here on wave motion. For example, the limiting slopes of the curves will give the partial specific volumes, $v_{34}=(\partial V/\partial M_3)_{M_4}$, $w\to 0=v_4+(\partial v/\partial w)_{w\to 0}$ and $v_{43}=(\partial V/\partial M_4)_{M_3}$, $w\to 1=v_3-(\partial v/\partial w)_{w\to 1}$, which together with v_3 and v_4 provide four experimental measures which a realistic theory of the equilibrium state of quantum liquids should fit.

[17] J. R. Pellam, Phys. Rev. **76**, 872 (1949).

where $u=u_1$ or u_2. Equations (23) show that the second sound mode carries a pressure fluctuation

$$P_2'=-\mu\frac{\rho c_1^2u_2^2}{c_1^2-u_2^2}(S_2'/S), \tag{27}$$

while first sound carries an entropy fluctuation

$$S_1'=\mu\frac{(\rho_s/\rho_n)S}{\rho(u_1^2-c_2^2)}P_1'. \tag{28}$$

However, these are not the only coupling effects which we may expect in practice. If, for example, we generate second sound in the conventional way, by a resistance strip carrying an alternating current, then the boundary conditions at the heater will be such that the first-sound *mode* must be generated at the same time. Picture the heater as a plane rigid wall, generating plane traveling waves by an oscillating outward entropy flux[18] $N(t)$: then, by the first of Eqs. (25), grad$P=0$ at the heater wall. Since the two wave modes generated have the same time variation, this means

$$P_1'=-(u_1/u_2)P_2', \text{ at the heater.} \tag{29}$$

Thus the coupling of modes at the wall leads to a bigger pressure component than does the coupling within the second mode. From (27), (28), and (29):

$$\frac{S_1'}{S_2'}=\mu^2\frac{(\rho_s/\rho_n)c_1^2u_1u_2}{(c_1^2-u_2^2)(u_1^2-c_2^2)}, \tag{30}$$

and hence, by the second of Eqs. (25),

$$S_2'=\frac{u_2N}{\rho c_2^2}\Big/\left[1+\frac{\mu^2(\rho_s/\rho_n)c_1^2u_2^2}{(c_1^2-u_2^2)(u_1^2-c_2^2)}\right], \text{ at the heater.} \tag{31}$$

If the oscillating flux N is periodic, then at increasing distances from the heater the pressure oscillations P_1' and P_2' will be alternately in and out of phase. If N_0 is the amplitude of N at the heater, then (neglecting μ^2) by (27), (29), and (31) the pressure amplitude will vary between the limits

$$P_0=\frac{\mu N_0}{S}\frac{u_1^2}{u_1+u_2}, \text{ and } P_0=\frac{\mu N_0}{S}\frac{u_1^2}{u_1-u_2}. \tag{32}$$

A rough estimate shows that amplitudes of grams per cm^2 should be readily produced in this way (indeed, for low temperatures and appreciable concentrations the cavitation threshold may be an effective limitation on second-sound amplitude†). It is suggested that measurements of this pressure effect be made to obtain an estimate of μ, and hence, when $\partial v/\partial w$ is determined, of ϵ.

[18] There will necessarily also be a constant (dc) flux, which does not affect this analysis and which we ignore.

† *Note added in proof:*—With positive temperature *pulses*, rather than continuous ac, the tension tending to cause cavitation would have the smaller value given by (27).

The excitation of standing waves of second sound in a cavity requires a more complicated analysis, which is not attempted here. The Pellam disk experiment[19] registers a force proportional to

$$\rho_n v_n^2+\rho_s v_s^2=(\rho_n/\rho_s)[J^2/\rho_n-2\mathbf{N}\cdot\mathbf{J}/S+N^2/S^2], \tag{33}$$

at the center of the cavity. It appears from the foregoing considerations that an analysis of this effect for mixtures,[20] as was attempted by Koide and Usui,[9] should take due account of the coupling measured by μ.

IV. EVALUATION OF RESULTS; DILUTE SOLUTIONS

The formulas (20′) are in terms of thermodynamic functions for mixtures, and their derivatives with respect to concentration, which are not known directly from practical measurements. This deficiency may be largely filled by combining the values of the functions for the pure He^3 and pure He^4 liquids with the extensive data on the partial vapor pressures of mixtures which have been obtained.[21] The link between the vapor pressures and the liquid functions is the equality of each of the chemical potentials in the two phases. This equality is expressed by the equations[22]

$$\begin{aligned} g-w(\partial g/\partial w)_{P,T}&=g_4+(kT/m_4)\ln(p_4/p_4^0),\\ g+(1-w)(\partial g/\partial w)_{P,T}&=g_3+(kT/m_3)\ln(p_3/p_3^0), \end{aligned} \tag{34}$$

where m_3 and m_4 are the atomic masses, p_3 and p_4 the partial pressures, and where g_3 and p_3^0 refer to pure He^3 liquid, g_4 and p_4^0 to pure He^4 liquid. (To allow for the nonideality of the vapor, the pressures p should be replaced by fugacities.[22]) In obtaining the other functions for the liquid from Eqs. (34), we have to remember that the latter are valid only on the saturation surface in the $P-T-w$ diagram. Thus, taking the difference of the two equations and differentiating along the line "$T=$constant" in the surface:

$$\left(\frac{\partial^2 g}{\partial w^2}\right)_{P,T}+\left(\frac{\partial v}{\partial w}\right)_{P,T}\left(\frac{\partial P_{\text{sat}}}{\partial w}\right)_T = kT\left[\frac{1}{m_3p_3}\left(\frac{\partial p_3}{\partial w}\right)_T-\frac{1}{m_4p_4}\left(\frac{\partial p_4}{\partial w}\right)_T\right].$$

Since the second term on the left may be neglected, this result gives the $w^2(\partial^2 g/\partial w^2)_{P,T}$ which occurs in the formula (20′) for c_2. $\bar{S}$ and $C_{P,w}$ are derived in the same way. Writing

$$\ln(p_3/p_3^0)=r_3, \quad \ln(p_4/p_4^0)=r_4 \tag{35}$$

for brevity, and neglecting terms in P_{sat} as before, we

[19] J. R. Pellam and W. B. Hanson, Phys. Rev. **85**, 216 (1952).
[20] B. Weinstock and J. R. Pellam, Phys. Rev. **89**, 521 (1953).
[21] H. S. Sommers, Jr., Phys. Rev. **88**, 113 (1952).
[22] See E. A. Guggenheim, *Thermodynamics* (North-Holland Publishing Company, Amsterdam, 1949), Chap. 5. For the purposes of this paper, we express the formulas in terms of the concentration by mass w.

have altogether:

$$\tilde{S}=S_4+(1-\epsilon)w(S_3-S_4)$$
$$-k\frac{\partial}{\partial T}\left[\frac{r_4T}{m_4}+(1-\epsilon)w\left(\frac{r_3}{m_3}-\frac{r_4}{m_4}\right)T\right],$$
$$C=wC_3+(1-w)C_4-kT\frac{\partial^2}{\partial T^2}\left[\frac{wr_3T}{m_3}+(1-w)\frac{r_4T}{m_4}\right], \quad (36)$$
$$\frac{\partial^2 g}{\partial w^2}=kT\frac{\partial}{\partial w}\left[\frac{r_3}{m_3}-\frac{r_4}{m_4}\right].$$

(To the approximation in which the P_{sat} term is neglected, C_P and C_v are not distinguished.) Thus, if the pure liquid data, the partial vapor pressures, and $\rho(P, T, w)$ are known, it is possible in principle to express ϵ and ρ_s/ρ_n in terms of u_1 and u_2.

The formulas (36) reduce to a more tractable and interesting form for the case of dilute solutions ($w\ll 1$), on which measurements of u_2 have actually been made and published.[3] It is known[21] that Henry's Law—the proportionality of solute vapor pressure to concentration—applies to sufficiently weak solutions of He^3.[23] We may then set

$$p_3=a(T)\cdot Xp_3^0+O(X^2), \quad p_4=(1-X)p_4^0+O(X^2), \quad (37)$$

where

$$X=\frac{m_4w}{m_3}\Big/\left[1+\left(\frac{m_4}{m_3}-1\right)w\right] \quad (38)$$

is the concentration of He^3 by molar fraction, the measure commonly quoted in the literature. If the solution were ideal, we would have $a=1$. The second of Eqs. (37) necessarily follows from the first, by the Duhem-Margules equation.[24] Substitution of (37) into (36) gives:

$$\tilde{S}=S_4+(1-\epsilon)\frac{m_3}{m_4}X(S_3-S_4)$$
$$+\frac{kX}{m_4}\left[1-(1-\epsilon)\frac{d(T\ln a)}{dT}-(1-\epsilon)\ln X\right],$$
$$C=C_4+X\left[\frac{m_3}{m_4}(C_3-C_4)-\frac{kT}{m_4}\frac{d^2(T\ln a)}{dT^2}\right], \quad (39)$$
$$w^2\left(\frac{\partial^2 g}{\partial w^2}\right)=\frac{kTX}{m_4},$$

+higher powers of X. Since $u_2^2-c_2^2$ vanishes as X^2 for dilute solutions, substitution of (39) in the second of (20′) gives u_2^2 as a function of ϵ, X, T, and ρ_s/ρ_n. If we assume with Pomeranchuk that the He^3 moves entirely with the normal fluid (i.e., set $\epsilon=1$), then we find

$$u_2^2=(\rho_s/\rho_n)[(S_4+kX/m_4)^2T/C(X)+kTX/m_4], \quad (40)$$

which is Pomeranchuk's result.[10] The above derivation of (40) shows that it is valid for just that range of concentrations for which Henry's Law is true. Corrections for higher concentrations, in terms of the deviations from Henry's Law, may be obtained from (36). We may expect ρ_s/ρ_n to be expandible as a power series in X,[25] so that according to (40)

$$[u_2(X)]^2=[u_2(0)]^2[1+XQ(T)+\cdots]. \quad (40')$$

If, on the other hand, $1-\epsilon$ does *not* vanish, then u_2^2 may not be expanded as a power series in X. We have instead an expansion of form

$$[u_2(X)]^2/[u_2(0)]^2=1$$
$$+XQ(T)+(X\ln X)R(T)+\cdots. \quad (41)$$

It follows that a sufficiently accurate examination of the dependence of u_2 on X for very small values of X (say 0.01 downward) would show whether or not $\epsilon=1$, i.e., whether or not $\rho_{2s}=0$, by the absence or presence of a $X\ln X$ term in the dependence. If such a term is present, then the determination of Q and R in (41) will serve to determine ϵ, and the dependence of ρ_s/ρ_n on X, separately. The numerical analysis depends on values of $a(T)$, Eq. (37), obtained from the vapor pressure data, and to a lesser extent on values of the entropy for pure He^3 liquid.[26] Q and R will increase very rapidly with decreasing temperature. For $\epsilon=1$, the part of Q not contributed by the variation of ρ_s/ρ_n with X is already of order 10^2 at 1.4°. It is therefore understandable that Lynton and Fairbank found a large increase of u_2 even for small concentrations, at such temperatures.

If $\epsilon\neq 1$, and varies with X, then for appreciable concentrations a knowledge of u_2, the vapor pressures, and the thermodynamic functions for the pure liquids, is not sufficient to determine ϵ and ρ_s/ρ_n separately. We need also (for example) the coupling factor μ and $v(X)$. In principle, μ might be found by comparing $u_1(X)$ with the values of $c_1(X)$ calculated from $P(\rho, T, X)$; but one would not expect the practical accuracy of this method to be good enough. However, as was remarked in Sec. III, μ might be found by measuring the pressure fluctuations in second sound; and there seems a reasonable hope that this method would be of tolerable accuracy.

V. DIFFUSION

In the preceding analysis we have ignored the possibility of *diffusion* of He^3 relative to He^4 [in addition to the reversible relative motion given by (3)] under a

[23] Application of Nernst's Law to the expression for S derived from (34) (or equally to $\tilde{S}$ in (36)) shows that Henry's Law must be violated at sufficiently low temperatures. The vapor pressure measurements only go down to 1.27°, and it seems unlikely that they can be carried much further.

[24] Reference 22, Eq. (5.20.3).

[25] This is not completely obvious. It would not be true if, for example, Tisza's relation $\rho_n/\rho=S/S_\lambda$ held for mixtures, because the expansion of S requires a term in $X\ln X$.

[26] Weinstock, Abraham, and Osborne, Phys. Rev. **89**, 787 (1953).

gradient of concentration and of the other thermodynamic variables. We shall see in this section that diffusion probably has a negligible influence on the propagation of free first- and second-sound waves. However, the *generation* of the waves at a solid surface cannot in general be consistently described without admitting diffusion.[27] At a solid wall the normal components of $\mathbf{J}$ and $\mathbf{J}_3$ must vanish separately; and consequently, if we did not allow diffusion, only for the Koide-Usui assumption ($\epsilon=0$) would the generation of second sound waves by the usual method be possible.

Beenakker *et al.*[28] have investigated the diffusion rate in very dilute solutions by measuring their thermal resistance. Arguing that thermal diffusion should be negligible[29] compared with concentration diffusion, they deduce from their measurements a concentration-diffusion coefficient D decreasing from about 2.5×10^{-2} cm^2/sec at 1.2° to about 4×10^{-4} cm^2/sec at 2.1°. Since the ratio of temperature gradient to concentration gradient is proportional to $(1/w)$ in second sound, whereas it is independent of w in the experiment quoted, the argument for neglecting thermal diffusion does not apply to second sound. However, we shall be concerned here simply with exploring qualitatively the consequences of diffusion, and accordingly use as a model the simplest equations which will serve this purpose—any particular model being, at this stage, provisional. We retain Eqs. (7), (9), (10), and (11), and replace (8) by

$$\partial(\rho w)/\partial t+\operatorname{div}[\rho w(\mathbf{v}_n+\mathbf{v}_3)]=0, \tag{42}$$

where

$$w\mathbf{v}_3=-D\operatorname{grad}w; \tag{43}$$

setting $w_s=0$, for simplicity, and neglecting thermal diffusion. We also neglect the coupling of entropy and pressure fluctuations, measured by μ of Sec. III, and solve the equations at constant pressure. If we define an operator

$$K=D\nabla^2\int dt\cdots, \tag{44}$$

then (to linear approximation as usual)

$$w\partial S/\partial t=S(1-K)\partial w/\partial t. \tag{45}$$

The wave equation for entropy and concentration fluctuations is hence

$$(1-K)\partial^2S/\partial t^2=[c_2^2-(\rho_s/\rho_n)(S\bar{S}T/C)K]\nabla^2S, \tag{46}$$

where $\bar{S}$ and c_2 are defined as in Sec. III, with $\epsilon=1$. If we now represent the time variation of S by the factor $\exp(2\pi ift)$, then the complex velocity of propagation u is given by substituting into (46):

$$K=2\pi iDf/u^2. \tag{44'}$$

Hence,

$$u^2[u^2-(c_2^2+ic_3^2)]=-i\alpha c_2^2c_3^2, \tag{47}$$

where

$$c_3^2=2\pi Df,\quad \alpha c_2^2=(\rho_s/\rho_n)S\bar{S}T/C. \tag{48}$$

The two roots of (47) correspond to a very slightly damped second sound and to a third very strongly damped "skin" mode. For the practical frequencies f and the Leiden values of D, $c_3^2\ll c_2^2$. Hence the roots are, to sufficient approximation,

$$u_2^2=[1+i(1-\alpha)(c_3/c_2)^2]c_2^2,\quad u_3^2=i\alpha c_3^2. \tag{49}$$

The extinction coefficient for second sound is thus at most of order Df^2/c_2^3 and hence will be negligible. In contrast, the mode corresponding to u_3 will be localized within a distance (from the source of the wave) of order $\sqrt{(D/f)}$: it will hence be confined in practice to a very thin skin around the source. There is thus a formal resemblance to the extra modes discussed by Kronig and Thellung.[30]

To satisfy the boundary conditions at the surface of a heater resistance, which is the conventional source of second sound, both second and third modes must be generated. By (45), the entropy and He^3-mass currents, in either mode, are related by

$$\mathbf{N}^{(q)}=(S/w)(1-K^{(q)})\mathbf{J}_3^{(q)};\quad q=2,3, \tag{50}$$

where the superscripts label the mode. By (49) we may set

$$1-K^{(2)}\simeq1,\quad 1-K^{(3)}\simeq-(1-\alpha)/\alpha; \tag{51}$$

and hence, since the normal component of $\mathbf{J}_3=\mathbf{J}_3^{(2)}+\mathbf{J}_3^{(3)}$ vanishes at the heater surface, we have

$$N^{(3)}/N=1-\alpha \text{ at the heater.} \tag{52}$$

Equation (52) gives the fraction of the "signal" lost into the damped mode, on the present model. For dilute solutions we may write it:

$$\frac{N^{(3)}}{N}=\frac{X}{m_4}\left\{\frac{k}{S_4}\left[\ln X+\frac{C_4}{S_4}+\frac{d(T\ln\alpha)}{dT}\right]+m_3\left(1-\frac{S_3}{S_4}\right)\right\}. \tag{52'}$$

Thus a fraction, of order X, of the signal is lost at the generator because of diffusion. An experimental study of this loss (or of the corresponding effect in the transimission of second sound through a thin conducting foil) might be complicated by the processes underlying the Kapitza temperature difference[31] at the boundary.[32] If the signal loss (52) is small, then we may expect that the formulas obtained in Sec. III for the pressure fluctuation in free second-sound waves will not be appre-

[27] This remark (and the impetus thereby to the work in this section) is due to F. London.

[28] Beenakker, Taconis, Lynton, Dokoupil, and Van Soest, Physica **18**, 433 (1952).

[29] Their argument for neglecting thermal diffusion in their experiment may at best be admitted provisionally, pending a realistic theoretical understanding of the magnitudes of the two coefficients; but their values for D are in any case presumably correct in order of magnitude, and will be used here as orders of magnitude.

[30] R. Kronig and A. Thellung, Physica **16**, 678 (1950).

[31] P. Kapitza, J. Phys. (U.S.S.R.) **4**, 181 (1941).

[32] I am indebted for this remark to J. R. Pellam.

ciably modified by diffusion; since (29) will still apply at a distance from the wall greater than the skin thickness but small compared with the wavelength.

It should be emphasized that the valid conclusions from the work in this section are qualitative and order-of-magnitude ones. In making the simplest possible modification, by (42) and (43), of the hydrodynamic equations, we have not taken account of the necessity for preserving the equations of conservation of energy and of momentum, and of "semi-conservation" (increase only) of entropy. It seems desirable that a study be made of the way in which the possible equations including diffusion are restricted by these conservation laws and the Onsager relations.[33] A detailed investigation—theoretical and experimental—of diffusion should be of some importance to the microscopic theory, in providing a clue to the way in which the He^3 component participates in the excitations of the liquid.

I am indebted to Professor F. London, Duke University, for first interesting me in this problem, for his continued interest and encouragement, and for valuable discussions; and to members of the Institute for Advanced Study, for criticisms of the manuscript.

APPENDIX A. THE EQUATIONS OF MOTION

Since

$$\delta(\rho\epsilon)=[g-w(\partial g/\partial w)_{P,T}]\delta\rho + (\partial g/\partial w)_{P,T}\delta(\rho w)+T\delta(\rho S), \quad \text{(A1)}$$

we have by (7), (8), and (9):

$$-\partial(\rho\epsilon)/\partial t=[g-w(\partial g/\partial w)_{P,T}]\,\mathrm{div}(\rho_n\mathbf{v}_n+\rho_s\mathbf{v}_s) + (\partial g/\partial w)_{P,T}\,\mathrm{div}(\rho w_n\mathbf{v}_n+\rho w_s\mathbf{v}_s)+T\,\mathrm{div}(\rho S\mathbf{v}_n). \quad \text{(A2)}$$

Limiting ourselves to terms quadratic and lower in the velocities, we may expect the two-fluid motion to satisfy as usual an energy-balance equation of form[14]

$$0=\partial(\tfrac{1}{2}\rho_n v_n^2+\tfrac{1}{2}\rho_s v_s^2+\rho\epsilon)/\partial t + \mathrm{div}(A_n\rho_n\mathbf{v}_n+A_s\rho_s\mathbf{v}_s), \quad \text{(A3)}$$

where $A_n=A_n(\rho, S, w)$, $A_s=A_s(\rho, S, w)$. We choose A_n and A_s such that (A3) may be reduced to the form:

$$0=\partial(\tfrac{1}{2}\rho_n v_n^2+\tfrac{1}{2}\rho_s v_s^2)/\partial t-\rho_n\mathbf{v}_n\cdot\mathbf{F}_n-\rho_s\mathbf{v}_s\cdot\mathbf{F}_s, \quad \text{(A4)}$$

where $\mathbf{F}_n$ and $\mathbf{F}_s$ are linear combinations of gradients of the thermodynamic functions:—i.e., with the terms remaining, in $\mathrm{div}(\rho_n\mathbf{v}_n)$ and $\mathrm{div}(\rho_s\mathbf{v}_s)$, cancelled identically. Equation (A4) may be written

$$0=\tfrac{1}{2}(v_n^2\dot\rho_n+v_s^2\dot\rho_s) + \rho_n\mathbf{v}_n\cdot(\dot{\mathbf{v}}_n-\mathbf{F}_n)+\rho_s\mathbf{v}_s\cdot(\dot{\mathbf{v}}_s-\mathbf{F}_s); \quad \text{(A4')}$$

and hence—since the first term of (A4') belongs to the higher powers of the velocities which we are neglecting—the form (A4) implies equations of motion:

$$\dot{\mathbf{v}}_n=\mathbf{F}_n, \quad \dot{\mathbf{v}}_s=\mathbf{F}_s. \quad \text{(A5)}$$

Thus our choice of A_n and A_s is just that designed to preserve the conventional form of the two-fluid dynamics. Substituting (A2) in (A3), we find that (A4) implies

$$A_n=g+(\partial g/\partial w)_{P,T}(w_n\rho_s-w_s\rho_n)/\rho_n+TS\rho/\rho_n,$$
$$A_s=g+(\partial g/\partial w)_{P,T}(w_s\rho_n-w_n\rho_s)/\rho_s, \quad \text{(A6)}$$

and

$$\mathbf{F}_n=-\mathrm{grad}A_n+(\partial g/\partial w)_{P,T}\,\mathrm{grad}(\rho w_n/\rho_n) + T\,\mathrm{grad}(\rho S/\rho_n),$$
$$\mathbf{F}_s=-\mathrm{grad}A_s+(\partial g/\partial w)_{P,T}\,\mathrm{grad}(\rho w_s/\rho_s). \quad \text{(A7)}$$

From (A5), (A6), and (A7) we obtain (10) and (11), which are evidently the only linear equations consistent with the forms of (A3) (energy flux vector) and (A5) (d'Alembert forces).

APPENDIX B. TRANSFORMATION FORMULAS

Expand ρ and S as functions of P, T and w, and substitute for w' by (15'):

$$\rho'=\left(\frac{\partial\rho}{\partial P}\right)_{T,w}P'+\left(\frac{\partial\rho}{\partial T}\right)_{P,w}T' + \epsilon w\left(\frac{\partial\rho}{\partial w}\right)_{P,T}\left(\frac{S'}{S}\right), \quad \text{(B1)}$$

$$S'=\left(\frac{\partial S}{\partial P}\right)_{T,w}P'+\left(\frac{\partial S}{\partial T}\right)_{P,w}T' + \epsilon w\left(\frac{\partial S}{\partial w}\right)_{P,T}\left(\frac{S'}{S}\right). \quad \text{(B2)}$$

Equation (B2) gives

$$T'=\left(\frac{\partial T}{\partial S}\right)_{P,w}\bar S\left(\frac{S'}{S}\right)+\left(\frac{\partial T}{\partial P}\right)_{S,w}P', \quad \text{(B3)}$$

which, substituted into (B1), yields (18). Similarly expanding g and $(\partial g/\partial w)_{P,T}$, we have

$$[g-w(\partial g/\partial w)_{P,T}]'+w(1-\epsilon)[(\partial g/\partial w)_{P,T}]' =[v-\epsilon\, w(\partial v/\partial w)_{P,T}]P'-\bar S T' - \epsilon^2 w^2(\partial^2 g/\partial w^2)_{P,T}(S'/S). \quad \text{(B4)}$$

Substituting (B3) into (B4) yields (19).

[33] For Onsager relations see S. R. de Groot, *Thermodynamics of Irreversible Processes* (North-Holland Publishing Company, Amsterdam, 1951).

Application of the Multiple Scattering Theory to Cloud-Chamber Measurements. II*

M. ANNIS,† H. S. BRIDGE, AND S. OLBERT
Physics Department and Laboratory for Nuclear Science, Massachusetts Institute of Technology, Cambridge, Massachusetts
(Received December 10, 1952)

The theory of multiple Coulomb scattering discussed in Part I has been applied to some specific problems in the analysis of data obtained with a multiplate cloud chamber. In particular, the problem of estimating the momentum (or, more exactly, the quantity $\Pi = p\beta$) for a single particle is discussed, and a procedure for determining mass using scattering and residual range is given for the case of a group of particles homogeneous in mass. In the case of an inhomogeneous group of particles, it is shown that the distribution function for values of the mean square angle of scattering in n plates can sometimes be used as a basis of separation into nearly homogeneous mass groups. In addition the distribution of the mean square angles provides an estimate of the error in Π or in the value of the mass. These methods are illustrated by a determination of the masses of the proton and meson using a mixture of these particles observed in a multiplate cloud chamber.

In the theory developed in Part I it was assumed that the probability for single Coulomb scattering goes abruptly to zero for angles greater than $\varphi_0 = \varphi_m a/r_n$, where φ_m is the screening angle as given by Molière, a is the Thomas-Fermi atomic radius, and r_n is the nuclear radius. As a result of this assumption the mean value of the scattering angles, for means of order two and higher, remains finite as contrasted with the result of Molière or Snyder and Scott where the mean square angle of scattering is infinite. Consequently either the mean of the absolute values of the scattering angles or the rms angle of scattering can be used in the above applications. Both cases are given.

The above assumption as to the cut-off angle for single scattering affects the value of the rms angle of scattering only slightly; it is shown, however, that the behavior of the "tail" of the distribution function depends critically on the choice of φ_0. Consequently, the value of Π or of the mass is not greatly dependent on the particular theory of multiple scattering used, but the probability of scattering through angles large compared with the rms angle is. The difficulty of identifying a nuclear scattering by this method is emphasized.

I. INTRODUCTION

MEASUREMENT of the multiple Coulomb scattering of particle tracks observed in photographic emulsions has proved a powerful tool in the determination of physical properties of the particles.[1,2] For example, the mass of a particle reaching the end of its range in the emulsion may be determined by a method which can be described schematically as follows: One divides the track into many small "cells" and measures for each of these cells the residual range and the angle of scattering. From the theoretical relations connecting the rms angle of scattering and the residual range to the momentum and mass of the particle one then computes the mass.

Consider now the analogous problem of estimating the mass of a particle which stops in one of the plates of a multiplate cloud chamber. One is tempted to follow a procedure very similar to that just outlined, i.e., to measure for each plate the projected angle of scattering and the residual range. However, there are some difficulties. While in the case of emulsions 50 to 100 cells may be available, most multiplate cloud chambers contain fewer than 15 plates and consequently the maximum number of cells is ~ 15. Under these conditions the mass determination for a single stopped particle is quite poor, indeed, so poor as to make the method of little value. If, however, one can group together particles of the same kind from different pictures, one has a statistically improved method of determining the mass. There are several ways in which this might be done. For example: (1) In some cases the particle can be identified by a characteristic interaction at the end of its range. (2) Simultaneous measurement of the specific ionization and residual range may be sufficient to give a crude identification of the particle. (3) From a single picture, one can calculate a rough mass value for the particle. This may be adequate for identification of the particle provided the possible mass values are limited by other information. This last method will be considered in greater detail in Sec. V.

Another more fundamental difficulty becomes apparent when the procedure just outlined is applied to cloud-chamber data. As Olbert has shown in a preceding paper[3] (quoted in what follows as "I"), the theory of multiple Coulomb scattering developed by Molière[4] or by Snyder and Scott[5] cannot be used without modification. The results obtained in I indicate that the effect of the finite size of the scattering nuclei cannot be completely neglected for the layers of heavy elements used in most multiplate cloud chambers (e.g., ~ 10 g cm^{-2} of lead).

For convenience the results from Part I which are needed in the present discussion are summarized in Sec. II below. References to particular equations in Part I are prefixed by I-. In Secs. III and IV we shall consider measurement of the momentum and mass of heavy particles, and, as a partial verification of the methods discussed, we give in Sec. V the results of a rough measurement of the masses of the proton and the meson. Finally in Sec. VI we consider the effect of the

* This work was supported in part by the joint program of the U. S. Office of Naval Research and the U. S. Atomic Energy Commission.
† Present address, Washington University, St. Louis, Missouri.
[1] Goldschmidt-Clermont, King, Muirhead, and Ritson, Proc. Phys. Soc. (London) **61**, 183 (1948).
[2] S. Lattimore, Nature **161**, 518 (1948).
[3] S. Olbert, Phys. Rev. **87**, 319 (1952).
[4] G. Molière, Z. Naturforsch. **2a**, 133 (1947); **3a**, 78 (1948).
[5] H. S. Snyder and W. T. Scott, Phys. Rev. **76**, 220 (1949).

finite nuclear size on the probability of large angle scattering.

II. SUMMARY OF MULTIPLE SCATTERING FORMULAS FROM I

In I the probability of a particle suffering a projected single scattering through an angle φ' in $d\varphi'$, in traversing a thickness t g cm^{-2} material, was approximated by,

$$\hat{f}_1(\varphi';\varphi_0)d\varphi'=\begin{cases}\frac{1}{2}Qd\varphi'/(\varphi'^2+\varphi_m'^2)^{\frac{3}{2}}, & |\varphi'|<\varphi_0;\\ 0, & |\varphi'|>\varphi_0.\end{cases} \tag{1}$$

Here φ_0 is the cut-off angle of single scattering resulting from the finite nuclear size and, according to I-5, is given by,

$$\varphi_0=\varphi_m a r_n^{-1}, \tag{2}$$

where $a=1.67\times10^4 r_e Z^{-\frac{1}{3}}$ is the Thomas-Fermi radius of the atom and r_n is of the order of the nuclear radius, $R_n=0.49 r_e A^{\frac{1}{3}}$ ($r_e=2.82\times10^{-13}$ cm is the classical radius of the electron); Q is defined by Eq. (4) and φ_m is the screening angle defined by Molière.[4] According to (I-3) φ_m is given by

$$\varphi_m=(1.14 m_e c Z^{\frac{1}{3}}/137p)\{1.13+3.76(Z/137\beta)^2\}^{\frac{1}{2}}. \tag{3}$$

Q is given in (I-2) by

$$Q=(4\pi Nt/A)(Ze^2/pc\beta)^2. \tag{4}$$

In Eqs. (3) and (4) p is the momentum of the scattered particle and βc its velocity. m_e is the mass of the electron, N, Avogadro's number, and e, the electronic charge. t is the thickness of scattering material in g cm^{-2}, and Z and A have the usual significance.

The distribution function for multiple scattering resulting from the assumptions of Eq. (1) has been derived in Part I. It is convenient to express this distribution in terms of a dimensionless variable $x=\varphi(2GQ)^{-\frac{1}{2}}$. Here φ is the projected angle of multiple scattering and G is Molière's scattering parameter given below. Calling $f(x;x_0)dx$ the probability that the scattering variable x lies between x and $x+dx$, the distribution function for x is represented by the following equation [see Eq. (I-22)]:

$$f(x;x_0)=\exp(-x^2)/\pi^{\frac{1}{2}}+(1/4G)f^{(1)}(x;x_0). \tag{5}$$

The symbols in Eq. (5) have the following meaning:

$$x_0=\varphi_0(2GQ)^{-\frac{1}{2}} \tag{6}$$

is the reduced cut-off angle and $f^{(1)}(x;x_0)$ is the correction function derived in I:

$$f^{(1)}(x;x_0)=\frac{2}{\pi^{\frac{1}{2}}}\exp(-x^2)\sum_{\nu=0}^{\infty}\alpha_\nu(x_0)x^{2\nu}, \tag{7}$$

where

$$\alpha_0(x_0)=\tfrac{1}{2}\left[\Psi(\tfrac{1}{2})+\frac{1-\exp(-x_0^2)}{x_0^2}-\mathrm{Ei}(-x_0^2)\right];$$

$$\alpha_1(x_0)=\mathrm{Ei}(-x_0^2)-1-\Psi(\tfrac{1}{2});\quad \Psi(\tfrac{1}{2})=-0.0365\cdots; \tag{8}$$

$$\alpha_\nu(x_0)=\frac{\pi^{\frac{1}{2}}}{2}\frac{I(x_0^2;\nu-2)}{\nu(\nu-1)\Gamma(\nu+\frac{1}{2})},\quad \nu=2,3,4,\cdots.$$

$$\mathrm{Ei}(-r)=-\int_r^\infty\frac{e^{-t}}{t}dt$$

is the exponential integral,[6] and

$$I(z;p)p!=\int_0^z e^{-t}t^p dt$$

is the incomplete gamma-function.[7] G is defined by the transcendental equation,

$$G=-\tfrac{1}{2}\ln\left(\frac{\gamma^2}{e}\frac{\varphi_m^2}{2GQ}\right), \tag{9}$$

where $\ln(\gamma^2/e)=0.154\cdots$ ($\ln\gamma$ is Euler's constant).

According to I the following useful approximation may be used to compute G:

$$G\approx 5.66+1.24\log_{10}[Z^{4/3}A^{-1}t/(1.13\beta^2+3.76(Z/137)^2)]. \tag{10}$$

Equation (10) is valid for all values of G greater than 3.

Finally the expected value of the mean square angle of scattering is given by [see (I-27) and (I-29)]:

$$\begin{aligned}\langle\varphi^2\rangle_{Av}&=GQ\left[1+\frac{1}{2G}\{\ln(\gamma x_0^2)-1-\Psi(\tfrac{1}{2})\}\right]\\&=Q[\ln(2\varphi_0/\varphi_m)-1].\end{aligned} \tag{11}$$

The mean of the absolute values of the angles of scattering obtained in a similar way is given by

$$\langle|\varphi|\rangle_{Av}=\left(\frac{2}{\pi}GQ\right)^{\frac{1}{2}}\left[1+\frac{1}{2G}\left(1-\alpha_0(x_0)+\frac{1-\exp(-x_0^2)}{x_0^2}-\frac{\pi^{\frac{1}{2}}}{x_0}\Phi(x_0)\right)\right],$$

where

$$\Phi(x_0)=\frac{2}{\pi^{\frac{1}{2}}}\int_0^{x_0}\exp(-t^2)dt \tag{11a}$$

is the error integral.

III. MEASUREMENT OF MOMENTUM

The quantity which can be computed from measurements of the projected angles of scattering ϕ is not the

[6] E. Jahnke and F. Emde, *Tables of Functions* (Dover Publications, New York, 1945).

[7] K. Pearson, *Tables of the Incomplete Gamma-Function* (Cambridge University Press, London, 1934).

TABLE I. The relative statistical error in Π for n between one and ten. The error has the same meaning as that given by Eq. (30) for $n>$ten; i.e., it corresponds to the $e^{-\frac{1}{2}}$ width of $\psi_n(s_2, \Pi)$. The calculation was done graphically.

n	$(\Delta\Pi)^+/\Pi_l$	$(\Delta\Pi)^-/\Pi_l$
1	0.775	0.597
2	0.536	0.364
3	0.432	0.350
4	0.373	0.319
5	0.332	0.297
6	0.297	0.277
7	0.277	0.259
8	0.263	0.241
9	0.244	0.230
10	0.229	0.214

momentum itself but the product of the momentum p and the velocity $c\beta$ of the particle, i.e., the quantity,

$$\Pi = pc\beta. \tag{12}$$

If a particle is scattered in several plates of a multiplate cloud chamber, one can form from the observed scattering angles any convenient average of the experimental data. If the ionization loss in the plates is neglected, the corresponding theoretical averages can be calculated from the distribution function $f(x; x_0)$ given by Eq. (5). From any of these averages one then finds the expected value of Π. For the theoretical averages we have

$$\begin{aligned}\langle|\varphi|^k\rangle_{Av} &= (2GQ)^{\frac{1}{2}k}\langle|x|^k\rangle_{Av} \\ &= (2GQ)^{\frac{1}{2}k}\int_{-\infty}^{+\infty}|x|^k f(x; x_0)dx.\end{aligned} \tag{13}$$

For $k=1$, evaluation of the right-hand side of Eq. (13) yields [see Eq. (11a)]

$$\langle|\varphi|\rangle_{Av} = K_1 l^{\frac{1}{2}} m_e c^3/\Pi, \tag{14}$$

where

$$K_1 = [8r_e^2 NZ^2A^{-1}G]^{\frac{1}{2}}\left[1+\frac{1}{2G}\left(0.9817+\frac{1-\exp(-x_0^2)}{2x_0^2}+\tfrac{1}{2}\,\mathrm{Ei}(-x_0^2)-\frac{\pi^{\frac{1}{2}}}{x_0}\Phi(x_0)\right)\right]. \tag{15}$$

If $x_0^2 \gg 1$, the asymptotic expansions of $\mathrm{Ei}(-x_0^2)$ and $\Phi(x_0)$ may be used to express K_1 as

$$K_1 \approx [8r_e^2 NZ^2A^{-1}G]^{\frac{1}{2}}\times\left[1+\frac{1}{2G}\left(0.9817+\frac{1}{2x_0^2}-\frac{\pi^{\frac{1}{2}}}{x_0}\right)\right]. \tag{16}$$

Although K_1 is a function of β through the functions G and x_0, analysis of Eqs. (2), (3), (6), (7), and (9) shows that K_1 is practically independent of β over a wide range of values for β. One must be cautioned, however, that the dependence of K_1 on β becomes more pronounced for low Z elements. If K_1 can be considered constant, Eq. (14) shows that the mean of the absolute value of the projected angle of multiple scattering varies inversely with Π.

For $k=2$, Eq. (13) yields [see Eq. (11)]

$$\langle\varphi^2\rangle_{Av}^{\frac{1}{2}} = K_2 l^{\frac{1}{2}} m_e c^2/\Pi, \tag{17}$$

where

$$\begin{aligned}K_2 &= [4\pi r_e^2 NZ^2A^{-1}\{\ln(2\varphi_0/\varphi_m)-1\}]^{\frac{1}{2}} \\ &= [4\pi r_e^2 NZ^2A^{-1}G(1+(1/2G)\{\ln(\gamma x_0^2) \\ &\qquad -1.0365\})]^{\frac{1}{2}}.\end{aligned} \tag{18}$$

Here K_2 is rigorously independent of β, being a function only of the constants A, Z, and t of the scattering material. This result follows from our assumption that φ_0/φ_m is independent of β, [see Eq. (2)]. Hence Π varies inversely as $\langle\varphi^2\rangle_{Av}^{\frac{1}{2}}$. If one drops the terms in $1/2G$, one obtains the value of K_2 in the so-called "normal approximation." Equation (18) becomes

$$K_2 \approx [4\pi r_e^2 NZ^2A^{-1}G]^{\frac{1}{2}} \approx (\pi/2)^{\frac{1}{2}}K_1. \tag{18a}$$

If the number of plates is sufficiently large, one may equate the theoretical averages to those observed experimentally, i.e., one may set

$$(s_k)^k = \langle|\varphi|^k\rangle_{Av}. \tag{19}$$

The observed means $(s_k)^k$ are by definition

$$(s_k)^k = \frac{1}{n}\sum_{i=1}^{n}|\varphi_i|^k, \tag{20}$$

where φ_i is the observed value of the scattering angle in the ith plate. Use of Eqs. (14) or (17) then enables one to calculate Π. However, if n is not large, a more rigorous treatment of the problem is necessary.

It is evident that in this case there is no longer a definite relation between $(s_k)^k$ and $\langle|\varphi|^k\rangle_{Av}$. To obtain the best estimate of Π and the standard deviation for this estimate, we must know the distribution in $(s_k)^k$. For $k=2$, this problem has been solved in I. According to I the variable χ, defined by

$$\chi^2 = \frac{1}{2GQ}\sum_{i=1}^{n}\varphi_i^2 = \frac{ns_2^2}{2GQ}, \tag{21}$$

has a distribution function represented by the following equation,

$$F_n(\chi; x_0) = \left[\frac{2}{\Gamma(n/2)}\chi^{n-1}\exp(-\chi^2)\right]\times\left[1+\frac{1}{2G}\sum_{\nu=0}^{\infty}\alpha_\nu^{(n)}(x_0)\chi^{2\nu}\right], \tag{22}$$

where

$$\alpha_\nu^{(n)}(x_0) = \frac{2}{\pi^{\frac{1}{2}}}\frac{\Gamma(1+n/2)\Gamma(\nu+\frac{1}{2})}{\Gamma(\nu+n/2)}\alpha_\nu(x_0),$$

and the $\alpha_\nu(x_0)$ are given in Eq. (8).

According to the definition of χ and the meaning of $F_n(\chi; x_0)$, the probability that, for a given Π, the rms angle of scattering lies between s_2 and s_2+ds_2 is

$$\psi_n(s_2, \Pi)ds_2 = F_n(\chi; x_0)(\partial\chi/\partial s_2)ds_2. \tag{23}$$

This probability can also be written as $\chi F_n(\chi; x_0)ds_2/s_2$. In the case of momentum measurements the estimate of Π can be based only on the data of one track, i.e., one has only one value of s_2. Under the assumption that all values of Π are *a priori* equally probable, the logical choice for Π is the "maximum likelihood estimate"[8] and is given by the solution of the equation

$$\partial\psi_n/\partial\Pi = (\partial/\partial\Pi)[\chi F_n(\chi; x_0)] = 0. \tag{24}$$

Since, for a given value of s_2, Π is a function of χ, the above equation is equivalent to

$$(\partial/\partial\chi)[\chi F_n(\chi; x_0)] = 0. \tag{25}$$

If one uses for F_n the "normal χ^2 distribution," i.e., if one neglects in Eq. (22) the terms proportional to $1/2G$, Eq. (25) becomes,

$$(\partial/\partial\chi)[\chi^n \exp(-\chi^2)] = 0, \tag{26}$$

which yields

$$\chi_l^2 \approx n/2. \tag{27}$$

Thus, from Eq. (21),

$$s_2 \approx (GQ)^{\frac{1}{2}} \tag{28}$$

or

$$\Pi_l \approx (m_e c^2/s_2)K_2 t^{\frac{1}{2}}. \tag{29}$$

One sees that this result is identical with that for large n [see Eq. (17)] in the case of the "normal approximation."

As a measure of the error we shall use the quantities $(\Delta\Pi)^+/\Pi_l$ and $(\Delta\Pi)^-/\Pi_l$ such that, if Π_l represents the position of the maximum of $\psi_n(s_2, \Pi)$, the function $\psi_n(s_2, \Pi)$ is $e^{-\frac{1}{2}}$ times its maximum value at the points $\Pi_l-(\Delta\Pi)^-$ and $\Pi_l+(\Delta\Pi)^+$, respectively. Table I gives the values of $(\Delta\Pi)^+/\Pi_l$ and $(\Delta\Pi)^-/\Pi_l$ for n between 1 and 10. For $n>10$ the following approximate formulas may be used:

$$\begin{aligned}\frac{(\Delta\Pi)^+}{\Pi_l} &= \left[1+\left(\frac{2}{n}\right)^{\frac{1}{2}}+\frac{2}{3n}+\frac{3}{4}\left(\frac{2}{n}\right)^{\frac{1}{2}}+\cdots\right]^{\frac{1}{2}}-1,\\ -\frac{(\Delta\Pi)^-}{\Pi_l} &= \left[1-\left(\frac{2}{n}\right)^{\frac{1}{2}}+\frac{2}{3n}-\frac{3}{4}\left(\frac{2}{n}\right)^{\frac{1}{2}}+\cdots\right]^{\frac{1}{2}}-1,\end{aligned} \tag{30}$$

which in the limit of large n reduce to

$$(\Delta\Pi)^+/\Pi_l = (\Delta\Pi)^-/\Pi_l = 1/(2n)^{\frac{1}{2}}. \tag{31}$$

From Table I the relative statistical error in the measurement of Π is, for $n=10$, approximately ± 20 percent. Since according to Eq. (31) the relative statistical error in the measurement of Π depends only on the number of plates traversed, it will be difficult to achieve an accuracy much better than this with a multiplate cloud chamber.

In addition to the statistical error, there is an experimental error arising from the uncertainty of the angular measurements. Let Δs_2 represent this experimental uncertainty in the value of s_2. From Eq. (17) the absolute value of the relative experimental error is

$$\Delta\Pi/\Pi = \Delta s_2/s_2. \tag{32}$$

The limit of accuracy for momentum measurements in a cloud chamber operated in a magnetic field is defined by the "maximum detectable momentum." In an analogous manner we introduce, using Eq. (29), a "maximum detectable Π."

$$\Pi_{\max} = (m_e c^2/\Delta s_2)K_2 t^{\frac{1}{2}}. \tag{33}$$

Using this definition, Eq. (32) may be written as follows:

$$\Delta\Pi/\Pi = \Pi/\Pi_{\max}. \tag{34}$$

As an example suppose that the plates are of lead, 2 cm thick, and that $\Delta s_2 = 0.5°$. Equation (18) gives $K_2 t^{\frac{1}{2}} = 3.42\times 10^3$ (deg) and Eq. (33) yields $\Pi_{\max} \sim 3.2$ Bev.

The procedure for the evaluation of Π and of the associated errors given above is based on the knowledge of the distribution in s_2 (Eq. 23). Since we do not have at our disposal a simple analytical expression for the distribution in s_1, a similar treatment of the errors in this case is not possible.

IV. MEASUREMENT OF MASS

As a second application of multiple scattering theory we shall consider the case of particles which reach the end of their range in one of the plates of the cloud chamber. We now have at our disposal an additional quantity, the residual range of the particle at each plate. From this quantity and from the scattering one can estimate the mass of the particle.

To simplify the procedure, it is useful to introduce a new variable η instead of the angle φ,

$$\eta = \varphi R^\alpha, \tag{35}$$

where R is the residual range and α is the constant appearing in Eq. (36) below. This new variable is a useful one because the following relation holds in all elements over a wide range of momenta ($0.05 < \Pi/(mc^2) < 2$)

$$R/mc^2 = A_Z(\Pi/mc^2)^{1/\alpha}, \tag{36}$$

where m is the mass of the particle, $\alpha = 0.55$ for all elements, and A_Z is a constant for a given scattering material ($A_{Pb} = 0.32$ g cm^{-2} Mev^{-1}, $A_{Al} = 0.20$ g cm^{-2} Mev^{-1}). The scattering variable $x = \varphi/(2GQ)^{\frac{1}{2}}$ which obeys the distribution given by Eq. (5), may be expressed in terms of η rather than in terms of φ, as follows:

$$x = \eta/\sqrt{2}\rho, \tag{37}$$

[8] See, for example, N. Arley and K. R. Buch, *Introduction to the Theory of Probability and Statistics* (John Wiley and Sons, Inc., New York, 1950), p. 137 ff.

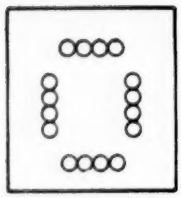

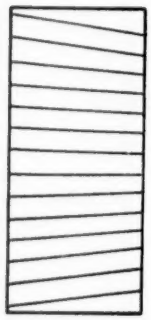

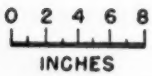

FIG. 1. Experimental arrangement for selecting stopped particles. A coincidence between the top tray, two or more G-M tubes in the bottom tray, and either or both side trays was required.

where

$$\rho=(GQ)^{\frac{1}{2}}R^{\alpha}=(4\pi r_e^2NZ^2A^{-1}lG)^{\frac{1}{2}}\times(m_ec^2A_Z)^{\alpha}(m_e/m)^{1-\alpha}. \quad (38)$$

Hence the variable η obeys the following distribution:

$$g(\eta;x_0)=f(x;x_0)dx/d\eta=\frac{1}{(2\pi)^{\frac{1}{2}}\rho}\exp\left(-\frac{\eta^2}{2\rho^2}\right)+\frac{1}{4\rho G(2\pi)^{\frac{1}{2}}}f^{(1)}\left(\frac{\eta}{\sqrt{2}\rho};x_0\right). \quad (39)$$

The advantage in using the above distribution lies in the fact that ρ is practically independent of the momentum (or velocity) of the scattered particle, and thus the distribution in η is the same for all plates of the cloud chamber. One may verify this by noting that (1) since the factor G is nearly constant for practically all values of β [see Eq. (10)] the parameter ρ is only a function of the characteristics of the scatterer and of the (unknown) mass of the scattered particle; (2) the dependence of the cut-off parameters x_0 on β may be disregarded, since x_0 appears only in the correction term of $g(\eta;x_0)$, and thus its accurate numerical value is of little influence on the distribution in η, except for $\eta\gg\rho$.

The explicit expressions for $\langle\eta^2\rangle_{Av}$ and $\langle|\eta|\rangle_{Av}$ follow directly from Eqs. (17) and (14), respectively. If one multiplies these equations by R^{α}, as defined by Eq. (36), one finds that

$$\langle\eta^2\rangle_{Av}^{\frac{1}{2}}=K_2l^{\frac{1}{2}}(A_Zm_ec^2)^{\alpha}(m_e/m)^{1-\alpha}, \quad (40)$$

and

$$\langle|\eta|\rangle_{Av}=K_1l^{\frac{1}{2}}(A_Zm_ec^2)^{\alpha}(m_e/m)^{1-\alpha}. \quad (41)$$

Table II shows calculated values of ρ, $\langle\eta^2\rangle_{Av}^{\frac{1}{2}}$ and $\langle|\eta|\rangle_{Av}$ for four different kinds of particles scattered in a 0.64-cm lead plate or in a 0.79-cm aluminum plate.

If the number n of observed scattering variables η_i is sufficiently large, one can simply equate the experimentally observed averages to the right-hand side of Eq. (40) or Eq. (41). Then one solves the resulting equation for m. In analogy with the measurement of momentum and Eqs. (20) and (19) we have

$$(S_k)^k=\frac{1}{n}\sum_{i=1}^{n}|\eta_i|^k, \quad (42)$$

and for large n,

$$(S_k)^k=\langle|\eta|^k\rangle_{Av}. \quad (43)$$

If n is not large it is again useful to have the distribution of the means, i.e., the distribution in $(S_k)^k$. Setting $\Psi_n(S_2,\rho)dS_2$ equal to the probability that a particle with the parameter $\rho(m)$ has a rms scattering variable between S_2 and S_2+dS_2 in traversing n plates of scattering material, we obtain from Eq. (22)

$$\Psi_n(S_2,\rho)=\left(\frac{n}{2\rho^2}\right)^{\frac{1}{2}}F_n\left\{\left(\frac{n}{2\rho^2}\right)^{\frac{1}{2}}S_2;x_0\right\}. \quad (44)$$

TABLE II. The values of the mass parameter ρ; the expected value of the rms of the variable η, $\langle\eta^2\rangle_{Av}^{\frac{1}{2}}$; and the expected value of the mean of the absolute values of the variable η, $\langle|\eta|\rangle_{Av}$ for different particles scattered in 7.3 g cm^{-2} of lead or 2.2 g cm^{-2} of Al.

	7.3 g cm^{-2} of Pb			2.2 g cm^{-2} of Al		
	ρ	$\langle\eta^2\rangle_{Av}^{\frac{1}{2}}$	$\langle\|\eta\|\rangle_{Av}$	ρ	$\langle\eta^2\rangle_{Av}^{\frac{1}{2}}$	$\langle\|\eta\|\rangle_{Av}$
μ-meson	58.5	59.3	46.7	10.6	12.20	9.01
π-meson	52.5	53.2	41.9	9.40	10.8	7.99
1000 m_e	29.5	29.9	23.5	5.30	6.08	4.51
proton	22.5	22.8	18.0	4.19	4.81	3.56

Differentiation of this equation with respect to S_2 shows that the maximum is given approximately by

$$(S_2)_{\text{most prob}} \approx [(n-1)/n]^{\frac{1}{2}}\rho. \tag{45}$$

[The exact expression is given in Eq. (I-41).]

Since the position of $(S_2)_{\text{most prob}}$ depends on ρ, it is evident that, for a mixture of particles with two different values of ρ, the resulting distribution in S_2 may consist of two well-separated parts. As we shall see in the following section, it is possible under some conditions to separate protons from π- or μ-mesons in a fairly unambiguous way using this method.

Thus the numerical values of ρ in Table II give an idea of the potentialities of the scattering method for the separation of particles of different masses.

V. EXPERIMENTAL RESULTS

We now turn to the discussion of a particular experiment which was not performed as a specific check of the present theory, but whose results give some confidence in the methods outlined above.

The experimental arrangement is shown in Fig. 1. It consisted of a cloud chamber 50 cm square and 16-cm illuminated depth. The chamber contained 14 lead plates 0.64 cm thick, and it was expanded by a penetrating shower detector of the type used by Tinlot[9] placed 0.7 meters above the chamber. Under these conditions most of the ionizing particles photographed in the chamber were protons and π-mesons. However, one would expect a few tracks of μ-mesons. Some of these arise from the decay of π-mesons which are produced in the nuclear event while others originate simply from unassociated μ-mesons. These latter traverse the chamber during its sensitive time and are recognized as not being of counter age. For our analysis, we have selected 72 pictures in which a particle appeared to stop after having traversed at least five lead plates.

In the case of any particular particle track, n then varies from a minimum of 5 to a maximum of 12, and individual mass measurements will have little significance. If, however, one can identify particle tracks from different pictures as having been caused by the same kind of particles, one can group all such data together to obtain a statistically significant value of $(S_k)^*$. For this purpose we have in what follows applied the third method mentioned in the introduction; i.e., we have used the experimental distribution in S_2 as a basis of separating meson tracks from proton tracks. After this procedure the separate data were grouped together and the mass values for the proton and meson calculated from Eq. (43).

To separate the protons from the mesons, we have chosen the following procedure: From the experimental data, we have computed for each accepted picture the quantity,

$$\xi = \left(\frac{n}{n-1}\right)^{\frac{1}{2}} S_2 = \left[\frac{1}{n-1}\sum_{i=1}^{n}(\varphi R^{\alpha})_i^2\right]^{\frac{1}{2}}, \tag{46}$$

[9] J. H. Tinlot, Phys. Rev. **73**, 1476 (1948).

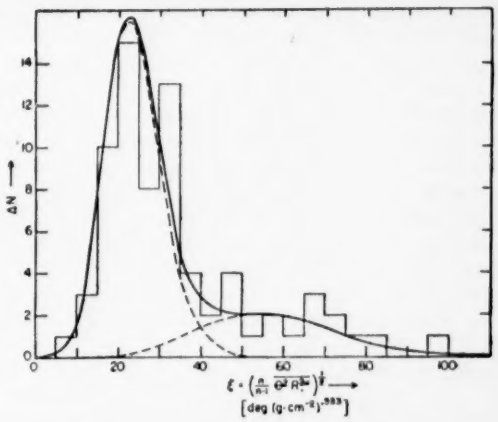

FIG. 2. The distribution in ξ for 72 stopped particles $[\xi^2 = \{1/(n-1)\}\Sigma\theta_i^2 R_i^{2\alpha}]$.

The histogram represents the observed distribution. The solid curve is the theoretical curve predicted by Eq. (49). The individual contributions by 55 protons and 17 mesons are indicated by the dashed curves.

where n is the number of Pb plates traversed by the particle in question. Since n varied from case to case, the position of the maximum of the distribution in S_2 would not be constant; however, according to Eqs. (45) and (46), the position of the maximum of the distribution in ξ is independent of n. Thus by the choice of the variable ξ one avoids an undue broadening of the distribution curve obtained by grouping together data corresponding to different values of n.

The 72 values of ξ obtained in this way have been plotted in the histogram shown in Fig. 2.‡ In order to compare this histogram with the theoretically predicted distribution in ξ, we have calculated values of the function:

$$G_n(\xi;\rho) = [(n-1)/2\rho^2]^{\frac{1}{2}} F_n\{[(n-1)/2\rho^2]^{\frac{1}{2}}\xi; x_0\} \tag{47}$$

separately for protons and mesons, taking as the average number of traversals observed per picture $n=7$. $G_n d\xi$ represents the probability of observing the variable ξ in the interval between ξ and $\xi+d\xi$, and it is normalized so that

$$\int_0^{\infty} G_n(\xi)d\xi = 1. \tag{48}$$

Evidently the observed distribution function should be represented by the following expression:

$$\Delta N = \{N_P(G_7)_{\text{proton}} + (72-N_P)(G_7)_{\text{meson}}\}\Delta\xi, \tag{49}$$

where ΔN is the number of cases where ξ lies between ξ and $\xi+\Delta\xi$, and N_P is the (unknown) number of protons. The best fit of Eq. (49) to the experimental data corresponds to $N_P = 55$, and therefore, $N_{\text{mes}} = 17$.

‡ *Note added in proof:*—The relation between the variable θ used in Figs. 2, 3, and 4, and the variable φ is given by Eq. (A4).

The curve defined by Eq. (50) with $N_P=55$ is represented by the solid line in Fig. 2.

After the number of protons and mesons has been established, it is not difficult to select the individual events corresponding to stopped protons and those corresponding to stopped mesons. Evidently it is most likely that the 55 values of ξ forming the *left* part of the histogram in Fig. 2 will correspond to protons and thus the remaining 17 values of ξ forming the "tail" of the histogram are due to the contribution of mesons. It turns out that the "separation value" of ξ given by the above procedure is 42.

By grouping together the 388 values of η corresponding to $\xi<42$, we obtain the following value for the proton mass

$$m_P=\left(1690\begin{matrix}+143\\-128\end{matrix}\right)m_e,$$

as calculating from Eq. (40); and

$$m_P=1610m_e,$$

calculated from Eq. (41). Similarly, the data contained in the group of tracks with $\xi>42$, 138 angles, yield for the meson mass

$$m_{\pi+\mu}=\left(213\begin{matrix}+32\\-26\end{matrix}\right)m_e$$

using Eq. (40), or

$$m_{\pi+\mu}=210m_e$$

using Eq. (41). The errors quoted are statistical and were obtained from a formula analogous to Eq. (31). The asymmetry in the error arises from the fact that $1/\rho$ is not a linear function of the mass.

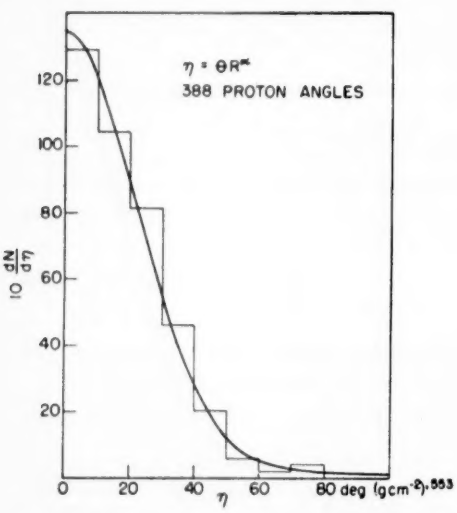

FIG. 3. The distribution in η for stopped particles with $\xi<42$. The histogram represents the observed distribution of 388 values of η. The curve represents the theoretical distribution computed for protons [Eq. (39)].

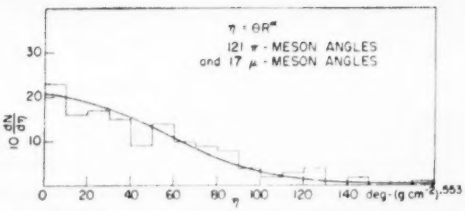

FIG. 4. The distribution in η for stopped particles with $\xi>42$. The histogram represents the observed distribution of 121 values of η obtained from "counter-age" tracks, and of 17 values of η obtained from post-expansion tracks. The curve represents the theoretical distribution computed for 121 scatterings of π-mesons and 17 scatterings of μ-mesons. [Eq. (39).]

Remembering that the mesons are mostly π-mesons, one sees that in all the above cases the experimental mass values are probably too small. Such a systematic discrepancy might be caused by the following effects: (a) the broadening of the distribution function introduced by the noise level scattering, (b) the bias introduced by our separation procedure for mesons and protons, (c) the decay of π-mesons in flight, and (d) scattering by other than electrostatic forces.

The first effect has been considered in I-Sec. IV, and its application to the present case is discussed in more detail in Appendix I. We note here that this effect is small for mesons but lowers the experimentally observed mass value of the proton by a few percent.

The second effect is more difficult to evaluate quantitatively. In our analysis we have assumed that all particles for which $\xi<42$ are protons and all particles for which $\xi>42$ are mesons. We estimate that this criterion mislabels two mesons and two protons. Thus our separation procedure makes 14 out of 388 proton angles too small and 14 out of 138 meson angles too large. Correspondingly, the experimental mass value of the proton should be slightly too high, and that of the meson appreciably too low.

Two of the π-mesons represented by the 14 counter-age meson tracks observed should have decayed before reaching the chamber. The expected value of the meson mass assuming that three of the tracks included in the analysis were post-expansion tracks of μ-mesons and that two π-mesons decayed before reaching the chamber is $255m_e$.

Finally, for the π-mesons and protons there is some nuclear scattering which modifies the observed mass values. The mean kinetic energies of the protons and mesons observed in the chamber are about 200 Mev and 100 Mev, respectively. Assuming that the total cross section for nuclear scattering is about geometric, one expects about one scattering angle in 25 to be modified by nuclear effects. In view of these uncertainties we have not attempted a rigorous correction of the data.

Figures 3 and 4 show the histograms of the observed distributions in η for protons and mesons, respectively. The solid lines represent the theoretical distributions as calculated from Eq. (39). While the agreement between

experiment and theory is satisfactory, we wish to emphasize that the determination of masses by the methods outlined above is as yet a rough procedure, and that a large amount of experimental work remains to be done before its accuracy can be considered as established.

VI. THE PROBLEM OF THE NUCLEAR SIZE, AND THE PROBABILITY OF LARGE ANGLE SCATTERING

Although the results discussed above show that there is no statistically significant discrepancy between experiment and theory, it is difficult to draw a definite conclusion as to whether the distribution function $f(x; x_0)$ is in better agreement with experiment than those given by Molière or by Williams. This results from the fact that, for the particular scattering layers used in our experiment (0.64-cm Pb plates) and for angles smaller than twice the rms value the values of the three distribution functions do not differ from one another by more than 3 percent. As far as the small angle scattering is concerned, the distribution $f(x; x_0)$ is noticably different from those given by Molière or Williams only for thicknesses of heavy materials greater than ~ 50 g cm^{-2}. One may verify this statement by comparing the three distributions in the limit as the angle of multiple scattering becomes zero. In the Gaussian approximation (Williams),[10]

$$f_W(0)=\frac{(GQ)^{\frac{1}{2}}}{\pi^{\frac{1}{2}}\sigma_W};\quad \sigma_W=\frac{E_s}{\sqrt{2}cp\beta}\left(\frac{t}{X_0}\right)^{\frac{1}{2}}, \tag{50}$$

where E_s = constant = 21 Mev and X_0 is the radiation length;[10] according to Molière,

$$f_M(0)=\frac{1}{\pi^{\frac{1}{2}}}\left(1+\frac{0.0365}{4G}\right),$$

and according to Eq. (5),

$$f(0; x_0)=\frac{1}{\pi^{\frac{1}{2}}}\left[1+\frac{1}{4G}\left\{0.0365+\frac{1-\exp(-x_0^2)}{x_0^2}-\mathrm{Ei}(-x_0^2)\right\}\right].$$

For thick layers of heavy scatterers x_0 becomes smaller than 1, and the value of $f(0; x_0)$ may exceed the value of $f_W(0)$ or of $f_M(0)$ by more than 5 percent. In Fig. 5 we illustrate this point by comparing the experimental results of Code[11] with the theoretical distributions. The solid curve is calculated by means of Eq. (5) and the dashed curve represents the Molière distribution which, for the small angles considered here, cannot be distinguished from the distribution of Williams.

Another basis for the comparison of the theories is the behavior of the "tail" of the distributions, i.e., the relative frequencies of scattering angles several times the rms value. Here the results of Williams and Molière differ as to order of magnitude. According to our modification of the Molière theory, the behavior of $f(x; x_0)$ for $x \gg 1$ depends strongly on the cut-off parameter x_0. Indeed, $f(x; x_0)$ approaches the Molière distribution [i.e., the distribution of single scattering, see Eq. (I-19)] for $x_0 \gg x$, and that of Williams (Gaussian distribution) for $x_0 \ll x$.

The controlling role of x_0 on the distribution function suggests some caution in the estimate of numerical values based on the behavior of the "tail." Evidently, in our highly schematic treatment of the effects of the finite nuclear size, Eq. (I-20) should be interpreted as giving the order of magnitude of x_0 rather than its accurate numerical value. In particular, there is no justification for identifying the effective radius for nuclear interaction R_n with that for electromagnetic interaction r_n. No quantitative results exist for lead, but the situation is indicated by the results of Amaldi *et al.* who have considered this problem for the Coulomb scattering of μ-mesons from light nuclei.[12] Their parameter b describing the nuclear dimensions, turns out to be about 30 percent smaller than R_n. At least this is the case for the coherent scattering of μ-mesons from protons, the latter being assumed point charges. The presence of incoherent scattering and the possibility of a finite value for the (electromagnetic) radius of the proton complicate further an accurate theoretical determination of r_n. In view of these difficulties we propose to express r_n as follows:

$$r_n=\Gamma R_n=0.49\Gamma r_e A^{\frac{1}{3}}, \tag{51}$$

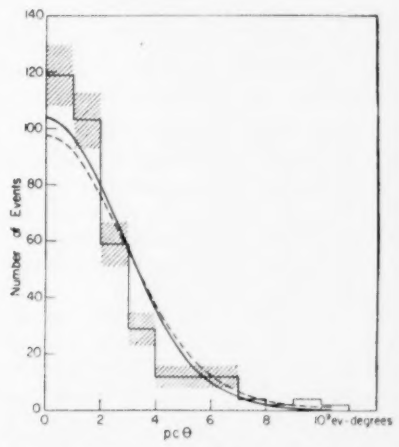

FIG. 5. The distribution in $(pc\theta)$ for cosmic-ray particles at sea level which traverse 3.8 cm of tungsten. The histogram represents the experimental results of Code with corresponding statistical errors. The solid curve was computed by means of Eq. (5); the dashed curve represents the Molière distribution.

[10] See B. Rossi and K. Greisen, Revs. Modern Phys. **13**, 265 (1941).

[11] F. L. Code, Phys. Rev. **59**, 229 (1941).

[12] Amaldi, Fidecaro, and Mariani, Nuovo cimento **7**, 1 (1950).

TABLE III. The integral scattering probability $P(q;\Gamma)$ tabulated as a function of thickness for aluminum, iron, and lead for values of Γ between zero and one. q is the projected angle of scattering φ expressed in units of $(GQ)^{\frac{1}{2}}$ and Γ is an arbitrary parameter which fixes the cut-off angle for single Coulomb scattering.

				(a) $\Gamma=1$						
	Al			Fe			Pb			
$q\backslash t$ g cm^{-2}	1	10	100	1	10	100	1	7.3	10	100
1.0	0.3244	0.3220	0.3113	0.3241	0.3196	0.3000	0.3236	0.3152	0.3125	0.2838
1.5	0.1494	0.1451	0.1318	0.1490	0.1421	0.1210	0.1487	0.1367	0.1340	0.1071
2.0	0.0657	0.0605	0.0471	0.0651	0.0571	0.0395	0.0649	0.0525	0.0496	0.0311
2.5	0.0310	0.0260	0.0148	0.0304	0.0226	0.0106	0.0300	0.0187	0.0166	0.00678
3.0	0.0168	0.0126	0.00419	0.0163	0.00939	0.00238	0.0157	0.00645	0.00521	0.00106
3.5	0.0104	0.00691	0.00108	0.0099	0.00400	0.00046	0.00906	0.00210	0.00151	0.00010
4.0	0.0071	0.00412	0.00025	0.0067	0.00167	0.00008	0.00554	0.00062	0.00039	0.00000
4.5	0.0051	0.00256	0.00005	0.0046	0.00065	0.00002	0.00367	0.00016	0.00009	
5.0	0.0038	0.00158	0.00001	0.0029	0.00022	0.00000	0.00160	0.00003	0.00002	
				(b) $\Gamma=0.70$						
1.0	0.3245	0.3226	0.3163	0.3243	0.3216	0.3081	0.3242	0.3193	0.3176	0.2935
1.5	0.1495	0.1459	0.1369	0.1492	0.1445	0.1284	0.1494	0.1420	0.1395	0.1152
2.0	0.0658	0.0613	0.0519	0.0654	0.0596	0.0446	0.0657	0.0574	0.0550	0.0360
2.5	0.0311	0.0269	0.0180	0.0307	0.0251	0.0133	0.0310	0.0228	0.0207	0.0090
3.0	0.0169	0.0135	0.0061	0.0165	0.0121	0.0034	0.0166	0.0094	0.0078	0.0018
3.5	0.0105	0.0078	0.0019	0.0102	0.0061	0.00083	0.0100	0.0040	0.0029	0.00030
4.0	0.0072	0.0050	0.00063	0.0069	0.0031	0.00016	0.00655	0.0016	0.0010	0.00004
4.5	0.0052	0.0034	0.00018	0.0050	0.00167	0.00004	0.00449	0.00055	0.00029	0.00001
5.0	0.0039	0.0017	0.00005	0.0035	0.00079	0.00001	0.0026	0.00020	0.00011	0.00000
				(c) $\Gamma=0.50$						
1.0	0.3245	0.3229	0.3192	0.3243	0.3222	0.3140	0.3244	0.3214	0.3204	0.3023
1.5	0.1495	0.1464	0.1408	0.1495	0.1455	0.1344	0.1498	0.1447	0.1434	0.1232
2.0	0.0659	0.0618	0.0554	0.0655	0.0607	0.0494	0.0662	0.0601	0.0586	0.0410
2.5	0.0312	0.0274	0.0211	0.0308	0.0263	0.0161	0.0314	0.0256	0.0240	0.0114
3.0	0.0170	0.0140	0.0084	0.0166	0.0130	0.0050	0.0170	0.0120	0.0106	0.0026
3.5	0.0106	0.0083	0.0035	0.0103	0.0073	0.0014	0.0105	0.0063	0.0053	0.00057
4.0	0.0073	0.0055	0.0014	0.0070	0.0045	0.00034	0.0071	0.0034	0.0025	0.00011
4.5	0.0053	0.0039	0.00055	0.0051	0.0029	0.00008	0.0050	0.0019	0.0013	0.00002
5.0	0.0041	0.0024	0.00018	0.0039	0.0013	0.00002	0.0033	0.0005	0.0003	0.00000
				(d) $\Gamma=0$ (Molière)						
1.0	0.3246	0.3232	0.3223	0.3245	0.3232	0.3223	0.3248	0.3236	0.3234	0.3225
1.5	0.1496	0.1468	0.1448	0.1497	0.1466	0.1447	0.1501	0.1475	0.1471	0.1450
2.0	0.0660	0.0622	0.0597	0.0657	0.0621	0.0596	0.0665	0.0631	0.0627	0.0600
2.5	0.0313	0.0278	0.0255	0.0310	0.0277	0.0254	0.0318	0.0287	0.0282	0.0258
3.0	0.0171	0.0144	0.0126	0.0168	0.0143	0.0126	0.0174	0.0151	0.0147	0.0129
3.5	0.0107	0.0088	0.00750	0.0105	0.00870	0.00745	0.0110	0.00923	0.00899	0.00767
4.0	0.0074	0.0060	0.00508	0.0072	0.00594	0.00505	0.00753	0.00632	0.00615	0.00520
4.5	0.0054	0.0044	0.00374	0.0053	0.00438	0.00372	0.00556	0.00466	0.00453	0.00383
5.0	0.0042	0.0035	0.00292	0.0042	0.00342	0.00290	0.00434	0.00364	0.00354	0.00299

where the dimensionless parameter Γ is to be determined experimentally. An underground experiment on the large-angle scattering of μ-mesons would seem to be the most reliable method for the determination of Γ, since the measurements would not be affected by the presence of particles (protons or π-mesons) with large cross sections for nuclear interactions.

To facilitate a comparison of the experimental results with the theoretically predicted distributions we tabulate below the integral distribution of multiple scattering, i.e., the quantity

$$P(q;\Gamma)=2\int_{q/\sqrt{2}}^{\infty} f(x;x_0)dx. \tag{52}$$

Tables IIIa to IIId give $P(q;\Gamma)$ for several thicknesses and for three different materials under various assumptions as to the magnitude of Γ. Note that q is the projected angle φ expressed in units of $\sigma=(GQ)^{\frac{1}{2}}$ (or the variable η in units of ρ), so that $P(q;\Gamma)$ represents the probability to observe an absolute value of the angle equal to or larger than q times the rms value. The data for lead have been given as a function of absorber thickness in Fig. 6. In particular note that Table IIId for $\Gamma=0$ (i.e., $x_0=\infty$), represents the *integral Molière distribution*. A comparison of the four tables shows that $P(q;\Gamma)$ depends strongly on the assumed value of Γ; the dependence is particularly pronounced in the case of lead (see Fig. 6).

ACKNOWLEDGMENT

The authors are greatly indebted to Professor Bruno Rossi for his active assistance in the preparation of this paper and to Dr. George Clark for many helpful discussions. We are also grateful to Mrs. Patricia Halpern for performing the numerical calculations.

APPENDIX I

The Effect of the Momentum Loss in the Plate

In the method of mass measurement given above we have neglected the momentum loss of the particle in traversing a single plate. We have also tacitly assumed that the residual range is accurately known whereas it is usually uncertain by the thickness of one scattering plate. We will now outline the actual procedure of measurement and show that its accuracy is not seriously affected by these two approximations.

In the measurements discussed in Sec. V values of η were calculated for each plate assuming that the particle traversed an integral number of plates below the one in which it was scattered. Let us call the plate in which the particle stopped plate number zero, and number successive plates above this one in increasing order. Thus the residual range is measured from the center of the scattering plate in question to the center of the plate in which the particle stops. Of course the actual point of stopping is uncertain, and the fractional error in the residual range becomes large for small plate numbers. In our calculation of mass values, therefore, the quantity η was only computed if the plate number was two or greater.

In order to justify this procedure we will calculate the correction to the mean square angle of scattering taking into account the momentum loss in the scatterer. In this case Π has to be considered as a function of the thickness t', $(0\leqslant t'\leqslant t)$, and is given at any point of the nth plate by

$$\Pi_n(t')=\langle\Pi\rangle_n\left(1+\frac{2t'-t}{2\bar{R}_n}\right)^{\alpha}, \tag{A1}$$

where $\bar{R}_n$ is the range measured from the mid-point of plate number n to the actual point of stopping, and $\langle\Pi\rangle_n$ is the corresponding value of $pc\beta$. Equation (A1) follows directly from Eq. (36).

As a consequence of Eq. (A1) the ms angle of scattering is now given by

$$\begin{aligned}\langle\varphi^2\rangle_{\text{av}}{}^{(n)}&=K_2{}^2(m_e c^2)^2\int_0^t\frac{dt'}{\Pi_n(t')}\\&=K_2{}^2\left(\frac{m_e c^2}{\langle\Pi\rangle_n}\right)^2 t\kappa_n(\epsilon),\end{aligned} \tag{A2}$$

where ϵt denotes the thickness which the particle penetrates in plate zero, and

$$\begin{aligned}\kappa_n(\epsilon)&=\frac{1}{t}\int_0^t dt'\Big/\left(1+\frac{2t'-t}{2\bar{R}_n}\right)^{2\alpha}\\&=\frac{n+\frac{1}{2}+\epsilon}{2\alpha-1}\left\{\left(\frac{n+\epsilon-\frac{1}{2}}{n+\epsilon-1}\right)^{2\alpha-1}-\left(\frac{n+\epsilon-\frac{1}{2}}{n+\epsilon}\right)^{2\alpha-1}\right\}.\end{aligned} \tag{A3}$$

A comparison of Eq. (A3) with Eq. (17) shows that the factor $\kappa_n(\epsilon)$ represents the correction for the momentum loss in the nth plate. Table IV shows

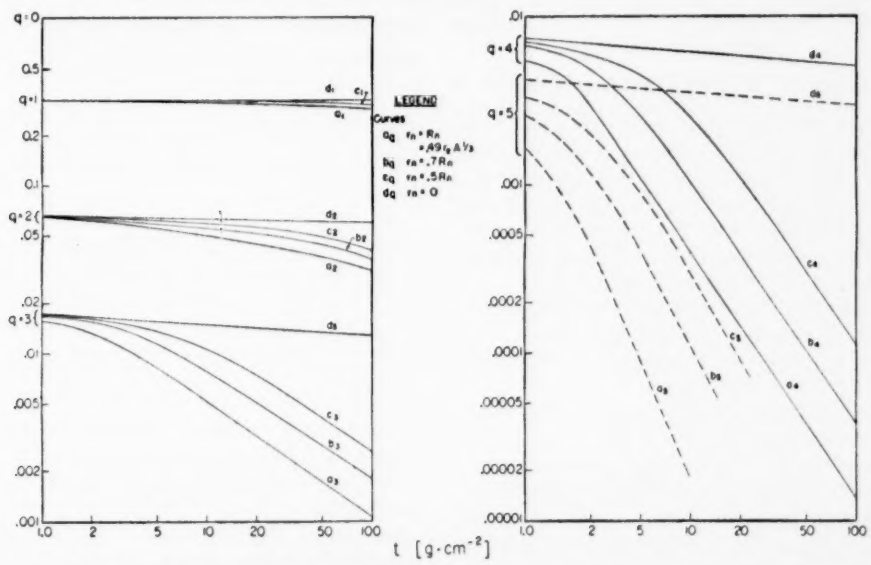

FIG. 6. The integral probability of multiple scattering, $P(q,\Gamma)$, for lead plotted as a function of the thickness t for various values of q. The quantity q represents the scattering angle φ expressed in units of $\sigma=(QG)^{\frac{1}{2}}$ or the variable η expressed in units of ρ. The four curves, a, b, c, and d, for each value of q correspond to different assumptions on the numerical value of the effective nuclear radius. Curves d_q represent the integral probability of the multiple scattering for point nuclei (Molière probability); curves a_q were computed under the assumption that the effective nuclear radius for Coulomb scattering is equal to the radius for nuclear interactions; curves b_q and c_q represent the intermediate cases.

TABLE IV. Numerical values of the correction function $\kappa_n(\epsilon)$. The body of the table gives the fractional increase in the mean square angle of scattering in the nth plate which results from the momentum loss which the particle suffers in traversing this plate. ϵt is the distance the particle penetrates into the plate in which it comes to rest.

$n \backslash \epsilon$	0.00	0.10	0.25	0.50	0.75	1.00
1	∞	1.54	1.25	1.12	1.07	1.05
2	1.05	1.04	1.03	1.03	1.02	1.02
3	1.02	1.02	1.01	1.01	1.01	1.01
4	1.01	1.01	1.01	1.01	1.01	1.01
5	1.01	1.01	1.01	1.00	1.00	1.00
6	1.00	1.00	1.00	1.00	1.00	1.00

numerical values of κ_n for a few values of ϵ and for n between one and six. The cases $\epsilon=1$ and $\epsilon=0$ give upper and lower limits for possible values of $\kappa_n(\epsilon)$. Note that, for $n>1$, κ_n differs from unity by 5 percent or less. Hence our procedure for computing the mass is justified.

To improve the statistical accuracy when only a limited amount of data is available, one would like to include measurements in the first plate. However, in this case the correction is appreciable and the first plate must be omitted unless the actual point of stopping is known. In some cases it is possible to determine the point of stopping quite accurately; e.g., the particle may stop in a plate and give rise to a visible decay product. Then one may use the exact value of the residual range measured from the center of the scattering plate to the point of stopping. The proper value of κ_n can be inferred from Table IV.

APPENDIX II

The Effect of "Noise Level" Scattering

The angular measurements which have been considered above are subject to two main sources of error; the track of a particle which suffers negligible real scattering in the gas between two plates is not straight because: (1) The track is made up of several "blobs" which sometimes correspond to δ-rays with an energy of several kilovolts. The center of the "blobs" will not in general define the trajectory of the particle and the extent to which the actual path can be determined is a function of the experimental conditions. (2) Even in the absence of the above effect there is an instrumental error in the determination of the scattering angles. This is due to the uncertainty in placing templates on the image of the track or in making measurements of the angles by any other means. We will call the combined effect of the above errors "noise level" scattering. Its effect on the observed angles of scattering was considered in I, Sec. IV.

It was shown there that in the "normal approximation" the expected value of the observed mean square angle of scattering is given by

$$\langle\theta^2\rangle_{Av}=(1+2\mu)\langle\varphi^2\rangle_{Av}, \tag{A4}$$

where $\langle\theta^2\rangle_{Av}$ is the expected value of the experimentally observed mean square scattering angle; $\langle\varphi^2\rangle_{Av}$ is the theoretically expected mean square scattering angle in the absence of "noise" [given by Eq. (17)] and μ is defined as:

$$\mu=\mathcal{T}_1^2/GQ. \tag{A5}$$

Here σ_1 is the standard deviation of the noise level scattering.

If we assume that there is no systematic error resulting from effect (1) above, σ_1 can be determined from a large number of measurements of the same scattering angle.

We have, however, used a somewhat different method and will now outline the procedure used to determine σ_1 experimentally. Let us call the observed angle between the particle track and an arbitrary line of reference ζ_i. (The observed angle of scattering θ_i is then given by the consecutive differences of ζ, i.e., $\theta_i=\zeta_{i+1}-\zeta_i$.) Consider now a large series of measurements of ζ on the same tracks by two independent observers. The observed angle ζ_i can be written as the sum of the true angle ϑ_i and the angle of noise level scattering γ_i. Thus for the two series of measurements,

$$\zeta_i=\vartheta_i+\gamma_i, \quad \text{and} \quad \zeta_i'=\vartheta_i+\gamma_i', \tag{A6}$$

since the true angle ϑ_i is the same for the two observers. The difference between two observations of the same angle is then just the difference in the noise level scattering, *viz.*,

$$\zeta_i-\zeta_i'=\gamma_i-\gamma_i'. \tag{A7}$$

We will assume that the mean square value of γ is independent of the value of ϑ, hence the mean square value of $\sigma_{\gamma-\gamma'}$ is given by

$$\sigma_{\gamma-\gamma'}^2=(1/n)\sum[(\gamma_i-\gamma_i')-\overline{(\gamma-\gamma')}]^2; \tag{A8}$$

and since the mean value of $\gamma-\gamma'$ is zero, Eq. (A8) becomes

$$\sigma_{\gamma-\gamma'}^2=(1/n)\sum(\zeta_i-\zeta_i')^2. \tag{A9}$$

If we assume that the distributions of γ_i and γ_i' are normal, the distribution of the difference $(\gamma_i-\gamma_i')$ is also normal. If, moreover, we assume that the two sets of observations have the same weight, we have for the mean square value of γ_i or γ_i',

$$\sigma_1^2=\tfrac{1}{2}\sigma_{\gamma-\gamma'}^2. \tag{A10}$$

Using this result we can determine the effect of the noise level scattering on the variable η and, therefore, upon the mass measurements. Let us call the value of η modified by the noise level scattering ω. In the mass measurement discussed in Sec. V we obtained from different particle tracks many values of ω for any given plate number i above the point of stopping. Hence we may express the expected value of ω in the ith plate as

$$\langle\omega_i^2\rangle_{Av}=\langle\theta_i^2\rangle_{Av}R_i^{2\alpha}=(1+2\mu_i)\langle\varphi_i^2\rangle_{Av}R_i^{2\alpha}, \tag{A11}$$

using Eqs. (35) and (A4). The averages are now func-

tions of i since μ depends on the momentum of the particle. Equation (A11) may also be written as

$$\langle\omega_i^2\rangle_{Av}=\left(1+\frac{2\sigma_1^2R_i^{2\alpha}}{\rho^2}\right)\langle\eta^2\rangle_{Av}\approx\langle\eta^2\rangle_{Av}+2\sigma_1^2R_i^{2\alpha}, \quad \text{(A12)}$$

since according to Eqs. (A7) and (38), σ_1 and ρ are independent of i.

Summing over i we have for a group of particles all of which penetrate n plates,

$$\langle\omega^2\rangle_{Av}=\langle\eta^2\rangle_{Av}+2\sigma_1^2\sum_{i=2}^{n}(il)^{2\alpha}/(n-1). \quad \text{(A13)}$$

The limits on the summation arise from the fact that we computed values of η for $n\geqslant 2$.

Using 55 values of $\zeta_i-\zeta_i'$ we evaluated σ_1 as 0.4 degrees. Using Eq. (A13) the mass of the proton is

$$m_P=1730m_e. \quad \text{(A14)}$$

Since the calculated correction for the noise level scattering depends on σ_1^2, it is quite sensitive to the evaluation of σ_1. In this evaluation our method of measuring angles was not the same as that used in the mass measurements; therefore, the correction is rather uncertain. We have performed the calculation chiefly as an illustration of the methods used.

PHYSICAL REVIEW VOLUME 89, NUMBER 6 MARCH 15, 1953

Pseudoscalar Matrix Element in Beta-Decay

M. RUDERMAN*
Columbia University, New York, New York
(Received December 3, 1952)

The interpretation of the β-spectrum of RaE seems to need a mixture of pseudoscalar and tensor interactions. Estimates of the necessary G_P give $G_P\gg G_T$ to compensate for the small pseudoscalar matrix element. This matrix element is greatly increased if the nucleon is in a potential which strongly mixes free particle states of positive and negative energies even though the diagonal terms are not large. Such an interaction arises from pseudoscalar meson theory. The pseudoscalar matrix element is calculated for the RaE decay assuming that the nucleons interact through pseudoscalar coupled pseudoscalar mesons. Exchange transitions, in which two nucleons exchange the charge and spin given to the electron and neutrino, predominate. The RaE spectrum can be fitted with $G_P\sim -G_T$. Exchange terms alter other momentum type matrix elements appreciably. Such effects are unimportant for gradient coupled pseudoscalar mesons.

I. INTRODUCTION

IN the β-decay of heavy nuclei the perturbation of the electron wave function by the Coulomb field of the nucleus plays a dominant role in determining the spectrum shape. This accounts for the allowed shape associated with most first forbidden transitions. Deviations from the allowed shape are small[1] except for the "unique forbidden" spectra ($\Delta I=2$, yes). The β-spectrum of RaE, assuming it is simple, is very different from the allowed or "unique forbidden" spectra. For many years this was explained as a second forbidden transition[2] ($\Delta I=2$, no).

Recently Petschek and Marshak[3] have pointed out that the shell model predicts unambiguously that the parity of RaE is odd. The final even-even nucleus should have even parity and the RaE β-decay cannot be second forbidden (no). Since a spin change greater than two gives much too large an ft value they attempted to interpret it as a first forbidden transition with $\Delta I=2, 1, 0$. All linear combinations of the β-interactions (S, V, A, T, P) not excluded by the Fierz condition were investigated. They found that the observed spectrum can be understood only if the decay is a $0\rightarrow 0$ transition. It is then possible to cancel those parts of the spectrum which usually dominate and give the allowed shape. The remaining terms give agreement with the measured RaE spectrum. The necessary cancellation is accomplished with a combination of tensor and pseudoscalar interactions such that

$$(G_P/G_T)\left[\int\beta\gamma_5\Big/\left(\int\beta\sigma\cdot\mathbf{r}/R\right)^*\right]\sim -\tfrac{1}{3}. \quad (1)$$

R is the nuclear radius $(e^2/2mc^2)A^{\frac{1}{3}}$. G_P and G_T are the Fermi constants for pseudoscalar and tensor β-interactions.[4] The increase in lifetime which results from the cancellation of the usually dominant terms in first forbidden transitions is enough to explain the large $\log ft$ of RaE.[5]

* National Science Foundation Postdoctoral Fellow on leave from University of California, Berkeley, California.

[1] All known first forbidden spectra with $\Delta I=1, 0$ have an allowed shape except RaE. This is to be expected only if there is no Fierz type interference between V and T, A and P, S and A. Only STP or VA are compatable with observed allowed and once forbidden spectra. See reference 6.

[2] E. J. Konopinski and G. E. Uhlenbeck, Phys. Rev. **85**, 308 (1952).

[3] R. E. Marshak and A. G. Petschek, Phys. Rev. **85**, 698 (1952).

[4] $\gamma_5=i\begin{pmatrix}0 & \mathrm{I}\\ \mathrm{I} & 0\end{pmatrix}$.

[5] E. J. Konopinski and L. M. Langer, *The Experimental Clarification of the Theory of Beta-Decay*, May, 1952 (to be published).

Ahrens, Feenberg, and Primakoff[6] have estimated the nuclear matrix element for the pseudoscalar interaction in $\Delta I=0$, (yes) transitions. In order to satisfy (1) they find

$$|G_P/G_T| \sim 1836A^{\frac{1}{3}}/Z = 133. \quad (2)$$

This large pseudoscalar coupling constant forced by the interpretation of the RaE spectrum is a peculiar feature. The β-decay of a free neutron is insensitive to the admixture of pseudoscalar interaction given in (2). If ψ_P and ψ_N satisfy Dirac equations for masses M_P and M_N,

$$\int d^4\chi(\psi_P^\dagger\gamma_5\psi_N)(\psi_e^\dagger\gamma_5\psi_\nu) = \frac{\hbar}{M_P+M_N}\int d^4\chi(\psi_P^\dagger\sigma_\mu\psi_N)\frac{\partial}{\partial\chi_\mu}(\psi_e^\dagger\gamma_5\psi_\nu). \quad (3)$$

For N a neutron and P a proton and an electron-neutrino energy of 1.3 Mev, (3) gives 0.1 percent the matrix elements of S, A, V, or T.

The very attractive hypothesis of a universal Fermi interaction among nucleons, electrons, neutrinos, and μ mesons must be abandoned unless $G_P \sim G_T$ or smaller. For the decay $\mu \to e+\nu+\nu$ according to (3) the matrix element of γ_5 is comparable to that of the other four interactions. Although the large pseudoscalar term of (2) does not affect the free neutron decay, its inclusion in μ decay gives a lifetime 10^5 shorter than observed.[7]

The average potential in which a nucleus moves inside of a nucleus is small next to the nucleon mass. It does not follow that the nucleon can be treated as almost free. Matrix elements of the potential off the energy shell (in the plane wave representation) can be much larger than the diagonal terms which yield the average. This is the case, for example, if a significant part of the nuclear force arises from pseudoscalar mesons with pseudoscalar coupling. The matrix element of γ_5 is then much greater than the estimate which leads to (2) and the otherwise weak pseudoscalar β-decay is greatly magnified. Cooperative transitions in which two nucleons exchange charge and momentum, which are in turn transferred to the electron and neutrino, predominate.

II. THE PSEUDOSCALAR BETA-DECAY INTERACTION

The Hamiltonian for pseudoscalar coupled mesons and nucleons interacting with the electron-neutrino field is

$$H = \int d\mathbf{x}\sum_{\alpha=1}^{3}\Big\{(\pi_\alpha)^2+(\nabla\varphi_\alpha)^2+(\varphi_\alpha)^2+\psi^*(\boldsymbol{\alpha}\cdot\mathbf{p}+\beta M)\psi \quad (4a)$$

$$+g\varphi_\alpha(\psi^*\beta\gamma_5\tau_\alpha\psi) \quad (4b)$$

$$+G_P\Phi\left(\psi^*\beta\gamma_5\left[\frac{\tau_1+i\tau_2}{2}\right]\psi\right), \quad (4c)$$

where

$$\Phi=(\psi_e^*\beta\gamma_5\psi), \quad \hbar=c=\mu=1, \quad (5)$$

and

$$[\pi(x),\varphi(x')]_- = -i\delta(x-x'),$$
$$[\psi_i^*(x),\psi_j(x')]_+ = \delta(x-x')\delta_{ij}.$$

Charge symmetric coupling is taken for the meson-nucleon interaction. Only pseudoscalar β-decay is considered here. To extract the major part of the β-decay matrix element is is useful to invoke the canonical transformation[8-10]

$$U=\exp(iS), \quad S=i\int(\psi^*\gamma_5\tau_\alpha\psi g\varphi_\alpha/2M)d\mathbf{x}, \quad (6)$$

so that

$$\bar{H}=U^{-1}HU$$

explicitly exhibits the nonrelativistic features of (4a) and (4b).

$$\bar{H}_{a+b}=\int d\mathbf{x}\sum_{\alpha=1}^{3}\Big\{(\pi_\alpha)^2+(\nabla\varphi_\alpha)^2+(\varphi_\alpha)^2+\psi^*(\boldsymbol{\alpha}\cdot\mathbf{p}+\beta M)\psi \quad (7a)$$

$$+\frac{g}{2M}\nabla\varphi_\alpha\cdot(\psi^*\tau_\alpha\boldsymbol{\sigma}\psi)+\frac{g^2}{2M}(\varphi_\alpha)^2(\psi^*\psi)\Big\}. \quad (7b)$$

Terms in higher powers of g have been omitted. The effect of all the omitted parts of (7) seems to be renormalization[11,12] of the pair coupling term of (7b),

$$g^2 \to \lambda g^2, \quad (8)$$

as long as only low energy meson-nucleon interactions are considered. The β coupling (4c) is also altered by (6).

$$\bar{H}_e=G_P\int d\mathbf{x}\Phi\Big\{\left(\psi^*\beta\gamma_5\left[\frac{\tau_1+i\tau_2}{2}\right]\psi\right)\left(1-\frac{\lambda g^2\varphi^2}{2M^2}\right) \quad (9a)$$

$$+\frac{\lambda g G_P}{2M}(\psi^*\beta\psi)(\varphi_1+i\varphi_2). \quad (9b)$$

(9b) does not contain the nuclear matrix element of γ_5 and can be much larger than (9a). The nucleon which is coupled to the electron-neutrino pair through (9b) does not change its charge. Rather the charge is taken from the meson field. The sources of this field, the neighboring nucleons, recoil to supply the spin, charge, and momentum carried off by the electron and neutrino.

In the interaction representation the lowest order (in λg^2) contribution to the β-decay with no real mesons

[6] Ahrens, Feenberg, and Primakoff, Phys. Rev. **87**, 663 (1952).
[7] The presence of pseudoscalar beta-interaction causes difficulty in understanding the absence of $\pi \to e+\nu$ [M. Ruderman and R. Finkelstein, Phys. Rev. **76**, 1458 (1949); M. Ruderman, Phys. Rev. **85**, 157 (1952)]. See, however, R. J. Finkelstein, Phys. Rev. **88**, 555 (1952).
[8] J. V. Lepore, Phys. Rev. **88**, 750 (1952).
[9] F. J. Dyson, Phys. Rev. **73**, 929 (1948).
[10] L. I. Foldy, Phys. Rev. **84**, 168 (1951).
[11] S. Drell and E. Henley, Phys. Rev. **88**, 1053 (1952).
[12] M. Ruderman, University of California Radiation Laboratory report 1876 July 1, 1952.

absorbed or emitted is the irreducible interaction.

$$H_\beta \equiv \frac{i}{2}\int dt'\epsilon(t,t')[\bar{H}_c(t),\bar{H}_b(t')]. \tag{10}$$

The transition amplitude for β-decay is then the matrix element of

$$\frac{1}{2\pi}\int_{-\infty}^{\infty} dt H_\beta.$$

The nonrelativistic limit of (10) is

$$\lambda G_P(g^2/4\pi)(\mu/2M)^2[\Phi(\mathbf{r}_2)(\tau_1+i\tau_2)_1(\boldsymbol{\sigma}\cdot\boldsymbol{\nabla})_1 \times V(r_{12})(1)_2+\Phi(\mathbf{r}_1)(\tau_1+i\tau_2)_2(\boldsymbol{\sigma}\cdot\boldsymbol{\nabla})_2 V(r_{12})(1)_1], \tag{11}$$

where

$$V(r_{12})=\exp(-\mu r_{12})/\mu^2 r_{12}. \tag{12}$$

The infinite correction to the matrix element for the decay of a single free nucleon, which is contained in (10), is included by renormalizing G_P in (9a) and will be ignored.[13]

III. ESTIMATE OF THE MATRIX ELEMENT FOR RaE

According to the shell model RaE has a neutron and a proton outside of a closed shell of 82 protons and 126 neutrons. Any changes in the structure of the core during the β-decay are neglected. The two nucleons outside of the core are assumed to be too far apart (about $A^{\frac{1}{3}}\hbar/\mu c$) to interact strongly with each other. It is in the spirit of the shell model to describe RaE by a Hartree wave function. The proton and neutron states of the core are the orthonormal sets

$$\psi_m{}^P \quad m=1,2,\cdots,82; \quad \psi_n{}^N \quad n=1,2,\cdots,126.$$

The beta-transition is the transfer of the extra core neutron from the state $\psi_I{}^N$ to the extra core proton state $\psi_F{}^P$. The matrix element of (11) for this transition is

$$2\lambda G_P(g^2/4\pi)(\mu/2M)^2\int\int d\mathbf{r}_1 d\mathbf{r}_2[\Phi(\mathbf{r}_2)\rho(\mathbf{r}_2) \times\langle\psi_F{}^{P*}(\mathbf{r}_1)\boldsymbol{\sigma}\psi_I{}^N(\mathbf{r}_1)\rangle\cdot\boldsymbol{\nabla}_1 V(r_{12}) \tag{13a}$$

$$-\sum_{n=1}^{126}\Phi(\mathbf{r}_1)\langle\psi_n{}^{N*}(\mathbf{r}_1)\psi_I{}^N(\mathbf{r}_1)\rangle \times\langle\psi_F{}^{P*}(\mathbf{r}_2)\boldsymbol{\sigma}\psi_n{}^N(\mathbf{r}_2)\rangle\cdot\boldsymbol{\nabla}_2 V(r_{12}) \tag{13b}$$

$$-\sum_{m=1}^{82}\Phi(\mathbf{r}_1)\langle\psi_F{}^{P*}(\mathbf{r}_1)\psi_m{}^P(\mathbf{r}_1)\rangle \times\langle\psi_m{}^{P*}(\mathbf{r}_2)\boldsymbol{\sigma}\psi_I{}^N(\mathbf{r}_2)\rangle\cdot\boldsymbol{\nabla}_2 V(r_{12}), \tag{13c}$$

where

$$\rho(r)=\rho_P(r)+\rho_N(r),$$

$$\rho_P(r)=\sum_{m=1}^{82}\psi_m{}^{P*}(r)\beta\psi_m{}^P(r)=(Z/A)\rho(r), \tag{14}$$

$$\rho_N(r)=\sum_{n=1}^{126}\psi_n{}^{N*}(r)\beta\psi_n{}^N(r)=(A-Z/A)\rho(r).$$

Equation (14) implies a uniform proton and neutron density throughout the core. Since $R\sim A^{\frac{1}{3}}\hbar/\mu c$,

$$\rho(r)=3\mu^3/4\pi, \quad r\leq R; \qquad =0, \quad r>R. \tag{15}$$

To evaluate (13b, c) it is necessary to know ψ^P and ψ^N but an estimate, independent of these functions, is obtained by the approximation

$$Y(r)\sim(4\pi/\mu)\delta(\mu r). \tag{16}$$

Equation (16) is certainly valid as long as the momentum transfers between nucleons 1 and 2 in (13b, c) are small next to μc. Substituting (16) in (13) and performing a partial integration, (13b) and (13c) become

$$-8\pi\lambda G_P(g^2/4\pi)(\mu/2M)^2\Phi(R) \times\int d\mathbf{r}[\tfrac{1}{2}\langle\psi_F{}^{P*}(\mathbf{r})\boldsymbol{\sigma}\cdot\boldsymbol{\nabla}\psi_I{}^N(\mathbf{r})\rangle\rho_N(r) \tag{17a}$$

$$-\tfrac{1}{2}\langle\psi_F{}^{P*}(\mathbf{r})\boldsymbol{\sigma}\cdot\boldsymbol{\nabla}\psi_I{}^N(\mathbf{r})\rangle\rho_P(r) \tag{17b}$$

$$-\langle\psi_F{}^{P*}(\mathbf{r})\boldsymbol{\sigma}\cdot\sum_{n=1}^{126}\boldsymbol{\nabla}\psi_n{}^N(\mathbf{r})\rangle\langle\psi_n{}^{N*}(\mathbf{r})\psi_I{}^N(\mathbf{r})\rangle \tag{17c}$$

$$\times\langle\psi_F{}^{P*}(\mathbf{r})\sum_{m=1}^{82}\boldsymbol{\nabla}\psi_m{}^P(r)\rangle\langle\psi_m{}^{P*}(\mathbf{r})\cdot\boldsymbol{\sigma}\psi_I{}^N(\mathbf{r})\rangle]\mu^{-4}. \tag{17d}$$

The variation of $\Phi(r)$ over the nucleus gives a much smaller contribution than (17) and has been neglected. (17c) and (17d) vanish if the core is everywhere isotropic. When (14) and (15) are used, (17a) and (17b) give

$$-3\lambda G_P(g^2/4\pi)(\mu/2M)^2 \times\Phi(R)\left(\frac{A-2Z}{A}\right)\int d\mathbf{r}\langle\psi_F{}^{P*}\boldsymbol{\sigma}\cdot\boldsymbol{\nabla}\psi_I{}^N\rangle\mu^{-1}. \tag{18}$$

The matrix element in (18) has been investigated by Ahrens and Feenberg.[14] They find

$$\int\boldsymbol{\sigma}\cdot\boldsymbol{\nabla}=\frac{Me^2Z\Lambda}{2\hbar}\int\frac{\boldsymbol{\sigma}\cdot\mathbf{r}}{R}. \tag{19}$$

Λ is a nuclear structure factor, estimated to be 1 for a heavy nucleus. Pursey,[15] using a specific model, deduces

[13] The mesic corrections to free nucleon beta-decay have been investigated by Kotani, Machida, Nakamura, Takebe, Umezawa, and Yoshimura. Prog. Theor. Phys. **6**, 1007 (1951). The correction to the allowed shape is of order $(\Delta p/M)^2(g^2/4\pi)(\mu/2M)$, which is quite negligible. The change in magnitude of the Fermi constant cannot be calculated. One could, in this way, get a large G_P for nucleons without spoiling the possibility of a universal Fermi interaction, but the mesic radiative corrections to the other nuclear beta-interactions could not change their order of magnitude.

[14] T. Ahrens and E. Feenberg, Phys. Rev. **86**, 64 (1952).

[15] D. L. Pursey, Phil. Mag. **42**, 1193 (1951).

(19) with A equal to 2. The estimate (19) makes it possible to compare (13b) and (13c) with (1) without knowledge of the initial and final nucleon states. The evaluation of (13a), however, needs the amplitudes of the extra core states near the boundary of the core. (13a) has been integrated for $\psi_F{}^P$ and $\psi_I{}^N$ solutions of the wave equation in a spherical well of radius R. For a 0→0 transition for the RaE decay the shell model predicts for $\psi_F{}^P$ an $h_{9/2}$ state and for $\psi_I{}^N$ a first excited (one node) $g_{9/2}$ state. With these wave functions and the definition (12), (13a) gives

$$-(1.7)\lambda G_P(g^2/4\pi)(\mu/2M)^2\Phi(R)\int\boldsymbol{\sigma}\cdot\mathbf{r}/R. \quad (20)$$

IV. FERMI CONSTANT FOR PSEUDOSCALAR BETA-DECAY

From (1), (18), (19), and (20)

$$G_P\sim -G_T\left(\frac{4\pi}{\lambda g^2}\right)(0.02\Lambda+0.04)^{-1}. \quad (21)$$

To fit the low energy properties of the two-nucleon system Lévy[16] uses a value of 12 for $(\lambda g^2/4)$. This results in $G_P\sim -1.4G_T$, a decrease of 10^2 from (2). Although the numerical results cannot be taken very seriously, it does appear possible to increase the pseudoscalar matrix element by several orders of magnitude over the results obtained from (3). If the nuclear force is due to gradient coupled pseudosclar mesons it is again necessary for $G_P\gg G_T$.

It is apparent from (18) that the ratio of pseudoscalar to $\int\boldsymbol{\sigma}\cdot\mathbf{r}$ will decrease for lighter nuclei. (18) vanishes for a symmetric nucleus. (13a) and (20) are significant only when ψ_F and ψ_I are states of high orbital momenta.

V. EXCHANGE MATRIX ELEMENTS FOR OTHER BETA-INTERACTIONS

Other beta-interactions are affected by the transformation (6), although none as much as the pseudoscalar. The first forbidden tensor which also gives 0→0 (yes) transitions becomes

$$\tfrac{1}{2}G_T\{\Phi(1)(\beta\boldsymbol{\sigma}\cdot\mathbf{r})_1(\tau_1+i\tau_2)_1 +\Phi(2)(\beta\boldsymbol{\sigma}\cdot\mathbf{r})_2(\tau_1+i\tau_2)_2\} \quad (22a)$$

$$-iG_T(g^2/4\pi)(\mu/2M)^2\{\Phi(1)(\tau_1+i\tau_2)_1(\boldsymbol{\sigma})_1 \cdot\boldsymbol{\nabla}_1Y(1,2)(\beta\boldsymbol{\alpha}\cdot\mathbf{r})_2+\Phi(2)(\tau_1+i\tau_2)_2(\boldsymbol{\sigma})_2 \cdot\boldsymbol{\nabla}_2Y(2,1)(\beta\boldsymbol{\alpha}\cdot\mathbf{r})_1\}. \quad (22b)$$

[16] Maurice M. Lévy, Phys. Rev. **88**, 725 (1952).

Unlike (9) the exchange term does not dominate. In the representation (6) nucleons 1 and 2 are moving in weak potentials so that

$$2M(\beta\boldsymbol{\alpha}\cdot\mathbf{r})_{1,2}\sim -i(3+\boldsymbol{\sigma}\cdot\mathbf{L})_{1,2}. \quad (23)$$

With the approximations which lead to (18), (22b) gives

$$G_T(g^2/4\pi)(\mu/2M)^2A^{-\frac{1}{3}} \times\int\boldsymbol{\sigma}\cdot\mathbf{r}\left[\Lambda\alpha Z\left(\frac{21}{4}-\frac{3Z}{A}\right)+5.1\left(\frac{\mu}{2M}\right)\right] \sim 0.04G_T\int\boldsymbol{\sigma}\cdot\mathbf{r}. \quad (24)$$

$\int\beta\boldsymbol{\sigma}\cdot\mathbf{r}$ is only slighly altered by the inclusion of (22b) and the estimate (21) is virtually unchanged. The exchange terms associated with momentum type matrix elements are more important. Corresponding to (21a) and (21b) these interactions become

$$\tfrac{1}{2}iG_T\{\Phi(1)(\tau_1+i\tau_2)_1(\beta\boldsymbol{\alpha})_1+\Phi(2)(\tau_1+i\tau_2)_2(\beta\boldsymbol{\alpha})_2\} \quad (25a)$$

$$+G_T(g^2/4\pi)(\mu/2M)^2\{\Phi(1)(\tau_1+i\tau_2)_1(\boldsymbol{\sigma})_1\cdot\boldsymbol{\nabla}_1Y(1,2)(\boldsymbol{\sigma})_2 +\Phi(2)(\tau_1+i\tau_2)_2(\boldsymbol{\sigma})_2\cdot\boldsymbol{\nabla}_2Y(1,2)(\boldsymbol{\sigma})_1\}, \quad (25b)$$

$$\tfrac{1}{2}iG_P\{\Phi(1)(\tau_1+i\tau_2)_1(\gamma_5)_1+\Phi(2)(\tau_1+i\tau_2)_2(\gamma_5)_2\} \quad (26a)$$

$$+iG_P(g^2/4\pi)(\mu/2M)^2\{\Phi(1)(\tau_1+i\tau_2)_1(\boldsymbol{\sigma})_1 \cdot\boldsymbol{\nabla}_1Y(1,2)(\tau_3)_2+\Phi(2)(\tau_1+i\tau_2)_2(\boldsymbol{\sigma})_2\cdot\boldsymbol{\nabla}_2Y(1,2)(\tau_3)_1 -\Phi(1)(\boldsymbol{\sigma}\tau_3)_1\cdot\boldsymbol{\nabla}_1Y(1,2)(\tau_1+i\tau_2)_2 -\Phi(2)(\boldsymbol{\sigma}\tau_3)_2\cdot\boldsymbol{\nabla}_2Y(1,2)(\tau_1+i\tau_2)_1\}, \quad (26b)$$

$$\tfrac{1}{2}G_V\{\Phi(1)(\tau_1+i\tau_2)_1(\boldsymbol{\alpha})_1+\Phi(2)(\tau_1+i\tau_2)(\boldsymbol{\alpha})_2\} \quad (27a)$$

$$-iG_V(g^2/4\pi)(\mu/2M)^2\{\Phi(1)(\tau_1+i\tau_2)_1(\boldsymbol{\sigma})_1 \cdot\boldsymbol{\nabla}_1Y(1,2)(\boldsymbol{\sigma}\tau_3)_2+\Phi(2)(\tau_1+i\tau_2)_2(\boldsymbol{\sigma})_2 \cdot\boldsymbol{\nabla}_2Y(1,2)(\boldsymbol{\sigma}\tau_3)_1-\Phi(1)(\tau_3\boldsymbol{\sigma})_1\cdot\boldsymbol{\nabla}_1Y(1,2) \times(\tau_1+i\tau_2)_2(\boldsymbol{\sigma})_2-\Phi(2)(\tau_3\boldsymbol{\sigma})_2 \cdot\boldsymbol{\nabla}_2Y(1,2)(\tau_1+i\tau_2)_1(\boldsymbol{\sigma})_1\}. \quad (27b)$$

For $(g^2/4\pi)(\mu/2M)^2\sim 1/12$, (a) and (b) can be comparable.

This investigation originated from a remark of Dr. S. Moszkowski on the possible importance of velocity ($\boldsymbol{\alpha}$) dependent potentials on the pseudoscalar matrix element. It is a pleasure to thank him and Professor Robert Serber for helpful discussion.

Effect of X-Ray Irradiation on the Self-Diffusion Coefficient of Na in NaCl†

DILLON MAPOTHER*
Carnegie Institute of Technology, Pittsburgh, Pennsylvania
(Received December 8, 1952)

The self-diffusion coefficient of the sodium ion in sodium chloride is decreased if the crystal is exposed to x-rays during the diffusion process. This effect was observed at temperatures under 550°C and was not observed at higher temperatures.

THE self-diffusion coefficient for the sodium ion in sodium chloride has been measured for samples which were subjected to x-ray irradiation during the diffusion process. The results indicate that the rate of diffusion is decreased by exposure to x-rays while diffusion is occurring.

The diffusion measurements were made using a radioactive tracer technique which was described in an earlier paper.[1] For the present work a small furnace was constructed to hold two crystal samples at the same temperature and permit radioactive sodium to diffuse from an evaporated film of sodium chloride on one face of each crystal. One crystal was situated about one inch from the window of a Machlett, type A-2, x-ray tube (molybdenum target) so that the evaporated face intercepted about 80 percent of the emergent x-ray beam. The x-ray tube was operated at 48 kv and 18 ma. The other sample was well shielded from the x-rays, and the two samples were located symmetrically in the furnace to minimize the possibility of dissimilar temperature gradients in the samples. The temperature was measured with thermocouples embedded in each sample. The temperature of the crystals was constant within ±1°C during an experiment. The samples were cleaved from single crystal sodium chloride supplied by the Harshaw Chemical Company.

After the radioactive sodium had been allowed to diffuse the samples were sectioned, and the distribution of radioactivity as a function of distance from the evaporated face was compared for the two samples.

Solution of the diffusion equation for the one-dimensional case approximated in these experiments shows the concentration of radioactive sodium to vary with depth x and time of diffusion t, according to the relation

$$C = C_0/(\pi Dt)^{\frac{1}{2}} \exp(-x^2/4Dt), \qquad (1)$$

where C_0 is a constant and D is the diffusion coefficient. Thus the points in a plot of logarithm of radioactive intensity *versus* distance squared should lie along a straight line whose slope is proportional to the diffusion coefficient. The data for one run have been plotted in this way in Fig. 1, and it will be noted that the points for the unirradiated sample do, in fact, fall along a straight line as do the deepest points for the irradiated sample. It can also be seen from Fig. 1 that the diffusion rate for the irradiated sample is substantially smaller in a thin layer next to the evaporated face, since the slope in this region is steeper and also the general level of radioactivity below this region is lower than in the case of the unirradiated sample. Below the layer in which the diffusion rate is retarded, the diffusion rate for the irradiated sample is approximately the same as for the unirradiated sample. The same behavior was observed when the experiment was repeated with the crystals interchanged with respect to irradiation. Data taken at 527°C, 496°C, and 462°C showed the same effect illustrated in Fig. 1.

The occurrence of this effect depends upon the temperature at which the diffusion takes place. For sodium chloride as for the other alkali halide crystals there is a fairly well defined temperature above which the acti-

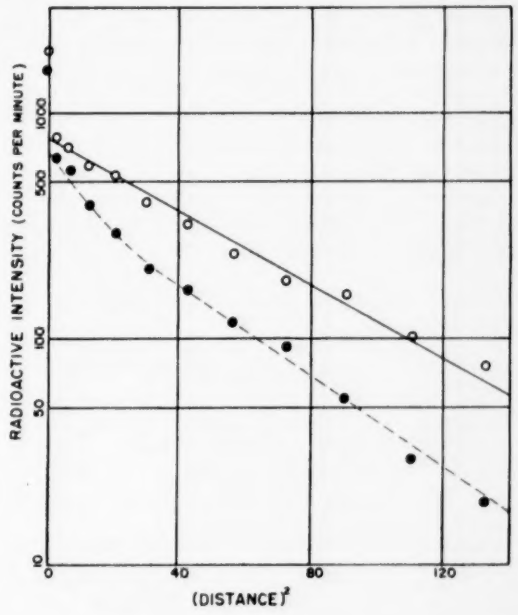

FIG. 1. Semilogarithmic plot of radioactive intensity *versus* square of distance below surface of crystal. Temperature of crystal 427°C. Diffusion time 3.75 days. Diffusion constant of unirradiated crystal 1.0×10^{-11} cm²/sec. Unit of length is 4.84×10^{-4} cm. ○ Unirradiated crystal. ● Irradiated crystal.

† This work received partial support from the U. S. Office of Naval Research.
* Now at the University of Illinois, Urbana, Illinois.
[1] Mapother, Crooks, and Maurer, J. Chem. Phys. **18**, 1231 (1950).

vation energy for diffusion has a distinctly higher value than in the lower temperature region. Above this temperature (which in the present case is about 550°C) the concentration of vacant lattice sites is believed to be determined by the temperature of the crystal and independent of the presence of impurity ions.[1] It is significant that the effect of x-ray irradiation shown in Fig. 1 was not present when the same experiments were performed at 567°C and 604°C.

This problem was suggested to the author by Professor R. J. Maurer, and the help of Dr. H. N. Crooks in performing these experiments is gratefully acknowledged. The author was assisted by a fellowship granted by the Westinghouse Corporation.

PHYSICAL REVIEW VOLUME 89, NUMBER 6 MARCH 15, 1953

Inelastic Scattering of Neutrons by Cd^{111}†

A. E. Francis, J. J. G. McCue, and Clark Goodman
Laboratory for Nuclear Science, Massachusetts Institute of Technology, Cambridge, Massachusetts

(Received November 10, 1952)

Neutrons with an energy spread of ±40 kev bombarded a disk of natural cadmium; among the products of bombardment was metastable Cd^{111m} produced by inelastic scattering. The yield of Cd^{111m} was measured from its threshold at 396 kev up to 1300 kev. Abrupt changes in the slope of the yield curve are interpreted as showing the onset of (n, n') excitation of higher levels. Such levels occur at 720 and 1150 kev. Below 720 kev, the Cd^{111m} was excited only by direct transition from the ground state. We have measured at 720 kev the cross section for this (n, n') event, which involves known changes of energy, spin, and parity. The cross section is about 10 millibarns.

THE existence of nuclear isomerism provides in some cases a practicable means of studying the inelastic scattering of neutrons. We have exploited this possibility in the case of Cd^{111}, a nuclide with an isomer, or metastable state, that has convenient half-life[1,2] and known spin.[3]

When a sufficiently energetic neutron is scattered from a nucleus, it may lose energy and leave the nucleus in an excited state. If this state is metastable, a gamma-ray or a conversion electron will be emitted later; detection of this radiation affords a means of tallying the inelastic scattering event. If the scattering leaves the nucleus in a state higher than the metastable one, the nucleus may make a transition to the metastable state before returning to the ground state. A curve showing the excitation of the metastable state as a function of neutron energy will therefore have a change of slope whenever a new excited state becomes energetically possible, provided that this state can decay to the metastable one. Moreover, if the neutron energy is such that the metastable state can be excited directly but not by decay, all metastable excitations will be caused by an inelastic scattering that leaves the nucleus in a known state. By measuring the cross section for such creation of the metastable state we measure the cross section for a *particular* inelastic scattering process.

TABLE I. Decay of metastable Cd^{111}.

Activity	49 min	8×10^{-3} sec
Conversion coefficient	2.2	0.06
K/L ratio	2.0	5.1
γ energy	150 kev	246 kev
K conversion energy	123 kev	219 kev
L conversion energy	146 kev	242 kev
K x-ray	23 kev	23 kev

Wiedenbeck[4] excited the 49-minute state of Cd^{111} by bombardment with x-rays and with electrons; he interprets these excitation curves as evidence for the existence of four excited levels above 1 Mev. Waldman and Miller[5] report two other levels in the same region. Hole,[6] using cadmium irradiated by neutrons, showed that the resulting metastable cadmium decays by the emission of two gamma-rays in cascade. Isotopically enriched cadmium showed[7] that the 49-minute state belongs to Cd^{111}. The energies of the gamma-rays were measured by Hole[6] and also by McGinnis,[8] who gives the gamma-ray energies as 149.6 kev and 246 kev. The 49-minute level is therefore 396 kev above the ground state. Deutsch and Stevenson[9] found that the 246-kev

† This work was supported by the U. S. Bureau of Ships and the U. S. Office of Naval Research. A portion of it was submitted by A. E. Francis (Lieutenant Commander, U.S.N.) in partial fulfillment of the requirements for the degree of Master of Science at the Massachusetts Institute of Technology.

[1] M. Dodé and B. Pontecorvo, Compt. rend. **207**, 287 (1938).

[2] M. L. Wiedenbeck, Phys. Rev. **66**, 36 (1944); Helmholtz, Hayward, and McGinnis, Phys. Rev. **75**, 1469 (1949).

[3] C. L. McGinnis, Phys. Rev. **81**, 734 (1951); Phys. Rev. **83**, 686 (1951); A. W. Sunyar, Phys. Rev. **83**, 864 (1951).

[4] M. L. Wiedenbeck, Phys. Rev. **67**, 92 (1945); see also reference 5.

[5] B. Waldman and W. C. Miller, Phys. Rev. **82**, 305 (1951).

[6] N. Hole, Arkiv Mat. Astron. Fysik **34B**, No. 19 (1947); also **36A**, No. 9 (1949).

[7] M. Goldhaber and C. O. Muehlhause, Phys. Rev. **74**, 1559 (1948).

[8] Helmholtz, Hayward, and McGinnis, Phys. Rev. **75**, 1469 (1949); C. L. McGinnis, Phys. Rev. **81**, 734 (1951).

[9] M. Deutsch and D. T. Stevenson, Phys. Rev. **76**, 184 (1949).

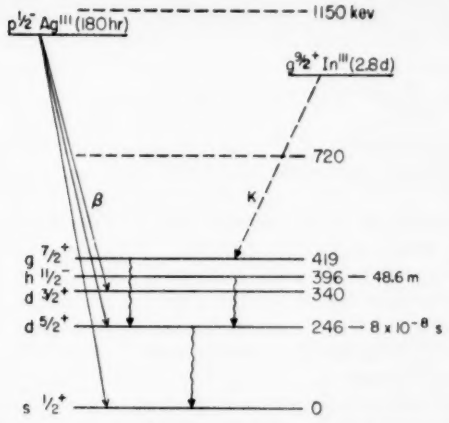

FIG. 1. Energy level diagram for Cd^{111}. The spin assignments and parities of the excited states are those of S. Johannson [Phys. Rev. **79**, 896 (1950)], McGinnis (reference 3), and Sunyar (reference 3). The two new levels found in the present work are shown at 720 and 1150 kev. Insufficient data are available to allow assignments of spins and parities for these states.

level has a half-life of 8×10^{-8} second; it is therefore the lower of the two levels. In addition to these two metastable levels, there is a 340-kev level observed in the β-decay of Ag^{111} (180 hr). A level at 419 kev has long been known, as a result of the work by Lawson and Cork[10] and by Bradt *et al.*[11] This level occurs in the decay of In^{111}. Figure 1 shows the lower levels and two new ones located in the present research.

The work reported in this paper falls into two parts. The first is a yield curve for the excitation of the 49-minute state by monoergic neutrons, as a function of neutron energy. This curve shows the relative cross section for creation of the 49-minute state by inelastic scattering of neutrons, and discloses two excited levels not hitherto reported. The second part is an absolute measurement of the cross section for creation of the 49-minute state by neutrons of a particular energy. This experimental cross section is in good agreement with the theoretical cross section computed by Hubscher and Margolis.[12]

I. THE EXCITATION FUNCTION

A. Experimental

Using neutrons with a total energy spread of about 80 kilovolts, we measured the yield of Cd^{111m} as a function of neutron energy up to 1400 kev. The neutrons resulted from the $Li^7(p, n)Be^7$ reaction in a rotating target of lithium metal on the Rockefeller electrostatic generator.[13] Neutron yield was measured with a cadmium-clad 8 in. long counter,[14] one meter from the lithium target, operating into a Model 100 amplifier[15] with 2-μsec clipping. The discriminator rejected counts due to gamma-rays.

Natural cadmium disks (99.8 percent pure), 3 cm in diameter and 0.16 cm thick, were located 4 cm from the target normal to and coaxial with the proton beam. Spectroscopic analysis showed that the only appreciable impurities were Cu and Pb.

After exposure, the disk was placed 3 mm from an anthracene crystal cemented with Canada balsam to an RCA 5819 photomultiplier tube. The crystal was about 3.7 cm in diameter and 8 mm thick; covering it was an aluminum reflector 6×10^{-3} mm thick. A cylinder of 1 mm mu-metal shielded the photomultiplier from magnetic fields, and the whole counter was encased in a light-tight lead shield 7.5 cm thick.

The accelerating potential for the photomultiplier came from a conventional electronically stabilized power supply, further stabilized by a bank of 12 type 5651 voltage-reference tubes[16] in series with a megohm. These tubes were in an enclosure to reduce thermal effects, and the power supply was never turned off during the experiment. The output of the photomultiplier fed a cathode-follower preamplifier working into a Model 100 amplifier with a delay line (0.8 μsec each way) for clipping.[17]

Background pulses were of two sorts, small and very large. We therefore used a single-channel differential discriminator, set to accept pulses in the range of 6 to 28 volts. With 1050 volts on the photomultiplier and the

TABLE II. Abundance and reaction products of cadmium isotopes. Radiative capture in Cd^{110}, which leads to the 48.6-min metastable state of particular interest, is found to be negligible at the neutron energies used in the present experiment. It is concluded that the fast neutron cross section for $Cd^{110}(n, \gamma)Cd^{111m}$ is much less than for $Cd^{110}(n, \gamma)Cd^{111}$. The 2.72-hr and 2.33-day half-lives of Cd^{117} and Cd^{115}, respectively, were observed, and appropriate corrections were made for their contributions to the observed activity. Since counting did not begin until several minutes after neutron irradiation, the activation, if any, of 2.3-min Cd^{113m} was not observed.

Isotope	Abundance	Possible product formed by exposure to neutrons	Half-life of product
Cd^{106}	1.22	$(n, \gamma)Cd^{107}$	6.7 hr
Cd^{108}	0.89	$(n, \gamma)Cd^{109}$	470 days
Cd^{110}	12.43	$(n, \gamma)Cd^{111m}$	48.6 min
		$(n, \gamma)Cd^{111}$	stable
Cd^{111}	12.8	$(n, n')Cd^{111m}$	48.6 min
		$(n, \gamma)Cd^{112}$	stable
Cd^{112}	24.1	$(n, \gamma)Cd^{113}$	stable
Cd^{113}	12.34	$(n, n')Cd^{113m}$	2.3 min
		$(n, \gamma)Cd^{114}$	stable
Cd^{114}	28.81	$(n, \gamma)Cd^{115}$	2.33 days
			43 days
Cd^{116}	7.66	$(n, \gamma)Cd^{117}$	2.72 hr

[10] J. L. Lawson and J. M. Cork, Phys. Rev. **57**, 982 (1940).
[11] Bradt *et al.*, Helv. Phys. Acta **19**, 77 (1946).
[12] L. Hubscher and B. Margolis (private communication) have applied the theory of W. Hauser and H. Feshbach [Phys. Rev. **87**, 366 (1952)] specifically to Cd^{111}.
[13] W. M. Preston and C. Goodman, Phys. Rev. **82**, 316 (1951); Hinchey, Stelson, and Preston, Phys. Rev. **86**, 483 (1952).
[14] A. Hanson and J. McKibben, Phys. Rev. **72**, 673 (1947).
[15] W. C. Elmore and M. Sands, *Electronics, Experimental Techniques* (McGraw-Hill Book Company, Inc., New York, 1949).
[16] W. A. Higinbotham, Rev. Sci. Instr. **22**, 429 (1951).
[17] See reference 15, p. 169.

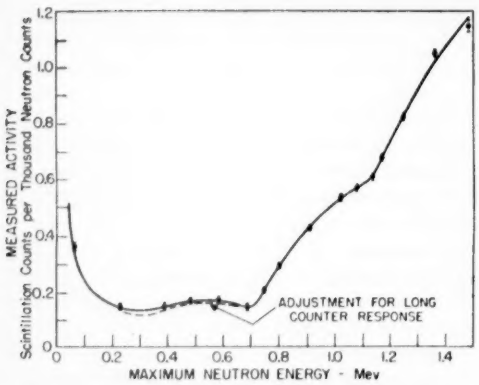
MEASURED ACTIVITY
Scintillation Counts per Thousand Neutron Counts
ADJUSTMENT FOR LONG COUNTER RESPONSE
MAXIMUM NEUTRON ENERGY - Mev

FIG. 2. Activity of disks as function of neutron energy.

amplifier gain at half-maximum, the pulses from Cd^{111} γ-activity were almost all counted. The ratio of desired counts to background counts was, with the lowest activities, as much as 10 times as large as the best ratio obtainable with an ordinary discriminator.

Because the 49-minute state decays in cascade, with internal conversion possible in each stage, Cd^{111m} produces several radiations. The various possibilities appear in Table I.[3] Practically all our Cd^{111} counts were from γ-rays, because the thickness of the Cd disks was about 25 times the range of the most energetic conversion electrons.

The many isotopes of Cd give rise to several unwanted activities. Table II[18] summarizes what may be expected. The large cross section of Cd for thermal neutrons is known[19] to be due to capture in Cd^{113}, the product being stable Cd^{114} with no metastable levels.

Exposure to the neutron flux lasted for 60 minutes for each disk, the beam current being about 6μa. Points on the uncorrected activation curve in Fig. 2 represent the total count in the period between 15 and 60 minutes after the end of the exposure. After obtaining Fig. 2, we exposed other disks to neutrons and counted for 3-minute intervals over periods of days.[20] From each resulting decay curve, we found what fraction of the total activity was due to Cd^{111m}. Figure 3 shows one such analysis. After one day, the decay curves such as Fig. 3 showed only the 2.33-day activity; in particular, 43-day Cd^{115} was not in evidence. In Fig. 4, the measured activity has been broken down into its components. The decay of each component was allowed for, so that the ordinates in Fig. 4 are the respective contributions to the activation curve in Fig. 2. The 15-minute interval between exposure and counting prevented any 2.3-minute activity of Cd^{113m} from making a detectable contribution.

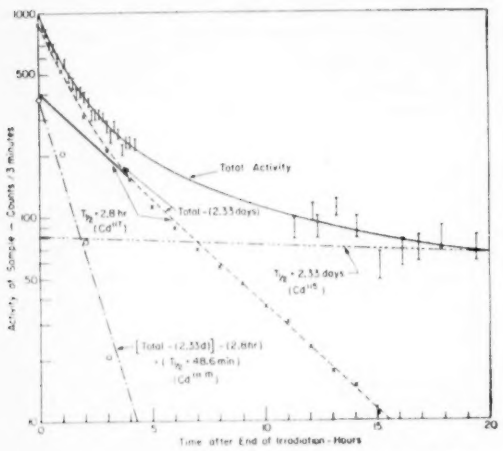

FIG. 3. Analysis of decay curve for irradiation of Cd by 592-kev neutrons.

The points on the total activation curve (Fig. 2) leave little doubt as to where the curve should be drawn. The points in Fig. 4, however, do not all fit on simple curves. It seems reasonable to assume that, when viewed with the resolution used in this experiment, the cross sections for formation of Cd^{115} and Cd^{117} vary slowly with neutron energy. We have therefore drawn simple smooth curves through the three sets of points. At each energy where the curves depart from the points, there is departure for at least two of the curves. The departure is such that, if more activity is ascribed to one component and less to another, the fit is very good for all curves. The single exception occurs at 950 kev, where the departures from the two lower curves cancel one another, and leave the departure from the 49-minute curve unexplained. This unexplained departure may indicate an excited level near 950 kev, which would produce a break in the curve at this energy. The evidence, however, is not conclusive.

Note that below about 400 kev, there is no detectable production of Cd^{111m}, which can in principle be formed by neutron capture in Cd^{110}. Since the natural abundances of Cd^{110} and Cd^{111} are nearly the same, we conclude that the cross section for formation of Cd^{111m} by capture is much smaller than the cross section for formation by inelastic scattering, when the latter mode of formation is energetically possible. Hughes[21] has obtained capture cross sections for neighboring elements at 1 Mev comparable in magnitude to the observed inelastic cross section of Cd^{111}. Since detectable amounts of Cd^{115} and Cd^{117} formed by radiative capture were observed, it is surprising that no appreciable production of Cd^{111m} resulted from $Cd^{110}(n, \gamma)$. Radiative capture cross sections decrease markedly with increasing neutron energy; therefore the absence below 400

[18] Table II is based on *Nuclear Data*, Circular 499 of the National Bureau of Standards (1950).

[19] A. J. Dempster, Phys. Rev. **71**, 144 (1947).

[20] During exposure, these foils were 2 cm from the lithium target. This small spacing introduced an additional spread in the neutron energy, but was needed in order to get enough activity to give a satisfactory number of counts.

[21] D. J. Hughes, private communication.

kev is adequate assurance that there was no contribution above this energy.

B. The Effect of Neutron Energy Spread

As measured by the position of the geometrical peak in the neutron yield,[22] the lithium target had a thickness of 60 kev at the (p, n) threshold. The resulting energy spread for neutrons emitted in the forward direction is 60 kev for 400-kev neutrons and 36 kev for 1500-kev neutrons. In addition, there was an energy spread because neutrons making any angle between 0 and 21 degrees with the forward direction could hit the disk. The spread from this cause alone is[23] 20 kev at 400 kev and 50 kev at 1500 kev. The neutron yield is nearly constant, at these energies, for angles between 0 and 21 degrees.[23] For the larger angles, however, the annular area intercepted at the disk is larger. The mean energy of neutrons striking the disk is less than the maximum energy E_{max} by 0.71 $(\Delta E)_\theta$, where $(\Delta E)_\theta$ is the total energy spread due to angle. The geometry of the scintillation counter discriminates to some extent against the activity at the edges of the disk. We therefore take the energy correction for angle to be 0.5 $(\Delta E)_\theta$, and the effective neutron energy to be $E=E_{max}-0.5\times[(\Delta E)_\theta+(\Delta E)_p]$, where $(\Delta E)_p$ is the total spread in neutron energy due to retardation of the protons in lithium. The term in brackets varies from 80 to 86 kev; calling it 80 kev throughout is an adequate approximation.

The breaks in the excitation curve come at thresholds for exciting new levels. The essential problem here is to locate such breaks; the effect of energy spread on the shape of the curve is relatively unimportant. If the minimum neutron energy is well above the threshold, it is sufficient to consider the mean energy as equal to the maximum energy minus half of the spread. Near a threshold, such a correction is not valid, because some of the neutrons counted are below the threshold. The correction for energy spread does not shift the position of the breaks, for the onset of a new activity depends on the maximum energy, not the mean energy. Figure 5 is obtained from the 49-minute curve of Fig. 4 by subtracting 40 kev from the energies of all points except those in intervals 0 to 80 kev above the breaks. Except at the first threshold, activity above a break is due partly to the excitation of a new state and partly to continuing excitation of the sort represented by the curve below the break. The latter component may be assumed to vary smoothly near the break. We therefore extrapolate each lower segment for a short distance beyond the break, and then shift it to the left by 40 kev. The corrected curve in Fig. 5 is then completed by extending each upper segment backward so that it joins the lower segment at the abscissa of a break in the uncorrected curve. The corrected curve closely approximates the effect of monoergic neutrons.

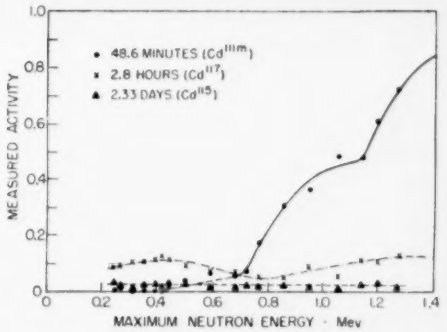

FIG. 4. Analysis of activity into its components.

II. THE CROSS SECTION

The corrected excitation curve in Fig. 5 gives the relative cross section for production of the 49-minute isomer by inelastic scattering. To get the actual cross section, we made a pair of exposures just after measuring the efficiencies of the long counter and the scintillation counter.

The long counter was calibrated by putting a 50 mg Ra—Be source at the point normally occupied by the lithium target. The fast neutron flux from the source had previously been determined by comparison with the 1.03 g Ra—Be source standardized by Dacey, Paine, and Goodman.[24] With the Ra—Be source at the place where the proton beam hit the lithium target, the over-all efficiency was 1.9×10^{-5}, with a probable error estimated at 10 percent.

The efficiency of the scintillation counter was measured by means of a standardized sample of Hg^{203}, whose 279-kev γ-rays were the nearest obtainable equivalent of the 246-kev γ-rays from Cd^{111m}. Hg^{203}, in the form of

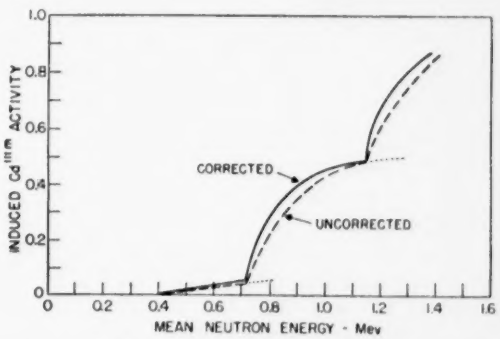

FIG. 5. The Cd^{111m} activity after correction for the spread in energy of the bombarding neutrons.

[22] R. Taschek and A. Hemmendinger, Phys. Rev. 74, 373 (1948).
[23] Willard, Preston, and Goodman, Technical Report No. 45, Laboratory for Nuclear Science and Engineering, Massachusetts Institute of Technology, 1950, unpublished.
[24] Dacey, Paine, and Goodman, Technical Report No. 23, Laboratory for Nuclear Science and Engineering, Massachusetts Institute of Technology, 1949 (unpublished).

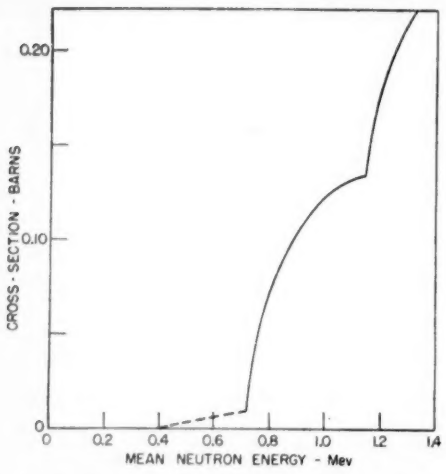

FIG. 6. The cross section for excitation of Cd^{111m} by inelastic scattering of neutrons.

the oxide, was sealed in a layer between two Lucite disks to imitate the geometry of the Cd disks. The Lucite was thick enough to stop the β-rays. A mechanically similar source consisting of Co^{60} on a filter-paper disk enveloped in Lucite was also prepared. The Co^{60} was pipetted from a solution with a disintegration rate that had been checked against a radium standard at the M.I.T. Radioactivity Center.[25] The method is that of Peacock.[26] As a check, the disintegration rate of the Co^{60} sample was also measured by the method of $\gamma-\gamma$ coincidences,[27] with the same result. Using the Co^{60} as a standard, we determined the efficiency of a brass-walled Geiger counter for the Co^{60} γ-rays (average energy 1.25 Mev). From this efficiency and the work of Bradt *et al.*,[11] the efficiency of the Geiger counter for 279-kev γ-rays was found, and the rate of γ-emission from the Hg^{203} sample determined. The Hg^{203} sample then served to measure the efficiency of the scintillation counter for 279-kev γ-rays. To avoid counts due to Hg x-rays, the gain of the amplifier was adjusted so that only pulses exceeding half the maximum height could pass the discriminator. The efficiency was 0.5 ± 0.1 percent.[28] The run to fix the cross section was made in the same way as the earlier ones, the mean neutron energy being 1270 kev. The amplifier gain following the scintillation counter was raised by 10 percent in order to compensate for the difference in scintillation pulses from 279-kev and 247-kev gammas. No attempt was made to correct for the difference in absorption of these two radiations in the crystal. The problem of the 150-kev γ-rays from Cd^{111} was alleviated by self-absorption in the cadmium (50 percent) and by the relatively large internal conversion coefficient (2.25). We have rather arbitrarily assumed that the efficiency of the counting apparatus was half as great for the 150-kev radiation as it was for 247 kev. If this estimate were wrong by 100 percent, the resulting error in cross section would be only 10 percent. Self-absorption in the cadmium eliminated the conversion electrons, and the discriminator stopped any pulses from x-rays. The over-all probability that a Cd^{111m} disintegration registered a count was 0.37 percent, with a probable error of about 30 percent. After the necessary corrections for isotopic constitution, unwanted activities, and Cd^{111m} decay, the cross section for creation of Cd^{111m} by 1270-kev neutrons is 0.21 ± 0.07 barn. Figure 6 shows the corrected curve of Fig. 5 plotted separately and scaled to fit the 1270-kev cross section.

The two upper segments of the curve are definitely concave downward. It is possible that the first segment should have the same sort of curvature, but here the data are equivocal. Re-examination of the half-life separations supports the idea that in Fig. 4 the Cd^{111} point at 506 kev is placed too high. There is no obvious defect, however, in the half-life separation at 592 kev (see Fig. 3). If the latter point is accepted, the cross section has a local maximum of 16 mb just below 600 kev. Although such a maximum cannot be ruled out, it seems physically unlikely, and the apparent errors in the other points at 592 kev in Fig. 4 imply that the Cd^{111} curve should be drawn as we show it, with the understanding that the lowest segment may have some curvature not revealed by the experiment.

It is of interest to compare the experimental cross section with that calculated by Hubscher and Margolis.[12] Unfortunately, such a comparison is meaningful only in the region below the first break in our curve, and in this region the large correction for unwanted activities subjects our cross section to considerable uncertainty. At 720 kev, the experiment gives 10 mb and the calculation gives 8.5 mb for spin 11/2 and only 1.3 mb for spin 13/2 (396-kev level). At 600 kev the experiment gives 6 mb and the calculation 3.5 mb for spin 11/2 and only 0.5 mb for spin 13/2. In this energy range our cross section can easily be wrong by as much as 50 percent. However, because of the strong dependence of cross section on spin change, the present agreement is quite good enough to serve as verification that the spin of the 396-kev level of Cd^{111} is 11/2. If separated Cd^{111} should become available in sufficient quantity, a more critical test of the theory would be possible. The comparison of measured and calculated cross sections may, therefore, be a practicable means of finding the spins of other metastable nuclides.

The authors wish to express their appreciation to Professor E. Guth for suggesting this problem and to Professor H. Feshbach, Dr. B. Margolis, and L. Hubscher for helpful discussions.

[25] The standardizing and pipetting of the Co^{60} solution were kindly performed by E. Backofen.

[26] W. C. Peacock, Ph.D. thesis, Massachusetts Institute of Technology, 1944 (unpublished) and Phys. Rev. **66**, 160 (1944).

[27] J. V. Dunworth, Rev. Sci. Instr. **11**, 167 (1940).

[28] Because of the change in amplifier gain, this efficiency is not applicable to Fig. 2.

Charge States of a Helium Beam in Hydrogen, Helium, Air, and Argon*

ELIAS SNITZER
Department of Physics and Institute for Nuclear Studies, University of Chicago, Chicago, Illinois
(Received November 28, 1952)

Measurements have been made of the fractions of a helium beam in the He^0, He^+, and He^{++} charge states in the energy range of 100 kev to 480 kev for beams in hydrogen, helium, air, and argon. For the four gases, the He^0 and He^+ components are equal for helium energies of 148 kev, 145 kev, 98 kev, and 115 kev, respectively. The ratios of the electron loss to electron capture cross sections between He^+ and He^{++} fitted a simple power dependence of $(\sigma_l/\sigma_c) \propto V^m$, where V is the velocity of the helium in the beam and m equals 6.1, 5.1, 5.2, and 6.3, respectively, for the four gases studied. For electron capture and electron loss between He^0 and He^+ the exponent m varies from 2.6, 2.0, 2.8, and 3.4 at 100 kev to 4.0, 4.0, 4.3, and 5.1 at 450 kev.

I. INTRODUCTION

WHEN a high energy ion beam passes through matter, it not only loses energy by exciting and ionizing the particles of the matter through which it traverses, but it also undergoes a process of charge exchange by capturing from, or losing electrons to, the matter being traversed. For singly charged ions such as protons and He^+, charge exchange between the neutral and singly ionized states does not become significant until the ion has been slowed down to where its velocity is comparable to the velocity of the outer electrons in the matter being traversed. The velocities at which exchange between multiply charged states is significant are higher. This paper relates the work done in determining the fractions of a helium beam in its three charge states, He^0, He^+, and He^{++}, for energies varying from 100 kev to 480 kev when the beam passes through hydrogen, helium, air, and argon.

The problem of the capture and loss of electrons by moving ions has been of interest since the discovery of canal rays. The earlier work has been reviewed by Rüchardt.[1] Singly charged alpha-particles were discovered by Henderson[2] in 1922. The experiments of Rutherford[3] on charge exchange for helium covered energies from 0.65 Mev to 6.78 Mev, and a considerable amount of work[4] on various ions for energies up to 100 kev has been reported, but no work has been done on helium in the interesting region of 100 kev to 500 kev, where most of the helium is in the single charged state. Recently, experiments have been carried out to determine the capture and loss cross sections for protons of energies from 20 kev to 400 kev.[5–9]

Besides the value in filling the gap for helium between Rutherford's high energy experiments and the work done up to 100 kev,[5,10–14] this problem is also of interest on other accounts. Accurate information regarding the fraction of a beam in a particular charge state is useful in experiments where the response of detectors and other apparatus is charge dependent. The process is important in the slowing down of fission fragments, for capture and loss of electrons is significant throughout the entire path of the fragment because of the large initial charge. The average charge of the ions in a beam affects the rate of energy loss by ionization and excitation of the medium, as indicated by the Bethe-Bloch formula. Also, the process of charge exchange itself contributes to the slowing down of the ion, for a cycle of capture and loss of an electron results in the creation of one ion pair.

II. DESCRIPTION OF APPARATUS

A. General

The singly ionized helium beam was produced by the University of Chicago 500 000-volt kevatron (Cockcroft-Walton generator). The beam was selected by a magnet H_1, which caused the accelerated He^+ ions to enter a port which made a 15° angle with the axis of the kevatron. The beam then entered the 74-cm long pipe A filled with the target gas. After passing through the pipe and undergoing charge exchange, the beam entered the evacuated magnetic deflection chamber B, where it was separated into its charged states. To maintain the gas pressure in the pipe without interfering either with the vacuum of the kevatron or the vacuum in the magnetic deflection chamber, one stage of differential pumping was used on either side of the pipe containing the gas. Differential pumping instead of a foil was used at the entrance to the pipe so as to make the apparatus durable and to avoid the difficulty of making and installing foils. Differential pumping had the additional advantage that it avoided difficulties

* This work was supported in part by a grant from the U. S. Atomic Energy Commission.

[1] E. Rüchardt, *Handbuch der Physik* (J. Springer, Berlin, 1933), Vol. **22**, No. 2, p. 103.
[2] G. H. Henderson, Proc. Roy. Soc. (London) **102**, 496 (1922).
[3] E. Rutherford, Phil. Mag. **47**, 277 (1924).
[4] A summary of the work done on protons, helium, and other ions is given in H. S. W. Massey and E. H. S. Burhop, *Electronic and Ionic Impact Phenomena* (Oxford University Press, London, 1952), Chap. VIII, Sec. 6.
[5] J. P. Keene, Phil. Mag. **40**, 369 (1949).
[6] T. Hall, Phys. Rev. **79**, 504 (1949).
[7] J. H. Montague, Phys. Rev. **81**, 1026 (1951).
[8] F. L. Ribe, Phys. Rev. **83**, 1217 (1951).
[9] H. Kanner, Phys. Rev. **84**, 1211 (1951).
[10] P. Rudnick, Phys. Rev. **38**, 1342 (1931).
[11] R. A. Smith, Proc. Cambridge Phil. Soc. **30**, 514 (1934).
[12] A. Rostagni, Nuovo cimento **12**, 134 (1935).
[13] F. Wolf, Ann. Physik **30**, 313 (1937).
[14] H. Meyer, Ann. Physik **37**, 69 (1940).

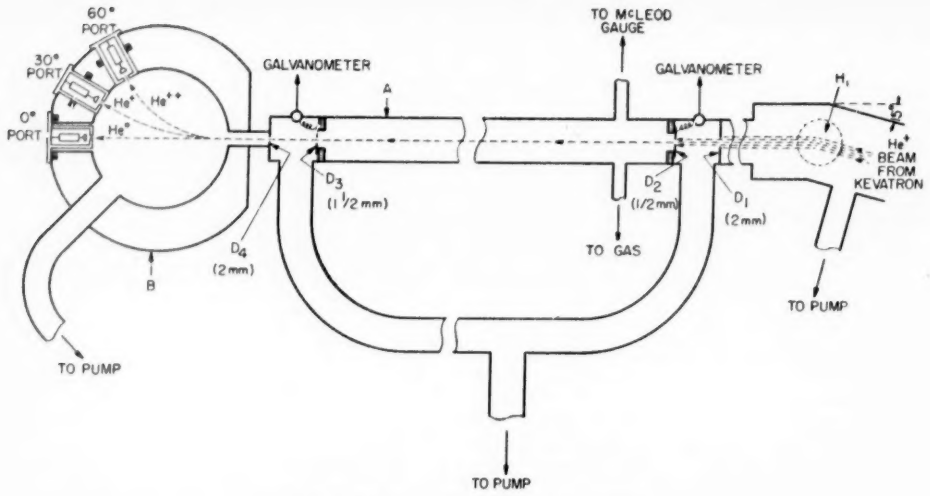

FIG. 1. Schematic drawing of the apparatus.

associated with determining the exact amount of slowing down of the beam as a result of passing through a foil. Of course, a foil could not be used at the emergent end of the pipe for the foil itself would have produced charge exchange. Figure 1 is a schematic drawing of the apparatus.

The energy of the beam particles was measured by the current drain through a resistor stack of 10^{10} ohms placed between the high voltage end of the kevatron and ground.

The pressure in the pipe was measured by a McLeod gauge. Pressures up to 8×10^{-2} mm of mercury were used in the pipe, but such a pressure did not cause the pressure in the magnetic deflection chamber to exceed 10^{-4} mm of mercury. The differential pumping sections were one inch long with two short lengths of $\frac{1}{2}$ in. i.d. tubing leading into the 2 in. i.d. tubing connecting to the vacuum pump.

The diameters of the holes through which the beam passed in entering and leaving the pipe are indicated in Fig. 1. Diaphragm D_2 was electrically insulated from the rest of the apparatus and connected to a galvanometer in order to use the current it collected as a monitor. Diaphragm D_3 was mounted behind another diaphragm with a $\frac{1}{4}$-in. hole and insulated from it. This arrangement greatly assisted alignment of the apparatus, for, when charge was collected on diaphragm D_3, the beam was no more than $\frac{1}{8}$ in. off from the center of D_3. The distance from D_2 to D_3 was 74 cm. The holes in D_1, D_2, D_3, and D_4 were aligned to within 0.005 in.

Except for one change, the magnetic deflection chamber and the magnet to provide its field were the same as used by Montague,[7] Ribe, and Kanner, and as described in detail by Montague. The change consisted of installing another port at 30° with respect to the incident beam direction. The magnet was water cooled. A dc motor-generator set rated at 220 volts and 6 amps activated the magnet. The output of the motor-generator set was controlled by a variable resistor in the self-excited shunt field of the generator.

B. The Detectors

The detectors each consisted of a thermistor Th_d enclosed in a nickel foil. (Figure 2 is a sketch of one of the detectors.) When the beam struck the foil the resultant heating of the foil and thermistor was measured by the change in resistance of the thermistor. The thermistors used were the type 27A thermistors manufactured by Western Electric.[15] These thermistors are beads of about $\frac{1}{2}$ mm in diameter with 0.001-in. nickel wire leads. The thermistor was enclosed in a cylindrical sheath of 0.001-in. thick nickel foil. The side of the cylindrical sheath facing the beam was flattened so that the entire beam struck the nickel surface perpendicularly. The flattened side of the sheath facing the beam was 5 mm high and 3 mm wide. Knife edges placed $\frac{1}{32}$ in. in front of the sheath stopped down the area exposed to the beam to 4 mm$\times2\frac{1}{2}$ mm. In this way, all the beam that entered the detector could hit only the nickel foil.

The nickel sheath was insulated from the thermistor by building up two globules G of glyptal paint on the wire leads on either side of the thermistor bead and having the nickel sheath rest on the hardened glyptal. The sheath was insulated from the thermistor so that the thermistor bead would not be electrically shorted out. Also, by this arrangement the sheath could be used to measure the charge collected, thus assisting in the alignment of the system by giving a rapid electrical response when the beam struck the detector.

The thermistor and sheath were mounted by solder-

[15] Becker, Green, and Pearson, Elec. Eng. 65, 711 (1946).

ing the leads from the thermistor to 0.008-in. thick nickel wires that were screwed fast to a piece of Lucite enclosed in the brass housing of the detector.

In addition to the detecting thermistor, another thermistor with approximately the same characteristics as the first was enclosed in the same housing in order to make possible the rapid and accurate reading of the ambient temperature. The additional thermistor Th_a was placed $\frac{1}{2}$ in. from the sheath of the detector thermistor, and out of sight from it so that the sheath could not radiate heat directly to it.

Leads from the thermistors and sheath were brought out through vacuum tight insulators at the base of the detector housing.

The geometry of all three detectors was alike. The detector in the 0° port was placed in an adjustable mounting which made possible adjustment in the position of the detector with respect to the beam. The 30° and 60° ports did not have such adjustable mountings, since the positions of the He^+ and He^{++} beams could easily be adjusted by the magnetic field.

III. EXPERIMENTAL PROCEDURE

The positioning of the beam so that it would pass through the differential pumping sections and enter the magnetic deflection chamber was facilitated by horizontal and vertical electrical deflecting plates placed at the exit end of the kevatron, the magnetic field H_1, and adjustable pole pieces on the analyzer magnet which permitted changes in the height of the magnetic deflection chamber B. The procedure followed was to first align the apparatus for a beam of given energy, then to admit gas to the pipe A. The helium, air, and argon were admitted through a needle valve, and the hydrogen via a palladium leak.

After gas was admitted, the beam was magnetically separated into its charged states. A rough indication of the correct current in the magnet to deflect the charged beams into their ports was obtained by observing beam currents collected on the nickel sheaths of the detectors. The exact value of the magnetic current was determined by taking a curve of the resistance change of the thermistor *versus* current in the magnet. In all cases the maximum heating occurred for the same magnet setting that gave the maximum charge collection. That being the case, in the later stages of the experiment the magnet settings were determined only by the maximum ion collection. Since the largest hole in the differential pumping system was 2 mm and the width of the detector entrances were $2\frac{1}{2}$ mm, the slight fluctuations in the current supply to the magnet could be tolerated. The beam currents were of the order of 10^{-8} ampere, but no attempt was made to get precise values by eliminating effects due to secondary electrons.

After allowing at least fifteen minutes for the temperature of the thermistors to come to equilibrium, their resistances were measured by a Wheatstone bridge. The resistances were measured several times with at least five minutes elapsing between measurements. Also, as a check that the correct magnet current was being used, sets of readings were taken for the current displaced either side of the original value. After the data were obtained, the thermistors were allowed to cool by deflecting the beam away from the apparatus and the resistance values of the thermistors at equilibrium with no heating were recorded. The above procedure was repeated for at least one more gas pressure to be sure that sufficient gas was admitted to the pipe for the beam to come to charge equilibrium.

The currents collected by diaphragm D_2 and the sheath in the 30° port were observed while the data were being taken so as to give an indication of the variation of beam intensity of the kevatron. Small fluctuations of the beam intensity were averaged out by the long time constant of the detector thermistor and sheath.

IV. ANALYSIS OF THE DATA

In this experiment, it was necessary to compare the intensities of three different beams each composed of particles of differing charge. This led to the selection of detectors whose response depended on the kinetic energy of the particles, and thus the measurements of beam intensities were reduced to the measurement of temperature changes.

Since the nickel sheath almost completely surrounded the thermistor, the assumption was made that the thermistor was at the same temperature as the sheath at equilibrium. Also, the small size of the thermistor and its leads as compared with the sheath further made this assumption justified.

In comparing beam intensities, essentially two steps were necessary. First, the change in resistance had to be converted to a temperature change, and then the temperature change converted into some arbitrary measure of beam intensity. Since the measurements were made after the detectors reached equilibrium temperatures, the latter stage was necessary since heat

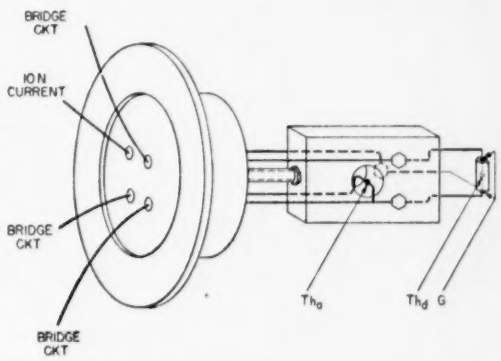

FIG. 2. Schematic drawing of the detector element, showing the beam-measuring thermistor Th_d and the thermistor for recording the ambient temperature Th_a.

TABLE I. Temperature *vs* resistance characteristics for the thermistor in the neutral (0° port) detector.[a]

R(ohms)	T(°C)
2175	15
1795	20
1495	25
1255	30
1060	35
899	40
768	45
658	50
506	55
490	60
425	65
372	70
326	75
287	80

[a] Notation: $R=R_0\exp[B(1/T-1/T_0)]$; $B=3183$ (1/°K); R = the resistance at temperature T; R_0 = the resistance at temperature T_0. For temperature changes less than 10°C the following is a good approximate formula:

$$T-T_0=\Delta T\cong-\frac{T_0^2}{B}\frac{\Delta R}{R_0}\left\{1+\left(\frac{1}{2}+\frac{1}{4}\frac{T_0}{B}\right)\frac{\Delta R}{R_0}\right\}.$$

was lost both by metallic conduction along the leads, and radiation from the nickel sheaths. The pressure in the deflection chamber was low enough so that gaseous conduction could be neglected.

The 27A thermistor is a solid semiconductor with a resistance of approximately 2000 ohms at 25°C and with a temperature coefficient of resistance at 25°C of about −0.034 ohms/ohm °C. The temperature is related to the resistance by the formula

$$R=R_0\exp[B(T^{-1}-T_0^{-1})], \tag{1}$$

where R is the resistance at temperature T, R_0 the resistance at temperature T_0, and B is a parameter depending on the materials from which the thermistor is made. For the limited temperature range of 0°C to 150°C, for which the 27A thermistor is designed, B is a constant and equal to 3183. A calibration curve was obtained by a temperature bath for temperatures from 13°C to 63°C. As would be expected from Eq. (1), when $\log R$ is plotted against $1/T$, the points fall on a straight line. The slope of this line was the same to within 2 percent for all six thermistors used and the rated values given by Western Electric. The resistance values at 25°C varied from 1450 to 1800 ohms as compared with the typical characteristics given by Western Electric of 2000 ohms±25 percent.

In converting from resistance to temperature, temperature changes larger than 5°C were obtained from the calibration curves. For temperature changes ΔT, less than 5°C, R in Eq. (1) was expanded in powers of ΔT, and terms beyond $(\Delta T)^2$ were dropped. This approximate equation, when solved for ΔT, gives

$$\Delta T\cong-\frac{T_0^2}{B}\frac{\Delta R}{R_0}\left\{1+\left(\frac{1}{2}+\frac{1}{4}\frac{T_0}{B}\right)\frac{\Delta R}{R_0}\right\}.$$

Temperature T_0 was obtained from the calibration curve for the thermistor used to measure the ambient temperature.

At equilibrium, the relation between beam intensity and temperature change is determined by the incoming heat being equal to the heat carried away by metallic conduction along the leads and radiation from the surface of the nickel sheath. At equilibrium, the incident power Q and the temperature change $\Delta T=T_d-T_a$, are related by the formula $Q=\alpha(\Delta T)+\beta(T_d^4-T_a^4)$, or

$$Q=[\alpha+4\beta T_a^3]\Delta T+6\beta T_a^2(\Delta T)^2+4\beta T_a(\Delta T)^3+\beta(\Delta T)^4, \tag{2}$$

where $\alpha(\Delta T)$ is the heat lost by metallic conduction and $\beta(T_d^4-T_a^4)$ the net heat lost by radiation. T_d and T_a are the detector and ambient temperatures, respectively. Q is a nonlinear function of ΔT, which for small temperature changes can be approximated by

$$Q=[\alpha+4\beta T_a^3](\Delta T). \tag{3}$$

To compare the temperature changes of the three detectors in order to get the fractions of the total beam in each of the charge states, an equivalent temperature change ΔT_e was obtained, which when substituted into Eq. (3) gave the same value for Q as would be obtained from substituting the measured temperature change ΔT into Eq. (2). By making the geometry of the detectors the same, α and β had the same values for the three detectors. If then, as was the case, the three detectors had the same ambient temperature T_a, the ratios of the beam intensities would be equal to the ratios of the ΔT_e's. If the two expressions for Q are equated and the resulting equation solved for ΔT_e, ΔT_e is expressed as a function of ΔT:

$$\Delta T_e=\Delta T+\frac{1}{(\alpha/\beta)+4T_a^3}[6T_a^2(\Delta T)^2+4T_a(\Delta T)^3+(\Delta T)^4]. \tag{3'}$$

When the temperature change ΔT is small, $\Delta T_e=\Delta T$ is a good approximation. For large ΔT the term in brackets must also be considered. The only unknown quantity on the right-hand side of Eq. (3′) is α/β. To obtain a curve of ΔT_e *versus* ΔT for a given value of T_a, sets of data were taken for large and for small temperature changes by varying the beam intensity from the kevatron for constant voltage. In this way, the physical quantities which were to be determined served to calibrate the detectors.

Table I gives the resistance-temperature characteristic of one of the thermistors used, and Table II gives the calibration for temperature change *versus* beam intensity for an ambient temperature of 300°K. Table III gives a typical set of data and results.

V. DESCRIPTION OF CAPTURE AND LOSS IN TERMS OF CROSS SECTIONS

Although the cross sections for electron capture and loss are functions of the velocity, the cross sections

are so large throughout the energy range of these experiments that gas pressures in the pipe sufficient to produce charge equilibrium in the emergent beam were low enough so that no appreciable diminution in beam energy took place. Thus in setting up equations to describe the approach to equilibrium in the pipe, we can treat the cross sections as independent of the velocity.

Let N_0, N_1, N_2 be, respectively, the numbers of He^0, He^+, and He^{++} ions in the beam. The cross sections σ_{ij} are defined by the first index referring to the initial charge state of the particle and the second to the charge state resulting from interaction with the medium, for example, σ_{01} is the cross section for He^0 to lose an electron and become He^+. The differential equations to be solved are

$$\begin{aligned} dN_0/dp &= -(L/kT)[(\sigma_{01}+\sigma_{02})N_0-\sigma_{10}N_1-\sigma_{20}N_2], \\ dN_1/dp &= -(L/kT)[-\sigma_{01}N_0 \\ &\qquad +(\sigma_{10}+\sigma_{12})N_1-\sigma_{21}N_2], \\ dN_2/dp &= -(L/kT)[-\sigma_{02}N_0 \\ &\qquad -\sigma_{12}N_1+(\sigma_{20}+\sigma_{21})N_2], \end{aligned} \tag{4}$$

subject to the condition

$$N_0+N_1+N_2=N_i=\text{const}, \tag{5}$$

where N_i is the total number of particles in the beam, p is the pressure, L the length of the pipe (74.0 cm), k the Boltzmann constant, and T the absolute temperature. The cross sections σ_{02} and σ_{20} refer to the capture or loss of two electrons in a single encounter. The equilibrium conditions may be found by setting the pressure derivatives equal to zero. Thus one obtains

$$\begin{aligned} \left.\frac{N_0}{N_1}\right|_{\text{equil}} &= \frac{\sigma_{10}\sigma_{21}+\sigma_{20}(\sigma_{12}+\sigma_{10})}{\sigma_{01}\sigma_{21}+\sigma_{21}\sigma_{02}+\sigma_{20}\sigma_{01}} \doteq \frac{\sigma_{10}}{\sigma_{01}}, \\ \left.\frac{N_2}{N_1}\right|_{\text{equil}} &= \frac{\sigma_{01}\sigma_{12}+\sigma_{02}(\sigma_{12}+\sigma_{10})}{\sigma_{21}\sigma_{01}+\sigma_{21}\sigma_{02}+\sigma_{20}\sigma_{01}} \doteq \frac{\sigma_{12}}{\sigma_{21}}, \end{aligned} \tag{6}$$

TABLE II. Conversion of temperature change to beam intensity for $T_a=300°K$.[a]

ΔT(°C)	ΔT_e
0	0
5	5.1
10	10.3
15	15.8
20	21.4
25	27.2
30	33.2
35	39.4
40	45.9
45	52.4
50	59.3
55	66.4
60	73.7
65	81.2
70	89.1

[a] Notation: T_d = the temperature of the detector; T_a = the ambient temperature; $\Delta T = T_d - T_a$; Q = incident power in beam; at equilibrium $Q = \alpha(\Delta T) + \beta(T_d^4 - T_a^4) = [\alpha + 4\beta T_a^3]\Delta T + 6\beta T_a(\Delta T)^2 + 4\beta T_a(\Delta T)^3 + \beta(\Delta T)^4$; $\alpha(\Delta T)$ = heat lost per second by metallic conduction along the leads; $\beta(T_d^4 - T_a^4)$ = heat lost per second by radiation from the surface of the nickel sheath; ΔT_e = temperature change such that $Q = [\alpha + 4\beta T_a^3]\Delta T_e$.

TABLE III. Typical set of data and results.[a] Beam energy = 400 kev.

Port	R_d	R_a	T_d	T_a	ΔT	ΔT_e	F_i
0°	871	1440	41.0	26.5	14.5	15.4	0.168
30°	274	1311	80.6	28.9	51.7	64.9	0.708
60°	1173	1560	39.0	28.3	10.7	11.3	0.123

[a] Notation: He^0 was detected in the 0° port; He^+ was detected in the 30° port; He^{++} was detected in the 60° port; R_d = the resistance in ohms of the detector thermistor; R_a = the resistance of the thermistor used to measure the ambient temperature; T_d = the temperature in °C of the detector thermistor; T_a = the ambient temperature; $\Delta T = T_d - T_a$; ΔT_e = the equivalent temperature change such that the incident power is proportional to ΔT_e (see Table II); F_i = the fraction of the total beam in the various charge states (He^0, He^+, He^{++}).

in which the simpler expressions at the right assume that the double electron cross sections are small compared to the others.

Although the primary purpose of this research was to obtain the equilibrium ratios, it was necessary to ascertain that sufficient gas had been admitted to the pipe to produce equilibrium, and in such tests a few measurements were made in which the change of the emergent beam from the pure He^+ from the kevatron to the final equilibrium mixture was followed as a function of pressure. The expressions for the initial rates of change of the numbers N_0, N_1, and N_2 may easily be found by imposing the conditions $N_0=N_2=0$ and $N_1=N_i$ on the original differential equations. Thus one obtains the initial pressure variations,

$$\begin{aligned} N_0/N_i &= (L/kT)\sigma_{10}p, \\ N_1/N_i &= 1-(L/kT)(\sigma_{10}+\sigma_{12})p, \\ N_2/N_i &= (L/kT)\sigma_{12}p. \end{aligned} \tag{7}$$

In the next section these equations will be used to obtain approximate values of the cross sections for two beam energies.

VI. RESULTS AND ERRORS

The results on the equilibrium distributions for the charge states of a helium beam after passing through hydrogen, helium, air, and argon are given in Figs. 3 and 4. Table IV gives the fractions of the total beam in each of the charge states in 20-kev steps. The values were obtained from the smooth curves drawn through the experimentally determined points. Table V is a summary of some of the features which facilitate a comparison of the data taken on the four gases.

The helium used was 99.8 percent pure with the remaining 0.2 percent hydrogen; it was obtained from the National Cylinder Gas Company. The hydrogen was admitted through a palladium leak which served the double purpose of being a valve and purifying the hydrogen. The argon was 99.9 percent pure and prepared by the Matheson Company. The air was dried and freed of CO_2 by passing the air from the laboratory through KOH, "Dryerite," and glass beads dusted with P_2O_5.

The objective of this research was to obtain the equilibrium ratios, leaving the problem of finding the

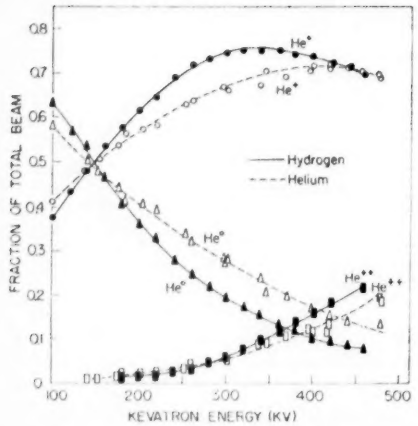

FIG. 3. Charge distribution as a function of energy for a helium beam in hydrogen and helium.

individual cross sections for a later effort. However, some rough estimates of the cross sections can be made from the data. The distribution of the beam in its charge states as a function of pressure was measured at 131 kev and 340 kev for helium as the target gas. By using Eqs. (7) for the initial change in charge as a function of pressure, rough estimates of the cross sections σ_{10} and σ_{12} can be obtained. Then, σ_{01} and σ_{21} can be determined by Eqs. (6) and the curves for helium. At 131 kev the values found are $\sigma_{01}=\sigma_{10}=1.72\times10^{-16}$ cm$^2\pm30$ percent. N_2 was small enough at this low energy so that it could be neglected. At 340 kev, the values of the cross sections found were $\sigma_{01}=8.3\times10^{-17}$ cm^2, $\sigma_{10}=3.1\times10^{-17}$ cm^2, $\sigma_{12}=1.4\times10^{-17}$ cm^2, and $\sigma_{21}=1.2\times10^{-16}$ cm^2. These values are correct to within 20 percent. Figure 5 shows the pressure variation at 340 kev.

As a check that all of the He^{++} beam was collected, the ratio of the intensities of the He^{++} and He^0 beams was measured by deflecting the He^{++} into the 30° port. The ratio so obtained agreed to within 2 percent of the value obtained in the usual way by having the He^{++} beam enter the 60° port. This check was made for helium gas and at 460 kev, where the He^{++} and He^0 beam intensities are comparable in magnitude. Also, for air at 130 kev the He^+ beam was detected by deflection into the 60° port. The He^+ to He^0 ratio was within 3 percent of the value obtained by He^+ detection in the 30° port. These checks also established that the 30° and 60° detectors were, in fact, equal in their response to the same beam.

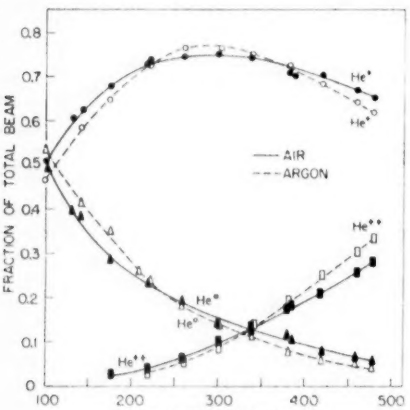

FIG. 4. Charge distribution of a helium beam as a function of energy in air and argon.

The errors in this experiment result mainly from the fluctuations in the kevatron beam. The errors can best be estimated by seeing how closely the points fall on a smooth curve. Each point represents the average of at least four sets of data and gives the results of one run. In the energy range from 200 kev to 400 kev, the error in the fraction of He^+ probably did not exceed 2 percent. Below 200 kev, the error in the He^+ beam was probably as high as 5 percent. This is due to the smaller beam intensities available at these lower energies. Above 400 kev, the beam fluctuations became more pronounced which probably resulted in an error in the He^+ beam of about 5 percent.

The beam energy was measured correctly to within 1 kev for energies up to 400 kev and to within 2 kev above 400 kev. The larger error at high energies was due to slight variations in the energy of the beam resulting from the beam fluctuations which affected the loading on the kevatron. The measurements of the resistances of the thermistors and their conversion into temperatures was correct to within 0.1°C for temperatures less than 10°C and for higher temperatures probably did not exceed 0.3°C.

VII. DISCUSSION

By Eqs. (6) the ratios of the capture and loss cross sections between He^0 and He^+, and between He^+ and He^{++} can be obtained from the equilibrium beam intensities, provided the assumption is made that the double captures and losses are negligible. Since the various theoretical calculations of the cross sections are based on approximations which lead to a power dependence on the energy, in Fig. 6, $\log(N_1/N_0)$ and $\log(N_2/N_1)$ are plotted *versus* $\log E$. Bohr[16] indicates that the loss cross section σ_l should be proportional to $1/V^n$, where n is a function of the atomic number Z of the material being traversed and the velocity of the particle, and varies from 0 to 2. n decreases with increasing Z and decreases for V less than $V_0=e^2/h$, the velocity of an electron in the first Bohr orbit. By the Born approximation, Brinkman and Kramers[17] found

[16] N. Bohr, Kgl. Danske Videnskab. Selskab, Mat.-fys. Medd. **18**, No. 8 (1948).

[17] H. C. Brinkman and H. A. Kramers, Proc. Akad. Amsterdam **33**, 973 (1930).

TABLE IV. Charge distribution for a helium beam in hydrogen, helium, dry air, and argon.[a]

Energy (kv)	Hydrogen F_0	Hydrogen F_1	Hydrogen F_2	Helium F_0	Helium F_1	Helium F_2	Dry air F_0	Dry air F_1	Dry air F_2	Argon F_0	Argon F_1	Argon F_2
100	0.63	0.37	···	0.59	0.41	···	0.50	0.50	···	0.53	0.47	···
120	0.57	0.43	···	0.54	0.45	···	0.43	0.57	···	0.48	0.52	···
140	0.52	0.48	···	0.51	0.48	0.01	0.38	0.62	···	0.42	0.58	···
160	0.47	0.53	···	0.47	0.52	0.015	0.34	0.66	···	0.37	0.63	···
180	0.41	0.57	0.015	0.43	0.55	0.02	0.28	0.69	0.025	0.33	0.67	···
200	0.36	0.62	0.02	0.40	0.57	0.025	0.26	0.71	0.03	0.28	0.70	0.02
220	0.32	0.66	0.025	0.38	0.59	0.03	0.23	0.73	0.035	0.24	0.73	0.03
240	0.28	0.69	0.03	0.35	0.61	0.035	0.21	0.74	0.05	0.21	0.75	0.04
260	0.25	0.72	0.035	0.32	0.63	0.04	0.19	0.75	0.065	0.18	0.77	0.055
280	0.22	0.73	0.05	0.30	0.65	0.05	0.17	0.75	0.08	0.16	0.77	0.07
300	0.19	0.75	0.06	0.28	0.67	0.06	0.15	0.76	0.095	0.15	0.77	0.085
320	0.17	0.75	0.075	0.25	0.68	0.07	0.14	0.75	0.11	0.13	0.76	0.11
340	0.15	0.76	0.095	0.23	0.69	0.085	0.13	0.74	0.13	0.11	0.75	0.13
360	0.13	0.75	0.12	0.21	0.70	0.095	0.12	0.73	0.15	0.095	0.74	0.16
380	0.12	0.74	0.14	0.19	0.71	0.11	0.11	0.72	0.17	0.085	0.73	0.19
400	0.10	0.74	0.16	0.17	0.71	0.12	0.095	0.71	0.19	0.07	0.71	0.22
420	0.095	0.73	0.18	0.16	0.71	0.13	0.08	0.70	0.21	0.06	0.69	0.25
440	0.085	0.72	0.20	0.14	0.71	0.15	0.07	0.69	0.24	0.055	0.66	0.28
460	0.08	0.70	0.22	0.13	0.70	0.17	0.065	0.68	0.26	0.05	0.64	0.30
480	···	···	···	0.11	0.68	0.20	0.055	0.66	0.29	0.045	0.62	0.33

[a] Notation: F_0 equals the fraction of He^0 in the beam; F_1 equals the fraction of He^+ in the beam; F_2 equals the fraction of He^{++} in the beam.

that the capture cross section σ_c was proportional to $1/V^{12}$, for $V \gg V_0$. Bohr[16] got a $1/V^6$ dependence for σ_c when $V > V_0$ and for material of large Z, by statistical considerations based on the assumption that the electron captured was one which in the substance had a velocity approximately equal to the velocity V of the particle. For velocities less than V_0 it would be expected that σ_c would be less sensitive to velocity, for σ_c cannot become significantly greater than the geometrical cross section. The above considerations indicate that σ_1/σ_c is proportional to V^m, where m increases with increasing V, and increases with increasing atomic number for Z large enough to make Bohr's statistical considerations valid ($Z > 5$).

Table VI gives the values of m for the gases studied.

In the energy range considered, m is a constant for exchange between He^+ and He^{++}. For exchange between He^0 and He^+ all the curves show the increase of m with velocity. The values of m for air and argon show the expected dependence on Z. Not very much can be said about the values of m for helium and hydrogen; the Bohr $1/V^6$ dependence breaks down because of the low atomic number, and Brinkman and Kramers' $1/V^{12}$ dependence does not apply because of the low value of V/V_0.

The energies at which $N_0 = N_1$ and $N_1 = N_2$ are of interest because they represent the energies at which $\sigma_{01} = \sigma_{10}$ and $\sigma_{12} = \sigma_{21}$. For proton beams the energy E_{01}, at which the capture and loss cross sections are equal corresponds to a velocity V_{01} of the proton,

TABLE V. Summary of data.[a]

	E_{01}	E_{02}	$(F_1)_{max}$	$(E_1)_{max}$	F_{02}
Hydrogen	148 kev	370 kev	0.76	340 kev	0.13
Helium	145	430	0.72	410	0.15
Air	98	340	0.76	300	0.13
Argon	115	330	0.77	290	0.12

[a] Notation: F_0 = fraction of He^0 in the beam; F_1 = fraction of He^+ in the beam; F_2 = fraction of He^{++} in the beam; E_{01} = energy at which $F_0 = F_1$; E_{02} = energy at which $F_0 = F_2$; $(F_1)_{max}$ = maximum value of F_1; $(E_1)_{max}$ = energy at which $F_1 = (F_1)_{max}$; F_{02} = the value of F_0 when $F_0 = F_2$.

TABLE VI. Values of the exponent m in the power dependence of σ_1/σ_c on V.[a]

	Charge exchange between He^0 and He^+				Charge exchange between He^+ and He^{++}	
	E_{01}	V_{01}/V_0	m at 100 kev	m at 450 kev	E_{12}	m
Hydrogen	148 kev	1.22	2.6	4.0	660 kev	6.1
Helium	145	1.21	2.0	4.0	800	5.1
Air	98	0.99	2.8	4.3	650	5.2
Argon	115	1.08	3.4	5.1	580	6.3

[a] Notation: E_{01} = energy at which the He^0 and He^+ equilibrium beams are equal; E_{12} = energy at which the He^+ and He^{++} equilibrium beams are equal; V_{01} = the velocity of helium at which it has the energy E_{01}; $V_0 = e^2/\hbar$, the velocity of an electron in the first Bohr orbit. For helium V_0 corresponds to the energy $E_0 = 99.2$ kev; m = the exponent of the power dependence of σ_1/σ_c on $V(\sigma_1/\sigma_c \propto V^m)$.

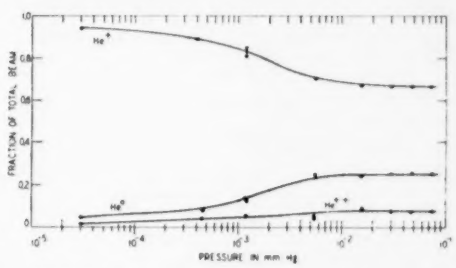

FIG. 5. Charge distribution as a function of pressure for a 340-kev helium beam emerging from a 74-cm long tube containing helium gas. The incident beam is all He^+.

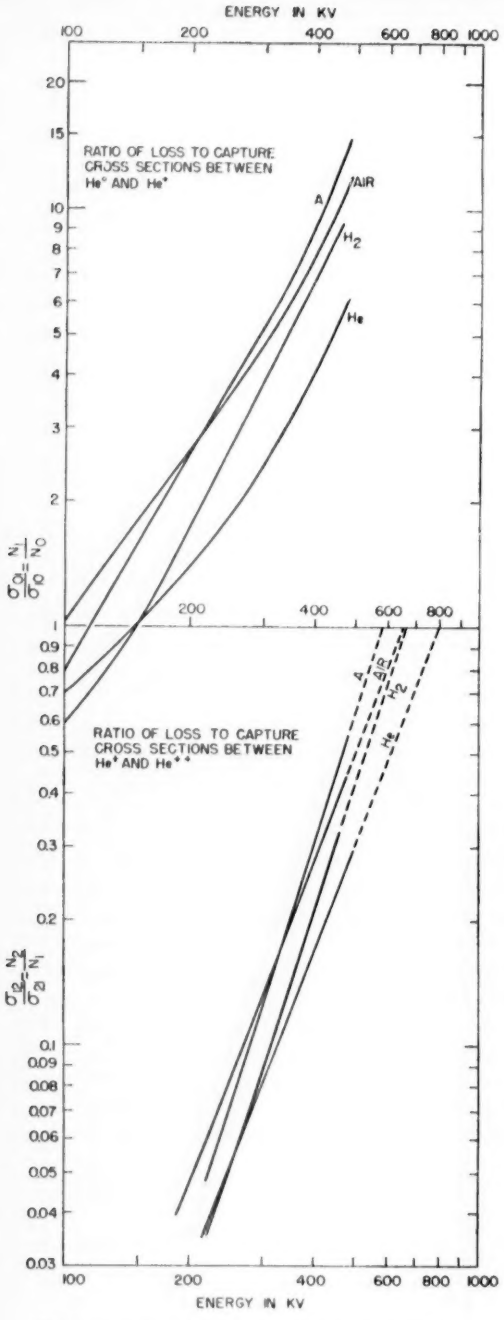
ENERGY IN KV
RATIO OF LOSS TO CAPTURE CROSS SECTIONS BETWEEN He° AND He+
A
AIR
H2
He
RATIO OF LOSS TO CAPTURE CROSS SECTIONS BETWEEN He+ AND He++
ENERGY IN KV

FIG. 6. The ratio of the loss to capture cross sections plotted as a function of beam energy.

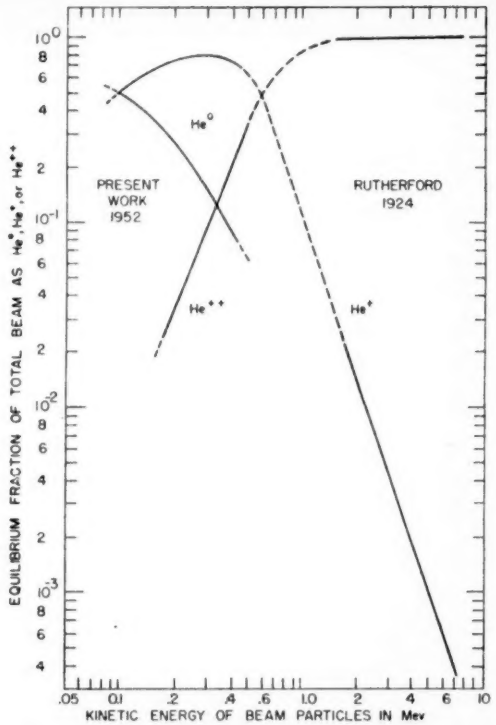

FIG. 7. Equilibrium charge distribution from 100 kev to 6 Mev for a helium beam traversing air.

approximately equal to V_0. For hydrogen beams in metals Hall[6] found $V_{01}=0.95V_0$, Montague and Ribe[8] got $V_{01}=1.44V_0$ for protons in hydrogen, and Kanner[9] got $V_{01}=1.0V_0$ for protons in air. Table VI gives V_{01}/V_0 for the present work. The agreement between the values of V_{01}/V_0 for hydrogen and helium beams in air is striking.

Table VI also gives the values of the energy E_{12} at which the capture and loss cross sections between He^+ and He^{++} are equal. These values were obtained by extrapolation (indicated by dashed lines in Fig. 6). The work by Rutherford[3] for a helium beam in air gave a value of $E_{12}=646$ kev, as compared with the value here obtained of $E_{12}=650\pm20$ kev.

Figure 7 gives the charge distribution as a function of energy for the present work and the data obtained by Rutherford, for a helium beam in air.

The author wishes to express his gratitude to Professor S. K. Allison who suggested the problem and extended the facilities of his laboratory for its solution. Mr. Gordon DuFloth was of great assistance in maintaining the equipment and taking data.

Nuclear Magnetic Moment of Pr^{141} from the Hyperfine Structure of Pr II

PETER BRIX*
Division of Physics, National Research Council, Ottawa, Canada
(Received November 10, 1952)

From the hyperfine structure of Pr II lines measured by White the magnetic interaction constant $a_{6s}=0.416\pm0.015$ cm^{-1} has been evaluated for the 6s electron in the configuration $4f^3(^4I)6s$. Application of the formula of Goudsmit and Fermi-Segrè yields the nuclear magnetic moment $\mu(Pr^{141})=+3.9\pm0.3$ nuclear magnetons.

NO precise value, of the order of precision attainable in the method of nuclear induction, has yet been found for the nuclear magnetic moment μ of Pr^{141}. A preliminary value $\mu=3.8$ nuclear magnetons has been derived[1] from the magnetic hyperfine structure (hfs) interaction constant a_{6s} of the 6s electron in Pr II. Recently Lew[2] measured the hfs due to the $4f^3$ electrons in Pr I and, independently, obtained the same result for μ from a_{4f}. In view of the theoretical uncertainties involved in any calculation of nuclear moments from hfs data of complex spectra, the agreement is very remarkable. Praseodymium is the first element for which the hfs of electronic states as different as 6s and 4f can be thus compared. It, therefore, seems justifiable to give a brief report of the calculations for Pr II, especially since the knowledge of a_{4f} now makes possible a more complete presentation.

The hfs of 170 lines of Pr II were measured by White[3] in 1929. Rosen, Harrison, and McNally[4] later classified 100 of these lines as transitions between $4f^3(^4I)6s\ a\ ^{3,5}I^\circ$ and higher even levels which originate mainly from $4f^3(^4I)6p$. They used the hfs data as a check on the analysis of the spectrum, and made a rough estimate of a_{6s}. Thus far, however, the large amount of information available from White's measurements had not been fully utilized.

The Pr II lines show characteristic hfs "flag patterns" with six components ($I=5/2$). Since in the classified transitions the total quantum numbers F are high, only the strong components can be observed.[5] For each line the separations of the components are simply given by the differences of the hfs intervals of the two levels involved. The hfs of the levels can, therefore, be deduced from White's data except for an additive constant which is the same for all levels. It is convenient to introduce a quantity Δ which is equal to the total hfs splitting of a level plus the separation between the hfs states with $F=J+I-1$ and $F=J+I-2$. The connection between Δ and the interval factor A is given by

$$\Delta=A(2IJ+2I+J-1).$$

This sum, Δ, can be shown to be nearly independent of nuclear quadrupole effects. One also has the advantage that the four best defined components out of each hfs pattern are used.

As an example, Table I shows the difference between the Δ values of $a^5I_6^\circ$ and $a^3I_6^\circ$ as obtained from combinations with various upper levels. The agreement is even better than that shown in Table I for most of the other levels belonging to the terms a^5I° and a^3I°. Up to ten independent determinations are available in some cases. The possibility of frequent cross checks indicates an accuracy of better than ±0.05 cm^{-1}, corresponding to about ±0.001 cm^{-1} for the A values.

The g sums as observed in the study of the Zeeman effect[4] show that $a\ ^{3,5}I^\circ$ and $z\ ^{3,5}H, I, K$ originate from a 6s and 6p electron, respectively, coupled to $4f^3\ ^4I^\circ$ and that good Russell Saunders coupling holds for the $^4I^\circ$. Under these assumptions the magnetic interaction constants of the 6s and 6p electrons can be evaluated in the usual way[5] from the experimental data. Since relativity corrections are negligible for the 4f electrons, Goudsmit's[6] formula for the hfs of a multiplet is applicable to the parent term $4f^3\ ^4I^\circ$. The contributions of the $4f^3$ configuration to the hfs of the various levels considered turn out to be nearly the same in all cases (see Table II). Only the small variations in these contributions enter into the evaluation of a_{6s} and μ. The influence upon the final result is less than 2 percent, and can be taken into account using $a_{4f}=0.02356$ cm^{-1}

TABLE I. Example of the evaluation of the hfs of Pr II levels from White's measurements: $\Delta(a^5I_6^\circ)-\Delta(a^3I_6^\circ)$ as obtained from pairs of lines originating from various upper levels.

Upper level	$\Delta(^5I_6)-\Delta(^3I_6)$ cm^{-1}
$z\ ^5K_6$	2.43
$z\ ^5K_7$	2.44
$z\ ^5I_6$	2.42
$z\ ^5H_6$	2.46
11_6	2.43
22_6	2.37
23_7	2.56
Mean	2.44

* National Research Laboratories Postdoctorate Fellow; on leave from II. Physikalisches Institut der Universität Göttingen, Göttingen, Germany.

[1] P. Brix, unpublished calculations, quoted by A. Steudel, Z. Physik **132**, 429 (1952).

[2] H. Lew, Phys. Rev. **89**, 530 (1953).

[3] H. E. White, Phys. Rev. **34**, 1397 (1929).

[4] Rosen, Harrison, and McNally, Phys. Rev. **60**, 722 (1941).

[5] See, e.g., H. Kopfermann, *Kernmomente* (Akademische Verlagsgesellschaft, Leipzig, 1940).

[6] S. Goudsmit, Phys. Rev. **37**, 663 (1931).

TABLE II: Calculated and observed values of $\Delta=(6J+4)A$ for the low odd levels of Pr II. The contributions due to the $4f^3$ electrons (according to Lew's value of a_{4f}) and to the 6s-electron (with $a_{6s}=0.416$ cm^{-1}) have been listed separately. All values in cm^{-1}.

Level	Δ_{calc} for (Jj) coupling from f^3	from 6s	total	Δ_{obs}	Obs-calc
$^5I_4^\circ$	+0.951	−1.165	−0.21	−0.21	0
$^5I_5^\circ$	+0.945	+1.414	+2.36	+2.20	−0.16
$^3I_5^\circ$	+0.915	−1.179	−0.26	−0.02	+0.24
$^5I_6^\circ$	+0.910	+1.387	+2.30	+2.21	−0.09
$^3I_6^\circ$	+0.902	−1.189	−0.29	−0.23	+0.06
$^5I_7^\circ$	+0.899	+1.367	+2.27	+2.21	−0.06
$^3I_7^\circ$	+0.901	−1.196	−0.30	−0.27	+0.03
$^5I_8^\circ$	+0.898	+1.352	+2.25	+2.25	0

as measured by Lew[2] for Pr I $4f^36s^2$. No appreciable effect should arise from the slightly different screening of the $4f$ electrons in Pr I and Pr II. Assuming a ratio[6] $a_{6p_{\frac{1}{2}}}/a_{6p_{\frac{3}{2}}}=6.66$, the following interaction constants have been obtained:

$$a_{6s}=0.416\pm0.015 \text{ cm}^{-1},$$
$$a_{6p_{\frac{1}{2}}}\approx 0.010 \text{ cm}^{-1}.$$

For the odd levels the agreement between observed and calculated hfs is shown in Table II. The calculated Δ values are for (Jj) coupling with $^5I_4^\circ$ and $^5I_8^\circ$ independent of coupling. For Δ_{obs} the additive constant has been chosen to give agreement for $^5I_4^\circ$. As was already known from the atomic g values,[4] Table II shows that a slight deviation from (Jj) coupling exists for the pairs of levels with equal J. For each of these pairs the differences $o-c$ have the signs expected from a mutual perturbation, and the sum rule holds within the accuracy of the experimental data.

For an evaluation of the nuclear magnetic moment from a_{6s} the quantity $Z_a^2(dn_a/dn)/n_a^3$ is needed. Although neither n_a nor dn_a/dn are directly known from the spectrum of Pr II, the quantity as a whole can be fairly accurately derived[7,8] from the position of the center of gravity of the $4f^3(^4I)6p$ configuration with respect to the center of gravity of $4f^3(^4I)6s$. From the value 23 600 cm^{-1} so obtained,[9] Fig. 7 of reference 8 gives

$$Z_a^2(dn_a/dn)/n_a^3=0.37_8 \quad \text{for} \quad 4f^3(^4I)6s.$$

This fits in well with the trend indicated by the directly known values for Ba II $4f^06s$ (0.346) and Eu II $4f^76s$ (0.406). The error for Pr II is not expected to exceed 5 percent.

The formula of Goudsmit and Fermi-Segrè,

$$a_s=0.008486[Z_a^2(dn_a/dn)/n_a^3]\times\kappa(\mu/I)Z(1-\delta)(1-\epsilon) \text{ cm}^{-1},$$

finally yields

$$\mu(\text{Pr}^{141})=+3.9\pm0.3 \text{ nuclear magnetons.}$$

The Rosenthal-Breit correction $\delta=0.05$ has been taken from calculations of Crawford and Schawlow;[10] the Bohr-Weisskopf correction ϵ can be neglected; and the relativity correction is $\kappa=1.472$.

Lew,[2] using hydrogen like wave functions for the $4f$ electrons, obtained $\mu=+3.8\pm\sim10$ percent from the magnetic interaction constant a_{4f}. A comparison of the two results seems to indicate that the various formulas used are more reliable than could have been expected from the theoretical uncertainties involved. This is rather important with respect to the isotope shift constants of some rare earth elements (e.g., cerium[7]) which also rely upon the validity, in complex spectra, of the Goudsmit-Fermi-Segrè formula and the determination of $Z_a^2(dn_a/dn)/n_a^3$ mentioned above.

I am very grateful to Dr. Lew for making available to me the results of his measurements in advance of publication.

[7] P. Brix and H. Frank, Z. Physik **127**, 289 (1950).
[8] P. Brix, Z. Physik **132**, 579 (1952).
[9] Only four even levels with low statistical weight are missing in the analysis of Rosen, Harrison, and McNally (reference 4). Their positions have been estimated.
[10] M. F. Crawford and A. L. Schawlow, Phys. Rev. **76**, 1310 (1949).

The Differential and Total Neutron Scattering Cross Sections of the Deuteron in the Energy Range 0.1 to 1.0 Mev

P. R. TUNNICLIFFE*
Atomic Energy Research Establishment, Harwell, Berkshire, England
(Received December 8, 1952)

The angular distribution of neutrons scattered by deuterons has been investigated by proportional counter techniques in the energy range 0.1 to 1.0 Mev. The distribution shows a very marked anisotropy at the higher energies which is still appreciable at 135 kev. Values for the total scattering cross sections are in agreement with earlier data down to 446 kev but apparently increase above the accepted value for the unbound thermal cross section.

I. INTRODUCTION

IN view of the large dimensions of the deuteron, it is expected that neutron scattering experiments at relatively low neutron energies will yield information concerning the nature of nuclear forces. Theoretical treatment of this three-body problem has been carried out by Buckingham and Massey,[1] and by Verde,[2] and recently by Buckingham, Hubbard, and Massey.[3] The treatment essentially yields isotropic scattering at neutron energies below 1 Mev.

Most of the experimental work published relating to the differential scattering cross section has been carried out for neutrons of about 2.5-Mev energy (Coon and Barschall;[4] Kruger, Shoupp, Watson, and Stallman;[5] Darby and Swann;[6] Caplehorn and Rundle[7]). The experimental results are somewhat conflicting, as pointed out by Caplehorn and Rundle. The later results favor ordinary or neutral type nuclear forces, while the earlier results are in better agreement with exchange or symmetrical theory forces. Recent work by Hamonda and de Montmollin[8] and by Wantuch[9] at higher neutron energies suggests that the theory is not adequate. The total scattering cross-section measurements of Aoki,[10] Nuckolls *et al.*,[11] Rainwater *et al.*,[12] Fermi and Marshall,[13] and Wollan, Schull, and Koehler[14] strongly favor the exchange type of force. Recent measurements of both the differential and total scattering cross sections have been reported by Walt, Okazaki, and Adair.[15] Their results support those of Coon and Barschall.

The corresponding theoretical treatment of neutron-proton scattering does not expect any appreciable anisotropy in the scattering at neutron energies of less than 10 Mev, and this has been confirmed by a number of authors (i.e., Kruger, Shoupp, and Stallman,[16] Bonner,[17] Coon and Barschall,[4] Laughlin and Kruger,[18] Barschall and Taschek,[19] Caplehorn and Rundle[7]). This isotropic scattering has been used as a cross check of the present experimental work.

II. EXPERIMENTAL METHOD

The measurements reported in this paper are based on a method described by Barschall and Kammer.[20] The pulse size distribution from a proportional counter containing deuterium gas is observed when the counter is irradiated with monoenergetic neutrons. The pulse size distribution is a direct measure of the distribution in energy of the recoiling deuterons, except for corrections for wall and end effects in the counters. We assume that, in the scattering of neutrons by deuterons in the energy range reported, only S and P wave scattering terms need be taken into account. Parallel observations were taken with a hydrogen filled counter to ensure that the method yielded isotropic scattering by protons.

The method of interpretation of the pulse distributions is outlined below. We use the notation E_n = neutron energy, E = recoil energy, E_m = maximum recoil energy, ϕ = angle of recoiling nucleus (laboratory system), θ = angle of scattering (center-of-mass system), $\sigma(\theta)$ = differential scattering cross section (center-of-mass system), σ_s = total scattering cross section, and M = mass of recoiling nucleus relative to the neutron mass. Then, from the conservation of momentum, E_m

* Now with Atomic Energy of Canada, Limited, Chalk River, Ontario, Canada.

[1] R. A. Buckingham and H. S. W. Massey, Proc. Roy. Soc. (London) **A179**, 123 (1941); Phys. Rev. **71**, 558 (1948).
[2] M. Verde, Helv. Phys. Acta **22**, 339 (1949).
[3] Buckingham, Hubbard, and Massey, Proc. Roy. Soc. (London) **A211**, 183 (1952).
[4] J. H. Coon and H. H. Barschall, Phys. Rev. **70**, 592 (1946).
[5] Kruger, Shoupp, Watson, and Stallman, Phys. Rev. **53**, 1014 (1938).
[6] J. F. Darby and J. B. Swan, Nature **161**, 22 (1948).
[7] W. F. Caplehorn and G. P. Rundle, Proc. Phys. Soc. (London) **64**, 546 (1951).
[8] I. Hamonda and G. de Montmollin, Phys. Rev. **83**, 1277 (1951).
[9] E. Wantuch, Phys. Rev. **84**, 169 (1951).
[10] H. Aoki, Proc. Phys.-Math. Soc. Japan **21**, 75 (1939).
[11] Nuckolls, Bailey, Bennett, Bergstralh, Richards, and Williams, Phys. Rev. **70**, 805 (1946).
[12] Rainwater, Havens, Dunning, and Wu, Phys. Rev. **73**, 733 (1948).
[13] E. Fermi and L. Marshall, Phys. Rev. **75**, 578 (1949).
[14] Wollan, Schull, and Koehler, Phys. Rev. **83**, 700 (1951).
[15] Walt, Okazaki, and Adair, Phys. Rev. **87**, 238 (1952).
[16] Kruger, Shoupp, and Stallman, Phys. Rev. **52**, 678 (1937).
[17] T. W. Bonner, Phys. Rev. **52**, 685 (1937).
[18] J. S. Laughlin and P. G. Kruger, Phys. Rev. **73**, 197 (1948).
[19] H. H. Barschall and R. F. Taschek, Phys. Rev. **75**, 1819 (1949).
[20] H. H. Barschall and M. H. Kammer, Phys. Rev. **58**, 590 (1940).

$=4ME_n/(M+1)^2$ and $E=E_m\cos^2\phi$. Since $\theta+2\phi=\pi$,

$$E=E_m(1-\cos\theta)/2. \tag{1}$$

If $p(E)$ is the probability per unit energy interval of a recoiling nucleus attaining energy E,

$$p(E)=\sigma(\theta)\pi(M+1)^2/\sigma_s E_n M. \tag{2}$$

Relations (1) and (2) show that the pulse size distribution is equivalent to a measurement of the differential scattering cross section in terms of $\cos\theta$.

In the case of hydrogen $\sigma(\theta)/\sigma_s=1/4\pi=$constant, and we obtain a uniform distribution.

The proportional counters used in these measurements have a cylindrical sensitive volume whose ends are electrically well defined and have been described in detail by Skyrme, Tunnicliffe, and Ward.[21] When neutrons are directed axially, the method of allowing for wall and end effects (i.e., for recoil particles leaving or entering the ends or striking the walls before expending all their energy) has been detailed for hydrogen. The pulse distribution for hydrogen is of the form

$$\phi_H(x)=1+\frac{R_0}{a}\frac{dI_1}{dx}+\frac{R_0}{b}\frac{dI_2}{dx}-\frac{R_0^2}{ab}\frac{dI_3}{dx},$$

where $\phi_H(x)$ is proportional to the number of pulses of size x per unit interval of size, $R_0=$maximum recoil proton range, $a=$radius, and $b=$length of sensitive volume of the counter, and where the normalization is such that $x=1$ is the maximum pulse size. The correction functions I_1, I_2, and I_3 have been computed.[21]

If we assume that the differential cross section of the deuteron can be written

$$\sigma(\theta)=\sigma_0(C_1+C_2\cos\theta+C_3\cos^2\theta)/4\pi C_1, \tag{3}$$

it can be shown that the pulse distribution from the deuterium-filled counter is of the form

$$\phi_D(x)=C_1\phi_1(x)+C_2\phi_2(x)+C_3\phi_3(x), \tag{4}$$

where

$$\phi_1(x)=1+\frac{R_0}{a}\frac{dI_4}{dx}+\frac{R_0}{b}\frac{dI_5}{dx}-\frac{R_0^2}{ab}\frac{dI_6}{dx},$$

$$\phi_2(x)=2(1-2x)+\frac{R_0}{a}\frac{dI_7}{dx}+\frac{R_0}{b}\frac{dI_8}{dx}-\frac{R_0^2}{ab}\frac{dI_9}{dx},$$

$$\phi_3(x)=(1-2x)^2+\frac{R_0}{a}\frac{dI_{10}}{dx}+\frac{R_0}{b}\frac{dI_{11}}{dx}-\frac{R_0^2}{ab}\frac{dI_{12}}{dx}.$$

The functions I_4, $I_5\cdots I_{12}$ arise from end and wall effects. They have been computed by methods similar to those outlined earlier[21] but assuming a linear range-energy relation for deuterons in the energy range of interest. This assumption should not give rise to inaccuracies in these functions of more than a few percent and has been a considerable saving in computing effort.

[21] Skyrme, Tunnicliffe, and Ward, Rev. Sci. Instr. **23**, 204 (1952).

The observed pulse distributions for deuterium were interpreted as follows. The best values of the coefficients C_1, C_2, C_3, and their standard deviations were obtained by making a least squares fit of Eq. (4) to the observations. From measurements with the hydrogen counter a value Φ was obtained for the total number of neutrons incident on the sensitive volume of the deuterium counter during the time taken to observe the pulse distribution. The value of σ_0 was obtained using the relation $C_1=\Phi b\rho\sigma_0$, which holds for the normalizations used, where $b=$length of the sensitive volume of the counter and $\rho=$number of deuterium atoms/cc of the filling. Integration of Eq. (3) gives the total scattering cross section,

$$\sigma_s=\sigma_0(1+C_3/3C_1). \tag{5}$$

Finally Eq. (3) was written in the more conventional form,

$$\sigma(\theta)=\sigma_0(1+\alpha\cos\theta+\beta\cos^2\theta)/4\pi, \tag{6}$$

where $\alpha=C_2/C_1$ and $\beta=C_3/C_1$.

III. EXPERIMENTAL APPARATUS

Monoenergetic neutrons were obtained from the $Li^7(p, n)Be^7$ reaction. An analyzed proton beam of energy up to 2.5 Mev from the Harwell electrostatic generator[22] with beam currents of 4μa was used. Targets of evaporated lithium fluoride on silver backings of thickness between 5 and 30 kev were mounted at the end of a thin aluminum thimble six inches long. The energy spread of the proton beam was controlled to about ±1 kev at the lower energies by an electron gun stabilizer and to about ±5 kev at higher energies by a slit placed in front of the target. Machine voltages were measured with a generating voltmeter calibrated using the $Li^7(p, n)Be^7$ threshold and neutron energies calculated using the known proton voltage.

Two counters were suspended in a light aluminum framework in a vertical plane intersecting the target and containing the proton beam and were orientated at angles of 20° above and below the direction of the beam. The counters were each about two and a half feet from the target. Apart from the beam analyzing magnet the nearest substantial mass of material was about nine feet from the target and counters.

One counter was filled with either pure deuterium at 78.1-cm pressure of mercury (16.3°C) or 30.7 cm of deuterium, 50.1 cm of argon, and 1.8 cm of carbon dioxide (20°C), and the other with either 79.6 cm of pure hydrogen (16.3°C) or 78.0 cm of pure methane (20°C). The fillings mentioned first were used for measurements below 450-kev neutron energy. The pure methane, hydrogen, and carbon dioxide were prepared by fractional distillation.[23] The deuterium was prepared by

[22] R. L. Fortescue and P. D. Hall, Proc. Inst. Elec. Engrs. (London) **96**, 77 (1949).

[23] The author is indebted to Dr. London of the Atomic Energy Research Establishment for preparation of the pure methane and to the Clarendon Laboratory, Oxford for the pure hydrogen.

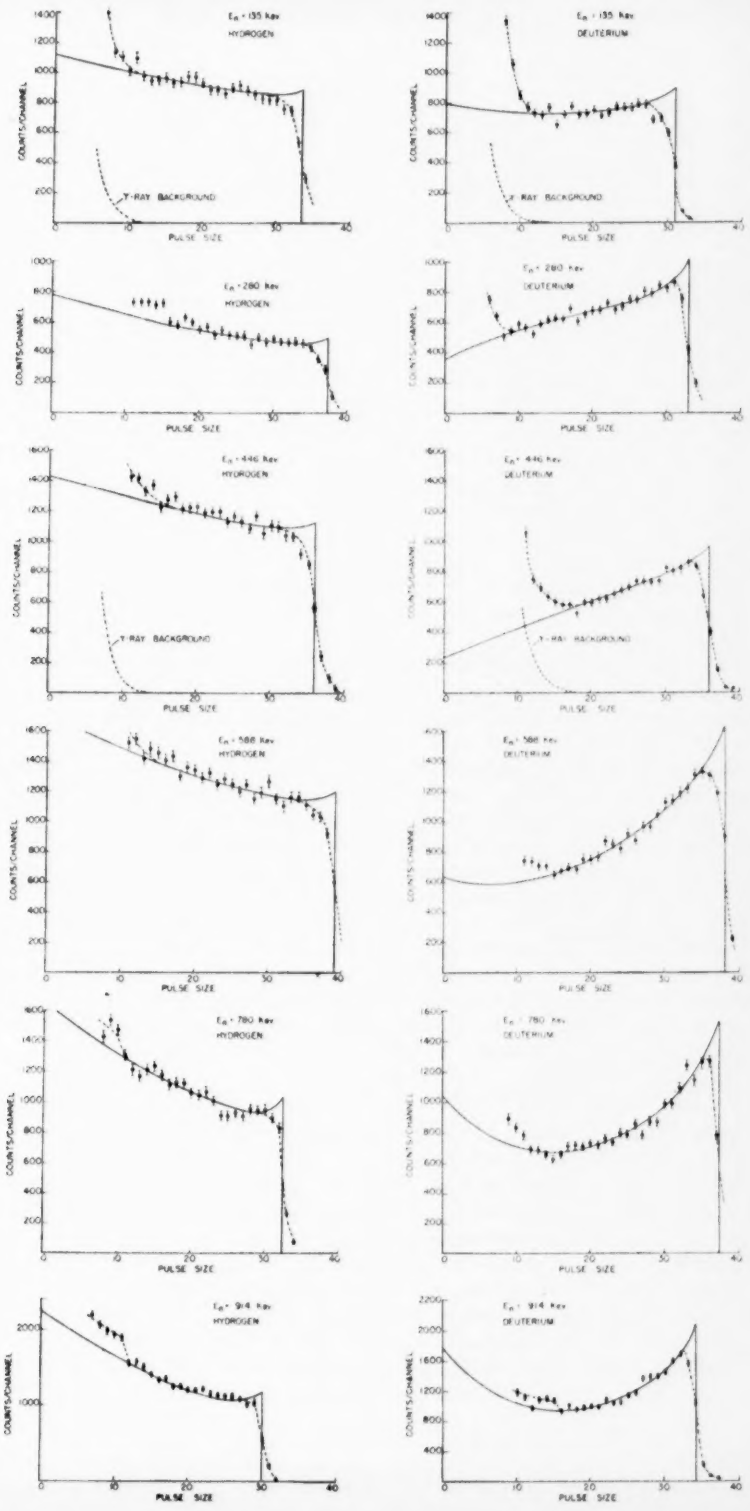

FIG. 1. Comparative pulse distributions obtained at various neutron energies E_n from counters containing hydrogen and deuterium. The solid lines are calculated assuming isotropic scattering in hydrogen and a mixture of S and P wave scattering in deuterium, allowing for end and wall effects.

TABLE I. Experimental values of the constants of Eqs. (5) and (6).

E_n kev	α	β	σ_0 cm$^2\times10^{-24}$	σ_s barns
135	-0.099 ± 0.039	0.111 ± 0.146	$4.6\ \pm0.07$	$4.8\ \pm0.34$
280	-0.470 ± 0.022	0.075 ± 0.082	3.70 ± 0.06	3.79 ± 0.22
446	-0.419 ± 0.092	0.055 ± 0.224	3.04 ± 0.09	3.10 ± 0.29
588	-0.496 ± 0.014	0.602 ± 0.125	2.62 ± 0.04	3.14 ± 0.20
780	-0.467 ± 0.036	0.838 ± 0.105	2.44 ± 0.04	3.18 ± 0.17
914	-0.333 ± 0.052	$1.17\ \pm0.13$	2.37 ± 0.04	3.29 ± 0.20

electrolysis of heavy water and purified by the method described by Wilson *et al.*[24] Mass spectrometer analyses[25] established the isotopic purity to be 98.25 percent D_2, 1.75 percent H_2.

Pulses from the counters were amplified by A.E.R.E. type 1008 linear amplifiers using the high frequency head amplifiers and fed in turn to a 30-channel pulse analyzer. Runs with each counter at a given neutron energy were taken with and without a neutron 'shadow cone' inserted between the counter and target to allow a correction to be made for scattered neutrons. This shadow cone consisted of a thin-walled aluminum can six inches long filled with water. Runs were monitored by measuring the integrated proton current received by the target.

The pulse distributions from the hydrogen containing counter were fitted to calculated curves immediately after they were obtained and showed that satisfactory experimental conditions had been established and were maintained during the series of measurements. They were used to determine the number of neutrons incident on the counter and hence on the deuterium counter during the corresponding run with the latter, after allowing for a small inverse square correction and using the integrated proton currents received by the target during the runs.

Runs were taken below the neutron threshold of the $Li^7(p, n)Be^7$ reaction with each filling to assess the gamma-ray background and to assist in rejecting points at the lower end of the distributions which might be modified by this background.

IV. RESULTS

The pulse distribution of comparison runs for the hydrogen and deuterium-filled counters are shown in Fig. 1. These data have been corrected for variations in pulse analyzer channel widths, for hydrogen content of the deuterium counter, and for scattered neutron background. The errors shown are standard deviations of the number of counts per channel. The solid lines are the theoretical curves calculated by the methods outlined in Sec. II. The maximum pulse size used in adjusting the pulse size scale of Eq. (4), and therefore entering into the value of C_1, has been assessed by taking the value at which the actual distribution falls to half the extrapolated value of the distribution which might be expected but for resolution effects. From previous experience[26] this assessment should not be in error by greater than 1 percent.

Correction for the hydrogen recoils in the deuterium counter was obtained in a straightforward manner using the hydrogen counter distribution at the corresponding neutron energy and allowing for the ratio of hydrogen in two counters and the lengths of the runs. Over the range of pulse sizes used, the scattered neutron background never amounted to more than a few percent. In carrying out the least squares fit of Eq. (4) to the experimental results the distributions were inspected and points at the upper and lower end of the runs discarded before making the analysis. In general, it was necessary to discard the upper three or four points since the upper ends of the distributions were smeared out by resolution effects in the counter and by the finite width of the incident neutron spectrum. The lower ends of the distributions were discarded where contributions of more than a few percent might have been made by the gamma-ray background and where a contribution could arise from the second neutron group from the $Li^7(p, n)Be^7$ reaction.[27]

The values of the constants α, β, σ_0, and σ_s obtained are listed as a function of neutron energy in Table I. The errors quoted for α, β, and σ_0 are standard deviations obtained from the analysis using the statistical accuracy of the experimental data. The restricted angular range has been allowed for automatically. A further uncertainty of 5 percent, assessed somewhat arbitrarily, has been added to the error of σ_s to allow for uncertainties in the neutron flux determination.

In treatment of the results it has been assumed that the ionization potential for the low energy recoil protons and deuterons used in this work is constant within the experimental accuracy and, therefore, that the pulse sizes were proportional to the recoil energies. This assumption is based on the work of Tunnicliffe and Ward.[26]

V. DISCUSSION AND CONCLUSIONS

It is concluded that neutron-deuteron scattering is markedly anisotropic at neutron energies of about 1 Mev. The anisotropy decreases with neutron energy but is still appreciable at 135-kev neutron energy. This magnitude of the anisotropy does not appear to be predicted by existing theoretical treatments. However, Buckingham, Hubbard, and Massey[3] point out that their calculations cannot be relied upon for neutron energies less than 2 Mev and propose to extend their calculations in more detail at low neutron energies. If an extrapolation of the trend of the experimentally observed anisotropy is permissible, it may be concluded

[24] Wilson, Beghian, Collie, Halban, and Bishop, Rev. Sci. Instr. **21**, 699 (1950).

[25] The author is indebted to the mass spectrometer group at the Atomic Energy Research Establishment for these analyses.

[26] P. R. Tunnicliffe and A. G. Ward, Proc. Phys. Soc. (London) **65**, 233 (1952).

[27] B. Hammermesh and V. Hummel, Phys. Rev. **78**, 73 (1950).

that these results tend to support those of Darby and Swan[6] and of Caplehorn and Rundle.[7]

The total cross-section values are in agreement within the experimental errors with the results of Nuckolls *et al.*[11] down to the lowest energies which they used (350 kev). The value 3.79 barns at 280 kev agrees within the experimental errors with the results of Walt, Okazaki, and Adair.[15] Both this value and the value of 4.8 barns at 135 kev are high in comparison with the unbound values of 3.3, 3.44, and 3.4 barns at very low neutron energies given, respectively, by Rainwater *et al.*,[12] Fermi and Marshall,[13] and by Wollan, Schull, and Koehler.[14] Owing to pressure of circumstances, it was not possible to repeat measurements and obtain adequate cross checks of these apparently anomalous cross sections in the time available. It would therefore seem desirable that the total cross section be investigated further below 500 kev.

The author is indebted to Dr. T. H. R. Skyrme for development of the method of handling the wall corrections, to Miss P. Dyson for much of the extensive numerical work, and to Mr. A. E. Pyrah for efficient maintenance and operation of the electrostatic generator. He wishes to thank the Director of the Atomic Energy Research Establishment for permission to publish this paper.

PHYSICAL REVIEW VOLUME 89, NUMBER 6 MARCH 15, 1953

A New Rigorous Lower Bound on the Range of the Triplet Neutron-Proton Interaction*

LESLIE L. FOLDY
Case Institute of Technology, Cleveland, Ohio
(Received December 1, 1952)

The experimental values of the electric quadrupole moment and percentage D state in the deuteron together with the effective triplet range of the neutron-proton interaction are employed to determine a rigorous lower bound on the "cut-off" range of the neutron-proton interaction. The latter is defined to be the range beyond which the deuteron wave functions have effectively their asymptotic form.

IT was first pointed out by Schwinger[1] that the existence of an electric quadrupole moment for the deuteron requires that the neutron-proton interaction in the triplet state have a finite range. By the use of approximate expressions for the deuteron quadrupole moment and percentage D state in the deuteron, Schwinger was further able to make an estimate of a lower bound on this range of 2.5×10^{-13} cm. More recently Broyles and Kivel[2] introduced an ingenious method for obtaining a *rigorous* lower bound on the triplet range. Before describing their approach it is necessary to give a more precise definition of the term "range" as it is used above. It is used here in the sense of the neutron-proton separation beyond which the deuteron S and D wave functions have effectively their asymptotic form. For an interaction which does not have a tail but cuts off sharply, it then represents the separation at which the cutoff occurs. For a long-tailed interaction, a precise definition is not so easy to formulate, and one must be satisfied with defining it as the neutron-proton separation beyond which the deviation of the actual deuteron wave function from its asymptotic form is sufficiently small to make no difference within the accuracy desired in the calculation of such quantities as the quadrupole moment, percentage D state, effective range, etc. To distinguish this range from such quantities as the effective range and intrinsic range, we shall refer to the range here defined as the "cut-off" range of the potential.

The method of Broyles and Kivel consists in completely ignoring the form of the interaction in the deuteron and concentrating attention on the deuteron wave function. Assuming then that these wave functions have their asymptotic form outside the cut-off range of the potential and an arbitrary form inside, they maximize the expression for the quadrupole moment of the deuteron by variation of the form of the wave functions inside the range of the interaction and the amplitude of the asymptotic forms outside the range of the interaction. This maximum quadrupole moment is then a monotonically increasing function of the range of the interaction, and the observed quadrupole moment then sets a lower bound on the range of the interaction. It is worth noting that the maximum quadrupole moment for a fixed range is obtained by having the wave functions vanish inside the range of interaction. The lower bound which these authors find for the cut-off range turns out to be 1.1×10^{-13} cm which is considerably below that estimated by Schwinger.

At least part of this last discrepancy can be at-

* This work was supported by the U. S. Atomic Energy Commission. Part of the work herein contained was carried out while the author was a summer visitor at Brookhaven National Laboratory. The hospitality extended to the author by this laboratory is gratefully acknowledged.

[1] J. Schwinger, Phys. Rev. **60**, 164 (1941).
[2] A. A. Broyles and B. Kivel, Phys. Rev. **77**, 839 (1950).

tributed to the fact that no condition is placed on the percentage of D state in the deuteron in the calculation of Broyles and Kivel. In fact, the lower bound on the range obtained by these authors turns out to correspond to a D state percentage of 35 percent which is much larger than is reasonable. To remedy this deficiency these authors and the present author[3] independently revised the original calculation by imposing the condition that the D state percentage in the deuteron be less than 5 percent. One then obtains for the lower bound on the range a value of 1.75×10^{-13} cm which is a substantial improvement but still considerably below Schwinger's value.

Since even in the improved calculation the maximum quadruple moment is obtained when the deuteron wave functions vanish inside the range of interaction, any improvement of the calculation must stem from a requirement that prevents this vanishing. Such a condition can be imposed by making use of the triplet *effective* range.[4,5] This is a quantity which can be expressed in terms of the deuteron wave functions in a manner which is relatively insensitive to the interaction potential and, consequently, is fairly well established from scattering experiments to have a value of about 1.70×10^{-13} cm. Actually, the quantity which we require is that usually designated by[4,5] $\rho_t(-\epsilon,-\epsilon)$ and defined in terms of the radial S and D wave functions of the deuteron, u and w, respectively, (normalized to $u^2+w^2\sim e^{-2\alpha r}$) by

$$\rho=\rho_t(-\epsilon,-\epsilon)=2\int_0^\infty[e^{-2\alpha r}-u^2-w^2]dr,$$

where $\alpha=(M\epsilon/h^2)^{\frac{1}{2}}$ is the reciprocal of the deuteron radius. The quantity which is experimentally determined is that designated as[4] $\rho_t(0,0)$, but the difference between this and $\rho_t(-\epsilon,-\epsilon)$ which depends on the shape dependence of the interaction potential is quite small, and the results we shall obtain are in any case not very sensitive to the exact value of the effective range.

Before proceeding with the actual calculation in this case, it is worth noting that a finite effective range already imposes of itself a lower bound on the range of the triplet neutron-proton interaction. For if we designate the range of the neutron-proton interaction by r_0, we have

$$\rho=2\int_0^\infty[e^{-2\alpha r}-u^2-w^2]dr=2\int_0^{r_0}[e^{-2\alpha r}-u^2-w^2]dr+2\int_{r_0}^\infty[e^{-2\alpha r}-u^2-w^2]dr=\frac{1-e^{-2\alpha r_0}}{\alpha}-2\int_0^{r_0}[u^2+w^2]dr+2\int_{r_0}^\infty[e^{-2\alpha r}-u^2-w^2]dr,$$

whence, since the last integral may easily be shown to be negative by the use of the asymptotic forms of u and w,

$$\rho\leqslant\frac{1-e^{-2\alpha r_0}}{\alpha},$$

and

$$r_0\geqslant-\frac{1}{2\alpha}\ln(1-\alpha\rho)=1.10\times10^{-13}\text{ cm}.$$

Because of this one might expect that the inclusion of the effective range as a condition on the maximization of the quadrupole moment would substantially raise the lower bound on the range obtained from the latter alone. We follow with the investigation of this problem.

CALCULATION

In what follows we shall use the "radius" of the deuteron, $(h^2/M\epsilon)^{\frac{1}{2}}$, where ϵ is the binding energy of the deuteron, as the unit of length. Writing u/r for the radial S function and w/r as the radial D function for the deuteron, we shall normalize these functions so that u is asymptotic to $(1-p^2)^{\frac{1}{2}}e^{-r}$ while w is asymptotic to $p(1+3/r+3/r^2)e^{-r}$, where p is a constant. In terms of these functions the quadrupole moment of the deuteron is given by

$$Q=\frac{1}{20}\int_0^\infty r^2[uw-w^2]dr\Big/\int_0^\infty[u^2+w^2]dr,\qquad(1)$$

the percentage D state by

$$\delta=\int_0^\infty w^2dr\Big/\int_0^\infty[u^2+w^2]dr,\qquad(2)$$

and the effective range of the triplet neutron-proton interaction by

$$\rho=2\int_0^\infty[e^{-2r}-u^2-w^2]dr.\qquad(3)$$

From (3) one has

$$\int_0^\infty[u^2+w^2]dr=\tfrac{1}{2}(1-\rho),\qquad(4)$$

whence we may write (1) and (2) in the form

$$Q=\frac{1}{10(1-\rho)}\int_0^\infty r^2[uw-w^2]dr,\qquad(5)$$

$$\delta=1-\frac{2}{1-\rho}\int_0^\infty u^2dr.\qquad(6)$$

Let r_0 be the cut-off range beyond which the potential (effectively) vanishes so that u and w take their

[3] A. A. Broyles and B. Kivel, Phys. Rev. **70**, 418 (1950); L. L. Foldy, Phys. Rev. **78**, 636 (1950).
[4] J. M. Blatt and J. D. Jackson, Phys. Rev. **76**, 18 (1949); H. A. Bethe, Phys. Rev. **76**, 38 (1949).
[5] H. Feshbach and J. Schwinger, Phys. Rev. **84**, 194 (1951).

asymptotic forms:

$$\left.\begin{aligned} u&=(1-p^2)^{\frac{1}{2}}e^{-r},\\ w&=p\left(1+\frac{3}{r}+\frac{3}{r^2}\right)e^{-r},\end{aligned}\right\}(r>r_0). \tag{7}$$

Also define

$$U^2=\int_0^{r_0}u^2dr, \tag{8}$$

$$W^2=\int_0^{r_0}w^2dr. \tag{9}$$

Then using these forms in (6) we find

$$\delta=1-\frac{2}{1-\rho}\{U^2+\tfrac{1}{2}(1-p^2)e^{-2r_0}\}, \tag{10}$$

so that U^2 is fixed once ρ, r_0, δ, and p are given. Also from (3) we may write

$$\rho=2\{\tfrac{1}{2}-U^2-W^2-\tfrac{1}{2}(1-p^2)e^{-2r_0}-\tfrac{1}{2}p^2K(r_0)\}, \tag{11}$$

where

$$K(r_0)=2\int_0^{r_0}\left[1+\frac{3}{r}+\frac{3}{r^2}\right]^2e^{-2r}dr. \tag{12}$$

Eliminating U^2 between (10) and (11) we obtain

$$\delta=1-\frac{2}{1-\rho}\{\tfrac{1}{2}-\tfrac{1}{2}\rho-W^2-\tfrac{1}{2}p^2K(r_0)\}, \tag{13}$$

so that W^2 is fixed when ρ, δ, r_0, and p are given.

Finally we may write (5) in the form

$$Q=\frac{1}{10(1-\rho)}\int_0^{r_0}r^2[8^{\frac{1}{2}}uw-w^2]dr + \frac{r_0^2}{10(1-\rho)}[pL(r_0)-p^2M(r_0)], \tag{14}$$

where

$$L(r_0)=\frac{8^{\frac{1}{2}}}{r_0^2}\int_{r_0}^{\infty}r^2\left[1+\frac{3}{r}+\frac{3}{r^2}\right]e^{-2r}dr, \tag{15}$$

$$M(r_0)=\frac{1}{r_0^2}\int_{0r}^{\infty}r^2\left[1+\frac{3}{r}+\frac{3}{r^2}\right]^2e^{-2r}dr. \tag{16}$$

Our problem now is to maximize this last expression for Q holding the quantities δ, ρ, and r_0 fixed, and varying p and the values of the functions u and w in the range $0\leqslant r\leqslant r_0$. We carry out this problem in two steps: first we maximize Q with respect to the functions u and w in the stated interval for a fixed value of p; then we maximize the resultant expression by variation of p.

By inspection one sees that we can maximize the expression (14) with respect to u and w holding p fixed by maximizing

$$\int_0^{r_0}r^2[8^{\frac{1}{2}}uw-w^2]dr,$$

subject to the conditions that U^2 and W^2 are held fixed. This is equivalent to the maximization of the quantity

$$q=\int_0^{r_0}r^2[8^{\frac{1}{2}}uw-w^2]dr/(U^2+W^2), \tag{17}$$

subject to the condition that W^2 is held fixed. We employ here the method of Broyles and Kivel combined with a Lagrange multiplier to take account of the subsidiary condition. To employ the method of Broyles and Kivel we write the integrations involved as summations whence we must maximize

$$q=\{\textstyle\sum_i r_i^2[8^{\frac{1}{2}}u_iw_i-w_i^2]\Delta r -\lambda\sum_i w_i^2\Delta r\}/\sum_i[u_i^2+w_i^2]\Delta r, \tag{18}$$

where λ is a Lagrange multiplier, with respect to variations of the u_i and w_i. As the above authors have shown, the maximum is obtained by setting u_i and w_i equal to zero in all intervals except that one for which the quantity

$$\{r_i^2[8^{\frac{1}{2}}u_iw_i-w_i^2]-\lambda w_i^2\}/\{u_i^2+w_i^2\} \tag{19}$$

has its maximum value. Hence we first proceed to maximize this last expression with respect to the ratio $\xi_i=u_i/w_i$. For this purpose let us write $\Lambda_i=\lambda/r_i^2$, whence we must maximize

$$r_i^2\{(8^{\frac{1}{2}}\xi_i-\xi_i^2-\Lambda_i\xi_i^2)/(1+\xi_i^2)\}$$

with respect to ξ_i. On differentiating and setting the result equal to zero, we find for the value of ξ_i maximizing (19),

$$\xi_i=\tfrac{1}{2}\{[\tfrac{1}{2}(1-\Lambda_i)^2+4]^{\frac{1}{2}}-2^{-\frac{1}{2}}(1-\Lambda_i)\},$$

and for the corresponding maximum value of (19)

$$q_i=r_i^2\left\{\frac{4}{2^{\frac{1}{2}}[\tfrac{1}{2}(1-\Lambda_i)^2+4]^{\frac{1}{2}}+\Lambda_i-1}-1\right\}.$$

Since, once we have found the interval in which (19) has its maximum value, we shall set u_i and w_i equal to zero in all other intervals, the subsidiary condition on the variation will take the form

$$\xi_i^2=\tfrac{1}{4}\{[\tfrac{1}{2}(1-\Lambda_i)^2+4]^{\frac{1}{2}}-2^{-\frac{1}{2}}(1-\Lambda_i)\}^2=W^2/U^2, \tag{20}$$

as an equation determining Λ_i. Since this equation does not involve r_i, the corresponding value of Λ_i does not depend on r_i. One then readily finds that so long as $U>2^{\frac{1}{2}}W$ (a condition which is satisfied in our case), the interval in which (19) takes its maximum value is that in which r_i^2 is a maximum, namely the interval for which $r_i=r_0$. This essentially solves the first part of our problem for we now know that u and w must be made to vanish everywhere except in the last infinitesi-

mal interval in the range $0 \leqslant r \leqslant r_0$. With this condition the expression (14) for the quadruple moment Q becomes

$$Q=\frac{r_0^2}{10(1-\rho)}\{8^{\frac{1}{2}}UW-W^2+pL(r_0)-p^2M(r_0)\}, \quad (21)$$

where U^2 and W^2 are functions of p through the relations (10), (13). The remainder of the problem now consists in maximizing this last expression with respect to p, for given δ, ρ, and r_0. This has been carried out numerically, using experimental values for δ and ρ, for a sequence of values of r_0. The value of r_0 corresponding to the observed quadrupole moment of the deuteron then represents a lower bound on the range of the triplet neutron-proton interaction. The experimental value for ρ which has been used is 1.70×10^{-13} cm. While there is some uncertainty in this value, the corresponding uncertainty in $(r_0)_{\min}$ is not of any significance. However, the percentage D state in the deuteron is not known very accurately, and hence the calculations were carried out for several values of δ. The results obtained are:

δ	$(r_0)_{\min}$
0.03	2.44×10^{-13} cm
0.04	2.16
0.05	1.97

CONCLUSION

We may note that another interpretation of the present result can be stated as follows: If it is desired to fit all of the available low energy data on the deuteron by a potential which vanishes at the minimum possible separation between proton and neutron, then the required potential is one which is infinitely repulsive for distances less than $(r_0)_{\min}$ and finite only in an infinitesimal interval at this distance. It seems rather remarkable that a potential interaction of this character, so at odds with our usual notions of internucleonic potentials, is capable of explaining this data. Of course, we must remember that higher energy neutron-proton scattering data in all probability conflict with this potential so we should not take it too seriously.

A further conclusion that we may draw from our results is that for a more reasonable potential, one which is attractive over most its range, it is necessary that the potential be appreciable for neutron-proton separations considerably greater than 2×10^{-13} cm. Unfortunately, the present calculation throws very little light on the question of exactly how long the tail of a long-tailed potential must be to be consistent with the experimental data, and it would seem that relatively detailed calculations with potentials of special shapes are required to answer this question. This is certainly a drawback for the practical application of the present results.

A point worth discussion before closing is the question as to what further information about the deuteron would be required to appreciably extend the present rigorous lower bound on the cut-off range. The most unrealistic feature of the wave functions that we have found above is the rapid variation of the wave functions with radius. To eliminate these sharp variations, it is necessary to have some information which bears on this question, and the feature which immediately comes to mind is the average value of the kinetic energy of the deuteron. When information is forthcoming which allows one to place a reasonable upper bound on the kinetic energy of the deuteron, it should be possible (though perhaps requiring a rather difficult calculation) to increase considerably the lower bound on the range beyond the value computed here.

We wish to express our thanks to Miss Jean Snover and participating members of her computation group at Brookhaven National Laboratory for the execution of the numerical calculations necessary to obtain the present results.

Effects of the Atmosphere on the Penetrating Cosmic Radiation

ROBERT L. CHASSON
Department of Physics, University of Nebraska, Lincoln, Nebraska
(Received November 10, 1952)

A comparison is made of the results of three independent studies of upper-atmospheric influences on the penetrating cosmic radiation. The results of Cotton and Curtis are in disagreement with those of Duperier and the author, who agree very closely on the value of the upper-atmospheric temperature coefficient for the hard radiation observed at sea level. The work of Cotton and Curtis is examined with regard to method of data reduction, whereupon it is suggested that they are possibly in error because of statistical inadequacy of the cosmic-ray data and an improper mode of application of meteorological data.

COTTON and Curtis[1,2] have reported calculations of the dependency of hard cosmic-ray intensity upon fluctuations of barometric pressure, the altitude of the 100-mb level of the atmosphere, and the mean temperature of the 100-mb region. Their results agree essentially with those of Duperier[3] for the barometric and pressure-altitude coefficients, but they find no significant correlation with upper-atmospheric temperature changes. The latter result contradicts the results of Duperier and those of the author.[4]

The cause for disagreement is not obvious, but it is interesting to compare the conditions of the experiment of Cotton and Curtis with those of Duperier and the author. Table I presents a summary of the three individual experiments. It is seen that the work of Duperier has roughly 5 times the statistical reliability of counting compared with Cotton and Curtis. The work of the author is almost 2½ times as reliable in this respect. Furthermore, there is a question about the proper use of meteorological data in conjunction with the cosmic-ray data. Using four different pairs of daily radiosonde records, Duperier calculated daily average pressure-altitude and temperature for the 100-mb region. He claimed that missing data for one station could be found with negligible error by interpolating data from nearest ascents for the one station and simultaneous ascents for the other. He then proceeded to employ these daily averages in his calculation of regression coefficients.

The present author had available only two daily radiosondes, at 0300 and 1500 GMT (Oakland Airport Weather Station; 12 km from Berkeley, California). Any attempt to interpolate missing data was doomed to failure because even known values of pressure-altitude and temperature could not be so reproduced, showing the impossibility of calculating meaningful daily averages for these parameters. Because of this, only cosmic-ray data collected during the 3-hour period bracketing the time of the radiosonde flight were used for regression calculations. Furthermore, separate calculations were made for morning and afternoon flight periods.

At first the author attempted to make daily average values for the atmospheric parameters, and these were compared with cosmic-ray intensity. He found agreement with Duperier, as did Cotton and Curtis, on all but the temperature coefficient. For the latter he obtained inconsistent results. Confinement of the data, as described above, yielded results that were substantially more significant over all, including agreement with Duperier on the temperature coefficient.

Cotton and Curtis used the results of two independent but simultaneous radiosonde ascents made twice daily. In light of the Berkeley experience, there is reason to doubt the accuracy of their daily averages for upper-atmospheric parameters. Duperier indicated that useful averages could be calculated from four daily ascents, and his ability to correctly interpolate values indicates that his use of an averaging procedure is somewhat more valid.

One is quite sure that there is an effect relating cosmic-ray intensity to atmospheric temperature, and

TABLE I. Comparison of experiments.

Authors	Angular aperture of telescope (to vertical)	Absorber	Datum period	Total No. of datum periods	Approx. av. counts per datum period	Temperature coefficient (percent/°C)
Cotton and Curtis	17°7′ (max)	12 in. concrete 10 cm Pb	24 hr	45	2.2×10^4	$-(0.023\pm0.027)$
Duperier	18°×60°	25 cm Pb	24 hr	125	1.8×10^5	$-(0.124\pm0.032)$
Duperier	36°×71°	40 cm Pb	24 hr	156	3×10^5	$-(0.075\pm0.010)$
Chasson	38°×60°	20 cm Pb	3 hr	78	7.3×10^4	$-(0.068\pm0.018)$

[1] E. S. Cotton and H. O. Curtis, Phys. Rev. **84**, 840 (1951).
[2] H. O. Curtis and E. S. Cotton, Phys. Rev. **88**, 173 (1952).
[3] A. Duperier, Proc. Phys. Soc. (London) **A62**, 684 (1949); Nature **167**, 312 (1951); J. Atmos. Terr. Phys. **1**, 296 (1951).
[4] R. L. Chasson, Ph.D. thesis, University of California, 1951 (unpublished). This work was supported by the joint program of the U. S. Office of Naval Research and the U. S. Atomic Energy Commision.

it is obvious that the whole atmosphere must be considered before a complete correlation is at all possible. But it is not unreasonable to believe that the upper-atmospheric temperature should exert an appreciably large influence in this respect. Duperier has shown that much better correlation and larger regression coefficients are obtained by considering the region between 50 and 200 mb instead of that between 100 and 200 mb. His results are in agreement with the known lifetime of charged pions and the value of the mean free path for primary radiation in the atmosphere. Furthermore, if one believes the explanation of the cosine-squared zenithal dependence of the hard intensity at low altitude, he would expect to find that the temperature coefficient would increase as telescope solid angle is decreased. This result has been found by Duperier. The use of relatively small solid angle in the experiment of Cotton and Curtis should thus yield a value of the coefficient larger than those found by Duperier and the author, although the small-angle telescope should not yield as good statistics unless appreciably longer periods of observation are used.

PHYSICAL REVIEW VOLUME 89 NUMBER 6 MARCH 15, 1953

Molière's Theory of Multiple Scattering

H. A. BETHE
Laboratory of Nuclear Studies, Cornell University, Ithaca, New York
(Received November 28, 1952)

Molière's theory of multiple scattering of electrons and other charged particles is here derived in a mathematically simpler way. The differential scattering law enters the theory only through a single parameter, the screening angle χ_a', Eq. (21). The angular distribution, except for the absolute scale of angles, depends again only on a single parameter b, Eq. (22). It is shown that b depends essentially only on the thickness of the scattering foil in g/cm², and is nearly independent of Z.

The transition to single scattering is re-investigated. An asymptotic formula is obtained which agrees essentially with that of Molière, Snyder, and Scott, but which remains accurate down to smaller angles, Eq. (38).

The theory of Goudsmit and Saunderson has a close *quantitative* relation to that of Molière, and a good approximation to their distribution function can be obtained by multiplying Molière's function by $(\theta/\sin\theta)$. This relation holds until the scattering angles become so large that only very few terms in the series of Goudsmit and Saunderson need to be taken into account.

I. INTRODUCTION

At least four different theories of the multiple scattering of electrons by atoms have been published which are mathematically closely related, and which can give exact results if carefully evaluated. They are the work of Molière,[1] Snyder, and Scott,[2,3] Goudsmit and Saunderson,[4] and Lewis.[5] Of these, the first two use immediately the approximation of small scattering angles and therefore an expansion in Bessel functions (see below) (or a Fourier integral for the distribution of projected angles). Goudsmit and Saunderson develop a theory valid for any angle by means of an expansion in Legendre polynomials. Lewis starts from the Legendre expansion and then goes over to the limit of small angles, thus establishing the connection between the first three methods.

The theories of Molière and of Goudsmit and Saunderson share one important advantage, namely that they do not assume any special form for the differential scattering cross section. In both theories it is shown that the scattering depends only on a single parameter describing the atomic screening, the critical angle χ_a, Eq. (16) of this paper. This angle can then be calculated, for instance, for the Fermi-Thomas distribution of electrons in an atom, or for any more accurate electron distribution if available. Molière has even included the *deviation* of the differential scattering from the Born approximation, Eq. (21), and Hanson, Lanzl, Lyman, and Scott[6] have shown that this inclusion is important for explaining their own experimental results as well as those of Kulchitsky, Latyshev, and Andrievsky[7] for heavy elements. Snyder and Scott, as well as Lewis, assume a special scattering law, *viz.*, that derived from the exponentially screened potential, $Ze^2r^{-1}e^{-r/a}$. Only *a posteriori* did Scott[3] state that the treatment of Snyder and Scott[2] is mathematically identical with Molière's and can therefore also be generalized to his differential scattering law.

The theory of Goudsmit and Saunderson has, of course, the further advantage that it is valid for all

[1] G. Molière, Z. Naturforsch. **3a**, 78 (1948).
[2] H. Snyder and W. T. Scott, Phys. Rev. **76**, 220 (1949).
[3] W. T. Scott, Phys. Rev. **85**, 245 (1952).
[4] S. A. Goudsmit and J. L. Saunderson, Phys. Rev. **57**, 24 and **58**, 36 (1940).
[5] H. W. Lewis, Phys. Rev. **78**, 526 (1950).
[6] Hanson, Lanzl, Lyman, and Scott, Phys. Rev. **84**, 634 (1951).
[7] L. A. Kulchitsky and G. D. Latyshev, Phys. Rev. **61**, 254 (1942); Andrievsky, Kulchitsky, and Latyshev, J. Phys. (U.S.S.R.) **6**, 279 (1943).

angles. On the other hand, the small-angle theories have the advantage of considerably greater transparency. This is particularly true of the theory of Molière, which remains analytical to the end.

To an accuracy of 1 percent or better, the angular distribution is given by the sum of 3 analytical terms, Eqs. (25) to (29), the first of which is the well-known Gaussian, while the second goes over into the single-scattering formula at large angles and the third is a correction. Both second and third terms are easily evaluated.

It is possible to combine the advantages of both types of theories because, up to quite large foil thicknesses and scattering angles, the Goudsmit-Saunderson result can be expressed in terms of the simpler Molière theory (Sec. 8). However, this is only possible if the total path length rather than the actual foil thickness, is used as the independent variable.

Snyder and Scott have calculated the distribution of projected angle, Goudsmit and Saunderson that of total scattering angle, and Molière both. We shall restrict ourselves to total scattering angle.

The aim of this paper is to give a simpler derivation of Molière's equations, to show how one is led in a straightforward way to Molière's "screening angle" χ_a, and to derive a simple asymptotic formula for the correction to single (Rutherford) scattering. In most places, the same notation as Molière's is used. His equations are quoted as M with the appropriate number.

II. DERIVATION

Molière derives his fundamental equation (M 4.4) by considering successive collisions. Like Molière, we assume that all scattering angles are small so that $\sin\theta$ may be replaced by θ, and the scattering problem is equivalent to diffusion in the plane of θ. Now let $\sigma(\chi)\chi d\chi$ be the differential scattering cross section into the angular interval $d\chi$, and $f(\theta, t)\theta d\theta$ the number of electrons in the angular interval $d\theta$ after traversing a thickness t. Then the standard transport equation is

$$\partial f(\theta,t)/\partial t = -Nf(\theta,t)\int\sigma(\chi)\chi d\chi + N\int f(\boldsymbol{\theta}',t)\sigma(\chi)d\boldsymbol{\chi}, \quad (1)$$

where N is the number of scattering atoms per cm^3, $\boldsymbol{\theta}'=\boldsymbol{\theta}-\boldsymbol{\chi}$ is the vector in the plane representing the direction of the electron before the last scattering, and $d\boldsymbol{\chi}=\chi d\chi d\phi/2\pi$, where ϕ denotes the azimuth of the vector $\boldsymbol{\chi}$ in the plane.

Now we make the same Fourier (Bessel) transformation as Molière, expanding

$$f(\theta,t)=\int_0^\infty \eta d\eta J_0(\eta\theta)g(\eta,t) \quad (2)$$

so that

$$g(\eta,t)=\int_0^\infty \theta d\theta J_0(\eta\theta)f(\theta,t). \quad (3)$$

Then the Fourier transformation of (1) yields, using the folding theorem,

$$\partial g(\eta,t)/\partial t = -g(\eta,t)N\int_0^\infty \sigma(\chi)\chi d\chi[1-J_0(\eta\chi)]. \quad (4)$$

This can be integrated over t, giving

$$g(\eta,t)=e^{\Omega(\eta)-\Omega_0} \quad (5)$$

in the notation of Molière, where

$$\Omega(\eta)=Nt\int_0^\infty \sigma(\chi)\chi d\chi J_0(\eta\chi), \quad (6)$$

and Ω_0 is the value of (6) for $\eta=0$, i.e., the total number of collisions. In (5) we have used the fact that $g(\eta, 0)=1$ for all η, which follows from the assumption that $f(\theta, 0)$ is a two-dimensional δ-function $\delta(\boldsymbol{\theta})$, i.e., the incident beam is exactly in the direction $\theta=0$.

Equations (2) and (5) are Molière's fundamental equations (M 4.4, 4.5). It is convenient to treat $\Omega(\eta)-\Omega_0$ *together*, rather than splitting them up because, as Molière himself has pointed out, the total number of collisions Ω_0 is irrelevant, and $\Omega_0-\Omega(\eta)$ is much smaller than Ω_0 for the values of η which are important; $\Omega_0-\Omega(\eta)$ may be called the "effective number of collisions." Inserting our results back into (2), we have

$$f(\theta,t)=\int_0^\infty \eta d\eta J_0(\eta\theta) \times\exp\left[-Nt\int_0^\infty \sigma(\chi)\chi d\chi\{1-J_0(\eta\chi)\}\right]. \quad (7)$$

This equation is exact for *any* scattering law,[8] provided only the angles are small compared with a radian.

III. TRANSFORMATION

The scattering from atoms is characterized by the fact that σ decreases rapidly and in simple manner, as χ^{-4}, for large χ, and is complicated only for angles of the order of

$$\chi_0=\lambda\!\!\!^{-}/a=\lambda\!\!\!^{-}/(0.885a_0Z^{-\frac{1}{3}}), \quad (8)$$

[8] The derivation of Eq. (7) in essentially the same form as in this section was shown to the author by Henry Hurwitz, Jr. in 1949, without knowledge of Molière's paper and before publication of the paper by Snyder and Scott. The derivation by Lewis (see reference 5) which starts from finite angles and spherical harmonics, could be simplified by using small angles and Bessel functions from the beginning, and would then become essentially identical with that given in this section. Lewis' result is equivalent with (7), but he uses a special scattering law before arriving at the formula corresponding to (7). Of course, Lewis' proof establishes at the same time the connection between the Goudsmit-Saunderson theory and that of Molière.

where λ is the de Broglie wavelength of the electron, a_0 the Bohr radius, and a the Fermi radius of the atom. For any reasonable foil thickness, the width of the multiple scattering distribution is very large compared with χ_0, and this is the reason for the essential simplicity of Molière's theory.

Following Molière, we set

$$Nt\sigma(\chi)\chi d\chi = 2\chi_c^2 \chi d\chi q(\chi)/\chi^4, \tag{9}$$

where q is the ratio of actual to Rutherford scattering, and

$$\chi_c^2 = 4\pi N t e^4 Z(Z+1)z^2/(pv)^2; \tag{10}$$

p is the momentum and v the velocity of the scattered particle of charge z. The factor $Z+1$ instead of Z is to take into account the scattering by the atomic electrons, as first suggested by Kulchitsky and Latyshev.[7] The physical meaning of χ_c is that the total probability of single scattering through an angle greater than χ_c is exactly one. This angle was already used by Williams[9] in his theory of multiple scattering. The ratio $q(\chi)$ is 1 for large χ and decreases to zero at $\chi=0$, the main drop occurring in the neighborhood of χ_0.

Inserting (9) into (6) and (5), we get

$$-\log g(\eta, t) = \Omega_0 - \Omega(\eta)$$
$$= 2\chi_c^2 \int_0^\infty \chi^{-3} d\chi [1 - J_0(\chi\eta)] q(\chi). \tag{11}$$

The important values of η will be of order $1/\chi_c$ or less.[10] Since q becomes appreciably different from 1 only for values of χ of order χ_0, and since χ_0 is much less than χ_c (of the order of 1/100), it is possible to split the integral at some angle k such that

$$\chi_0 \ll k \ll 1/\eta \sim \chi_c. \tag{11a}$$

Then, for the part of the integral from k to infinity, $q(\chi)$ can be replaced by unity and the integral evaluated analytically. For the part from 0 to k, on the other hand, the argument of the Bessel function is small and we may write

$$1 - J_0(\chi\eta) = \tfrac{1}{4}\chi^2\eta^2, \tag{12}$$

which will make it possible to reduce the integral to a universal one, independently of η.

The analytical integral may be written:

$$\int_k^\infty d\chi \chi^{-3}[1 - J_0(\chi\eta)] = \eta^2 \int_{k\eta}^\infty dt t^{-3}[1 - J_0(t)]$$
$$\equiv \tfrac{1}{4}\eta^2 I_1(k\eta). \tag{13}$$

The integral I_1, defined by (13), can be integrated by parts and gives, since the lower limit $x = k\eta$ is small:

$$I_1(x) = 4\int_x^\infty \frac{dt}{t^3}[1 - J_0(t)] = \frac{2}{x^2}[1 - J_0(x)] + \frac{J_1(x)}{x}$$
$$+ \int_x^\infty \frac{dt}{t} J_0(t) = 1 - \ln x + \ln 2 - C + O(x^2), \tag{14}$$

where $C = 0.577\cdots$ is Euler's constant.

The lower range of integration gives, using (12),

$$\int_0^k d\chi \chi^{-3} q(\chi)[1 - J_0(\chi\eta)] = \tfrac{1}{4}\eta^2 \int_0^k q(\chi) d\chi/\chi$$
$$\equiv \tfrac{1}{4}\eta^2 I_2(k). \tag{15}$$

Molière now defines the characteristic screening angle χ_a by the equation[11]

$$-\ln \chi_a = \lim_{k=\infty}\left[\int_0^k q(\chi) d\chi/\chi + \tfrac{1}{2} - \ln k\right]. \tag{16}$$

Then, taking together (11) and (13) to (16), we get

$$\Omega_0 - \Omega(\eta) = \tfrac{1}{2}(\chi_c\eta)^2[-\ln(\chi_a\eta) + \tfrac{1}{2} + \ln 2 - C], \tag{17}$$

Putting then $\chi_c\eta = y$, we get

$$\Omega_0 - \Omega(\eta) = \tfrac{1}{4}y^2[b - \ln(\tfrac{1}{4}y^2)], \tag{18}$$

where

$$b = \ln(\chi_c/\chi_a)^2 + 1 - 2C \equiv \ln(\chi_c/\chi_a')^2. \tag{19}$$

Then, setting

$$\theta/\chi_c = \lambda, \tag{19a}$$

we get Molière's transformed equation

$$f(\theta)\theta d\theta = \lambda d\lambda \int_0^\infty y dy J_0(\lambda y) \exp[\tfrac{1}{4}y^2(-b + \ln \tfrac{1}{4}y^2)], \tag{20}$$

which is very much simpler in form than (7).

The derivation was based on the inequality (11a) and will, therefore, fail if η is of order $1/\chi_0$, or y of order $\chi_c/\chi_0 \sim e^{\frac{1}{2}b}$. Indeed, the exponent in (20) has a minimum when $y = y_1 = 2e^{\frac{1}{2}(b-1)}$; thereafter it increases and becomes in fact positive infinite as y goes to infinity. This increase is spurious and due to the approximation (11a); therefore, the integral should only be extended to $y = y_1$. How little difference this makes can be seen from the fact that the exponential, for $y = y_1$, has the value $\exp(-\frac{1}{4}y_1^2) = \exp(-e^{b-1})$. Since $e^b \sim (\chi_c/\chi_a)^2$ is about the number of collisions Ω_0, the formula (20) is correct to the relative order $e^{-\Omega_0/e}$. For foils of moderate thickness, the number of collisions is 1000 to 100 000 so

[9] E. J. Williams, Phys. Rev. **58**, 306 (1940).

[10] This is most easily seen from Eq. (17) according to which $g(\eta, t) = \exp[\Omega_0 - \Omega(\eta)]$ becomes extremely small when $\chi, \eta \gg 1$. The use of (17) to justify (11a) may seem circular because (17) itself is based on the assumption (11a); but the only part of (11a) actually used in deriving (17) is that $\eta\chi_0 \ll 1$. Our method will therefore be in error if, and only if, $\eta\chi_0$ is of the order 1, in which case (17) gives $g \sim \exp[-\frac{1}{4}(\chi_c/\chi_0)^2]$ which is exceedingly small (see the end of this section).

[11] The term $\frac{1}{2}$ would not need to be in the definition. It is included by Molière in order that χ_a be exactly λ/a for an exponentially screened potential, $V(r) = (Ze^2/r)e^{-r/a}$.

that the error would be only e^{-400} to $e^{-40\,000}$! Actually, the error in (17) for values of y of order 1 is more important; it gives corrections to $f(\theta)$ of order $1/\Omega_0$ with a small numerical factor.[12*]

IV. THE SCREENING ANGLE

Perhaps the most important result of Molière's theory is that the scattering is described by a single parameter, the screening angle χ_a'. The angular distribution depends only on the ratio of the "unit probability angle" χ_c, Eq. (9), which describes the foil thickness, to the screening angle χ_a' which describes the scattering atom. The distribution function $f(\theta)$ is entirely independent of the shape of the differential cross section $d\sigma$ provided only $d\sigma$ goes over into the Rutherford law for large angles. In most other[2,3,5] derivations of exact theories of multiple scattering, an explicit assumption was made about the differential cross section, namely the Born-approximation cross section for an exponentially screened potential. This potential is not a good approximation to the actual atomic potential, and the only rigorous published proofs that the shape of the potential is immaterial for the multiple scattering, are those of Molière and of Goudsmit and Saunderson.

For the actual determination of the screening angle χ_a, Molière uses his own calculation[13] of the *single* scattering by a Thomas-Fermi potential which does not make use of the Born approximation, the solution being accomplished by means of the WKB method. An exact formula for the differential cross section in terms of an integral is given in Molière's paper,[13] Eq. (4, 6), but his final evaluation of integrals over the Fermi function is numerical and only approximate; it yields

$$\chi_a^2=\chi_0^2(1.13+3.76\alpha^2), \quad \chi_a'^2=1.167\chi_a^2, \tag{21}$$

with α the usual parameter,

$$\alpha=zZe^2/\hbar v. \tag{21a}$$

The term in α^2 represents the deviation from the Born approximation. We now insert (21) and the definitions (8) and (10) of χ_0 and χ_c into the definition of b, Eq. (19); this gives

$$e^b=\frac{\chi_c^2}{\chi_a'^2}=\frac{\chi_c^2}{1.167\chi_a^2}$$
$$=4\pi N_0 t\left(\frac{h}{mc}\right)^2\frac{(Z+1)Z^{\frac{1}{3}}z^2 0.885^2}{\beta^2 A 1.167(1.13+3.76\alpha^2)}$$
$$=\frac{6680t}{\beta^2}\frac{(Z+1)Z^{\frac{1}{3}}z^2}{A(1+3.34\alpha^2)}, \tag{22}$$

where t is measured in g/cm², $\beta=v/c$, A is the atomic weight, and $N_0=6.02\times10^{23}$ is Avogadro's number. The relations $p\lambda=h$ and $a_0=\hbar^2/me^2$ have been used. It is interesting that the Z dependent last factor in (22) never deviates much from 1; its values for $z=1$ and $v=c$ are given in Table I. This means that the effective "number of collisions" per g/cm² is nearly the same for all elements.

TABLE I. Last factor in Eq. (22) as a function of atomic number.

Z	1*	6	10	20	30	40	50	70	92
$\frac{(Z+1)Z^{\frac{1}{3}}}{A(1+3.34\alpha^2)}$	1.00	1.05	1.15	1.32	1.27	1.20	1.00	0.90	0.70

* Deuterium; for hydrogen the factor is 2.00.

Hanson, Lanzl, Lyman, and Scott[6] have pointed out that the Thomas-Fermi potential is not suitable for substances of low atomic number, such as Be, and that in fact their experiments indicate a somewhat larger χ_a for this substance than that required by the Thomas-Fermi atom. If the potential of the atom is known, it is easy to insert it in (16) and thus to derive χ_a.

V. EVALUATION

Molière has given a satisfactory evaluation of (20) for all angles. He defines the new parameter B by the transcendental equation

$$B-\ln B=b, \tag{23}$$

and the variable ϑ by

$$\vartheta=\lambda B^{-\frac{1}{2}}=\theta/(\chi_c B^{\frac{1}{2}}). \tag{24}$$

It will also be useful to use

$$x=\vartheta^2. \tag{24a}$$

The value of B is usually between 5 and 20. The integration variable is now changed to

$$u=B^{\frac{1}{2}}y, \tag{24b}$$

and the distribution function is expanded in a power series in $1/B$, which gives

$$f(\theta)\theta d\theta=\vartheta d\vartheta[f^{(0)}(\vartheta)+B^{-1}f^{(1)}(\vartheta)+B^{-2}f^{(2)}(\vartheta)+\cdots], \tag{25}$$

where

$$f^{(n)}(\vartheta)=n!^{-1}\int_0^\infty u du J_0(\vartheta u)\times\exp(-\tfrac{1}{4}u^2)[\tfrac{1}{4}u^2\ln(\tfrac{1}{4}u^2)]^n. \tag{26}$$

[12] Exactly the same formulas as in this section were already obtained by Molière. The only difference is that he used in the proof a rather complicated series of Hankel functions, whereas we used the simple Bessel function J_0 so that every step in our derivation can be easily followed. This simplification made it possible to show in a more logical way why just the quantity χ_a, Eq. (16), enters the theory. Finally, it also makes possible a more precise estimate of the errors.

* *Note added in proof:*—We have not taken into account any spin or relativity corrections, except for the use of the relativistically correct denominator $(pv)^2$ in (10). These corrections are appreciable only at numerically large single-scattering angles χ, and therefore will not materially affect the small-angle multiple scattering treated in this section. In the region where single scattering predominates, it should still be a good approximation to consider the quantity R which will be calculated in Section VI, as the ratio of actual to correct single scattering.

[13] G. Molière, Z. Naturforsch. **2a**, 133 (1947).

TABLE II. Comparison of the asymptotic formulas for scattering with the exact theory.

ϑ	$f^{(0)}$	$f^{(1)}$	$f^{(2)}$	$\frac{1}{2}\vartheta^4 f^{(1)}$	$\frac{1}{2}\vartheta^4 f^{(2)}$
0	2	0.8456	2.4929	0	0
0.2	1.9216	0.7038	2.0694	0.0006	0.0008
0.4	1.7214	0.3437	1.0488	0.0044	0.0034
0.6	1.4094	−0.0777	−0.0044	−0.0050	−0.0003
0.8	1.0546	−0.3981	−0.6068	−0.0815	−0.1246
1	0.7338	−0.5285	−0.6359	−0.2642	−0.318
1.2	0.4738	−0.4770	−0.3086	−0.4946	−0.320
1.4	0.2817	−0.3183	0.0525	−0.6113	0.101
1.6	0.1546	−0.1396	0.2423	−0.4573	0.669
1.8	0.0783	−0.0006	0.2386	−0.0032	1.251
2	0.0366	+0.0782	0.1316	0.6258	1.053
2.2	0.01581	0.1054	0.0196	1.2347	0.475
2.4	0.00630	0.1008	−0.0467	1.6718	−0.775
2.6	0.00232	0.08262	−0.0649	1.8877	−1.483
2.8	0.00079	0.06247	−0.0546	1.9200	−1.676
3	0.000250	0.04550	−0.03568	1.8429	−1.448
3.2	7.3×10^{-5}	0.03288	−0.01923	1.7240	−1.008
3.4	1.9×10^{-5}	0.02402	−0.00847	1.6050	−0.566
3.6	4.7×10^{-6}	0.01791	−0.00264	1.5038	−0.222
3.8	1.1×10^{-6}	0.01366	0.00005	1.4237	0.005
	$1000\,f^{(0)}$	$1000\,f^{(1)}$	$1000\,f^{(2)}$		
4	2.3×10^{-4}	10.638	1.0741	1.3617	0.1375
4.5	3×10^{-5}	6.140	1.2294	1.2588	0.2521
5	2×10^{-6}	3.831	0.8326	1.1972	0.2602
5.5	2×10^{-10}	2.527	0.5368	1.1563	0.2456
6	5×10^{-12}	1.739	0.3495	1.1275	0.2264
7	1×10^{-18}	0.9080	0.1584	1.0901	0.1901
8	3×10^{-26}	0.5211	0.0783	1.0679	0.1604
9	1×10^{-32}	0.3208	0.0417	1.0523	0.1369
10	1×10^{-40}	0.2084	0.0237	1.0419	0.1186

For the first two functions $f^{(n)}$, he gives simple analytical formulas,

$$f^{(0)}=2e^{-x}, \tag{27}$$

$$f^{(1)}=2e^{-x}(x-1)[\overline{\mathrm{Ei}}(x)-\ln x]-2(1-2e^{-x}), \tag{28}$$

where $\overline{\mathrm{Ei}}$ is defined in Jahnke-Emde.[14]

The next partial function $f^{(2)}$ is given by Molière in terms of a definite integral, *viz.*

$$\tfrac{1}{4}e^x f^{(2)}=[\Psi^2(2)+\Psi'(2)](x^2-4x+2)+\int_0^1 t^{-3}dt[\ln t/(1-t)-\Psi(2)][(1-t)^2e^{xt}-1-(x-2)t-(\tfrac{1}{2}x^2-2x+1)t^2], \tag{29}$$

where $\Psi(n)=d\ln\Gamma(n+1)/dn$, as defined by Jahnke and Emde. We have not found any way to evaluate the integral analytically, but a power series was obtained by Dr. Max Goldstein of the Los Alamos Scientific Laboratory, *viz.*

$$\text{Integral}=\sum_{n=0}^{\infty}\frac{1}{n+1}[\Psi(n)+C-\Psi(2)]\times\left[\frac{x^{n+3}}{(n+3)!}-\frac{2x^{n+2}}{(n+2)!}+\frac{x^{n+1}}{(n+1)!}\right]. \tag{29a}$$

Dr. Goldstein was able to use this series to evaluate $f^{(2)}$ for ϑ up to 10, or x up to 100. Various transformations of (29a) were found but none proved more practical than the series itself.

In Table II, we give the functions $f^{(0)}$, $f^{(1)}$, and $f^{(2)}$ more accurately and over a wider interval of ϑ than Molière.[15] We also give $\frac{1}{2}\vartheta^4 f^{(i)}$, $i=1$ and 2, because these functions determine the ratio to Rutherford scattering at large angles, Eq. (32), and are easier to interpolate than the f's themselves. As will be shown, the functions $f^{(0)}$ to $f^{(2)}$ are sufficient to determine the distribution function to about 1 percent or better for any angle.

For small angles, i.e., ϑ less than about 2, the Gaussian $f^{(0)}$ is the dominant term. In this region, $f^{(1)}$ is in general less than $f^{(0)}$, so that the correction to the Gaussian is of order $1/B$, i.e., of the order of 10 percent. Hanson *et al.*,[6] have pointed out that a better approximation than $f^{(0)}$ in this region is given by a Gaussian of slightly *smaller* width: The angle at which the intensity has dropped to $1/e$ of the maximum, is

$$\theta_w=\chi_c(B-1.2)^{\frac{1}{2}} \tag{30}$$

rather than $\theta_w=\chi_c B^{\frac{1}{2}}$, and a Gaussian of width (30) is the better approximation mentioned.

The formula for the width of the multiple scattering peak can be understood simply as follows: The width can in principle be found by calculating the average of χ^2 from the single-scattering law, but since $\sigma(\chi)$ is proportional to χ^{-4}, the integral $\int\chi^2\sigma(\chi)\chi d\chi$ diverges logarithmically at large χ. Now a reasonable way to cut off this divergence is to extend the integral to $\chi=\theta_w$, the width of the multiple scattering peak itself. This leads to the transcendental equation (23) for the width parameter, B.

For *larger angles*, $\vartheta>2$, the function $f^{(1)}$ in (28) becomes larger than $f^{(0)}$. Indeed, for very large ϑ, (28) goes over into the single scattering law $f^{(1)}=2\vartheta^{-4}$, while $f^{(0)}$ decreases exponentially. Now the fortunate point is that $f^{(2)}$ and the higher $f^{(n)}$ behave for large ϑ as ϑ^{-2n-2} and the series (25) therefore converges even faster at large ϑ than at moderate ones. Therefore, $f^{(0)}+B^{-1}f^{(1)}$ will be a good approximate representation of the distribution at *any* angle. If an accuracy of 1

[14] E. Jahnke and F. Emde, *Table of Functions* (Dover Publications, New York, 1945), pp. 1 and 2.

[15] In general, agreement with Molière is good, the maximum error being about 3 units of the last significant figure carried by him. The only major error in Molière's table is $f^{(2)}(\vartheta)$ for $\vartheta=3.5$ for which he gives +0.0052, while the correct value is −0.0051. This mistake had caused us considerable trouble in trying to obtain smooth distributions.

percent is desired, and if B is of order 10, the function $f^{(2)}$ must be included. This is sufficient, even at large angles where $f^{(1)}$ is the dominant term, because $f^{(2)}$ is smaller than $f^{(1)}$ in this region, as can be seen both from Table II and from the asymptotic formula (34), and $f^{(3)}$ is presumably still smaller.

VI. ASYMPTOTIC FORMULA

In the limit of large angles, the distribution function tends toward the Rutherford single-scattering law. According to (9), (19a), and (24), this is

$$f_R(\theta)\theta d\theta = 2d\lambda/\lambda^3 = (2/B)d\vartheta/\vartheta^3. \tag{31}$$

Therefore the ratio of actual to Rutherford scattering is, using (25),

$$R = f/f_R = \tfrac{1}{2}\vartheta^4(f^{(1)} + B^{-1}f^{(2)} + \cdots), \tag{32}$$

neglecting the Gaussian term $Bf^{(0)}$. The relative magnitude of this term can be seen from Table I.

For $f^{(1)}$, Molière (M 9.3a) gives the asymptotic expression

$$R_1 \equiv \tfrac{1}{2}\vartheta^4 f^{(1)} = (1 - 5\vartheta^{-2})^{-4/5}, \tag{33}$$

whose expansion in inverse powers of ϑ agrees with that of the exact expression (28) up to and including the term of order ϑ^{-4} and agrees reasonably well with it even in higher orders. Similarly, the asymptotic behavior of $f^{(2)}$ is

$$R_2 \equiv \tfrac{1}{2}\vartheta^4 f^{(2)} = 8\vartheta^{-2}(\ln\vartheta + C - \tfrac{3}{2})/1 - 9\vartheta^{-2} - 24\vartheta^{-4}. \tag{34}$$

In (34), $C - \frac{3}{2}$ may be replaced by ln0.4 which differs from it by only 0.0065. Equation (34) is about 6 percent too high at $\vartheta = 6$, 1.2 percent high at $\vartheta = 8$, and 0.2 percent high at $\vartheta = 10$. The error of Eq. (33) is much smaller; in parts per thousand, it is

For $\vartheta =$	3	3.2	3.6	4	5	6	8	10
Error =	+40	−8	−17	−9	−1.4	−0.8	−0.5	−0.1

The most obvious way to obtain an asymptotic formula for R is to expand (33) and (34) in inverse powers of ϑ and neglect all terms of order ϑ^{-4} and higher. This procedure, however, is obviously very inaccurate since the higher terms in the series expansion of (33) have very large coefficients. A much better convergent series is obtained by taking the *reciprocal*,

$$R_1^{-1} = (1 - 5\vartheta^{-2})^{4/5} = 1 - 4\vartheta^{-2} - 2\vartheta^{-4} - \cdots. \tag{35}$$

Because of the denominator occurring in its first term, (34) gives a simple result when combined with (33), namely (including order ϑ^{-4}),

$$R^{-1} = 1 - 4\vartheta^{-2}[1 + 2B^{-1}\ln(0.4\vartheta)] + 2\vartheta^{-4}(12B^{-1} - 1). \tag{36}$$

Here $R = R_1 + (R_2/B)$ is the ratio of actual to Rutherford scattering, so that R^{-1} is the ratio of Rutherford to actual. A term of order $B^{-2}\vartheta^{-4}$, arising from $f^{(3)}$, has been neglected.

A further simplification of (36) can be effected by noting that in most practical cases B is of the order of 10, so that the last term in (36) is very small. We may then write

$$R^{-1} = 1 - 4\vartheta^{-2}[1 + 2B^{-1}\ln(2\vartheta/5)]. \tag{37}$$

Here we may re-insert the value of ϑ and B from (23), (24), (19) and get for the ratio of *Rutherford to actual* scattering without further approximation,

$$1/R = 1 - 8(\chi_c^2/\theta^2)\ln(2\theta/5\chi_a'). \tag{38}$$

In Table III, we have compared the asymptotic formulas (36) and (37) with the exact value of R for two values of B and various values of ϑ. The ratio of the first to the second term in Molière's series (25), $Bf^{(0)}/f^{(1)}$, is also listed: this ratio is small in the asymptotic region. It is seen from the table that for $B = 14$, the simpler asymptotic expression (37) is excellent, down to $\vartheta = 2.4$, i.e., right down to the point where the Gaussian begins to dominate. For $B = 7.3$, the agreement is not quite so good, and the more complicated expression (36) is somewhat better than the simple (37), although a larger correction than the last term of (36) would improve the agreement. Anyway, also for $B = 7.3$ the agreement is good down to $\vartheta = 3$. The fact that $f^{(1)}$ and $f^{(2)}$ combine in such a simple way to give the asymptotic formula (38) may seem somewhat mysterious from the derivation given here. A more natural derivation is given in Appendix A.

The main difference between (38) and previous asymptotic formulas is that (38) gives $1/R$ rather than R, and that the asymptotic series for $1/R$ obviously converges much better than that for R. Otherwise, in agreement with the theories of Molière and of Snyder and Scott, (38) has a logarithmic dependence of the correction term on ϑ, in addition to the $1/\vartheta^2$ dependence. Other theories, e.g., that of Butler,[16] failed to get the logarithmic dependence but had $\ln(\chi_c/\chi_a)$ instead.

As was pointed out before, χ_c^2/θ^2 is the probability of having a single scattering through an angle greater than θ in the foil. The correction term in (38) is roughly 50 times greater than this probability. This shows that the approach to single scattering is extremely slow as has been pointed out in the earlier papers.

VII. COMPARISON WITH EXPERIMENT

Hanson, Lanzl, Lyman, and Scott[6] have shown that Molière's theory is in almost perfect agreement with their experiments, up to angles ϑ (Sec. 5) of about 2 or

TABLE III. Comparison of asymptotic formulas with exact value.

ϑ	4	3.6	3.2	3	2.8	2.6	2.4	2.2
$B = 14$								
Exact	1.373	1.49$_8$	1.70$_5$	1.87$_8$	2.14	2.52	3.08	3.84
Eq. (37)	1.362	1.48$_8$	1.68	1.84	2.07$_8$	2.47$_8$	3.22	5.30
$Bf^{(0)}/f^{(1)}$	0.0003	0.004	0.031	0.077	0.18	0.39	0.88	2.10
$B = 7.3$								
Exact	1.378	1.477	1.610	1.71$_8$	1.87	2.07		
Eq. (36)	1.384	1.49$_6$	1.68	1.82	2.01$_8$	2.29		
Eq. (37)	1.393	1.513	1.71$_8$	1.87	2.10$_8$	2.45		
$Bf^{(0)}/f^{(1)}$	0.0001	0.005	0.015	0.04	0.09	0.20		

[16] S. T. Butler, Proc. Phys. Soc. (London) **A63**, 599 (1950).

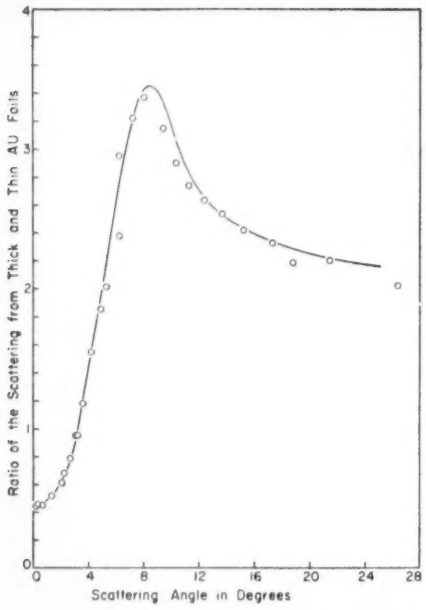

FIG. 1. Comparison of the experiments of Hanson *et al.* with the theory. Abscissa is scattering angle; ordinate is the ratio of the scattering by two gold foils differing by a factor 2 in thickness.

3 (their Fig. 3). They showed that similarly good agreement exists with the earlier experiments of Andrievsky, Kulchitsky, and Latyshev.[7]

At larger angles, the analysis was made somewhat difficult by the absence of accurate tables of Molière's functions for these angles. Hanson *et al.*, interpolated between Molière's tables and his asymptotic formula, which do not fit accurately together. This is especially apparent in their Fig. 4 which gives the ratio of the scattering by two gold foils having a ratio 2 in thickness: Molière's asymptotic formula gives smaller scattering ratios than observed.

In Fig. 1, we have compared the experiments with our more accurate Table II, which we have already shown to agree with our asymptotic formula (38) in Table III. The agreement is seen to be excellent. At large angles, our theoretical curve now lies slightly above the measurements, whereas Hanson's lay below. The position of the maximum now agrees exactly with experiment while Hanson's was shifted somewhat toward larger angles.

VIII. COMPARISON WITH THE THEORY OF GOUDSMIT AND SAUNDERSON

Goudsmit and Saunderson[4] have shown that for any angle, small or large, the angular distribution is given *exactly* by

$$f(t,\theta)=\sum(l+\tfrac{1}{2})P_l(\theta)$$
$$\times\exp\left\{-Nt\int\sigma(\chi)\sin\chi d\chi[1-P_l(\chi)]\right\}, \quad (39)$$

where $f(t,\theta)\sin\theta d\theta$ is the number of electrons between θ and $\theta+d\theta$.

It should be noted that the quantity t means actually the distance travelled along the path of the electron. No attempt is being made in this paper to take into account the "detour factor," i.e., the difference between the distance travelled and the foil thickness, produced by the crooked path. This problem has been considered by Wang and Guth.[17]

Lewis[5] has pointed out that expression (39) goes over into the small-angle expression of Molière, Snyder, and Scott if we replace $\sin\theta$ by θ and P_l by the well-known formula[18]

$$P_l(\theta)=J_0((l+\tfrac{1}{2})\theta), \quad (40)$$

which is valid for small θ regardless of whether l is small or large. To obtain (7), $l+\frac{1}{2}$ is replaced by η and the sum over l by an integral over η.

The approximation made by Molière therefore consists of 3 parts, *viz.* (a) the replacement of the sum over l by an integral, (b) approximations made in the exponential in (39), and (c) the use of the approximate formula (40) in the factor $P_l(\theta)$. Concerning (a), we may use the Euler summation formula,

$$\sum_{l=0}^{\infty}g(l+\tfrac{1}{2})=\int_0^{\infty}g(\eta)d\eta+\frac{1}{24}g'(0)+\cdots. \quad (41)$$

Now in our case, according to (20),

$$g(\eta)=\eta J_0(\eta\theta)\exp[\tfrac{1}{4}\eta^2(-b+\ln\tfrac{1}{4}\eta^2\chi_c^2)], \quad (42)$$

and therefore

$$g'(0)=1, \quad (42a)$$

from which

$$f_{GS}(t,\theta)=f_M(t,\theta)+1/24+\cdots. \quad (43)$$

(GS = Goudsmit and Saunderson, M = Molière). In the Gaussian region, $f_M\approx 1/\chi_c^2$ so that the correction term 1/24 is very small as long as the critical angle χ_c is small compared with a radian. In the single-scattering region where θ is large, higher-order corrections in the Euler formula become important; the correction 1/24 should certainly not be used when f_M is of the order of 1/24 or less, and it should generally be regarded as an estimate of error rather than as a useful correction.

Now we investigate the errors introduced in the *exponent* of (39). First of all, it is now necessary to use the exact Rutherford formula,

$$Nt\sigma(\chi)\sin\chi d\chi=2\chi_c^2q(\chi)\frac{\sin\chi d\chi}{4(1-\cos\chi)^2}, \quad (44)$$

where χ_c is still given by (10). For angles χ small compared with a radian, (44) goes over into our old

[17] M. C. Wang and E. Guth, Phys. Rev. **84**, 1092 (1951).

[18] This formula is slightly more accurate than that given by Lewis, Eq. (19), in which $l+\frac{1}{2}$ is replaced by l.

formula (9). As in Sec. 3, we break the integral up into two parts, from 0 to k and from k to π, and, similarly to (11a) we choose k such that

$$\chi_0 \ll k \ll 1/l. \tag{44a}$$

Then, in the region from 0 to k, we may use the formula

$$1-P_l(\chi)=\tfrac{1}{4}l(l+1)\chi^2 \tag{45}$$

and replace (44) by (9); then we get

$$\int_0^k Nt\sigma(\chi)\sin\chi d\chi[1-P_l(\chi)] = \tfrac{1}{2}\chi_c^2 l(l+1)\int_0^k (d\chi/\chi)q(\chi), \tag{46}$$

in complete analogy with (15). The screening angle χ_a may then be introduced by (16), in analogy with Goudsmit and Saunderson.

In the interval $\chi > k$, we replace $q(\chi)$ by 1, as in (13). Then, for $l=1$, this part of the integral is elementary:

$$\tfrac{1}{2}\chi_c^2\int_k^\pi \frac{\sin\chi d\chi}{1-\cos\chi}=\tfrac{1}{2}\chi_c^2\ln(1-\cos\chi)\Big|_k^\pi=\chi_c^2\ln(2/k). \tag{47}$$

For other values of l, Goudsmit and Saunderson have shown that

$$Nt\int_k^\pi \sigma(\chi)\sin\chi d\chi[1-P_l(\chi)] = \tfrac{1}{2}\chi_c^2 l(l+1)\left[\ln(2/k)-\left(\tfrac{1}{2}+\tfrac{1}{3}+\cdots+\frac{1}{l}\right)\right]. \tag{48}$$

GS have omitted the proof of this formula as too lengthy; Lewis has given a proof which is somewhat complicated. An elementary proof is given in Appendix B.

Adding (46) and (48), and using (16) and (19), we get for the GS exponent,

$$\begin{aligned} Q_l &\equiv \int_0^\pi Nt\sigma(\chi)\sin\chi d\chi[1-P_l(\chi)] \\ &= \tfrac{1}{2}\chi_c^2 l(l+1)\left[\ln 2/\chi_a-\tfrac{1}{2}-\left(\tfrac{1}{2}+\tfrac{1}{3}+\cdots+\frac{1}{l}\right)\right] \\ &= \tfrac{1}{2}\chi_c^2 l(l+1) \\ &\quad\times\left[-\ln\chi_a'+\ln 2+C-\left(1+\tfrac{1}{2}+\cdots+\frac{1}{l}\right)\right]; \end{aligned} \tag{49}$$

or, using the well-known formula[19]

$$1+\tfrac{1}{2}+\tfrac{1}{3}+\cdots+\frac{1}{l}=\Psi(l)+C, \tag{50}$$

[19] See reference 14, p. 19.

with $\Psi(x)=d\ln\Gamma(x+1)/dx$, we get

$$Q_l=\tfrac{1}{2}\chi_c^2 l(l+1)[-\ln(\tfrac{1}{2}\chi_a')-\Psi(l)]. \tag{51}$$

This very simple formula is correct for all l which satisfy (44a). This limitation is the same as that of (11a) and, like the latter, introduces errors of the order of $1/\Omega_0$ at most, with Ω_0 the number of collisions (see end of Sec. 3).

We now use for Ψ the asymptotic formula,[18]

$$\Psi(l)=\ln(l+\tfrac{1}{2})+\frac{1}{24}(l+\tfrac{1}{2})^{-2}+\cdots. \tag{52}$$

Neglecting the second term, setting $l+\frac{1}{2}=\eta=y/\chi_c$, and introducing b from (19), (51) becomes

$$Q_l=\tfrac{1}{4}\chi_c^2 l(l+1)[b-\ln(\tfrac{1}{4}y^2)]. \tag{53}$$

This differs from Molière's formula, (18), only by having the factor $l(l+1)$ instead of $(l+\frac{1}{2})^2$ outside the bracket.

The neglect of the second term in (52) is obviously justified for large l. Indeed, for large l it must be expected that the Goudsmit-Saunderson theory *should* give the same as Molière's because in this case the rapid oscillation of $P_l(\chi)$ destroys the contributions to the integral Q_l from large angles χ, while for small angles the approximations (9) and (40) are justified. However, this argument does not hold for small l, especially for $l=1$, and in this case 3 approximations are made in Molière's theory: the replacement of the Rutherford law (44) by (9), the replacement of the Legendre polynomial by the Bessel function (40), and that of the upper limit π of the angular integration by infinity. Equation (52) shows then that these approximations compensate almost exactly, the error being only 0.019 for $l=1$.

According to (53), the factor η^2 in Molière's exponent, e.g., in Eq. (17), should be replaced by $l(l+1)$. In other words, the integrand in (20) should be multiplied by

$$\exp[\tfrac{1}{16}\chi_c^2(b-\ln\tfrac{1}{4}y^2)]. \tag{54}$$

Now, according to the beginning of Sec. 5, the most important values of y are of order $B^{-\frac{1}{2}}$, making the parenthesis in (54) equal to B, according to (23). Therefore,

$$f_{GS}\approx f_M\exp(\tfrac{1}{16}\chi_c^2 B). \tag{55}$$

Finally, we consider the factor $P_l(\theta)$ in (39). Molière [reference 13, Eq. (A.1)] has derived a formula considerably more accurate than (40), *viz.*

$$P_l(\theta)=(\theta/\sin\theta)^{\frac{1}{2}}J_0((l+\tfrac{1}{2})\theta). \tag{56}$$

At an angle as large as 90°, this formula gives 1.067, 0.032, and -0.502, respectively, for $l=0$, 1, and 2, as compared with the correct values 1, 0 and -0.5. For all except very low l, the expression remains good even up to values of θ close to 180°, and breaks down only in the immediate neighborhood of 180°. For small angles, the approximation is, of course, particularly good.

Combining the three corrections, we get the approximate formula

$$f_{GS}=(\theta/\sin\theta)^{\frac{1}{2}}\exp(\tfrac{1}{16}\chi_c^2B)f_M+1/24. \quad (57)$$

From its derivation, this formula should be good approximately for $\chi_c^2B\leqslant 1$, i.e., until the Gaussian has a width of about one radian. At this point, the exponential in (57) gives a correction of only 6 percent so that it can in general be neglected. For larger values of χ_c^2B, i.e., larger thickness of foil, only 2 or 3 terms in the Goudsmit-Saunderson formula (39) need to be taken into account so that this formula becomes very easy to handle directly. For smaller thickness, (57) may be used, and since both the exponential and the 1/24 are in general unimportant, the angular distribution may simply be written

$$f_M(\theta)(\theta\sin\theta)^{\frac{1}{2}}d\theta, \quad (58)$$

where f_M is the Molière distribution function as calculated in this paper.

As pointed out in the beginning of this section, t is the total length of path of the electron, rather than the foil thickness t'. The difference $t-t'$ gives effects of the same order as the difference between the Goudsmit-Saunderson and the Molière distribution.

Lewis[5] has shown how the energy loss can be taken into account and has calculated the lateral distribution in space.

I am greatly indebted to Dr. Max Goldstein of the Los Alamos Scientific Laboratory for the calculation of Table II and the development of methods which made this calculation possible. I also wish to thank Dr. Hanson of the University of Illinois for drawing my attention to Molière's theory and for discussion of the experiments, to Stanley Cohen of Cornell University for help with Table I and the figure, and to Dr. Henry Hurwitz of the Knolls Atomic Power Laboratory for showing me the essentials of the proof of Sec. 2 in 1949.

APPENDIX A. ALTERNATIVE DERIVATION OF ASYMPTOTIC FORMULA

We consider the region of large angles in which $f^{(1)}$, Eq. (28) dominates over all other contributions. According to Table II, $f^{(0)}$ becomes unimportant for $\vartheta>3$. We shall neglect all terms which decrease exponentially with ϑ, such as $f^{(0)}$, but keep terms which decrease as inverse powers, ϑ^{-n}. We have shown at the end of Sec. 5 that $f^{(3)}$ can be neglected to an accuracy of 1 percent or better, so that we need consider only $f^{(1)}$ and $f^{(2)}$.

We shall now show that it is possible to combine these two terms, by re-arrangement of terms in the expansion (25). For this purpose, we start again from the exact formula (20) but introduce $\lambda y=z$, rather than u, as the integration variable. We then write the exponent of the exponential as follows:

$$\tfrac{1}{4}y^2(-b+\ln\tfrac{1}{4}y^2)$$
$$=(z^2/4\lambda^2)[-b-2\ln(2\lambda/k)+2\ln(z/k)], \quad (61)$$

where k is a numerical constant which will be determined later to our convenience. We further introduce the abbreviations

$$\beta\equiv\vartheta_1^{-2}\equiv[b+2\ln(2\lambda/k)]/\lambda^2. \quad (62)$$

Since b is in general large compared to the logarithm, the ϑ_1, defined in (62) is close to ϑ of (24) but is not identical with it. In our asymptotic region, ϑ_1 is large and β small.

The distribution function (20) becomes now

$$f(\theta)\theta d\theta=(d\lambda/\lambda)\int_0^\infty zdzJ_0(z)$$
$$\times\exp(-\tfrac{1}{4}\beta z^2)\exp[(z^2/2\lambda^2)\ln(z/k)]. \quad (63)$$

Expanding the last exponential, the first term will, upon integration, give a function like $f^{(0)}$ which decreases exponentially with angle λ, and can therefore be neglected. The second term will give a funcion like $f^{(1)}$ which will be our main contribution. The third term gives, except for a constant factor $(8\lambda^4)^{-1}$:

$$F^{(2)}=\int_0^\infty zdzJ_0(z)\exp(-\tfrac{1}{4}\beta z^2)z^4(\ln z/k)^2. \quad (64)$$

Our simplification will now be achieved by making $F^{(2)}$ equal to zero by appropriate choice of the free numerical constant k. Then the distribution function is reduced to $F^{(1)}$ alone.

In the limit of small β, the integral (64) can be evaluated analytically and gives

$$\lim_{\beta=0}F^{(2)}=-128(\tfrac{3}{2}+\ln 2-C-\ln k). \quad (65)$$

To make this zero, we have to choose

$$k=5.0325 \quad (65a)$$

or nearly 5. The result (65) is closely related to Molière's asymptotic formula for $f^{(2)}$, Eq. (34).

For somewhat larger β, it is possible to estimate k by considering the integral (63) in the complex plane. We first substitute for $J_0(z)$ the real part of the Hankel function $H_0^{(1)}(z)$. Then we replace the integral along the positive real axis of z by one along the following contour: We follow the imaginary axis up to $z=2i/\beta$ and then go parallel to the positive real axis. To evaluate the integral along the imaginary axis, we write $z=ix$, with x real, and get for the integral in (63):

$$-\mathrm{Re}\int_0^{2/\beta}xdxH_0^{(1)}(ix)e^{\frac{1}{4}\beta x^2}$$
$$\times\exp[-(x^2/2\lambda^2)\{\ln(x/k)+\pi i/2\}]. \quad (66)$$

Since most of the contribution comes from large x, see Eq. (70), we may replace the Hankel function by its asymptotic expression,

$$H_0^{(1)}(ix)=-i(2/\pi x)^{\frac{1}{2}}e^{-x}. \quad (67)$$

As in Eq. (25), it is now simplest to expand the last exponential in (66). The first term in this expansion, 1 is purely real. The integral in (66) is then purely imaginary, which means that the integral along the imaginary axis gives no contribution at all. This leaves only the second part of the contour parallel to the real axis which obviously gives a contribution proportional to the value of the integrand at $x=2/\beta$ which is about $\exp(-x+\frac{1}{4}\beta x^2)=\exp(-1/\beta)=\exp(-\vartheta_1^2)$. This explains the exponential decrease of $f^{(0)}$, Eq. (27). (For β moderate or large, this term is of course large.)

The second term in the expansion of the exponential is

$$-(x^2/2\lambda^2)[\ln(x/k)+\pi i/2]. \tag{68}$$

Only the imaginary part matters, so that the integral becomes

$$(\pi/2)^{\frac{1}{2}}(2\lambda^2)^{-1}\int_0^{2/\beta} x^3\exp(-x+\tfrac{1}{4}\beta x^2)x^{-\frac{1}{2}}dx. \tag{69}$$

We now consider the integrand of (69), which we define as

$$x^3\exp(-x+\tfrac{1}{4}\beta x^2). \tag{69a}$$

The factor $x^{-\frac{1}{2}}$ is better included with dx as will be shown below, Eq. (72). This integrand has a maximum at

$$x_1=\beta^{-1}[1-(1-6\beta)^{\frac{1}{2}}]. \tag{70}$$

In the limit of small β which interests us particularly, x_1 has the value 3. This is large enough to use the asymptotic formula (67) but is very small compared with $2/\beta$. The main contribution to the integral (69) comes then from the neighborhood of x_1 and the integral can be evaluated by a saddle point method. The resulting asymptotic formula is similar to (35). For larger β, x_1 increases; for $\beta=\frac{1}{6}$, it reaches the value $1/\beta=6$. For still larger β, there is no longer any solution x_1: The integrand (69a) then has no maximum for real x but increases monotonically to $x=2/\beta$. Then the main contribution comes from the neighborhood of that point: We get into the region where the Gaussian dominates. Thus we should expect that our asymptotic theory will hold reasonably well for $\beta\ll\frac{1}{6}$ or $\vartheta_1^2\gg 6$, $\vartheta_1>2.45$. This is in agreement with Table III which shows that at about $\vartheta=2.45$, formula (37) breaks down and simultaneously the Gaussian $f^{(0)}$ becomes more important than $f^{(1)}$.

We now turn to the third term in the expansion of the exponential in (66) which is

$$-(x^2/2\lambda^2)^2[\ln(x/k)+\pi i/2]^2. \tag{71}$$

The imaginary part of this which is the only part giving a contribution, yields the integral

$$F^{(2)}\sim\int x^5\exp(-x+\tfrac{1}{4}\beta x^2)\ \ln(x/k)x^{-\frac{1}{2}}dx. \tag{72}$$

If β is neglected, the integrand is x^5e^{-x} and has a maximum at $x=5$. Therefore the integral, evaluated by the method of steepest descent, will be zero if k is set equal to 5. It was shown in (65a) that this is very nearly correct, the exact value of k being 5.0325. This is the reason why we included $x^{-\frac{1}{2}}$ with dx; had we included it with the integrand, the maximum would occur at $x_2=4.5$ which would give less accurate results.

For finite values of β, the exponential has a maximum at

$$x_2=\beta^{-1}[1-(1-10\beta)^{\frac{1}{2}}]. \tag{73}$$

The method of steepest descent will therefore fail for $\beta>\frac{1}{10}$ or $\vartheta_1<10^{\frac{1}{2}}=3.16$; at this point, $x_2=10$. For smaller β, the method can be applied and shows that $F^{(2)}=0$, if we set

$$k=x_2. \tag{73a}$$

Therefore, if we define ϑ_1 by (62) and insert for k the value (73), the distribution function is given by $f^{(1)}(\vartheta_1)$ alone, without any contribution $f^{(2)}$.

According to (73), k depends on ϑ_1 so that ϑ_1 is defined by an implicit equation which is not convenient. However, in the region in which the method is useful at all, (73) may be expanded, giving[20]

$$k=x_2=5/(1-5\beta/2+\cdots). \tag{74}$$

The useful range is somewhat better covered by putting

$$k=5/(1-3\beta). \tag{74a}$$

This is accurate within better than 1 percent for $\vartheta_1>4$, $\beta<\frac{1}{16}$. Inserting into (62), we get then

$$\lambda^2\vartheta_1^{-2}=b+2\ln(2\lambda/5)+2\ln(1-3\vartheta_1^{-2}), \tag{75}$$

which is still implicit but now very simple.

The last term in (75) is small and can therefore be treated approximately. In particular, it will be shown presently that ϑ_1 is very nearly equal to ϑ in the region $\vartheta_1\sim 3.5$, i.e., where the asymptotic treatment just begins to be valid and where therefore $\ln(1-3\vartheta_1^{-2})$ is as large as it can get. Therefore we replace ϑ_1 by ϑ in the last term of (75), and we can then get a relation between ϑ and ϑ_1, using (24) and (23):

$$\begin{aligned}\vartheta_1&=B^{\frac{1}{2}}\vartheta[B+2\ln(2\vartheta/5)+2\ln(1-3\vartheta^{-2})]^{-\frac{1}{2}}\\&=B^{\frac{1}{2}}\vartheta[B+2\ln(0.4\vartheta-1.2\vartheta^{-1})]^{-\frac{1}{2}}.\end{aligned} \tag{76}$$

From this it follows that $\vartheta\approx\vartheta_1$ in the important region. Furthermore, this result provides a check on the theory of this Appendix: Molière's $f^{(2)}$ vanishes for $\vartheta=3.80$ (Table II) so that his distribution function is given by $B^{-1}f^{(1)}(\vartheta)$ alone for this particular value of ϑ. On the other hand, our ϑ_1 is so defined that the distribution function is $B^{-1}f^{(1)}(\vartheta_1)$ for *all* (sufficiently large) ϑ_1. Therefore we should have $\vartheta_1=\vartheta$ at the ϑ for which Molière's $f^{(2)}$ vanishes. The agreement is reasonably satisfactory.

[20] This expansion in the denominator is somewhat more accurate than a direct expansion, and will actually be more convenient Eq. (76).

The ratio to Rutherford scattering, (32), becomes now, using (63), (31), (62), (26):

$$R=\int zdzJ_0(z)\exp(-\tfrac{1}{4}z^2/\vartheta_1^2)\tfrac{1}{4}z^2\ln(z/k)$$
$$=\tfrac{1}{2}\vartheta_1^4 f^{(1)}(\vartheta_1). \tag{77}$$

Since the value of k matters only for the part proportional to $\exp(-\vartheta_1^2)$, it is often convenient to use (77) directly with (76) and Table II. Alternatively, we may use the asymptotic formula (33), getting

$$R=(1-5\vartheta_1^{-2})^{-6/5}. \tag{78}$$

Inserting (76), expanding the reciprocal of R and dropping terms of relative order B^{-2} or ϑ^{-6} leads directly to our old formula (36).

Finally, we may write down our complex integral (66) without expanding the exponential; it is

$$(2/\pi)^{\frac{1}{2}}\int x^{\frac{1}{2}}dx\exp(-x+\tfrac{1}{4}\beta x^2)$$
$$\cdot\exp[-\tfrac{1}{2}x^2\lambda^{-2}\ln(x/k)]\sin(\pi x^2/4\lambda^2). \tag{79}$$

The approximation used earlier in this Appendix, of considering only $f^{(1)}$, is equivalent to replacing the sine by its argument. Since the important x are around 3, and λ is very large (greater than 10) in the single-scattering region, this is a good approximation.

APPENDIX B. DERIVATION OF THE GOUDSMIT-SAUNDERSON FORMULA

We shall here prove Eq. (48). Since k is chosen to satisfy (44a), we may neglect screening. Setting $\cos\chi=x$, we thus have to calculate [see (44)]

$$K_l=2\int_{-1}^{1-\epsilon}dx(1-x)^{-2}[1-P_l(x)], \tag{81}$$

where $\epsilon\approx\frac{1}{2}k^2$ and the factor 2 is inserted for convenience in the following. Because of (44a), P_l at $\chi=k$ satisfies (45), or, since we now use x as the argument:

$$1-P_l(1-\epsilon)=\tfrac{1}{2}l(l+1)\epsilon. \tag{82}$$

We first integrate (81) by parts:

$$K_l=2\frac{1-P_l(x)}{1-x}\Bigg|_{-1}^{1-\epsilon}+\int_{-1}^{1-\epsilon}\frac{2dx}{1-x}P_l'(x). \tag{83}$$

The integrated part gives, according to (82)

$$l(l+1)-1+P_l(-1). \tag{83a}$$

In the integral, we write

$$\frac{2}{1-x}=\frac{1+x}{1-x}+1=\frac{1-x^2}{(1-x)^2}+1. \tag{83b}$$

Then the term with 1 can be integrated, giving

$$1-P_l(-1), \tag{83c}$$

which cancels the last two terms of (83a) (a term of order ϵ has been neglected). In the other term, we perform another integration by parts, giving

$$K_l=l(l+1)+\frac{1}{1-x}(1-x^2)P_l'\Bigg|_{-1}^{1-\epsilon}$$
$$-\int_{-1}^{1-\epsilon}\frac{dx}{1-x}\frac{d}{dx}[(1-x^2)P_l']. \tag{84}$$

Using (82) one finds that the second term cancels the first. In the last term, we use the differential equation for the Legendre polynomials and get

$$K_l=l(l+1)A_l, \tag{85}$$

$$A_l=\int_{-1}^{1-\epsilon}dxP_l/(1-x), \tag{85a}$$

which is a considerable simplification.

In order to be able to extend the integral to 1 rather than $1-\epsilon$, we take the difference

$$A_{l-1}-A_l=\int_{-1}^{1}dx(P_{l-1}-P_l)/(1-x). \tag{86}$$

Here we use the relation between spherical harmonics,[21]

$$l(P_{l-1}-xP_l)=(1-x^2)P_l'. \tag{87}$$

Then (86) becomes

$$A_{l-1}-A_l=l^{-1}\int_{-1}^{1}dx(1+x)P_l'-\int_{-1}^{1}P_l dx. \tag{88}$$

Integrating the first integral once more by parts, and using the fact that

$$\int P_l dx=0 \tag{89}$$

for any $l\neq 0$ (orthogonality), we get

$$A_{l-1}-A_l=l^{-1}(1+x)P_l\big|_{-1}^{1}=2/l. \tag{90}$$

Inserting back into (85), we find then

$$K_l=l(l+1)\left[A_1-2\left(\tfrac{1}{2}+\tfrac{1}{3}+\cdots+\frac{1}{l}\right)\right]; \tag{91}$$

and inserting $A_1=\frac{1}{2}K_1$ from (47), we have proved Eq. (48).

[21] See reference 14, p. 115.

Short-Lived Cerium Isotopes from Uranium Fission†

A. A. Caretto, Jr.,* and S. Katcoff
Chemistry Department, Brookhaven National Laboratory, Upton, New York
(Received November 25, 1952)

It was demonstrated that the previously reported 1.8-hr Ce^{145} and 4.5-hr Pr^{145} do not occur among the uranium fission products. Ce^{146} and Pr^{146} were briefly reinvestigated: the former decays with a half-life of 13.9±0.6 minutes and emits β-rays of 0.9-Mev maximum energy followed by soft γ-rays; the latter decays with a half-life of 24.4±0.5 minutes and its maximum β-ray energy is 3.8 Mev. In addition, it was shown that any undiscovered short-lived Ce fission products must decay with half-lives shorter than 6 minutes.

A STUDY was made of short-lived cerium isotopes, produced by fission of uranium to confirm, or disprove, the existence of 1.8-hr Ce^{145} and 4.5-hr Pr^{145}.[1–3]

The chemical procedure used was a modification of the method of Boldridge and Hume,[4] which is based on the fact that ceric iodate is insoluble in 6 *N* nitric acid while all trivalent rare earth iodates remain in solution. The following changes were found necessary in order to obtain sufficient radiochemical purity: (1) Two rare earth fluoride precipitations were made instead of one, and rhodium was used as hold-back carrier; (2) the cerium was passed through six precipitation cycles as $Ce(IO_3)_4$ instead of three, and barium was used as hold-back carrier twice; (3) three zirconium iodate precipitations were made instead of one. When the praseodymium daughters were isolated from cerium, ceric iodate was precipitated at least six times.

Seven irradiations of uranyl nitrate followed by separation of cerium yielded decay curves showing the 14.6-min Ce^{146}–24.6-min Pr^{146} chain and 33-hour Ce^{143}. In no case was any 1.8-hr Ce observed or any other half-time between 24.6-min and 33-hrs. Also, on four irradiations a Pr fraction was isolated from pure cerium which had decayed for times between 30 minutes and 2.5 hours. The Pr decay curves showed the 24.6-min Pr and the 13.8-day Pr^{143}, but no 4.5-hr Pr or any other intermediate half-time. These experiments show conclusively that the previously reported Ce^{145}–Pr^{145} chain does not occur among the uranium fission products. If it did occur with a fission yield greater than 0.1 percent, it would have been easily observed in these decay curves; the yield expected for mass 145 is about 4 percent. The previously reported Ce^{145}–Pr^{145} chain was probably due to contamination, perhaps by 2.0-hr Nd^{149} and 3.7-hr La^{141}. Only one or two $Ce(IO_3)_4$ precipitations were done formerly, while in the present work far greater purity was achieved. The report of 0.8-sec Xe^{145} [3] is also based on insufficiently purified cerium and is therefore probably in error.

The Ce^{146}–Pr^{146} chain, previously reported by Götte,[5] and Schuman,[6] was observed and investigated further. Pure cerium and praseodymium fission products were quickly isolated and their activities followed with an end-window Geiger tube through a series of aluminum absorbers. The half-life of Pr^{146} was found to be 24.4 ±0.5 minutes as determined from twelve decay curves, each followed for four to nine half-lives. The maximum beta-energy was found to be 3.8 Mev from the absorption curves which gave a Feather plot range of 1900 mg/cm². Schuman[6] reported 24.6±0.3 minutes for the half-life, about 3 Mev for the maximum β-ray energy, and 1.4 Mev for the γ-ray energy.

A growth of activity was observed in the cerium fractions when measured through absorbers thicker than 50 mg/cm². This resulted from the fact that the beta-rays of the Ce^{146} are soft and easily absorbed relative to the energetic Pr^{146} betas. The four growth-decay curves obtained with enough absorber to completely remove the Ce^{146} beta-rays were analyzed to determine the half-life of Ce^{146}, as follows. The observed activity at various times was subtracted from the asymptote (corresponding to the 24.4-min half-life of the daughter) which the curves approach after about three hours. The resulting difference curves were exponential and corresponded to the decay of the Ce^{146} through a factor of about 20 with a half-life of 13.9±0.6 minutes. Schuman's value[6] was 14.6±0.8 minutes determined by counting a series of cerium aliquots that were periodically cleaned of Pr daughter activity. The maximum β-ray energy of the Ce^{146} was found by analyzing absorption curves obtained for the Ce^{146}–Pr^{146} mixture. The observed half-thickness value in aluminum for the Ce^{146} β-rays was 31 mg/cm², which corresponds[7] to about 0.9-Mev maximum energy. It was also found that 13.9-min Ce emits soft γ-rays, probably between

† Work performed under the auspices of the U. S. Atomic Energy Commision.
* Present address: Department of Chemistry, University of Rochester, Rochester, New York.

[1] N. E. Ballou, *Radiochemical Studies: The Fission Products* (McGraw-Hill Book Company, Inc., New York, 1951), Paper No. 173, National Nuclear Energy Series, Plutonium Project Record, Vol. 9, Div. IV.
[2] S. Katcoff, Paper No. 174 of reference 1.
[3] Dillard, Adams, Finston, and Turkevich, Paper No. 68 of reference 1.
[4] W. F. Boldridge and D. N. Hume, Paper No. 294 of reference 1.
[5] H. Götte, Z. Naturforsch. **1**, 377 (1946).
[6] R. P. Schuman, Metallurgical Laboratory Reports CN-2799, March, 1945 and CN-2929, April, 1945 (unpublished).
[7] D. W. Engelkemeir, Figs. I–7 of "Introduction to Part I," *Radiochemical Studies: The Fission Products*, p. 18, reference 1.

0.2 and 0.3 Mev. This is based on an analysis of two runs in which the cerium fractions were measured through three lead absorbers (2, 3, and 4 g/cm²). A more thorough investigation of these radiations is planned by means of a scintillation spectrometer.

In the above cerium runs counting was begun as soon as 28 minutes after the irradiation and 3.5 minutes after the final separation from Pr. Since no component shorter than 13.9-min was seen, it is concluded that any other short-lived Ce fission products must have half-times shorter than 6 minutes.

One of the authors (A.A.C.) wishes to express his appreciation to Dr. R. W. Dodson and the staff of the Chemistry Department for the opportunity to carry out this work at the Brookhaven National Laboratory during the past summer.

PHYSICAL REVIEW VOLUME 89, NUMBER 6 MARCH 15, 1953

Gamma-Radiation from Interaction of 14-Mev Neutrons with Iron

V. E. SCHERRER, R. THEUS, AND W. R. FAUST
Radiation Division, Naval Research Laboratory, Washington, D. C.

(Received September 19, 1952)

Experiments have been performed to observe gamma-rays produced by the interaction of 14-Mev neutrons with iron. Although the gamma-spectrum appears to be continuous below 3.0 Mev, there may be discrete gamma-rays at 3.3, 4.4, 5.8, 7.1, and 8.75 Mev. The total cross section for gamma-ray production is 4.6±0.5 barns.

I. INTRODUCTION

SOME observations[1,2] of the gamma-radiation produced by interaction of fast neutrons with matter have been carried out primarily by absorption techniques. To obtain better resolution, we have made measurements with a spectrometer consisting of a single crystal of NaI(Tl) in conjunction with an eighteen-channel pulse-height analyzer. The spectra examined so far appear to consist of a low energy continuum overlaid by a series of discrete lines or bands at higher energies.

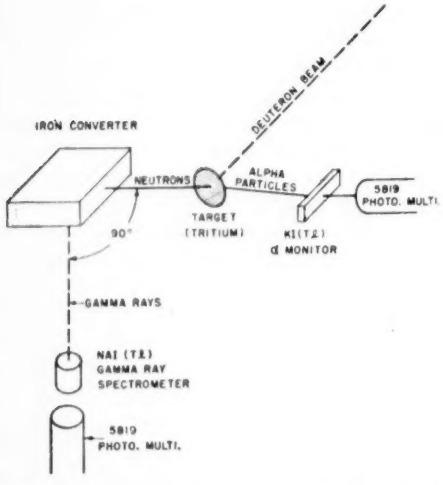

FIG. 1. Schematic representation of the experimental arrangement showing accelerator target, alpha-monitor, iron converter, and crystal detector.

II. DESCRIPTION OF THE EXPERIMENT

A 250-kilovolt Cockcroft-Walton accelerator[3] employing the $T(d,n)He^4$ reaction was used as a source[4] of 14-Mev neutrons, which were allowed to fall upon an iron converter arranged as shown in Fig. 1.

The converter and the accelerator monitor were so placed that whenever an alpha-particle entered the monitor a corresponding neutron entered the converter. The iron converter, approximately 0.75 inelastic neutron mean free paths long, was just wide enough to cover the "coincidence neutron beam." On the average a gamma-ray traveled about 0.25 mean free paths before leaving the converter and reaching the detector.

A block diagram of the electronic arrangement is shown in Fig. 2. A single crystal of NaI(Tl) and a 5819 photomultiplier in conjunction with an eighteen-channel pulse-height analyzer detected the gamma-rays produced in the converter. The multichannel analyzer was gated only by coincidences between the alpha-monitor and the spectrometer, thereby eliminating background counts from direct neutrons on the crystal as well as radiation scattered off the walls of the room. The amplifier discriminator in the alpha-channel was set to eliminate counts from the $D(d,n)He^3$ reaction, from electrons and low level noise. Scalers were placed at all points in the system that gave useful information.

Figure 3 shows typical calibration curves with the 4.45-Mev line of Po-Be and the two gamma-lines of

[1] D. F. Lea, Proc. Roy. Soc. (London) **150**, 637 (1935).
[2] J. H. Coon, private communication.
[3] Bergstralh, Dunning, Durand, Ellison, Howerton, and Slavin (to be published).
[4] Graves, Rodrigues, Goldblatt, and Meyer, Rev. Sci. Instr. **20**, 579 (1949).

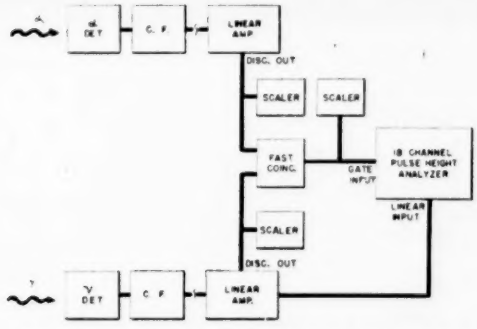

FIG. 2. Block diagram of electronic equipment used in the experiment.

Co^{60}. These curves, after correction for the statistics of the 5819 photomultiplier tube and the finite channel width of the discriminator, resemble the theoretical response due to scattering and absorption of the gamma-rays in the crystal.

III. SPECTROMETER RESPONSE

The pulse-height distribution produced by an arbitrary spectrum of gamma-rays falling upon a crystal spectrometer can always be expressed in terms of the incident spectrum and various system parameters. The resulting integral equation may be inverted to obtain thereby the energy spectrum of the incident radiation. To formulate an expression for the spectrometer pulse-height distribution, let $d\sigma(E')/dE'$ represent the differential cross section (in barns/Mev) for gamma-ray production of energy E', and $K(E', E)$ the relative probability of finding a pulse whose height lies in the interval between E and $E+dE$ whenever a gamma-ray of energy E' interacts with the crystal. It can then be shown that the pulse-height distribution $M(E)$ is

$$\frac{N_\alpha}{h_0}\frac{r}{4\pi}\eta\times 10^{-24}\int_0^l Adl\int_0^\infty dE'K(E',E)\frac{d\sigma}{dE'}\times\int_{t_1}^{t_2} dh e^{-h\mu_1(E')}(1-e^{-D\mu_2(E')}).$$

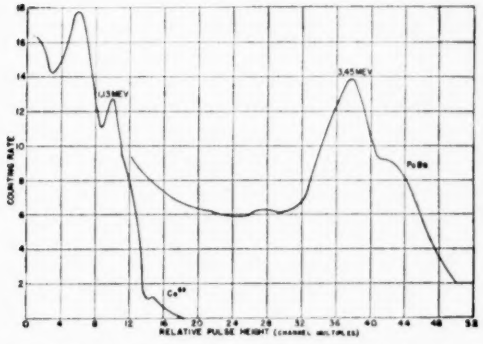

FIG. 3. Calibration curves of the spectrometer, obtained for Co^{60} and Po-Be gamma-rays.

Here, N_α represents the number of neutrons falling on the iron converter which are in coincidence with the alpha-monitor. The converter to detector solid angle is Ω, and the quantities t_1, t_2, and D refer to converter and crystal dimensions as indicated in Fig. 4. h_0 is the width of the coincidence neutron beam falling on the converter. The μ_1, μ_2 are gamma-ray absorption coefficients for converter and crystal, respectively, and are functions of the integration variable E'. Attenuation of the direct neutron beam in the converter is represented by A and was computed from the transport cross section and atomic density η for iron.

A possible method of analyzing the spectrum is to first subtract out apparent lines or bands which appear as maxima in the pulse-height distribution. This can be done if the relative pulse-height distribution $K(E', E)$ is known for each line energy. $K(E', E)$ can be obtained from calibration curves or estimated theoretically. The cross section σ_0 for gamma-ray production at the energy E_0, is obtained from the integral equation for the pulse-height distribution by setting $d\sigma/dE' = \sigma_0\delta(E'-E_0)$. After all apparent lines have been subtracted, the remaining portion of the pulse-height distribution is treated as a continuum and an approximate solution of the integral equation for $d\sigma/dE$ is obtained by use of a simple form of $K(E', E)$.

IV. RESULTS

Coincidence counting data was taken on a multichannel analyzer for a given number of neutrons (or alpha-monitor counts) with the converter both in and out of the "coincidence neutron beam." The machine rate was held constant during both runs so that the accidental rate was the same. The ratio of converter in to converter out counting rate was between 5 and 10, so generally the "background" was small. True counting data was obtained by subtraction of results obtained with the converter and out of the beam. Figure 5 is a plot of a representative set of data in counts per neutron per Mev. Probable errors in the counting data are indicated by the length of the vertical lines. Peaks occurring at electron energies of 2.5, 3.4,

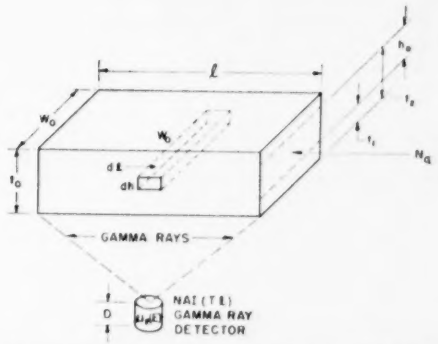

FIG. 4. Arrangement of iron converter and detector.

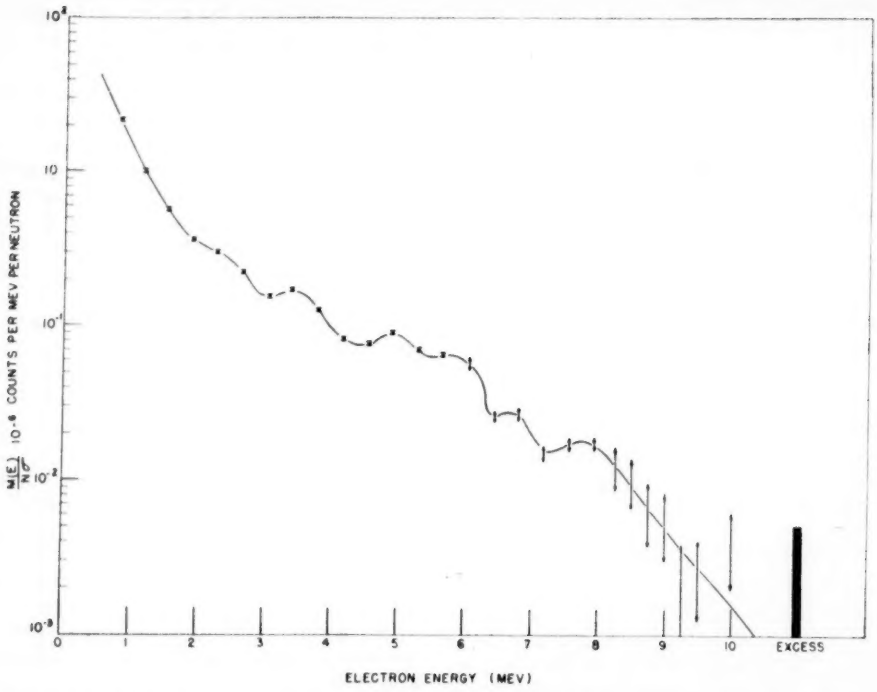

FIG. 5. Pulse-height distribution owing to iron gamma-rays. Ordinate is in counts per Mev per neutron and is the difference between converter-in and converter-out data.

4.80, 6.1, and 7.75 Mev were attributed to lines or bands in the gamma-ray spectrum at energies of 3.3, 4.4, 5.8, 7.1, and 8.75 Mev, respectively, and were subtracted from the data as described previously. An approximate solution of the integral equation was applied to the remaining portion of the distribution, which resulted in a continuous spectral distribution. Figure 6 shows the line or band spectra with their total production cross section, the estimated total cross section for all gamma-rays above 9.0 Mev and the part of the spectrum which appears continuous. No great significance should be placed on the shape of the continuum; however, the total cross section for this region is correct even though its distribution may be in error. The total cross section for the production of gamma-rays of all energies is 4.6±0.5 barns. The error indicated in the cross section arises mainly upon uncertainties in the analysis and not from counting statistics. Error in energy assignment is of the order of 0.2 Mev.

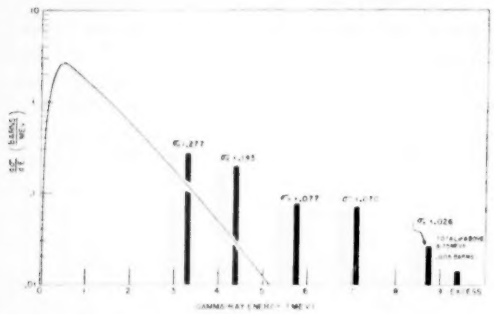

FIG. 6. Computed spectral distribution of iron gamma-rays. Ordinate is in barns per Mev for the "continuous portion" of the spectrum. Total cross sections are given for the line spectra.

In conclusion the authors wish to thank Dr. E. H. Krause and Dr. M. H. Johnson for their active interest and support. The authors also wish to express their indebtedness to Mr. A. P. Flanick for aid in performing the experiments.

Total Fast Neutron Cross Sections of Co, Ga, Se, Cd, Te, Pt, Au, Hg, and Th†

M. WALT,* R. L. BECKER,‡ A. OKAZAKI, AND R. E. FIELDS
University of Wisconsin, Madison, Wisconsin
(Received December 8, 1952)

The total neutron cross sections of Co, Ga, Se, Cd, Te, Pt, Au, Hg, and Th were measured as a function of neutron energy from 0.1 to 3 Mev. An estimate of the error caused by neutrons scattered into the detector was made by measuring the apparent cross section as a function of sample diameter. The results give additional evidence that, neglecting resonance structure, total neutron cross-section curves have characteristic shapes which change slowly with atomic weight.

IT has been pointed out[1] that if total neutron cross sections divided by the nuclear geometrical area are plotted as a function of the neutron energy and of the atomic weight, the result is a smooth surface containing broad maxima and minima. This regular behavior of the total neutron cross sections of various elements has created interest in measuring the cross sections of hitherto uninvestigated elements to see if they conform to these regularities. The present experiment was undertaken to supplement existing data.

Total cross sections were measured by transmission experiments as described by Miller *et al.*[2] Fast neutrons for energies above about 1 Mev were produced by bombarding a zirconium-tritium target with protons from an electrostatic generator. Below 1 Mev a lithium target was used. Cylindrical samples about one inch in diameter of the elements studied were placed midway between the neutron source and the detector; the distance from source to detector was fourteen inches. With the exception of the measurements on Te, Au, and Se above 1.5 Mev, neutrons were detected by a hydrogen recoil (pulse) ionization chamber. The high energy Te, Au, and Se data were taken with a scintillation detector using a stilbene phosphor mounted on an RCA 5819

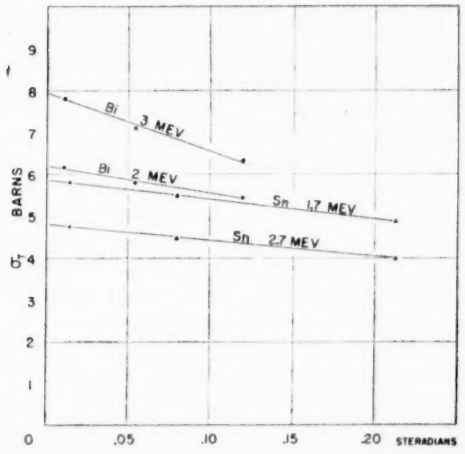

FIG. 1. Variation of the apparent total neutron cross section of Sn and Bi as a function of the solid angle subtended by the sample at the source and at the detector.

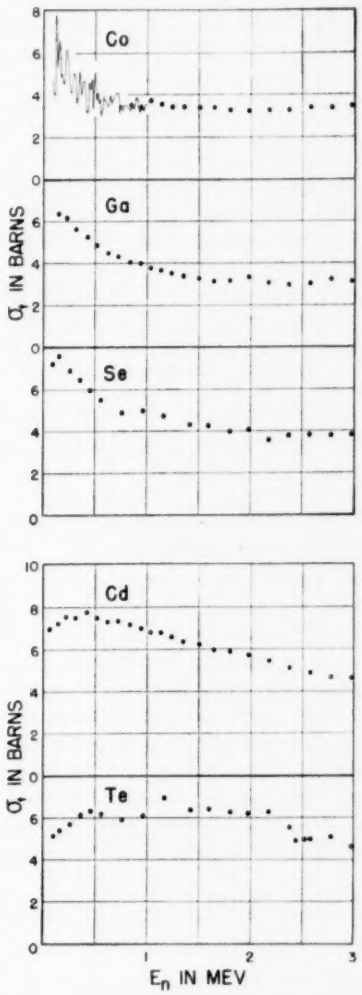

FIG. 2. Total neutron cross sections of Co, Ga, Se, Cd, and Te.

† Work supported by the U. S. Atomic Energy Commission and the Wisconsin Alumni Research Foundation.
* U. S. Atomic Energy Commission predoctoral fellow.
‡ National Science Foundation predoctoral fellow.
[1] H. H. Barschall, Phys. Rev. **86**, 431 (1952).
[2] Miller, Adair, Bockelman, and Darden, Phys. Rev. **88**, 83 (1952).

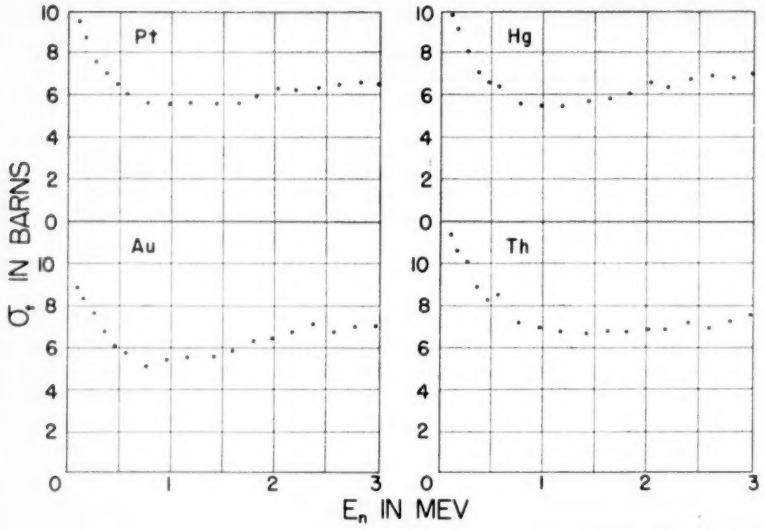

FIG. 3. Total neutron cross sections of Pt, Au, Hg, and Th.

photomultiplier tube. Background, which was measured by shielding the detector from the source by a paraffin cone, was less than 2 percent with the recoil counter and less than 10 percent with the scintillation detector. The recoil counter background was produced by neutrons reflected from the floor and walls of the room while the background of the scintillation counter was due primarily to x-rays from the electrostatic generator. The data for neutron energies below 200 kev were taken at 115° with respect to the incident proton beam. All other measurements were made with neutrons produced at 0° to the incident protons.

Before cross sections could be determined, it was necessary to correct the measured transmissions for the effect of neutrons scattered into the detector by the sample. The correction was made assuming that the neutrons were scattered isotropically. However, angular distributions[3] of scattered neutrons calculated from the continuum model show a strong forward maximum which becomes more pronounced with increasing energy and increasing atomic weight. Therefore, the isotropic correction was expected to be too small, and an experiment was undertaken to determine the magnitude of the resultant error. The experiment consisted of measuring the apparent transmission of samples of Sn and Bi as a function of the solid angle subtended by the sample at the source and detector. The apparent transmission increased with sample size because of the increase in the number of neutrons scattered into the detector. Figure 1 gives the apparent cross sections of Sn and of Bi for three different samples of the same thickness but different diameters. Assuming that the theoretical angular distributions of reference 3 are valid, the calculated apparent cross sections are very nearly a linear function of the solid angle subtended by the sample at the source and detector for the range of sample sizes used. Hence it is reasonable to assume that a straight line extrapolation of the data of Fig. 1 to 0 steradians will give the true cross sections.

As Sn and Bi are typical of medium and heavy elements, the in-scattering error for the elements measured can be estimated from the Sn and Bi data. At 3 Mev for 1-in. samples and a source-to-detector distance of 14 in., the measured cross section would be 4 percent low for the case of Bi and about 2 percent low for Sn. The isotropic correction was about ½ percent so the data shown in Figs. 2 and 3 are probably low as much as 3 percent for the heavy elements at the highest energy.

Figures 2 and 3 give the total cross section of Co, Ga, Se, Cd, Te, Pt, Au, Hg, and Th as a function of neutron energy. No effort was made to resolve individual resonances. The resolution was determined by the target thickness and was about 25 kev for the data taken with tritium targets and 50 kev for the Li target work.

The measured cross sections fit smoothly on the surface giving cross section as a function of atomic weight and neutron energy shown in reference 1.

We wish to thank Dr. J. H. Coon and Dr. C. W. Zabel of the Los Alamos Scientific Laboratory for the loan of most of the samples used in the experiments.

[3] Final Report of the Fast Neutron Data Project, January 31, 1951, Atomic Energy Commission Report NYO-636 (unpublished).

Direct Comparison of m/e for the Positron and the Electron*

L. A. PAGE, P. STEHLE, AND S. B. GUNST
University of Pittsburgh, Pittsburgh, Pennsylvania
(Received December 1, 1952)

A relativistic, double-focusing mass spectrometer has been built to operate with 55-kev electrons. It has reversible electric field and fixed magnetic field. Positrons from Na^{22} and electrons from a hot filament alternately follow identical trajectories in opposing directions. The magnitude of the electric field required to focus is used as the measure of m/e. Seventeen positron runs were made intermediate in time between twelve electron runs. The rms deviation of the data lies within the standard deviation associated with positron counting. The result is

$$\frac{(m/e)^- - (m/e)^+}{m/e} = (26 \pm 71) \times 10^{-6},$$

where the uncertainty is the standard deviation.

I. INTRODUCTION

EARLY experimental comparisons between m/e for the positron and the electron[1] indicated equality within 15 percent and, later,[2] within 2 percent. Because many atomic constants are known to much greater precision,[3] and because of the possibility of a difference between $(m/e)^-$ and $(m/e)^+$, a number of investigators have recently suggested the need for a direct precision comparison.[4,5] A mass spectrometer built for this purpose is described, as are the results of the experimental comparison.

II. METHOD

If a particle with a mass-charge ratio m/e follows a certain trajectory from point 1 to point 2 under the influence of fields $\mathbf{E}$, $\mathbf{H}$, then a particle with a mass-charge ratio $-m/e$ will follow the same trajectory from point 2 to point 1 under the influence of fields $-\mathbf{E}$, $\mathbf{H}$. In the present experiment a family of trajectories between points 1 and 2 is furnished representing the focusing in angle and energy of a source at 1 on a detector at 2 or vice versa. If, however, the particles have slightly different magnitudes of m/e, correspondingly different magnitudes of $\mathbf{E}$ will be needed to achieve focus. One has

$$\frac{\delta(m/e)}{m/e} = -\left(1-\frac{v^2}{c^2}\right)^{-1}\frac{\delta E}{E},$$

for the case where the particle speed v is constant along the central trajectory.

III. DESCRIPTION OF APPARATUS

A simplified plan view of the mass spectrometer is shown in Fig. 1. An electromagnet, with rectangular poles between which the rectangular part of the vacuum chamber is clamped, provides a nearly uniform vertical magnetic field over the volume of the chamber. Electrostatic deflector plates CC (stainless steel with adjacent planes lapped flat and parallel) have a potential difference between them, the average potential being near ground. These act as a velocity selector. The purely magnetic deflection between D and E defines the momentum. It will be shown below that by suitable choice of λ, ρ, and ϕ the apparatus is made double-focusing. The controls for varying ρ and ϕ are not shown.

At A there is a line source of positive β-rays (0.5 mC Na^{22}). A portion of the positron spectrum entering the mass spectrometer through slit B is brought to a focus on slit E by adjusting the electric field between plates CC. This selects a velocity to match the momentum defined by the magnetic field, which is held fixed. In terms of the fractional change in voltage across the velocity selector, the beam has a width at half-maximum approximately equal to the defining slit width divided by ρ ($\sim$0.009 in./3 in.$=$0.003). The horizontal angle range and the fractional energy range accepted are of the order of magnitude of the velocity-selector plate spacing divided by ρ ($\sim$0.115 in./3 in.$=$0.038). Vertical angles are limited by the height of aperture H and of slit B, and are the same for electrons and for positrons.

The situation for a positron run is indicated in Fig. 1. A bundle of positron trajectories from slit B to slit E is schematically represented. The trajectories emerging from the spectrometer at E are stopped down at aperture H, pass through the housing I, and terminate at the end-window Geiger-Mueller counter GMC. Aperture H limits the width of the beam to the usable width of the counter window.

For an electron run the velocity-selector voltage is reversed. The injector housing I is held at a negative potential so that electrons from the hot tungsten filament J are accelerated toward the aperture H. An aluminum scattering foil G (0.2 mg/cm^2), retracted during positron runs, is now placed across H. The foil

* Work supported in part by the U. S. Office of Naval Research, and done in the Sarah Mellon Scaife Radiation Laboratory.
[1] J. Thibaud, Phys. Rev. **45**, 781 (1934).
[2] A. H. Spees and C. T. Zahn, Phys. Rev. **58**, 861 (1940).
[3] Jesse W. M. DuMond and E. Richard Cohen, Phys. Rev. **82**, 555 (1951); Muller, Hoyt, Klein, and Du Mond, Phys. Rev. **88**, 775 (1952). We are indebted to Professor DuMond for communicating some recent results prior to publication.
[4] J. W. M. DuMond, Phys. Rev. **81**, 468 (1951).
[5] Arne Hedgran and David A. Lind, Phys. Rev. **82**, 126 (1951).

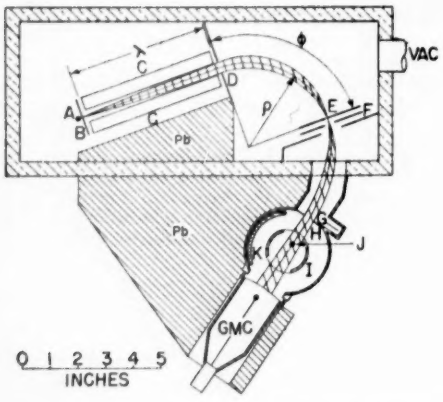

FIG. 1. Plan view of double-focusing mass spectrometer. Spacing between plates *CC* and the widths of slits *B*, *E*, and rough-slit *D* are grossly exaggerated in order to show a bundle of particle trajectories. The magnetic field is uniform over the rectangular part of the vacuum chamber and is out of the paper. The vacuum chamber height between magnet pole faces is 1⅛ in.

is bombarded uniformly by electrons from the injector and thus, through multiple scattering, provides trajectories of acceptable angles at each point of the aperture. All acceptable energies are provided by modulating the injector voltage at an audiofrequency, the amplitude being large compared with the range of acceptable energies. The current provided by the injector is monitored by measuring the current collected at rough-slit *F*. During electron injection the counter window is protected by closing the nonmagnetic gate *K*.

Electrons arrive at slit *B* twice during each modulation cycle and are collected on the positron source-holder *A*. The signal is amplified and detected on a heterodyne analyzer. The average injector voltage is adjusted to give a null first-harmonic response. This means that the modulation voltage is centered about the mean acceptable energy. The second-harmonic signal is then taken as a measure of the electron beam.

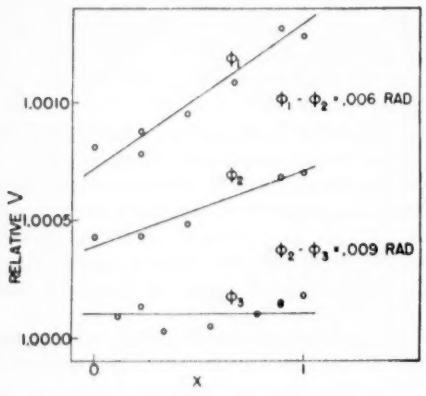

FIG. 2. Velocity-selector voltage V to focus electrons as a function of scanning-slit position x for three different values of momentum-selector angle ϕ. (The aperture H has unit width in x on this plot.)

The magnet is excited by current from an electronically regulated 300-volt supply.[6] Fluctuations in current are detected by balancing the potential difference across a precision resistor against a standard cell and are compensated by hand adjustment. To allow the magnet yoke to reach equilibrium it is found necessary to permit magnet-coil current to flow continuously for several days. The field in the spectrometer is approximately 100 gauss.

Fluctuating magnetic fields due to dc machinery in the city (streetcars, etc.) were so large relative to the field in the spectrometer that final adjustment and runs had to be made in a magnetically quiet location outside the city. The improvement in magnetic-field stability was a hundredfold.

The velocity-selector voltage is provided by a 4-kv regulated rf power supply immersed in oil.[7] The output appears across an 8-meg chain whose center point is grounded. The regulating signal is obtained by comparison of the potential at a point on this chain with that across a type 5651 voltage regulating tube. For measuring the velocity-selector voltage, an independent 16-meg potential divider is connected across the output terminals. The center of this chain is also grounded. A precision potentiometer measures the potential difference between ground and either the plus or minus 1-volt (nominal) points on the potential divider. The measured potential differences are designated by a symbol V (with or without a subscript) in the remainder of the paper. These readings are a measure of both the potential difference between the velocity-selector plates and the average potential of the plates with respect to ground. This latter voltage acts longitudinally and therefore enters only relative to the beam energy and not to the velocity-selector voltage, thus being reduced in effect by a factor of about fifteen.

The electron-injector voltage is provided by an rf voltage quadrupler immersed in oil. The maximum output is 60 kv dc. Because the injector potential is modulated, no regulation is necessary. The audiofrequency modulation (75 cps) is impressed by a transformer whose output is 10 kv peak. The injector power supply is not operated during positron runs, but it is so arranged that the same direct current flows in the primary of the rf transformer during electron and positron runs. This circuit is the only one in the immediate vicinity of the spectrometer whose operation is different for electron and positron runs.

IV. FOCUSING PROCEDURE

Elementary considerations show that a linear, crossed-field velocity selector in series with a magnetic momentum selector, operating in a common magnetic

[6] Hausman, Bender, and Reilley, Phys. Rev. **82**, 773 (1951).

[7] We are indebted to Professor R. S. Bender for the design of this circuit.

field, focuses a nonrelativistic particle to first order in initial angle when the total transit time is half a cyclotron period. The combination also focuses to first order in initial energy provided the path lengths in the two selectors are equal. Thus, in Fig. 1 one would have $\phi=\frac{1}{2}\pi$ and $\rho=2\lambda/\pi$ nonrelativistically.

Because of the paucity of low energy positrons it was necessary to run at slightly relativistic energies (~55 kev). Under these circumstances the focusing conditions are altered. For example, time-dilation during velocity selection necessitates lengthening the velocity selector. In addition the angle ϕ must be decreased from $\frac{1}{2}\pi$. These effects are of order v^2/c^2.

The values of the parameters for best focus are determined experimentally using the electron beam. Criteria for good focus are: (a) The line width should be consistent with the geometry; (b) if the width of aperture H is subdivided, the focusing potential of the velocity-selector should be the same for all subdivisions. When these criteria are satisfied, besides having a narrow line, the location in voltage V of the line does not depend on the details of the electron energy spectrum.

To find the best focus, the following procedure was used.

(a) For given ρ and ϕ the electron-injector assembly is moved until the central trajectory enters D in a direction parallel to the plates CC.

(b) For the same ρ and ϕ the focusing potential V is determined as a function of the position x of a scanning slit, one-fourth the width of H and temporarily installed at H.

For suitable ρ, $V(x)$ is an essentially linear function, the slope depending on ϕ. The value of ϕ can then be adjusted to make this slope vanish. Figure 2 shows $V(x)$ for three values of ϕ in the neighborhood of a good focus. A check on the focus so obtained is afforded by offsetting the injector voltage from the usual value which gives a null first-harmonic response. Offsets of ± 3.5 kv induce no significant change in $V(x)$.

After achieving a focus as described, the scanning slit at H is removed from the apparatus. With this slit removed, a check on the state of the focus is made from time to time by running electrons with the foil G retracted. This alters the spectrum of energies provided. No change in location in V of the electron line, or in its width, has ever been observed for the two positions of foil G.

The curve of zero slope in Fig. 2 indicates the state of focus used in taking the final data.

V. EXPERIMENTAL PROCEDURE

Using the electron beam, the resolution function, beam *versus* velocity-selector voltage V, was found to be a gaussian. Positron counts were then taken at various values of V. Figure 3(a) shows the results of these runs superimposed on the electron line-shape. It

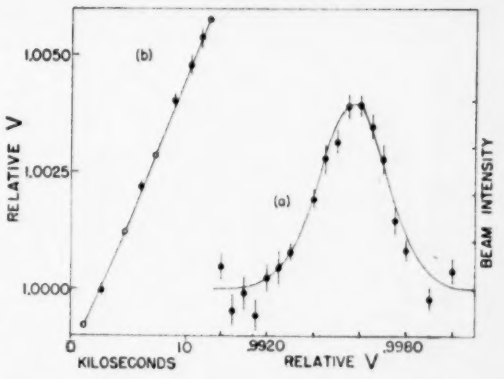

FIG. 3(a). Comparison between observed electron and positron line-shapes. The curve (Gaussian) is for electrons. The points are positron counting rates with standard counting errors attached. (b). Preliminary sequence of runs showing electron points as circles (V^- *versus* time) and positron points as dots (V^+ *versus* time). The errors attached to the latter are standard deviations due to counting N_R-N_L. Straight line segments connect electron points.

is concluded that the positron line-shape is the same as that for electrons. Secular drifting of the line position in V was allowed for by frequent locations of the half-beam points with electrons. This drift is a smooth function of time and can be largely attributed to the temperature dependence of the 16-meg potential divider.

After showing that the electron and positron line-shapes are identical, the procedure is to sandwich pairs of positron runs between electron runs. During a sequence of runs, the magnetic-field current is continuously monitored as described previously, and the balance is held within three parts per million.

Electron Runs

Gate K (Fig. 1) is closed to protect the counter. Scattering foil G is inserted across aperture H. The average injector voltage is adjusted to give a null first-harmonic signal from the electron collector; then the second-harmonic signal is detected. Values V_L and V_R of the velocity-selector voltage are found which pass half the peak electron beam. During this process the current from the injector to rough-slit F is monitored. If it fluctuates more than 1 percent, the reading of V is discarded. Each half-beam point is located once or twice. The total elapsed time during the readings is about one minute. The location V^- of the electron line is then $(V_L+V_R)/2$.

The ratio of peak beam current to noise was 80:1. The dc beam current was $\sim 10^{-10}$ amp.

Positron Runs

Gate K is opened, scattering foil G is retracted from aperture H. The leads from the velocity-selector plates CC are disconnected from the ends of the resistor

TABLE I. Results for two sequences of positron and electron runs.

Particle*	Elapsed time kilosec	Potentiometer volts V_L	Potentiometer volts V_R	Counts in 800 sec N_L	Counts in 800 sec N_R	Volts to focus V^-	Volts to focus V^+	δV volts
First sequence of runs								
−	2.3	0.9301	0.9334	···	···	0.93175	···	···
+	3.6	0.9301	0.9333	592	613	···	0.93181	−0.00009
+	5.2	0.9301	0.9333	559	701	···	0.93242	+0.00032
−	6.4	0.93055	0.93395	···	···	0.93225	···	···
−	10.8	0.9311	0.93463	···	···	0.93288	···	···
+	12.1	0.9315	0.9347	619	625	···	0.93313	0.00000
+	13.8	0.9315	0.9347	625	671	···	0.93333	−0.00013
−	15.0	0.93195	0.93545	···	···	0.93370	···	···
+	16.3	0.9325	0.9350	632	736	···	0.93427	+0.00028
+	18.5	0.9330	0.9362	677	623	···	0.93433	−0.00016
−	19.8	0.9330	0.93658	···	···	0.93470	···	···
+	21.0	0.9334	0.9366	602	647	···	0.93523	+0.00015
+	22.6	0.9334	0.9366	559	678	···	0.93560	+0.00012
−	23.8	0.93405	0.93746	···	···	0.93576	···	···
+	26.0	0.9345	0.9377	646	680	···	0.93627	−0.00001
−	27.1	0.93478	0.93832	···	···	0.93655	···	···
Second sequence of runs								
−	2.6	0.92543	0.9288	···	···	0.92711	···	···
+	3.8	0.9254	0.9286	598	645	···	0.92724	−0.00007
+	5.6	0.9257	0.9289	567	589	···	0.92741	−0.00021
−	6.9	0.9262	0.9295	···	···	0.92785	···	···
+	8.6	0.9264	0.9296	600	659	···	0.92830	+0.00015
+	10.7	0.9266	0.9298	582	649	···	0.92851	+0.00002
−	12.0	0.92705	0.93048	···	···	0.92876	···	···
+	13.2	0.9273	0.9305	618	681	···	0.92922	+0.00021
+	14.8	0.9278	0.9310	633	598	···	0.92922	−0.00012
−	15.8	0.9278	0.9313	···	···	0.92955	···	···
+	16.9	0.9284	0.9316	674	625	···	0.92975	+0.00001
+	18.6	0.9284	0.9316	674	662	···	0.92994	−0.00010
−	19.6	0.9285	0.93193	···	···	0.93021	···	···
+	20.8	0.9290	0.9322	648	607	···	0.93039	···
+	22.5	0.9290	0.9322	657	628	···	0.93045	···
−	23.6	0.92875	0.93205	···	···	0.93040	···	···
+	24.9	0.9288	0.9320	710	659	···	0.93014	···
+	26.6	0.9284	0.9316	563	711	···	0.93074	···
−	27.6	0.92883	0.93227	···	···	0.93055	···	···
−	28.1	0.9288	0.9323	···	···	0.93055	···	···

* Electron runs are designated by the symbol −, positron runs by +.

chains and are reconnected with reversed polarity. The direct current in the primary of the rf transformer of the injector power-supply is set at the value observed during the previous electron run. V is set at a value well off the curve and the background counting rate is checked.

Counts are then taken for 400 sec, at, say, voltage V_L as determined from the previous electron run, or at a value slightly displaced in anticipation of a drift. Then counts are taken for 800 sec at $V_R = V_L + 0.0032$ volt and again for 400 sec at V_L. The total number of counts at V_L is recorded as N_L, that at V_R as N_R. In this way effects of the slope, the curvature, and the rate of change of curvature of the focusing potential as a function of time are eliminated. This procedure is called a "run" and, as will be shown, yields the value of positron focusing voltage V^+ at the center of gravity of the counting time for that run. If, for a given pair of positron runs, V_L is set up first, then for the next pair, one sets up V_R first, and vice versa.

For the final data, two sequences of runs were made. Between these sequences the leads from the velocity-selector power-supply to the resistor chains were reversed, so as to average out any effect of leakage currents and any asymmetry of the velocity-selector voltage about ground. Measured leakage currents never exceeded 10^{-5} of the current in the 8-meg chain.

VI. RESULTS

Table I shows, in the first six columns, the raw data obtained for the final sequences of runs. The values for V^-, the location of the electron peak as obtained directly from columns three and four, are tabulated in column seven and shown in Figs. 4 and 5.

The total number of counts obtained during a run, N_L+N_R, should remain constant. In general, however, N_R is not equal to N_L, indicating that the positron focusing potential V^+ differs from the mean potential $(V_L+V_R)/2$ by an amount ΔV. The magnitude of ΔV is derived from the known beam height and width as follows.

If $\langle B\rangle$ is the average number of background counts in 800 sec, then $\frac{1}{2}\langle N_L+N_R\rangle-\langle B\rangle$ is the height of the Gaussian 0.0016 volt from its center. The width of the Gaussian curve is taken to be the average of the electron widths, and is 0.00343 volt. The peak height of the Gaussian is then $1.828[\frac{1}{2}\langle N_L+N_R\rangle-\langle B\rangle]=239.8$ counts/800 sec. The slope of the Gaussian at the ±0.0016-volt points is 9.908 counts/(800 sec×0.0001 volt). Thus, since

$$\Delta V=\tfrac{1}{2}(N_R-N_L)dV/dN,$$

we have

$$\Delta V=(N_R-N_L)/19.82.$$

The uncertainty in ΔV arises from the uncertainty in N_R-N_L and also from that in the quantity 19.82, while the uncertainty in the latter arises from that in the electron line width, that in $\langle N_R+N_L\rangle$, and that in $\langle B\rangle$. The rms deviation of the line width is 2.6 percent. The standard deviation of $\frac{1}{2}\langle N_R+N_L\rangle-\langle B\rangle$ is 17.1 percent, so that the uncertainty in the quantity 19.82 is 17.3 percent. The uncertainty in (N_R-N_L) is $\langle N_R+N_L\rangle^{\frac{1}{2}}=35.6$ counts/800 sec, or 0.00018 volt in each V^+.

The values of V^+ so obtained (with only the 0.00018-volt error attached), together with the values of V^-

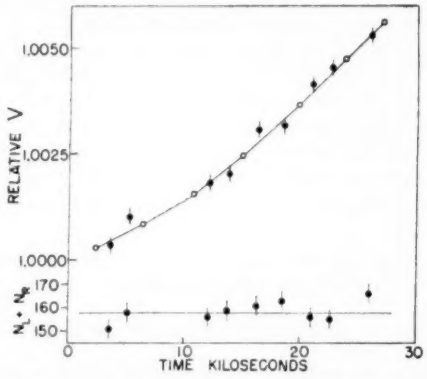

FIG. 4. Final data, first sequence of runs. Electron points are shown as circles, and are joined by straight line segments. Positron points are shown as dots with standard deviations arising from the counting errors in N_R-N_L. Also shown is N_L+N_R for each positron run (here expressed as counts per 100 sec) with a standard statistical error.

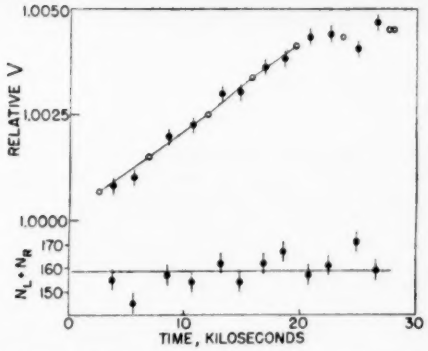

FIG. 5. Final data, second sequence of runs. Same notation as in Fig. 4. Data beyond 20 ksec is not used for final result (see Table I).

are plotted in Figs. 4 and 5 for the final sequences of runs. The sum N_R+N_L is plotted on the same time scale. The results of a preliminary sequence, observed when V^- and V^+ varied rapidly with time, are plotted in Fig. 3(b). These preliminary results are not used in subsequent computations and are shown only to indicate the validity of the method used to locate the positron points in time. Results shown in Fig. 5 for times exceeding 20 ksec also are not used in subsequent computations since a heat source was removed and returned to the laboratory during this period.

The value of V^- corresponding to the time of each positron point is found by linear interpolation between adjacent electron points. The difference δV between V^+ and the interpolated value of V^- is tabulated in the last column of Table I. The average δV is 53×10^{-6} volt for the first sequence and -14×10^{-6} volt for the second sequence. These in turn are averaged with equal weights.

Attached to this final average is a standard deviation compounded from the statistical uncertainties of the individual points and the uncertainty in the average of ΔV stemming from the quantity 19.82.

The seventeen values of δV have an rms deviation of 0.00015 volt which compares favorably with the standard deviation associated with counting (N_R-N_L), namely 0.00018 volt.

The difference of the mass-charge ratios is connected with the difference in focusing potentials δV through the factor $(1-v^2/c^2)^{-1}$. This is evaluated from the magnitude of voltage V, the known ratio of the potential divider used to measure the velocity-selector voltage, and the geometric parameters. The factor is 1.23.

The final result is

$$\frac{(m/e)^- - (m/e)^+}{m/e} = (26\pm71)\times10^{-6}.$$

VII. ACKNOWLEDGMENTS

The authors are grateful to Professor A. J. Allen whose constant assistance made the experiment possible, and to Professor R. S. Bender who designed some of the electronic apparatus and made many helpful suggestions. The assistance of other members of the laboratory, particularly Mr. R. F. Weise, Mr. J. F. Kane, and Mr. E. M. Perkins, in the design and construction of equipment is acknowledged with thanks.

Loans of apparatus from the Gulf Research and Development Company, the Westinghouse Research Laboratories, and the Westinghouse Atomic Power Division are respectfully acknowledged.

Finally, the authors deeply appreciate the constant cooperation of Dr. and Mrs. T. Lyle Hazlett who generously permitted the use of a building at their summer home during the final stages of the experiment.

Applications of Variational Principles to Scattering Problems*

SAUL ALTSHULER
Department of Physics, Iowa State College, Ames, Iowa
(Received November 17, 1952)

The Schwinger variational principle is reduced to a convenient form by using trial solutions of the form $\Sigma_i c_i u_i(x)$. The reliability of the formalism for polynomial trial solutions is studied for several fields, and wherever possible comparisons are made with phase shifts determined from other variational principles.

The forward scattering amplitude is determined variationally for scattering in the static field of the hydrogen atom, and it is demonstrated that the undisturbed wave as trial solution provides more accurate results for all incident energies than second Born approximation. The improved variational estimate of the total cross section for this field approaches that of Born at the higher energies.

I. INTRODUCTION

A VARIATIONAL formulation of the collision problem equivalent to the Schrödinger statement (Schrödinger equation and appropriate boundary conditions) means that the latter must be obtained as a necessary and sufficient condition for the stationary property of a suitable quantity. Schwinger[1,2] has shown that the transition probability amplitude can be exhibited in stationary form. Using the notation of linear operator algebra, the stationary functional for the transition amplitude is given by

$$T_{ba}=\frac{(\psi_b', V\varphi_a)(\varphi_b, V\psi_a)}{(\psi_b', V\psi_a)-(\psi_b', VGV\psi_a)}. \tag{1}$$

Here, the transition amplitude describes the transition from φ_a to φ_b, the φ's being unperturbed states. It is easy to show that the stationary property of T_{ba} with respect to independent arbitrary variations of ψ_b' and ψ_a leads to the integral equation describing the collision as well as the associated adjoint integral equation, namely,

$$\psi_a=\varphi_a+GV\psi_a, \tag{2}$$

$$\psi_b'=\varphi_b+G^\dagger V^\dagger\psi_b', \tag{3}$$

where the superscript dagger indicates Hermitian adjoint. In all collisions conserving the total energy, V is real and symmetric. G is symmetric because the Hamiltonian is Hermitian. It should be observed that Eq. (1) is an identity for exact solutions since

$$T_{ba}=(\varphi_b, V\psi_a)=(\psi_b', [V-VGV]\psi_a)=(\psi_b', V\varphi_a).$$

This result follows directly if Eqs. (2) and (3) are employed. If Hartree units are used, the exact relation between the scattering amplitude and the transition amplitude is given by

$$f(b\leftarrow a)=-(1/4\pi)T_{ba}. \tag{4}$$

It is to be pointed out that the Schwinger principle, Eq. (1), is the only available variational principle which treats inelastic as well as elastic collisions on the same footing. However, chiefly because of analytical difficulties involved in evaluating the matrix element containing the Green's function, there has as yet been no application of this procedure to atomic collision problems involving more than two particles. In fact, this matrix element is exactly the same as the integral in second Born approximation when φ_a and φ_b are used as trial solutions. Equation (1) then becomes

$$T_{ba}=\frac{(\varphi_b, V\varphi_a)}{\{1-(\varphi_b VGV\varphi_a)/(\varphi_b, V\varphi_a)\}}=(\varphi_b, V\varphi_a)+(\varphi_b, VGV\varphi_a)+\cdots. \tag{5}$$

Thus, the use of unperturbed wave functions furnishes more information than the second Born approximation. However, since the variational principle is only meaningful for trial wave functions which are good approximations to the true solutions, it cannot be said *a priori* that the presence of the extra terms in Eq. (5) produces a more accurate answer than the second Born approximation. Nevertheless, example 4 in the section on applications indicates that such is indeed the case for all incident energies.

For the purpose of computing phase shifts in the case of spherically symmetric fields, it is easy to show from Eq. (1) that the stationary functional for $k\tan\delta_0$ is given by

$$k\tan\delta_0=\frac{\left(\int_0^\infty u(x)\sin kx V(x)dx\right)^2}{\int_0^\infty u^2(x)V(x)dx-\int_0^\infty\int_0^\infty u(x)V(x)G(x,x')V(x')u(x')dxdx'}, \tag{6}$$

* The research reported in this paper has been sponsored by the Geophysics Research Directorate of the Air Force Cambridge Research Center, Air Research and Development Command under Contract AF 19(122)-469. This material comprises part of a dissertation presented to the University of Southern California Graduate School in partial fulfilment of the requirements for the degree of Doctor of Philosophy in the Department of Physics.

[1] J. Schwinger, *Lectures in Nuclear Physics*, Harvard University, 1947 (unpublished).

where $u(x)$ is defined by

$$u''(x)+k^2u(x)+V(x)u(x)=0,$$

and

$$G(x, x')=1/k\ \sin kx_<\cos kx_>,$$

$$x_>=\text{greater of } x, x'. \quad x_<=\text{lesser of } x, x'.$$

Similarly expressions may be written for the higher order phase shifts.

Hulthén[3] has derived a variational principle for the phase shifts which differs from the Schwinger principle in that the Schrödinger differential equation, rather than the integral equation, is derived as a necessary and sufficient condition for the stationary character of a suitable functional. Applications of this principle were made by Hulthén[3,4] and by Massey and Moiseiwitsch.[5] The structure of the Hulthén principle is such that the trial solutions must be normalized to the correct asymptotic form. Inspection of Eq. (1) indicates that this is not necessary when employing the Schwinger principle. Kohn[6] derived a modification of the Hulthén principle which allows the use of trial solutions not having the correct asymptotic form in cases where the interaction range is finite. The Kohn modification also affords a further improvement in that a unique determination of the phase is possible; this is not the case with the Hulthén principle, which is quadratic in the phase.

The reliability of the Schwinger formalism, Eq. (6), for simple trial solutions of the form $\sum_i c_i x^i$ has been investigated for several fields. Wherever possible, the phase shift estimates are compared to values obtained numerically, by exact calculations, or to values from the application of the Hulthén principle by other workers.

Even for the two-particle problems it is desirable to calculate the scattering amplitude of the entire plane wave without having to determine separately the phase shifts of each partial wave. Such an investigation has been carried out for the field $-(1+1/r)e^{-2r}$, the static field of the hydrogen atom, by means of Eq. (5). This field is arrived at by averaging the potential energy of an electron in the presence of the hydrogen atom over the ground state of the hydrogenic electron. The scattering of an electron from this field represents the solution of the problem of electron scattering from hydrogen atoms, if exchange and polarization effects are ignored. It is demonstrated that the forward scattering amplitude following from Eq. (5) is better than second Born approximation for all incident energies.

II. APPLICATIONS

We first show that for trial solutions of the form $\sum_i c_i u_i(x)$, $u_i(0)=0$, $k\tan\delta$ can be reduced to a form quite convenient for calculation and, incidentally, that $\tan\delta$ is uniquely determined. Substituting the trial solution

$$\sum_{i=1}^{N} c_i u_i(x)$$

directly into Eq. (6) leads to

$$k\tan\delta=\frac{c_\alpha c_\beta A_\alpha B_\beta}{(c_\alpha c_\beta)(D_{\alpha\beta}-E_{\alpha\beta})}; \quad \alpha, \beta=1, 2\cdots, N. \quad (7)$$

Here we use the summation convention, and we have set

$$A_i=\int_0^\infty \sin kx V(x)u_i(x)dx=B_i,$$

$$D_{ij}=\int u_i(x)u_j(x)V(x)dx=D_{ji},$$

$$E_{ij}=\int\int u_i(x)V(x)G(x, x')V(x')u_j(x')dxdx'=E_{ji}.$$

The symmetry of the E_{ij} follows from the symmetry of $G(x, x')$. Multiplying and transposing, let us define

$$Q\equiv[(k\tan\delta)M_{\alpha\beta}-A_\alpha B_\beta]c_\alpha c_\beta=0,$$

where we have put

$$M_{\alpha\beta}=D_{\alpha\beta}-E_{\alpha\beta}.$$

Now, employing the stationary property, $\partial Q/\partial c_i=0$, yields the N linear equations:

$$[(k\tan\delta)M_{i\beta}-A_iB_\beta]c_\beta=0.$$

The compatibility condition for this system then leads to the Nth order determinant,

$$|(k\tan\delta)M_{ij}-A_iB_j|=0. \quad (8)$$

Examination of the matrix (A_iB_j) shows it is of rank one. It is then easy to show that, of the N possible roots for $k\tan\delta$, only one is nonzero.[6] That is, $\tan\delta$ is uniquely determined. Defining $A_iB_j=N_{ij}$, the solution for $k\tan\delta$

[2] *Seminar on Recent Developments in the Theory of Wave Propagation*, Institute for Mathematics and Mechanics, New York University, (notes prepared by H. E. Moses) 1949–1950 (unpublished).

[3] L. Hulthén, Kgl. Fysiograf. Sällskap. Lund, Förh. **14**, No. 21 (1944)

[4] L. Hulthén, Die Xieme Congres des Mathematiciens Scandanaves, Copenhagen, 1946

[5] H. S. W. Massey and B. L. Moiseiwitsch, Proc. Roy. Soc. (London) **205A**, 483 (1951).

[6] W. Kohn, Phys. Rev. **74**, 1763 (1948).

from Eq. (8) may be reduced to the final form

$$k\tan\delta=\frac{\begin{vmatrix}N_{11} & N_{12}\cdots N_{1n}\\ M_{21} & M_{22}\cdots M_{2n}\\ \vdots & \\ M_{n1} & M_{n2}\cdots M_{nn}\end{vmatrix}+\begin{vmatrix}M_{11} & M_{12}\cdots M_{1n}\\ N_{21} & N_{22}\cdots N_{2n}\\ M_{31} & M_{32}\cdots M_{3n}\\ \vdots & \\ M_{n1} & M_{n2}\cdots M_{nn}\end{vmatrix}+\text{etc. (to } N \text{ determinants)}}{|M_{ij}|}. \tag{9}$$

1. Square Well

The first application of the Schwinger principle is to the square well defined in dimensionless units by

$$V=\lambda f(x);\quad f(x)=1,\ 0<x<1;\quad 0,\ x>1.$$

Simple wave functions of the form x, $c_1x+c_2x^2$ were used. A parallel calculation with the same trial wave functions was carried out using Kohn's modification of Hulthén's variational principle, which is referred to here as the Kohn-Hulthén method. Briefly, the Kohn-Hulthén principle asserts that the logarithmic derivative, $L=u'(a)/u(a)$, appearing in the following expression, is stationary, where a is some point in the asymptotic region:

$$\int_0^a\{-u'^2+k^2u^2+V(x)u^2\}dx+Lu^2(a)=0.$$

The results of the calculation using both variation principles appear in Fig. 1, which portrays the zero-energy scattering amplitude X in terms of which the total scattering cross section is $4\pi X^2$. That is,

$$X=\lim_{k\to 0}\frac{\tan\delta}{k}.$$

X is plotted as a function of λ so that the effect of different binding strengths may be observed. For comparison the exact solution is included in the figure. It is apparent from Fig. 1 that the Schwinger principle furnishes more accurate results than the Kohn-Hulthén method for a given trial solution. (The value $\lambda=4.014$ gives the correct binding energy for the deuteron.)

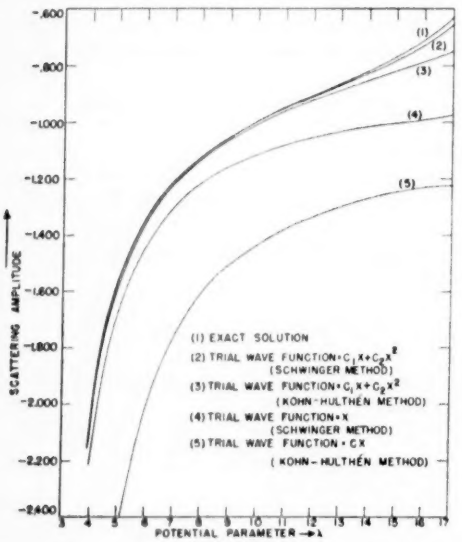
SCATTERING AMPLITUDE
POTENTIAL PARAMETER → λ
(1) EXACT SOLUTION
(2) TRIAL WAVE FUNCTION = C1X + C2X2 (SCHWINGER METHOD)
(3) TRIAL WAVE FUNCTION = C1X + C2X2 (KOHN-HULTHÉN METHOD)
(4) TRIAL WAVE FUNCTION = X (SCHWINGER METHOD)
(5) TRIAL WAVE FUNCTION = CX (KOHN-HULTHÉN METHOD)

FIG. 1. Square-well scattering amplitude as a function of $\lambda=2\mu V_0r_0^2/\hbar^2$.

2. Static Field of the Hydrogen Atom (One Dimension)

In Hartree units the static field of the hydrogen atom is given by

$$V(r)=-(1+1/r)e^{-2r}.$$

Massey and Moisewitsch[5] have calculated the zero-order phase shift using the Hulthén method. The trial solution which they utilized was

$$\sin kr+(a+be^{-r})(1-e^{-r})\cos kr.$$

This problem was treated by the Schwinger procedure using Eq. (9). Trial solutions $c_1x+c_2x^2$ and $c_1x+c_2x^2+c_3x^3$ were used. Since the Schwinger expression, Eq. (6), is independent of a normalization constant, these trial solutions are essentially one and two parameter functions, respectively. The results of this calculation appear in Table I along with the Massey-Moisewitsch estimates. A few exact phases obtained numerically[7] are listed for comparison.

3. The Yukawa Field

The first variational estimate of the zero-order phase shift for scattering in the field be^{-x}/x was made by Hulthén[3] using his original variation principle. The best trial solution used is given by

$$u(x)=f(x)\cos\delta\sin kx+g(x)\sin\delta\cos kx,$$

with $f(x)=1+c_1e^{-x}+c_2e^{-2x}$, $g(x)=(1-e^{-x})(1+he^{-x})$. Here, c_1, c_2, h are the variation parameters. For $b=2.64$, corresponding to the ^3S field and $k^2=0.225$, the result

[7] S. Chandrasekhar and F. Breen, Astrophys. J. **103**, 41 (1946).

arrived at by Hulthén was

$$\delta = 2.03367.$$

Reference to this work indicates that considerable labor was involved. Again employing the Schwinger method, in the convenient form of Eq. (9), the phase shift estimate for this problem was carried out with simple trial solutions

$$\sum_{i=1}^{2} c_i x^i, \quad \sum_{i=1}^{3} c_i x^i, \quad \text{and} \quad \sum_{i=1}^{4} c_i x^i.$$

The results were $\delta = 1.736$, 1.937, 1.939, respectively. The lack of significant improvement in the last case is not surprising since, in the interaction region which is most effective in determining the scattering, x^4 is negligible.

Clearly, excellent estimates of zero-order phase shift can be made in a very convenient manner even with simple trial solutions of a polynomial type. Other trial solutions of the form $\sum_i c_i u_i(x)$ would undoubtedly furnish better results although some of the E_{ij} integrals could possibly become so difficult that resort to numerical methods might prove necessary. It is a simple matter to generalize Eq. (9) for the higher order phases; the form of Eq. (9) is exactly the same and only the individual matrix elements would differ.

4. Static Field of the Hydrogen Atom (3 Dimensions)

This problem is concerned with the solution of

$$(\nabla^2 + k_0^2)\psi = V\psi, \tag{10}$$

where $V = -2(1+1/r)e^{-2r}$. The solution was obtained using Eq. (5) by calculation the forward transition amplitude and invoking the cross-section theorem[8] in order to find the total cross section. If T_{aa} is the forward transition amplitude, then the total transition probability,

$$w = 2\pi \sum_a |T_{aa}|^2 \delta(E_a - E_a), \tag{11}$$

provides the total cross section σ by means of the cross-section theorem,

$$-\mathrm{Im}(T_{aa}/k_0) = w/k_0 = \sigma. \tag{12}$$

Here, the units are defined by Eq. (10). The total cross section, after using Eq. (4), is then

$$\sigma = (4\pi/k_0)\ \mathrm{Im} f(\mathbf{k}_0 - \mathbf{k}_0). \tag{13}$$

Since Eq. (13) is true exactly, the question arises as to its meaning when approximate forward scattering amplitudes are employed. By introducing a coefficient λ as a measure of the perturbation strength to label the orders of approximation, it is not difficult to establish by using Eqs. (11) and (12), that the accuracy for the total cross section is diminished by one order in λ when, in applying the cross-section theorem, approximate values of the forward scattering amplitude are used. In particular, the forward amplitude when evaluated to within the second Born approximation can only provide the total cross section in first Born approximation. It follows that there is no point in applying the cross-section theorem unless a higher approximation for the forward transition amplitude than that of a second Born can be determined. Although the restriction to the forward direction provides a significant simplification to the task of evaluating the amplitude in second Born approximation, it is a far more difficult problem than that of determining the first-order total cross section directly, i.e., angular integration of Born amplitudes. This difficulty is due to the presence of the Green's function in the second Born matrix element. But the utility of the cross-section theorem is restored if one calculates the forward transition amplitude by means of the variation principle. Alternatively, the cross-section theorem can be used to test the accuracy of the variation principle, for if a better total cross section than first Born is obtained from a variational evaluation of the forward transition amplitude, then it follows that the forward amplitude is determined to an accuracy greater than that given by the second Born approximation. This was the basis for testing the Schwinger principle for the trial solution $e^{i\mathbf{k}_0\cdot\mathbf{r}}$ in connection with scattering in the static field of the hydrogen atom. As pointed out in Sec. I, [Eq. (5)] the matrix element containing the Green's function is exactly the integral which arises in the second Born approximation and, as we shall see, the variational principle with unperturbed wave function as trial solution is capable of producing better results for the forward amplitude, for all incident energies, than that of the second Born approximation.

Accordingly, we write the Schwinger principle, [Eq. (1)], explicitly for the trial solutions,

$$\psi_a = e^{i\mathbf{k}_0\cdot\mathbf{r}}, \quad \psi_b' = e^{i\mathbf{k}\cdot\mathbf{r}},$$

TABLE I. Comparative zero-order phase shifts as a function of incident wave number k in Hartree units. Column A gives the Hulthén method used by Massey and Moisewitsch. Column B gives the Schwinger method with trial solution $c_1x+c_2x^2$. Column C gives the Schwinger method using $c_1x+c_2x+c_3x^2$. Column D gives the exact phase shift.

k	A	B	C	D
0.1	0.721	0.646	0.695	0.730
0.2	0.972		0.950	0.9731
0.4	1.057		1.045	1.0458
0.6	1.020		1.017	
1.0	0.904		0.901	0.9057
1.5	0.783		0.767	
2.0	0.694		0.636	

[8] B. A. Lippman and J. Schwinger, Phys. Rev. 79, 469 (1950).

as

$$T_{ba}\equiv T(\mathbf{k}\leftarrow\mathbf{k}_0)=\frac{\left(\int d\mathbf{r}e^{-i\mathbf{k}\cdot\mathbf{r}}V(\mathbf{r})e^{i\mathbf{k}_0\cdot\mathbf{r}}\right)^2}{\int d\mathbf{r}e^{-i\mathbf{k}\cdot\mathbf{r}}V(\mathbf{r})e^{i\mathbf{k}_0\cdot\mathbf{r}}-\int\int d\mathbf{r}d\mathbf{r}'e^{-i\mathbf{k}\cdot\mathbf{r}}\frac{V(\mathbf{r})e^{i\mathbf{k}|\mathbf{r}-\mathbf{r}'|}}{-4\pi|\mathbf{r}-\mathbf{r}'|}V(\mathbf{r}')e^{i\mathbf{k}_0\cdot\mathbf{r}'}}. \tag{14}$$

We ignore normalization constants since the Schwinger principle is indifferent to the normalization of trial solutions. The integral containing the Green's function is most conveniently evaluated in momentum representation. This integral may then be written

$$\lim_{\epsilon\to 0}\int\frac{d\mathbf{k}'}{(2\pi)^3}\frac{(\mathbf{k}|V|\mathbf{k}')(\mathbf{k}'|V|\mathbf{k}_0)}{k_0^2-k^2+\epsilon i};\quad \epsilon>0, \tag{15}$$

where the matrices $(\mathbf{k}|V|\mathbf{k}')$ are the first Born transition amplitudes. For the static field of hydrogen [Eq. (10)], this quantity by a straight forward integration is

$$(\mathbf{k}|V|\mathbf{k}')=-8\pi(8+K^2)/(4+K^2)^2, \tag{16}$$

where $\mathbf{K}=\mathbf{k}-\mathbf{k}'$. Since we are concerned with the forward transition amplitude, the integral in Eq. (15) may be evaluated by standard contour methods with the result

$$\lim_{\epsilon\to 0}\int\frac{d\mathbf{k}}{(2\pi)^3}\frac{|(\mathbf{k}|V|\mathbf{k}_0)|^2}{k_0^2-k^2+\epsilon i}=\frac{-4\pi(Bi+A)}{96(1+k_0^2)^3}, \tag{17}$$

where

$$A=39k_0^4+106k_0^2+75,\quad B=56k_0^5+144k_0^3+96k_0.$$

On using Eq. (4), the variational result for the forward scattering amplitude is

$$f_{\text{var}}(\mathbf{k}_0\leftarrow\mathbf{k}_0)=\frac{96(1+k_0^2)^3}{96(1+k_0^2)^3-(A+Bi)}. \tag{18}$$

On applying the cross-section theorem, Eq. (13), the total cross section in units of πa_0^2 (a_0 = first Bohr radius) is given by

$$\sigma_{\text{var}}=\frac{3072(1+k_0^2)^3(7k_0^4+18k_0^2+12)}{(96k_0^6+249k_0^4+182k_0^2+21)^2+64k_0^2(7k_0^4+18k_0^2+12)^2}. \tag{19}$$

To find the total cross section in Born approximation it is only required to perform the integration over solid angle of the differential cross section obtained from the Born amplitudes in Eq. (16). That is

$$\sigma_B=\int|f_B(\mathbf{k}\leftarrow\mathbf{k}_0)|^2d\Omega,$$

where

$$f_B(\mathbf{k}\leftarrow\mathbf{k}_0)=-\frac{1}{4\pi}T_B(\mathbf{k}\leftarrow\mathbf{k}_0)=-\frac{1}{4\pi}\left\{\frac{-8\pi(8+K^2)}{(4+K^2)^2}\right\}.$$

The integral is an elementary one, and the result[9] is

$$\sigma_B=\frac{7k_0^4+18k_0^2+12}{3(1+k_0^2)^3}, \tag{20}$$

in units of πa_0^2. On using the integral in Eq. (17), the forward scattering amplitude in the second Born approximation is given by

$$f_{\text{2nd Born}}(\mathbf{k}_0\leftarrow\mathbf{k}_0)=-\frac{1}{4\pi}T(\mathbf{k}_0\leftarrow\mathbf{k}_0)=-\frac{1}{4\pi}\left\{-4\pi-\frac{4\pi(A+Bi)}{96(1+k_0^2)^3}\right\}. \tag{21}$$

[The first term, (-4π), in curly brackets is the forward Born amplitude which follows from Eq. (16).] On applying the cross-section theorem using Eq. (21), we obtain precisely σ_B as given in Eq. (20). This is the result to be expected by virtue of the previous discussion.

TABLE II. Comparative total cross sections in units of πa_0^2 for electron scattering in the static field of the hydrogen atom.

k_0 (Hartree units)	Eq. (19)	Eq. (20)	Phase shifts
0	83.59	4	...
0.2	35.54	3.77	68.34
0.4	12.99	3.22	19.05
0.6	6.28	2.57	8.12
0.8	3.63	1.99	4.27
1.0	2.34	1.54	2.62
1.323	1.34	1.04	1.40
1.5	1.05	0.854	0.885[a]
2.0	0.587	0.522	0.410[a]
3.0	0.260	0.247	
5.0	0.0935	0.0917	
8.0	0.0365	0.0362	
10.0	0.0233	0.0232	
.			
.			
.			
$k_0\to\infty$	$(7/3)k_0^{-2}$	$(7/3)k_0^{-2}$	

[a] These are calculated from zero-order phase shift alone, obtained variationally in reference 5.

[9] This result may also be found in N. F. Mott and H. S. W. Massey, *Theory of Atomic Collisions* (Clarendon Press, Oxford, 1949), second edition, p. 185.

That the variational determination of σ, Eq. (19), is actually superior to σ_B can be seen by reference to Table II. This table includes a few values calculated from zero- and first-order phase shifts obtained numerically by Chandrasekhar and Breen.[7] It is also interesting to observe that $\sigma_{var} \rightarrow \sigma_{Born}$ as $k_0 \rightarrow \infty$. We may therefore conclude on the basis of the discussion of the cross-section theorem that the forward amplitude as obtained variationally with the undisturbed wave as the trial solution is indeed better than that determined from the second Born approximation for all incident energies.

SUMMARY

(a) Good estimates of the of the phase shift may be conveniently made variationally with polynomial type wave functions.

(b) For a given trial solution the Schwinger formalism appears to furnish estimates of the phase shift superior to the Hulthén-Kohn method.

(c) Of particular advantage, in comparison with the Hulthén method, is the fact that in the Schwinger principle the trial wave functions need not be normalized to the correct asymptotic form.

(d) For the undisturbed wave as trial solution, the forward scattering amplitude is determined more accurately variationally for all incident energies than by use of the second Born approximation.

(e) The improved estimate of the total cross section, σ_{var}, still underestimates the correct value at the low incident energies and approaches the Born approximation for the higher energies in a continuous manner.

The author wishes to thank Dr. J. F. Carlson for his kind interest and helpful discussions.

PHYSICAL REVIEW VOLUME 89, NUMBER 6 MARCH 15, 1953

The Absolute Determination of Resonant Energies for the Radiative Capture of Protons by Boron, Carbon, Fluorine, Magnesium, and Aluminum in the Energy Range below 500 kev

S. E. HUNT AND W. M. JONES
Research Laboratory, Associated Electrical Industries, Ltd., Aldermaston, Berkshire, England
(Received November 26, 1952)

An absolute electrostatic analyzer of deflecting angle $\pi/2\sqrt{2}$ radians has been used to measure and stabilize the energy of the proton beam from an air insulated electrostic generator. The following resonant energies for proton capture by some of the light elements have been measured:

$B^{11}(p,\gamma)C^{12}$	163.8±0.3 kev.
$C^{13}(p,\gamma)N^{14}$	456.8±0.5 kev.
$F^{19}(p,\gamma)Ne^{20*}$	224.4±0.4 kev.
$Mg^{26}(p,\gamma)Al^{27}$	314.8±0.5, 338.5±0.5, 389.4±0.5, 436.5±0.4, 454.2±0.3, 484.0±1.0 kev.
$Mg^{24}(p,\gamma)Al^{25*}$	418.0±0.5 kev.
$Al^{27}(p,\gamma)Si^{28}$	226.3±1.5, 294.1±0.5, 325.6±0.4, 404.7±0.4, 438.5±0.5, 504.0±0.6 kev.

The high energy resolution of one thousand obtained has made accurate determination of the half-widths of these resonances possible.

INTRODUCTION

THE construction of the 63.6° electrostatic analyzer and its use to measure absolutely and stabilize the energy of the beam from an electrostatic generator have been described in a previous paper.[1]

The uncertainty of the measurements is about one part in a thousand except for the very weak resonances.

The agreement of the absolute values obtained for the strong lithium resonance at 441.5 kev and the fluorine resonances at 340.4 and 483.1 kev[1] with recent precise determinations by other workers[2–4] confirms the claim for high absolute accuracy.

The resonances investigated in the present work have not, in general, been measured to this accuracy previously, and it is hoped that precise determinations of nuclear resonances, and hence of nuclear energy level spacing, will be of use in testing theories on nuclear structure, whilst for closely spaced levels precise energy determinations are necessary in order to provide definite identification.

Because of the high energy resolution and stability of the beam, it has been possible to measure the natural half-widths of many resonances to an accuracy not previously obtained.

EXPERIMENTAL DETAILS

The energy of the beam could be varied continuously and target currents up to 25 microamperes were obtained. These were fed into a beam current integrator and timing unit which stopped the γ-ray counts when the target had received a predetermined charge.

[1] S. E. Hunt Proc. Phys. Soc. (London) **A65**, 982 (1952).
[2] E. L. Hudspeth and C. P. Swann, Phys. Rev. **75**, 1272 (1949).
[3] W. A. Fowler and C. C. Lauritsen, Phys. Rev. **76**, 314 (1949).
[4] A. H. Morrish, Phys. Rev. **76**, 1651 (1949).

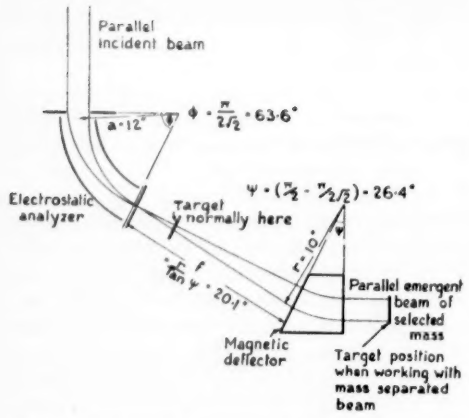
Parallel incident beam
a=12°
Φ = π/2√2 = 63·6°
Ψ = (π/2 − π/2√2) = 26·4°
Electrostatic analyzer
Target normally here
r = 10"
r tan Ψ = 20·4"
Parallel emergent beam of selected mass
Magnetic deflector
Target position when working with mass separated beam

FIG. 1. Diagrammatic representation of the electrostatic analyzer and deflector magnet.

In normal operation the target was placed a short distance from the exit slit of the electrostatic analyzer to allow the finely focused beam to diverge and prevent damage resulting from local overheating of the target surface. When there was any uncertainty as to which mass component of the beam produced an observed resonance, mass separation was effected by placing a small triangular magnet after the electrostatic analyzer. The first focal point of the magnet was made to coincide with the exit slit of the analyzer so that the two formed a telescopic system, and the deflecting angle of the magnet was complementary to that of the analyzer to produce a horizontal emergent beam. A Mu metal shield was fitted over the analyzer for these exposures to reduce the stray magnetic field from the magnet.

The system is illustrated diagrammatically in Fig. 1.

It was possible to observe the 224.4-kev fluorine resonance using the mass 1 and mass 2 components of the beam and the 163.8-kev boron resonance using mass 1, mass 2, and mass 3 components.

ABSOLUTE ACCURACY

The errors associated with the determinations have been discussed in detail elsewhere.[1] It has been estimated that systematic errors associated with geometrical measurements on the electrostatic analyzer and the measurement of the voltages applied to the deflector plates are less than five parts in ten thousand. The main source of random error was the uncertainty in estimating exactly the point of maximum yield from a curve drawn through the experimental points. This varied considerably, being about 5 parts in 10^4 for the single determination of a fairly strong, sharp resonance to about 3 parts in 10^3 for that of a weak, broad resonance. The errors were approximately half this when scintillation counters were used for detection. They were further reduced by making between five and ten independent determinations of each resonance. This had the advantage that other small random errors associated with the estimation of target thickness and the measurement of deflector voltages also tended to be minimized. The results quoted are the mean values of these several determinations and the uncertainties were obtained by adding the standard deviation of this mean value to the estimated systematic error.

TARGETS

The target materials were deposited on carefully cleaned and polished copper backings. These were heated to a temperature of between 200 and 250°C during irradiation and were situated close to a liquid nitrogen cooled baffle. This has been found to be effective in stopping the contamination of the target surface by condensed oil from the diffusion pumps.[1]

Boron and separated magnesium isotope targets were deposited by the Isotope Division A.E.R.E., Harwell, using a mass spectrograph. Natural magnesium and aluminum were deposited by vacuum evaporation of the metal from molybdenum boats and tungsten filaments, respectively.

Some boron targets were also prepared by evaporation from graphite boats. The target thickness was estimated from the total amount of boron plus boron carbides evaporated.[5]

Fluorine targets were prepared by evaporating calcium, lithium, and magnesium fluorides from molybdenum boats.

In all evaporations the target thickness in micrograms per square centimeter was estimated from the total weight of material evaporated and the geometry of the evaporation. The accuracy of this method was tested by evaporating aluminum on to a larger surface and estimating the thickness of the deposit by direct weighing of the backing using a microbalance. The two estimates of target thickness agreed to within two percent.

It was not found possible to evaporate carbon, and it was considered undesirable to dilute the target by evaporating a carbon compound. Carbon targets were, therefore, prepared by depositing soot from a Calor gas flame on to a copper backing, on which a very thin ($\sim$100 ev) calcium fluoride target had been previously deposited. It was then possible to estimate the thickness of the carbon targets in energy units directly from the observed displacements of the fluorine resonances.

The thickness of other targets in energy units was estimated from published stopping power curves, when available, and from Bethe's formula.[6]

Tangen[7] and Morrish[4] have shown that the true resonant energy is given by $E_0 = E - \Delta E/2$, where E is the observed energy of maximum yield and ΔE is the thickness of the target in energy units. In order to

[5] N. V. Sidgwick, *Chemical Elements and Their Compounds* (Clarendon Press, Oxford, 1950), Vol. 1, p. 368.

[6] M. S. Livingston and H. A. Bethe, Revs. Modern Phys. **9**, 263 (1937).

[7] R. Tangen, Kgl. Norske Videnskab. Selskabs Skrifter No. 1 (1946).

minimize the uncertainty in ΔE targets were kept as thin as possible, so far as this was consistent with obtaining measurable yields. Thicknesses between 100 ev and 2 kev were used for most of the determinations in the present work, except in the case of carbon, for which uncertainties in the stopping power of the target material were not relevant.

The thickness of the targets in energy units was further checked by rotating them through an angle of 60° with respect to the proton beam. This effectively doubled the target thickness and the resonance peak was displaced by a further energy of $\Delta E/2$.

Tangen[7] has shown that if Γ is the experimentally observed half-width of a resonance, then Γ_0, the true half-width, is given by $\Gamma_0=(\Gamma^2-\Delta E^2)^{\frac{1}{2}}$. This correction applies only when ΔE is small compared with Γ_0. Estimates of half-width were therefore made only when this condition obtained. When the observed half-width did not greatly exceed the thickness of the thinnest target on which it was observed, this was given as an upper limit of the possible natural half-width.

Resonances were also observed using thick targets in the case of carbon and aluminium. The resonant energy was taken as the point of inflection in the experimental curve. The values were in good agreement with those obtained from the thin target yield curves, although the points of inflection could not be located with the same accuracy as could the peaks of thin target yield curves. Since thick target yield curves represent the integral of thin target yield curves they were, however, useful in confirming that no measurable resonance had been omitted.

DETECTION

Initially the γ-rays were detected by using an end window type Geiger-Müller counter with a lead radiator. The solid angle subtended by the counter at the target was arranged to be as large as possible.

In order to rotate the target through 60° with respect to the incident beam, a brass tube with flanges inclined at an angle of 60° was interposed between the analyzer and target flange. This rotated both target and detector without affecting the geometrical efficiency of detection.

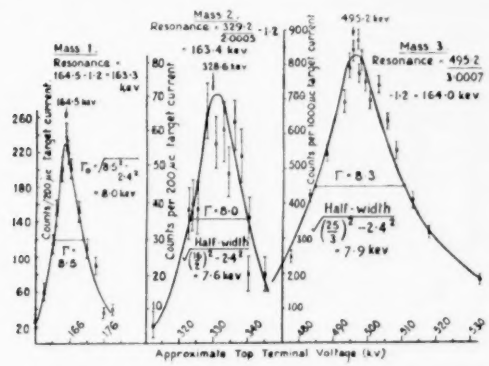
Mass 1
Resonance = 164·5 ± 1·2 = 163·3 kev
164·5 kev
Γ = 8·5
Γ₀ = √(8·5² − 2·4²) = 8·0 kev
Mass 2
Resonance = 329·2 / 2·0005 ± 1·2 = 163·4 kev
328·6 kev
Γ = 8·0
Half-width = √((25/3)² − 2·4²) = 7·6 kev
495·2 kev
Mass 3
Resonance = 495·2 / 3·0007 ± 1·2 = 164·0 kev
Γ = 8·3
Half-width = √((25/3)² − 2·4²) = 7·9 kev
Counts/200 μc Target current
Counts per 200 μc Target current
Counts per 1000 μc Target current
Approximate Top Terminal Voltage (kv)

FIG. 2. The boron resonance observed using mass 1, mass 2, and mass 3 components of the beam.

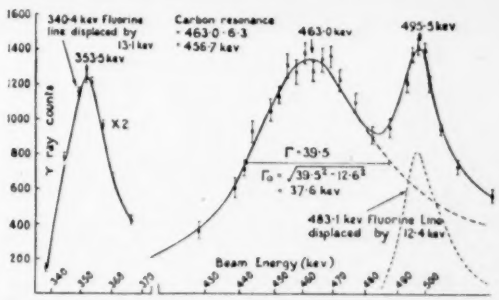
340·4 kev Fluorine line displaced by 13·1 kev
353·5 kev
Carbon resonance = 463·0 ± 6·3 = 456·7 kev
463·0 kev
495·5 kev
X 2
γ ray counts
Γ = 39·5
Γ₀ = √(39·5² − 12·6²) = 37·6 kev
483·1 kev Fluorine Line displaced by 12·4 kev
Beam Energy (kev)

FIG. 3. The carbon resonance observed using a carbon target deposited on a 100-ev thick calcium fluoride target.

In later exposures the sensitivity of detection was improved by using a scintillation counter consisting of a thallium activated sodium iodide crystal and an E.M.I. type 5311 photomultiplier.

When using both Geiger counters and scintillation counters, background counts were reduced as far as possible by using thick lead shielding. The background was estimated by placing a clean brass surface in front of the target and repeating the exposures. The estimated background has been subtracted from all experimental points shown in the figures.

DISCUSSION OF RESULTS

Boron. $B^{11}(p,\gamma)C^{12*}$

The mean value of ten independent determinations of the energy of the boron resonance was 163.8 kev with a standard deviation of 0.2 kev. The total uncertainty after allowing for possible systematic errors is ±0.3 kev. A mean value of 7.3±0.5 kev was obtained for the natural half-width of the resonance. Typical curves obtained using mass 1, 2, and 3 components of the beam are shown in Fig. 2.

Another precise determination of this resonance has been made by Morrish[4] using an electrostatic analyzer calibrated by deflecting a low energy electron beam. He quotes a value of 162.8 kev with an uncertainty of ±0.2 kev, though it appears that this latter figure refers to the internal consistency of this results, as the probable errors associated with the calibration of the apparatus are quoted as 0.3 percent.[4,8] His value for the natural half-width was 4.5±1.5 kev. The disagreement of both these measurements with those obtained in the present work is somewhat greater than the combined errors.

Earlier and less precise determinations made by other workers have been listed by Morrish.

[8] Allison, Frankel, Hall, Montague, Morrish, and Warshaw, Rev. Sci. Instr. **20**, 735 (1949).

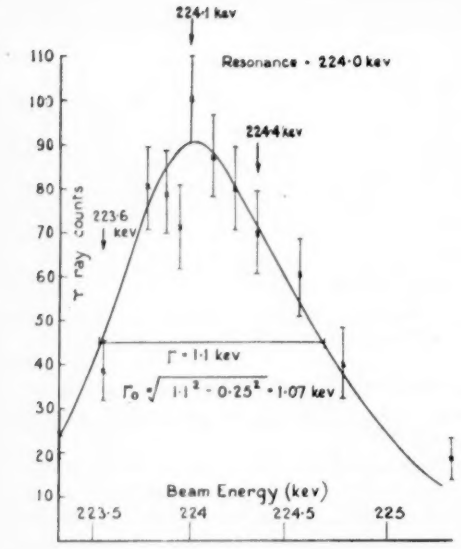

FIG. 4. The weak fluorine resonance at 224.4 kev observed on a calcium fluoride target of thickness 250 ev.

Carbon. $C^{12}(p,\gamma)N^{13}$

The mean value of five determinations, using targets of thickness in energy units between 5 and 15 kev deposited over thin calcium fluoride targets, was 456.8 kev, the total uncertainty was ±0.5 kev, and the mean half-width was 39.5±1.0 kev. A typical curve is shown in Fig. 3. It will be seen that the fluorine resonance at 340.4 kev was displaced by 13.1 kev and the peak at 483.1 kev by 12.4 kev. The thickness of the carbon target at the energy of the carbon resonance was therefore taken as 12.6 kev. This represents a mean value for the thickness since it is seen from the broadening of the fluorine lines that the carbon deposition was not uniformly thick.

One of the thin calcium fluoride targets was irradiated before the deposition of the soot target, and the yield from the two fluorine resonance was found to be negligible between 400 and 475 kev. It was, therefore, reasonable to assume that the yield from these resonances did not affect the position of the carbon peak observed in the composite targets. Some uncertainty was introduced in the half-width measurements since the yield from the upper fluorine resonance started to be appreciable at about 480 kev. It was possible, however, to analyze the combined curve with a fair degree of accuracy by assuming that the upper fluorine resonance was broadened by the same amount as the lower one. Additional irradiations were also made of carbon targets deposited directly on the copper backings. The exact shape of the carbon resonance could then be followed in the absence of the fluorine lines. An estimate of the target thickness was necessary to obtain the natural half-width from the experimentally observed half-width. This was taken as twice the displacement of the carbon peak itself from the mean corrected value of the resonance previously determined.

The values of the half-width so obtained were in good agreement with those obtained from the composite targets.

Previous determinations of this resonance have been summarized by Hornyak, Lauritsen, Morrison, and Fowler.[9] The highest precision previously quoted being for a determination by Fowler and Lauritsen[3] of 456±2 kev with a half-width of 35 kev; this measurement was made relative to the 441.5-kev-lithium resonance.

Fluorine. $F^{19}(p,\gamma)Ne^{20*}$

The measurement of the strong resonances at 340.4 ±0.5 and 483.1±0.5 kev has been reported previously.[1] A resonance of approximately one three-hundredth of the yield of the 340.4 line has been observed. The mean of ten determinations was 224.4±0.4 kev, and the half-width of the resonance, observed on a target of thickness in energy units 0.25 kev, was 1.1 kev. The natural half-width of the resonance is therefore estimated to be 1.0±0.3 kev.

A typical resonance curve is shown in Fig. 4. This resonance has been observed previously by Tangen[7] who measured the resonant energy as 222±2 kev and gave the half-width as less than 2 kev, which was the thickness in energy units of the target used.

Magnesium

Magnesium occurs in three isotopic forms Mg^{24}, Mg^{25}, and Mg^{26}. The compound nuclei Al^{25} and Al^{26} produced on proton capture by the two lower isotopes decay by positron emission, while Mg^{26} produces the stable isotope Al^{27}.

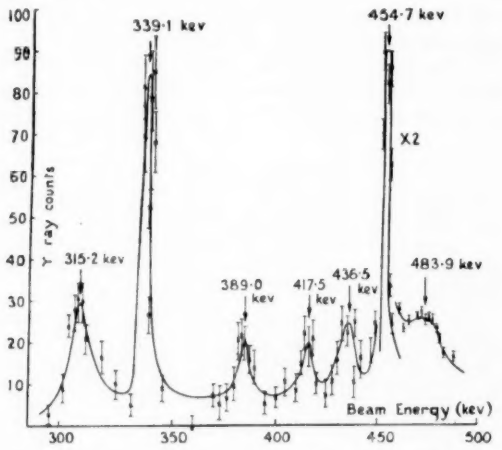

FIG. 5. The magnesium resonances observed on a target of thickness 1.1 kev.

[9] Hornyak, Lauritsen, Morrison, and Fowler, Revs. Modern Phys. 22, 291 (1950).

On bombarding metallic magnesium targets, (p,γ) resonance were observed at the following energies: 314.8±0.5, 338.5±0.5, 389.4±0.5, 418.0±0.5, 436.5 ±0.4, 454.2±0.3, and 484.0±1.0 kev, with respective half-widths of: 4.0±1.0, 2.5±1.0, 4.0±1.0, 4.0±0.5, 4.0±1.0, <1.0, and 10±2 kev. A typical experimental curve is shown in Fig. 5.

It was thought that the formation of oxide films on the metallic target surfaces might increase their effective thicknesses considerably and thus produce errors in the target correction. The displacement of the strong 454.2-kev line on rotating the targets through 60° indicated that any oxide layers were of negligible thickness. This was also confirmed by observing this resonance on magnesium fluoride targets, when the absolute determinations and measurements relative to the fluorine lines were in excellent agreement with those obtained using metallic targets.

Tangen has observed all the above resonances to an accuracy of about 1 percent,[7] and the present observations are mainly within the limits of experimental error which he quoted, or sufficiently near to his values to allow positive identification, except for the weak broad resonance at 484±1.0 kev. The discrepancy between the present determination and Tangen's value of 494±5 kev was thought to be sufficiently serious to produce doubts on the identification of this resonance, but no other resonance was observed up to 510 kv so that it seems probable that the two measurements refer to the same resonance.

From the absence of positron emission Tangen ascribed all but the 418.0-kev resonance to the Mg^{26} isotope. This he originally ascribed to Mg^{25}, although Grotdal[10] later ascribed it to the Mg^{24} isotope. The resonance has been observed using separated Mg^{24} in the present work, thus confirming Grotdal's result.

Aluminum. $Al^{27}(p,\gamma)Si^{28}$

Aluminum resonances have been observed at the following energies using thin targets: 294.1±0.5, 325.6 ±0.4, 404.7±0.4, 438.5±0.5, and 504.0±0.6, and using a thick aluminum disk as a target a further weak resonance has been detected at 226.3±1.5 kev.

The half-widths of the resonances observed on a 1.0-kev thick target were only slightly greater than the thickness of the target. From thick target yield curves the width of the stronger 504.0- and 404.7-kev lines were both estimated to be 0.7±0.3 kev, while the weaker resonances all had a half-width of about or slightly less than 1 kev. Typical resonance curves are shown in Fig. 6.

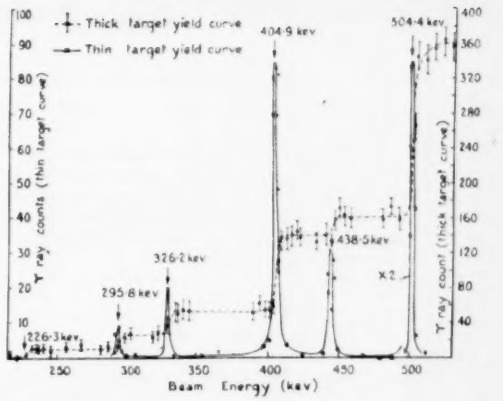

FIG. 6. Thick and thin target resonance curves for aluminum.

The aluminum resonances in this energy range have been investigated previously by Gentner[11] who reported a sharp resonance at 425 kev and by Tangen who reported resonances at 225±3, 295±3, 325±3, 404±3, 443±5, and 503±5 kev. The present results are in good agreement with those of Tangen. However, it is interesting to note that from Tangen's results the levels of Si^{28} can be arranged into a system of doublets of separation 34.0 kev, the spacing between the doublets being twice this. The errors associated with the fit are within the experimental errors quoted by Tangen. It was hoped that more precise determinations would demonstrate the regularity more convincingly, but the errors associated with the fitting of a regular doublet system to the present results are far greater than the experimental errors.

The only half-width measurement quoted previously is Tangen's value of less than 0.5 kev for the strong 404.7-kev line.

The authors wish to express their thanks to Professor J. Rotblat for his constructive criticism, and Mr. D. R. Chick and Mr. D. P. R. Petrie for their continued interest in the program of research.

They would also like to thank Mr. D. A. Hancock and Mr. R. Griffin for assisting in the experimental work, and members of the workshop staff for the production of apparatus.

Thanks are also due Dr. T. E. Allibone, F.R.S., for permission to publish this paper.

[10] Grotdal, Lönjö, Tangen, and Bergström, Phys. Rev. **77**, 296 (1950).

[11] W. Gentner, Z. Physik. **107**, 354 (1937).

Fission Neutron Spectrum of U^{235}

DAVID B. NICODEMUS* AND HANS H. STAUB†
University of California, Los Alamos Scientific Laboratory, Los Alamos, New Mexico
(Received November 26, 1952)

A high pressure ionization chamber has been used to measure the energy distribution of proton recoils from the neutrons which are emitted during the thermal neutron fission of U^{235}. The energy spectrum of the fission neutrons is obtained by applying suitable wall corrections and by using 2.5-Mev $d-d$ neutrons for an energy calibration. Measurements were made in the range from 1 to 4 Mev, and within the experimental errors, the resulting fission spectrum follows Watt's [B. E. Watt, Phys. Rev. **87**, 1037 (1952)] semi-empirical relation, $N(E)=e^{-E}\sinh\sqrt{(2E)}$.

I. INTRODUCTION

THE energy spectrum of neutrons arising from the fission of U^{235} induced by thermal neutrons was investigated by Bloch and Staub[1] in 1943 at Stanford University. The slow neutrons used to induce fission in 2.93 kg of normal uranium were produced by first modulating a cyclotron beam of 2.6-Mev deuterons and then admitting the $Be-d$ neutrons into a large, graphite lined box in which the slow neutrons had a lifetime of about 2 milliseconds. Approximately centered in the box were the uranium sample and a high pressure ionization chamber filled with a mixture of hydrogen and argon. The ion pulses from the chamber were fed through an amplifier which was modulated so as to register counts only after the burst of fast cyclotron neutrons had decayed. These measurements extended over a range of neutron energies from 0.7 to 3.3 Mev, and showed a maximum in the fission spectrum at 0.8 Mev and a half maximum value at about 2 Mev. It was found, however, that these results were affected by some inelastic scattering in the rather heavy iron walls of the ionization chamber and possibly in the walls of the box. In addition, the accuracy of the measurements was greatly limited by the low intensity of primary slow neutrons that resulted from the modulation scheme needed to eliminate the background of fast neutrons. The present measurements (carried on during the early part of 1944) were undertaken as an attempt to obtain a more accurate fission spectrum. The results, although not in strong disagreement with the Stanford measurements, did indeed show a larger abundance of higher energy neutrons. Since the results of the present measurements have not previously been available in a complete form, they are reported here and compared briefly with subsequent data.

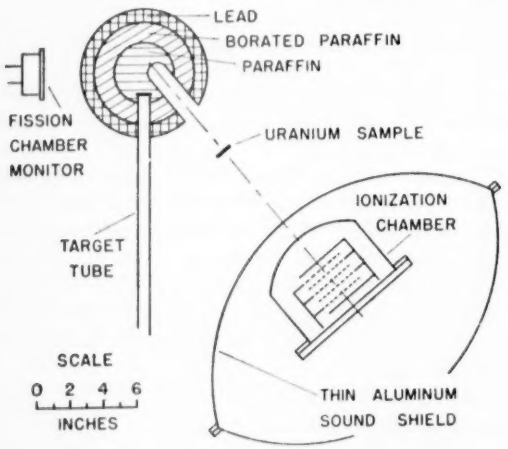

FIG. 1. Experimental arrangement. The target of the Van de Graaff accelerator is surrounded by a spherical paraffin moderator and lead shield. Thermal neutrons to irradiate the uranium sample originate from a 1¼-in. diameter howitzer in the moderator.

II. APPARATUS AND EXPERIMENTAL ARRANGEMENT

Three sets of measurements were made using different amounts of fissionable material and also slightly different experimental arrangements. They will be referred to as runs A, B, and C, respectively.

Run A: using 2.93 kg normal uranium.
Run B: using 243 g normal uranium.
Run C: using 2 g of material enriched in U^{235}.

In all three runs, the thermal neutrons to induce fission were obtained by moderating neutrons from the $Li(p, n)$ reaction produced in a Van de Graaff generator. The accelerating voltage was chosen so that the energies of the neutrons from the reaction would not exceed a few hundred kilovolts. The lithium target in each run was surrounded by a suitable paraffin moderator and lead shield, chosen so as to provide both an adequate flux of thermal neutrons and a low background of fast neutrons and gamma-rays. A typical arrangement is shown in Fig. 1, which is the geometry used during run C. The neutron beam was monitored both by a fission chamber placed near the target assembly and by means of a current integrator for the accelerated beam. The uranium sample was placed approximately midway between the target and the chamber, the distances being chosen to insure a reasonable collimation of the fission neutrons which entered the chamber directly, without allowing too large a possibility of other fission neutrons

* Now at Oregon State College, Corvallis, Oregon.
† Now at the Physikalisches Institut, University of Zürich, Zürich, Switzerland.
[1] F. Bloch and H. Staub, Los Alamos Declassified Report No. 934, 1943 (unpublished).

being inelastically scattered in the moderator and subsequently being detected. Perfect collimation of the fission neutrons was assumed in the calculation of the wall effects.

The ionization chamber used in these measurements was the same one used at Stanford.[1] A complete description of this chamber is also given by Rossi and Staub.[2] Since lower gas pressures were used here than in the earlier Stanford measurements, it was possible to use a thinner $\frac{1}{8}$-in. steel chamber housing. Although the steel back plate of the chamber was $\frac{7}{16}$ in. in thickness, estimates of the inelastic scattering in the chamber walls indicated that its effect on the spectrum was small compared to the random statistical errors in the measurements. The chamber was filled with a mixture of purified hydrogen and argon to a total absolute pressure of 220 lb/in.^{2} giving a stopping power of 5.68. The gas mixture also contained a trace of oxygen, because it was essential that the ions be collected without gas multiplication which might otherwise occur near the wire grids of the chamber electrodes. The chamber was operated at 8700 volts. The ion pulses were fed through a single 1603 tube preamplifier into a linear amplifier whose time constants were a few milliseconds. Appreciable microphonics resulted from the use of these relatively long time constants needed for ion collection. The microphonics, which were induced largely in the woven grid structure of the collecting electrodes, were greatly reduced in the present measurements by the construction of a sound shield consisting of a thin-walled evacuated metal shell. The chamber and preamplifier were suspended by rubber within the sound shield, and the entire arrangement likewise suspended by suitably loaded springs. In spite of the sound shield, the noise level in the vicinity of the electrostatic generator, together with the radiation background, prohibited the measurements to extend below 1 Mev.

During run A, the energy distribution of the proton recoils was measured by feeding the amplified pulses into an electronic differential pulse-height analyzer, similar to the one used in the Stanford measurements.[1] Photographic recording[3] of the pulses was used for runs B and C. Repeated background measurements were taken during all runs with the uranium sample removed. Linearity and reproducibility of the amplifying and recording system were checked during each run by means of artificial pulses fed directly to the collecting system of the chamber. An energy calibration of the recorded pulse heights was obtained between runs by separate measurements with 2.5-Mev $d-d$ neutrons. In addition, the $d-d$ measurements provided a check on the accuracy of the entire experimental method and the wall effect calculations. A typical recoil pulse-height distribution and calculated neutron spectrum from such a calibration run is given by Rossi and Staub.[2]

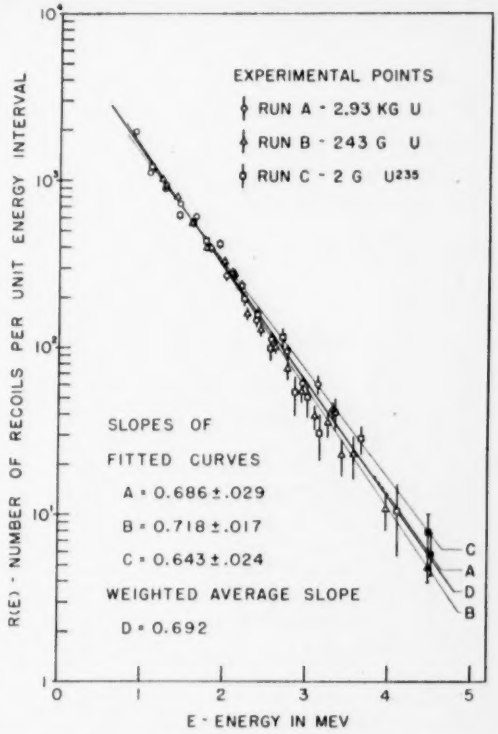

FIG. 2. Measured energy distribution of proton recoils. The data are corrected for background and interval width. The solid points at 4.5 Mev are calculated points.

III. MEASUREMENTS AND RESULTS

The semilogarithmic plot in Fig. 2 shows the number of proton recoil pulses per unit energy interval as a function of the pulse height in Mev. The three sets of data plotted for the runs A, B, and C have been arbitrarily normalized at 1.6 Mev. No pronounced departure from linearity is indicated by the data, and therefore since the assumption of a simple exponential recoil distribution greatly simplifies the calculations of the wall effects, a straight line fit has been made for each of the three sets of data by the method of least squares. Although a linear fit could be made in each case with reasonably good accuracy, there is admittedly no theoretical justification for this simplifying procedure. The calculated magnitudes of the slopes of the three fitted curves together with their standard probable errors are:

$$\text{Slope } A = 0.686 \pm 0.029,$$
$$\text{Slope } B = 0.718 \pm 0.017,$$
$$\text{Slope } C = 0.643 \pm 0.024.$$

The overlapping of these values is shown in Fig. 2 by the calculated points and their errors at 4.5 Mev.

[2] B. Rossi and H. Staub, *Ionization Chambers and Counters* (McGraw-Hill Book Company, Inc., New York, 1949), National Nuclear Energy Series, Div. V, Vol. 2, Sec. 7.11.

[3] The authors are indebted to N. Nereson for the use of his photographic recording apparatus.

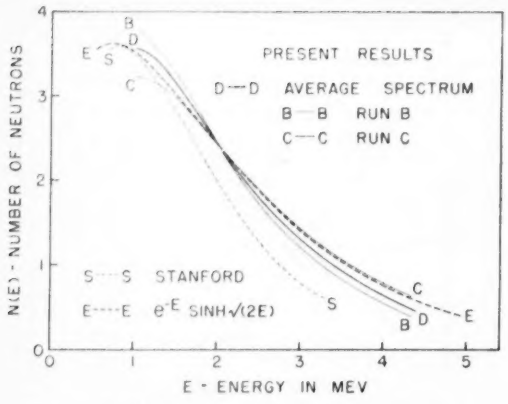

FIG. 3. Energy spectrum of U^{235} fission neutrons.

The fact that the slope for the fitted curve C is less than those of the other two runs probably has only slight significance, although it suggests the possible effect of inelastic scattering in the larger samples of normal uranium used in runs A and B. However, the Stanford measurements had shown no appreciable distortion of the $d-d$ spectrum measured with and without the 2.93-kg disk of uranium placed between the $d-d$ neutron source and the chamber.

Since the differences between the three values of the slopes given above are of the same order as their errors, and especially in view of the rather large wall effects, we have taken 0.692, the weighted average value of the three slopes, to represent our most reliable estimate of the proper recoil distribution and this is shown by curve D (Fig. 2). Furthermore, we have assumed the distributions given by curves B and C to represent the approximate limits of accuracy of the mean distribution.

The energy spectrum of the fission neutrons can readily be calculated from a given proton recoil distribution. If the wall effects are negligible, then $N(E)$ the number of neutrons per unit energy interval is given by

$$N(E)=-\frac{E}{n\cdot\sigma(E)\cdot d}\frac{dR(E)}{dE},$$

where $R(E)$ is the observed number of recoils per unit energy interval, n the number of hydrogen nuclei per cm^3, d the depth of the chamber, and $\sigma(E)$ the cross section for scattering which is assumed to be isotropic in the center-of-mass system. However, when the range of the proton recoils becomes comparable with the dimensions of the collecting volume, the neutron distribution is given by

$$N(E)=-\frac{E}{n\cdot\sigma(E)\cdot d\cdot\alpha(E)}\left[\frac{dR(E)}{dE}-f(E)\right],$$

where $\alpha(E)$ and $f(E)$ are functions which depend essentially on the geometry and the stopping power. The evaluation of these functions is discussed in detail elsewhere.[1] The calculation of the wall effects for this chamber was done at Stanford by Bloch, Hamermesh, and Weinstock. In the present measurements the chamber geometry was not altered, and thus only the appropriate corrections for the different stopping power had to be made in the analysis of the data. Values of the neutron-proton scattering cross sections used were taken from Bohm and Richman.[4]

The calculated fission spectra for each of the three recoil distributions B, C, and D are shown by the correspondingly labeled curves in Fig. 3 which give the number of fission neutrons on an arbitrary scale as a function of their energy in Mev. The three spectra are normalized at 2 Mev which is fairly close to the estimated average energy of the fission neutrons. The present measurements do not extend below 1 Mev, and hence do not quite reach the maximum in the fission spectrum at about 0.8 Mev indicated by the Stanford results which are shown by curve S (Fig. 3). The trend of the curves B, C, and D, however, suggests rather strongly the presence of a maximum in the region slightly below 1 Mev. Some additional evidence for such a maximum was obtained by the present authors from other measurements of the fission spectrum taken with a parallel-plate chamber with a thin paraffin radiator and using electron collection. These latter measurements extended between 0.5 and 1.5 Mev. Because of large wall effect corrections and rather high backgrounds in the lower energy region, no great reliability could be attributed to the results obtained below 1 Mev. The spectrum obtained showed a maximum near 1 Mev, and coincided with the present results in the region between 1 and 1.5 Mev.

Subsequent investigations[5–8] of the fission spectrum of U^{235} have shown good agreement with Watt's[6] semi-empirical relation $N(E)=e^{-E}\sinh\sqrt{(2E)}$, where E is the neutron energy in Mev. This relation is given by curve E in Fig. 3 for comparison with the present results. Curve E is likewise normalized at 2 Mev, and falls between our mean spectrum shown by curve D and that obtained from run C over the entire range of measurement from 1 to 4 Mev.

The neutron spectrum from the fission of Pu^{239} was measured at the same time as run C for U^{235} and under the same geometry. Samples of the two materials were periodically interchanged during the measurement. The slopes of the proton recoil distributions as plotted in Fig. 2 differed by only one percent, showing that the neutron spectra from the fission of the two materials were identical within the statistical accuracy of the data.

[4] D. Bohm and C. Richman, Phys. Rev. **71**, 32 (1947).
[5] B. E. Watt, Phys. Rev. **87**, 1037 (1952).
[6] N. Nereson, Phys. Rev. **85**, 600 (1952).
[7] Bonner, Ferrell, and Rinehart, Phys. Rev. **87**, 1032 (1952).
[8] D. L. Hill, Phys. Rev. **87**, 1034 (1952).

The Radioactive Decay of Tungsten 187

J. M. Cork, M. K. Brice, W. H. Nester, J. M. LeBlanc, and D. W. Martin
Department of Physics, University of Michigan, Ann Arbor, Michigan

(Received December 10, 1952)

Using sources derived from neutron capture in enriched (97.5 percent) W^{186}, about 40 internally converted electron lines are recorded in photographic magnetic spectrometers. Their interpretation leads to the evaluation of 14 gamma-rays in rhenium 187, seven of which had not been previously observed. It is possible to arrange these transitions in a consistent level scheme for the rhenium 187 nucleus. The K/L ratios are determined for five of the gamma-rays and the multipolarity and nature of the transitions proposed.

THE first observation of radioactivity in tungsten induced by slow neutrons was made in 1935, and the half-life was reported[1] to be 23 hours. Many subsequent investigations[2] have dealt with the emitted beta- and gamma-radiations and have shown the activity to be identified with the isotope of mass 187. The beta-spectrum appeared to be complex with components having maximum energies at about 0.6 and 1.3 Mev. A maximum of seven gamma-rays have been noted by various observers. The results of some of the later investigations[3–7] are shown assembled in Table I.

In the present investigation tungsten 186 was obtained from the Oak Ridge National Laboratory, enriched from its normal abundance of 29.2 percent up to 97.5 percent. The specimens were irradiated in the Argonne heavy water pile and were promptly transferred to serve as sources in photographic, magnetic spectrometers of high resolution. Throughout the complete energy range some 39 electron conversion lines have been found with energies as tabulated in Table II. These electron energies are found to fit very satisfactorily the work functions of rhenium ($Z=75$) as expected, following beta-emission from tungsten ($Z=74$). They may be interpreted to show the existence of 14 gamma-rays, seven of which had not been previously observed. For the strong low energy gamma-rays the L_1, L_2, and L_3 lines could be resolved and the M and N lines observed. For one of the gamma-rays of high energy only a K conversion line was noted. The half-life has been followed through several octaves and found to be 24.0 ± 0.1 hours, and all conversion lines decay with this same period.

The agreement between the energies found for five of the gamma-rays and the corresponding energies as expressed by DuMond *et al.*, with their high precision spectrometer, is well within our experimental error, which is believed to be not greater than ±0.2 percent. In scanning the numbers representing the gamma-energies, certain equivalent arithmetic combinations are apparent. It is thus possible, on the basis of energy values alone, to suggest a nuclear level scheme for rhenium 187. For several of the electron groups, satisfactory traces of the photographic plates could be made by a Leeds and Northrup recording microphotometer. When suitably corrected for the variation in emulsion sensitivity with energy, it is thus possible to evaluate the K/L ratios. These values as observed for particular gamma-rays are shown in column 3 of Table III. The gamma-rays are arbitrarily designated by numbers increasing with increasing energy, as shown in column 1.

TABLE I. Summary of beta- and gamma-energies of previous investigators.

Item	Investigator 3	4	5	6	7
β_1	0.6 Mev	0.65		0.63	
β_2	1.3	1.34		1.33	
γ_1				0.078	0.07200
γ_2		0.129	0.133	0.138	0.13425
γ_3			0.204		
γ_4	0.48	0.462	0.478	0.480	0.47952
γ_5	0.69	0.652	0.615	0.618	0.61889
γ_6			0.680	0.696	0.68606
γ_7			0.767		

TABLE II. Energies of electron conversion lines.

Electron energy (kev)	Interpretation	Energy sum (kev)	Electron energy (kev)	Interpretation	Energy sum (kev)
34.5	K	106.2	174.7	K	246.4
42.1	K	113.8	194.0	L_1	206.5
46.7	Auger (α_1-L_1)		203.3	M	206.2
49.0	Auger (α_1-L_3)		226.8	L_1	239.3
50.5	Auger (α_2-L_3)		234.0	L_1	246.5
59.6	L_1	72.1	408.2	K	479.9
61.6	L_3	72.1	441.8	K	513.5
62.9	K	134.6	468.0	L_2	480.0
69.4	M_2	72.1	476.4	M	479.3
71.7	N	72.3	480.0	N	480.6
94.2	L_3	106.2	547.4	K	619.1
101.4	L_1	113.9	554.0	K	625.7
111.0	M_3	113.7	606.8	L	619.3
121.8	L_1	134.3	613.5	L	626.0
122.3	L_2	134.3	614.8	K	686.5
123.6	L_3	134.1	674	L	686
131.4	M_1	134.3	702.9	K	774.6
133.5	N	134.1	763.0	L	775.0
134.6	K	206.3	794.0	K	865.7
167.5	K	239.2			

[1] McLennan, Grimmett, and Read, Nature **135**, 147 (1935).
[2] See K. Way, Nuclear Data (National Bureau of Standards Circular 499, 1950).
[3] L. Miller and C. Curtiss, Phys. Rev. **70**, 983 (1946).
[4] Hole, Benes, and Hedgran, Arkiv. Mat. Astron. Fysik **A35**, No. 35 (1948).
[5] P. Levy, Oak Ridge National Laboratory Report 312, 1949 (unpublished).
[6] Beach, Peacock, and Wilkinson, Phys. Rev. **75**, 211 (1949).
[7] Muller, Hoyt, Klein, and DuMond, Phys. Rev. **88**, 775 (1952).

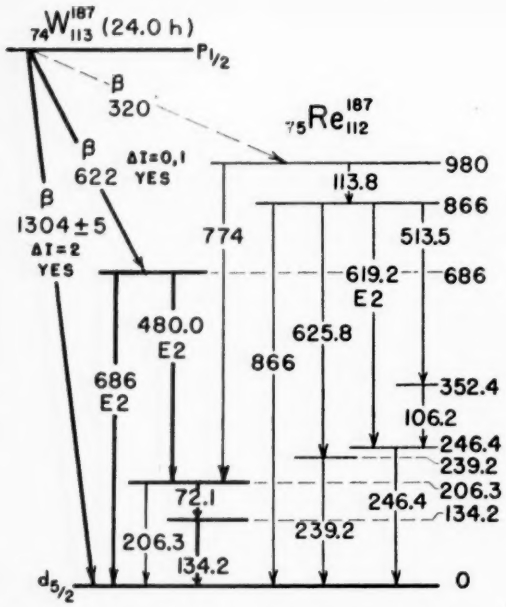

FIG. 1. Energy levels in Re^{187} following β-emission in W^{187}.

A complementary study of the electron distribution from the tungsten specimens has been made by Mr. A. E. Stoddard in this laboratory, using the double-focusing magnetic spectrometer. From a resolution of the beta-spectrum two upper energy limits are found to be 1.304 and 0.622 Mev, with a branching ratio of 1 to 4. The 1.30-Mev beta-ray is first-forbidden with a spin change of two and a change in parity. It appears certain that no other beta-ray with an energy greater than 330 kev exists, but it is not impossible that some lower energy transition may occur. The log(ft) value for the 0.622-Mev beta-ray is 6.2, indicating that it also is forbidden with $\Delta I = 0$ or 1, and a probable change of parity.

From the observed values of the K/L ratio, the radiation lifetime, and the quantity Z^2/W, where W is the energy, it is possible to employ the known empirical relationships[8] and speculate on the multipolarity and the nature of the transition for many of the gamma-rays. This information is an aid in arranging the nuclear levels in any proposed plan, such as is shown in Fig. 1. It may be noted that the placement of the curve relating K/L ratio and Z^2/W for $M2$ radiation by Goldhaber and Sunyar was based entirely upon the 134-kev gamma-ray in W^{187}. A half-life of 5×10^{-7} sec had been observed[9] for an excited state in rhenium and the K/L ratio had been reported to be 5.1. The present observed value of 5.5 ± 0.5 is in agreement with this. It is, however, now possible to note that the L_3/L_1 ratio is only about 1/60, which from observed[10] empirical and theoretical relationships would indicate that the transition is $M1$ or perhaps $M1$ plus $E2$.

[8] M. Goldhaber and A. Sunyar, Phys. Rev. **83**, 906 (1951).

TABLE III. Gamma-energies from W^{187}.

Number	Energy (kev)	K/L ratio	Number	Energy (kev)	K/L ratio
1	72.1		8	480.0	4.2±0.5
2	106.2		9	513.5	
3	113.8		10	619.2	4.0±1.0
4	134.3	5.5±0.5	11	625.8	
5	206.3	4.0±0.5	12	686	5.0±1.0
6	239.2		13	774	
7	246.4		14	866	

The level arrangement shown in Fig. 1 includes as a small part, shown in heavy lines, the previously suggested order[7] for four of the gamma-rays. The observed beta-rays fit well, with an additional transition of 320 kev required. It seems quite likely that the transitions of energy 480, 619, and 686 kev are all $E2$, both from their K/L values and the fact that the L shell conversion seems to occur largely in the L_2 subshell. The delay of 5×10^{-7} second might occur in any one of several of the levels. The ground state in rhenium has been found[11] to be a $d_{5/2}$ level. While shell theory predicts for the W^{187} ground state a $p_{1/2}$ level, it might have been expected that a $d_{3/2}$ state would exist as was found[12] for the very similar nucleus, osmium 189. This would, however, be incompatible with the beta-transition of maximum energy being first-forbidden. It is not possible to assign spin values to all levels on the basis of present information.

This project received the joint support of the U. S. Atomic Energy Commission and the U. S. Office of Naval Research.

Note added in proof:—The electron line at 480 kev could also be interpreted as a K line for a gamma-ray at 552 kev, as observed by Sunyar [Bull. Am. Phys. Soc. **28**, Z3 (1953)] by a scintillation method. It fits the scheme of Fig. 1 as a transition between the levels at 134.2 and 686 kev.

[9] McGowan, DeBenedetti, and Francis, Phys. Rev. **75**, 1761 (1949); Bunyan, Lunby, and Walker, Proc. Phys. Soc. (London) **A62**, 253 (1949).
[10] J. Mihelich, Phys. Rev. **87**, 646 (1952).
[11] Meggers, King, and Bacher, Phys. Rev. **38**, 1258 (1931).
[12] K. Murakawa and S. Suwa, Phys. Rev. **87**, 1048 (1952).

Magnetic Moments of Odd-Odd Nuclei and the Strong Spin-Orbit Coupling Shell Model*

H. M. SCHWARTZ
Department of Physics, University of Arkansas, Fayetteville, Arkansas

(Received September 19, 1952)

Using the extreme *jj* coupling model and employing semi-empirical g factors, magnetic moments are computed for those odd-odd nuclei for which I and μ measurements exist (Table I). The results are suggestive as to relevant coupling properties of such nuclei, but as yet not sufficient for definite conclusions. As an aid to possible future work, this note includes a tabulation (Table II) of computed magnetic moments for some odd-odd nuclei for which tentative spin assignments are possible, employing both free nucleon and semi-empirical g factors and based on pure *LS* and *jj* two-nucleon states.

THE extreme *jj* coupling model has been recently applied to the calculation of magnetic moments of odd-odd nuclei by Feenberg,[1] who pointed out its particular success in the case of K^{40}. Since the Schmidt g factors[2] entering in these calculations are known to deviate considerably from the measured values for most nuclei, the question arises as to the scope of validity of such calculations. It has been suggested[3] that in nuclei (such as B^{10}, N^{14}, Na^{22}, V^{50}) whose odd proton and odd neutron belong the the same l, j-orbital, there is an approximate mutual cancellation of the respective deviations from the Schmidt limits. This suggestion is consistent with the following tentative conjecture: The magnetic moments of those odd-odd nuclei (excepting Li^6) which admit of a definite configuration assignment $(l_p, j_p; l_n, j_n)$, are given to a first approximation by the pure *jj* coupling formula

$$\mu(Z,N)=\frac{1}{2}\left[(g_p+g_n)I+(g_p-g_n)\frac{j_p(j_p+1)-j_n(j_n+1)}{I+1}\right], \quad (1)$$

with g_p and g_n representing the *empirical* g factors of the nuclei $(Z, N-1)$ and $(Z-1, N)$, respectively (and with the customary meaning of the other symbols). Such a result can be expected to have approximate validity if (a) the deviations of odd A magnetic moments from the Schmidt values are due largely to interaction of the odd nucleon with the core, and (b) if *jj* coupling is in fact an adequate approximation. Conversely, if premise (b) were to become definitely established, then the study of μ for odd-odd nuclei could shed some light on (a).

The results presented in Table I seem to be in accord with the above conjecture.[4] Unfortunately, they are subject to two severe limitations: the number of definitely established μ and I values is quite small, and the number of corresponding g_n is even smaller. In both Tables I and II, some of the empirical g values had to be estimated from measured μ of neighboring nuclei with the same odd nucleon l and j values. An examination of the set of measured odd A magnetic moments lends support to the expectation that in most cases the error committed by such an interpolation is not serious, when precision is not required. Whenever it appeared impossible to make a reliable estimate, the correspond-

TABLE I. Magnetic moments of some odd-odd nuclei for which measurements exist.

Nucleus	Measured I ($\hbar$)	Measured μ (nm)	Configuration[a] proton	Configuration[a] neutron	Computed μ using free-nucleon g	Empirical odd nucleon g proton	Empirical odd nucleon g neutron	Computed μ using available empirical g
B^{10}	3	1.80	$1p_{3/2}^-$	$1p_{3/2}^-$	1.88	(2.0)	−0.786	1.82
N^{14}	1	0.404	$1p_{1/2}^-$	$1p_{1/2}^-$	0.37	(−0.58)	1.40	0.41
K^{40}	4	−1.30[b]	$1d_{3/2}^-$	$1f_{7/2}^+$	−1.70	0.261	···	−1.54
V^{50}	?	$0.557I$	$1f_{7/2}$	$1f_{7/2}^-$	$0.55\,I$	1.43	···	$0.44\,I$
Co^{60}	(5)	3.0±0.5	$1f_{7/2}^-$	$2p_{3/2}$	3.88	1.33	···	2.73
Rb^{86}	2	(−1.68)	$1f_{5/2}$	$1g_{9/2}^-$	−2.13	0.54	(−0.22)	−1.72
Cs^{134}	4	2.96	$1g_{7/2}$	$2d_{3/2}$	2.18	0.737	(0.55)	2.80
Lu^{176}	≧7	4.2±0.8	$1g_{7/2}$	$1h_{9/2}$	2.85 ($I=7$)	(0.83)	···	3.8 ($I=7$)
					3.28 ($I=8$)			4.5 ($I=8$)
					3.71 ($I=9$)			5.0 ($I=9$)

[a] The superscripts − and + indicate closed shells or subshells minus or plus one particle, respectively.
[b] Eisinger, Bederson, and Feld, Phys. Rev. **86**, 73 (1952).

* This work was supported in part by the U. S. Atomic Energy Commission.

[1] E. Feenberg, Phys. Rev. **76**, 1275 (1949).
[2] T. Schmidt, Z. Physik **106**, 358 (1937). This paper employs the free nucleon model.
[3] I. Talmi, Phys. Rev. **83**, 1248 (1951).
[4] The experimental μ were taken from the compilation by P. F. Klinkenberg [Revs. Modern Phys. **24**, 63 (1952)], in which μ-values obtained from optical hyperfine structure are corrected for the effect of finite nuclear size. For V^{50} and Cs^{134}, see Walchi, Leyshon, and Scheitlin, Phys. Rev. **86**, 618 (1952), and Jaccarino, Bederson, and Stroke, Phys. Rev. **87**, 676 (1952).

TABLE II. Computed magnetic moments for some odd-odd nuclei for which measurements do not now exist.

Nucleus	Assigned I ($\hbar$)	Configuration[a] proton	neutron	LS states	$\mu(LS)$ (nm)	$\mu(jj)$ $j_p j_n$	$j_p' j_n$[b]	$j_p j_n'$	$j_p' j_n'$	$\mu(jj)$ using available empirical g
P^{32}	1	$2s_{1/2}^+$	$1d_{3/2}$	^3D	−0.440	−0.440	···	···	···	−0.12
K^{42}	2	$1d_{3/2}^-$	$1f_{7/2}$	$^1D, ^3P, ^3D, ^3F$	0, −0.120, 0.293, 0.080	−1.72	−1.50	1.02	2.46	
$Ga^{66,68}$	1	$(2p_{3/2}^+$	$2p_{3/2})$	$^1P, ^3S, ^3P, ^3D$	$\frac{1}{2}$, 0.88, 0.69, 0.310	0.627	−1.46	2.84	0.373	
$Ga^{66,68}$[c]	1	$(2p_{3/2}^+$	$1f_{5/2})$	^3D	−0.94	−0.94	···	···	···	
As^{72}	2	$(1f_{5/2}$	$1g_{9/2})$	$^1D, ^3P, ^3D, ^3F$	−0.334, −0.620, 0.015, −0.141	−2.13	−1.89	0.864	2.08	
As^{72}	2	$(1f_{5/2}$	$2p_{1/2})$	$^1D, ^3D, ^3F$	2.67, 2.51, 1.86	0.379	3.88	0.420	6.24	
Br^{80*} (4.4 hr)	5	$2p_{3/2}$	$1g_{9/2}$	$^1H, ^3G, ^3H$	1, 1.08, 1.11	0.091	−2.18	5.28	···	0.142
Y^{90}	2	$2p_{1/2}$	$2d_{5/2}^+$	$^1D, ^3P, ^3D, ^3F$	0.334, 0.380, 0.572, 0.301	−1.61	−0.981	0.883	3.29	−0.84
In^{114*} (50 days)	5	$(1g_{9/2}^-$	$3s_{1/2})$	^3G	4.88	4.88	···	···	···	4.87
In^{114*}	5	$(1g_{9/2}^-$	$2d_{3/2})$	$^1H, ^3G, ^3H, ^3I$	3.67, 4.28, 3.69, 3.16	6.99	2.86	4.89	0.045	
Sb^{124}	3	$1g_{7/2}^+$	$3s_{1/2}$	^3G	3.09	3.09	···	···	···	3.13
$Au^{192,194}$, $Au^{196,198}$	2	$2d_{3/2}$	$3p_{1/2}$	$^1D, ^3P, ^3D, ^3F$	1.67, 2.38, 1.68, 1.19	0.762	4.05	−1.19	3.30	0.836
Tl^{204}	2	$(3s_{1/2}^-$	$3p_{3/2})$	^3P	0.88	0.88	···	···	···	1.05
Tl^{204}	2	$(3s_{1/2}^-$	$2f_{5/2})$	^3F	−0.59	−0.59	···	···	···	
Tl^{204}	2	$(2d_{3/2}$	$3p_{1/2})$	$^1D, ^3P, ^3D, ^3F$	1.67, 2.38, 1.68, 1.19	0.762	4.05	−1.19	3.30	
Bi^{204}	3	$(1h_{9/2}^+$	$3p_{3/2})$	^3G	3.85	3.85	···	···	···	
RaE^{210}	2	$(1h_{9/2}^+$	$3d_{5/2}^+)$	^3F	3.43	3.43	···	···	···	

[a] See footnote a to Table I.
[b] A dash signifies reversal of I, s orientation.
[c] See reference 10.

ing free-nucleon g factors were employed. If in case of V^{50} and Co^{60} we employ g_n corresponding to $\mu \sim -1$, a mean value fitted to the diagram of measured μ-values, one finds $\mu(V^{50}) = 0.57I$, and $\mu(Co^{60}) = 3.65$. With similar g_n, one finds μ (K^{42}) $= -1.0$ (see Table II).

Lu^{176}, whose spin is still unknown, is included in Table I because of the indication that it is possible to have here a normal configuration assignment[5] and a spin close to the experimental lower bound. A discussion leading to different conclusions has been published recently.[6]

Table II lists a few odd-odd nuclei, of half-lives exceeding one hour, for which spin assignments can now be made, at least tentatively. These assignments are based on Nordheim's rules[7] and on an analysis of beta-decay schemes compiled by King.[8] Because of existing uncertainty as to the actual coupling schemes that obtain for the ground and first excited states of various nuclei, computed values for the two-particle LS and jj coupling type states corresponding to the given configurations and I, are also included in this table.[9] At the same time only those nuclei are listed for which the computed μ are either the same for all states, or else are sufficiently distinct for the LS and jj states to present the possibility of μ measurement discrimination between them. Although the latter group do not comprise any examples strictly similar to K^{40}, for which μ for the *expected* jj coupling scheme is definitely distinguished (by its sign) from those given by the other coupling possibilities, it will be observed that such a situation does obtain in the case of $Ga^{66,68}$, Br^{80*} (4.4 hr), $Au^{192,194,196,198}$, and Tl^{204} if the configurations which belong to them are, respectively, $p_{1/2} - p_{3/2}$, $p_{1/2} - g_{9/2}$, $d_{3/2} - p_{3/2}$, $d_{3/2} - p_{3/2}$ instead of those listed in the table.

In both Tables I and II parentheses enclosing a quantity indicate some uncertainty regarding it. A few cases with uncertainty in the configuration assignment are included in the tabulation.[10] These indicate a possibility of resolving such uncertainties when the corresponding I and μ measurements become available.

The author takes pleasure in expressing his indebtedness to Professor Feenberg for stimulating discussion concerning the subject of this note.

[5] See entry for Lu^{176} in Table II, L. W. Nordheim, Revs. Modern Phys. **23**, 322 (1951), p. 326.
[6] P. F. Klinkenberg, Physica **17**, 715 (1951).
[7] L. W. Nordheim, Phys. Rev. **78**, 294 (1950). These rules appear to admit of some exceptions.
[8] Richard King (unpublished).
[9] A similar tabulation for Y^{90} is given in reference 1, to which the reader is referred for relevant discussion.

[10] Recent Ga^{68} and Ga^{68} disintegration measurements [A. Mukerji and P. Preiswerk, Helv. Phys. Acta **25**, 387 (1952)] support the following respective configuration assignments: $p_{3/2}f_{5/2}$, $p_{3/2}p_{3/2}$.

Letters to the Editor

PUBLICATION of brief reports of important discoveries in physics may be secured by addressing them to this department. The closing date for this department is five weeks prior to the date of issue. No proof will be sent to the authors. The Board of Editors does not hold itself responsible for the opinions expressed by the correspondents. Communications should not exceed 600 words in length and should be submitted in duplicate.

The Temperature Dependence of Drift Mobility in Germanium

R. LAWRANCE*
Department of Supply, Commonwealth of Australia
(Received November 18, 1952)

THE occurrence of values of current gain greater than 3.1 in *n*-type germanium triodes has been attributed by Sittner[1] to hole traps. If this explanation is correct, a study of the drift mobility of holes in *n*-type germanium at low temperatures should indicate such trapping. Haynes and Shockley[2] have pointed out that trapping will not influence the temperature dependence of the Hall mobility.

In the present experiments, a modification reported by Lawrance and Gibson[3] to the method of Haynes and Shockley[2] has been used to measure the drift mobility of holes in 0.02 ohm-meter resistivity single crystal *n*-type germanium in the temperature range 100°K to 360°K. This method involves the use of a dc emitter current and a pulsed sweeping field.

As the temperature is lowered the drift mobility increases and then decreases rapidly as trapping occurs. By increasing the emitter current so that the ratio of the number of holes trapped to the number available becomes small, the trapping is observed to occur at a lower temperature. The temperature at which trapping occurs for a given emitter current is variable from specimen to specimen and depends upon surface treatment and the age of the specimen. It is therefore concluded that these traps are on the surface. The traps may be completely filled and made ineffective by illuminating the specimen with light from a tungsten lamp, and by this means it has been possible to carry out the drift mobility measurements at temperatures much lower than those at which trapping cannot be eliminated by increasing the emitter current alone.

Initial experiments have given a temperature variation of drift mobility proportional to T^{-3}, but this has been found to be due to strains produced by differential expansion of the germanium and the "perspex" base. Subsequent experiments in which the germanium was free to move relative to the base have given a $T^{-2.3}$ relationship, in substantial agreement with the results for the Hall mobility of holes published by Dunlap.[4] The Hall mobility for electrons in the sample of germanium used by the author has been measured by Dr. E. H. Putley of this establishment and found to vary as T^{-1}.

It is interesting to note that, in the case where the germanium was under stress, the drift mobility was higher than it should have been at any given temperature. The holes were therefore moving faster than they would have done in a strain-free lattice at the same temperature.

The accompanying graph (Fig. 1) shows the relationship between $\log\mu$ and $\log T$ over the temperature range already stated. It is not possible at present to calculate the trap depth from these measurements, since the present method of measuring in the trapping region is a complicated function of the delay time.

A fuller account of this work is to be published elsewhere.

The author wishes to acknowledge the helpful guidance of Dr. A. F. Gibson of this establishment. He is indebted to the Chief Scientist, British Ministry of Supply and to the Controller of H.B.M. Stationery Office, England for permission to publish this letter.

* Attached to Telecommunications Research Establishment, Great Melvern, Worcester, England.
[1] W. R. Sittner, Proc. Inst. Radio Engrs. **40**, 448 (1952).
[2] J. R. Haynes and W. Shockley, Phys. Rev. **81**, 835 (1951).
[3] R. Lawrance and A. F. Gibson, Proc. Phys. Soc. (London) **B65**, 994 (1952).
[4] W. C. Dunlap, Phys. Rev. **79**, 286 (1950).

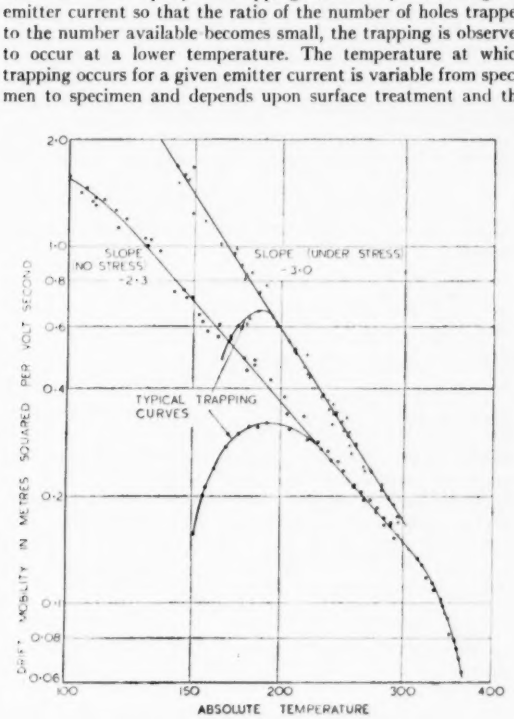

FIG. 1. The drift mobility of holes in *n*-type germanium as a function of temperature.

Proton-Proton Scattering for a Nucleon Isobar Model

FRANK T. SOLMITZ*
University of Chicago, Chicago, Illinois
(Received February 2, 1953)

A NUMBER of phenomenological static potentials have been used in the analysis of p–p scattering.[1] It has been found to be quite difficult to account for the experimentally observed large isotropic cross section at high energies (about 5 mb/sterad in the energy interval of 100 to 350 Mev[2]) with a potential which also fits the low energy experiments; only Jastrow's hard core model gives reasonably good agreement with the data.

We have investigated the effect of excited isobaric states on the p–p scattering. The particular model used was based on the strong coupling approximation of meson theory.[3] According to the pseudoscalar charge-symmetric theory in the strong coupling approximation, nucleons can exist in states with any half-odd integral spin and isotopic spin (spin and isotopic spin being equal in a given state). The energy of such a state is proportional to $(\text{spin}+\frac{1}{2})^2$. The interaction energy of two nucleons is of the form $[\Omega V(r)+T'U(r)]$, V and U being functions of the distance between the two nucleons only, and Ω and T' depending on the spins and isotopic spins.[4] With respect to states in which both nucleons have spin $\frac{1}{2}$, the interaction reduces to that obtained in the weak coupling approximation:

$$\Omega=(1/9)(\tau_1\cdot\tau_2)(\sigma_1\cdot\sigma_2),\quad T'=(1/27)(\tau_1\cdot\tau_2)S_{12}.$$

T' is a somewhat unusual tensor force in the sense that it has an effect on the ^1S scattering.

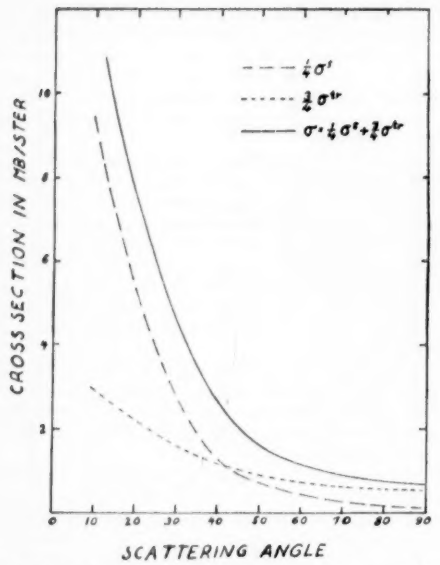

FIG. 1. Differential cross sections in the center-of-mass system for $p-p$ scattering at 300 Mev.

In the present work the excitation energy of the first excited state (i.e., one nucleon in an isobaric state) was taken to be 265 Mev; the effect of all higher excited states was neglected. Two Yukawa potentials of the same parametric range were used for V and U. The depths of the potentials and the parametric range were adjusted so as to obtain a fit with the low energy $p-p$ scattering data. The depths of V and U so determined were 34 Mev and 145 Mev, respectively, and the parametric range 2.0×10^{-13} cm. (This determination is, of course, not unique since low energy scattering yields only two parameters, the scattering length and the effective range.) The scattering at 300 Mev (in the lab system) was then calculated with the model described; the resulting differential cross sections are presented in Fig. 1. The results are in sharp conflict with the large, flat cross section found experimentally. Both ^1S and ^1D phase shifts were found to be negative, leading to destructive S–D interference at 90°. In the Jastrow model the ^1S phase shift becomes positive at high energies, resulting in constructive S–D interference at 90°. Coupling to excited states always seems to result in a negative contribution to the phase shifts and therefore cannot change the sign of the ^1S or ^1D phase shifts. The triplet scattering at 90° could be increased by increasing the depth of the tensor potential U, but estimates indicate that even for the maximum possible depth the cross section at 90° would still be much too small.

The present work does not rule out all conceivable types of nucleon isobar models, but it seems to indicate that such models do not promise any great improvement over the conventional interactions in accounting for the known $p-p$ scattering data.

A more detailed account of this work will be published shortly.

Ideas similar to the one explored here have been suggested by Breit[5] and by Raphael and Schwinger.[6]

The author would like to thank Professor M. L. Goldberger and Professor G. Wentzel for their invaluable help and guidance.

* U. S. Atomic Energy Commission, Predoctoral Fellow.
[1] R. S. Christian and H. P. Noyes, Phys. Rev. **79**, 85 (1950); R. Jastrow, Phys. Rev. **79**, 389 (1950); **81**, 636 (1951); L. J. B. Goldfarb and D. Feldman, Phys. Rev. **88**, 1099 (1952).
[2] R. S. Christian, Repts. Progr. Phys. **15**, 68 (1952).
[3] G. Wentzel, Revs. Modern Phys. **19**, 1 (1947).
[4] M. Fierz, Helv. Phys. Acta **17**, 181 (1944); **18**, 158 (1945).
[5] G. Breit, *Proceedings of the International Conference on Nuclear Physics* (Institute for Nuclear Studies, Chicago, 1951), p. 107.
[6] R. B. Raphael and J. Schwinger, Bull. Am. Phys. Soc. **28**, No. 1, 44 (1953).

Nonexistence of Stable Isobars with Odd Mass Number

S. SENGUPTA
Physics Laboratory, Krishnagar College, Krishnagar, Calcutta, India
(Received October 17, 1952)

THREE very important characteristics in the distribution of stable nuclei are well known. These are (1) instability of odd-odd nuclei for $A>14$; (2) existence of stable isobars for even-even nuclei; (3) nonexistence of stable isobars for odd mass nuclei.

The first two of the above facts were explained by Bethe and Bacher[1] on the assumption of a strong attractive like-particle force between paired nucleons. Combining this with the saturation property of the nuclear forces Fuchs[2] made a remarkable analysis of the distribution of stable nuclei and succeeded in explaining many of its important features. Still his analysis does not make it quite clear why in all cases of nuclei with odd mass number we get only one stable nucleus and no isobars. We want to show in the present note that a formal proof of this fact can be easily given on the basis of like-particle forces and saturation of nuclear forces.

Let $B_Z(N, Z)$ and $B_N(N, Z)$ be the binding energies of the last even proton and neutron in the nucleus (N, Z) and let the corresponding quantities for odd particles be B_Z' and B_N'. Let both N and Z be even. Then we can write

$$\begin{aligned} B_Z(N, Z)-B_Z'(N, Z-1)&=\delta+B_{ZZ},\\ B_N(N, Z)-B_N'(N-1, Z)&=\delta+B_{NN}, \end{aligned} \tag{1}$$

where δ is the pairing energy of proton and neutron, which is the same for both particles owing to the charge symmetry of the nuclear forces. B_{ZZ} and B_{NN} are defined by $B_{ZZ}=\partial B_Z/\partial Z$ and $B_{NN}=\partial B_N/\partial N$ and measure the regular change in B_Z and B_N apart from the pairing effect, with proton and neutron numbers, respectively. We also define the quantities B_{NZ} and B_{ZN} by $B_{NZ}=\partial B_N/\partial Z$ and $B_{ZN}=\partial B_Z/\partial N$. Fuchs[2] has shown that the saturation property of the nuclear forces gives

$$B_{ZZ}<0;\quad B_{NN}<0;\quad B_{NZ}=B_{ZN}>0. \tag{2}$$

We now consider the three odd mass isobaric nuclei $(N, Z+1)$, $(N+1, Z)$, and $(N+2, Z-1)$. Let us suppose that $(N+1, Z)$ is β^--active. Then from the well-known β^--stability condition[3] we write

$$B_N'(N+1, Z)-B_Z'(N, Z+1)<M_N-M_H, \tag{3}$$

where M_N and M_H are the masses of the neutron and the hydrogen atom, respectively. Now we have

$$\begin{aligned} B_N(N+2, Z-1)&=B_N'(N+1, Z)+\delta+B_{NN}-B_{NZ},\\ B_Z(N+1, Z)&=B_Z'(N, Z+1)+\delta-B_{ZZ}+B_{ZN}. \end{aligned} \tag{4}$$

Hence,

$$\begin{aligned} B_N(N+2, Z-1)-B_Z(N+1, Z)=&B_N'(N+1, Z)\\ &-B_Z'(N, Z+1)+B_{ZZ}+B_{NN}-2B_{NZ}. \end{aligned}$$

Keeping in mind (2) and (3), it is easily seen that the right-hand side of (5) must be less than M_N-M_H. Therefore, we conclude that if the nucleus $(N+1, Z)$ is β^--active, then the nucleus $(N+2, Z-1)$ and hence the nuclei $(N+3, Z-2)$, $(N+4, Z-3)$, etc. will also be β^--active. Again, suppose that the nucleus $(N+1, Z)$ is K-capturing or β^+-active. Then we can write

$$B_N(N+2, Z-1)-B_Z(N+1, Z)>M_N-M_H. \tag{6}$$

From (5) and (2) we at once get

$$B_N'(N+1, Z)-B_Z'(N, Z+1)>M_N-M_H. \tag{7}$$

Therefore, the nucleus $(N, Z+1)$ and hence the nuclei $(N-1, Z+2)$, $(N-2, Z+3)$, etc. must also be K-capturing or β^+-active.

Thus, we find that for isobaric odd mass nuclei, if any nucleus is β^--active, then all nuclei with higher neutron numbers must also be β^--active; and if a nucleus is K-capturing or β^+-active, then

all nuclei with higher proton numbers are also K-capturing or β^+-active.

If now we have a stable nucleus (N, Z) for a certain odd value of the mass number, then $(N+1, Z-1)$ must be β^--active and $(N-1, Z+1)$ either K-capturing or β^+-active. From what has already been pointed out, it is clear that all nuclei on the higher neutron number side of (N, Z) will then be β^--active and all nuclei on the higher proton number side of (N, Z) will be K-capturing or β^+-active. Thus for a particular odd mass number we shall have only one stable nucleus, all other isobars being unstable.

Let us now consider what happens if the above argument is applied to the case of an even mass nucleus. For such nuclei we can distinguish between the even-even and odd-odd nuclei. Let (N, Z) be an even-even nucleus which is β^--active. Then we have

$$B_N(N, Z) - B_Z'(N-1, Z+1) < M_N - M_H. \quad (8)$$

Now since,

$$B_N'(N+1, Z-1) = B_N(N, Z) - \delta + B_{NN} - B_{NZ},$$
$$B_Z(N, Z) = B_Z'(N-1, Z+1) + \delta - B_{ZZ} + B_{NZ},$$

we have

$$B_N'(N+1, Z-1) - B_Z(N, Z) = B_N(N, Z) - B_Z'(N-1, Z+1) - 2\delta + B_{NN} + B_{ZZ} - 2B_{NZ} < M_N - M_H, \quad (9)$$

because δ is positive and $(B_{NN}+B_{ZZ}-2B_{NZ})$ is negative. Thus the odd-odd nucleus $(N+1, Z-1)$ must be β^--active. But this same argument applied now to the even-even nucleus $(N+2, Z-2)$ leads to a different result. For $B_N(N+2, Z-2)$ and $B_Z'(N+1, Z-1)$ we write

$$B_N(N+2, Z-2) = B_N'(N+1, Z-1) + \delta + B_{NN} - B_{NZ},$$
$$B_Z'(N+1, Z-1) = B_Z(N, Z) - \delta - B_{ZZ} + B_{NZ}.$$

Thus we get

$$B_N(N+2, Z-2) - B_Z'(N+1, Z-1) = B_N'(N+1, Z-1) - B_Z(N, Z) + 2\delta + B_{NN} + B_{ZZ} - 2B_{NZ}. \quad (10)$$

Since δ is positive and $(B_{NN}+B_{ZZ}-2B_{NZ})$ is negative, we cannot conclude from the above equation that the left-hand side will be less than $M_N - M_H$. It may or may not be, depending on the relative magnitudes of δ and $(B_{NN}+B_{ZZ}-2B_{NZ})$. This shows that the even-even nucleus $(N+2, Z-2)$ may be stable in spite of the fact that the odd-odd nucleus $(N+1, Z-1)$ is β^--active, and thus the existence of stable isobars for even mass nuclei becomes possible.

[1] H. A. Bethe and R. F. Bacher, Revs. Modern Phys. **8**, 83 (1936).
[2] K. Fuchs, Proc. Cambridge Phil. Soc. **35**, 242 (1939).
[3] S. Jha and G. P. Dube, Indian J. Phys. **26**, 15 (1952).

Crystallization of Silicon from a Floating Liquid Zone

PAUL H. KECK AND MARCEL J. E. GOLAY
Signal Corps Engineering Laboratories, Fort Monmouth, New Jersey
(Received January 27, 1953)

CRYSTALLIZATION of silicon from a melt is of great interest as an initial step in the preparation of transistor devices. Since molten silicon is very active, there is no crucible material known of which one could be sure that no impurities are being introduced during the melting process. Fused silica, which is considered the best refractory material for melting silicon, is slightly reduced to silicon monoxide by the melt. The extent to which these reduction products affect the electrical properties of silicon is not known. This situation lends attractiveness to the method described below, which permits crystallization of silicon from the melt without having recourse to any crucible material.

The suspected high value of the surface tension of liquid silicon pointed to the possibility that a suitably large zone of molten silicon could be held stable between two vertically aligned, solid rods, and this surmise was verified indeed by experiment. A piece of silicon which had the shape of a rod was held vertically and clamped at both ends. A heater element consisting of a short tantalum cylinder was mounted around the center portion of the rod. Heating this cylinder to incandescence caused a short section of the silicon to melt. The molten zone which developed and assumed the shape of a pear was held stable between the solid parts of the silicon rod by surface tension. The molten zone was then caused to travel slowly along the silicon rod by moving downwards or upwards the bracket to which the upper and lower clamps holding the silicon piece were attached. This constitutes a method of vertical zone melting with a floating liquid zone requiring no container for its support. The silicon rod shown in Fig. 1 was recrystallized by this method. Another possible application of this method is the growth of a single crystal from a polycrystalline mass. For this a seed crystal is placed against one end of the polycrystalline rod, and an initial floating zone of liquid silicon is formed at the joint. Then the seed crystal together with the silicon rod is slowly moved while the crystal grows from the melt and the floating liquid zone travels along the silicon piece. Thus the polycrystalline mass can be converted into a single crystal almost to its support.

FIG. 1. Silicon recrystallized from a floating liquid zone. The comparison scale is in inches.

The new method is not limited to silicon; it may find useful applications for a number of materials.

We wish to express our appreciation for fruitful discussions of this work with Mr. E. L. Manning and Dr. B. Bradshaw. Moreover, it is a pleasure to acknowledge the enthusiastic help of Lt. W. Van Horn and Mr. J. Soled in experimentation.

Ferroelectricity in Oxides of Face-Centered Cubic Structure

W. R. COOK, JR., AND HANS JAFFE
Brush Development Company, Cleveland, Ohio
(Received February 2, 1953)

IN a recent letter[1] we reported on dielectric and x-ray observations on cubic cadmium niobate ($Cd_2Nb_2O_7$) and lead niobate ($Pb_2Nb_2O_7$) to which we ascribed the fluorite structure. B. C. Frazer of Brookhaven National Laboratory has pointed out to us that the structure of $Cd_2Nb_2O_7$ was studied by Byström[2] in 1944 who found it to be of the pyrochlore ($NaCaNb_2O_6F$) type. This structure type is face-centered cubic with dimensions double that of the fluorite structure. We have confirmed the presence of additional faint lines of a doubled cell for $Cd_2Nb_2O_7$.

The pyrochlore structure differs from the fluorite structure in the following ways:

There is a regular alternation of cations in the (fluorite) cation positions and a regular omission of one of the eight oxygens in a manner which leaves the larger cation surrounded by eight oxygens but reduces the coordination around the smaller cation to six. These six oxygens are equally displaced from the symmetrical fluorite positions towards the smaller cation.

We have now found a strictly cubic pattern of unit cell 10.561 $\pm$0.001A for a lead niobate which is deficient in lead, approximating the composition $Pb_{1.4}Nb_2O_{5.4}$. The diffraction line in-

tensities are very similar to those of $Cd_2Nb_2O_7$. The dielectric constant is 200 at room temperature and rises to about 500 at $-196°C$.

The interesting ferroelectric properties found in $Cd_2Nb_2O_7$ are variable. The dielectric constant and Curie point vary markedly in disks from the same mix, with the highest Curie point at $-103°C$ on a disk with a dielectric constant of 450 at room temperature. The remanent charge density of the latter sample as shown by a hysteresis loop is 3.2 microcoulomb per centimeter[2] near $-196°C$.

Further work to determine accurate locations of the oxygens in $Cd_2Nb_2O_7$ and $Pb_2Nb_2O_7$ is underway.

[1] W. R. Cook, Jr. and H. Jaffe, Phys. Rev. **88**, 1426 (1952).
[2] A. Byström, Arkiv Kemi, Mineral. Geol. **18A**, No. 21 (1944) [discussed in A. F. Wells, *Structural Inorganic Chemistry* (Oxford University Press, London, 1950), second edition, p. 504].

Variational Methods for Periodic Lattices and Artificial Dielectrics*

CARSON FLAMMER
Stanford Research Institute, Stanford, California
(Received January 30, 1953)

IN a recent paper, Kohn[1] has given a valuable variational principle for the determination of the propagating solutions of the Schrödinger equation within a unit cell of a periodic lattice. Of late, the cellular method has also been found useful in the analysis of artificial dielectrics which consist of arrays of conducting obstacles embedded in a dielectric medium.[2,3] Such artificial dielectrics are useful in the form of lenses at microwave frequencies. It is of interest, therefore, to obtain the electromagnetic analog of Kohn's variational principle.

The electromagnetic problem is the following:

$$(\nabla\times\nabla\times-k^2)\begin{matrix}\mathbf{E}(\mathbf{r})\\ \mathbf{H}(\mathbf{r})\end{matrix}=0, \quad \mathbf{r} \text{ within } V, \tag{1}$$

$$\mathbf{n}\times\mathbf{E}(\mathbf{r})=0, \quad \mathbf{r} \text{ on } \sigma, \tag{2}$$

$$\mathbf{n}\times\begin{matrix}\mathbf{E}(\mathbf{r}')\\ \mathbf{H}(\mathbf{r}')\end{matrix}=-\exp(i\boldsymbol{\kappa}\cdot\boldsymbol{\tau}_r)\mathbf{n}\times\begin{matrix}\mathbf{E}(\mathbf{r})\\ \mathbf{H}(\mathbf{r})\end{matrix}, \quad \mathbf{r} \text{ on } \Sigma. \tag{3}$$

Here σ denotes the surface of the object within a unit cell, while V and Σ denote the volume and surface of the unit cell; $\mathbf{n}$ is the outward normal at the designated point; $\boldsymbol{\kappa}$ is the wave-number vector; and $\boldsymbol{\tau}_r$ is the vector which translates a given face of the unit cell into coincidence with its conjugate, i.e., $\boldsymbol{\tau}_r=\mathbf{r}'-\mathbf{r}$. Only the transverse components need be subjected to the boundary conditions on Σ, because the normal components then automatically satisfy them in consequence of the Maxwell equations $\nabla\times\mathbf{E}=ik\sqrt{(\mu/\epsilon)}\mathbf{H}$, $\nabla\times\mathbf{H}=-ik\sqrt{(\epsilon/\mu)}\mathbf{E}$.

With the aid of the vector analog of Green's theorem, the first variation of the functional,

$$I=[ik\sqrt{(\mu/\epsilon)}]^{-1}\int_V \mathbf{E}^*\cdot(\nabla\times\nabla\times-k^2)\mathbf{E}dV, \tag{4}$$

is easily shown to be

$$\delta I=\int_{\sigma+\Sigma}(\mathbf{n}\times\mathbf{E}^*\cdot\delta\mathbf{H}-\mathbf{n}\times\delta\mathbf{E}\cdot\mathbf{H}^*)dS, \tag{5}$$

if $\nabla\times\delta\mathbf{E}=ik\sqrt{(\mu/\epsilon)}\delta\mathbf{H}$. Transforming the part of Eq. (5) over Σ in the manner of Kohn, we find that the desired variational principle is

$$\mathrm{Re}\Big\{[ik\sqrt{(\mu/\epsilon)^{-1}}]\int_V \mathbf{E}^*\cdot(\nabla\times\nabla\times-k^2)\mathbf{E}dV+\int_\sigma \mathbf{n}\times\mathbf{E}\cdot\mathbf{H}^*dS$$
$$+\int_\Sigma \mathbf{n}\times\mathbf{E}(\mathbf{r})\cdot\mathbf{H}^*(\mathbf{r}')\exp(i\boldsymbol{\kappa}\cdot\boldsymbol{\tau}_r)dS\Big\}=\text{stationary}. \tag{6}$$

If the trial functions $\mathbf{E}$, $\mathbf{H}$ satisfy the vector wave Eq. (1) and the boundary condition of Eq. (2), the variational principle becomes

$$\mathrm{Re}\int_\Sigma \mathbf{n}\times\mathbf{E}(\mathbf{r})\cdot\mathbf{H}^*(\mathbf{r}')\exp(i\boldsymbol{\kappa}\cdot\boldsymbol{\tau}_r)dS=\text{stationary}. \tag{7}$$

Equation (7) may be cast into the form

$$\mathrm{Re}\int_\Sigma \delta\mathbf{E}(\mathbf{r})\cdot[\mathbf{n}\times\mathbf{H}^*(\mathbf{r})+\mathbf{n}\times\mathbf{H}^*(\mathbf{r}')\exp(i\boldsymbol{\kappa}\cdot\boldsymbol{\tau}_r)]dS$$
$$+\mathrm{Re}\int_\Sigma \delta\mathbf{H}(\mathbf{r})\cdot[\mathbf{n}\times\mathbf{E}^*(\mathbf{r})+\mathbf{n}\times\mathbf{E}^*(\mathbf{r}')\exp(i\boldsymbol{\kappa}\cdot\boldsymbol{\tau}_r)]dS=0, \tag{8}$$

by adding two terms which vanish by virtue of the vector Green's theorem.

In the same way that the method of Slater[4] follows from the equation analogous to Eq. (8) in the atomic case, as shown by Kohn, so the electromagnetic extension of Slater's method follows from Eq. (8). In this method, the boundary conditions of Eq. (3) are satisfied at only a finite number of points. When series expansions of vector functions, containing as many arbitrary coefficients as there are equations, are substituted for $\mathbf{E}$ and $\mathbf{H}$, a compatibility equation is obtained which yields the desired relation between $\boldsymbol{\kappa}$ and k. The surface $k=$constant in $\boldsymbol{\kappa}$-space is the analog of the index surface in crystal optics and is, in general, two-sheeted. When the wave propagating in the artificial dielectric is approximately plane, the relevant refractive index is $|\boldsymbol{\kappa}|/k$ to a first approximation and is a function of the direction of the wave normal and of the polarization of the wave.

As a case in point, we have applied Slater's method to the case when the objects are infinitesimally thin, circular disks and the unit cell is a rectangular parallepiped. There are two independent field distributions to be considered. Using series of oblate spheroidal vector wave functions which satisfy the boundary conditions on the disk, as in the recently obtained vector wave function solution of the diffraction of electromagnetic waves by circular disks and apertures,[5] we have satisfied the boundary conditions at the midpoints of the faces of the unit cell. The resulting surfaces $k=$constant in $\boldsymbol{\kappa}$-space are prolate spheroids at low frequencies. The employment of the variational principle of Eq. (7) should lead to more accurate forms of the surfaces at higher frequencies.

The general form of the variational principle, Eq. (6), may be expected to be useful in the case of objects for which there are available no vector wave functions that can be used to satisfy completely the boundary conditions on the object within a unit cell.

* This work has been supported by the Signal Corps Engineering Laboratories, Fort Monmouth, New Jersey.
[1] W. Kohn, Phys. Rev. **87**, 472 (1952).
[2] S. Pasternack, University of Pennsylvania Laboratory Report (unpublished).
[3] D. Slepian, thesis, Harvard University, 1949 (unpublished).
[4] J. C. Slater, Phys. Rev. **45**, 794 (1934).
[5] C. Flammer, Stanford Research Institute Technical Report No. 27 (to be published).

A General Relativistic Approach to Short-Range Forces

HENRI AMAR
Lafayette College, Easton, Pennsylvania
(Received October 24, 1952)

ORDINARY Newtonian gravitational forces are far too small to account for nuclear interactions. However, it is possible to modify the law of gravitation in such a way as to get unusually strong gravitational attractions in the very small forces. To do so we propose the following generalized law of gravitation

$$R_{\mu\nu}= \quad =(\Lambda g\cdots)_{\mu\nu}, \tag{1}$$

where $g_{\alpha\beta}$ is the metric tensor, $R_{\mu\nu}$ the Riemann-Christoffel tensor, and $\Lambda\ldots^{\cdots}$ some multiplicative tensor such that the right side of (1) is covariant of second rank. The first simplest cases are

$$R_{\mu\nu}=\Lambda g_{\mu\nu} \tag{1a}$$

and

$$R_{\mu\nu}=\Lambda_\mu{}^\sigma g_{\sigma\nu}. \tag{1b}$$

Professor Bargmann and Professor Einstein in a private communication gave us the simple proof that in (1a) Λ is necessarily

a constant. Equation (1a) is Einstein's "cosmological" equation and its solution is well known.

Applying (1b) to the spherically symmetric problem we made a special choice[1] of Λ_β^α which led us to the following solution:

$$ds^2=\gamma dl^2-\gamma^{-1}dr^2-r^2\sin^2\theta d\phi^2-r^2d\theta^2, \qquad (2)$$

where $\gamma=1-(2m/r)\exp(l/r)$ and l is introduced as a universal length, arbitrarily chosen equal to the electronic Compton wavelength; $\exp(l/r)$ is $1+10^{-10}$ for $r=1$ cm and is much closer to unity at larger distances. So that (2) is essentially equivalent to Schwarzschild's line element, and all results of general relativity remain unchanged. However, the corresponding gravitational potential $V=-(m/r)\exp(l/r)$, equivalent to Newton's for all macroscopic considerations, is remarkably large in the small. In the nuclear range, for two nucleons such gravitational interaction is of the order of 2 Mev (magnitude of the binding energy of the deuteron).

We have mentioned the calculation above only to illustrate the potentiality of general relativistic methods in dealing with the very small. Other alternatives are being investigated and will be presented when the calculations are completely carried through.

[1] Namely, Λ_β^α diagonal, the four elements being chosen so that

$$\Lambda_1^1=\Lambda_2^2, \quad \Lambda_2^2=\frac{l}{r^2}(g_{44}-1), \quad \Lambda_4^4=\Lambda_4^4=-\left(1+\frac{l}{2r}\right)\Lambda_2^2.$$

Generation of *F* Centers at Low Temperature

FREDERICK SEITZ
University of Illinois, Urbana, Illinois
(Received January 29, 1953)

MARTIENSSEN[1] has demonstrated that the α-band in KBr can be bleached by irradiating with light absorbed in the α-band. This effect has been observed at -183°C. The quantum efficiency is low and the bleaching is accompanied by a green-blue fluorescence of unspecified quantum efficiency, but designated as "lebhaft." Since the α-band is believed[2] to be associated with the production of an exciton localized at a vacant halogen-ion site, this result suggests that the shifts of nuclear coordinates and lattice oscillations stimulated, when the halogen-ions around the vacancy absorb and emit light quanta, promote sufficient diffusion for the vacancies to disappear, presumably at dislocations or in formation of aggregates without a distinctly observable band. The process appears to be associated with an ideal limiting type of point thermal "spike" accompanying the readjustment of nuclear coordinates after a change of electronic state. We shall assume that half the 6 ev absorbed is reemitted as light, and the remaining 3 ev is divided equally in thermal spikes accompanying absorption and emission. Since at least eighteen neighboring ions participate in this readjustment in a major way, and since about 1.5 ev presumably is available for vibrational quanta in each readjustment, the initial spike temperature should correspond to no more than 0.1 ev per ion, or to an average temperature of about 400°K. It is possible, however, that even this low spike temperature is adequate to promote diffusion because the equilibrium nuclear configuration for the initially degenerate excited state is close to the saddle point for the migration process in the ground state; relatively small thermal oscillations are sufficient to guarantee an appreciable probability for the jumping process each time a light quantum is absorbed in the α-band. It would be exceedingly valuable to know if the α-band formed at liquid hydrogen or helium temperatures can be bleached in the same way at these low temperatures. If this is the case, the results appear to throw penetrating light on the way in which *F* and *V* centers are generated at very low temperatures by x-rays, a problem recently reviewed by Markham.[3] The writer proposes the following speculative solutions.

(1) The x-ray quanta produce energetic photoelectrons which dissipate their energy in the formation of electrons, holes, and excitons, the agents ultimately responsible for production of color centers. Initially the electrons and holes become trapped at incipient negative- and positive-ion vacancies (jogs at Taylor-Orowan dislocations) where they may annihilate one another if sufficiently close. The excitons also end their lives at incipient vacancies[4] producing point thermal spikes analogous to those described above, only of higher intensity by a factor of three or four since a luminescent quantum is not emitted as frequently. These spikes may be violent enough to promote evaporation of incipient vacancies and thereby form normal vacancies near the dislocations. However, we shall assume tentatively that the electrons and holes present play an essential role. If not, it should be possible to produce color centers at very low temperatures by irradiating in the tail of the fundamental band, as is possible[5] at nitrogen and higher temperatures. This highly important experiment apparently has not yet been carried out.

(2) It is assumed that many incipient vacancies occur in the form of neighboring pairs of opposite sign, because of the electrostatic attraction. When one member of a pair captures an electron or hole, the two centers repell one another strongly. Such electrostatic repulsive forces, operating in conjunction with the thermal spikes, have the effect of causing incipient vacancies to evaporate, forming isolated vacancies and clusters in the region around the dislocation.[6] This gas will be more widely dispersed at liquid nitrogen temperature than at hydrogen or helium temperatures because of the higher density of thermal quanta at the higher temperature. Some of the vacancies are present in the form of coupled pairs of positive- and negative-ion vacancies, the most mobile agent containing a halogen-ion vacancy. However, pairs, like isolated positive-ion vacancies, do not contribute an absorption peak in the tail of the fundamental band.

(3) The α-band is stronger than the *F* band when the crystal is radiated at hydrogen temperatures (Martienssen[1] Fig. 3) because the separation of neighboring centers is sufficiently small that many electrons and holes trapped at vacancies annihilate by tunneling (see page 408 of the second reference in footnote 4 for comment on tunneling). At liquid nitrogen temperatures the vacancies become more widely dispersed, and a higher ratio of number of *F* to α-centers prevails. The spacing between centers is sufficiently close, if they are formed at helium temperatures, that annihilation of electrons and holes is enhanced when the electrons in the *F* centers are raised to the first excited state.

(4) When a coupled pair of vacancies captures an electron, the positive-ion vacancy is, with the aid of the accompanying thermal spike, expelled for several lattice spacings even at helium temperatures, as a result of the electrostatic repulsion of the electron and the positive-ion vacancy. Hence the *F* center formed is essentially normal. In contrast, the thermal spike is not sufficient to aid the escape of the halogen-ion vacancy, because of the higher barrier for migration. When the crystal is warmed to 78°C, the hole escapes from the pair giving the current pulse observed by Dutton.[7] The free hole is either captured by a positive-ion vacancy to form a V_1 center, or annihilates an electron at an *F* center. The *H* center of Duerig and Markham[8] is a vacancy pair on which a hole is trapped, that is, is a V_1 center to which a halogen-ion vacancy is attached.

(5) It is assumed that the density of incipient vacancies in a normal specimen is so small that the absorption arising from incipient *F* and *V* centers is not observable in crystals of normal thickness.

I am indebted to Professor R. J. Maurer and Dr. J. J. Markham for discussions of this Letter.

[1] W. Martienssen, Nachr. Akad. Wiss. Göttingen, Math-physik Kl. **11**, 111 (1952).
[2] Delbecq, Pringsheim, and Yuster, J. Chem. Phys. **19**, 574 (1951).
[3] J. J. Markham, Phys. Rev. **88**, 500 (1952).
[4] F. Seitz, Phys. Rev. **80**, 239 (1950); Revs. Modern Phys. **23**, 328 (1951).
[5] A. Smakula, Z. Physik **63**, 762 (1930); L. Apker and E. Taft, Phys. Rev. **79**, 964ff (1950).
[6] This solvent action of electrons and holes is described by the writer (F. Seitz) in Revs. Modern Phys. **18**, 384 (1946). See p. 403ff.
[7] Dutton, Heller, and Maurer, Phys. Rev. **84**, 363 (1951).
[8] W. H. Duerig and J. J. Markham, Phys. Rev. **88**, 1043 (1952). The term *H* center is now used by these investigators to designate the new bands described on p. 1049 of this paper.

Low Angle X-Ray Diffraction with Long Wavelengths

BURTON HENKE AND JESSE W. M. DUMOND
California Institute of Technology, Pasadena, California
(Received January 30, 1953)

THE use of long wavelengths in the investigation of submicroscopic structures by low angle diffraction methods is of considerable interest for the following reasons. First, the effects of multiple scattering, multiple refractions,[1] and of electron density fluctuations within the particles become or can be made vanishingly small for these wavelengths. This makes the direct application of a relatively simple theory of low angle diffraction[2] more feasible. Second, the larger angles of scattering for the long wavelengths open up to experimental observation the very important central portion of the diffraction pattern. And finally, the sizes of the particles and the thinness of the sample mountings appropriate to these wavelengths permit direct comparison studies with the electron microscope. These provide valuable complementary information as to the nature of packing and other gross features of the material. For larger particles, these studies would permit a dependable verification by means of the electron microscope of the low angle diffraction method.

Very few workers have attempted investigations of this sort in the long wavelength region.[3] Perhaps this has been because of the necessity of working in vacuum and with very low x-ray production efficiencies. In order to meet such problems a new type of diffraction unit has been developed at this laboratory which is designed to operate at such wavelengths as Cr-K, Al-K, Cu-L, O-K, and C-K lines (2.3, 8.3, 13.3, 23.6, and 44.5 angstroms, respectively).

The central feature of the instrument is the use of a nearly cylindrical totally reflecting mirror, which forms a point-focused image of the source. (See Fig. 1.) This mirror is ground and

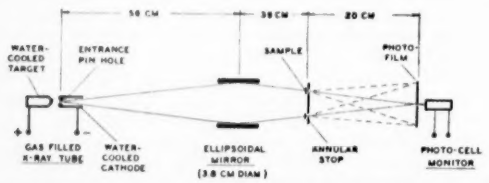

FIG. 1. Sketch of a high intensity, lowangle diffraction unit for soft x-radiation. A large solid angle of x-ray beam is totally reflected and point-focused by an ellipsoidal mirror, ground and polished from Pyrex. Reflection angles are very nearly equal to the critical angle of reflection for the desired line radiation so that all harder background radiation is essentially "cut off."

polished into an ellipsoidal section from Pyrex. In this way a solid angle of radiation is used which is from one hundred to several thousand times that of comparable pinhole geometries.

The principal problem involved in the effective monochromatization of long wavelengths is the suppression of the continuous background radiation. This, however, rapidly diminishes in comparison with the associated characteristic radiation for the longer wavelengths.[4] Effectively complete suppression of this background has been possible by a combination of methods. A specially designed gas-filled x-ray tube has been developed to give a high intensity of x-radiation in the direction of 180° from that of the electron beam by placing the entrance pinhole inside the cathode focusing cup. Soft continuous radiation in this "back" direction should be a minimum. Next the mirror is constructed of such diameter as to present angles of reflection only at the critical angle for the desired line radiation. In this way all radiation that is harder is effectively "cut off." Then the soft component that remains is rapidly absorbed by the filter action of an appropriately chosen substrate on which the sample is supported. Spectrographic checks of the radiation at the focal point have revealed no effective background.

A preliminary study has been made at 13.3A of the same Dow Latex sample which has been investigated by others of this laboratory[5] at the Cu K-1.54A. One of these diffraction photographs (ten-hour exposure) is shown in Fig. 2. Measurements

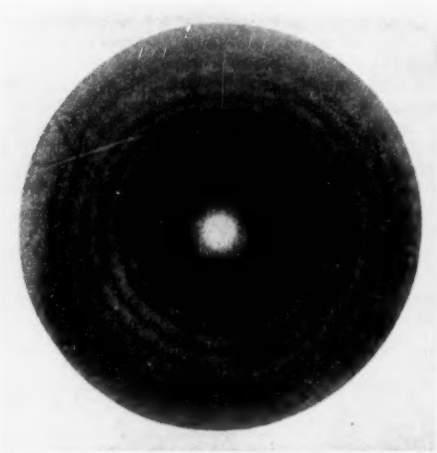

FIG. 2. A low angle diffraction photograph of the Dow Latex spherical particles taken with Cu-L 13.3A radiation. The sample-to-film distance is 20 cm. The separation of each pair of short, straight, parallel scratches is 1.88 cm. A few preliminary measurements of the rings indicate a particle diameter of 2720±20A.

based on the Guinier formula for a homogeneous system of spheres randomly spaced yields a value of 2720±20A for the diameters, which is in good agreement with that at the shorter wavelength.

A report on this work, including studies of the Dow Latex at other wavelengths along with parallel measurements with the electron microscope, will be forthcoming.

We wish to acknowledge the generous support of this research by the U. S. Office of Naval Research. We would also like to acknowledge the very valuable assistance of Mr. Herbert Henrikson on the mechanical layout of the instrument.

[1] R. von Nardroff, Phys. Rev. **28**, 240 (1926).
[2] A. Guinier, Ann. Phys. **12**, 161 (1939).
[3] K. L. Yudowitch, J. Appl. Phys. **20**, 174 (1949).
[4] E. C. Unnewehr, Phys. Rev. **22**, 529 (1923).
[5] Danielson, Shenfil, and DuMond, J. Appl. Phys. **23**, 860 (1952).

Resolution of the "Photon Difference Method"

J. GOLDEMBERG* AND L. KATZ
Physics Department, University of Saskatchewan, Saskatoon, Saskatchewan, Canada
(Received February 2, 1953)

SINCE its formulation[1,2] the "photon difference method" has been used extensively in betatron work for obtaining cross sections from activation curves. The resulting cross sections so obtained are, in general, quite smooth and present the usual resonance shape of photonuclear reactions. Recently, however,[3–7] experiments have been performed in which the neutrons emitted in the photonuclear reactions are detected directly. These activation curves are usually more complex, since in some cases there are several isotopes present as well as neutrons from $(\gamma, 2n)$ and (γ, np) processes. Thus the cross sections obtained from the "photon difference method" sometimes present very "odd" shapes and occasionally show two different peaks. Since this method of solution is liable to give rise to damped oscillations in the cross-section curve if small errors are present in the activation curves, some questions may arise as to the validity of interpreting the humps in the high energy side of the cross-section curves as contributions from the $(\gamma, 2n)$ and (γ, np) reactions.[3–6]

To gain confidence in the method we decided to mix two samples (copper and lead), in which the peaks of the (γ, n) reactions occur at different energies, and measure the resulting activation curve. By changing the relative amounts of these samples it is possible to represent the various cases which occur in practice.

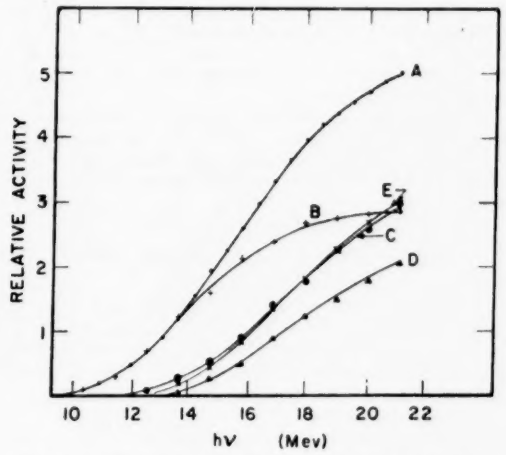

FIG. 1. Neutron yield curves. (A) Sample of Cu (0.45 mole) and Pb (0.072 mole) irradiated simultaneously. (B) Pb sample only. (C) Cu sample only. (D) Curve A minus curve B. (E) Curve D corrected for photon absorption in sample.

The first experiment consisted in mixing 0.45 mole of copper and 0.072 mole of lead, which should result in about the same number of disintegrations from each of the elements. This represents those cases where the elements measured have two isotopes of about equal abundance with close thresholds. The activation curves for each of the samples (Pb and Cu) and for both together were measured in the arrangement described[5] on the same day. This was done to make conditions reproducible as closely as possible. The combined curve was taken with a lead disk sandwiched between two copper disks. The results are shown in Fig. 1. Also plotted in the same figure is the copper curve (D) obtained by subtracting the lead curve (B) from the (copper +lead) curve (A). Applying a correction for absorption of the beam reaching the rear sample, curve (E) is obtained, which is to be compared with the copper curve measured directly (C). Figure 2 shows the cross sections obtained by applying the "photon difference method" to the activation curves (A), (B), and (C). The difference (C″) between the cross-section curves (A′) and (B′) is to be compared to the cross section (C′) calculated directly.

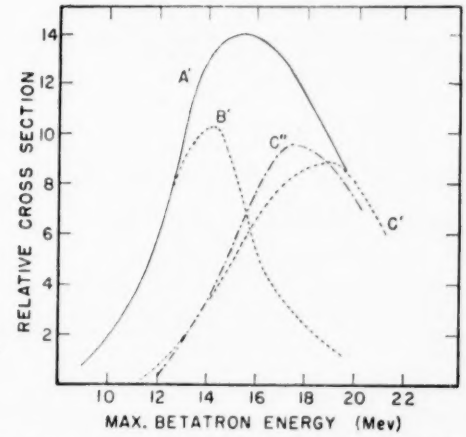

FIG. 2. Cross-section curves. (A′) Calculated from yield curve A. (B′) Calculated from yield curve B. (C′) Calculated from yield curve C. (C″) Difference between cross sections A′ and B′.

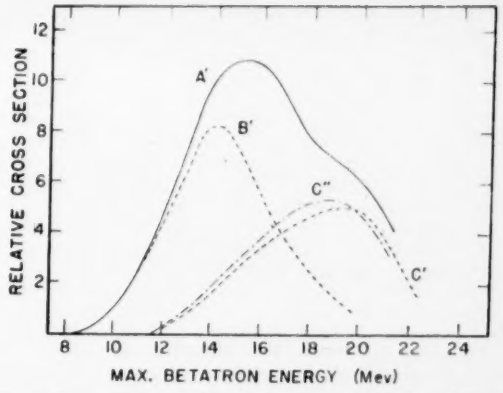

FIG. 3. Cross-section curves from yield curves similar to those of Fig. 1, except that 0.23 mole of Cu and 0.072 mole of Pb were used. Notation as in Fig. 2.

Figure 3 shows the results for a mixture of 0.23 mole of copper and 0.072 mole of lead analyzed in the same manner. This combination was chosen to represent some of the $(\gamma, 2n)$ reactions.

It must be emphasized that small changes in the activation curves can *distort* the shape of the cross sections; thus accurate measurements are necessary for obtaining reliable results with the "photon difference method."

* On leave of absence from Departamento de Fisica, Universidade de São Paulo, São Paulo, Brazil.

[1] Johns, Katz, Douglas, and Haslam, Phys. Rev. **80**, 1062 (1950).
[2] L. Katz and A. G. W. Cameron, Can. J. Phys. **29**, 518 (1951).
[3] Halpern, Nathans, and Mann, Phys. Rev. **88**, 619 (1952).
[4] Halpern, Mann, and Nathans, Phys. Rev. **88**, 958 (1952).
[5] R. Montalbetti and L. Katz (to be published).
[6] J. Goldemberg and L. Katz (to be published).
[7] E. A. Whalin and A. O. Hanson, private communication.

Photoproduction of Neutral Mesons in Hydrogen at High Energies*

R. L. WALKER, D. C. OAKLEY, AND A. V. TOLLESTRUP
California Institute of Technology, Pasadena, California
(Received February 2, 1953)

PRELIMINARY measurements have been made with the newly operating California Institute of Technology synchrotron on the cross section for photoproduction of neutral pions in hydrogen at photon energies up to 450 Mev. The differential cross section at 90° in the laboratory system was measured in the manner of Silverman and Stearns,[1] by observing the recoil proton in coincidence with one decay photon from the π^0. The energy and angle of the recoil proton define, through the conservation laws, both the energy of the incident photon, and the meson angle. The meson angle in the present measurements was 90° in the laboratory system, which corresponds to 107° to 111° in the center-of-mass system, depending on the photon energy.

The arrangement of target and counters is shown schematically in Fig. 1. Recoil protons were counted with a coincidence-anticoincidence scintillation crystal "telescope" which measured their range and their specific ionization (given by the pulse height in the first counter). Decay photons from the π^0's were detected in a γ-ray counter consisting of an anticoincidence scintillator followed by a $\frac{1}{4}$-inch lead converter and two scintillators in coincidence. The calculated efficiency of this detector for counting the π^0

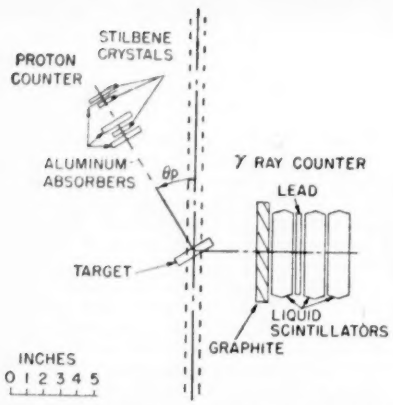

FIG. 1. Experimental arrangement. The proton angle θ_p was near 32° in the present measurements.

associated with an observed recoil proton was between 0.15 and 0.28 in this experiment, depending on the incident photon energy.

Measurements were made with polyethylene and graphite targets and a subtraction made to obtain the cross section in hydrogen. The "carbon background" was between 15 and 40 percent, depending on the photon energy.

The bremsstrahlung spectrum assumed in calculating the cross sections was normalized to give the same total energy in the x-ray beam as measured by a Cornell type ionization chamber with 1-inch copper walls. We are indebted to R. Littauer and the Cornell synchrotron group for both the design of this chamber and its absolute calibration.

The measured cross section at 90° is shown as a function of the incident photon energy in Fig. 2, together with the data of Silverman and Stearns[1] at lower energies. The existence of a maximum in this cross section has been the subject of considerable discussion and is predicted, for example, in the theory of Brueckner and Watson.[2] This theory assumes that the π^0 photo-

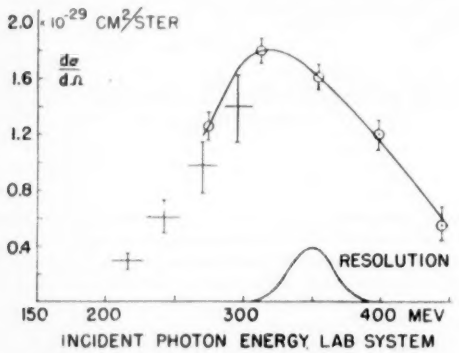

FIG. 2. Differential cross section at 90° in the laboratory system for the photoproduction of neutral pions in hydrogen. The crosses at lower energies are the data of Silverman and Stearns.[1] The indicated errors include estimated instrumental errors in so far as they affect the *relative* cross section.

production involves a resonant interaction between meson and nucleon in a state of isotopic spin and angular momentum $\frac{3}{2}$. Whereas this theory is probably not unique in giving a maximum in the cross section, an interpretation in terms of a resonance is suggested by the sharpness of the observed maximum. The observed cross section at 90° falls off above the maximum considerably more rapidly than the curve given by Brueckner and Watson.[2]

Further work is being undertaken to obtain data with somewhat better energy resolution and to investigate the angular distribution.

Because of the importance of the data at 400 and 445 Mev, we have tried to investigate the extent to which these points might be in error because of uncertainties in the upper end of the incident bremsstrahlung spectrum, arising in part from an uncertainty in the synchrotron energy itself. This has been done by making measurements at three different "nominal" synchrotron energies, E_0=480, 420, and 370 Mev and taking a weighted average for Fig. 2 in such a way that the internal consistency of the three sets of data is as great as possible.

From this analysis, which is given in Fig. 3, it is concluded that the errors introduced by uncertainties in the upper end of the incident bremsstrahlung spectrum are probably less than 10 percent for the 400-Mev point, and 25 percent for the 445-Mev point.

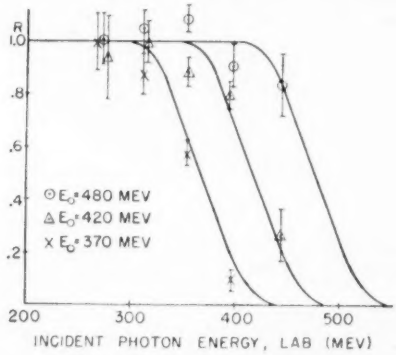

FIG. 3. Internal consistency of data taken at three different "nominal" synchrotron energies E_0=480, 420, and 370 Mev (obtained from a magnetic field integrator). For each E_0 is plotted the ratio R of counts observed to the counts which would be expected if the incident bremsstrahlung spectrum did not fall off near E_0, and if the cross section of Fig. 2 were correct. The three curves have been drawn in such a way that the energies at which R=0.5 are in the same ratio as the three "nominal" energies E_0 but with an absolute scale adjusted to make the two lower curves agree with the data as well as possible. This determines the curve for E_0=480 Mev, and thus the correction factor $1/R$=1/0.85 to be applied to the cross section at 445 Mev as measured with E_0=480.

This experiment owes much to the work of all the members of the synchrotron group, and we wish to acknowledge especially the contributions of Dr. R. F. Bacher, Dr. M. L. Sands, Dr. R. V. Langmuir, Dr. J. G. Teasdale, Dr. V. Z. Peterson, Dr. J. C. Keck, and our chief engineer, Bruce Rule.

* This work was supported by the U. S. Atomic Energy Commission.

[1] A. Silverman and M. Stearns, Phys. Rev. **83**, 853 (1951); Phys. Rev. **88**, 1225 (1952).

[2] K. A. Brueckner and K. M. Watson, Phys. Rev. **86**, 923 (1952).

The (n, γ) and $(n, 2n)$ Reactions in Iodine*

H. C. MARTIN AND R. F. TASCHEK

Los Alamos Scientific Laboratory, University of California, Los Alamos, New Mexico

(Received January 29, 1953)

CROSS sections for the $I^{127}(n, \gamma)I^{128}$ reaction from 0.25 to 1.6 Mev and the $I^{127}(n, 2n)I^{126}$ reaction from 12 to 18 Mev have been measured by irradiating NaI(Tl) crystals and observing the induced activity with a photomultiplier. The crystals thus served both as targets and as nearly 100 percent efficient detectors.

For the (n, γ) reaction, monoergic neutrons were provided by bombarding a tritium gas target[1] with a monatomic proton beam from the 2.7-Mev electrostatic accelerator. The NaI(Tl) crystals were irradiated at 10 cm and 0° from the gas target; the energy of the neutrons from the $T(p, n)He^3$ reaction[2] was selected by

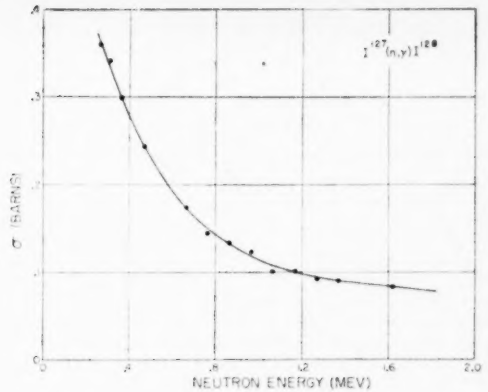

FIG. 1. Cross section for the $I^{127}(n, \gamma)I^{128}$ reaction.

varying the proton energy. Several clear cubic crystals weighing from 2.5 to 5 grams were used in obtaining the data. Each crystal was placed in a cadmium-shielded test tube and covered with mineral oil; for each datum a crystal was irradiated for 1600 seconds. A flat-response long counter,[2] also at 0°, monitored the neutron flux during the irradiation. The absolute flux was determined by comparison with a standard RaBe source, calibrated to ±5 percent, placed at the gas target. In each case the transmission of the sample was measured so that a correction could be made for attenuation of the neutron beam in passing through the crystal.

After irradiation the crystals were submerged in a mineral oil well on a 5819 photomultiplier, and their activities were detected by feeding pulses from the photomultiplier to an amplifier and scaler. In all cases clean 25-minute activities due to I^{128} were observed. Extrapolation of the detecting system's integral bias curve to zero bias indicated that about 98 percent of all pulses from the scintillator were above normal operating bias. Within experimental error, the value obtained for the cross section at a given neutron energy was found to be independent of the size of the activated crystal. No induced activity was observed in a crystal that was irradiated behind a 30-cm long tungsten shadow-cone, indicating a negligible slow neutron background.

Figure 1 shows the (n, γ) cross section as a function of neutron energy. The estimated error in the absolute values is ±7 percent; the energy spread for each datum is about 50 kev. The cross section is very nearly proportional to $1/E$ in this energy range. These results are essentially in agreement with values for the (n, γ) cross section that have been obtained at several isolated points.[4]

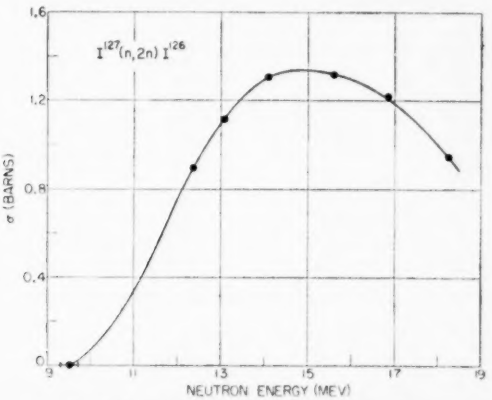

FIG. 2. Cross section for the $I^{127}(n, 2n)I^{126}$ reaction.

A relative $(n, 2n)$ activation curve was obtained by placing the NaI(Tl) crystals at appropriate angles around the tritium gas target at a distance of 12 cm and accelerating monatomic deuterons to 2.00 Mev to produce the $T(d, n)He^4$ reaction.[2] The crystals were counted as in the case of the (n, γ) reaction, and for each crystal the 13.1-day I^{126} activity was observed for about 40 days with no longer-lived period becoming apparent. While the error in the relative activities of the crystals is only about ±4 percent, the cross-section values shown in Fig. 2 depend upon the angular distribution of the $T(d, n)He^4$ neutrons, which is known to about ±10 percent. For a deuteron energy of 2 Mev, at the angular positions where the crystals were irradiated, the laboratory differential cross sections for neutrons shown in Table I have been used. These values seem most consistent with presently available data on the $T(d, n)He^4$ reaction.[2,5] To fix the absolute value of the $(n, 2n)$ cross section, a crystal was irradiated with 14.1-Mev neutrons produced by a Cockcroft-Walton accelerator, with the absolute neutron flux monitored to ±5 percent by observing the alpha-particles from the $T(d, n)He^4$ reaction. The error in the absolute value of the $(n, 2n)$ cross section at 14.1 Mev is estimated to be ±6 percent. The neutron energy spread at each point is about 0.7 Mev; the threshold of 9.52±0.20 Mev is determined from the value reported for the (γ, n) reaction.[6]

TABLE I. Laboratory differential cross sections for $T(d, n)He^4$ neutrons at a deuteron energy of 2 Mev.

θ_{lab} deg	0	52.5	75	127.5	150
$\sigma(\theta_{lab})$ mb/sterad	23.0	13.4	10.1	8.0	8.0

We are indebted to Mr. Arthur Frentrop for the irradiation at the Cockcroft-Walton accelerator.

* Work done under the auspices of the U. S. Atomic Energy Commission.
[1] Jarvis, Hemmendinger, Argo, and Taschek, Phys. Rev. **79**, 929 (1950).
[2] Hanson, Taschek, and Williams, Revs. Modern Phys. **21**, 635 (1949).
[3] A. O. Hanson and J. L. McKibben, Phys. Rev. **72**, 673 (1947).
[4] U. S. Atomic Energy Commission Report AECU-2040.
[5] T. F. Stratton and G. D. Freir, Phys. Rev. **88**, 261 (1952).
[6] Ogle, Brown, and Carson, Phys. Rev. **78**, 63 (1950).

Precision Measurement of Co^{60} Gamma-Radiation

G. LINDSTRÖM, A. HEDGRAN, AND D. E. ALBURGER*
Nobel Institute of Physics, Stockholm, Sweden
(Received January 19, 1953)

BECAUSE of the usefulness of Co^{60} as a gamma-ray standard, Lind, Brown, and DuMond have made[1] precision determinations of the gamma-ray energies from this isotope. Their values of 1.1715±0.0010 Mev and 1.3316±0.0010 Mev are based on curved crystal spectrometer measurements of wavelengths. Recently it was reported[2] by Muller, Hoyt, Klein, and DuMond that an unsuspected nonlinearity was present in the crystal spectrometer at the time of the Co^{60} experiments. From Fig. 7 of their paper it can be seen that if a correction is made for this, it would raise the Co^{60} values by about 0.1 percent.

In order to obtain a check on the Co^{60} gamma-rays, we have determined their energies in the following way. The K line of the highly converted 1.41-Mev transition occurring in the decay of 20-min RaC (electron energy about 1.32 Mev) was first measured absolutely in a semicircular focusing uniform field spectrometer. The technique was similar to that previously described[3] in connection with ThC″ measurements except that both photographic and counter detection were used. In the latter case a NaI gamma-ray monitor counter was employed to correct for decay. Sources consisted of tungsten wires 20 microns in diameter on which the activity had been collected electrostatically. Measurements of both the magnetic field along the path in terms of the proton resonance and the source to slit (or image) distance were done according to previous procedures. The weighted average of two counter and two photographic measurements gives a momentum

of 5874.4±0.6 gauss-cm for the extrapolated high energy edge of the line. This corresponds to a RaC′ transition energy of 1.4158 ±0.0002 Mev, if finite line width effects are not taken into account.

The RaC line was then compared in the 50-cm radius double-focusing spectrometer with the K shell internal conversion electrons due to the 1.33-Mev Co^{60} transition. The cobalt sources were 3×15 mm electrolytic deposits on copper backings. Source thickness effects prevented the use of a spectrometer resolution better than 0.25 percent, but this was sufficient to resolve the L line well enough so that the extrapolated high energy edge of the K line was practically unaffected. The $K/(L+M)$ ratios of both cobalt transitions were found to be close to 10. For the RaC runs the sources were collected on copper strips 3 mm wide and a gamma-ray monitor corrected for decay. Using a slit 3 mm wide to accurately define the position of the sources, the extrapolated edges of the RaC and Co^{60} conversion lines were compared and found to be about 0.08 percent apart. By using the weighted average of three comparisons and adding the Ni K shell binding energy of 8.337 kev,[4] the cobalt gamma-ray is found to have a value of 1.3325±0.0003 Mev.

The two cobalt K conversion lines were then compared in the double-focusing spectrometer in order to obtain their momentum ratio. Because these are ∼10 percent apart in momentum, it was considered advisable to accurately check the linearity of the instrument over this range. This was done by first making an absolute determination in the semicircular spectrometer of the strong RaC line at 1.02 Mev. The momentum of its extrapolated edge was found from photographic measurements to be 4839.8 ±0.8 gauss-cm. Together with the 1.32-Mev electrons of RaC, these two lines represented well-established momentum points and could be used to study the linearity of the double-focusing spectrometer. The difference between the calibration constants derived from these two lines was 2 parts in 10^4, which is within the combined probable errors of the absolute values. This indicates that the error in the comparison of the two cobalt lines due to uncertainties in the linearity is probably not more than 1 part in 10^4. The value of the lower energy cobalt gamma-ray based on four comparisons between the 1.17- and 1.33-Mev conversion lines is 1.1728±0.0005 Mev. It is seen that although both of the present values of the Co^{60} gamma-rays agree with those of Lind, Brown, and DuMond within the combined probable errors they are, in fact, about 0.1 percent higher.

The authors are indebted to Dr. W. Forsling for chemical preparation of the Co^{60} plating solution.

* National Science Foundation fellow on leave from Brookhaven National Laboratory.

[1] Lind, Brown, and DuMond, Phys. Rev. **76**, 1838 (1949).
[2] Muller, Hoyt, Klein, and DuMond, Phys. Rev. **88**, 775 (1952).
[3] G. Lindström, Phys. Rev. **87**, 678 (1952).
[4] Hill, Church, and Mihelich, Rev. Sci. Instr. **23**, 523 (1952).

The Mass Relation of Heavy Particles

H. ENATSU*
Columbia University, New York, New York
(Received January 13, 1952)

In a previous note[1,2] on the mass spectrum of heavy particles, our calculation of self-energies was carried out only for the case of nucleons. We have now extended our treatment to the case of heavy nucleons. Before presenting our results, we should like to outline the method used. (A) We assume derivative couplings for interactions between nucleons (and heavy nucleons) and mesons. (B) Self-energies of nucleons and heavy nucleons are calculated to the second order in the coupling constants by using the method described in the preceding paper.[1] (C) Self-energy divergences are canceled out by mixing two kinds of mesons. (D) The mass relations are derived from the conditions of the elimination of logarithmic divergences and are independent of the charge of the mesons.

Let us assume the following interactions:

$$i\frac{g}{\kappa_0}\bar{\psi}_N\gamma_5\gamma_\nu\psi_N\frac{\partial\phi_\pi}{\partial x_\nu}+\text{h.c.}, \tag{1}$$

$$i\frac{G}{\mu_0}\bar{\psi}_V\gamma_\nu\psi_N\frac{\partial\phi_c}{\partial x_\nu}+\text{h.c.}, \tag{2}$$

and

$$i\frac{L}{\kappa_0}\bar{\psi}_V\gamma_5\gamma_\nu\psi_V\frac{\partial\phi_\pi}{\partial x_\nu}+\text{h.c.}, \tag{3}$$

where ψ_N, ψ_V, ϕ_π, and ϕ_c are the wave functions for nucleons ($m=1836\ m_e$), heavy nucleons (m_1), π-mesons ($\kappa=276\ m_e$), and cohesive mesons (μ), respectively. The couplings (1) and (2) have been considered already for the case of nucleons in the previous note.[1] In order to eliminate self-energy divergences of heavy nucleons caused by the interaction (2), we must introduce another new interaction. Generally speaking, we have no restriction on the choice of the new coupling. However, the hypothesis of symmetry between nucleons and heavy nucleons seems most suitable at the present stage. In fact, as will be shown in the following, we can achieve the desired compensation of divergences by assuming the form (3). In connection with these interactions, it is interesting to refer back to the proposal made by Pais[3] on the types of couplings of heavy particles. According to him, the so-called strong couplings can be written in the forms

$$(N_0N_0\pi_0), \tag{4}$$

$$(N_0N_1\pi_1), \tag{5}$$

$$(N_1N_1\pi_0), \tag{6}$$

or

$$(N_iN_j\pi_k);\quad i+j+k=\text{even},$$

which correspond to (1), (2), and (3) above.

Now, the expression for the mass relation can be written as

$$\frac{\mu^2}{x^2}=\frac{1}{120\beta-105}\left\{(2\beta-1)\left(75\frac{\kappa^2}{x^2}+65\right)-(60\beta^3-75\beta^2+66\beta+6)\right\}, \tag{7}$$

where

$$\beta=y/x.$$

In the case of self-energies of nucleons, $x=m$, $y=m_1$, and $\beta=m_1/m$. On the other hand, in the case of heavy nucleons, $x=m_1$, $y=m$, and $\beta=m/m_1$ because of the symmetry between nucleons and heavy nucleons. Using the relation (7), we have computed the mass values of cohesive mesons for the cases of heavy nucleons and the results are given in Table I. It may be worth pointing out that in both cases mass values are of the order

TABLE I. Masses of cohesive mesons for the corresponding masses of heavy nucleons.

Case of the nucleon[a] self-energy		Case of the heavy nucleon self-energy	
m_1	μ	m_1	μ
1836 m_e	1474[b] m_e	1836 m_e	1474 m_e
1900	1378	1900	1645
2000	1263	2000	2107
2100	1152	2098	$+\infty$
2200	1042	2220[c]	···
2220	1019	2222	0
2230	1006	2230	412
2240	995	2240	595
2250	988	2250	715
2260	973	2260	819
2270	963	2270	884
2280	949	2280	970
2290	937	2290	1029
2300	923	2300	1078
2350	857	2350	1269
2400	787	2400	1400

[a] Nucleon = 1836 m_e, π-meson = 276 m_e.
[b] Professor N. M. Kroll pointed out that the self-energy of the nucleon caused by the interaction $(N_0N_0\pi_1)$, which is of the scalar type with vector coupling, should be zero with the computation method suggested by him. However, in the present note we have regarded $(N_0N_0\pi_1)$ as a special case of $(N_0N_1\pi_1)$ in the limit of $m_1\to m$, which gives us nonvanishing values. The author is much indebted to Dr. Kroll for discussion on this point.
[c] For this case we have no real mass value.

of magnitude given by recent experiments. Here we have another possibility of being able to explain the existence of various heavy particles and, at the same time, to remove part of the infinities. Nevertheless, we should like to remark in a general sense about the provisional character of our theory. First, it has been recognized that higher order corrections might seriously modify the results obtained. Second, the consequence of the mass relation (7) is of such a radical nature that we cannot determine discrete values for the masses of elementary particles. We feel that, besides the phenomenological prescription of the compensation, another principle would be necessary for us to solve this problem. Third, granted that we ignore such a circumstance for a time, we are still required to introduce more cohesive mesons in order to be consistent with the experimental fact that there may be numerous mesons. For instance, the evidence for χ-mesons ($\sim 1470\ m_e$) and ζ-mesons ($\sim 550\ m_e$) suggests a possibility of considering two kinds of cohesive mesons, namely, c_1 mesons ($\sim 1474\ m_e$) for the nucleon, and c_2 mesons ($\sim 595\ m_e$) for the heavy nucleon. Of course, the latter gives rise to a new infinity for the nucleon which may be canceled out by assuming a third cohesive meson. Finally, we are still not sure of a scheme to take into account the τ-meson and κ-meson (if it is a Fermion).

At any rate, we may conclude from this work that there may be intimate relations between masses of elementary particles and some of the divergences inherent in the current field theory.

The writer wishes to express his thanks to H. Yukawa, R. Serber, A. Pais, N. M. Kroll, and G. J. Yevick for their kind discussion.

* On leave from Kyoto University, Kyoto, Japan.
[1] H. Enatsu, Prog. Theoret. Phys. **6**, 643 (1951); Phys. Rev. **85**, 484 (1952).
[2] Enatsu, Hasegawa, and Pac (to be published). The decay and production of heavy particles will be treated in this paper. It will be seen that our argument proceeds in almost the same way as that of Pais except for the internal mass relations. The results obtained are not in disagreement with experiments.
[3] A. Pais, Phys. Rev. **86**, 663 (1952); Nambu, Nishijima, and Yamaguchi, Prog. Theoret. Phys. **6**, 615 (1951); S. Oneda, Prog. Theoret. Phys. **6**, 633 (1951).

Pure Nuclear Quadrupole Spectrum of Bi^{209} in Bismuth-Triphenyl*

H. G. Robinson,† H. G. Dehmelt, and Walter Gordy
Department of Physics, Duke University, Durham, North Carolina
(Received January 23, 1953)

PURE nuclear quadrupole resonance in solids, observed first by Dehmelt and Krüger[1] in 1949, has now been found for several nuclei. This type of spectrum has, however, not been previously investigated for Bi.

The only stable bismuth-isotope, Bi^{209}, has a spin $I=9/2$ well established from optical spectra.[2] The quadrupole moment also has been optically determined[3] as $Q(Bi^{209})=0.39\times10^{-24}$ cm². Corresponding to the spin value of 9/2, the nuclear quadrupole spectrum is expected to consist of four lines, all of which have been found in $Bi\phi_3$ by use of super-regenerative detection techniques described by Dehmelt and Krüger.[1] The observed frequencies which are given in Table I can be fitted to the theoretical values[4] for the case of deviation from axial symmetry:

$$\nu_1=(1/24)eQq_{zz}[1+9.03333\epsilon^2-45.690667\epsilon^4],$$
$$\nu_2=(2/24)eQq_{zz}[1-1.338095\epsilon^2+11.7224048\epsilon^4],$$
$$\nu_3=(3/24)eQq_{zz}[1-0.185714\epsilon^2-0.12329457\epsilon^4],$$
$$\nu_4=(4/24)eQq_{zz}[1-0.080952\epsilon^2-0.00425796\epsilon^4],$$

ν_1 to ν_4 corresponding to the transitions $\pm\frac{1}{2}\leftrightarrow\pm\frac{3}{2}$, $\pm\frac{3}{2}\leftrightarrow\pm5/2$, and so on.

The calculated frequencies ν_1, ν_2, ν_3 are obtained when ν_4 is assumed equal to the observed value and $\epsilon^2=7.875\times10^{-3}$ is used for the asymmetry parameter. The quadrupole coupling constant then is $eQq_{zz}=669.06\pm0.13$ Mc/sec.

In $Bi\phi_3$, bismuth forms three covalent bonds with some ionic character. The structure can be described as

$$\begin{matrix}\phi\\ Bi^{+}-\phi\\ \phi^{-}\end{matrix},$$

since from the difference of the electronegativity values $x_{Bi}=1.8$ and $x_C=2.5$, about 35 percent ($\approx\frac{1}{3}$) ionic character is expected.[5] The rather large observed Bi coupling reveals that the Bi bonding orbitals are not pure p but have significant s character. It is s admixture which accounts for the fact that an appreciable field gradient exists, and therefore, quadrupole coupling is observed in the $Bi\phi_3$ molecule. Three pure p bonds would lead to a vanishing field gradient q_{zz}.

The quadrupole coupling constant found in the molecule can be expressed as fractions of the coupling constant for an unbalanced atomic $6p$ electron:[6]

$$eQq_{zz}(Bi\phi_3)=3\alpha(1+2\beta)eQq_{zz}(p),$$

α denoting the fractional s admixture and β the ionic character of the Bi−C bonds. The coupling per $6p$ electron, $eQq_{zz}(p)$, can be evaluated from the doublet separation of a single p electron in the $6s^26p^3$ configuration of atomic Bi. A simple but probably not very accurate approach is linear extrapolation from the measured doublet separation of $6p$ for Bi V, which equals 2.8×10^4 cm^{-1}, and of $6s^26p$ for Bi III, which is equal to 2.18×10^{-6} cm^{-1}; in this way one obtains $\Delta\nu(p,\text{Bi I})=1.4\times10^4$ cm^{-1}. With $Z_1=79$ this gives $q_{zz}(p,\text{Bi I})=5.2\times10^{16}$ esu. With the optical value of Q this yields

$$eQq_{zz}(p)=1500\text{ Mc/sec}.$$

Comparison with the value observed in the $Bi\phi_3$ molecule leads to

$$3\alpha(1+2\beta)=669/1500.$$

From this, with $\beta=0.35$, one obtains 8 to 9 percent s admixture, which is in accordance with general expectations of hybridization in the nitrogen group of elements.

The rather large asymmetry of the field gradient, $\epsilon\approx9$ percent, could be caused by bond strains which are to be expected for this rather bulky molecule in the crystalline state.

The $BiCl_3$ quadrupole spectrum has also been investigated. A number of lines have been found, but the spectrum has not yet been analyzed.

TABLE I. Comparison between calculated and measured frequencies.

	Measured Mc/sec	Calculated Mc/sec	Line half-width kc/sec
ν_1	29.785	29.7815	~25
ν_2	55.214	55.2075	~15
ν_3	83.516	83.5089	~20
ν_4	111.438	assumed	~20

* Supported by the U. S. Office of Ordnance Research.
† Shell Fellow.
[1] H. G. Dehmelt and H. Krüger, Z. Physik **129**, 401 (1951); R. V. Pound, Phys. Rev. **79**, 685 (1950).
[2] S. Goudsmit and E. Back, Z. Physik **43**, 321 (1927).
[3] H. Schuler and T. Schmidt, Z. Physik **99**, 717 (1936).
[4] These frequency values can be obtained either from a secular equation similar to that given by H. Krüger, Z. Physik **130**, 371 (1951) or evaluated by perturbation methods, a general formula for which is given by R. Bersohn, J. Chem. Phys. **20**, 1505 (1952).
[5] W. Gordy, J. Chem. Phys. **19**, 792 (1951).
[6] Gordy, Trambarulo, and Smith, *Microwave Spectroscopy* (John Wiley and Sons, Inc., New York, to be published); C. H. Townes and B. P. Dailey, J. Chem. Phys. **17**, 782 (1949).

The Diamagnetism of an Enclosed Electron Gas

H. A. Nye
University of Buffalo, Buffalo, New York
(Received December 8, 1952)

IN recent papers, Osborne[1] and Steele[2] discuss the diamagnetism of a free electron gas in a finite container from the point of view of number theory. In these papers interesting effects are uncovered

which depend upon the size and the shape of the container, but in the limit of large volume, the results obtained for Landau diamagnetism and the Haas-van Alphen effect agree with those obtained by many previous authors. This last result should not appear to be surprising. One of these authors,[1] however, criticizes the procedure in previous calculations of ignoring the contributions of surface electrons to the partition function, on the grounds that completely different results could be obtained by methods which one has no *a priori* reason for rejecting. More specifically, reference is made to the discrepancy between the results obtained by making the approximation of neglecting surface states before or after differentiating the partition function with respect to the magnetic field. This discrepancy has been discussed by Teller[3] and Van Vleck,[4] who concluded that while the contribution of the surface states to the partition function is negligible in the limit of large volume, the direct contribution of these electrons to the magnetic moment must be included if the procedure is followed of summing over states after differentiating the partition function. Osborne rejects this explanation by pointing out that Van Vleck omitted certain states, and by stating that if these states are included, completely unreasonable results are obtained. It is the purpose of this letter to indicate that a consistent inclusion of effects, of the order of those contributed by the omitted states referred to, leaves the results of Van Vleck unaltered.

Van Vleck considers the electrons to be enclosed in a container of cylindrical shape, the axis of the cylinder being parallel to the magnetic field. The inner electrons are treated as being completely free, and the Schrödinger equation for the motion of a free electron in a plane perpendicular to the magnetic field is solved in polar coordinates, with the result that the energy levels are given by

$$W=(n_1+|n_1|+2n_2+1)h\nu, \tag{1}$$

where n_1 is the azimuth quantum number, n_2 the radial quantum number, and ν the Larmor frequency. The partition function is taken to be

$$Z=\sum_{n_1}\sum_{n_2=0}^{\infty}\exp[-(n_1+|n_1|+2n_2+1)h\nu/kT], \tag{2}$$

where n_1 is to be summed over only those values of n_1 corresponding to inner electrons. Van Vleck takes the lower limit on this summation to be $n_1=-\pi eHR^2/hc$, R being the radius of the container; this value for the limit is obtained by considering the semiclassical equation

$$n_1=\pi eH(r^2-d^2)/hc \tag{3}$$

(r being the radius of the circular orbit and d the distance of its center from the origin) and by ruling out values of n_1 which would give $d>R$, on the assumption that $R\gg r$. The upper limit is taken to be $n_1=-1$, since, if $R\gg r$, only a negligible number of orbits encircle the origin (have positive n_1). It is this last assumption to which objection has been raised by Osborne. It is true that the sum in (2) includes many states for which the assumption $R\gg r$ is not valid, and hence states of positive n_1 should be included. For these states, however, the r^2 term in Eq. (3) cannot be ignored, and it is easy to see that the consistent inclusion of states of positive n_1, i.e., the correction of both the upper and lower limits on n_1, leads to results identical with those given by Van Vleck. If one introduces the principal quantum number $n=(n_1+|n_1|+2n_2)/2$, Eq. (1) becomes

$$W=(2n+1)h\nu, \tag{4}$$

and (2) becomes

$$Z=\sum_{n=0}^{\infty}\sum_{n_1}\exp[-(2n+1)h\nu/kT]. \tag{5}$$

It is clear that the upper limit on n_1 should be taken to be n. However, since the classical radius of the orbit is given by

$$r^2=hcn/\pi eH, \tag{6}$$

Eq. (3) can be written as

$$n_1=n-\pi eHd^2/hc, \tag{7}$$

and Van Vleck's criterion gives for the lower limit $n_1=n-\pi eHR^2/hc$. Thus, the correction of both the limits leads to all the results given by Van Vleck. It is thus seen that the inclusion of the orbits which enclose the origin does not lead to unreasonable results.

[1] M. F. M. Osborne, Phys. Rev. **88**, 438 (1952).
[2] M. C. Steele, Phys. Rev. **88**, 451 (1952).
[3] E. Teller, Z. Physik **67**, 311 (1931).
[4] J. H. Van Vleck, *The Theory of Electric and Magnetic Susceptibilities* (Oxford University Press, London, 1932), p. 353.

Activation Cross Sections Measured with Antimony-Beryllium Photoneutrons. II

CLYDE KIMBALL AND BERNARD HAMERMESH
Argonne National Laboratory, Lemont, Illinois
(Received February 2, 1953)

ADDITIONAL measurements of activation cross sections using Sb–Be photoneutrons (energy≦25 kev) have been made using the technique described by Hummel and Hamermesh.[1]

Table I contains a list of these cross sections relative to Seren's[2] thermal cross section for the given element.

TABLE I. Natural atom cross sections for (Sb–Be).

Isotope ($A+1$)	Half-life	Natural atom cross section (millibarns)	Percent error
Co^{60}	10.7 min	7.7[a]	30
Cu^{64}	12.8 hr	85	25
Ge^{75}	82 min	14	10
Ba^{139}	85 min	53	10
W^{187}	24.1 hr	119	15

[a] This value is an upper limit. The very small number of counts above background made it difficult to obtain good half-life values. The value in the table is obtained by assigning to the 10.7-min activity all counts above background corresponding to a half-life of less than thirty minutes.

[1] V. Hummel and B. Hamermesh, Phys. Rev. **82**, 67 (1951)
[2] Seren, Friedlander, and Turkel, Phys. Rev. **72**, 888 (1947).

Influence of the Nuclear Quadrupole Moment on the $\alpha-\gamma$ Angular Correlation in Radiothorium

A. ABRAGAM AND R. V. POUND
Harvard University, Cambridge, Massachusetts
(Received February 4, 1953)

IT is well known that the angular correlation between two nuclear radiations can be affected by magnetic fields, either atomic or applied, acting on the magnetic moment of the nucleus in its intermediate state. No attention seems to have been paid so far, in this connection, to the quadrupole moment of the nucleus. The influence of the quadrupole coupling on the angular correlations and the possibility of using this effect to measure the quadrupole moments of short-lived isomers are discussed in detail in a forthcoming paper by Abragam, Bloembergen, and Pound. The purpose of the present letter is to show that such coupling provides an explanation for the discrepancy between experimental and theoretical values of the $\alpha-\gamma$ correlation in the disintegration of radiothorium which has recently been investigated by two different groups.[1,2] Their results agree within experimental error.

The correlation is given in reference 1 as

$$W(\theta)=1+6.9\cos^2\theta-7.07\cos^4\theta,$$

or, if we rewrite it in terms of Legendre polynomials,

$$W(\theta)=1+0.30P_2-0.86P_4.$$

The theoretical correlation resulting from the most plausible disintegration scheme ($I_a=0$, quadrupole α-emission, $I_b=2$, quadrupole γ-emission, $I_c=0$) is $W=\cos^2\theta-\cos^4\theta$ or $1+(5/7)P_2-(12/7)P_4$. It is seen that the experimental correlation is weaker

than the theoretical one. The experimental coefficients of the second and fourth Legendre polynomials are, respectively, smaller than the theoretical ones by the factors $G_2=0.42$ and $G_4=0.50$.

Such a weakening can be produced by the interaction of the quadrupole moment in the intermediate state with the gradient of the electric field at the nucleus. If we assume that the field has axial symmetry and that all directions of its axis are equally probable (as for a crystalline powder), it can be shown that for a nucleus of spin 2,

$$G_2^{\text{theor}}=(1/35)[8(1+16x^2)^{-1}+12(1+9x^2)^{-1}+2(1+x^2)^{-1}+13],$$
$$G_4^{\text{theor}}=(1/63)[6(1+16x^2)^{-1}+16(1+9x^2)^{-1}+12(1+x^2)^{-1}+29].$$

In this formula $x=2\pi\nu\tau$, where τ is the lifetime of the intermediate state and $h\nu$ the energy difference between the states $M_b=0$ and $M_b=\pm1$ of the quadrupole moment in the axial field.

G_2 and G_4 are decreasing functions of x which vary very slowly for $x>1$.

$$G_2(0)=G_4(0)=1;$$
$$G_2(1)=0.45, \quad G_4(1)=0.59,$$
$$G_2(\infty)=0.37, \quad G_4(\infty)=0.46.$$

If we take $\tau=10^{-8}$ sec,[1,2] $x=1$ corresponds to a frequency ν of 15 Mc/sec. Much higher quadrupole interactions have been observed in nuclear resonance experiments, and values of x much higher than 1 are by no means unlikely.

It follows from this that G_2 and G_4, and therefore the correlation, are practically independent of the value of the gradient of the electric field as long as it is large enough (ν higher than 15 Mc/sec). This is particularly important in view of the fact that after the α-emission, the nucleus, which has a recoil energy higher than 100 kev, can occupy any position with respect to the surrounding atoms or molecules. Such circumstances are favorable for large electric field gradients with considerable variation in magnitude and direction from one radioactive nucleus to another. For $x>1$ the agreement with experiment is very good.

The near constancy of the G's for $x>1$ explains why both experimental groups obtain almost identical results using different source materials. A departure of the electric field from axial symmetry is not likely to affect the previous results drastically.

The fact that G_4 is larger than G_2, theoretically and experimentally, suggests very strongly that the influence of atomic magnetic fields on the correlation is very small. It can be shown[3] that a magnetic field, whether atomic or applied, affects the higher harmonics most strongly and would lead to $G_4 \ll G_2$.

The nuclear electric quadrupole interaction in the intermediate state appears to offer explanation of discrepancies observed in many other angular correlation experiments. Other examples will be discussed in the later paper.

[1] Beling, Feld, and Halpern, Phys. Rev. **84**, 155 (1951).
[2] Battey, Madansky, and Rasetti, Phys. Rev. **89**, 182 (1953).
[3] Alder, Helv. Phys. Acta **25**, 234 (1952).

Neutron Capture Cross Sections for Production of Sc^{46} and Sr^{85}†

W. S. Lyon
Analytical Chemistry Division, Oak Ridge National Laboratory, Oak Ridge, Tennessee
(Received December 29, 1952)

CONSIDERABLE uncertainty exists in the literature concerning the thermal neutron capture cross section for production of both 85-day Sc^{46} and 65-day Sr^{85}. Tabulated nuclear data[1] give conflicting values for Sc^{46} and none for Sr^{85}.

Bethe[2] has reported >13 barns for the reaction $Sc^{45}(n,\gamma)Sc^{46}$. Seren *et al.*[3] report 22 b. Recently Pomerance[4] has measured the capture cross section for pile neutrons using the pile oscillator. He finds 23±1.5 barns.

Samples of spectroscopically pure Sc_2O_3 together with weighed pieces of Al–Mn alloy of known Mn concentration were irradiated in the Oak Ridge National Laboratory graphite reactor for eight hours. Upon removal from the reactor the decay of the monitor metal was followed in a calibrated high pressure ionization chamber, and the activity of the product 2.59-hour Mn^{56} was determined. The neutron flux was then calculated using the expression

$$A=Nf\sigma(1-e^{-\lambda t}),$$

where $\sigma=13$ barns.

Samples of the irradiated Sc_2O_3 were then weighed on an analytical balance, and the activity of the daughter Sc^{46} determined from ion chamber measurements. After correction for decay from pile discharge time, the pile neutron cross section for Sc^{46} was calculated as above and found to be 21.6±2 barns. Goldhaber and Muehlhause[5] have reported a 20-sec isomer of Sc^{46} which has an activation cross section of 10±4 barns. Thus the cross section for direct production to the ground state 85-day activity is 12 barns, and the value of 22 barns is the "effective" production cross section for the longer-lived activity.

Sr^{85} is a K electron capturing nuclide whose decay scheme has only recently been completely elucidated by Sunyar *et al.*[6] These workers have established that Sr^{85m}, which is the 70-min excited state initially produced, decays to Sr^{85} (65-day) in 86 percent of the disintegrations. Recently Harrison and Seymour[7] have reported an "effective" production cross section of Sr^{85} of 0.3±0.1 measured relative to the 5-mb cross section for the Sr^{89} 53-day activity.

The thermal neutron cross section for production of Sr^{85} has been obtained by use of $SrCO_3$ enriched to a Sr^{84} concentration of 45.95 percent.[8] Samples of $SrCO_3$ together with cobalt monitor metal were irradiated in the Oak Ridge National Laboratory graphite reactor for two weeks. After cooling one week, the $SrCO_3$ and Co metal were weighed, and the activity produced in them was read on the calibrated high pressure ionization chamber. By use of the decay scheme noted above, the activity of product Sr^{85} was calculated. The "effective" isotopic capture cross section for the production of Sr^{85} was then calculated and found to be 1.2±0.1 barns.

To establish that the γ-activity observed was due solely to radiation from the primary product nuclides, portions of the irradiated material were examined on a NaI(Tl) crystal γ-ray spectrometer equipped with a linear amplifier and differential and integral pulse-height selector. The γ-spectra so obtained indicated the activities to be pure Sc^{46} and Sr^{85}.

Table I is a summary of the results.

TABLE I. Capture cross sections for pile neutrons.

Target atom	Product atom	"Effective" isotopic capture cross section (barns)	Atomic capture cross section (barns)
Sc^{45}	Sc^{46}	21.6±2	21.6±2
Sr^{84}	Sr^{85}	1.2±0.1	0.0066±0.0006

† Based on work performed by the U. S. Atomic Energy Commission.
[1] K. Way *et al.*, *Nuclear Data*, National Bureau of Standards Circular 499, and Supplements 1, 2, 3 (1951).
[2] W. Bothe, Z. Naturforsch. **1**, 179 (1946).
[3] Seren, Friedlander, and Turkel, Phys. Rev. **72**, 88 (1947).
[4] H. Pomerance, private communication, November, 1952.
[5] M. Goldhaber and C. O. Muehlhause, Phys. Rev. **74**, 1877 (1948).
[6] Sunyar, Mihelich, Scharff-Goldhaber, Goldhaber, Wall, and Deutsch, Phys. Rev. **86**, 1023 (1952).
[7] G. E. Harrison and F. D. Seymour, Proc. Phys. Soc. (London) **A65**, 958 (1952).
[8] Electromagnetically enriched isotope supplied by the Isotope Research and Production Division, Y-12 Plant, Carbide and Carbon Chemicals Corporation, Oak Ridge, Tennessee.

Angular Distribution of Particles from Stars*

R. W. Waniek and Taiichiro Ohtsuka
Cyclotron Laboratory, Harvard University, Cambridge, Massachusetts
(Received February 2, 1953)

IN our recent communications[1,2] we have described the experimental arrangement and some preliminary results obtained on stars induced by high energy neutrons in 200-μ Ilford G5 plates.

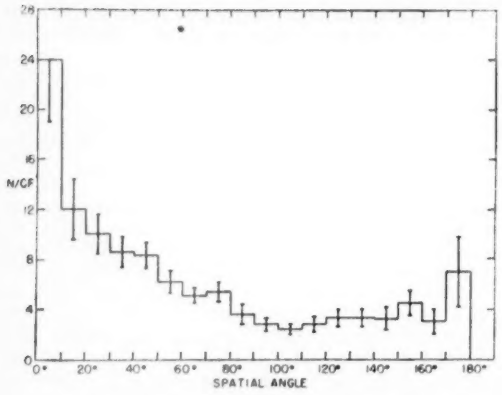

FIG. 1. Number of prongs *vs* spatial angle in 10° intervals. (Plate exposed at 0°.)

We intend to report here on the angular distribution of the particles emitted.

To our knowledge similar studies so far have been made only on the distribution projected onto the plane of the emulsion. However, this can be regarded only as an approximation to the three-dimensional phenomenon, and consequently, what is of interest is the distribution in space.

We have carried out the measurement of about 1000 stars for the two plates exposed[2] determining the angular distribution in space for each prong. This was obtained in the conventional way by observing the angle of dip together with the projected angle. Particular care was taken in determining the shrinkage factor which affects the angle of dip and hence could be a source of possible distortion of the distribution.

The results obtained from the plate exposed to the higher effective neutron energy[2] are given in Fig. 1. The width of the channels is selected as 10° because the intrinsic angular resolution, taking into account all possible sources of error (range, dip, shrinkage factor), is estimated to be about ±2°.

The forward tendency in the emission of the prongs is apparent. This spatial angular distribution includes all types of events (1 to 5 prongs) and particles of all energies. The discrimination between $n-p$ scattering events due to the interaction of the

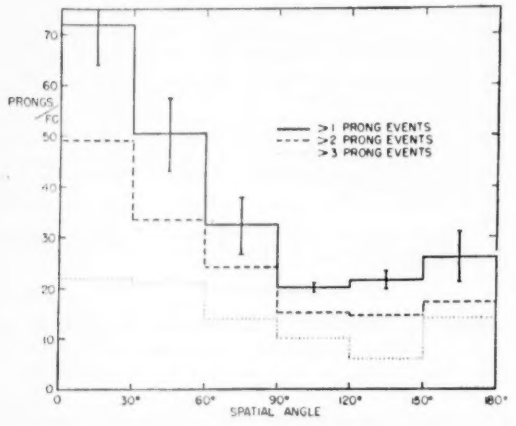

FIG. 2. Number of prongs *vs* spatial angle, in 30° intervals, for different classes of events. (Plate exposed at 0°.)

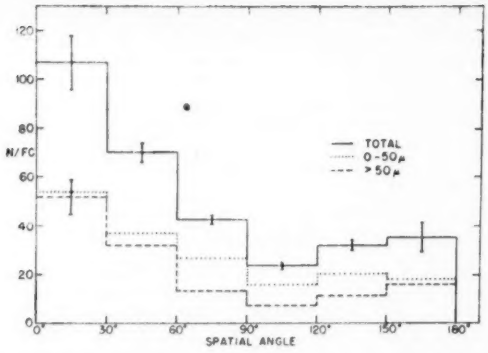

FIG. 3. Number of prongs *vs* spatial angle, in 30° intervals, with range subdivisions from all types of events. (Plate exposed at 0°.)

neutrons with the hydrogen in the emulsion and *bona fide* one-prong events is made difficult by the uncertainties in the flux determination, shape of the spectrum, and effective cross section. Therefore in Fig. 2, we show results obtained by excluding all one-prong events, together with the results in which the two and three prongs respectively are excluded. The channel has been widened to 30° in order to avoid large statistical fluctuations. The forward trend is seen to prevail up to three-prong events. As for the larger types of events, a conclusive answer cannot be provided due to the lack of statistics, although the distribution seems to be nearly isotropic. One might expect that the peak in the forward direction is due to the high energy knock-on particles. In order to investigate this point we have plotted the angular distribution of Fig. 1 subdivided into prongs with actual ranges over and under 50 microns (Fig. 3).

It turns out that not only the high energy particles but also the low energy ones are peaked to an appreciable extent in the forward direction, a fact which remains true for at least up to three-prong events. This is not easy to interpret if the stars examined originate in the heavier elements because the low energy particles are normally attributed to the evaporative component of the star generating process. From consideration of the measured cross sections it seems unlikely that the light elements are contributing to a very appreciable extent, although direct confirmation is still lacking.

This anomaly is less pronounced in the plate exposed to the lower effective neutron energy, which seems to indicate that this phenomenon is caused mainly by the high energy peak of the neutron spectrum.

We wish to express our indebtness to Mr. Sang C. Kim for his valuable assistance in scanning the plates.

* Supported by the joint program of the U. S. Office of Naval Research and the U. S. Atomic Energy Commission.

[1] R. W. Waniek and T. Ohtsuka, Bull. Am. Phys. Soc. **27**, No. 1, 26 (1953).

[2] R. W. Waniek and T. Ohtsuka, Phys. Rev. **89**, 882 (1953).

Errata

An Application of the Cellular Method to Silicon, D. K. HOLMES [Phys. Rev. **87**, 782 (1952)]. The following acknowledgement should have been included: "This work was suggested by Prof. F. Seitz, and its completion was made possible by his constant help and advice."

Energy Loss of Cosmic-Ray Mu-Mesons in Sodium Iodide Crystals, ALVIN HUDSON AND ROBERT HOFSTADTER [Phys. Rev. **88**, 589 (1952)]. The small quantity $\xi\beta^2$ should be subtracted from the right-hand side of Eq. (4). The same quantity, $\xi\beta^2$, should also be added to the term 0.37ξ appearing on the last line of p. 593. These corrections involve an argument used to explain the straggling theory in an intuitive way and do not affect any of the results, figures, or other equations of the original paper.

The Density Effect for the Ionization Loss in Various Materials, R. M. STERNHEIMER [Phys. Rev. **88**, 851 (1952)]. In Eqs. (22), (43), (44), and (45), replace $\ln[4mv^2/3.17\pi b^3ne^2 \times(1-\beta^2)]$ by $\ln[mv^2/3.17\pi b^2ne^2(1-\beta^2)]$. This correction does not affect the values of δ.

PHYSICAL REVIEW VOLUME 89, NUMBER 6 MARCH 15, 1953

Author Index to Volume 89

References with (A) are to abstracts of papers presented at meetings of the American Physical Society, and those with (T) designate title only. References with (L) are to Letters to the Editor.

Abragam, A. and R. V. Pound. Influence of nuclear quadrupole moment on α-γ angular correlation in RaTh—1306(L)
—— (see Fields, R. E.)—908(A)
Abraham, Bernard M. (see Weinstock, Bernard)—787
Accardo, C. A. (see Lehovec, K.)—20
Adair, R. K., A. Okazaki, and M. Walt. Scattering of neutrons by deuterons—1165
Adams, E. N. II. Magnetic susceptibility of diamagnetic electron gas—role of small effective electron mass—633
Affleck, J. H. and L. V. Holroyd. Use of Ba^{140} in studies of oxide coated cathodes—893(A)
Ahrens, L. H. (see Aldrich, L. T.)—631
Alburger, D. E. and S. Thulin. Identification of 7-hr Mo^{93m}—1146(L)
—— (see Lindström, A.)—1303(L)
Aldrich, L. T., L. F. Herzog, W. K. Holyk, F. B. Whiting and L. H. Ahrens. Variations in isotopic abundances of Sr—631
Allen, James S. and W. K. Jentschke. Electron-neutrino angular correlation in β-decay of He^6—902(A)
Allis, W. P. and D. J. Rose. Transition from free to ambipolar diffusion—335(A)
Almy, G. M. (see Butler, W. A.)—893(A)
Alpert, D. Researches in ultra-high vacuum—902(T)
Alpert, Morris (see Nielsen, J. Rud)—895(A)
Altshuler, Saul. Applications of variational principles to scattering problems—1278
—— Excitation cross section for He atoms—1093(L)
Amar, Henri. General-relativistic approach to short-range forces—1298(L)
Ames, D. P., M. E. Bunker, L. M. Langer, and B. M. Sorenson. Disintegration of Sr^{91} and Y^{91m}—903(A)
Anderson, C. D. (see Leighton, R. B.)—148
Andrew, Alan and Clifton R. Davidson. Induced thermoelectric potential from radiation damage—876(L)
Andrews, Donald H. (see Haley, Floyd C.)—821
Annis, Martin, H. S. Bridge, and S. Olbert. Application of multiple scattering theory to cloud-chamber measurements—1216
Antal, J. J. and A. H. Weber. Structure of surface of glass and of Bi films deposited on glass—900(A)
Antonoff, George. Kinks in vapor pressure p *vs* temperature curves—915(A)
—— New theory of aggregates as supplement to van't Hoff's theory of solutions—915(A)
—— **and Raymond Madrazo, Jr.** Angular points in densities of water *vs* temperature—899(A)
Apker, L. Photoelectric emission from solids—902(T)
—— (see Huntington, H. B.)—352
Atkins, K. R. Heat pulses in liquid He II below 1°K—526(L)
Atkinson, W. R. and R. G. Fowler. Plane supersonic flow patterns in ionized media—906(A)
—— (see Fowler, R. G.)—336(A)
Austern, N. Validity of Born approximation in stripping—318(L)

Bair, J. K. (see Kington, J. D.)—530(L)
Bandyopadhyay, G. New equation in affine field laws—1161(L)
Barber, W. C., G. E. Becker, and E. L. Chu. Electron-electron scattering at 6.1 Mev—950
Barkas, Walter H. Range correction for electron pickup—1019
—— **and Helge Tyren.** Physical analysis of Be and C disintegration induced by 330-Mev protons—1
—— (see Wilson, H. W.)—758
Barker, W. A. and Z. V. Chraplyvy. Amplified Dirac equation and Lamb-Retherford shift—913(A)
—— **and Z. V. Chraplyvy.** Conversion of amplified Dirac equation to approximately relativistic form—446
Barnes, B. T. Electron velocity distributions in Hg-A discharge—335(A)
Baroody, E. M. Energy loss of medium-fast electrons in metals—910(A)
Barrett, Paul H., G. Cocconi, and Y. Eisenberg. Search for "T-tracks" in photographic plates—656(L)
Bartholomew, G. A. and B. B. Kinsey. Neutron capture γ-rays from Sc, V, Mn, Co, and Cu—386
—— (see Kinsey, B. B.)—375
Bartlett, J. H. and G. J. Dienes. Combined pairs of vacancies in Cu—848
Barton, R. (see Kip, A. F.)—518(L)
Battat, M. E. and F. L. Ribe. Formation of He^6 by 14-Mev neutron bombardment of Li and Be—80
Battey, James, L. Madansky, and F. Rasetti. α-γ angular correlation in RaTh—182
Becker, G. E. (see Barber, W. C.)—950
Becker, R. L., M. Walt, and A. Okazaki. Total cross sections for fast neutrons—904(A)
—— (see Fields, R. E.)—908(A)
—— (see Walt, M.)—1271
Belinfante, F. J. Special-relativistic linear gravitational theory—914(A)
Belser, Richard B. Frictional adhesion of metal to glass, quartz, and ceramic surfaces—915(A)
—— Improved techniques in aging of thin metal films—911(A)
—— Technique of soldering to thin metal films—915(A)
Bendt, Philip J. Neutron scattering by coupled paramagnetic ions—561
Benedict, T. S. and W. Shockley. Microwave observation of collision frequency of electrons in Ge—1152(L)
Bentley, W. (see Elson, R.)—320(L)

Benveniste, Jack and Bruce Cork. Inelastic events induced by 32-Mev protons on He—422
Bergmann, Peter G. and Ralph Schiller. Classical and quantum field theories in Lagrangian formalism—4
—— **and Robb Thomson.** Spin and angular momentum in general relativity—400
—— (see Goldberg, Joshua N.)—278
Berkowitz, Ami E. (see Franklin, Alan D.)—1171
Bethe, H. A. Molière's theory of multiple scattering—1256
Bhowmik, B. Negative primaries as part of cosmic radiation—327(L)
Billington, H. B. (see Roberts, J. H.)—905(A)
Biondi, Manfred A. Dissociative attachment of thermal electrons to I_2 molecules—337(A)
—— (see Chanin, Lorne M.)—337(A)
Birkhoff, R. D. (see Maerker, R. E.)—1159(L)
Birnbaum, G. and A. A. Maryott. High pressure inversion spectrum of ND_3 near 1500 Mc—895(A)
Birnbaum, Milton, Eric M. Harth, Leo Seren, and Ralph Tobin. Activity ratio method for measuring energy stability of betatrons—897(A)
Blatt, John M. β-decay interaction—83; 914(A)
—— β-decay of triton—86
Bloch, F. (see Wangsness, R. K.)—728
Bloembergen, N. and G. M. Temmer. Nuclear magnetic resonance of aligned radioactive nuclei—883(L)
Bohm, David. Causal interpretation of quantum theory—319(L)
—— Proof that probability density approaches $|\psi|^2$ in causal interpretation of quantum theory—458
Bohr, Aage and Ben R. Mottelson. Interpretation of isomeric transitions of electric quadrupole type—316(L)
Bolgiano, P., L. Madansky, and F. Rasetti. Continuous γ-ray spectrum accompanying β-decay—679
Borowitz, Sidney and Bernard Friedman. Variational principles for three-body scattering problems—441
Borsellino, A. Momentum transfer and angle of divergence of pairs produced by photons—1023
Bostick, W. H., M. A. Levine, and L. S. Combes. Photographic and spectrographic evidence of the pinch effect in N_2—339(A)
Bowell, E. (see Lockett, E. E.)—657(L)
Bozorth, R. M. and R. W. Hamming. Measurement of magnetostriction in single crystals—865
—— **and J. G. Walker.** Magnetic crystal anisotropy and magnetostriction of Fe-Ni alloys—624
Braught, Gene (see Conn, Willi M.)—898(A)
Breit, G. and R. M. Thaler. Relativistic corrections to magnetic moments of nuclear particles—1177
Bretscher, M. M. (see McFarland, C. E.)—892(A)
Brice, M. K. (see Cork, J. M.)—1291
—— (see LeBlanc, J. M.)—907(A)
Brickl, David E. (see Griffith, Wayland)—451
Bridge, H. S. (see Annis, Martin)—1216
Brix, Peter. Nuclear magnetic moment of Pr^{141} from hfs of Pr II—1245
Brock, E. G., A. L. Houde, and E. A. Coomes. Periodic deviations in Schottky effect for Mo—851
Broida, H. P. OH rotational distributions in mixtures of H_2O in high frequency discharge—336(A)
—— **and W. R. Kane.** Rotational intensity distributions of OH and OD in electrodeless discharge through water vapor—1053
Brolley, John E., Jr. Isomeric branching and threshold behavior of $Mo^{92}(n,2n)Mo^{91}$—877(L)
Bromley, D. A., J. A. Bruner, and H. W. Fulbright. Angular distributions of protons from $F^{19}(d,p)F^{20}$—396
—— (see Fulbright, H. W.)—892(A)
Broyles, C. D. and S. K. Haynes. K-fluorescence yield summary—912(A)
——, **D. A. Thomas, and S. K. Haynes.** Measurement and interpretation of the K-Auger intensities of Sn^{113}, Cs^{137}, and Au^{198}—715
Bruce, C. R. Homogeneity mapping of permanent magnet field for chemical effect studies in nuclear resonance—896(A)
Brueckner, K. A. Multiple scattering correction to impulse approximation in two-body system—834
—— Multiple scattering effects in pion-deuteron scattering—909(A)
Bruner, J. A. (see Bromley, D. A.)—396
—— (see Fulbright, H. W.)—892(A)
Budini, P. Energy loss and Čerenkov radiation of relativistic ionizing particle—1147(L)
Bunker, M. E. (see Ames, D. P.)—903(A)
Burbidge, G. R. and A. H. de Borde. Mesonic Auger effect—189
Burstein, E., J. J. Oberly, and J. W. Davisson. Infrared photoconductivity due to neutral impurities in Si—331(L)
Bushkovitch, A. B. (see Jones, L. C.)—895(A)
Butler, S. T. and E. E. Salpeter. Angular distribution of (d,t) reactions—891(A)
Butler, W. A. and G. M. Almy. Photoprotons from Mo^{100} and Mo^{92}—893(A)

Caird, R. S. and Allan C. G. Mitchell. Rb^{84m}—573; 903(A)
Callaway, Joseph (see Herman, Frank)—518(L)
Camac, M., J. B. Platt, and H. J. Schulte. Z-dependence of mesic x-ray yield—905(A)
—— (see Schulte, H. J.)—905(A)
Cameron, John R., Robert H. Davis, Ajay S. Divatia, Frederic J. Eppling, and Richard W. Hill. Elastic scattering of α-particles by O^{16}—909(A)
—— (see Jackson, H. L.)—365
Caretto, A. A., Jr., and S. Katcoff. Shortlived Ce isotopes from U fission—1267
Carlson, R. R. (see Kington, J. D.)—530(L)
Carroll, E. E., Jr. (see Stephens, W. E.)—893(A)
Carter, R. S. (see Palevsky, H.)—910(A)
Carver, J. H., R. D. Edge, and D. H. Wilkinson. Cross section for $Ta^{181}(\gamma,2n)Ta^{179}$ at 17.6 Mev—658(L)
Casson, Harvey. Nuclear γ-rays from low energy proton bombardment of Na, Mg, and Al—809
Chang, C. H., C. S. Cook, and H. Primakoff. Transmission of electrons through thin metallic foils—910(A)
Chang, W. Y., G. del Castillo, and Leon Grodzins. Sea level penetrating showers—408
Chanin, Lorne M. and Manfred A. Biondi. Mobilities of thermal ions in noble gases—337(A)
Chasson, Robert L. Effects of atmosphere on penetrating cosmic radiation—1255
Chen, Tien Chi and F. London. Entropy of liquid He^3—1038
Chew, Geoffrey F. Pion-nucleon scattering when coupling is weak and extended—591
—— Theoretical approach to pion-nucleon interaction—904(T)
Chraplyvy, Z. V. Approximate two-body relativistic wave equations—912(A)
—— (see Barker, W. A.)—446; 913(A)
Christy, R. F. Coupling of angular momenta in nuclear reactions—839
Chu, E. L. (see Barber, W. C.)—950
Clark, D. D. (see Igo, G. J.)—879(L)
Clarke, R. L. (see Paul, E. B.)—892(A)
Class, C. M. and S. S. Hanna. Angular correlation in decay of Li^8—877(L)
Cleland, Marshall R. Fast neutron scintillation spectrometer—896(A)
Clifford, R. P. Extensometer for rubber—341(A)
Cocconi, G. (see Barrett, Paul H.)—656(L)
Coester, F. Symmetry of S-matrix—619; 913(A)
Cohen, S. G. (see Jaffe, A. A.)—454

Cole, Richard W. Exchange magnetic moments of nuclei with almost closed shells of nucleons—883(L)
Colgate, S. A. and F. C. Gilbert. Electron-positron annihilation in flight—790
Colladay, G. S. (see Juenker, D. W.)—894(A)
Collins, T. L. Atomic masses of light elements—909(T)
Combes, L. S. (see Bostick, W. H.)—339(A)
Conant, F. S. (see Hall, G. L.)—342(A)
Conklin, G. L. (see Mandeville, C. E.)—559
Conn, Willi M. and Gene Braught. Separation of incident and emitted radiations in solar furnace by rotating sectors —898(A)
Conner, J. P. Cloud-chamber study of scattering of fast neutrons in O_2—712
Cook, C. F. and J. R. Smith. Cross section for $D(d,p)H^3$—785
Cook, C. J. (see Jorgensen, T.)—897(A)
Cook, C. S. (see Chang, C. H.)—910(A)
—— (see Whalen, J. A.)—902(A)
Cook, W. R., Jr., and Hans Jaffe. Ferroelectricity in oxides of face-centered cubic structure—1297(L)
Coomes, E. A., J. A. Dezoteus, and J. F. Whalen. Patch effect for thermionic emission from polycrystalline Ta —894(A)
—— (see Brock, E. G.)—851
—— (see Juenker, D. W.)—894(A)
Coor, T. (see Hafner, E. M.)—204
Cork, Bruce. Elastic scattering of protons from He^4—78
—— (see Benveniste, Jack)—422
Cork, J. M., M. K. Brice, W. H. Nester, J. M. LeBlanc, and D. W. Martin. Radioactive decay of W^{187}—2191
—— (see LeBlanc, J. M.)—907(A)
Coryell, Charles D., Pierre Lévêque, and Harold G. Richter. Isomerism for Cd^{117}, In^{117}, and In^{118}—903(A)
Cüer, P. and J. J. Jung. Angular distribution of $Be^9(d,t)Be^8$ at low energy—1151(L)
Curtis, C. D. Bremsstrahlung cross section of 60-Mev electrons in Pb—123

Damm, C. C. Secondaries of penetrating showers—826
Danielson, G. C. (see Shaw, William C.)—900(A)
—— (see Smith, J. F.)—911(A)
Dannis, Mark L. Plasticizers for polyvinyl chloride—341(A)
Darden, Sperry (see Nereson, Norris)—775
Date, Muneyuki (see Okamura, Tosihiko)—525(L)
Daunt, J. G. (see Kaplan, B.)—907(A)
—— (see Smith, T. S.)—654(L)
Davidson, Clifton R. (see Andrew, Alan)—876(L)
Davidson, J. P. and E. Feenberg. Deviations from *LS* coupling in spheroidal core nuclear model—856
Davis, Robert H. (see Cameron, John R.)—909(A)
—— (see Herb, R. G.)—897(A)
Davisson, J. W. (see Burstein, E.)—331(L)
Day, Robert B. Inelastic scattering of neutrons—908(A)
Dayhoff, Edward S., Sol Triebwasser, and Willis E. Lamb, Jr. Fine structure of the H atom—106
—— (see Triebwasser, Sol)—98
Dayton, Irving E. *Z*-dependence of pair production cross section at 1.33 and 2.62 Mev—544
de Borde, A. H. (see Burbidge, G. R.)—189
Dehmelt, H. G. (see Robinson, H. G.)—1305(L)
de Klerk, D., R. P. Hudson, and J. R. Pellam. Normal fluid concentration in liquid He II below 1°K—662(L)
——, **R. P. Hudson, and J. R. Pellam.** Second-sound velocity measurements below 1°K—326(L)
Delaney, C. F. G. and J. H. J. Poole. Half-life of Ca^{45}—529(L)
del Castillo, G. (see Chang, W. Y.)—408
del Río, C. S. and V. L. Telegdi. Inelastic nuclear scattering of photons by Rh^{103}—909(A)
Dennison, D. M. (see Ivash, E. V.)—895(A)
—— (see Gopalakrishnan, K.)—908(A)
Deverall, G. V., K. W. Meissner, and G. J. Zissis. Hfs of resonance lines of In I—895(A)
Dewdney, John W. (see Geiger, James S.)—621
Dezoteus, J. A. (see Coomes, E. A.)—894(A)
Diamond, R. M. Mo^{99}—1149(L)
Dicke, Robert H. Effect of collisions upon Doppler width of spectral lines—472
Dienes, G. J. Entropies of activation in metallic diffusion —185
—— (see Bartlett, J. H.)—848
Divatia, Ajay S. (see Cameron, John R.)—909(A)
—— (see Herb, R. G.)—897(A)
Donahue, D. J., K. W. Jones, M. T. McEllistrem, and H. T. Richards. Electrostatic analysis of nuclear reaction energies —824; 892(A)
Donaven, T. W. (see Kundu, D. N.)—1200
Donn, Bertram. Theory of interstellar grains—898(A)
Dousmanis, G. C. (see Sanders, T. M.)—1158(L)
Duckworth, Henry E. (see Geiger, James S.)—621
Dudley, J. M. (see Rosengren, J. W.)—603
Duerig, William H. and Jordan J. Markham. Rates of coloration of KCl and KBr during x-irradiation at 78°K—900(A)
Duffield, Robert B. and John R. Huizenga. Photofission and photoneutron emission in U—1040
—— **and L. M. Langer.** Decay of Zn^{69}—854
—— (see Huizenga, John R.)—893(A)
—— (see Langer, L. M.)—907(A)
Dugdale, J. S. and D. K. C. MacDonald. Thermal expansion of solids—832
DuMond, Jesse W. M. (see Henke, Burton)—1300(L)
Durbin, Richard P. (see Goodell, Warren F., Jr.)—724
Dyke, W. P. and J. K. Trolan. Field emission: Large current densities, space charge, and vacuum arc—799

Eager, R. L. and D. B. Langmuir. Self-diffusion of Ta—911(A)
Early, Harold C. (see Smith, Haldon L.)—338(A)
Easterday, Harry T. and Heinrich A. Medicus. Isomeric transitions in Tc^{93} and Tc^{96}—752
Eatherly, W. P. and J. D. McClelland. Anisotropic susceptibility of polycrystalline graphite—661(L)
Edge, R. D. (see Carver, J. H.)—658(L)
Eichholz, G. G. Characteristics of thin plastic scintillation phosphors—912(A)
—— Half-life of W^{187}—525(L)
Einstein, Albert. Unified field theory—321(L)
Eisberg, R. M. (see Igo, G. J.)—879(L)
Eisenberg, Y. (see Barrett, Paul H.)—656(L)
Ekstein, H. Multiple scattering and radiation damping—490
Elenbass, W. Similarity conditions of high pressure discharges—338(A)
Elliott, R. J. Paramagnetism of uranyl-like ions—659(L)
Elson, R., W. Bentley, A. Ghiorso, and Q. Van Winkle. Thermal neutron fission and capture cross section of U^{232} —320(L)
Enatsu, H. Mass relation of heavy particles—1304(L)
Engelkemeir, D. W. (see Wagner, F., Jr.)—502
Eppling, Frederic J. (see Cameron, John R.)—909(A)
—— (see Jackson, H. L.)—365
Epstein, Saul T. Causal interpretation of quantum mechanics —319(L)
Esaki, Leo. Properties of thermally treated Ge—1026
—— Thermal treatment of Si rectifiers—398

Faire, A. C. (see Fundingsland, O. T.)—337(A)
Falconer, John I., Jr. Irregularities in radiation along positive column of high pressure Hg arc—342(A)
Falk, C. E. (see Hafner, E. M.)—204
Falkoff, David L. Quantum-mechanical methods in classical physics—340(A)
Faust, W. R. (see Scherrer, V. E.)—1268
Feenberg, E. (see Davidson, J. P.)—856

Feingold, A. M. Ground state of N^{14}—318(L)
Feld, Bernard T. Angular and energy distributions in photomeson production—330(L)
Feldman, David. Charge independence of nuclear forces—1159(L)
Ferguson, Eldon E. Normal coordinate analysis of 1, 3, 5-trifluoro-benzene—895(A)
Fields, R. E., R. L. Becker, and R. K. Adair. Total n-p scattering cross section at 2.5 Mev—908(A)
—— (see Walt, M.)—1271
Firor, J. W. (see Fonger, W. H.)—891(A)
Fischer, Heinz. Hydrogen spectra from channel of spark discharge with increased energy—336(A)
Fite, Wade L. Production of negative ions and noise in negative ion beams—411
Fivel, Daniel I. (see Plass, Gilbert N.)—898(A)
Flammer, Carson. Variational methods for periodic lattices and artificial dielectrics—1298(L)
Foldy, Leslie L. New rigorous lower bound on range of triplet n-p interaction—1251
Fong, Peter. Asymmetric fission—332(L)
Fonger, W. H., J. W. Firor, and J. A. Simpson. Recurring daily cycles of nucleonic component intensity—891(A)
Foote, H. L., Jr. (see Sailor, V. L.)—904(A)
Fosdick, L. D. and H. M. James. Approximate treatment of order-disorder transitions in simple cubic Ising lattice—901(A)
Foster, John S., Jr., E. O. Lawrence, and E. J. Lofgren. High vacuum, high speed ion pump—338(A)
Fowler, R. G., W. R. Atkinson, and R. J. Lee. Shock waves in expansion of low pressure sparks—336(A)
—— **and H. C. Rose.** Ion concentrations in shock-type spark discharge tubes—906(A)
—— (see Atkinson, W. R.)—906(A)
Fowler, William A. (see Kraus, Alfred A., Jr.)—299
Fox, R. E., W. M. Hickam, and T. Kjeldaas, Jr. Ionization probability curves near threshold—336(A); 555
Francis, A. E., J. J. G. McCue, and Clark Goodman. Inelastic scattering of neutrons by Cd^{111}—1232
Francis, Norman C. Photoproduction of π^0-mesons in H and D—766
—— **and Kenneth M. Watson.** Relation between photoproduction and scattering cross sections for π-mesons in complex nuclei—328(L)
Frank, V. and O. Gram Jeppesen. Hall coefficient of Ca—1153(L)
Frankl, D. R. and T. A. Read. Effects of F-centers on internal friction of rocksalt single crystals—663(L)
Franklin, Alan D. and Ami E. Berkowitz. Approach to saturation in dilute ferromagnetics—1171
Fred, Mark, and Frank S. Tomkins. Nuclear spin of $_{95}Am^{241}$—318(L)
Freedman, Melvin S., Arthur H. Jaffey, Frank Wagner, Jr., and Jack May. Radiations of Th^{231}(UY)—302
—— (see Wagner, F., Jr.)—502
Freeman, B. E. and J. L. McHale. Barrier penetration effects for light nuclei—223
French, A. P. (see Kraus, Alfred A., Jr.)—299
Fretter, W. B., M. M. May, and M. P. Nakada. V^0 particles—168
Friedman, Bernard (see Borowitz, Sidney)—441
Frieman, E. A. and L. Motz. p-p reaction and energy production in sun—648
Fry, W. F. Li^9 disintegration in photographic emulsion—325(L)
Fukuda, H. Multiple meson production by high energy nucleon-nucleon collisions—842
Fulbright, H. W., D. A. Bromley, and J. A. Bruner. Angular distributions of protons from $F^{19}(d,p)F^{20}$—892(A)
—— (see Bromley, D. A.)—396
Fumi, Fausto G. and Robert G. Parr. Electronic spectra of diatomic molecules: O_2 molecule—895(A)
Fundingsland, O. T., A. C. Faire, and A. J. Penico. Microwave method for measuring mean energy transfer per collision and velocity dependence of collision cross section for slow electrons in gases—337(A)
Furst, Milton and Hartmut Kallmann. Energy transfer in complex solutions—912(A)
——, **Hartmut Kallmann, and Bernard Kramer.** Absolute light emission efficiency of crystal anthracene for γ-ray excitation—416

Gager, W. B. (see Smith, T. S.)—654(L)
Galonsky, Aaron I. (see Jackson, Herbert L.)—365; 370
Gandy, Harold W. Cathodoluminescent studies of (BaSr)O—912(A)
Gehman, S. D. Physics of rubber—341(A)
Geiger, James S., Benjamin G. Hogg, Henry E. Duckworth, and John W. Dewdney. Zr^{92}—Mo^{92} and Zr^{94}—Mo^{94} pairs and Zr^{96}—Mo^{96}—Ru^{96} triplet—621
Gelinas, R. W. and S. S. Hanna. Magnetic analysis of d-Be reactions—483
Geltman, S. and H. Margenau. Theory of mobility of He_2^+ in He—337(A)
Ghiorso, A. (see Elson, R.)—320(L)
—— (see Hulet, E. K.)—878(L)
—— (see Rasmussen, J. O., Jr.)—33
Gilbert, F. C. (see Colgate, S. A.)—790
Gilley, L. W. (see Lagemann, R. T.)—906(A)
Gilvarry, J. J. Relativity precession of asteroid Icarus—1046
Gingrich, N. S., C. G. Shull, and M. K. Wilkinson. Magnetic structure of Mn antimonide—910(A)
Glauber, Roy and Verner Schomaker. Theory of electron diffraction—667
Glockler, George (see McCulloh, K. E.)—145
Golay, Marcel J. E. (see Keck, Paul H.)—1297(L)
Goldberg, E. Levels of Al^{26} from $Mg^{24}(d,n)Al^{25}$—760
—— (see Jackson, H. L.)—365
Goldberg, Joshua N. Strong conservation laws and equations of motion in covariant field theories—263
——, **John W. Trischka, and Peter G. Bergmann.** Electric resonance transitions in tapered electric field—278
Goldemberg, J. and L. Katz. Resolution of "photon difference method"—1300(L)
Goldhaber, Gerson. Elastic pion-hydrogen scattering in photographic emulsions—1187
Goldhaber, M. Core isomerism—remarks on Mo^{93m}—1146(L)
—— (see Kraushaar, J. J.)—1081
Goldman, L. M. Elastic scattering of 6.5-Mev protons from Cu—349
Goldschmidt-Clermont, Y., L. S. Osborne, and M. B. Scott. Photoproduction of neutral mesons in H—329(L)
Goldstein, Herbert, J. Ernest Wilkins, Jr., and L. V. Spencer. Systematic calculations of γ-ray penetration—1150(L)
Goldstein, Louis. Theory of liquid He II—597
Gonzales, O. D. (see White, David)—593
Goodell, Warren, F., Jr., Howard H. Loar, Richard P. Durbin, and William W. Havens, Jr. Neutron energy distribution from proton bombardment of Li, Be, and C at 375 Mev—724
Goodenough, John B. Theory of deviation from close packing in hexagonal metal crystals—282
Goodman, Clark (see Francis, A. E.)—1232
Gopalakrishnan, K., A. deShalit, and J. W. Mihelich. Neutron deficient isotopes of Hg—908(A)
Gora, E. Lower limit for interaction time in photon-photon scattering—913(A)
Gordon, M. M. and J. G. Jones. Variational procedure for electron-hydrogen scattering—913(A)
Gordy, W. (see Robinson, H. G.)—1305(L)

Goucher, F. S. and M. B. Prince. Interpretation of α-values in p-n junction transistors—651
Graves, Elizabeth R. and Louis Rosen. Distribution in energy of neutrons from interaction of 14-Mev neutrons with some elements—343
Green, H. S. First-order meson wave equations—965
—— (see Messel, H.)—315(L)
Gregory, Christopher. Conservation of quanta for non-local fields—1199
Griffith, Wayland and David E. Brickl. Diffraction of strong shock waves—451
Grodzins, Leon (see Chang, W. Y.)—408
Gui, K. E. New type of rubber fatigue test—341(A)
Gunst, S. B. (see Page, L. A.)—1273
Güttinger, Werner. Quantum field theory in light of distribution analysis—1004
Hafner, E. M., W. F. Hornyak, C. E. Falk, G. Snow, and T. Coor. Total n-p scattering cross section at 4.75 Mev—204
Hagstrum, Homer D. Effect of adsorption of common gases on electron ejection by noble gas ions—338(A)
—— Electron ejection from Mo by He^+, He^{++}, and He_2^+—244
Hales, R. W. and B. J. Moyer. Atomic number dependence of neutral meson yield from proton bombardment—1047
Haley, Floyd C. and Donald H. Andrews. Anomalous critical current effect in superconducting NbN—821
Hall, G. L. and F. S. Conant. Firestone shear flexometer—342(A)
Hall, Harry H., Daniel T. Hedden, and Thomas J. Turner. Activation energies of Se-Te alloys—340(A)
Hamermesh, Bernard. Measurement of neutron-capture γ-rays—896(T)
—— (see Kimball, Clyde)—1306(L)
Hamming, R. W. (see Bozorth, R. M.)—865
Hanna, S. S. (see Class, C. M.)—877(L)
—— (see Gelinas, R. W.)—483
Hannam, H. J. (see Lindemann, W. W.)—900(A)
Hanson, A. O. (see Whalin, E. A.)—324(L)
Hanson, H. P. Mixing of states and antiferromagnetism—1154(L)
Hardy, George F. and John K. Hulm. Superconducting silicides and germanides—884(L)
Härm, Richard (see Spitzer, Lyman, Jr.)—977
Harris, E. G. and M. A. Melkanoff. Quadrupole moment of Li^7—914(A)
Harris, Gerard G. and T. J. B. Shanley. γ-rays from μ-meson capture in Pb—983
Harris, S. P. Neutron resonances in Xe—904(A)
Harrison, F. B. (see Jackson, Jasper A.)—322(L)
Hart, Edward W. Structure of deformation bands—521(L)
Harth, Eric M. (see Birnbaum, Milton)—897(A)
Hatch, Albert J. and H. Bartel Williams. Theory of high frequency secondary electron resonance discharge mechanism—339(A)
—— (see Williams, H. Bartel)—339(A)
Havens, William W., Jr. (see Goodell, Warren F., Jr.)—724
Haxby, B. V. and P. Wargo. Effect of evaporation products from BaO coated cathode on secondary emission of MgO thin films—893(A)
Haynes, S. K. (see Broyles, C. D.)—715; 912(A)
Hedden, Daniel T. (see Hall, Harry H.)—340(A)
Hedgran, A. (see Lindström, G.)—1303(L)
Hellund, E. J. Decay of resonance radiation by spontaneous emission—919
Henke, Burton and Jesse W. M. DuMond. Low angle x-ray diffraction with long wavelengths—1300(L)
Herb, R. G., Robert H. Davis, Ajay S. Divatia, and D. Saxon. Evapor-ion pump—897(A)
Herlin, Melvin A. (see Mayper, Victor, Jr.)—523(L)
Herman, Frank and Joseph Callaway. Electronic structure of Ge crystal—518(L)
Herzog, L. F. (see Aldrich, L. T.)—631
Hickam, W. M. (see Fox, R. E.)—336(A); 555
Hildebrand, Roger H. Charge-independence in meson production—904(T)
—— Neutral meson production in n-p collisions—1090
Hill, David Lawrence and John Archibald Wheeler. Nuclear constitution and interpretation of fission phenomena—1102
Hill, R. D. and J. W. Mihelich. Probable existence of $E3+M4$ mixture in isomeric transition—323(L)
—— (see Swan, J. B.)—907(A)
Hill, Richard W. (see Cameron, John R.)—909(A)
—— (see Jackson, H. L.)—365
Hjalmar, Elis and Hilding Slätis. Q-values for $N^{14}(\alpha,p)O^{17}$—1151(L)
Hobson, J. P. and W. A. Nierenberg. Statistics of two-dimensional, hexagonal net—662(L)
Hoffman, Banesh. Relativity of size—49
—— Similarity theory of relativity and Dirac-Schrödinger theory of electrons—52
Hofstadter, Robert (see Hudson, A.)—1309(L)
—— (see Kantz, Asher)—607
Hogg, Benjamin G. (see Geiger, James S.)—621
Holmes, D. K. Application of cellular method to Si, erratum—1308(L)
Holroyd, L. V. (see Affleck, J. H.)—893(A)
Holt, J. R. and T. N. Marsham. States of S^{33} and Si^{29} from (d,p) stripping—665(L)
Holyk, W. K. (see Aldrich, L. T.)—631
Hope, J. Tensor force interaction between shell closed except for single vacancy and external nucleon—884(L)
Hornyak, W. F. (see Hafner, E. M.)—204
Horton, G. K. and R. T. Sharp. Approximate wave functions for unbound relativistic particles in Coulomb field—885(L)
Hotz, H. P. (see Porter, F. T.)—903(A); 938
Houde, A. L. (see Brock, E. G.)—851
Huddleston, Charles M. and Allan C. G. Mitchell. Nuclear spectra of Rb^{82} and Rb^{84}—903(A)
Hudson, A. and R. Hofstadter. Energy loss of cosmic-ray μ-mesons in NaI crystals, erratum—1309(L)
Hudson, D. E. (see Shaw, William C.)—900(A)
Hudson, R. P. (see de Klerk, D.)—326(L); 662(L)
Hughes, D. J. (see Palevsky, H.)—910(A)
—— (see Seidl, F. G. P.)—897(A)
Hughes, Vernon (see Perl, William)—886(L)
Huizenga, J. R. Neutron binding-energies of heavy elements and some applications—904(T)
—— **and Robert B. Duffield.** Relative photofission and photoneutron cross sections for U^{238}—893(A)
—— (see Duffield, Robert B.)—1042
—— (see Wagner, F., Jr.)—502
Hulet, E. K., S. G. Thompson, and A. Ghiorso. Spontaneous fission rate of Cf^{246}—878(L)
Hulm, John K. (see Hardy, George F.)—884(L)
—— (see Matthias, B. T.)—439
Hunt, R. Allen and Robert H. Schuler. Saturation in x-ray coloration of corundum single crystals—664(L)
Hunt, S. E. and W. M. Jones. Absolute determination of resonant energies for radiative capture of protons by B, C, F, Mg, and Al below 500 kev—1283
Huntington, H. B. Extension of Makinson's theory of photoelectric emission to periodic potential—357
—— **and L. Apker.** Transition probability for photoelectric emission from semiconductors—352
Hutchison, Clyde A., Jr., and Leonard S. Singer. Paramagnetic resonance absorption in salts of V and Mn—256
Huxford, W. S. (see Olsen, H. N.)—336(A)

Igo, G. J., D. D. Clark, and R. M. Eisberg. Statistical fluctuations in ionization by 31.5-Mev protons—879(L)
Ivash, E. V. and D. M. Dennison. Molecular constants of CH_3OH—895(A)
Ivey, Henry F. Spectral location of absorption due to color centers in alkaline earth halide crystals—322(L)

Jackson, Herbert L. and Aaron I. Galonsky. Excited states of N^{13} nucleus—370
——, **A. I. Galonsky, F. J. Eppling, R. W. Hill, E. Goldberg, and J. R. Cameron.** $C^{12}(p,p)C^{12}$ differential cross section—365
Jackson, J. David and Harry Schiff. Electron capture by protons passing through H_2—359
Jackson, Jasper A. and F. B. Harrison. Slow component in decay of scintillation phosphors—322(L)
Jacobsohn, B. A. Test for charge independence in high energy nucleon-nucleon scattering—881(L)
Jaffe, A. A. and S. G. Cohen. Disintegration of RaD—454
Jaffe, Hans (see Cook, W. R., Jr.)—1297(L)
Jaffey, Arthur H. (see Freedman, Melvin S.)—302
James, Hubert M. (see Fosdick, L. D.)—901(A)
—— (see Krieger, Theodore J.)—901(A)
Jamgochian, E. (see Lehovec, K.)—20
Jensen, Erling. Coincidence measurements with β-ray spectrometers—909(T)
Jentschke, W. K. (see Allen, James S.)—902(A)
—— (see Remley, M. E.)—1194
Jeppesen, O. Gram (see Frank, V.)—1153(L)
Johnson, C. Peter, Jr. Unified field theory—320(L)
Johnson, J. B. Experiments and thoughts on secondary emission—902(T)
Johnson, N. R. (see Sheline, R. K.)—520(L)
Johnson, Vivian A. Galvanomagnetic effects in semiconductors—910(T)
—— **and W. J. Whitesell.** Theory of magnetoresistive effect in semiconductors—941
Johnston, H. L. (see White, David)—593
Jones, E. (see Jorgensen, T.)—897(A)
Jones, J. G. (see Gordon, M. M.)—913(A)
Jones, K. W. (see Donahue, D. J.)—824; 892(A)
Jones, L. C., A. B. Bushkovitch, C. A. Potter, and A. G. Rouse. Variation of mutual collision diameters with mix ratio in binary mixtures in microwave pressure broadening—895(A)
Jones, Mark W. Respiration of plant tissue cultures as function of x-ray dose—899(A)
Jones, W. M. (see Hunt, S. E.)—1283
Jorgensen, T., E. Jones, and C. J. Cook. Extrapolated ionization ranges for 10- to 250-kv protons in various gases—897(A)
Juenker, D. W., G. S. Colladay, and E. A. Coomes. Analysis of Schottky deviation for highly refractory metals—894(A)
Jung, J. J. (see Cüer, P.)—1151(L)

Kahn, Arnold H. and C. Kittel. *F*-center wave functions and electronic *g*-values in KCl crystals—315(L)
Kallmann, Hartmut, Bernard Kramer, and Arnold Perlmutter. Induced conductivity in luminescent powders. II. Ac impedance measurements—700
—— (see Furst, Milton)—416; 912(A)
Kane, W. R. (see Broida, H. P.)—1053
Kantz, Asher and Robert Hofstadter. Electron-induced showers in Cu—607
Kaplan, B. and J. G. Daunt. Current noise in partially superconducting resistors at temperatures down to 2°K—907(A)
Katcoff, S. (see Caretto, A. A., Jr.)—1267
Katz, L. (see Goldemberg, J.)—1300(L)
Keck, Paul H. and Marcel J. E. Golay. Crystallization of Si from floating liquid zone—1297(L)
Keesom, P. H., K. Lark-Horovitz, and N. Perlman. Influence of neutron bombardment on low temperature atomic heat of Si—900(A)
Keller, Joseph B. Bohm's "interpretation of quantum theory in terms of 'hidden' variables"—1040
Kenty, Carl. Afterglow spectra observable in incandescent lamps—336(A)
—— **and D. A. Larson.** Enhancement of green continuum of Hg by rare gas—180
Kerman, R. O., W. E. Kreger, and P. G. Kruger. *p-p* scattering at 5.77 Mev using photographic techniques—908(A)
Kimball, Clyde and Bernard Hamermesh. Activation cross sections measured with Sb–Be photoneutrons—1306(L)
King, D. T., Nathan Seeman, and Maurice M. Shapiro. Mass measurements of heavy mesons—891(A)
King, J. S. and W. C. Parkinson. Angular distribution of protons from V^{52}—1080
Kington, J. D., J. K. Bair, R. R. Carlson, and H. B. Willard. Mass difference $Si^{27}-Al^{27}$—530(L)
Kinsey, B. B. and G. A. Bartholomew. Neutron capture γ-rays from Ti, Cr, Fe, Ni, and Zn—375
—— (see Bartholomew, G. A.)—386
Kip, A. F., C. Kittel, A. M. Portis, R. Barton, and F. H. Spedding. Microwave resonance absorption in Gd metal—518(L)
Kitagaki, T. Focusing method for large accelerators—1161(L)
Kittel, C. (see Kahn, Arnold H.)—315(L)
—— (see Kip, A. F.)—518(L)
Kjeldaas, T., Jr. (see Fox, R. E.)—336(A); 555
Klein, Abraham, Symmetric pseudoscalar theory of nuclear forces—1158(L)
Klick, Clifford C. Luminescence and photoconductivity in CdS at absorption edge—274
Kofoed-Hansen, O. and Aage Winther. Cross terms in β-decay—526(L)
Kofsky, Irving L. Crystal diodes in electronics laboratory—340(A)
Koster, G. F. Localized functions in molecules and crystals—67
Kramer, Bernard (see Furst, Milton)—416
—— (see Kallmann, Hartmut)—700
Kraus, Alfred A., Jr., A. P. French, William A. Fowler, and C. C. Lauritsen. Angular distribution of γ-rays and short range α-particles from $N^{15}(p,\alpha\gamma)C^{12}$—299
Kraushaar, J. J. and M. Goldhaber. Direction and polarization correlations of successive γ-rays—1081
Kreger, W. E. (see Kerman, R. O.)—908(A)
Krieger, Theodore J. and Hubert M. James. Theory of successive rotational transitions in crystals—901(A)
Krone, R. W. (see Teener, J. W.)—892(A)
Krotkov, R. V. (see Scheidegger, A. E.)—1096
Kruger, P. G. (see Kerman, R. O.)—908(A)
—— (see Remley, M. E.)—1194
Krumhansl, James A. and N. Schwartz. Calculation of *F*-center energy levels—1154(L)
—— (see Steele, Earl L.)—901(A)
Kruse, U. E., N. F. Ramsey, and B. J. Malenka. Electric scattering of deuterons—655(L)
Kruskal, Martin. Instabilities of completely ionized plasma—335(A)
Kundu, D. N., T. W. Donaven, M. L. Pool, and J. K. Long. Nuclear reactions with 21-Mev He^3 in cyclotron—1200
Kurşunoğlu, B. (see Rickayzen, G.)—522(L)

Lagemann, R. T. and L. W. Gilley. Ultrasonic velocity, density, and compressibility of supercooled H_2O and D_2O—906(A)
Lamb, Willis E., Jr. (see Dayhoff, Edward S.)—106
—— (see Triebwasser, Sol)—98
Lampert, Murray A. and Alan D. White. New microwave technique for study of discharges in gases—337(A)

Landon, H. H. (see Sailor, V. L.)—904(A)
Langer, L. M., R. B. Duffield, and C. W. Stanley. Radioactivity of Cs^{135}—907(A)
—— (see Ames, D. P.)—903(A)
—— (see Duffield, R. B.)—854
Langmuir, David B. Observations on "direct-current etch"—911(A)
—— (see Eager, R. L.)—911(A)
Larach, Simon and John Turkevich. Interaction of Mn activator ions in Zn-orthosilicate phosphors—1060
Lark-Horovitz, K. (see Keesom, P. H.)—900(A)
Larson, D. A. (see Kenty, C.)—180
Lauritsen, C. C. (see Kraus, Alfred A., Jr.)—299
Lawrance, R. Temperature dependence of drift mobility in Ge—1295(L)
Lawrence, E. O. (see Foster, John S., Jr.)—338(A)
LeBlanc, J. M., W. H. Nester, D. W. Martin, M. K. Brice, and J. M. Cork. γ-radiation from radioactive Cs^{136}—907(A)
—— (see Cork, J. M.)—1291
Lee, R. J. (see Fowler, R. G.)—336(A)
Lehovec, K., C. A. Accardo, and E. Jamgochian. Light emission produced by current injected into green SiC crystal—20
Leighton, R. B., S. D. Wanlass, and C. D. Anderson. Decay of V^0-particles—148
Lévêque, Pierre (see Coryell, Charles D.)—903(A)
Levine, M. A. (see Bostick, W. H.)—339(A)
Levinger, J. S. Effects of radioactive disintegrations on inner electrons of atom—908(A)
Levinson, Norman. Certain explicit relationships between phase shift and scattering potential—755
Lew, Hin. Ground state hfs and nuclear magnetic moment of Pr—530(L)
—— **and Günter Wessel.** Hfs of ground state of Al—894(A)
Lewis, H. W. (see Simmons, B. E.)—905(A)
Liang, C. Y. (see Nielsen, J. Rud)—895(A)
Lindemann, W. W. and H. J. Hannam. Flicker noise caused by interface layer—900(A)
Lindenfeld, P., A. Sachs, and J. Steinberger. Internal pair production of γ-rays of mesonic origin; alternate modes of π^0-decay—531
Lindner, Manfred. Heavy isotopes of Mg and Si—1150(L)
Lindström, G., A. Hedgran, and D. E. Alburger. Precision measurement of Co^{60} γ-radiation—1303(L)
Livingston, M. S. Design considerations for very high energy accelerators—339(T)
Loar, Howard H. (see Goodell, Warren F., Jr.)—724
Lockett, E. E. and E. Bowell. Thermal neutron absorption cross section of Sc—657(L)
Lofgren, E. J. (see Foster, John S., Jr.)—338(A)
Long, J. K. (see Kundu, D. N.)—1200
Luborsky, Fred E. and Stanley I. Reynolds. Frequency spectra from point-to-plane corona—338(A)
Lyon, W. S. Neutron capture cross sections for production of Sc^{46} and Sr^{85}—1307(L)
Lyons, Harold (see Nuckolls, R. G.)—1101
Lyons, W. James. Viscoelastic properties as functions of distribution of activation energies—342(A)

MacDonald, D. K. C. (see Dugdale, J. S.)—832
MacDonald, William M. (see Richardson, John M.)—913(A)
Madansky, L. (see Battey, James)—182
—— (see Bolgiano, P.)—679
Madrazo, Raymond, Jr. (see Antonoff, George)—899(A)
Maerker, R. E. and R. D. Birkhoff. Experimental K to $L+M$ ratios for internal conversion lines—1159(L)
Malenka, B. J. (see Kruse, U. E.)—655(L)
Mandeville, C. E., E. Shapiro, R. I. Mendenhall, E. R. Zucker, and G. L. Conklin. γ-radiations from Zr^{95} and Nb^{95}—559
Mapother, Dillon. Effect of x-ray irradiation on self-diffusion coefficient of Na in NaCl—1231
Margenau, H. (see Geltman, S.)—337(A)
Markham, Jordan J. Second-order acoustic fields: relations between energy and intensity—972
—— (see Duerig, William H.)—900(A)
Marsham, T. N. (see Holt, J. R.)—665(L)
Martin, André and Loup Verlet. p-p scattering at intermediate energies—519(L)
Martin, D. W. (see Cork, J. M.)—1291
—— (see LeBlanc, J. M.)—907(A)
Martin, H. C. and R. F. Taschek. (n,γ) and $(n,2n)$ reactions in I—1302(L)
Maryott, A. A. (see Birnbaum, G.)—895(A)
Matland, C. G. Quenching of Hg resonance radiation (2537A) by N_2—338(A)
Matossi, Frank and Sol Nudelman. Influence of electric fields on luminescence—660(L)
Matsuda, H. (see Ogata, K.)—27; 333(L)
Matthias, B. T. and J. K. Hulm. Superconducting properties of $CoSi_2$—439
Mattson, R. H. and A. van der Ziel. Shot noise in Ge filaments—899(A)
Max, L. W. (see Taylor, T. Smith)—899(A)
May, Jack (see Freedman, Melvin S.)—302
May, M. M. (see Fretter, W. B.)—168
Mayper, Victor, Jr., and Melvin A. Herlin. Second-sound velocity below 1°K as function of pressure—523(L)
McClelland, J. D. (see Eatherly, W. P.)—661(L)
McClure, G. W. Specific primary ionization of H_2, He, Ne, and A by high energy electrons—335(A)
McCue, J. J. G. (see Francis, A. E.)—1232
McCulloh, K. E. and George Glockler. Electronic emission spectrum of $C^{13}O^{16}$—145
McCusker, C. B. A., H. Messel, D. D. Millar, and N. A. Porter. Experimental investigation of nucleon cascade in water—1172
McEllistrem, M. T. (see Donahue, D. J.)—824; 892(A)
McFarland, Charles E., M. M. Bretscher, and F. B. Shull. Magnetic analysis of protons from $Cr^{52}(d,p)Cr^{53}$ and $Ni^{59}(d,p)Ni^{60}$—892(A)
—— **and Franklin B. Shull.** Magnetic analysis of $Sr^{88}(d,p)Sr^{89}$—489
McFarland, Robert H. and Robert E. Swanson. Sensitized fluorescence studies using photomultiplier detection method—911(A)
—— (see Swanson, Robert E.)—911(A)
McHale, J. L. (see Freeman, B. E.)—223
Medicus, G. and G. Wehner. Investigation of cathode sputtering by means of probe measurements—339(A)
—— (see Wehner, G.)—339(A)
Medicus, Heinrich A. (see Easterday, Harry T.)—752
Meinke, W. Wayne (see Schott, G. L.)—1156(L)
Meissner, K. W. (see Deverall, G. V.)—895(A)
Melkanoff, M. A. (see Harris, E. G.)—914(A)
Mendenhall, R. I. (see Mandeville, C. E.)—559
Merzbacher, E. (see Simmons, B. E.)—905(A)
Messel, H. and H. S. Green. Suggested scheme for meson production—315(L)
—— (see McCusker, C. B. A.)—1172
Meyer, D. I. and F. H. Schmidt. Precise measurement of "F" line of ThB—908(A)
Mihelich, J. W. Disintegration of Re^{188m}—907(A)
—— (see Gopalakrishnan, K.)—908(A)
—— (see Hill, R. D.)—323(L)
Millar, D. D. (see McCusker, C. B. A.)—1172
Miller, R. F. Dipole moment of β-propiolactone—341(A)
Miller, William (see Motz, J. W.)—968
Mitchell, Allan C. G. (see Caird, R. S.)—573; 903(A)
—— (see Huddleston, Charles M.)—903(A)
Mize, J. P. and D. J. Zaffarano. β-spectrum of S^{35}—902(A)

Mizushima, Masataka (see Putcha, Venkateswarlu)—896(A)
Molnar, J. P. (see Phelps, A. V.)—1202
Moore, Marvin G. Quasi-relativistic theory of gravitation —587
Moorhouse, R. G. Pair creation in intermediate coupling theory—958
Morrison, S. R. Adsorption of O_2 on ZnO—900(A)
Morrow, J. C. Vapor-liquid equilibria in He^3-He^4 solutions —1034
Moses, H. E. Canonical transformation for electron-positron field coupled to time-independent electromagnetic field—115
Moszkowski, Steven A. Lifetimes of nuclear isomers—474
Mottelson, Ben R. (see Bohr, Aage)—316(L)
Motz, J. W., William Miller, and H. O. Wyckoff. 11-Mev thick target bremsstrahlung—968
Motz, Lloyd. Gauge invariance and classical electrodynamics —60
—— (see Frieman, E. A.)—648
Mower, Lyman. Tables for second Born approximation scattering from various potential fields—947
Moyer, B. J. (see Hales, R. W.)—1047

Nakada, M. P. (see Fretter, W. B.)—168
Nakamura, Seitaro. Meson theory of β-decay and ΔL-forbidden transitions—16
Nereson, Norris and Sperry Darden. Average neutron total cross sections in 3- to 12-Mev region—775
Nester, W. H. (see Cork, J. M.)—1291
—— (see LeBlanc, J. M.)—907(A)
Newton, J. O. and B. Rose. γ-radiation from Am^{241}—1157(L)
Nicodemus, David B. and Hans H. Staub. Fission neutron spectrum of U^{235}—1288
Niday, J. B. (see Turkevich, A.)—552
Nielsen, J. Rud, C. Y. Liang, D. C. Smith, and Morris Alpert. Vibrational spectra and calculated thermodynamic properties of CCl_3CF_2Cl and CCl_3CFCl_2—895(A)
Nierenberg, W. A. (see Hobson, J. P.)—662(L)
Nomura, K. C. Secondary electron emission of MgO single crystals with excess O_2—894(A)
Novey, T. B. Experimental energy and angular distributions of inner bremsstrahlung—672
Nuckolls, R. G., L. J. Rueger, and Harold Lyons. Microwave absorption spectrum of ND_3—1101
Nudelman, Sol (see Matossi, Frank)—660
Nye, H. A. Diamagnetism of enclosed electron gas—1305(L)

Oakley, D. C. (see Walker, R. L.)—1301(L)
Oberly, J. J. (see Burstein, E.)—331(L)
Ogata, K. and H. Matsuda. Atomic mass of P^{31}—333(L)
—— **and H. Matsuda.** Masses of light atoms—27
Ohtsuka, Taiichiro (see Waniek, R. W.)—882(L);1307
Okamura, Toshiko, Yosiharu Torizuka, and Muneyuki Date. Paramagnetic resonance in copper acetate at 47 000 Mc/sec—525(L)
Okazaki, A. (see Adair, R. K.)—1165
—— (see Becker, R. L.)—904(A)
—— (see Walt, M.)—1271
Olbert, S. (see Annis, Martin)—1216
Olsen, H. N. and W. S. Huxford. Time variation of ion concentration in flash discharge plasmas—336(A)
Olsen, K. M. (see Pfann, W. G.)—322(L)
O'Meara, F. E. Enhanced reactor—982
O'Rourke, R. C. Multiple Compton scattering of low energy γ-radiation—999
Osborne, Darrell W. (see Weinstock, Bernard)—787
Osborne, L. S. (see Goldschmidt-Clermont, Y.)—329(L)
Overhauser, Albert W. Paramagnetic relaxation in metals —689

Packard, R. G. Streaming potentials developed across porous diaphragms for sinusoidal flow—906(A)
Page, L. A., P. Stehle, and S. B. Gunst. Direct comparison of m/e for positron and electron—1273
Pake, G. E. (see Sands, R. H.)—896(A)
—— (see Townsend, J.)—606
—— (see Wilson, C. W., III)—896(A)
Palevsky, H., R. S. Carter, and D. J. Hughes. Magnetic inelastic scattering of neutrons in Fe—910(A)
—— (see Seidl, F. G. P.)—897(A)
Parkinson, W. C. (see King, J. S.)—1080
Parmenter, R. H. Acousto-electric effect—990
Parr, Robert G. (see Fumi, Fausto G.)—895(A)
Parzen, G. Electronic energy bands in metals—237
—— **and T. Wainwright.** Calculation of energy bands in crystals—901(A)
Paul, E. B. and R. L. Clarke. Yield of long-range α-particles from $F^{19}(p,\alpha)O^{16}$—892(A)
Pearlman, N. (see Keesom, P. H.)—900(A)
Peaslee, D. C. Fermi term in β-ν correlation—1148(L)
Pellam, John R. (see de Klerk, D.)—326(L); 662(L)
—— (see Weinstock, Bernard)—521(L)
Penico, A. J. (see Fundingsland, O. T.)—337(A)
Perl, William and Vernon Hughes. Non-radiative relativistic contribution to magnetic moment of $^3S_1$ He—886(L)
Perlmutter, Arnold (see Kallmann, Hartmut)—700
Petermann, A. Divergence of perturbation expansion—1160(L)
Peterson, R. W. Rate of evolution of constituents of oxide coated cathode as function of molar composition of coating —894(A)
Pfann, W. G. and K. M. Olsen. Purification and prevention of segregation in single crystals of Ge—322(L)
Phelps, A. V. and J. P. Molnar. Lifetimes of metastable states of noble gases—1202
Phillips, G. C. Accurate determination of disintegration energies—896(T)
Plass, Gilbert N. and Daniel I. Fivel. Contributions of Doppler effect to radiation exchange in stratosphere —898(A)
Platt, J. B. (see Camac, M.)—905(A)
—— (see Schulte, H. J.)—905(A)
Pool, M. L. (see Kundu, D. N.)—1200
Poole, J. H. J. (see Delaney, C. F. G.)—529(L)
Pope, N. K. Entropy of fusion of monatomic liquids—899(A)
Porter, F. T. and H. P. Hotz. Upper limit for atomic orbital electron ejection accompanying K capture in Fe^{55}—903(A); 938
—— (see Primakoff, H.)—903(A); 930
—— (see Whalen, J. A.)—902(A)
Porter, N. A. (see McCusker, C. B. A.)—1172
Portis, A. M. (see Kip, A. F.)—518(L)
Portnoy, W. M. (see Swann, J. B.)—907(A)
Potter, C. A. (see Jones, L. C.)—895(A)
Pound, R. V. (see Abragam, A.)—1306(L)
—— (see Watkins, G. D.)—658(L)
Pressly, E. C. Air mass between observer and outer space —654
Price, P. J. Macroscopic theory of superfluid He^3-He^4 mixtures—1209
Primakoff, H. and F. T. Porter. Atomic excitation and ionization accompanying orbital electron capture by nuclei —903(A); 930
—— (see Chang, C. H.)—910(A)
Prince, M. B. (see Goucher, F. S.)—651
Pruett, Charles H. (see Roggenkamp, Paul L.)—903(A)
Pugh, Emerson M. (see Schindler, Albert I.)—295
Putcha, Venkateswarlu and Masataka Mizushima. Possible microwave absorption in molecules belonging to point groups $D_{2d}=V_d$ and T_d—896(A)

Racah, G. and I. Talmi. Pairing property of nuclear interactions—913(A)
Rado, George T. Theory of microwave permeability tensor and Faraday effect in nonsaturated ferromagnetic materials —529(L)
Ramsey, Norman F. Pseudo-quadrupole effect for nuclei in molecules—527(L)
—— (see Kruse, U. E.)—655(L)
Rasetti, F. (see Battey, James)—182
—— (see Bolgiano, P.)—679
Rasmussen, J. O., Jr., S. G. Thompson, and A. Ghiorso. α-radioactivity in 82-neutron region—33
Raychaudhuri, Amalkumar. Arbitrary concentrations of matter and Schwarzschild singularity—417
Read, T. A. (see Frankl, D. R.)—663(L)
Reddan, M. J. Clean-up of He in arc discharge—339(A)
Remley, M. E., W. K. Jentschke, and P. G. Kruger. n-p scattering using organic crystal scintillation detectors—1194
Reynolds, Stanley I. (see Luborsky, Fred E.)—338(A)
Ribe, F. L. (see Battat, M. E.)—80
Rice, O. K. Irreversible processes with application to He II and Knudsen effect in gases—793
Richards, Hans Kohn. Measurement of ionizing radiation by frequency variation—897(A)
Richards, H. T. Level classification by resonance scattering of protons and alphas—909(T)
—— (see Donahue, D. J.)—824; 892(A)
Richardson, J. Reginald (see Sachs, Donald C.)—1163
Richardson, John M. and William M. MacDonald. Variation method in quantum statistics—913(A)
Richter, Harold G. (see Coryell, Charles D.)—903(A)
Rickayzen, G. and B. Kurşunoğlu. Unified field theory and Born-Infeld electrodynamics—522(L)
Roberts, J. H., W. O. Solano, D. E. Wood, and H. B. Billington. Measurement of energy of isotropic fast neutrons with Li^6 loaded emulsions—905(A)
—— (see Solano, W. O.)—892(A)
—— (see Weddell, J. B.)—891(A)
Robinson, H. G., H. G. Dehmelt, and W. Gordy. Pure nuclear quadrupole spectrum of Bi^{209} in Bi-triphenyl—1305(L)
Roggenkamp, Paul L., Charles H. Pruett, and Roger G. Wilkinson. Excited levels of Ti^{48}—903(A)
Rose, B. (see Newton, J. O.)—1157(L)
Rose, D. J. (see Allis, W. P.)—335(A)
Rose, H. C. (see Fowler, R. G.)—906(A)
Rosen, Louis (see Graves, Elizabeth R.)—343
Rosenblum, G. (see Stephens, W. E.)—893(A)
Rosengren, J. W. and J. M. Dudley. High energy photoproton production by 322-bremsstrahlung—603
Rothstein, Jerome. Solids subjected to constant rate of generation of lattice defects—901(A)
Rouse, A. G. (see Jones, L. C.)—895(A)
Ruby, Stanley L. (see Rustad, Brice M.)—880(L)
Ruderman, M. Pseudoscalar matrix element in β-decay—1227
Rueger, L. J. (see Nuckolls, R. G.)—1101
Rustad, Brice M. and Stanley L. Ruby. Correlation between electron and recoil nucleus in He^6 decay—880(L)

Sachs, A. (see Lindenfeld, P.)—531
Sachs, Donald C. and J. Reginald Richardson. Mean excitation potentials—1163
Sailor, V. L., H. L. Foote, Jr., and H. H. Landon. Slow neutron resonances in Sm and Y—904(A)
Salpeter, E. E. Lamb shift for H and D—92
—— (see Butler, S. T.)—891(A)
Salzman, F. Photopion production from single nucleon —913(A)
Sanders, T. M., Jr., A. L. Schawlow, G. C. Dousmanis, and C. H. Townes. Microwave spectrum of free OH radical —1158(L)
Sands, R. H. and G. E. Pake. Anomalous results in attempt to determine spin of Si^{29}—896(A)
Sard, R. D. Recent research on μ-mesons—909(T)
Savitt, J. Propagation of explosive produced air shocks —906(A)
Saxon, D. (see Herb, R. G.)—897(A)
Schawlow, A. L. (see Sanders, T. M.)—1158(L)
Scheidegger, A. E. and R. V. Krotkov. Relativistic statistical thermodynamics—1096
Scherrer, V. E., R. Theus, and W. R. Faust. γ-radiation from interaction of 14-Mev neutrons with Fe—1268
Schiff, Harry (see Jackson, J. David)—359
Schiller, Ralph (see Bergmann, Peter G.)—4
Schindler, Albert I. and Emerson M. Pugh. Hall effect of Cu-Ni alloys—295
Schmidt, F. H. (see Meyer, D. I.)—908(A)
Schmitt, Roman A. and Nathan Sugarman. U photofission yields—1155(L)
Schomaker, Verner (see Glauber, Roy)—667
Schott, G. L. and W. Wayne Meinke. Assignment of Y^{92} and Y^{94}—1156(L)
Schuler, Robert H. (see Hunt, R. Allan)—664(L)
Schulte, H. J., J. B. Platt, and M. Camac. X-rays from mesic C atom—905(A)
—— (see Camac, M.)—905(A)
Schwartz, H. M. Magnetic moments of odd-odd nuclei and strong spin-orbit coupling shell model—1293
Schwartz, N. (see Krumhansl, J. A.)—1154(L)
Schwetman, Herbert D. (see Williams, Corre)—899(A)
Scott, E. J. Technique for secondary electron emission measurements—894(A)
Scott, G. G. Gyromagnetic ratio of supermalloy—618
Scott, M. B. (see Goldschmidt-Clermont, Y.)—329(L)
Seagondollar, L. W. (see Teener, J. W.)—892(A)
Seeman, Nathan (see King, D. T.)—891(A)
Seidl, F. G. P., D. J. Hughes, and H. Palevsky. Velocity spectrometer using μsec neutron shutter—897(A)
Seitz, Frederick. Generation of F-centers at low temperatures —1299(L)
Sengupta, S. Non-existence of stable isobars with odd mass number—1296(L)
Seren, Leo (see Birnbaum, Milton)—897(A)
Shanley, T. J. B. (see Harris, Gerard G.)—983
Shapiro, E. (see Mandeville, C. E.)—559
Shapiro, Maurice M. (see King, D. T.)—891(A)
Sharp, R. T. (see Horton, G. K.)—885(L)
Shaw, William C., D. E. Hudson, and G. C. Danielson. Electrical characteristics of crystalline B—900(A)
Sheline, R. K. and N. R. Johnson. New long-lived Mg^{28} isotope—520(L)
Sherman, Noah. Diurnal variations in intensity of cosmic rays underground—25
Shockley, W. (see Benedict, T. S.)—1152(L)
Shull, C. G. (see Gingrich, N. S.)—910(A)
Shull, Franklin B. (see McFarland, Charles E.)—489; 892(A)
Simmons, B. E., H. W. Lewis, and E. Merzbacher. Production of characteristic x-rays by proton bombardment—905(A)
Simon, A. and T. A. Welton. Production of polarized particles in nuclear reactions—886(L)
Simpson, J. A. Properties of cosmic-ray intensity variations —891(T)
—— (see Fonger, W. H.)—891(A)
Singer, Leonard S. (see Hutchison, Clyde A.)—256
Slätis, Hilding (see Hjalmar, Elis)—1151(L)
Smith, D. C. (see Nielsen, J. Rud)—895(A)
Smith, Haldon L. and Harold C. Early. Rocket measurement of upper atmosphere density by Paschen's law—338(A)
Smith, J. F. and G. C. Danielson. Diffusion of Na in sodium tungsten bronze—911(A)
Smith, J. R. (see Cook, C. F.)—785

Smith, T. S., W. B. Gager, and J. G. Daunt. Properties of superconductors below 1°K—654
Snitzer, Elias. Charge states of He beam in H_2, He_2, air, and A_2—898(A); 1237
Snow, G. (see Hafner, E. M.)—204
Solano, W. O. and J. H. Roberts. Spin of 7.4-Mev state of Li^7—892(A)
—— (see Roberts, J. H.)—905(A)
Solmitz, Frank T. p-p scattering for nucleon isobar model—1295(L)
Sorenson, B. M. (see Ames, D. P.)—903(A)
Spedding, F. H. (see Kip, A. F.)—518(L)
Spencer, L. V. (see Goldstein, Herbert)—1150(L)
Spitzer, Lyman, Jr., and Richard Härm. Transport phenomena in completely ionized gas—977
Stanley, C. W. (see Langer, L. M.)—907(A)
Staub, Hans H. (see Nicodemus, David B.)—1288
Steele, Earl L. and James A. Krumhansl. Cellular calculation of band structure for BaO—901(A)
Steffen, Rolf M. Angular momenta of excited states of Pt^{196}—665(L)
—— Effect of chemical binding and phase on angular correlations—903(A)
Stehle, P. (see Page, L. A.)—1273
Stehney, Andrew F. and Nathan Sugarman. Characteristics of Br^{87}, a delayed-neutron activity—194
Stein, Robert P. Electrical fields in Crookes dark space of low pressure glow discharge in air and N_2—134
Steinberger, J. (see Lindenfeld, P.)—531
Stephens, W. E., M. E. Toms, E. E. Carroll, Jr. and G. Rosenblum. Energy distributions of photoprotons from heavy elements—893(A)
Sternheimer, R. M. Density effect for ionization loss in various materials, erratum—1309(L)
—— Energy loss of fast charged particle by Čerenkov radiation—1148(L)
Stout, Virgil L. Luminescence and thermionic emission of BaO—310
Strauch, Karl. Interaction of protons with free and bound neutrons in the 100-Mev region—340(T)
Sugarman, Nathan. Genetics of Ge^{78}–As^{78} fission chain—570
—— (see Schmitt, Roman A.)—1155(L)
—— (see Stehney, Andrew F.)—194
Summerfield, Mary B. Inexpensive, easily controlled process for developing 400-micron nuclear emulsions—340(A)
Swan, J. B., W. M. Portnoy, and R. D. Hill. Isomeric Pt^{193}—907(A)
Swanson, Don R Interpretation of high energy p-p scattering—740
—— Polarization effects in nucleon-nucleon scattering—749
Swanson, Robert E. and Robert H. McFarland. Intensity variations in sensitized fluorescence—911(A)
—— (see McFarland, Robert H.)—911(A)
Swenson, C. A. Blocked capillary method for determining melting pressures: Melting curve of He from 1.5° to 4°K—538
Swim, Richard T. Flow of He II through narrow slits—906(A)
Synge, J. L. Primitive quantization in relativistic two-body problem—467

Talmi, Igal. Evaluation of energy matrix of tensor forces—1065
—— (see Racah, G.)—913(A)
Tannenwald, Peter E. Disintegration of He by 90-Mev neutrons—508
Taschek, R. F. (see Martin, H. C.)—1302(L)
Taylor, Norman L. and T. Smith Taylor. Design and construction of universal test mattress—899(A)
Taylor, T. Smith and L. W. Max. Research on comfort, relaxation, and quality of sleep—899(A)
—— (see Taylor, Norman L.)—899(A)
Teasdale, Tom S. Frozen moments in superconducting sphere—907(A)
Teener, J. W., L. W. Seagondollar, and R. W. Krone. γ-rays from proton bombardment of Na^{23}—892(A)
Telegdi, V. L. (see del Rio, C. S.)—909(A)
Temmer, G. M. (see Bloembergen, N.)—883(L)
Thaler, R. M. (see Breit, G.)—1177
Theus, R. (see Scherrer, V. E.)—1268
Thomas, D. A. (see Broyles, C. D.)—715
Thompson, Lewis C. γ-rays produced by inelastic scattering of 14-Mev neutrons—905(A)
Thompson, S. G. (see Hulet, E. K.)—878(L)
—— (see Rasmussen, J. O., Jr.)—33
Thomson, Robb (see Bergmann, Peter G.)—400
Thulin, S. (see Alburger, D. E.)—1146(L)
Ting, Yu and Dudley Williams. Nuclear gyromagnetic ratios—595
Tobin, Ralph (see Birnbaum, Milton)—897(A)
Tollestrup, A. V. (see Walker, R. L.)—1301(L)
Tomita, Kazuhisa. States of solid CH_4 as inferred from nuclear magnetic resonance—429
Tomkins, Frank S. (see Fred, Mark)—318(L)
Tompkins, A. (see Turkevich, A.)—552
Toms, M. E. (see Stephens, W. E.)—893(A)
Torizuka, Yosiharu (see Okamura, Tosihiko)—525(L)
Townes, C. H. (see Sanders, T. M., Jr.)—1158(L)
Townsend, Jonathan. Detection of weak electron paramagnetic resonance—911(T)
——, **S. I. Weissman, and G. E. Pake.** Hfs in paramagnetic resonance of $(SO_3)_2NO^{--}$ ion—606
Trainor, L. E. H. and Ta-You Wu. Symmetry requirements in electron scattering by atom—273
Treiman, S. B. Effect of equatorial ring current on cosmic-ray intensity—130
Triebwasser, Sol, Edward S. Dayhoff, and Willis E. Lamb, Jr. Fine structure of H atom—98
—— (see Dayhoff, Edward S.)—106
Trischka, John W. (see Goldberg, Joshua N.)—278
Trolan, J. K. (see Dyke, W. P.)—799
Tunnicliffe, P. R. Differential and total neutron scattering cross sections of deuteron in energy range 0.1 to 1.0 Mev—1247
Turkevich, A., J. B. Niday, and A. Tompkins. Radiochemical studies on fission of Th^{232} with Li+D neutrons—552
Turkevich, John (see Larach, Simon)—1060
Turner, Thomas J. (see Hall, Harry H.)—340(A)
Tyler, W. W. and A. C. Wilson, Jr. Thermal conductivity, electrical resistivity, and thermoelectric power of graphite—870
Tyren, Helge (see Barkas, Walter H.)—1

Van Allen, J. A. Cosmic-ray intensity above atmosphere near geomagnetic pole—891(T)
van der Ziel, A. Shot noise in semiconductors—900(A)
—— (see Mattson, R. H.)—899(A)
Van Horn, D. D. Diffusion and motion of phase in binary alloys—910(A)
Van Hove, Leon. Occurrence of singularities in elastic frequency distribution of crystal—1189
van Kampen, N. G. S-matrix and causality condition. I. Maxwell field—1072
Van Winkle, Q. (see Elson, R.)—320(L)
Varney, Robert N. Drift velocity of ions in O_2, N_2, and CO_2—337(A); 708
Verlet, Loup (see Martin, André)—519(L)
von Krzywoblocki, M. Z. Boundary layer theory—906(A)

Wagner, Frank, Jr., M. S. Freedman, D. W. Engelkemeir, and J. R. Huizenga. Radiations of 6.7-day U^{237}—502
—— (see Freedman, Melvin S.)—302
Wainwright, T. (see Parzen, G.)—901(A)
Walker, J. G. (see Bozorth, R. M.)—624
Walker, R. L., D. C. Oakley, and A. V. Tollestrup. Photoproduction of neutral mesons in H at high energies—1301(L)
Walt, M., R. L. Becker, A. Okazaki, and R. E. Fields. Total fast neutron cross sections of Co, Ga, Se, Cd, Te, Pt, Au, Hg, and Th—1271
—— (see Adair, R. K.)—1165
—— (see Becker, R. L.)—904(A)
Wangsness, Roald K. Antiferromagnetic resonance above Curie temperature—142
—— **and F. Bloch.** Dynamical theory of nuclear induction—728
Waniek, R. W. and Taiichiro Ohtsuka. Angular distribution of particles from stars—1307(L)
—— **and Taiichiro Ohtsuka.** Nuclear stars in emulsions—882(L)
Wanlass, S. D. (see Leighton, R. B.)—148
Wannier, Gregory H. Threshold law for ionization of atoms by electrons—336(A)
Wargo, P. (see Haxby, B. V.)—893(A)
Watkins, G. D. and R. V. Pound. Intensities of nuclear magnetic resonances in cubic crystals—658(L)
Watson, Kenneth M. Multiple scattering and many-body problem—applications to photomeson production in complex nuclei—575
—— Photoproduction and multiple scattering of mesons within atomic nuclei—904(T)
—— (see Francis, Norman C.)—328(L)
Weaver, H. E., Jr. Magnetic moments of Si^{29}, S^{33}, Zn^{67}, As^{75}, Se^{77}, Te^{123}, and Te^{125}—923
Weber, A. H. (see Antal, J. J.)—900(A)
Weddell, J. B. and J. H. Roberts. Angular distribution and differential cross section of $Li^6(n,\alpha)H^3$—891(A)
Wehner, G. and G. Medicus. Sputtering at low ion velocities—339(A)
—— (see Medicus, G.)—339(A)
Weinstock, Bernard, Bernard M. Abraham, and Darrell W. Osborne. Nuclear alignment and entropy of liquid He^3—787
—— **and John R. Pellam.** Thermal Rayleigh disk measurements in He^3-He^4 mixtures—521(L)
Weissman, S. I. (see Townsend, J.)—606
Welton, T. A. (see Simon, A.)—886(L)
Wentzel, G. Three-nucleon interactions in Yukawa theory—684
Werle, J. Higher order corrections in meson theory of nuclear forces—527(L)
Wessel, Günter (see Lew, Hin)—894(A)
Whalen, J. A., F. T. Porter, and C. S. Cook. High energy negatron spectrum of Sc^{46}—902(A)
Whalen, J. F. (see Coomes, E. A.)—894(A)
Whalin, E. A. and A. O. Hanson. Observation of the $(\gamma,2n)$ reaction in Ta—324(L)
Wheeler, John Archibald (see Hill, David Lawrence)—1102
White, Alan D. (see Lampert, Murray A.)—337(A)
White, David, O. D. Gonzales, and H. L. Johnson. Heat conduction of boundary layer in liquid He II—593
Whitesell, W. J. (see Johnson, V. A.)—941
Whiting, F. B. (see Aldrich, L. T.)—631
Wilkins, J. Ernest, Jr. (see Goldstein, Herbert)—1150(L)
Wilkinson, D. H. (see Carver, J. H.)—658(L)
Wilkinson, M. K. (see Gingrich, N. S.)—910(A)
Wilkinson, Roger G. (see Roggenkamp, Paul L.)—903(A)
Willard, H. B. (see Kington, J. D.)—530(L)
Williams, Corre and Herbert D. Schwetman. Analysis of bridged-T network by Laplace transformations—899(A)
Williams, Dudley (see Ting, Yu)—595
Williams, H. Bartel and Albert J. Hatch. Confirmatory measurements in high frequency secondary electron resonance discharge mechanism—339(A)
—— (see Hatch, Albert J.)—339(A)
Williams, R. W. New particles in cosmic rays—340(T)
Wilson, A. C., Jr. (see Tyler, W. W.)—870
Wilson, C. W. III and G. E. Pake. Nuclear magnetic relaxation in polytetrafluoro-ethylene and polyethylene—896(A)
Wilson, H. W. and Walter H. Barkas. Test of charge symmetry hypothesis: Positive to negative pion production ratio obtained in bombarding C with α-particles and protons—758
Winans, J. G. Possible inconsistency in customary use of vectors—914(A)
Winston, Harvey. Comparison of Slater's and Peckar's treatments of perturbed periodic potentials—317(L)
Winther, Aage (see Kofoed-Hansen, O.)—526(L)
Witmer, Enos E. Excited energy levels of nuclei as rational multiples of electron mass—905(A)
Wittels, M. Lattice expansion of quartz due to fast neutron bombardment—656(L)
Witten, Louis. Ionizing and heating plasma—335(A)
Wood, D. E. (see Roberts, J. H.)—905(A)
Woodhouse, R. L. Effect of weak magnetic field on constricted arc in fluorescent lamp—342(A)
Worley, R. Edwin. Third Ryberg series of N_2—864
Wright, Byron T. Spectrometer measurement on high energy positrons of Na^{22}—902(A)
Wu, Ta-You. Spectrum of discrete eigenvalues in negative atomic ion—629
—— (see Trainor, L. E. H.)—273
Wyckoff, H. O. (see Motz, J. W.)—968
Wyly, L. D. and A. Zucker. Activities in light nuclei from nitrogen ion bombardment—524(L)

Zaffarano, D. J. (see Mize, J. P.)—902(A)
Zissis, G. J. (see Deverall, G. V.)—895(A)
Zucker, A. (see Wyly, L. D.)—524(L)
Zucker, E. R. (see Mandeville, C. E.)—559

Analytic Subject Index to Volume 89

References with (A) are to abstracts of papers presented at meetings of the American Physical Society. References with (L) are to Letters to the Editor.

Absorption of radiation (see **Radiation**)
Acoustics
Acousto-electric effect, R. H. Parmenter—990
Second-order acoustic fields: relations between energy and intensity, Jordan J. Markham—972
Ultrasonic velocity of supercooled H_2O and D_2O, R. T. Lagemann and L. W. Gilley—906(A)
Adsorption
Effect of adsorption of common gases on electron ejection by noble gas ions, Homer D. Hagstrum—338(A)
Of O_2 on ZnO, S. R. Morrison—900(A)
Afterglow (see **Discharge of electricity in gases**)
Alloys (see **Crystalline state**)
Annihilation (see **Pair production and annihilation**)
Antiferroelectric phenomena (see **Dielectrics and dielectric properties**)
Antiferromagnetism (see **Magnetic properties**)
Arcs (see **Discharge of electricity in gases**)
Astrophysics
p-p reaction and energy production in sun, E. A. Frieman and L. Motz—648
Relativity precession of asteroid Icarus, J. J. Gilvarry—1046
Theory of interstellar grains, Bertram Donn—898(A)
Atmosphere
Air mass between observer and outer space, E. C. Pressly—654
Contributions of Doppler effect to radiation exchange in stratosphere, Gilbert N. Plass and Daniel I. Fivel—898(A)
Rocket measurement of upper atmosphere density by Paschen's law, Haldon L. Smith and Harold C. Early—338(A)
Atomic and molecular beams
Charge states of He beam in H_2, He_2, air, and A_2, Elias Snitzer—898(A); 1237
Electric resonance transitions in tapered electric field, Joshua N. Goldberg, John W. Trischka, and Peter G. Bergmann—278
Atomic mass
Masses of light atoms, K. Ogata and H. Matsuda—27
P^{31} atomic mass, K. Ogata and H. Matsuda—333(L)
$Si^{27}-Al^{27}$ mass difference, J. D. Kington, J. K. Bair, R. R. Carlson, and H. B. Willard—530(L)
$Zr^{92}-Mo^{92}$ and $Zr^{94}-Mo^{94}$ pairs and $Zr^{96}-Mo^{96}-Ru^{96}$ triplet, James S. Geiger, Benjamin G. Hogg, Henry E. Duckworth, and John W. Dewdney—621
Atomic structure and spectra
Amplified Dirac equation and Lamb-Retherford shift, W. A. Barker and Z. V. Chraplyvy—913(A)
Atomic excitation and ionization accompanying orbital electron capture by nuclei, H. Primakoff and F. T. Porter—903(A); 930
Enhancement of green continuum of Hg by rare gas, C. Kenty and D. A. Larson—180
Excitation cross section for He atoms, Saul Altshuler—1093(L)
Fine structure of H atom. V, Sol Triebwasser, Edward S. Dayhoff, and Willis E. Lamb, Jr.—98; VI, Edward S. Dayhoff, Sol Triebwasser, and Willis E. Lamb, Jr.—106
Hydrogen spectra from channel of spark discharge with increased energy, Heinz Fischer—336(A)
Lamb shift for H and D, E. E. Salpeter—92
Lifetimes of metastable states of noble gases, A. V. Phelps and J. P. Molnar—1202
Mesonic Auger effect, G. R. Burbidge and A. H. de Borde—189
Nonradiative relativistic contribution to magnetic moment of $^3S_1$ He, William Perl and Vernon Hughes—886(L)
Spectrum of discrete eigenvalues in negative atomic ion, Ta-You Wu—629
Upper limit for atomic orbital electron ejection accompanying K capture in Fe^{55}, F. T. Porter and H. P. Hotz—903(A); 938

Biophysics
Comfort, relaxation, and quality of sleep, T. Smith Taylor and L. W. Max—899(A)
Respiration of plant tissue cultures as function of x-ray dose, Mark W. Jones—899(A)
Universal test mattress, Norman L. Taylor and T. Smith Taylor—899(A)
Boson theory (see **Field theory**)
Bremsstrahlung (see **Radiation**)
Broadening of spectral lines
Effect of collisions upon Doppler width of spectral lines, Robert H. Dicke—472
Electric resonance transitions in tapered electric field, Joshua N. Goldberg, John W. Trischka, and Peter G. Bergmann—278
Variation of mutual collision diameters with mix ratio in binary mixtures in microwave pressure broadening, L. C. Jones, A. B. Bushkovitch, C. A. Potter, and A. G. Rouse—895(A)

Compton effect (see **Radiation**)
Conductivity, electrical (see **Electrical conductivity**)
Conductivity, thermal (see **Thermal properties**)
Cosmic radiation
Application of multiple scattering theory to cloud-chamber measurements, Martin Annis, H. S. Bridge, and S. Olbert—1216
Diurnal variations in intensity underground, Noah Sherman—25
Effect of equatorial ring current on cosmic-ray intensity, S. B. Treiman—130
Effects of atmosphere on penetrating cosmic radiation, Robert L. Chasson—1255
Electron-induced showers in Cu, Asher Kantz and Robert Hofstadter—607
Energy loss of cosmic-ray μ-mesons in NaI crystals, erratum, A. Hudson and R. Hofstadter—1309(L)
γ-rays from μ^- meson capture in Pb, Gerard G. Harris and T. J. B. Shanley—983
Mass measurements of heavy mesons, D. T. King, Nathan Seeman, and Maurice M. Shapiro—891(A)
Negative primaries as part of cosmic radiation, B. Bhowmik—327(L)
Nucleon cascade in water, C. B. A. McCusker, H. Messel, D. D. Millar, and N. A. Porter—1172
Recurring daily cycles of nucleonic component intensity, W. H. Fonger, J. W. Firor, and J. A. Simpson—891(A)
Sea level penetrating showers, W. Y. Chang, G. del Castillo, and Leon Grodzins—408
Secondaries of penetrating showers, C. C. Damm—826
"T-tracks" in photographic plates, Paul H. Barrett, G. Cocconi, and Y. Eisenberg—656(L)
V^0 decay, R. B. Leighton, S. D. Wanlass, and C. D. Anderson—148
V^0 particles, W. B. Fretter, M. M. May, and M. P. Nakada—168

Crystal counters (see **Methods and instruments**)
Crystalline state
Acousto-electric effect, R. H. Parmenter—990
Activation energies of Se-Te alloys, Harry H. Hall, Daniel T. Hedden, and Thomas J. Turner—340(A)
Anisotropic susceptibility of polycrystalline graphite, W. P. Eatherly and J. D. McClelland—661(L)
Application of cellular method to Si, erratum, D. K. Holmes—1308(L)
Calculation of energy bands in crystals, G. Parzen and T. Wainwright—901(A)
Calculation of *F*-center energy levels, J. A. Krumhansl and N. Schwartz—1154(L)
Cellular calculation of band structure for BaO, Earl L. Steele and James A. Krumhansl—901(A)
Combined pairs of vacancies in Cu, J. H. Bartlett and G. J. Dienes—848
Comparison of Slater's and Peckar's treatments of perturbed periodic potentials, Harvey Winston—317(L)
Crystallization of Si from floating liquid zone, Paul H. Keck and Marcel J. E. Golay—1297(L)
Deviation from close packing in hexagonal metal crystals, theory, John B. Goodenough—282
Diffusion and motion of phase in binary alloys, D. D. Van Horn—910(A)
Effect of x-ray irradiation on self-diffusion coefficient of Na in NaCl, Dillon Mapother—1231
Effects of *F*-centers on internal friction of rocksalt single crystals, D. R. Frankl and T. A. Read—663(L)
Electrical characteristics of crystalline B, William C. Shaw, D. E. Hudson, and G. C. Danielson—900(A)
Electronic energy bands in metals, G. Parzen—237
Electronic structure of Ge crystal, Frank Herman and Joseph Callaway—518(L)
Energy loss of medium-fast electrons in metals, E. M. Baroody—910(A)
Entropies of activation in metallic diffusion, G. J. Dienes—185
Extension of Makinson's theory of photoelectric emission to periodic potential, H. B. Huntington—357
F-center wave functions and electronic *g*-values in KCl crystals, Arnold H. Kahn and C. Kittel—315(L)
Frictional adhesion of metal to glass, quartz, and ceramic surfaces, Richard B. Belser—915(A)
Generation of *F*-centers at low temperatures, Frederick Seitz—1299(L)
Hall coefficient of Ca, V. Frank and O. Gram Jeppesen—1153(L)
Hall effect of Cu-Ni alloys, Albert I. Schindler and Emerson M. Pugh—295
Lattice expansion of quartz due to fast neutron bombardment, M. Wittels—656(L)
Light emission produced by current injected into green SiC crystal, K. Lehovec, C. A. Accardo, and E. Jamgochian—20
Localized functions in molecules and crystals, G. F. Koster—67
Magnetic crystal anisotropy and magnetostriction of Fe-Ni alloys, R. M. Bozorth and J. G. Walker—624
Magnetic structure of Mn antimonide, N. S. Gingrich, C. G. Shull, and M. K. Wilkinson—910(A)
Measurement of magnetostriction in single crystals, R. M. Bozorth and R. W. Hamming—865
Observations on "direct-current etch," David B. Langmuir—911(A)
Order-disorder transitions in simple cubic Ising lattice, L. D. Fosdick and H. M. James—901(A)
Purification and prevention of segregation in single crystals of Ge, W. G. Pfann and K. M. Olsen—322(L)
Rates of coloration of KCl and KBr during x-irradiation at 78°K, William H. Duerig and Jordan J. Markham—900(A)
Saturation in x-ray coloration of corundum single crystals, R. Allan Hunt and Robert H. Schuler—664(L)
Singularities in elastic frequency distribution of crystal, Leon Van Hove—1189
Solids subjected to constant rate of generation of lattice defects, Jerome Rothstein—901(A)
Spectral location of absorption due to color centers in alkaline earth halide crystals, Henry F. Ivey—322(L)
States of solid CH_4 as inferred from nuclear magnetic resonance, Kazuhisa Tomita—429
Statistics of two-dimensional, hexagonal net, J. P. Hobson and W. A. Nierenberg—662(L)
Structure of deformation bands, Edward W. Hart—521(L)
Successive rotational transitions in crystals, theory, Theodore J. Krieger and Hubert M. James—901(A)
Variational methods for periodic lattices and artificial dielectrics, Carson Flammer—1298(L)

Diamagnetism (see **Magnetic properties**)
Dielectrics and dielectric properties
Dipole moment of β-propiolactone, R. F. Miller—341(A)
Ferroelectricity in oxides of fcc structure, W. R. Cook, Jr., and Hans Jaffe—1297(L)
Variational methods for periodic lattices and artificial dielectrics, Carson Flammer—1298(L)
Diffraction of electrons (see **Electron diffraction**)
Diffusion
In binary alloys, D. D. Van Horn—910(A)
Effect of x-ray irradiation on self-diffusion coefficient of Na in NaCl, Dillon Mapother—1231
Entropies of activation in metallic diffusion, G. J. Dienes—185
Of Na in sodium tungsten bronze, J. F. Smith and G. C. Danielson—911(A)
Ta self-diffusion, R. L. Eager and D. B. Langmuir—911(A)
Transition from free to ambipolar diffusion, W. P. Allis and D. J. Rose—335(A)
Discharge of electricity in gases
Afterglow spectra observable in incandescent lamps, Carl Kenty—336(A)
Clean-up of He in arc discharge, M. J. Reddan—339(A)
Dissociative attachment of thermal electrons to I_2 molecules, Manfred Biondi—337(A)
Drift velocity of ions in O_2, N_2, and CO_2, Robert N. Varney—337(A); 708
Effect of weak magnetic field on constricted arc in fluorescent lamp, R. L. Woodhouse—342(A)
Electrical fields in Crookes dark space of low pressure glow discharge in air and N_2, Robert P. Stein—134
Electron velocity distributions in Hg-A discharge, B. T. Barnes—335(A)
Field emission: Large current densities, space charge, and vacuum arc, W. P. Dyke and J. K. Trolan—799
Frequency spectra from point-to-plane corona, Fred E. Luborsky and Stanley I. Reynolds—338(A)
High frequency secondary electron resonance discharge mechanism, theory, Albert J. Hatch and H. Bartel Williams—339(A)
Hydrogen spectra from channel of spark discharge with increased energy, Heinz Fischer—336(A)
Instabilities of completely ionized plasma, Martin Kruskal—335(A)
Ion concentrations in shock-type spark discharge tubes, R. G. Fowler and H. C. Rose—906(A)
Ionizing and heating a plasma, Louis Witten—335(A)
Irregularities in radiation along positive column of high pressure Hg arc, John K. Falconer, Jr.—342(A)

Discharge of electricity in gases (continued)
Measurements in high frequency secondary electron resonance discharge mechanism, H. Bartel Williams and Albert J. Hatch—339(A)
Microwave method for measuring mean energy transfer per collision and velocity dependence of collision cross section for slow electrons in gases, O. T. Fundingsland, A. C. Faire, and A. J. Penico—337(A)
Microwave technique for discharges in gases, Murray A. Lampert and Alan D. White—337(A)
OH rotational distributions in mixtures of H_2O in high frequency discharge, H. P. Broida—336(A)
Pinch effect in N_2, W. H. Bostick, M. A. Levine, and L. S. Combes—339(A)
Production of negative ions and noise in negative ion beams, Wade L. Fite—411
Rotational intensity distributions of OH and OD in electrodeless discharge through water vapor, H. P. Broida and W. R. Kane—1053
Shock waves in expansion of low pressure sparks, R. G. Fowler, W. R. Atkinson, and R. J. Lee—336(A)
Similarity conditions of high pressure discharges, W. Elenbass—338(A)
Time variation of ion concentration in flash discharge plasmas, H. N. Olsen and W. S. Huxford—336(A)
Transition from free to ambipolar diffusion, W. P. Allis and D. J. Rose—335(A)
Disintegration and excitation of nucleus (see **Nuclear reactions**)
Doppler effect (see **Radiation**)

Electrical circuits (see **Methods and instruments**)
Electrical conductivity and resistance (see also **Semiconductors; Superconductivity**)
Electrical characteristics of crystalline B, William C. Shaw, D. E. Hudson, and G. C. Danielson—900(A)
Of graphite, W. W. Tyler and A. C. Wilson, Jr.—870
Magnetoresistive effect in semiconductors, theory, V. A. Johnson and W. J. Whitesell—941
Transport phenomena in completely ionized gas, Lyman Spitzer, Jr., and Richard Härm—977
Electrodynamics (see **Electromagnetic theory and electrodynamics**)
Electromagnetic theory and electrodynamics (see also **Quantum electrodynamics**)
Gauge invariance and classical electrodynamics, Lloyd Motz—60
Electron diffraction
Theory of electron diffraction, Roy Glauber and Verner Schomaker—667
Electronic tubes (see **Methods and instruments**)
Electrons and positrons (see also **Electromagnetic theory and electrodynamics; Pair production and annihilation**)
m/e for positron and electron, L. A. Page, P. Stehle, and S. B. Gunst—1273
Electrons, secondary
Effect of evaporation products from BaO coated cathode on secondary emission of MgO thin films, B. V. Haxby and P. Wargo—893(A)
Electron ejection from Mo by He^+, He^{++}, and He_2^+, Homer D. Hagstrum—244
Emission measurement technique, E. J. Scott—894(A)
From MgO single crystals with excess O_2, K. C. Nomura—894(A)
Electrons, thermionic (see **Thermionic emission**)
Energy loss of particles (see **Range and energy loss of particles**)
Energy states of atoms (see **Atomic structure and spectra**)
Energy states of molecules (see **Molecular structure and spectra**)
Energy states of nucleus (see **Nuclear reactions; Nuclear spectra; Nuclear theory**)
Errata
Application of cellular method to Si, D. K. Holmes—1308(L)
Density effect for the ionization loss in various materials, R. M. Sternheimer—1309(L)
Energy loss of cosmic-ray μ-mesons in NaI crystals, A. Hudson and R. Hofstadter—1309(L)
Excitation of atoms and molecules (see **Atomic structure and spectra; Molecular structure and spectra**)
Excitation of nuclei (see **Nuclear reactions; Nuclear spectra; Nuclear theory**)

Faraday effect (see **Magneto-optical effects**)
Ferroelectric phenomena (see **Dielectrics and dielectric properties**)
Ferromagnetism (see **Magnetic properties**)
Field currents
Field emission: Large current densities, space charge, and vacuum arc, W. P. Dyke and J. K. Trolan—799
Field theory (see also **Quantum electrodynamics**)
Charge independence of nuclear forces, David Feldman—1159(L)
Classical and quantum field theories in Lagrangian formalism, Peter G. Bergmann and Ralph Schiller—4
Conservation of quanta for non-local fields, Christopher Gregory—1199
Conversion of amplified Dirac equation to approximately relativistic form, W. A. Barker and Z. V. Chraplyvy—446
Divergence of perturbation expansion, A. Petermann—1160(L)
First-order meson wave equations, H. S. Green—965
Higher order corrections in meson theory of nuclear forces, J. Werle—527(L)
Mass relation of heavy particles, H. Enatsu—1304(L)
Meson theory of β-decay and L-forbidden transitions, Seitaro Nakamura—16
New equation in affine field laws, G. Bandyopadhyay—1161(L)
Pair creation in intermediate coupling theory, R. G. Moorhouse—958
Photopion production from single nucleon, F. Salzman—913(A)
Quantum field theory in light of distribution analysis, Werner Güttinger—1004
Spherically symmetric solutions in nonsymmetrical field
Strong conservation laws and equations of motion in covariant field theories, Joshua N. Goldberg—263
Symmetric pseudoscalar theory of nuclear forces, Abraham Klein—1158(L)
Three-nucleon interactions in Yukawa theory, G. Wentzel—684
Unified field theory, C. Peter Johnson, Jr.—320(L); Albert Einstein—321(L)
Unified field theory and Born-Infeld electrodynamics, G. Rickayzen and B. Kurşunoğlu—522(L)
Films, properties of
Aging of thin metal films, Richard B. Belser—911(A)
Soldering to thin metal films, Richard B. Belser—915(A)
Structure of surface of glass and of Bi films deposited on glass, J. J. Antal and A. H. Weber—900(A)
Fine structure (see **Atomic structure and spectra; Hyperfine structure**)
Fission of nucleus (see **Nuclear fission**)
Fluctuation phenomena (see **Noise**)
Fluid dynamics
Boundary layer theory, M. Z. von Krzywoblocki—906(A)
Streaming potentials developed across porous diaphragms for sinusoidal flow, R. G. Packard—906(A)
Fluorescence (see **Luminescence**)

Gamma-rays (see also **Nuclear reactions; Nuclear spectra; Radioactivity**)
Precision measurement of Co^{60} γ-radiation, G. Lindström, A. Hedgran, and D. E. Alburger—1303(L)
Systematic calculations of γ-ray penetration, Herbert Goldstein, J. Ernest Wilkins, Jr., and L. V. Spencer—1150(L)
Gases
Transport phenomena in completely ionized gas, Lyman Spitzer, Jr., and Richard Härm—977
Geophysics
Variations in isotopic abundances of Sr, L. T. Aldrich, L. F. Herzog, W. K. Holyk, F. B. Whiting, and L. H. Ahrens—631
Gravitation (see **Relativity and gravitation**)
Gyromagnetization (see **Magnetic properties**)

Hall effect
Of Ca, V. Frank and O. Gram Jeppesen—1153(L)
Of Cu-Ni alloys, Albert I. Schindler and Emerson M. Pugh—295
Of crystalline B, William C. Shaw, D. E. Hudson, and G. C. Danielson—900(A)
Heat capacity (see **Thermal properties**)
Helium, liquid
Blocked capillary method for determining melting pressures: Melting curve of He from 1.5°K to 4°K, C. A. Swenson—538
Entropy of liquid He^3, Tien Chi Chen and F. London—1038
Flow of He II through narrow slits, Richard T. Swim—906(A)
Heat conduction of boundary layer in liquid He II, David White, O. D. Gonzales, and H. L. Johnston—593
Heat pulses in liquid He II below 1°K, K. R. Atkins—526(L)
Irreversible processes with application to He II and Knudsen effect in gases, O. K. Rice—793
Liquid He II, theory, Louis Goldstein—597
Macroscopic theory of superfluid He^3–He^4 mixtures, P. J. Price—1209
Normal fluid concentration in liquid He II below 1°K, D. de Klerk, R. P. Hudson, and J. R. Pellam—662(L)
Nuclear alignment and entropy of liquid He^3, Bernard Weinstock, Bernard M. Abraham, and Darrell W. Osborne—787
Second-sound velocity below 1°K as function of pressure, Victor Mayper, Jr., and Melvin A. Herlin—523(L)
Second-sound velocity measurements below 1°K, D. de Klerk, R. P. Hudson, and J. R. Pellam—326(L)
Thermal Rayleigh disk measurements in He^3–He^4 mixtures, Bernard Weinstock and John R. Pellam—521(L)
Vapor-liquid equilibria in He^3–He^4 solutions, J. C. Morrow—1034
Hyperfine structure (see also **Nuclear moments and spin**)
Of Al ground state, Hin Lew and Günter Wessel—894(A)
Of In I resonance lines, G. V. Deverall, K. W. Meissner, and G. J. Zissis—895(A)
Nuclear spin of $_{95}Am^{241}$, Mark Fred and Frank S. Tomkins—318(L)
In paramagnetic resonance of $(SO_3)_2NO^{--}$ ion, J. Townsend, S. I. Weissman, and G. E. Pake—606
Pr ground state hfs and nuclear magnetic moment, Hin Lew—530(L)
Of Pr^{141}, Peter Brix—1245

Instruments (see **Methods and instruments**)
Internal conversion (see **Nuclear spectra**)
Ionization
Charge states of He beam in H_2, He_2, air, and A_2, Elias Snitzer—898(A); 1237
Ionization probability curves near threshold, R. E. Fox, W. M. Hickam, and T. Kjeldaas, Jr.—336(A); 555
Specific primary ionization of H_2, He, Ne, and A by high energy electrons, G. W. McClure—335(A)
Statistical fluctuations in ionization by 31.5-Mev protons, G. J. Igo, D. D. Clark, and R. M. Eisberg—879(L)
Threshold law for ionization of atoms by electrons, Gregory H. Wannier—336(A)
Ions
Drift velocity of ions in O_2, N_2, and CO_2, Robert N. Varney—337(A); 708
Effect of adsorption of common gases on electron ejection by noble gas ions, Homer D. Hagstrum—338(A)
Electron ejection from Mo by He^+, He^{++}, and He_2^+, Homer D. Hagstrum—244
High vacuum, high speed ion pump, John S. Foster, E. O. Lawrence, and E. J. Lofgren—338(A)
Ion concentration in shock-type spark discharge tubes, R. G. Fowler and H. C. Rose—906(A)
Production of negative ions and noise in negative ion beams, Wade L. Fite—411
Sputtering at low ion velocities, G. Wehner and G. Medicus—339(A)
Time variation of ion concentration in flash discharge plasmas, H. N. Olsen and W. S. Huxford—336(A)
Ions and electrons, mobility (see also **Semiconductors**)
Drift velocity of ions in O_2, N_2, and CO, Robert N. Varney—337(A); 708
Mobilities of thermal ions in noble gases, Lorne M. Chanin and Manfred A. Biondi—337(A)
Mobility of He_2^+ in He, theory, S. Geltman and H. Margenau—337(A)
Temperature dependence of drift mobility in Ge, R. Lawrance—1295(L)
Isomers, nuclear (see **Nuclear isomers**)
Isotopes (see **Atomic mass; Radioactivity**)

Kinetic theory of gases (see **Gases; Statistical mechanics and thermodynamics**)

Liquid helium (see **Helium, liquid**)
Liquids (see also **Fluid dynamics**)
Angular points in densities of water *vs* temperature, George Antonoff and Raymond Madrazo, Jr.—899(A)
Entropy of fusion of monatomic liquids, N. K. Pope—899(A)
New theory of aggregates as supplement to van't Hoff's theory of solutions, George Antonoff—915(A)
Ultrasonic velocity, density, and compressibility of supercooled H_2O and D_2O, R. T. Lagemann and L. W. Gilley—906(A)
Luminescence
Absolute light emission efficiency of crystal anthracene for γ-ray excitation, Milton Furst, Hartmut Kallmann, and Bernard Kramer—416
Of BaO, Virgil L. Stout—310
In CdS at absorption edge, Clifford C. Klick—274
Cathodoluminescent studies of (BaSr)O, Harold W. Gandy—912(A)
Energy transfer in complex solutions, Milton Furst and Hartmut Kallmann—912(A)
Induced conductivity in luminescent powders. II. Ac impedance measurements, Hartmut Kallmann, Bernard Kramer, and Arnold Perlmutter—700
Influence of electric fields on luminescence, Frank Matossi and Sol Nudelman—660(L)
Intensity variations in sensitized fluorescence, Robert E. Swanson and Robert H. McFarland—911(A)
K-fluorescence yield summary, C. D. Broyles and S. K. Haynes—912(A)
Light emission produced by current injected into green SiC crystal, K. Lehovec, C. A. Accardo, and E. Jamgochian—20

Luminescence (continued)
Sensitized fluorescence studies using photomultiplier detection method, Robert H. McFarland and Robert E. Swanson—911(A)
Slow component in decay of scintillation phosphors, Jasper A. Jackson and F. B. Harrison—322(L)
Thin plastic scintillation phosphors, G. G. Eichholz—912(A)

Magnetic properties (see also **Crystalline state; Magnetic resonance absorption; Nuclear moments and spin**)
Anisotropic susceptibility of polycrystalline graphite, W. P. Eatherly and J. D. McClelland—661(L)
Approach to saturation in dilute ferromagnetics, Alan D. Franklin and Ami E. Berkowitz—1171
Diamagnetism of enclosed electron gas, H. A. Nye—1305(L)
Gyromagnetic ratio of supermalloy, G. G. Scott—618
Interaction of Mn activator ions in Zn-orthosilicate phosphors, Simon Larach and John Turkevich—1060
Magnetic crystal anisotropy and magnetostriction of Fe-Ni alloys, R. M. Bozorth and J. G. Walter—624
Magnetic structure of Mn antimonide, N. S. Gingrich, C. G. Shull, and M. K. Wilkinson—910(A)
Magnetic susceptibility of diamagnetic electron gas—role of small effective electron mass, E. N. Adams II—633
Magnetostriction in single crystals, R. M. Bozorth and R. W. Hamming—865
Microwave permeability tensor and Faraday effect in nonsaturated ferromagnetic materials, theory, George T. Rado—529(L)
Mixing of states and antiferromagnetism, H. P. Hanson—1154(L)
Paramagnetism of uranyl-like ions, R. J. Elliott—659(L)
Magnetic and electric resonance absorption (see also **Nuclear moments and spin**)
Antiferromagnetic resonance above Curie temperature, Roald K. Wangsness—142
Dynamical theory of nuclear induction, R. K. Wangsness and F. Bloch—728
Electronic resonance transitions in tapered electric field, Joshua N. Goldberg, John W. Trischka, and Peter G. Bergmann—278
Homogeneity mapping of permanent magnet field for chemical effect studies in nuclear resonance, C. R. Bruce—896(A)
Intensities of nuclear magnetic resonances in cubic crystals, G. D. Watkins and R. V. Pound—658(L)
Microwave resonance absorption in Gd metal, A. F. Kip, C. Kittel, A. M. Portis, R. Barton, and F. H. Spedding—518(L)
Nuclear magnetic relaxation in polytetrafluoro-ethylene and polyethylene, C. W. Wilson III and G. E. Pake—896(A)
Nuclear magnetic resonance of aligned radioactive nuclei, N. Bloembergen and G. M. Temmer—883(A)
Paramagnetic relaxation in metals, Albert W. Overhauser—689
Paramagnetic resonance absorption in salts of V and Mn, Clyde A. Hutchinson, Jr., and Leonard S. Singer—256
Paramagnetic resonance in copper acetate at 47 000 Mc, Tosihiko Okamura, Yosiharu Torizuka, and Muneyuki Date—525(L)
Pure nuclear quadrupole spectrum of Bi^{209} in Bi-triphenyl, H. G. Robinson, H. G. Dehmelt, and W. Gordy—1305(L)
States of solid CH_4 as inferred from nuclear magnetic resonance, Kazuhisa Tomita—429
Magneto-optical effects
Microwave permeability tensor and Faraday effect in nonsaturated materials, theory, George T. Rado—529(L)
Magnetostriction (see **Magnetic properties**)
Mass defects (see **Atomic mass**)

Mathematical methods
Analysis of bridged-T network by Laplace transformations, Corre Williams and Herbert D. Schwetman—899(A)
Possible inconsistency in customary use of vectors, J. G. Winans—914(A)
Measurements (see **Methods and instruments**)
Mechanics, quantum—atomic structure and spectra (see **Atomic structure and spectra**)
Mechanics, quantum—general (see **Quantum mechanics**)
Mechanics, quantum—molecular structure and spectra (see **Molecular structure and spectra**)
Mechanics, quantum—nuclear (see **Nuclear theory**)
Mechanics, quantum—of solid bodies (see **Crystalline state**)
Mechanics, statistical (see **Statistical mechanics**)
Meson field theory (see **Field theory**)
Mesons (see also **Cosmic radiation**)
Angular and energy distributions in photomeson production, Bernard T. Feld—330(L)
Atomic number dependence of neutral meson yield from proton bombardment, R. W. Hales and B. J. Moyer—1047
Elastic pion-hydrogen scattering in photographic emulsions, Gerson Goldhaber—1187
Energy loss of cosmic-ray μ-mesons in NaI crystals, erratum, A. Hudson and R. Hofstadter—1309(L)
γ-rays from μ^- meson capture in Pb, Gerard G. Harris and T. J. B. Shanley—983
Internal pair production of γ-rays of mesonic origin; alternate modes of π^0 decay, P. Lindenfeld, A. Sachs, and J. Steinberger—531
Li^9 disintegration in photographic emulsion, W. F. Fry—325(L)
Mass measurements of heavy meson, D. T. King, Nathan Seeman, and Maurice M. Shapiro—891(A)
Mesonic Auger effect, G. R. Burbidge and A. H. de Borde—189
Multiple meson production by high energy nucleon-nucleon collision, H. Fukuda—842
Multiple scattering and many-body problem—applications to photomeson production in complex nuclei, Kenneth M. Watson—575
Multiple scattering effects in pion-deuteron scattering, K. A. Brueckner—909(A)
Neutral meson production in n-p collisions, Roger H. Hildebrand—1090
Photopion production from single nucleon, F. Salzman—913(A)
Photoproduction of neutral mesons in H, Y. Goldschmidt-Clermont, L. S. Osborne, and M. B. Scott—329(L)
Photoproduction of neutral mesons in H at high energies, R. L. Walker, D. C. Oakley, and A. V. Tollestrup—1301(L)
Photoproduction of π^0 mesons in H and D, Norman C. Francis—766
Pion-nucleon scattering when coupling is weak and extended, Geoffrey F. Chew—591
Relation between photoproduction and scattering cross sections for π-mesons in complex nuclei, Norman C. Francis and Kenneth M. Watson—328(L)
Suggested scheme for meson production, H. Messel and H. S. Green—315(L)
Test of charge symmetry hypothesis: Positive to negative pion production ratio obtained in bombarding C with α-particles and protons, H. W. Wilson and Walter H. Barkas—758
V^0 decay, R. B. Leighton, S. D. Wanlass, and C. D. Anderson—148
V^0 particles, W. B. Fretter, M. M. May, and M. P. Nakada—168
X-rays from mesic C atom, H. J. Schulte, J. B. Platt, and M. Camac—905(A)

Z-dependence of mesic x-ray yield, M. Camac, J. B. Platt, and H. J. Schulte—905(A)
Metals (see **Crystalline state**)
Metastable atoms and molecules (see **Atomic structure and spectra; Molecular structure and spectra**)
Methods and instruments
Activity ratio method for measuring energy stability of betatrons, Milton Birnbaum, Eric M. Harth, Leo Seren, and Ralph Tobin—897(A)
Aging of thin metal films, Richard B. Belser—911(A)
Analysis of bridged-T network by Laplace transformations, Corre Williams and Herbert D. Schwetman—899(A)
Blocked capillary method for determining melting pressures, C. A. Swenson—538
Crystal diodes in electronics laboratory, Irving L. Kofsky—340(A)
Crystallization of Si from floating liquid zone, Paul H. Keck and Marcel J. E. Golay—1297(L)
Evapor-ion pump, R. G. Herb, Robert H. Davis, Ajay S. Divatia, and D. Saxon—897(A)
Extensometer for rubber, R. P. Clifford—341(A)
Fast neutron scintillation spectrometer, Marshall R. Cleland—896(A)
Firestone shear flexometer, G. L. Hall and F. S. Conant—342(A)
Focusing method for large accelerators, T. Kitagaki—1161(L)
High vacuum, high speed ion pump, John S. Foster, Jr., E. O. Lawrence, and E. J. Lofgren—338(A)
Homogeneity mapping of permanent magnet field for chemical effect studies in nuclear resonance, C. R. Bruce—896(A)
Interpretation of α-values in p-n junction transistors, F. S. Goucher and M. B. Prince—651
Measurement of energy of isotropic fast neutrons with Li^6 loaded emulsions, J. H. Roberts, W. O. Solano, D. E. Wood, and H. B. Billington—905(A)
Measurement of ionizing radiation by frequency variation, Hans Kohn Richards—897(A)
Microwave method for measuring mean energy transfer per collision, O. T. Fundingsland, A. C. Faire, and A. J. Penico—337(A)
Microwave technique for discharges in gases, Murray A. Lampert and Alan D. White—337(A)
Plasticizers for polyvinyl chloride, Mark L. Dannis—341(A)
Process for developing 400-micron nuclear emulsions, Mary B. Summerfield—340(A)
Resolution of "photon difference method," J. Goldemberg and L. Katz—1300(L)
Secondary electron emission measurement technique, E. J. Scott—894(A)
Separation of incident and emitted radiations in solar furnace by rotating sectors, Willi M. Conn and Gene Braught—898(A)
Soldering to thin metal films, Richard B. Belser—915(A)
Universal test mattress, Norman L. Taylor and T. Smith Taylor—899(A)
Velocity spectrometer using μsec neutron shutter, F. G. P. Seidl, D. J. Hughes, and H. Palevsky—897(A)
Microwaves and microwave spectra (see also **Molecular structure and spectra**)
Fine structure of H atom. V, Sol Triebwasser, Edward S. Dayhoff, and Willis E. Lamb, Jr.—98; VI, Edward S. Dayhoff, Sol Triebwasser, and Willis E. Lamb, Jr.—106
Microwave absorption spectrum of ND_3, R. G. Nuckolls, L. J. Rueger, and Harold Lyons—1101
Microwave method for measuring mean energy transfer per collision, O. T. Fundingsland, A. C. Faire, and A. J. Penico—337(A)
Microwave spectrum of free OH radical, T. M. Sanders, Jr., A. L. Schawlow, G. C. Dousmanis, and C. H. Townes—1158(L)
Microwave technique for discharges in gases, Murray A. Lampert and Aian D. White—337(A)
Possible microwave absorption in molecules belonging to point groups $D_{2d} \equiv V_d$ and T_d, Venkateswarlu Putcha and Masataka Mizushima—896(A)
Variation of mutual collision diameters with mix ratio in binary mixtures in microwave pressure broadening, L. C. Jones, A. B. Bushkovitch, C. A. Potter, and A. G. Rouse—895(A)
Mobility of ions and electrons (see **Ions and electrons, mobility**)
Molecular beams (see **Atomic and molecular beams**)
Molecular structure and spectra (see also **Microwaves and microwave spectra; Raman spectra**)
Of CH_3OH, E. V. Ivash and D. M. Dennison—895(A)
Electronic emission spectrum of $C^{13}O^{16}$, K. E. McCulloh and George Glockler—145
Electronic spectra of diatomic molecules: O_2, Fausto G. Fumi and Robert G. Parr—895(A)
High pressure inversion spectrum of ND_3 near 1500 Mc, G. Birnbaum and A. A. Maryott—895(A)
Microwave absorption spectrum of ND_3, R. G. Nuckolls, L. J. Rueger, and Harold Lyons—1101
Microwave spectrum of free OH radical, T. M. Sanders, Jr., A. L. Schawlow, G. C. Dousmanis, and C. H. Townes—1158(L)
N_2, third Rydberg series, R. Edwin Worley—863
Normal coordinate analysis of 1, 3, 5-trifluoro-benzene, Eldon E. Ferguson—895(A)
OH rotational distributions in mixtures of H_2O in high frequency discharge, H. P. Broida—336(A)
Possible microwave absorption in molecules belonging to point groups $D_{2d} \equiv V_d$ and I_d, Venkateswarlu Putcha and Masataka Mizushima—896(A)
Pseudo-quadrupole effect for nuclei in molecules, Norman F. Ramsey—527(L)
Rotational intensity distributions of OH and OD in electrodeless discharge through water vapor, H. P. Broida and W. R. Kane—1053
Vibrational spectra and calculated thermodynamic properties of CCl_3CF_2Cl and CCl_3CFCl_2, J. Rud Nielsen, C. Y. Liang, D. C. Smith, and Morris Alpert—895(A)
Moments, nuclear (see **Nuclear moments and spin**)

Neutrino (see also **Radioactivity; Nuclear spectra**)
Electron-neutrino angular correlation in β-decay of He^6, James S. Allen and W. K. Jentschke—902(A)
Noise
Current noise in partially superconducting resistors at temperatures down to 2°K, B. Kaplan and J. G. Daunt—907(A)
Flicker noise causes by interface layer, W. W. Lindemann and H. J. Hannam—900(A)
Production of negative ions and noise in negative ion beams, Wade L. Fite—411
Shot noise in Ge filaments, R. H. Mattson and A. van der Ziel—899(A)
Shot noise in semiconductors, A. van der Ziel—900(A)
Nuclear fission (see also **Nuclear reactions**)
Asymmetric fission, Peter Fong—332(L)
Cf^{246} spontaneous fission rate, E. K. Hulet, S. G. Thompson, and A. Ghiorso—878(L)
Enhanced reactor, F. E. O'Meara—982
Genetics of Ge^{78}–As^{78} fission chain, Nathan Sugarman—570
Nuclear constitution and interpretation of fission phenomena, David Lawrence Hill and John Archibald Wheeler—1102

Nuclear fission (continued)
Radiochemical studies on fission of Th^{232} with Li+D neutrons, A. Turkevich, J. B. Niday, and A. Tompkins—552
Relative photofission and photoneutron cross sections for U^{238}, John R. Huizenga and Robert B. Duffield—893(A)
Short-lived Ce isotopes from U fission, A. A. Caretto, Jr., and S. Katcoff—1267
Thermal neutron fission and capture cross section of U^{233}, R. Elson, W. Bentley A. Ghiorso, and Q. Van Winkle—320(L)
U photofission and photoneutron emission, Robert B. Duffield and John R. Huizenga—1040
U photofission yields, Roman A. Schmitt and Nathan Sugarman—1155(L)
U^{235} fission neutron spectrum, David B. Nicodemus and Hans H. Staub—1288
Nuclear induction (see **Magnetic and electric resonance absorption; Nuclear moments and spin**)
Nuclear isomers (see also **Nuclear spectra; Radioactivity**)
Of Cd^{117}, In^{117}, and In^{118}, Charles D. Coryell, Pierre Lévêque, and Harold G. Richter—903(A)
Core isomerism—remarks on Mo^{93m}, M. Goldhaber—1146(L)
Interpretation of isomeric transitions of electric quadrupole type, Aage Bohr and Ben R. Mottelson—316(L)
Isomeric branching and threshold behavior of $Mo^{92}(n,2n)$-Mo^{91}, John E. Brolley, Jr.—877(L)
Lifetimes, Steven A. Moszkowski—474
Pt^{193m}, J. B. Swan, W. M. Portnoy, and R. D. Hill—907(A)
Probable existence of $E3+M4$ mixture in isomeric transition, R. D. Hill and J. W. Mihelich—323(L)
Re^{185m} disintegration, J. W. Mihelich—907(A)
Rb^{84m}, R. S. Caird and Allan C. G. Mitchell—573; 903(A)
7-hr Mo^{93m}, D. E. Alburger and S. Thulin—1146(L)
Tc^{93} and Tc^{96} isomeric transitions, Harry T. Easterday and Heinrich A. Medicus—752
Y^{91m} disintegration, D. P. Ames, M. E. Bunker, L. M. Langer, and B. M. Sorenson—903(A)
Nuclear moments and spin (see also **Hyperfine structure**)
Of $_{95}Am^{241}$, Mark Fred and Frank S. Tomkins—318(L)
Anomalous results in attempt to determine spin of Si^{29}, R. H. Sands and G. E. Pake—896(A)
Exchange magnetic moments of nuclei with almost closed shells of nucleons, Richard W. Cole—883(L)
Influence of nuclear quadrupole moment on α-γ angular correlation in RaTh, A. Abragam and R. V. Pound—1306(L)
Magnetic moments of odd-odd nuclei and strong spin-orbit coupling shell model, H. M. Schwartz—1293
Magnetic moments of Si^{29}, S^{33}, Zn^{67}, As^{75}, Se^{77}, Te^{123}, and Te^{125}, H. E. Weaver, Jr.—923
Nuclear gyromagnetic ratios, Yu Ting and Dudley Williams—595
Nuclear magnetic moment of Pr^{141} from hfs of Pr II, Peter Brix—1245
Pr ground state hfs and nuclear magnetic moment, Hin Lew—530(L)
Pure nuclear quadrupole spectrum of Bi^{209} in Bi-triphenyl, H. G. Robinson, H. G. Dehmelt, and W. Gordy—1305(L)
Quadrupole moment of Li^7, E. G. Harris and M. A. Melkanoff 914(A)
Spin of 7.4-Mev state of Li^7, W. O. Solano and J. H. Roberts—892(A)
Nuclear photoeffects
Cross section for $Ta^{181}(\gamma,2n)Ta^{179}$ at 17.6 Mev, J. H. Carver, R. D. Edge, and D. H. Wilkinson—658(L)
Energy distributions of photoprotons from heavy elements, W. E. Stephens, M. E. Toms, E. E. Carroll, Jr., and G. Rosenblum—893(A)
High energy photoproton production by 322-bremsstrahlung, J. W. Rosengren and J. M. Dudley—603
Photopion production from single nucleon, F. Salzman—913(A)
Photoproduction of neutral mesons in H at high energies, R. L. Walker, D. C. Oakley, and A. V. Tollestrup—1301(L)
Photoproduction of π^0 mesons in H and D, Norman C. Francis—766
Photoprotons from Mo^{100} and Mo^{92}, W. A. Butler and G. M. Almy—893(A)
Relation between photoproduction and scattering cross sections for π-mesons in complex nuclei, Norman C. Francis and Kenneth M. Watson—328(L)
Relative photofission and photoneutron cross sections for U^{238}, John R. Huizenga and Robert B. Duffield—893(A)
Resolution of "photon difference method," J. Goldemberg and L. Katz—1300(L)
$Ta(\gamma,2n)$ reaction, E. A. Whalin and A. O. Hanson—324(L)
U photofission and photoneutron emission, Robert B. Duffield and John R. Huizenga—1040
U photofission yields, Roman A. Schmitt and Nathan Sugarman—1155(L)
Nuclear reactions (see also **Nuclear photoeffects; Nuclear spectra; Radioactivity**)
Activation cross sections measured with Sb-Be photoneutrons, Clyde Kimball and Bernard Hamermesh—1306(L)
Activities in light nuclei from nitrogen ion bombardment, L. D. Wyly and A. Zucker—524(L)
Al^{27} levels from $Mg^{24}(d,n)Al^{25}$, E. Goldberg—760
Angular distribution and differential cross section of $Li^6(n,\alpha)H^3$, J. B. Weddell and J. H. Roberts—891(A)
Angular distribution of $Be^9(d,t)Be^8$ at low energy, P. Cüer and J. J. Jung—1151(L)
Angular distribution of (d,t) reactions, S. T. Butler and E. E. Salpeter—891(A)
Angular distribution of γ-rays and short range α-particles from $N^{15}(p,\alpha\gamma)C^{12}$, Alfred A. Kraus, Jr., A. P. French, William A. Fowler, and C. C. Lauritsen—299
Angular distribution of particles from stars, R. W. Waniek and Taiichiro Ohtsuka—1307(L)
Angular distribution of protons from V^{51}, J. S. King and W. C. Parkinson—1080
Angular distributions of protons from $F^{19}(d,p)F^{20}$, D. A. Bromley, J. A. Bruner, and H. W. Fulbright—396; H. W. Fulbright, D. A. Bromley, and J. A. Bruner—892(A)
Average neutron total cross sections in 3- to 12-Mev region, Norris Nereson and Sperry Darden—775
Barrier penetration effects for light nuclei, B. E. Freeman and J. L. McHale—223
Be and C disintegration induced by 330-Mev protons, Walter H. Barkas and Helge Tyren—1
Coupling of angular momenta in nuclear reactions, R. F. Christy—839
Cross section for $D(d,p)H^3$, C. F. Cook and J. R. Smith—785
Disintegration of He by 90-Mev neutrons, Peter E. Tannenwald—508
Electrostatic analysis of nuclear reaction energies, D. J. Donahue, K. W. Jones, M. T. McEllistrem, and H. T. Richards—824; 892(A)
Excited energy levels of nuclei as rational multiples of electron mass, Enos E. Witmer—905(A)
γ-radiation from interaction of 14-Mev neutrons with Fe, V. E. Scherrer, R. Theus, and W. R. Faust—1268
γ-rays from proton bombardment of Na^{23}, J. W. Teener, L. W. Seagondollar, and R. W. Krone—892(A)
He^6 formation by 14-Mev neutron bombardment of Li and Be, M. E. Battat and F. L. Ribe—80
Inelastic events induced by 32-Mev protons on He, Jack Benveniste and Bruce Cork—422

Inelastic scattering of neutrons by Cd^{111}, A. E. Francis, J. J. G. McCue, and Clark Goodman—1232
Isomeric branching and threshold behavior of $Mo^{93}(n,2n)Mo^{91}$, John E. Brolley, Jr.—877(L)
Li^9 disintegration in photographic emulsion, W. F. Fry—325(L)
Magnetic analysis of *d*-Be reactions, R. W. Gelinas and S. S. Hanna—483
Magnetic analysis of protons from $Cr^{53}(d,p)Cr^{53}$ and $Ni^{58}(d,p)Ni^{59}$, C. E. McFarland, M. M. Bretscher, and F. B. Shull—892(A)
Magnetic analysis of $Sr^{88}(d,p)Sr^{89}$, Charles E. McFarland and Franklin B. Shull—489
Neutron capture cross sections for production of Sc^{46} and Sr^{85}, W. S. Lyon—1307(L)
Neutron capture γ-rays from Sc, V, Mn, Co, and Cu, G. A. Bartholomew and B. B. Kinsey—386
Neutron capture γ-rays from Ti, Cr, Fe, Ni, and Zn, B. B. Kinsey and G. A. Bartholomew—375
Neutron energy distribution from proton bombardment of Li, Be, and C at 375 Mev, Warren F. Goodell, Jr., Howard H. Loar, Richard P. Durbin, and William W. Havens, Jr.—724
(n,γ) and $(n,2n)$ reactions in I, H. C. Martin and R. F. Taschek—1302(L)
Neutron resonances in Xe, S. P. Harris—904(A)
N^{13} excited states, Herbert L. Jackson and Aaron I. Galonsky—370
Nuclear γ-rays from low energy proton bombardment of Na, Mg, and Al, Harvey Casson—809
Nuclear reactions with 21-Mev He^3 in cyclotron, D. N. Kundu, T. W. Donaven, M. L. Pool, and J. K. Long—1200
Nuclear stars in emulsions, R. W. Waniek and Taiichiro Ohtsuka—882(L)
Production of polarized particles in nuclear reactions, A. Simon and T. A. Welton—886(L)
p-p reaction and energy production in sun, E. A. Frieman and L. Motz—648
Q-values for $N^{14}(\alpha,p)O^{17}$, Elis Hjalmar and Hilding Slätis—1151(L)
Resonant energies for radiative capture of protons by B, C, F, Mg, and Al below 500 kev, S. E. Hunt and W. M. Jones—1283
$Si^{27}-Al^{27}$ mass difference, J. D. Kington, J. K. Bair, R. R. Carlson, and H. B. Willard—530(L)
Slow neutron resonances in Sm and Y, V. L. Sailor, H. L. Foote, Jr., and H. H. Landon—904(A)
Spin of 7.4-Mev state of Li^7, W. O. Solano and J. H. Roberts—892(A)
States of S^{33} and Si^{29} from (d,p) stripping, J. R. Holt and T. N. Marsham—665(L)
Thermal neutron absorption cross section of Sc, E. E. Lockett and E. Bowell—657(L)
Thermal neutron fission and capture cross section of U^{233}, R. Elson, W. Bentley, A. Ghiorso, and Q. Van Winkle—320(L)
Total cross sections for fast neutrons, R. L. Becker, M. Walt, and A. Okazaki—904(A)
Total fast neutron cross sections of Co, Ga, Se, Cd, Te, Pt, Au, Hg, and Th, M. Walt, R. L. Becker, A. Okazaki, and R. E. Fields—1271
Yield of long-range α-particles from $F^{19}(p,\alpha)O^{16}$, E. B. Paul and R. L. Clarke—892(A)

Nuclear spectra (see also **Nuclear reactions; Radioactivity**)
α-γ angular correlation in RaTh, James Battey, L. Madansky, and F. Rasetti—182
Am^{241} γ-radiation, J. O. Newton and B. Rose—1157(L)
Angular correlation in Li^8 decay, C. M. Class and S. S. Hanna—877(L)
Angular distribution of γ-rays and short range α-particles from $N^{15}(p,\alpha\gamma)C^{12}$, Alfred A. Kraus, Jr., A. P. French, William A. Fowler, and C. C. Lauritsen—299
Angular momenta of excited states of Pt^{196}, Rolf M. Steffen—665(L)
Of Br^{87}, a delayed-neutron activity, Andrew F. Stehney and Nathan Sugarman—194
Of Cs^{138}, L. M. Langer, R. B. Duffield, and C. W. Stanley—907(A)
Cs^{134} γ-rays, J. M. LeBlanc, W. H. Nester, D. W. Martin, M. K. Brice, and J. M. Cork—907(A)
Continuous γ-ray spectrum accompanying β-decay, P. Bolgiano, L. Madansky, and F. Rasetti—679
Core isomerism—remarkson Mo^{93m}, M. Goldhaber—1146(L)
Correlation between electron and recoil nucleus in He^6 decay, Brice M. Rustad and Stanley L. Ruby—880(L)
Cross terms in β-decay, O. Kofoed-Hansen and Aage Winther—526(L)
Direction and polarization correlations of successive γ-rays, J. J. Kraushaar and M. Goldhaber—1081
Effect of chemical binding and phase on angular correlations, Rolf M. Steffen—903(A)
Electron-neutrino angular correlation in β-decay of He^6, James S. Allen and W. K. Jentschke—902(A)
Experimental K to $L+M$ ratios for internal conversion lines, R. E. Merker and R. D. Birkhoff—1159(L)
"*F*" line of Th B, D. I. Meyer and F. H. Schmidt—908(A)
Fermi term in β-ν correlation, D. C. Peaslee—1148(L)
γ-rays from proton bombardment of Na^{23}, J. W. Teener, L. W. Seagondollar, and R. W. Krone—892(A)
Influence of nuclear quadrupole moment on α-γ angular correlation in RaTh, A. Abragam and R. V. Pound—1306(L)
Interpretation of isomeric transitions of electric quadrupole type, Aage Bohr and Ben R. Mottelson—316(L)
K-Auger intensities of Sn^{113}, Cs^{137}, and Au^{198}, C. D. Broyles, D. A. Thomas, and S. K. Haynes—715
Lifetimes of nuclear isomers, Steven A. Moszkowski—474
Meson theory of β-decay and ΔL-forbidden transitions, Seitaro Nakamura—16
Mo^{99}, R. M. Diamond—1149(L)
Neutron capture γ-rays from Sc, V, Mn, Co, and Cu, G. A. Bartholomew and B. B. Kinsey—386
Neutron capture γ-rays from Ti, Cr, Fe, Ni, and Zn, B. B. Kinsey and G. A. Bartholomew—375
Neutron deficient isotopes of Hg, K. Gopalakrishnan, A. deShalit, and J. W. Mihelich—908(A)
Nuclear γ-rays from low energy proton bombardment of Na, Mg, and Al, Harvey Casson—809
Pt^{193m}, J. B. Swan, W. M. Portnoy, and R. D. Hill—907(A)
Precision measurement of Co^{60} γ-radiation, G. Lindström, A. Hedgran, and D. E. Alburger—1303(L)
Probable existence of $E3+M4$ mixture in isomeric transition, R. D. Hill and J. W. Mihelich—323(L)
Of RaD, A. A. Jaffe and S. G. Cohen—454
Of Re^{188m}, J. W. Mihelich—907(A)
Of Rb^{82} and Rb^{84}, Charles M. Huddleston and Allan C. G. Mitchell—903(A)
Rb^{84m}, R. S. Caird and Allan C. G. Mitchell—573; 903(A)
Sc^{46} high energy negatron spectrum, J. A. Whalen, F. T. Porter, and C. S. Cook—902(A)
7-hr Mo^{93m}, D. E. Alburger and S. Thulin—1146(L)
Of 6.7-day U^{237}, F. Wagner, Jr., M. S. Freedman, D. W. Engelkemeir, and J. R. Huizenga—502
Na^{22} high energy positrons, Byron T. Wright—902(A)
Spin of 7.4-Mev state of Li^7, W. O. Solano and J. H. Roberts—892(A)
Of Sr^{91} and Y^{91m}, D. P. Ames, M. E. Bunker, L. M. Langer, and B. M. Sorenson—903(A)

Nuclear Spectra (continued)
S^{35} β-spectrum, J. P. Mize and D. J. Zaffarano—902(A)
Tc^{93} and Tc^{96} isomeric transitions, Harry T. Easterday and Heinrich A. Medicus—752
Of Th^{231}(UY), Melvin S. Freedman, Arthur H. Jaffey, Frank Wagner, Jr., and Jack May—302
Ti^{48} excited levels, Paul L. Roggenkamp, Charles H. Pruett, and Roger G. Wilkinson—903(A)
Zn^{69} decay, R. B. Duffield and L. M. Langer—854
Zr^{95} and Nb^{95} γ-radiations, C. E. Mandeville, E. Shapiro, R. I. Mendenhall, E. R. Zucker, and G. L. Conklin—559
Nuclear theory (see also **Nuclear reactions; Nuclear spectra**)
Barrier penetration effects for light nuclei, B. E. Freeman and J. L. McHale—223
β-decay interaction, John M. Blatt—83; 914(A)
β-decay of triton, John Blatt—86
Charge independence of nuclear forces, David Feldman—1159(L)
Coupling of angular momenta in nuclear reactions, R. F. Christy—839
Cross terms in β-decay, O. Kofoed-Hansen and Aage Winther—526(L)
Deviations from LS coupling in spheroidal core nuclear model, J. P. Davidson and E. Feenberg—856
Evaluation of energy matrix of tensor forces, Igal Talmi—1065
Exchange magnetic moments of nuclei with almost closed shells of nucleons, Richard W. Cole—883(L)
Fermi term in β-ν correlation, D. C. Peaslee—1148(L)
Ground state of N^{14}, A. M. Feingold—318(L)
Lifetimes of nuclear isomers, Steven A. Moszkowski—474
Magnetic moments of odd-odd nuclei and strong spin-orbit coupling shell model, H. M. Schwartz—1293
New rigorous lower bound on range of triplet n-p interaction, Leslie L. Foldy—1251
Nonexistence of stable isobars with odd mass number, S. Sengupta—1296(L)
Nuclear constitution and interpretation of fission phenomena, David Lawrence Hill and John Archibald Wheeler—1102
Pairing property of nuclear interactions, G. Racah—913(A)
Production of polarized particles in nuclear reactions, A. Simon and T. A. Welton—886(L)
Pseudoscalar matrix element in β-decay, M. Ruderman—1227
Relativistic corrections to magnetic moments of nuclear particles, G. Breit and R. M. Thaler—1177
Tensor force interaction between shell closed except for single vacancy and external nucleon, J. Hope—884(L)
Validity of Born approximation in stripping, N. Austern—318(L)

Optical instruments (see **Methods and instruments**)

Pair production and annihilation
Electron-positron annihilation in flight, S. A. Colgate and F. C. Gilbert—790
Internal pair production of γ-rays of mesonic origin; alternate modes of π^0 decay, P. Lindenfeld, A. Sachs, and J. Steinberger—531
Momentum transfer and angle of divergence of pairs produced by photons, A. Borsellino—1023
Z-dependence of pair production cross section at 1.33 and 2.62 Mev, Irving E. Dayton—544
Phosphors and phosphorescence (see **Luminescence**)
Photoconductivity
In CdS at absorption edge, Clifford C. Klick—274
Induced conductivity in luminescent powders. II. Ac impedance measurements, Hartmut Kallmann, Bernard Kramer, and Arnold Perlmutter—700
Infrared photoconductivity due to neutral impurities in Si, E. Burstein, J. J. Oberly, and J. W. Davisson—331(L)
Photodisintegration (see **Nuclear photoeffects**)
Photoelectric effect
Extension of Makinson's theory of photoelectric emission to periodic potential, H. B. Huntington—357
Transition probability for photoelectric emission from semiconductors, H. B. Huntington and L. Apker—352
Photography and photographic emulsions (see also **Methods and instruments**)
Process for developing 400-micron nuclear emulsions, Mary B. Summerfield—340(A)
Photons (see **Gamma-rays; Radiation; X-rays**)
Polymers
Extensometer for rubber, R. P. Clifford—341(A)
Firestone shear flexometer, G. L. Hall and F. S. Conant—342(A)
Physics of rubber, S. D. Gehman—341(A)
Plasticizers for polyvinyl chloride, Mark L. Dannis—341(A)
Rubber fatigue test, K. E. Gui—341(A)
Viscoelastic properties as functions of distribution of activation energies, W. James Lyons—342(A)
Positrons (see **Electrons and positrons**)
Proceedings of the American Physical Society
Fifth Annual Conference on Gaseous Electronics at Princeton University and RCA Laboratories, Princeton, New Jersey, September 4, 5, and 6, 1952—335
Autumn Meeting of the New England Section at the University of New Hampshire, Durham, New Hampshire, October 25, 1952—340
Ohio Section Meeting at Akron University, Akron, Ohio, October 31 and November 1, 1952—341
Thanksgiving Meeting at Washington University, St. Louis, Missouri, November 28 and 29, 1952 [Bull. Am. Phys. Soc. **27**, No. 5 (1952)]—888

Quantum electrodynamics (see also **Field theory**)
Canonical transformation for electron-positron field coupled to time-independent electromagnetic field, H. E. Moses—115
Divergence of perturbation expansion, A. Petermann—1160(L)
Lamb shift for H and D, E. E. Salpeter—92
Lower limit for interaction time in photon-photon scattering, E. Gora—913(A)
Momentum transfer and angle of divergence of pairs produced by photons, A. Borsellino—1023
Pair creation in intermediate coupling theory, R. G. Moorhouse—958
Quantum field theory in light of distribution analysis, Werner Güttinger—1004
S-matrix and causality condition. I. Maxwell field, N. G. van Kampen—1072
Unified field theory and Born-Infeld electrodynamics, G. Rickayzen and B. Kurşunoğlu—522(L)
Quantum mechanics
Approximate two-body relativistic wave equations, Z. V. Chraplyvy—912(A)
Approximate wave functions for unbound relativistic particles in Coulomb field, G. K. Horton and R. T. Sharp—885(L)
Bohm's "interpretation of quantum theory in terms of 'hidden' variables," Joseph B. Keller—1040
Causal interpretation of quantum mechanics, Saul T. Epstein—319(L); David Bohm—319(L)
Classical and quantum field theories in Lagrangian formalism, Peter G. Bergmann and Ralph Schiller—4
Conversion of amplified Dirac equation to approximately relativistic form, W. A. Barker and Z. V. Chraplyvy—446
Primitive quantization in relativistic two-body problem, J. L. Synge—467

Proof that probability density approaches $|\psi|^2$ in causal interpretation of quantum theory, David Bohm—458
Quantum-mechanical methods in classical physics, David L. Falkoff—340(A)
Similarity theory of relativity and Dirac-Schrödinger theory of electrons, Banesh Hoffmann—52
Symmetry of S-matrix, F. Coester—519; 913(A)
Variation method in quantum statistics, John M. Richardson and William M. MacDonald—913(A)
Variational principles for three-body scattering problems, Sidney Borowitz and Bernard Friedman—441

Quenching of radiation (see **Radiation**)

Radiation (see also **Gamma-rays; Thermal radiation; X-rays**)
Bremsstrahlung cross section of 60-Mev electrons in Pb, C. D. Curtis—123
Contributions of Doppler effect to radiation exchange in stratosphere, Gilbert N. Plass and Daniel I. Fivel—898(A)
Decay of resonance radiation by spontaneous emission, E. J. Hellund—919
11-Mev thick target bremsstrahlung, J. W. Motz, William Miller, and H. O. Wyckoff—968
Energy loss and Čerenkov radiation of relativistic ionizing particle, P. Budini—1147(L)
Energy loss of fast charged particle by Čerenkov radiation, R. M. Sternheimer—1309(L)
Experimental energy and angular distributions of inner bremsstrahlung, T. B. Novey—672
Inelastic nuclear scattering of photons by Rh^{102}, C. S. del Río and V. L. Telegdi—909(A)
Lower limit for interaction time in photon-photon scattering, E. Gora—913(A)
Multiple Compton scattering of low energy γ-radiation, R. C. O'Rourke—999
Quenching of Hg resonance radiation (2537A) by N_2, C. G. Matland—338(A)
Systematic calculations of γ-ray penetration, Herbert Goldstein, J. Ernest Wilkins, Jr., and L. V. Spencer—1150(L)

Radioactivity (see also **Nuclear reactions; Nuclear spectra**)
α-γ angular correlation in RaTh, James Battey, L. Madansky, and F. Rasetti—182
α-radioactivity in 82-neutron region, J. O. Rasmussen, Jr., S. G. Thompson, and A. Ghiorso—33
Am^{241} γ-radiation, J. O. Newton and B. Rose—1157(L)
Atomic excitation and ionization accompanying orbital electron capture by nuclei, H. Primakoff and F. T Porter—903(A); 930
β-decay interaction, John M. Blatt—83; 914(A)
β-decay of triton, John Blatt—86
Of Br^{87}, a delayed-neutron activity, Andrew F. Stehney and Nathan Sugarman—194
Ca^{45} half-life, C. F. G. Delaney and J. H. J. Poole—529(L)
Of Cs^{138}, L. M. Langer, R. B. Duffield, and C. W. Stanley—907(A)
Continuous γ-ray spectrum accompanying β-decay, P. Bolgiano, L. Madansky, and F. Rasetti—679
Correlation between electron and recoil nucleus in He^6 decay, Brice M. Rustad and Stanley L. Ruby—880(L)
Effects of radioactive disintegrations on inner electrons of atom, J. S. Levinger—908(A)
Experimental energy and angular distributions of inner bremsstrahlung, T. B. Novey—672
"F" line of Th B, D. I. Meyer and F. H. Schmidt—908(A)
Genetics of Ge^{78}—As^{78} fission chain, Nathan Sugarman—570
Influence of nuclear quadrupole moment on α-γ angular correlation in RaTh, A. Abragam and R. V. Pound—1306(L)
Mg and Si heavy isotopes, Manfred Lindner—1150(L)
Mg^{28}, a new long-lived isotope, R. K. Sheline and N. R. Johnson—520(L)
Mo^{99}, R. M. Diamond—1149(L)
Of RaD, A. A. Jaffe and S. G. Cohen—454
Short-lived Ce isotopes from U fission, A. A. Caretto, Jr., and S. Katcoff—1267
Of 6.7-day U^{237}, F. Wagner, Jr., M. S. Freedman, D. W. Engelkemeir, and J. R. Huizenga—502
Of Th^{231}(UY), Melvin S. Freedman, Arthur H. Jaffey, Frank Wagner, Jr., and Jack May—302
W^{187} half-life, G. G. Eichholz—525(L)
Upper limit for atomic orbital electron ejection accompanying K-capture in Fe^{55}, F. T. Porter and H. P. Hotz—903(A); 938
Y^{92} and Y^{94} assignment, G. L. Schott and W. Wayne Meinke—1156(L)

Range and energy loss of particles
Density effect for ionization loss in various materials, erratum, R. M. Sternheimer—1309(L)
Electron capture by protons passing through H_2, J. David Jackson and Harry Schiff—359
Energy loss and Čerenkov radiation of relativistic ionizing particle, P. Budini—1147(L)
Energy loss of cosmic-ray μ-mesons in NaI crystals, erratum, A. Hudson and R. Hofstadter—1309(L)
Energy loss of fast charged particle by Čerenkov radiation, R. M. Sternheimer—1148(L)
Energy loss of medium-fast electrons in metals, E. M. Baroody—910(A)
Extrapolated ionization ranges for 10- to 250-kv protons in various gases, T. Jorgensen, E. Jones, and C. J. Cook—897(A)
Mean excitation potentials, Donald C. Sachs and J. Reginald Richardson—1163
Range correction for electron pickup, Walter H. Barkas—1019
Specific primary ionization of H_2, He, Ne, and A by high electrons, G. W. McClure—335(A)
Statistical fluctuations in ionization by 31.5-Mev protons, G. J. Igo, D. D. Clark, and R. M. Eisberg—879(L)
Transmission of electrons through thin metallic foils, C. H. Chang, C. S. Cook, and H. Primakoff—910(A)

Rectifiers (see **Electrical conductivity and resistance; Semiconductors**)

Relativity and gravitation
Arbitrary concentrations of matter and Schwarzschild singularity, Amalkumar Raychaudhuri—417
General-relativistic approach to short-range forces, Henri Amar—1298(L)
New equation in affine field laws, G. Bandyopadhyay—1161(L)
Primitive quantization in relativistic two-body problem, J. L. Synge—467
Quasi-relativistic theory of gravitation, Marvin G. Moore 587
Relativity of size, Banesh Hoffmann—49
Relativity precession of asteroid Icarus, J. J. Gilvarry—1046
Similarity theory of relativity and Dirac-Schrödinger theory of electrons, Banesh Hoffmann—52
Special-relativistic linear gravitational theory, F. J. Belinfante—914(A)
Spin and angular momentum in general relativity, Peter G. Bergmann and Robb Thomson—400
Unified field theory, C. Peter Johnson, Jr.—320(L); Albert Einstein—321(L)
Unified field theory and Born-Infeld electrodynamics, G. Rickayzen and B. Kurşunoğlu—522(L)

Resistance, electrical (see **Electrical conductivity and resistance**)

Resonance radiation
Decay of resonance radiation by spontaneous emission, E. J. Hellund—919
Quenching of Hg resonance radiation (2537A) by N_2, C. G. Matland—338(A)

Scattering of electrons, mesons, neutrons, protons, deuterons, and ions (see also **Electron diffraction; Nuclear reactions**)
Application of multiple scattering theory to cloud-chamber measurements, Martin Annis, H. S. Bridge, and S. Olbert—1216
Average neutron total cross sections in 3- to 12-Mev region, Norris Nereson and Sperry Darden—775
Bremsstrahlung cross section of 60-Mev electrons in Pb, C. D. Curtis—123
$C^{12}(p,p)C^{12}$ differential cross section, H. L. Jackson, A. I. Galonsky, F. J. Eppling, R. W. Hill, E. Goldberg, and J. R. Cameron—365
Certain explicit relationships between phase shift and scattering potential, Norman Levinson—755
Charge independence of nuclear forces, David Feldman—1159(L)
Cloud-chamber study of scattering of fast neutrons in O_2, J. P. Conner—712
Differential and total neutron scattering cross sections of deuteron in energy range 0.1 to 1.0 Mev, P. R. Tunnicliffe—1247
Distribution in energy of neutrons from interaction of 14-Mev neutrons with some elements, Elizabeth R. Graves and Louis Rosen—343
Elastic pion-hydrogen scattering in photographic emulsions, Gerson Goldhaber—1187
Elastic scattering of α-particles by O^{16}, John R. Cameron, Robert H. Davis, Ajay S. Divatia, Frederic J. Eppling, and Richard W. Hill—909(A)
Elastic scattering of protons from He^4, Bruce Cork—78
Elastic scattering of 6.5-Mev protons from Cu, L. M. Goldman—349
Electric scattering of deuterons, U. E. Kruse, N. F. Ramsey, and B. J. Malenka—655(L)
Electron-electron scattering at 6.1 Mev, W. C. Barber, G. E. Becker, and E. L. Chu—950
Excitation cross section for He atoms, Saul Altshuler—1093(L)
γ-rays produced by inelastic scattering of 14-Mev neutrons, Lewis C. Thompson—905(A)
Inelastic events induced by 32-Mev protons on He, Jack Benveniste and Bruce Cork—422
Inelastic scattering of neutrons, Robert B. Day—908(A)
Inelastic scattering of neutrons by Cd^{111}, A. E. Francis, J. J. G. McCue, and Clark Goodman—1232
Interpretation of high energy p-p scattering, Don R. Swanson—740
Magnetic inelastic scattering of neutrons in Fe, H. Palevsky, R. S. Carter, and D. J. Hughes—910(A)
Molière's theory of multiple scattering, H. A. Bethe—1256
Multiple scattering and many-body problem—applications to photomeson production in complex nuclei, Kenneth M. Watson—575
Multiple scattering and radiation damping, H. Ekstein—490
Multiple scattering correction to impulse approximation in two-body system, K. A. Brueckner—834
Multiple scattering effects in pion-deuteron scattering, K. A. Brueckner—909(A)
n-p scattering using organic crystal scintillation detectors, M. E. Remley, W. K. Jentschke, and P. G. Kruger—1194
Neutron resonances in Xe, S. P. Harris—904(A)
Neutron scattering by coupled paramagnetic ions, Philip J. Bendt—561
Of neutrons by coupled paramagnetic ions, Philip J. Bendt—561
Of neutrons by deuterons, R. K. Adair, A. Okazaki, and M. Walt—1165
Pion-nucleon scattering when coupling is weak and extended, Geoffrey F. Chew—591
Polarization effects in nucleon-nucleon scattering, Don R. Swanson—749
p-p scattering at 5.77 Mev using photographic techniques, R. O. Kerman, W. E. Kreger, and P. G. Kruger—908(A)
p-p scattering at intermediate energies, Andre Martin and Loup Verlet—519(L)
p-p scattering for nucleon isobar model, Frank T. Solmitz—1295(L)
Relation between photoproduction and scattering cross sections for π-mesons in complex nuclei, Norman C. Francis and Kenneth M. Watson—328(L)
Slow neutron resonances in Sm and Y, V. L. Sailor, H. L. Foote, Jr., and H. H. Landon—904(A)
Symmetry requirements in electron scattering by atom, L. E. H. Trainor and Ta-You Wu—273
Tables for second Born approximation scattering from various potential fields, Lyman Mower—947
Test for charge independence in high energy nucleon-nucleon scattering, B. A. Jacobsohn—881(L)
Total cross sections for fast neutrons, R. L. Becker, M. Walt, and A. Okazaki—904(A)
Total fast neutron cross sections of Co, Ga, Se, Cd, Te, Pt, Au, Hg, and Th, M. Walt, R. L. Becker, A. Okazaki, and R. E. Fields—1271
Total n-p scattering cross section at 4.75 Mev, E. M. Hafner, W. F. Hornyak, C. E. Falk, G. Snow, and T. Coor—204; at 2.5 Mev, R. E. Fields, R. L. Becker, and R. K. Adair—908(A)
Transmission of electrons through thin metallic foils, C. H. Chang, C. S. Cook, and H. Primakoff—910(A)
Validity of Born approximation in stripping, N. Austern—318(L)
Variational principles for three-body scattering problems, Sidney Borowitz and Bernard Friedman—441
Variational principles in scattering, Saul Altshuler—1278
Variational procedure for electron-hydrogen scattering, M. M. Gordon and J. G. Jones—913(A)
Velocity dependence of collision cross section for slow electrons in gases, O. T. Fundingsland, A. C. Faire, and A. J. Penico—337(A)

Scattering of radiation (see **Radiation**)

Scintillation counters (see **Methods and instruments**)

Secondary electrons (see **Electrons, secondary**)

Semiconductors (see also **Electrical conductivity and resistance**)
Influence of neutron bombardment on low temperature atomic heat of Si, P. H. Keesom, K. Lark-Horovitz, and N. Pearlman—900(A)
Interpretation of α-values in p-n junction transistors, F. S. Goucher and M. B. Prince—561
Magnetoresistive effect in semiconductors, theory, V. A. Johnson and W. J. Whitesell—941
Microwave observation of collision frequency of electrons in Ge, T. S. Benedict and W. Shockley—1152(L)
Properties of thermally treated Ge, Leo Esaki—1026
Shot noise in Ge filaments, R. H. Mattson and A. van der Ziel—899(A)
Shot noise in semiconductors, A. van der Ziel—900(A)
Temperature dependence of drift mobility in Ge, R. Lawrance—1295(L)
Thermal treatment of Si rectifiers, Leo Esaki—398
Transition probability for photoelectric emission from semiconductors, H. B. Huntington and L. Apker—352

Shock waves (see also **Explosion phenomena; Supersonics**)
Diffraction of strong shock waves, Wayland Griffith and David E. Brickl—451

In expansion of low pressure sparks, R. G. Fowler, W. R. Atkinson, and R. J. Lee—336(A)
Ion concentrations in shock-type spark discharge tubes, R. G. Fowler and H. C. Rose—906(A)
Propagation of explosive produced air shocks, J. Savitt—906(A)
Solid state (see **Crystalline state**)
Sound (see **Acoustics**)
Spallation (see **Nuclear reactions**)
Spark discharge (see **Discharge of electricity in gases**)
Specific heat (see **Thermal properties**)
Spectra, atomic (see **Atomic structure and spectra**)
Spectra, general
Afterglow spectra observable in incandescent lamps, Carl Kenty—336(A)
Effect of collisions upon Doppler width of spectral lines, Robert H. Dicke—472
Spectra, microwave (see **Microwaves and microwave spectra**)
Spectra, molecular (see **Molecular structure and spectra**)
Spectra, nuclear (see **Nuclear spectra**)
Spectra, x-ray (see **X-rays**)
Spectroscopy, technique (see **Methods and instruments**)
Spinor fields (see **Field theory**)
Statistical mechanics and thermodynamics
Entropy of fusion of monatomic liquids, N. K. Pope—899(A)
New theory of aggregates as supplement to van't Hoff's theory of solutions, George Antonoff—915(A)
Relativistic statistical thermodynamics, A. E. Scheidegger and R. V. Krotkov—1096
Variation method in quantum statistics, John M. Richardson and William M MacDonald—913(A)
Superconductivity (see also **Electrical conductivity and resistance**)
Anomalous critical current effect in superconducting NbN, Floyd C. Haley and Donald H. Andrews—821
Of $CoSi_2$, B. T. Matthias and J. K. Hulm—439
Current noise in partially superconducting resistors at temperatures down to 2°K, B. Kaplan and J. G. Daunt—907(A)
Frozen moments in superconducting sphere, Tom S. Teasdale—907(A)
Properties of superconductors below 1°K, T. S. Smith, W. B. Gager, and J. G. Daunt—654
Superconducting silicides and germanides, George F. Hardy and John K. Hulm—884(L)
Supersonics (see also **Shock waves**)
Plane supersonic flow patterns in ionized media, W. R. Atkinson and R. G. Fowler—906(A)

Thermal conductivity (see **Thermal properties**)
Thermal expansion (see **Thermal properties**)
Thermal properties
Angular points in densities of water *vs* temperature, George Antonoff and Raymond Madrazo, Jr.—899(A)
Entropy of fusion of monatomic liquids, N. K. Pope—899(A)
Influence of neutron bombardment on low temperature atomic heat, P. H. Keesom, K. Lark-Horovitz, and N. Pearlman—900(A)
Kinks in vapor pressure p *vs* temperature curves, George Antonoff—915(A)
Thermal conductivity of graphite, W. W. Tyler and A. C. Wilson, Jr.—870
Thermal expansion of solids, J. S. Dugdale and D. K. C. MacDonald—832
Transport phenomena in completely ionized gas, Lyman Spitzer, Jr., and Richard Härm—977
Thermionic emission, emitting surfaces
Analysis of Schottky deviation for highly refractory metals, D. W. Juenker, G. S. Colladay, and E. A. Coomes—894(A)
Of BaO, Virgil L. Stout—310
Effect of evaporation products from BaO coated cathode on secondary emission of MgO thin films, B. V. Haxby and P. Wargo—893(A)
Patch effect for thermionic emission from polycrystalline Ta, E. A. Coomes, J. A. Dezoteus, and J. F. Whalen—894(A)
Periodic deviations in Schottky effect for Mo, E. G. Brock, A. L. Houde, and E. A. Coomes—851
Probe measurements of cathode sputtering, G. Medicus and G. Wehner—339(A)
Rate of evolution of constituents of oxide coated cathode as function of molar composition of coating, R. W. Peterson—894(A)
Sputtering at low ion velocities, G. Wehner and G. Medicus—339(A)
Use of Ba^{140} in studies of oxide coated cathodes, J. H. Affleck and L. V. Holroyd—893(A)
Thermodynamics (see **Statistical mechanics and thermodynamics**)
Thermoelectric and thermomagnetic effects
Induced thermoelectric potential from radiation damage, Alan Andrew and Clifton R. Davidson—876(L)
Thermoelectric power of graphite, W. W. Tyler and A. C. Wilson, Jr.—870

Ultrasonics (see **Acoustics**)

Vacuum tubes (see **Methods and instruments**)

Wave mechanics (see **Quantum mechanics**)

X-rays
Low angle x-ray diffraction with long wavelengths, Burton Henke and Jesse W. M. DuMond—1300(L)
From mesic C atom, H. J. Schulte, J. B. Platt, and M. Camac—905(A)
Production of characteristic x-rays by proton bombardment, B. E. Simmons, H. W. Lewis, and E. Merzbacher—905(A)
Z-dependence of mesic x-ray yield, M. Camac, J. B. Platt, and H. J. Schulte—905(A)

THE AMERICAN INSTITUTE OF PHYSICS

INCORPORATED

57 East 55 Street New York 22, N.Y.

MEMBER SOCIETIES:

American Physical Society
KARL K. DARROW, *Secretary*, Columbia University, New York 27, New York.

Optical Society of America
ARTHUR C. HARDY, *Secretary*, Massachusetts Institute of Technology, Cambridge 39, Massachusetts.

Acoustical Society of America
WALLACE WATERFALL, *Secretary*, 57 East 55th Street, New York 22, New York.

Society of Rheology
G. J. DIENES, *Secretary*, Brookhaven National Laboratory, Upton, Long Island, New York.

American Association of Physics Teachers
R. F. PATON, *Secretary*, University of Illinois, Urbana, Illinois.

AFFILIATED SOCIETIES:

American Crystallographic Association
American Society for Metals
Electron Microscope Society of America
Physical Society of Pittsburgh
Physics Club of Chicago
Physics Club of Philadelphia
Cleveland Physics Society
Physics Club of the Lehigh Valley
Sigma Pi Sigma

ASSOCIATES:

Over seventy-five leading industrial enterprises and other institutions which contribute to the support of the Institute.

JOURNALS:

The Physical Review
S. A. GOUDSMIT, *Editor*, Brookhaven National Laboratory, Upton, Long Island, New York.

Reviews of Modern Physics
J. W. BUCHTA, *Editor*, University of Minnesota, Minneapolis, Minnesota.

Journal of the Optical Society of America
WALLACE R. BROCK, *Editor*, National Bureau of Standards, Washington 25, D. C.

The Journal of the Acoustical Society of America
FLOYD A. FIRESTONE, *Editor*, 57 East 55th Street, New York 22, New York.

American Journal of Physics
THOMAS H. OSGOOD, *Editor*, Michigan State College, East Lansing, Michigan.

The Review of Scientific Instruments
GAYLORD P. HARNWELL, *Editor*, Randal Morgan Laboratory of Physics, University of Pennsylvania, Philadelphia, Pennsylvania.

The Journal of Chemical Physics
CLYDE A. HUTCHISON, JR., *Editor*, Institute for Nuclear Studies, University of Chicago, Chicago 37, Illinois.

Journal of Applied Physics
ELMER HUTCHISSON, *Editor*, Case Institute of Technology, Cleveland 6, Ohio.

Physics Today
GAYLORD P. HARNWELL, *Editorial Director*; ROBERT R. DAVIS, *Managing Editor*, American Institute of Physics, 57 East 55 Street, New York 22, New York.

OFFICERS
GEORGE R. HARRISON, *Chairman*
Massachusetts Institute of Technology
GEORGE B. PEGRAM, *Treasurer*
Columbia University

GOVERNING BOARD
J. W. BUCHTA
KARL K. DARROW
G. J. DIENES
S. A. GOUDSMIT
GEORGE R. HARRISON
FREDERICK V. HUNT
DEANE B. JUDD
HUGH S. KNOWLES
C. C. LAURITSEN
WILLIAM F. MEGGERS
PHILIP M. MORSE
BRIAN O'BRIEN
GEORGE B. PEGRAM
I. I. RABI
DUANE ROLLER
FREDERICK SEITZ
WILLIAM SHOCKLEY
RICHARD M. SUTTON
J. H. VAN VLECK
MARK W. ZEMANSKY

Consultant on Printing
MELVIN LOOS

ADMINISTRATIVE STAFF
HENRY A. BARTON, *Director*
WALLACE WATERFALL, *Executive Secretary*
THEODORE VORBURGER, *Advertising Manager*
RUTH F. BRYANS, *Publication Manager*
BETTY H. GOODFRIEND, *Assistant Secretary*
EILEEN B. NEUBERGER, *Circulation Manager*
KATHRYN SETZE, *Assistant Treasurer*

THE American Institute of Physics was founded in 1931 as a federation of leading societies in the field of Physics. It combines into one operating agency those functions on behalf of physics which can best be done by the Societies jointly. Its purpose is the advancement and diffusion of physics and its applications to human welfare. To this end it publishes for itself or the Societies the nine journals listed on this page; promotes unity and effectiveness of effort among all who are interested in physics; renders numerous direct services to physicists and to the public; and cooperates with government agencies, national associations, educational institutions, technical industries, and others in such manner as to realize the opportunities and fulfill the responsibilities of physics as an important and constructive human activity.

CONTENTS

THE PHYSICAL REVIEW SECOND SERIES, VOLUME 89, NO. 6 MARCH 15, 1953

Mean Excitation Potentials . . . DONALD C. SACHS AND J. REGINALD RICHARDSON 1163
Scattering of Neutrons by Deuterons . . . R. K. ADAIR, A. OKAZAKI, AND M. WALT 1165
Approach to Saturation in Dilute Ferromagnetics . . . ALAN D. FRANKLIN AND ARI E. BERKOWITZ 1171
Experimental Investigation of the Nucleon Cascade in Water . . . C. B. A. MCCUSKER, H. MESSEL, D. D. MILLAR, AND N. A. PORTER 1172
Relativistic Corrections to the Magnetic Moments of Nuclear Particles . . G. BREIT AND R. M. THALER 1177
Study of Elastic Pion-Hydrogen Scattering in Photographic Emulsions . . . GERSON GOLDHABER 1187
Occurrence of Singularities in the Elastic Frequency Distribution of a Crystal . . . LÉON VAN HOVE 1189
Neutron-Proton Scattering Using Organic Crystal Scintillation Detectors . . . M. E. REMLEY, W. K. JENTSCHKE, AND P. G. KRUGER 1194
Conservation of Quanta for Nonlocal Fields . . . CHRISTOPHER GREGORY 1199
Nuclear Reactions with 21-Mev He^3 in a Cyclotron . . . D. N. KUNDU, T. W. DONAVEN, M. L. POOL, AND JOHN K. LONG 1200
Lifetimes of Metastable States of Noble Gases . . . A. V. PHELPS AND J. P. MOLNAR 1202
Macroscopic Theory of Superfluid He^3-He^4 Mixtures . . . P. J. PRICE 1209
Application of the Multiple Scattering Theory to Cloud-Chamber Measurements. II . . . M. ANNIS, H. S. BRIDGE, AND S. OLBERT 1216
Pseudoscalar Matrix Element in Beta-Decay . . . M. RUDERMAN 1227
Effect of X-Ray Irradiation on the Self-Diffusion Coefficient of Na in NaCl . . . [DILLON MAPOTHER 1231
Inelastic Scattering of Neutrons by Cd^{111} . . . A. E. FRANCIS, J. J. G. MCCUE, AND CLARK GOODMAN 1232
Charge States of a Helium Beam in Hydrogen, Helium, Air, and Argon . . . ELIAS SNITZER 1237
Nuclear Magnetic Moment of Pr^{141} from the Hyperfine Structure of Pr II . . . PETER BRIX 1245
Differential and Total Neutron Scattering Cross Sections of the Deuteron in the Energy Range 0.1 to 1.0 Mev . . . P. R. TUNNICLIFFE 1247
New Rigorous Lower Bound on the Range of the Triplet Neutron-Proton Interaction . LESLIE L. FOLDY 1251
Effects of the Atmosphere on the Penetrating Cosmic Radiation . . . ROBERT L. CHASSON 1255
Moliére's Theory of Multiple Scattering . . . H. A. BETHE 1256
Short-Lived Cerium Isotopes from Uranium Fission . . . A. A. CARETTO, JR., AND S. KATCOFF 1267
Gamma-Radiation from Interaction of 14-Mev Neutrons with Iron . . . V. E. SCHERRER, R. THEUS, AND W. R. FAUST 1268
Total Fast Neutron Cross Sections of Co, Ga, Se, Cd, Te, Pt, Au, Hg, and Th . . . M. WALT, R. L. BECKER, A. OKAZAKI, AND R. E. FIELDS 1271
Direct Comparison of m/e for the Positron and the Electron . L. A. PAGE, P. STEELE, AND S. B. GUNST 1273
Applications of Variational Principles to Scattering Problems . . . SAUL ALTSHULER 1278
Absolute Determination of Resonant Energies for the Radiative Capture of Protons by Boron, Carbon, Fluorine, Magnesium, and Aluminum in the Energy Range below 500 kev . . . S. E. HUNT AND W. M. JONES 1283
Fission Neutron Spectrum of U^{235} . . . DAVID B. NICODEMUS AND HANS H. STAUB 1288
Radioactive Decay of Tungsten 187 . . . J. M. CORK, M. K. BRICE, W. H. NESTER, J. M. LE BLANC, AND D. W. MARTIN 1291
Magnetic Moments of Odd-Odd Nuclei and the Strong Spin-Orbit Coupling Shell Model . H. M. SCHWARZ 1293

Letters to the Editor:

Temperature Dependence of Drift Mobility in Germanium . . . R. LAWRENCE 1295
Proton-Proton Scattering for a Nucleon Isobar Model . . . FRANK T. SOLMITZ 1295
Nonexistence of Stable Isobars with Odd Mass Numbers . . . S. SENGUPTA 1296
Crystallization of Silicon from a Floating Liquid Zone . . . PAUL H. KECK AND MARCEL J. E. GOLAY 1297
Ferroelectricity in Oxides of Face-Centered Cubic Structure . . . W. R. COOK, JR., AND HANS JAFFE 1297
Variational Methods for Periodic Lattices and Artificial Dielectrics . . . CARSON FLAMMER 1298
General Relativistic Approach to Short-Range Forces . . . HENRI ARMAND 1298
Generation of *F* Centers at Low Temperature . . . FREDERICK SEITZ 1299
Low Angle X-Ray Diffraction with Long Wavelengths . . . BURTON HENRY AND JESSE W. M. DUMOND 1300
Resolution of the "Proton Difference Method" . . . J. GOLDEMBERG AND L. KATZ 1300
Photoproduction of Neutral Mesons in Hydrogen at High Energies . . . R. L. WALKER, D. C. OAKLEY, AND A. V. TOLLESTRUP 1301
(n,γ) and $(n,2n)$ Reactions in Iodine . . . H. C. MARTIN AND R. F. TASCHEK 1302
Precision Measurement of Co Gamma-Radiation . . . G. LINDSTRÖM, A. HEDGRAN, AND D. E. ALBURGER 1303
Mass Relation of Heavy Particles . . . H. ENATSU 1304
Pure Nuclear Quadrupole Spectrum of Bi^{209} in Bismuth-Trihalogen . . . H. G. ROBINSON, H. G. DEMMELT, AND WALTER GORDY 1305
Diamagnetism of an Enclosed Electron Gas . . . H. A. NYE 1305
Activation Cross Sections Measured with Antimony-Beryllium Photoneutrons. II . . . CLYDE KIMBALL AND BERNARD MARGOLIS 1306
Influence of the Nuclear Quadrupole Moment on the $\alpha-\gamma$ Angular Correlation in Radiothorium . . . A. ABRAGAM AND R. V. POUND 1306
Neutron Capture Cross Sections for Production of Sr^{89} and Sr^{90} . . . W. S. LYON 1307
Angular Distribution of Particles from Stars . . . R. W. WAINIOKI AND TAKICHIRO CHITOSE 1307

Errata . . . 1308
Author Index to Volume 89 . . . 1309
Analytical Subject Index to Volume 89 . . . 1320

LANCASTER PRESS, INC., LANCASTER, PA.